3455

INVESTIGATIONS OF HYDROGEN-BONDED ORGANIC SOLIDS BY X-RAY CRYSTALLOGRAPHY AND EXPERIMENTAL CHARGE DENSITIES

A Thesis

Submitted for the Degree of

Doctor of Philosophy

By

T. R. ANUPAMA

Chemistry and Physics of Materials Unit

JAWAHARLAL NEHRU CENTRE FOR ADVANCED

SCIENTIFIC RESEARCH (A Deemed University)

BANGALORE 560 064, INDIA

MAY 2003
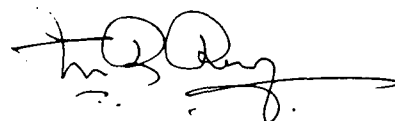
To Amma, Appa, Archana and Balaji

DECLARATION

I hereby declare that the matter embodied in this thesis entitled "**Investigations of hydrogen-bonded organic solids by X-ray crystallography and experimental charge densities**" is the result of investigations carried out by me at the Chemistry and Physics of Materials Unit, Jawaharlal Nehru Centre for Advanced Scientific Research, Bangalore, India, under the supervision of Professor C. N. R. Rao, *FRS* and Professor G. U. Kulkarni.

In keeping with the general practice of reporting scientific observations, due acknowledgement has been made whenever the work described has been based on the findings of the other investigators. Any omission that might have occurred by oversight or error of judgement is regretted.
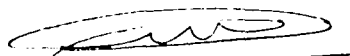
T. R. ANUPAMA

CERTIFICATE

Certified that the work described in this thesis titled "**INVESTIGATIONS OF HYDROGEN-BONDED ORGANIC SOLIDS BY X-RAY CRYSTALLOGRAPHY AND EXPERIMENTAL CHARGE DENSITIES**" has been carried out under our supervision at the Chemistry and Physics of Materials Unit, Jawaharlal Nehru Centre for Advanced Scientific Research, Bangalore, India.

Prof. C. N. R. Rao

Prof. G. U. Kulkarni

ACKNOWLEDGEMENTS

CONTENTS

INVESTIGATIONS OF HYDROGEN-BONDED ORGANIC SOLIDS BY X-RAY CRYSTALLOGRAPHY AND EXPERIMENTAL CHARGE DENSITIES

PART 1 X-RAY CRYSTALLOGRAPHIC INVESTIGATIONS OF THE SUPRAMOLECULAR ARCHITECTURES IN HYDROGEN-BONDED ORGANIC SOLIDS

1. SUPRAMOLCEULAR ARCHITECTURES FORMED BY HYDROGEN-BONDED ORGANIC SOLIDS: AN OVERVIEW

2. SCOPE OF THE PRESENT INVESTIGATIONS

3. EXPERIMENTAL

4. RESULTS AND DISCUSSION

4. RESULTS AND DISCUSSION

PREFACE

The Thesis consists of two parts, Part 1 dealing with X-ray crystallographic investigations of supramolecular architectures in hydrogen-bonded organic solids and Part 2 with the experimental charge density investigations of hydrogen-bonded organic solids. In both these parts, the underlying theme is the study of the crucial role and properties of the hydrogen bond in the molecular systems.

In **Part 1**, the following systems have been investigated:

Channels formed by four-membered networks of trimesic acid,

Layered hydrogen-bonded structures formed by dinitrobenzoic acids,

Layered hydrogen-bonded structures formed by aliphatic dicarboxylic acids with aza-aromatics,

Solvent-directed self-assembly of adducts formed by 4,4'-bipyridine with cyanuric acid and N-methylcyanuric acid,

Cyanurate mimics of hydrogen bonding patterns of nucleic acids,

Organic channel structures formed by the hydrogen bonding interaction of melamine with cyanuric and trithiocyanuric acid,

Organic porous solids formed by trithiocyanuric acid with 4,4'-bipyridine, and

Metal-organic assembly in the silver salt of cyanuric acid.

Of the various systems listed above, specially noteworthy are the synthesis of the organic porous solid containing channels, formed by trithiocyanuric acid and 4,4'-bipyridine, accommodating aromatic guests, the rosette structure formed between cyanuric acid and melamine and the novel metal-organic hybrid layered structure in silver cyanurate.

Part 2 of the thesis deals with the experimental charge density studies of hydrogen-bonded crystals. The investigations have provided useful correlations of the various charge density descriptors with the hydrogen-acceptor distance, the variation of the positive curvature of the electron density at the bond critical point being particularly exact. Based on the disposition of the lone-pairs of electrons on the participating donor and acceptor atoms in a series of O-H$\cdots$O hydrogen bonds and the bond paths, it has been possible to provide a complete description of the hydrogen bond. These investigations have provided new insights into the hydrogen bond in terms of the location of the bond critical point and its relation to the geometry of the lone-pairs.

***

List of acronyms and formulae

D	Donor
A	Acceptor
2D	Two-dimensional
3D	Three-dimensional
CSD	Cambridge Structural Database
CCDC	Cambridge Crystallographic Data Centre
AIM	Atoms in Molecules
BCP	Bond critical point
BP	Bond path
CP	Critical point
CCP	Cage critical point
RCP	Ring critical point
LP	Lone-pair
ρ	electron density in $e\text{Å}^{-3}$
$\nabla^2\rho$	Laplacian of the electron density in $e\text{Å}^{-5}$
$\lambda_1, \lambda_2, \lambda_3$	Curvatures of the electron density in $e\text{Å}^{-5}$
ε	ellipticity ($= \dfrac{\lambda_1}{\lambda_2} - 1$)

<u>Residuals</u>

Statistical factors are defined as

$$R_{int} = \frac{\sum (I - <I>)}{\sum I} \qquad R_{merge} = \left[\frac{\sum |F_o|^2 - |F_o(mean)|^2}{\sum |F_o|^2} \right]$$

$$R_1 = \frac{\sum K^{-1}|F_o| - |F_c|}{\sum K^{-1}|F_o|} \qquad wR_2 = \left[\frac{\sum w(K^{-1}|F_o| - |F_c|)^2}{\sum wK^{-2}|F_o|^2} \right]^{1/2}$$

$$GOF = \left[\frac{\sum w(K^{-1}|F_o| - |F_c|)^2}{n - p} \right]^{1/2}$$

I is the Bragg intensity, $|F_o|$ and $|F_c|$ are the moduli of the observed and the calculated structure factors, respectively, K is the scale factor, w is the statistical weight, p is the number of refined parameters, and n is the number of used data.

PART 1

X-RAY CRYSTALLOGRAPHIC INVESTIGATIONS OF THE SUPRAMOLECULAR ARCHITECTURES IN HYDROGEN-BONDED ORGANIC SOLIDS*

SUMMARY

A variety of organic solids with supramolecular architectures involving O-H⋯O, N-H⋯O, O-H⋯N, N-H⋯N and other hydrogen bonds are known. In the present study, we have prepared adducts between different donor and acceptor molecules by co-crystallization to obtain molecular-recognition directed supramolecular assemblies consisting of two-dimensional layered networks, cavities, three-dimensional channels, and related structures. The important systems investigated are the following: trimesic acid solvates, adducts of 4,4'-bipyridine with 3,5-dinitrobenzoic acid and 3,5-dinitro-4-methylbenzoic acid, complex of 1,4-diiodobenzene with 3,5-dinitrobenzoic acid, co-crystals formed by aliphatic dicarboxylic acids with 2,4,6-triaminopyrimidine, co-crystals of 4,4'-bipyridine with cyanuric acid and *N*-methylcyanuric acid, adduct of 9-ethyladenine with *N*-methylcyanuric acid, complexes of melamine with cyanuric and trithiocyanuric acids, adducts of trithiocyanuric acid with 4,4'-bipyridine, and a silver cyanurate complex. The highlights of the results of X-ray crystallographic studies on these systems are presented below.

The solvent employed for the crystallization has a significant effect on the hydrogen-bonded structure of 1,3,5-benzenetricarboxylic acid (trimesic acid). Thus, trimesic acid crystallized from DMF/benzene yields a crystal structure comprising of 2D molecular tapes between TMA and DMF. Crystallization from methanol/benzene, however, gives 4-membered networks with a polymeric chain of O-H···O hydrogen bonded methanol molecules inside the channels. Crystallization of trimesic acid with acetone yields a structure identical to that obtained from methanol/benzene, with the acetone molecules residing in the channels.

Layered hydrogen-bonded structures formed by 3,5-dinitrobenzoic acid and 3,5-dinitro-4-methylbenzoic acid with 4,4'-bipyridine involve single O-H···N and C-H···O hydrogen bonds between the acid and the bipyridyl rings. Also, the adduct formed by 3,5-dinitro-4-methyl benzoic acid, 4,4'-bipyridine and anthracene, is stabilized by the formation of the pairwise O-H···N/C-H···O hydrogen bonds.

The crystal structure of the complex of 3,5-dinitrobenzoic acid and 1,4-diiodobenzene consists of bifurcated I···O interactions, that help to bring two molecules of the acid closer forming hydrogen bonds with each other. There are centrosymmetric O-H···O hydrogen-bonded synthons between the carboxylic acid groups of the adjacent molecules. This pattern gives rise to a helical type of arrangement in the crystal structure.

Layered hydrogen-bonded structures formed by aliphatic dicarboxylic acids with 2,4,6-triaminopyrimidine yield different hydrogen bonding patterns depending on the number of $-CH_2$ groups in the acid molecule. The hydrogen-bonded molecular

complexes of the aliphatic diacids with 2,4,6-triaminopyrimidine show crossed ribbon networks in the case of the odd carbon malonic and glutaric acids and a two-dimensional sheet in the case of the even carbon adipic acid.

Co-crystallization of cyanuric acid and 4,4'-bipyridine gives two different types of molecular complexes on varying the solvent of crystallization. A 2:1 adduct is formed from methanol and a 1:1 adduct from water. Such a difference is attributed to the different hydrogen-bonded networks formed within the crystal structures of cyanuric acid upon crystallization from methanol and water. *N*-methylcyanuric acid, when crystallized from methanol or water forms two different chain structures but consist of a single type of hydrogen-bonded chains. The presence of the methyl group does not favour cyclic hydrogen-bonded dimers. Only one type of hydrogen bond network is obtained in the adduct of *N*-methylcyanuric acid and 4,4'-bipyridine, irrespective of the solvent of crystallization.

A unique molecular complex is formed by *N*-methylcyanuric acid with 9-ethyladenine. This complex is stabilized by homomeric and heteromeric hydrogen bond patterns. These patterns are different from those observed in the crystal structures of the pure phases. Such a complexation can mimic the role of the nucleobases thymine (T) or uracil (U) in complementary base pairing with adenine (A). The formation of this complex can be regarded as a substitution reaction through noncovalent synthesis with the lattice substitution of *N*-methylcyanuric acid in between a pair of ethyladenine molecules in the resulting two-dimensional sheets.

1:1 co-crystals of cyanuric acid and melamine (as well as trithiocyanuric acid and melamine) have been obtained by hydrothermal synthesis. The structure is

stabilized by antiparallel, triple, N-H···O– N-H···N– N-H···O hydrogen bonds (sulphur replaces oxygen in the trithiocyanuric acid-melamine adduct). A hexameric, rosette structure giving rise to channels was obtained in both the cases. A unique feature of this rosette is all the hydrogen bond donor and acceptor groups in both cyanuric acid (and trithiocyanuric acid) and melamine molecules are used in hydrogen bond formation.

The supramolecular hydrogen bond assemblies obtained from the crystallization of trithiocyanuric acid and 4,4'-bipyridine along with a variety of aromatic guest molecules, give rise to interesting channel structures. This host-guest assembly is stabilized by a three-point C-H···S– N-H···N– C-H···S recognition pattern and centrosymmetric N-H···S hydrogen-bonded dimers. Benzene, toluene and xylenes are accommodated in the channels while mesitylene is not. In the case of the xylenes, the para isomer can be accommodated reversibly.

A hybrid layer compound containing silver sheets and an organic spacer (cyanuric acid) has been synthesized that shows interesting molecular recognition synthons and electrical properties. The structure consists of two-dimensional sheets of positively charged silver atoms that are pillared by cyanurate anions. Perpendicular to the silver sheets, the cyanuric acid molecules are held to each other through single N-H···O hydrogen-bonded chains. Dative bonds are formed by the silver ions with oxygen and nitrogen atoms.

1. SUPRAMOLECULAR ARCHITECTURES FORMED IN HYDROGEN-BONDED ORGANIC SOLIDS: AN OVERVIEW

1.1 Introduction

Properties of molecular crystals, consisting of organic molecules, organometallics or coordination complexes, depend on the structure as well as the three-dimensional architecture adopted in the crystalline form. Interest in these materials stems from the potential to manipulate solid-state properties of single crystals by systematically varying the molecular structure and properties of the molecular sub-units. This crucial link between the structure of a molecular assembly and its solid-state reactivity was clearly demonstrated by the pioneering studies of Schmidt,[1] who showed that different solid-state packing arrangements (i.e., polymorphs, α, β and γ) of *trans*-cinnamic acids led to distinctly different photodimerization behaviours (see Scheme 1.1).
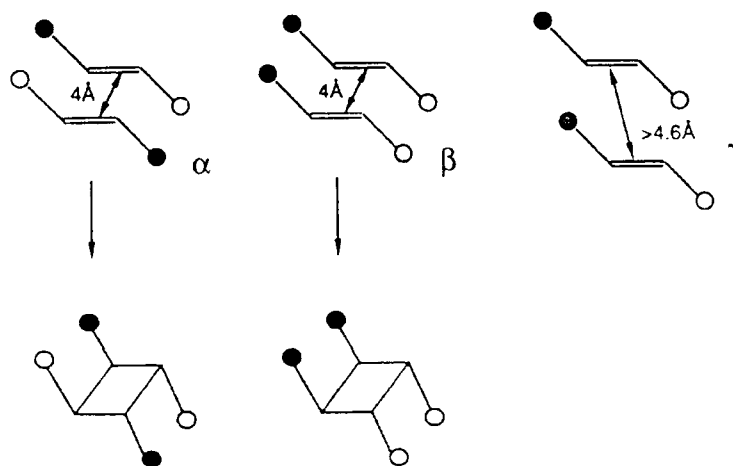
Scheme 1.1 Photoactive (α and β) and photostable (γ) forms of trans-cinnamic acids.[1]

In connection with this discovery, Schmidt suggested the term 'crystal engineering', which has since been used to describe the design and synthetic strategies of molecules or functional materials.[2]

1.2 Intermolecular interactions

The process of crystal engineering is a study in balance and interaction. Chemistry of the covalent bond is not so concerned with subtle equilibria because the energetic barriers between the reactants and the products are orders of magnitude larger than those that separate, for instance, hydrogen-bonded pairs from free acids. In order to rationalize and predict the structures of molecular solids, it is pertinent to take into account the relative strengths of the non-bonding (intermolecular) contacts that mesh neighbouring molecules in a three-dimensional array. Noncovalent (or non-bonding) interactions are responsible for the bulk of the information that passes through living systems. These forces are the fundamental causes for the crystallization and dissolution of organic molecules as well. As many of these interactions are destroyed in solution, their study in the solid state becomes essential. Crystallization of a pure substance is accompanied by a reduction in the translational freedom, which leads to a decrease in entropy. Simultaneously, there is a gain in the enthalpy. This enthalpy gain arises from a balance of the attractive and the repulsive forces between the molecules in a crystal. The attractive forces are of two kinds: dispersion and electrostatic (or Coulombic) interactions. These interactions are classified based on their distance dependence and their directionality. Dispersion interactions are attractive, but weak and nondirectional. Electrostatic interactions have a markedly

directional character, notable among these are hydrogen bonding and charge transfer interactions. There are long range forces that are effective over distances greater than 10 nm down to ~ 0.2 nm. These are the weak van der Waals forces (< 8 kJ mol^{-1}) which are nondirectional, although they are responsible for bringing nonpolar molecules together and aligning them.

The basis of molecular recognition is the presence of information in the reacting components, this information being expressed by the potential of one of the components to enter into noncovalent interaction with the other components, and by its electronic and steric requirements. The various distance dependencies and directionalities discussed above give rise to an overall stabilizing arrangement. Such arrangements result in the close-packing of molecules in a molecular crystal. Kitaigorodskii described this concept as the close-packing model.[3] Thus, it has been shown that for molecules of arbitrary shapes, close packing is possible only in a limited number of space groups, a prediction that proved to be in agreement with the analysis based on the data from the Cambridge Structural Database (CSD).

1.3 The hydrogen bond

The hydrogen bond is probably the strongest of all the non-covalent, weak intermolecular interactions.[4,5] Traditionally, it has been thought to be essentially an electrostatic interaction between a proton and a highly electronegative acceptor atom such as oxygen or nitrogen, the latter usually possessing a lone pair of electrons. It is now well established that the high electron density regions in ethylenic and acetylenic bonds[6] as well as the π-face of aromatic or heteroaromatic rings[7] can virtually act as

acceptors. The other known acceptors include sulfur[8] and halogen atoms.[9] The O-H, N-H and F-H groups are some examples of hydrogen bond donors. Less electronegative groups such as C-H and S-H, also act as proton donors.[10] The basic geometrical criteria for a hydrogen bond, D-H$\cdots$A-X (D:donor, A:acceptor) require that the hydrogen bonding distance ($d_{H\ldots A}$) should be less than the sum of the van der Waals radii of the H and A atoms with a donor-hydrogen-acceptor angle (θ) close to 180° as well as a nearly planar DHAX system (Figure 1.1a). The actual ranges of these parameters vary depending on the donor and acceptor groups. Hydrogen bonds cover a wide energy spectrum (Figure 1.1b), ranging from a covalent-type of bond to a weak dipolar attraction.
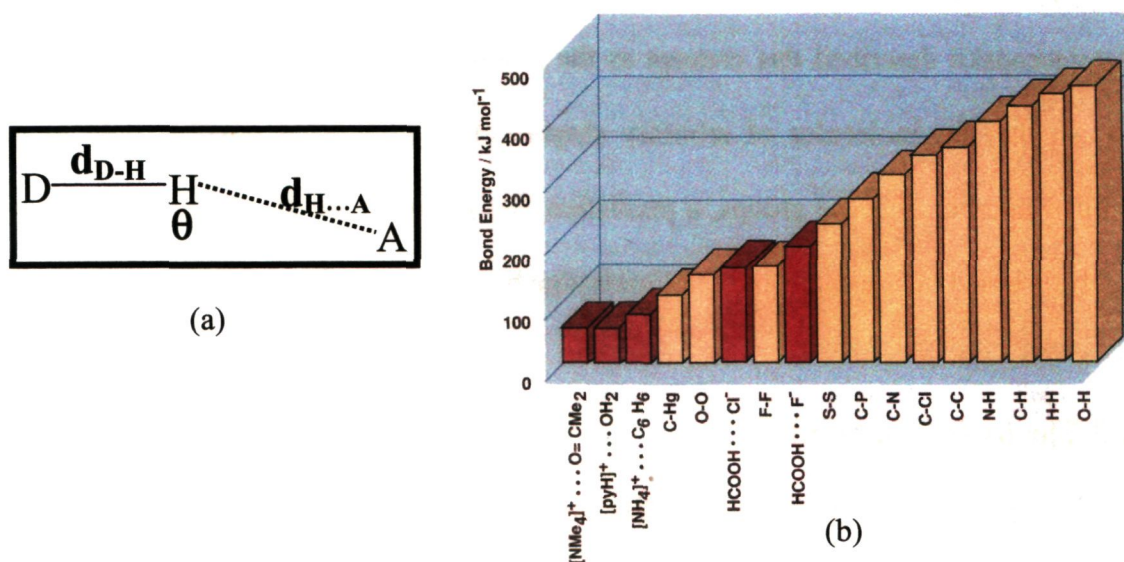
Figure 1.1: *(a) Geometrical attributes of a hydrogen bond, (b) Bond energies for a range of common σ-bonds compared with a number of strong hydrogen bonds.*

A broad classification of the hydrogen bond into strong, moderate and weak has been based on a variety of methods such as IR,[11] Raman and NMR,[12] use of potential functions,[4] isotope effects,[13] besides purely geometrical criteria using

crystallographic techniques.[14] Statistical surveys of the hydrogen bond geometries using structural databases such as the CSD[15] have been carried out in the last two decades from which a number of publications have resulted.[16]

The hydrogen bond plays a vital role in determining the shapes and biological properties of macromolecules such as the proteins and the nucleic acids.[5,17] They aid molecular recognition, forming large assemblies. Etter[18] carried out extensive studies on hydrogen bonds and proposed a set of guidelines based on graph theory, for encoding hydrogen bond patterns in organic solids. The four basic hydrogen bond motifs (**D**:dimer, **C**:chain, **S**:intramolecular bond, **R**:ring) are illustrated in some examples in Figure 1.2.
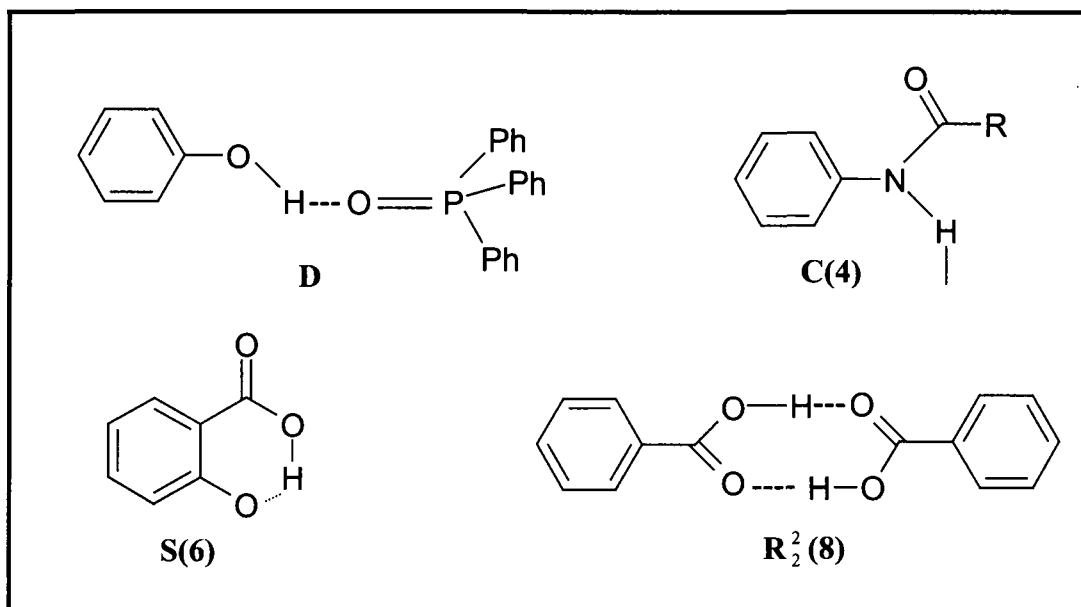
***Figure 1.2:** Graph set notations for some hydrogen-bonded motifs[18]*

Today, we understand the nature of the hydrogen bond in some detail because of the theoretical developments. The very first attempts were made by Pauling who used an electrostatic model[19] and showed trends in the observed hydrogen bond energies.[20] Tsubomura and Coulson[21] applied the perturbation theory to estimate the contribution of various energy components to the hydrogen bond energy. Bader rationalized the observed shifts in the D-H force constants with an electrostatic model.[22] Such early theoretical studies on hydrogen bond, especially using molecular orbital or semi-empirical calculations have been reviewed by many authors.[23] Morokuma *et al*[24] developed an energy partitioning method based on Hartree-Fock SCF formalism to study the nature of hydrogen bonding. Rao *et al*[25] have reviewed results of semi-empirical and ab-initio studies of hydrogen-bonded complexes.

1.4 Supramolecular design and the prediction of crystal structures

Construction of molecular assemblies employing noncovalent bonds has been referred to as noncovalent synthesis by Lehn[26] and Whitesides.[27] It is analogous to molecular synthesis (1-100 Å length scales) except that weak noncovalent bonds control the structure of the solid state (with much larger length scales of 10-1000 Å). This new methodology has indeed started to bridge the gap between molecular and macromolecular structures.[28] In recent years, a number of multimolecular assemblies have been synthesized employing these noncovalent bonds, which has led to the birth of a highly interdisciplinary field of chemical research – supramolecular chemistry. Supramolecular chemistry was defined in the words of Lehn,[26] "Just as there is a field of *molecular chemistry* based on the covalent bond, there is a field of *supramolecular*

chemistry, the chemistry of molecular assemblies and of the intermolecular bond."

This is depicted in Scheme 1.2. Following Lehn's analogy, if molecules formed by covalent bonds, are the targets in organic synthesis, crystals assembled via intermolecular interactions may be considered as targets in supramolecular synthesis.[29]

Among the numerous noncovalent bonds, hydrogen bonds such as O-H···O, N-H···O and C-H···O have been widely used, as the nature of these bonds is well understood both theoretically and experimentally than other bonds. There are also a few examples available in the literature using non-hydrogen bonds in the design and synthesis of supramolecular assemblies. The non-hydrogen bonds are due to those of the type Cl···O, Br···O, I···O, I···I, O···I, N···Cl and so on. There are a few examples where such interactions have been made use of in the synthesis of supramolecular assemblies. For instance, the 1:1 supramolecular assembly between 1,4-dinitrobenzene and 1,4-diiodobenzene formed through I···O interactions is a representative example.[30]
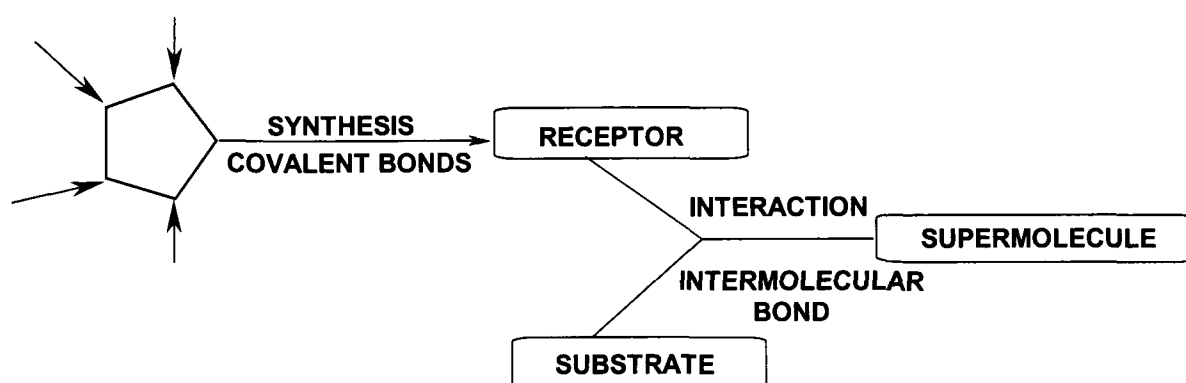
Scheme 1.2 *From molecular to supramolecular chemistry: molecules and supermolecules.*

The noncovalent interactions discussed above can be combined to generate *supramolecular synthons*. The term 'synthon' was first introduced by Corey, who defined it as 'structural units within molecules which can be formed and/or assembled by known or conceivable synthetic operations.[31,32] The use of this term has been extended by Desiraju to describe supramolecular subunits. The identification and use of robust synthons considerably mitigates the difficulties involved in crystal structure design or prediction. Some examples of synthons based on strong and weak hydrogen bonds are illustrated in Scheme 1.3.
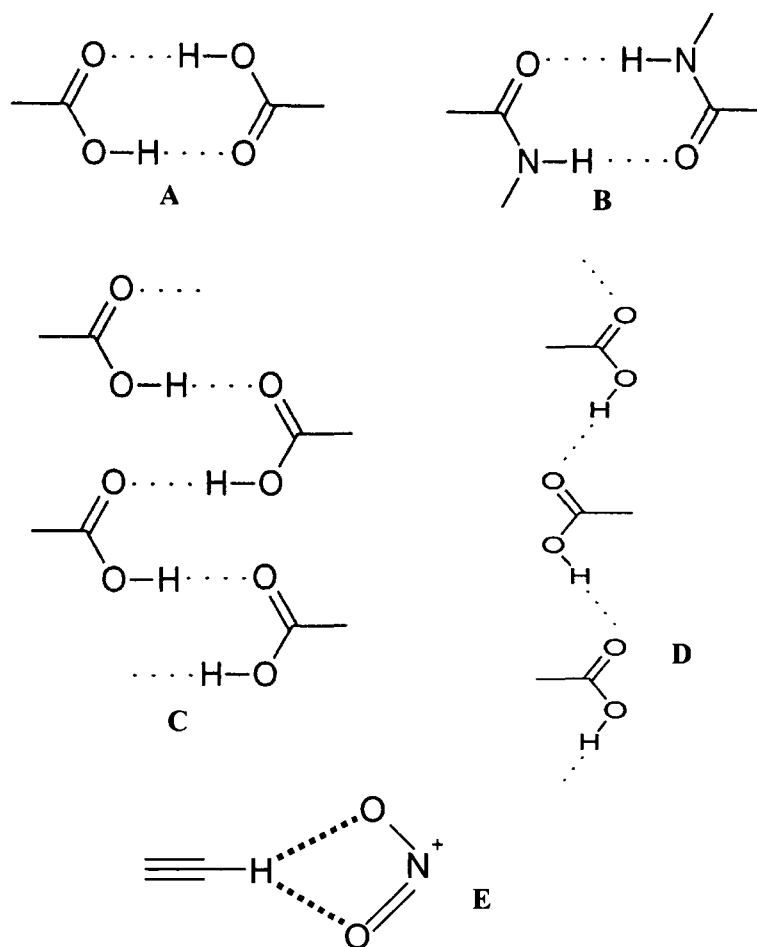
Scheme 1.3 *Representative supramolecular synthons*
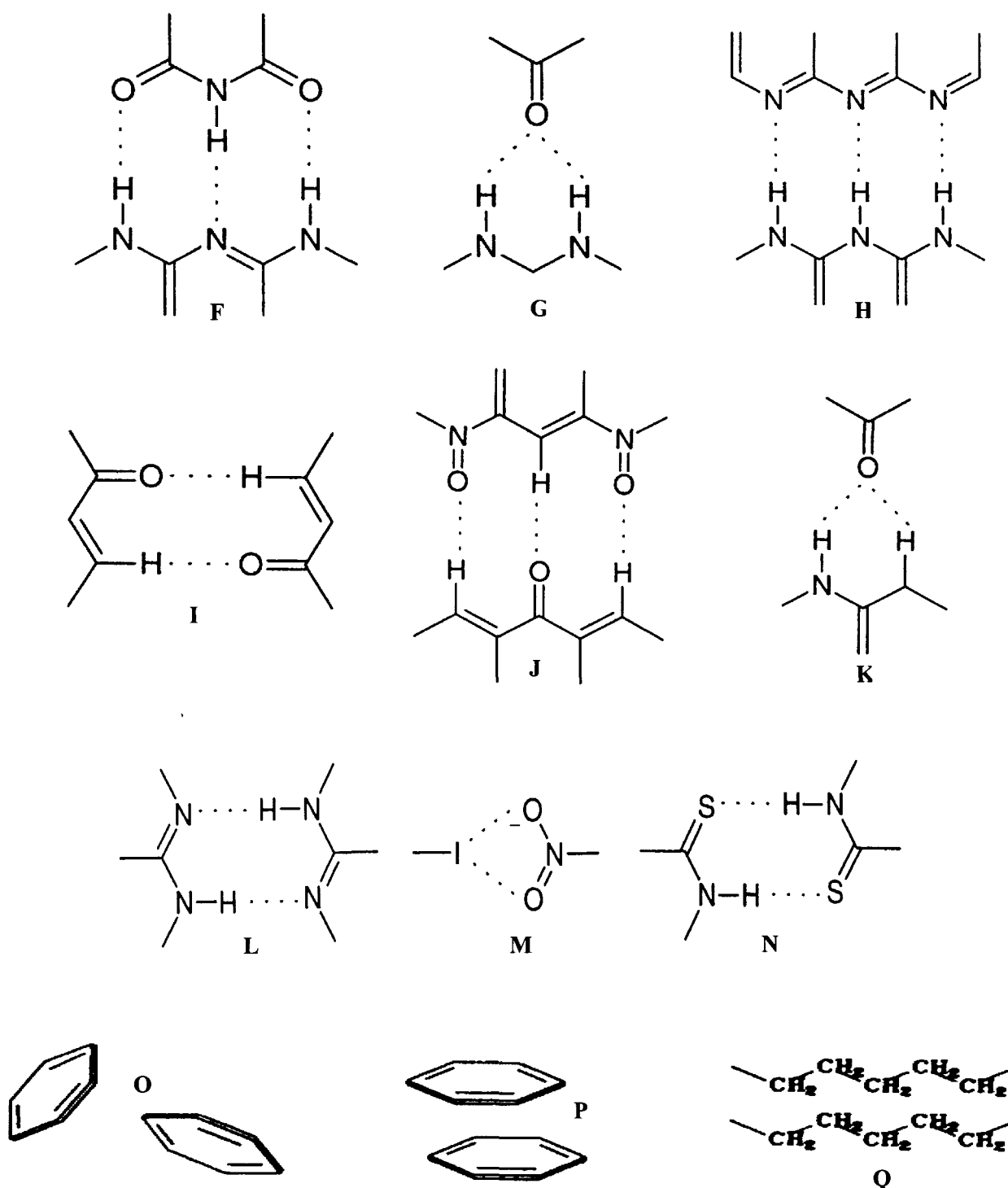
Scheme 1.3 *Representative supramolecular synthons (continued).*

1.4.1 Engineering strategies based on strong hydrogen bonds

The strongest and most directional of all hydrogen bonds are the ones in which the hydrogen atom is bound to a highly electronegative donor and acceptor, such as F, O and N. These are considered as 'classical' or 'conventional' hydrogen bonds. Their directionality and distinct geometrical features have been extensively discussed and reviewed.[33-38] Following is a discussion on the known conventional hydrogen bonds like O-H···O, N-H···O, O-H···N and N-H···N bonds.

The carboxylic acid dimer synthon (**A** in Scheme 1.3) is utilized in the arrangement of aromatic carboxylic acids like benzoic,[39] terephthalic,[40] isophthalic,[41] trimesic[42] and adamantane-1,3,5,7-tetracarboxylic acid[43] to produce zero-dimensional dimers, one-dimensional linear tapes, two-dimensional sheets and three-dimensional diamondoid structures, respectively (see Figure 1.3).
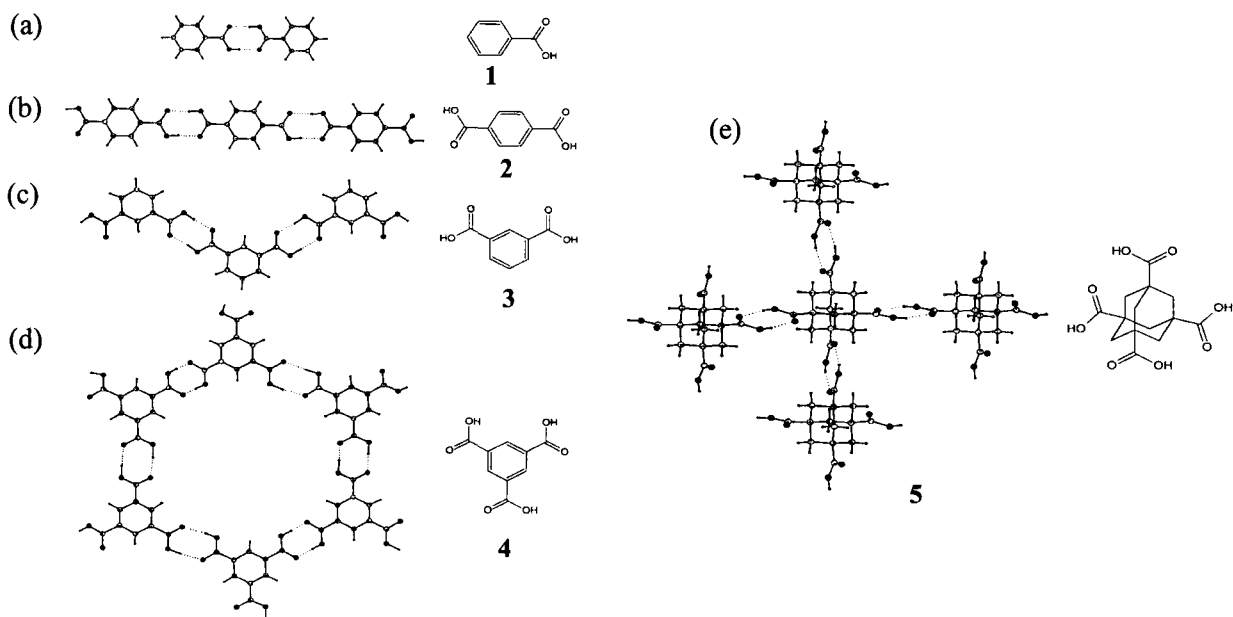
Figure 1.3: The carboxylic acid dimer coupling utilized in (a) benzoic acid 1,[39] (b) terephthalic acid 2,[40] (c) isophthalic acid 3,[41] (d) trimesic acid 4,[42] (e) adamantane-1,3,5,7-tetracarboxylic acid 5.[43]

There have been extensive, pioneering studies on hydrogen-bonded structures formed by the carboxylic acid synthon, by Leiserowitz and Etter.[18,44]

The oxocarbon acids, ($H_2C_nO_n$), have served as new building blocks to be utilized in the crystal engineering of organic materials. Braga *et al*[45] have reported the formation of linear O-H$\cdots$O bonds between the five-membered croconic acid, **6** (n=5), molecules, resulting in sheets of large tetrameric rings. The unusual aspect of these hydrogen-bonded sheets is that they are pleated in an 'accordion' pattern in three dimensions and shifted to avoid overlap between molecules in different layers (see Figure 1.4). The four-membered squaric acid, **7** (n=4) also forms large tetrameric rings resulting in flat sheets.[46]

6

7
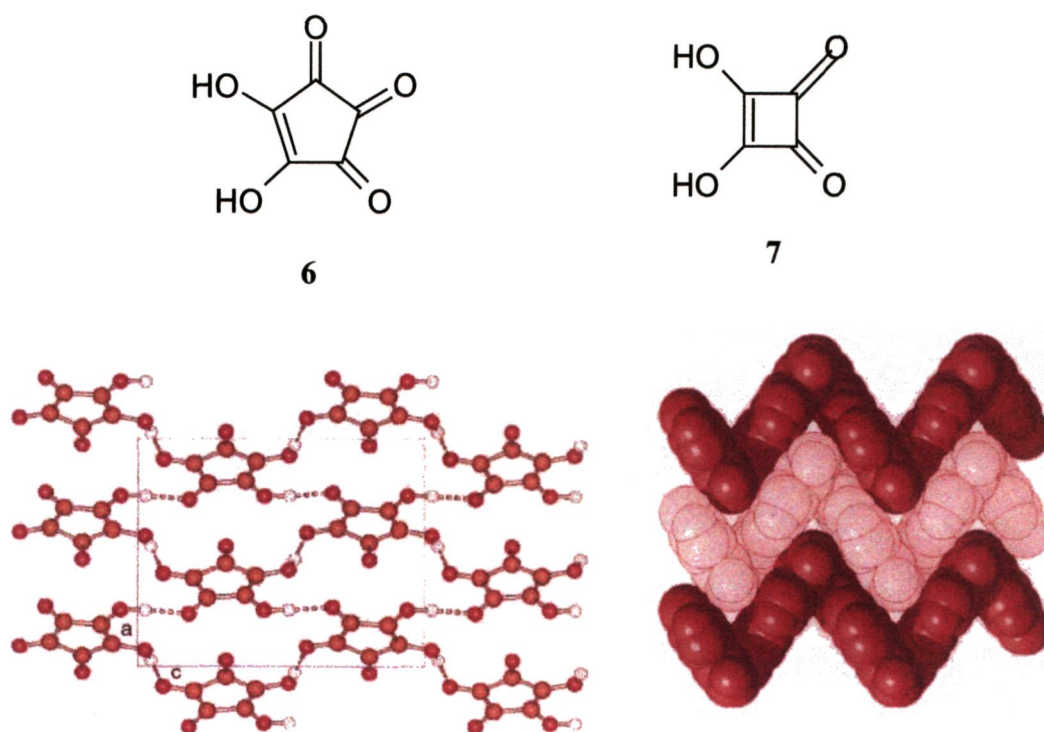
***Figure 1.4:** A pleated sheet (left) and an 'accordion' type arrangement (right) of croconic acid[45]*

Within the last decade, a sizeable number of supramolecular complexes that act as host lattices for smaller organic molecule guests within their interiors have been prepared.[47] Some examples are the open-ended cavitands,[48] covalently scaled carcerands,[49] and self-assembled hydrogen-bonded capsules.[50] Calixarenes have had a great impact in the history of porous solids.[51] The role of intramolecular hydrogen bonds in calixarenes have been reviewed by Rudkevich.[52] Circular, cooperative arrays of intramolecular O-H⋯O bonds in calixarenes, **8**, are shown in Figure 1.5a.[53] Such a cooperative network of O-H⋯O bonds accounts for the crown-like conformation of resorcinarenes, **9** (Figure 1.5b). Six molecules of resorcinarenes may assemble to form a spectacular spherical cavity of diameter 17.7 Å and internal volume of 1375 Å^3.[54]
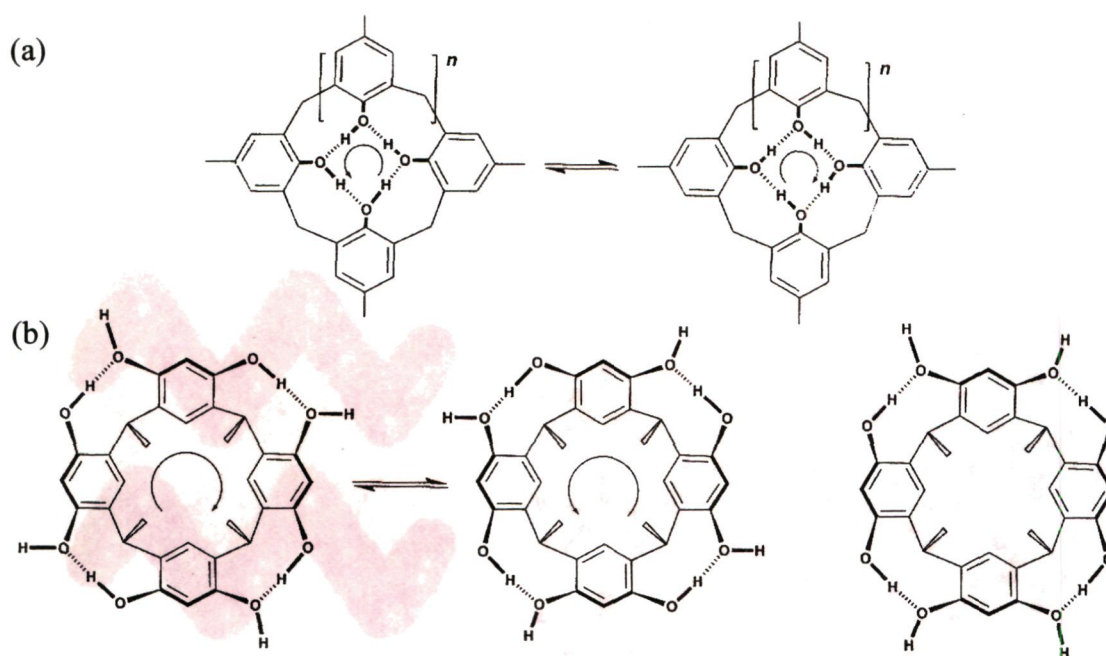
Figure 1.5: *Arrays of intramolecular hydrogen bonds in (a) unsubstituted calixarenes* **8**[53] *and (b) resorcinarenes* **9**.[54]

As explained earlier, trimesic acid contains an infinite O-H···O bonded chicken-wire motif formed by the dimerization of the COOH groups. The two-dimensional sheets interlace one another, thus filling the voids. Herbstein *et al*[55] have reported the first noninterlaced trimesic acid structures (again containing O-H···O dimers) containing disordered alkane guests. Later, Kolotuchin at al[56] synthesized a series of trimesic acid inclusion complexes with pyrene and ethanol molecules residing as guests in the cavities (depicted in Figure 1.6).
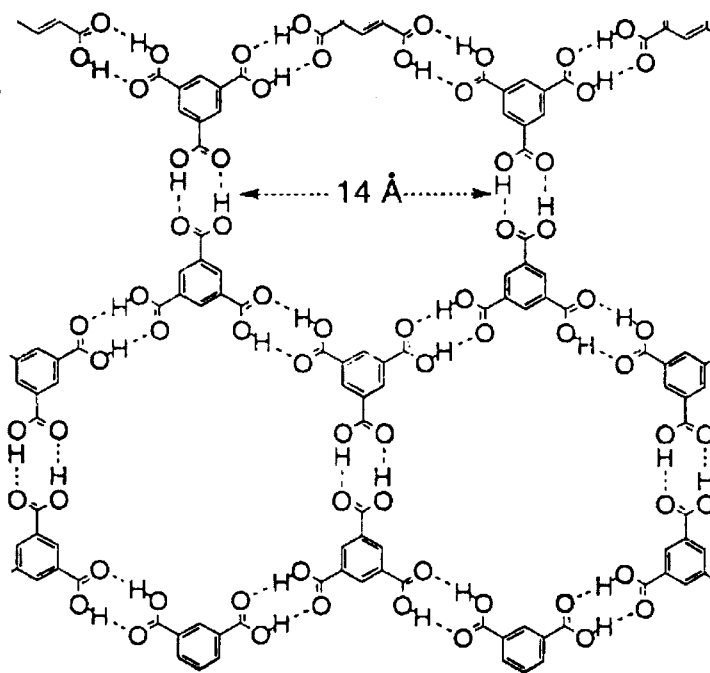
Figure 1.6: *The chicken-wire network of trimesic acid where all the donors and acceptors are utilized in the formation of O-H···O hydrogen bonds. The holes are filled by extensive interpenetration of independent networks.*[56]

An X-ray structural study of the high-energy cyclic form of the water hexamer trapped in an organic supramolecular complex with bimesityl dicarboxylic acid, **10**,

through O-H⋯O bonds has been carried out[57] (see Figure 1.7). The formation of catemeric (single) O-H⋯O hydrogen-bonded motifs in this complex is contrary to the ubiquitous centrosymmetric dimer motifs. A recent CSD analysis has shown that the dimer motif is found in 90% of the crystal structures reported for acids, while the catemer motif is found only in 4% of the reported structures.
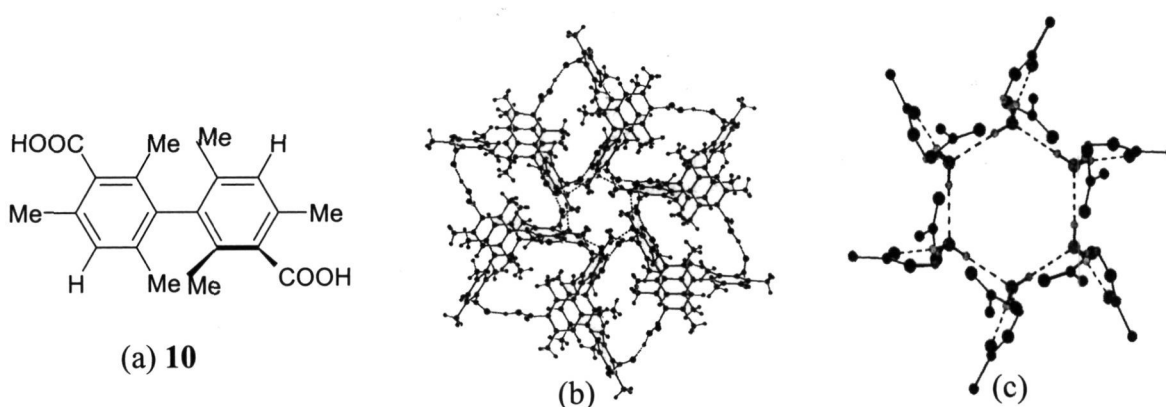
Figure 1.7: *(a) bimesityl dicarboxylic acid **10**, (b) The crystal packing of **10**.H₂O, (c) The water hexamer with the acid molecules (only –COOH are shown for clarity).*[57]

Very short O-H⋯O bonds occur in monobasic salts of diacids.[58] These bonds are usually formed between an acid and its conjugate base (O-H⋯O⁻) or in the hydrates of strong acids (O⁺-H⋯O). They have a quasi-covalent character with H⋯O distances in the range 1.2 to 1.5 Å (O⋯O, 2.2 – 2.5 Å) and θ in the range of 170° to 180°, with energy of ~ 63 to 170 kJ mol⁻¹ in contrast to strong hydrogen bonds (H⋯O, 1.5 - 2.2 Å, O⋯O, 2.5 – 3.2 Å, E = 17 – 63 kJ mol⁻¹). The O-H⋯O bonds formed by resonance assistance through π bonds (RAHB) are unusually short.[59] A cooperative network of O-H⋯O and O-H⋯N hydrogen-bonded synthons appear in the crystal

18

structure of 2,3,5,7-pyrazinetetracaboxylic acid.[60] A motif compared to the COOH unit in its directionality and predictability is the amide unit (CONH$_2$). The crystal structure of benzamide, **11** contains centrosymmetric N-H$\cdots$O dimers linked into α networks[61] (Figure 1.8). Combination of such α networks can be used to generate β networks, one such example being the β network formed by 3,3'-ureylenedipropionic acid, where there is a co-existence of O-H$\cdots$O and N-H$\cdots$O bonds. Another interesting example where the α networks are linked into β networks by O-H$\cdots$N hydrogen bonds is in the co-crystal of an oxalamide derivative with 1,2-(bis-4,4'-bipyridyl) ethylene.[62]

11
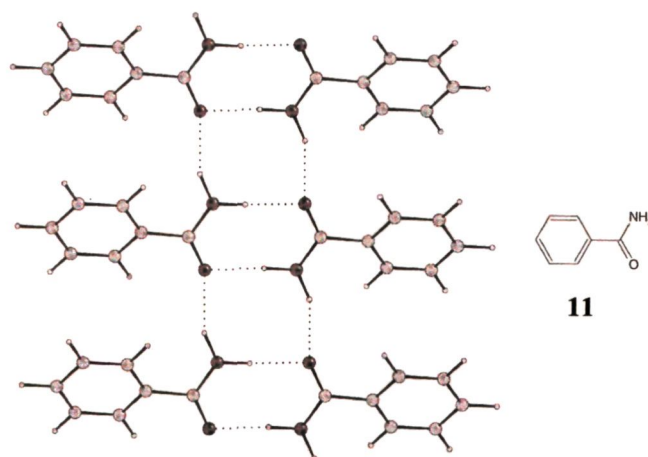
Figure 1.8: *Centrosymmetric N-H$\cdots$O dimers in benzamide - α-network.*[61]

The tuning of the stoichiometry of supramolecular complexes represents a distinct step forward towards crystal engineering.[63] In the complexes of melamine with succinimide (1:1), glutarimide (1:2) and 1-N-propylthymine (1:3), the availability of the imide carbonyl acceptor sites affords a handle to tune the crystal structures.[64]

The 1:2 complex of melamine (**12**) and glutarimide (**13**) formed by antiparallel N-H···O and N-H···N bonds is shown in Figure 1.9.
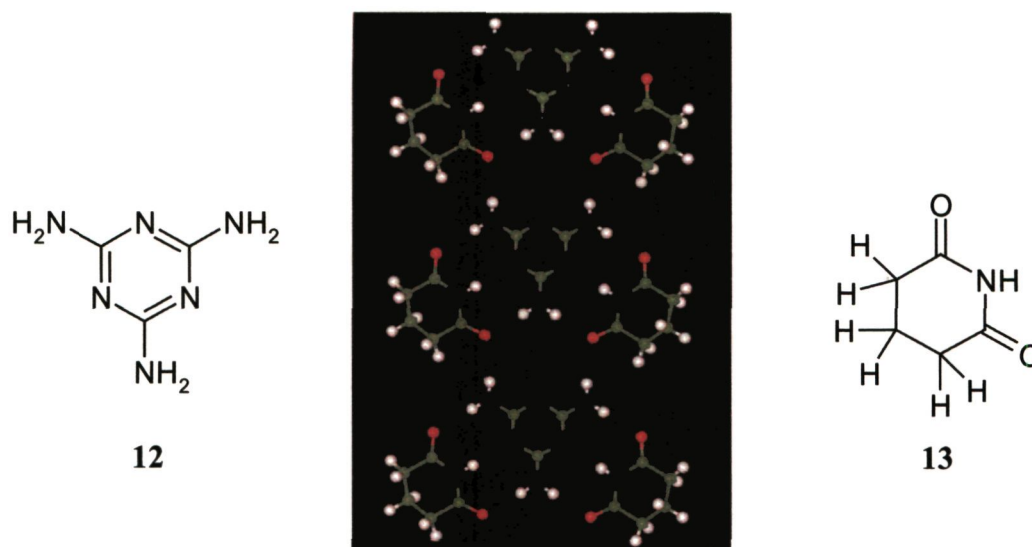
Figure 1.9: *X-ray crystal structure of the 1:2 complex between melamine 12 and glutarimide 13.*[64]

An interesting example of a two-dimensional structural motif/synthon is that of the tetrahedral shaped sulfamide functionality. Figure 1.10 depicts the N-H···O bonds formed between N,N'-disubstituted sulfamide (**14**). Gong *et al*[65] have shown that the formation of molecular layers is tunable by changing the substituents of the sulfamide molecules and that their incorporation into self-assembled monolayers (SAMs) would significantly enhance the stability of the monolayers. All the S atoms of the 2D network lie in the same plane, resulting in the formation of a sheet of sulfamide moieties (see Figure 1.10). There are N-H···O hydrogen bonds between the sulfamide moieties.
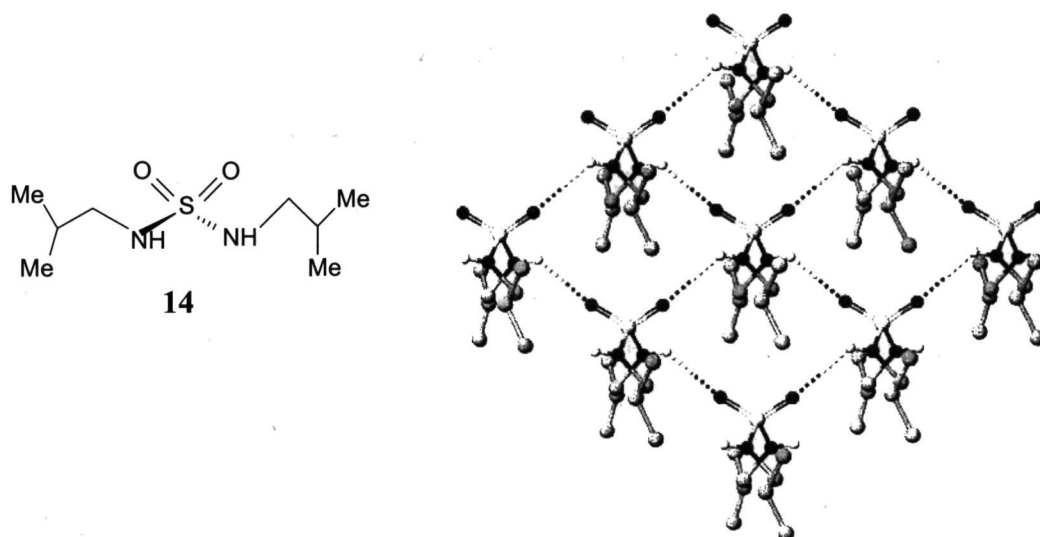
Figure 1.10: *One molecular layer held together by the 2D-hydrogen-bonded sulfamide network. The isobutyl groups pack above and below the 2D-network.*[65]

Whitesides and co-workers[66] have studied the complexes formed between substitued melamine (**12**) and substituted cyanuric acid (**15**). Three antiparallel N-H⋯O and N-H⋯N bonds stabilize the structure forming linear and crinkled tapes
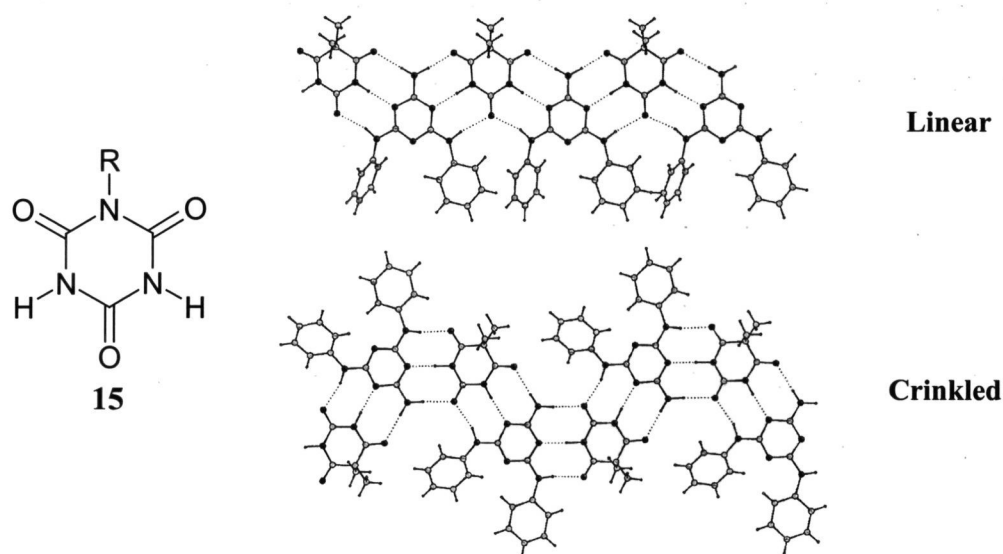
Linear

Crinkled

Figure 1.11: *Linear and crinkled tapes in substituted melamine (12)-cyanurates (15).*[66]

(Figure 1.11).

The highly stable nitroxide radical, 5,6-chloro-2-(N-tert-butyl-N-aminoxyl)benzimidazole (**16**)[67] crystallizes with N-H⋯O dimeric pairs (Figure 1.12). These hydrogen bonds act as structural scaffolds to hold the radicals in proximity. Susceptibility measurements in this radical show dimeric antiferromagnetic exchange coupling.
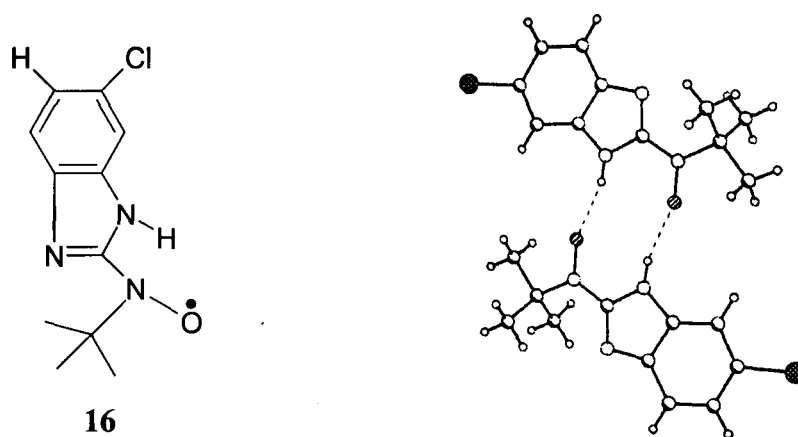
Figure 1.12: A dimeric pair of the nitroxide radical.[67]

1.4.2 Engineering strategies based on weak hydrogen bonds

When a hydrogen atom involved in intermolecular hydrogen bonding is bound to a less electronegative atom, the interaction becomes weaker compared to the strength of the previously discussed classical (or 'hard') hydrogen bonds. Indeed, C-H⋯O interactions have been shown to share many of the characteristics of stronger hydrogen bonds formed with the more conventional proton donors such as N-H and O-H.[10,68] Such non-classical hydrogen bonds with C-H as the proton donor and the π-face

22

of an aromatic ring, acetylene or ethylene bond as the acceptor are referred to as 'soft'

hydrogen bonds. The controversy concerning the nature of such weak hydrogen bonds

has been dispelled by crystallographic statistical analysis. There appears to be little

doubt that these interactions are directional and electrostatic in nature just like the

strong hydrogen bonds.[69] Statistical surveys from crystallographic data regarding the

directional behaviour of C-H$\cdots$N/$\cdots$Cl and $\cdots$F interactions have been carried out by

Taylor and Kennard[70] and Thalladi *et al.*[71]

An interesting example of supramolecular aggregates of diaryl sulfones (**17a-**

d) formed solely by C-H$\cdots$O hydrogen bonds was reported by Glidewell *et al.*[72] In

these structures, the aromatic C-H donors preclude the possibility of hard hydrogen

bonding and the SO_2 group acts as the acceptor. The C-H$\cdots$O interactions lead to

aggregates, which can be zero-dimensional (Figure 1.13a), one-dimensional (Figure

1.13b), two-dimensional (Figure 1.13c) or three-dimensional (Figure 1.13d).

17a
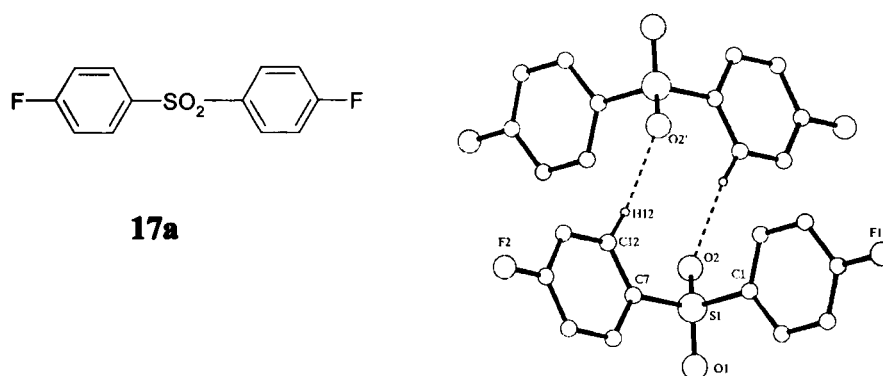
Figure 1.13a: A centrosymmetric R_2^2 (10) ring.[72]

17b
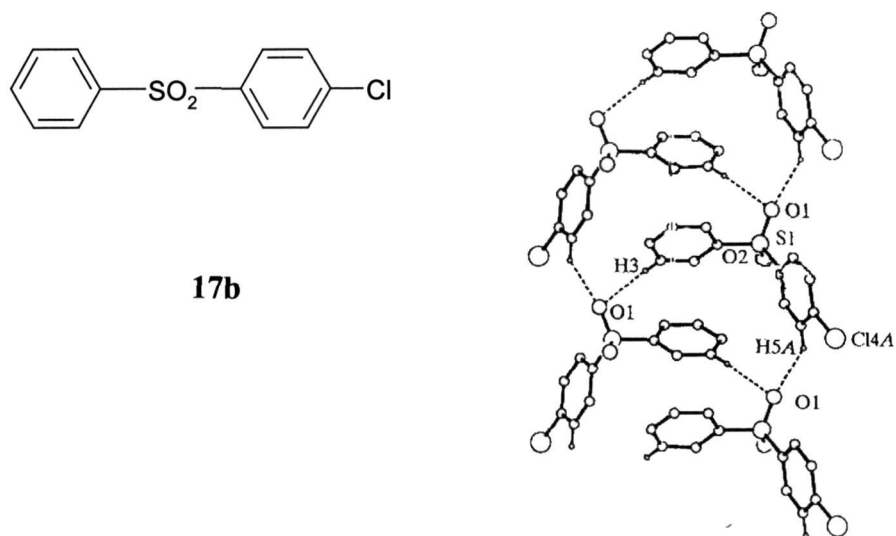
Figure 1.13b: *Part of the crystal structure of* **17b** *showing a chain of fused* R_3^2 *(16) rings.*[72]

17c
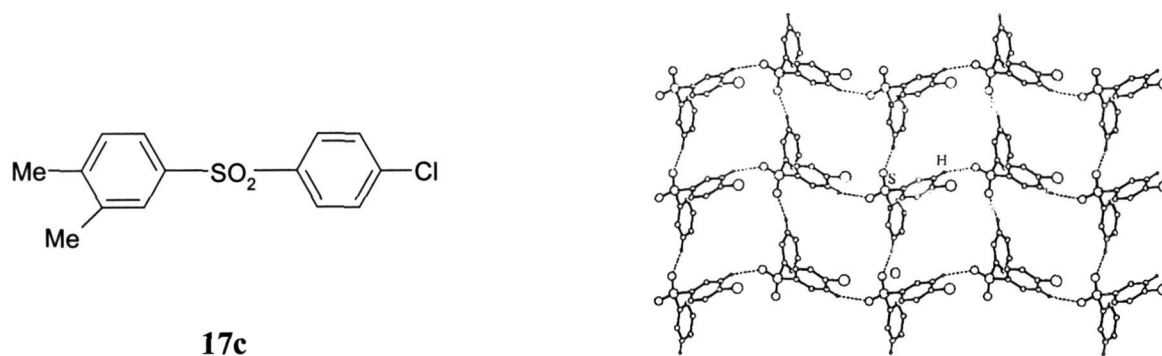
Figure 1.13c: *Part of the crystal structure of* **17c** *showing a (4,4) net of* R_4^4 *(24) rings.*[72]

17d
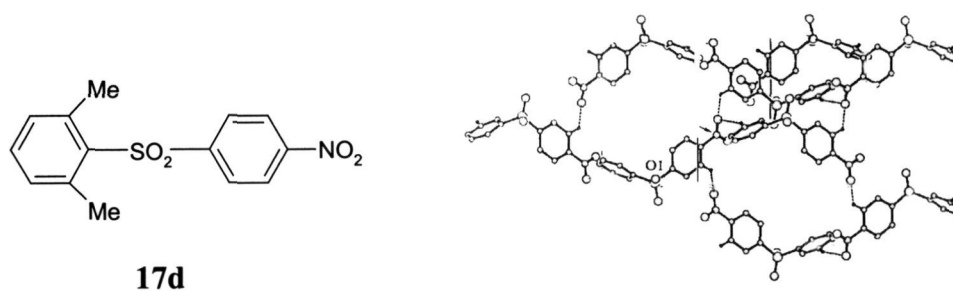
Figure 1.13d: *Part of the crystal structure of* **17d** *showing a (4,4) net of* R_4^2 *(20) and* R_4^4 *(32) rings.*[72]

Robinson *et al*[73] have exploited the proximity of terminal alkynes, such as those in 1,3,5-triethynyl-benzene (**18**), to participate in bifurcated interactions (the same donor forms hydrogen bonds to two acceptors) with nitro groups in 1,3,5-trinitrobenzene (**19**) resulting in an organic solid containing a hexameric hydrogen-bonded array. The carboxylic acid dimer synthon **A** can be replaced by the synthon **E** which can give geometrically similar arrays as that found in trimesic acid (Figure 1.3d). In reality, the crystal structure does not contain the predicted hexameric arrays and instead, contains alternate tapes of **18** and **19** linked by $C\equiv C\text{-}H\cdots O_2N$ and $Ar\text{-}H\cdots O_2N$ contacts (Figure 1.14).
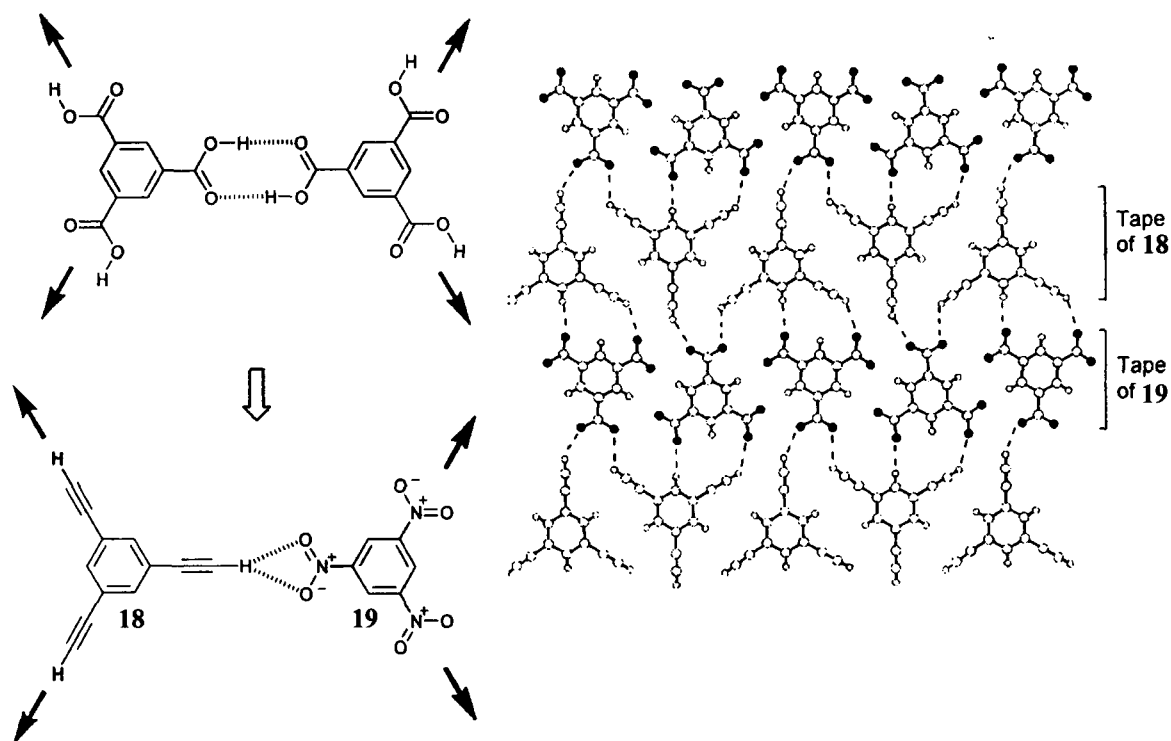
Figure 1.14: The carboxylic acid dimer coupling is structurally analogous to the coupling **18.19**. The filled arrows represent the directions of hydrogen bonding. The co-crystal of **18** and **19**.[73]

4-(4-Ethynyl phenyl)ethynyl pyridine (**20**) crystallizes in the form of polar

crystals in which the molecules are directed in straight hydrogen-bonded tapes through

C(sp)-H$\cdots$N hydrogen bonds.[74] The hydrogen bonds induce non-linear optical activity

in this compound. It is shown to be eight times more SHG (Second Harmonic

Generation) active than crystalline urea.[75] The C-H$\cdots$N bonds are very short (H$\cdots$N

distance of 2.32 Å, C$\cdots$N, 3.27 Å) and exactly linear (θ, 180°) (see Figure 1.15).
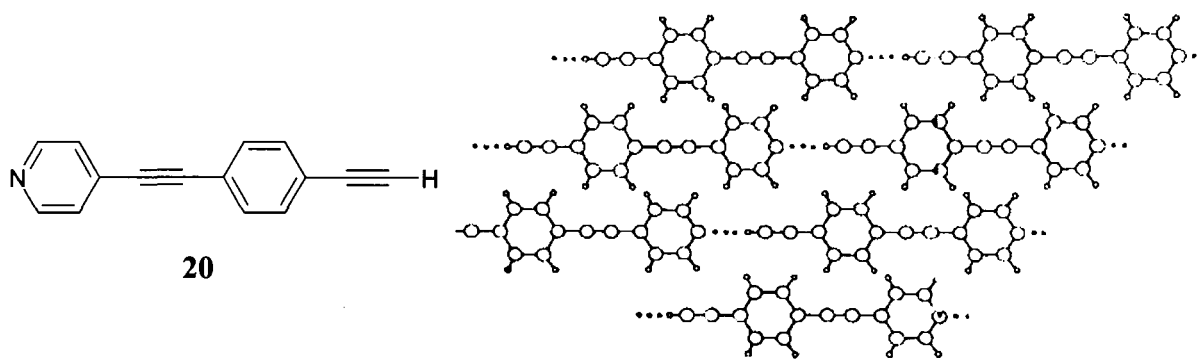
Figure 1.15: *Packing arrangement of **20** in the crystal. C(sp)-H$\cdots$N bonds shown by dotted lines.*[74]

The C-H$\cdots\pi$ bond[76] plays a crucial role in controlling the crystal packing of

many organic compounds. It is significant in determining the conformation and

chiroptical property of some of the compounds. These interactions have been used to

achieve third dimensional control of the crystal structure of 1,3,5-trisubstituted

triazine[77] molecule (**21**), which has led to its octupolar NLO activity (Figure 1.16).

This molecule adopts noncentrosymmetric packing. The *para* methyl group forms C-

H$\cdots\pi$ interactions in such an orientation that sustains 3D-chirality.

21
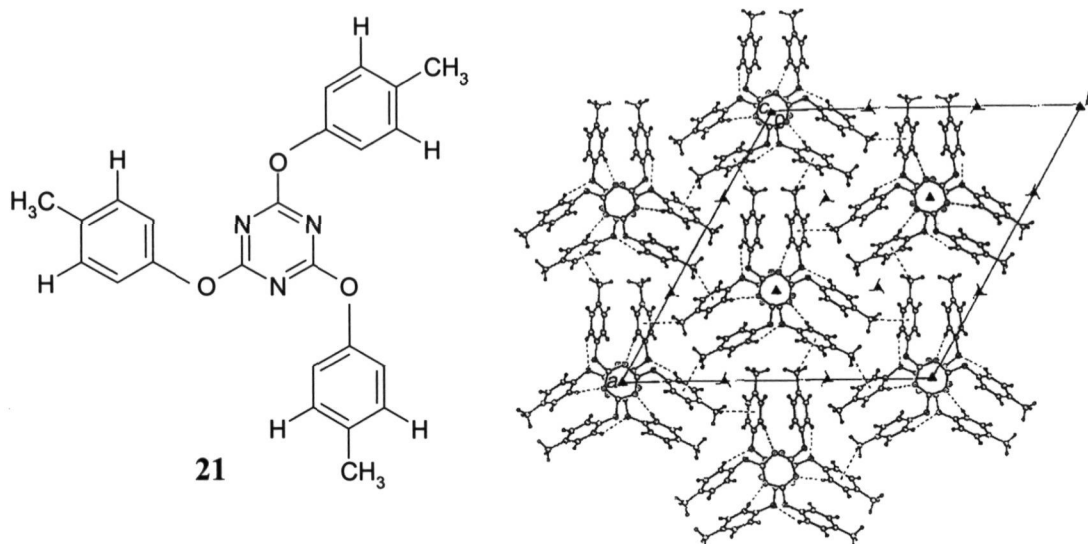
Figure 1.16: Octupolar trigonal network structure in 21. The 3-fold, 3_1- and 3_2-axes are depicted.[77]

N-H···π interactions between a substrate (**22**) and synthetic receptor (**23**) stabilizes the complex (shown in Figure 1.17) in non-polar solvents.[78] The use of various conformationally rigid substrates complexed with the receptor have shown that amide-aromatic hydrogen bonds can have a vital effect on the recognition properties of host-guest complexes in a non-polar medium. The N-H···π interactions are of special importance in biological systems.[79]
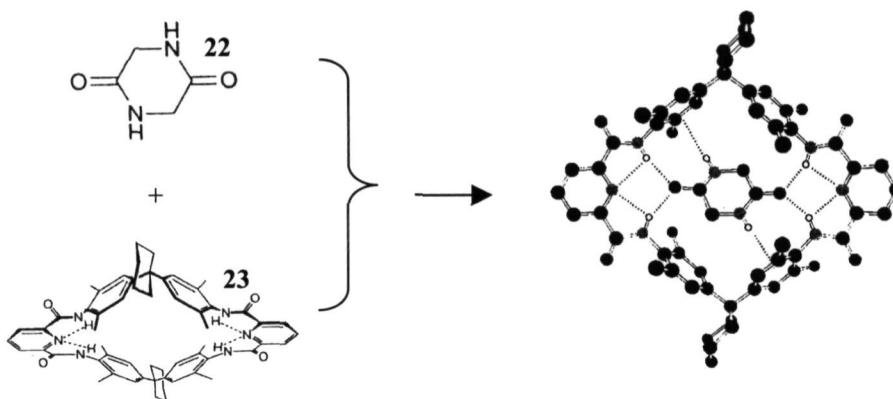
Figure 1.17: X-ray crystal structure of the 22.23 complex. The amide N-H groups of 22 are directed towards the faces of the aromatic side-walls of the cavity.[78]

Cowan *et al*[80] have reported the first N-H···C bond formed between an N-heterocyclic carbene 1,3-dimesityl imidazole-2-ylidene (**24**) and diphenylamine (**25**). Only the N-H···C contact (H···C, 2.30 Å and θ=179°) is shown in Figure 1.18. There are also C-H···π interactions between the phenyl and mesityl rings, which are not shown in the figure. There are also several examples of O-H···π (aromatic) hydrogen bonds documented in the literature.[81]
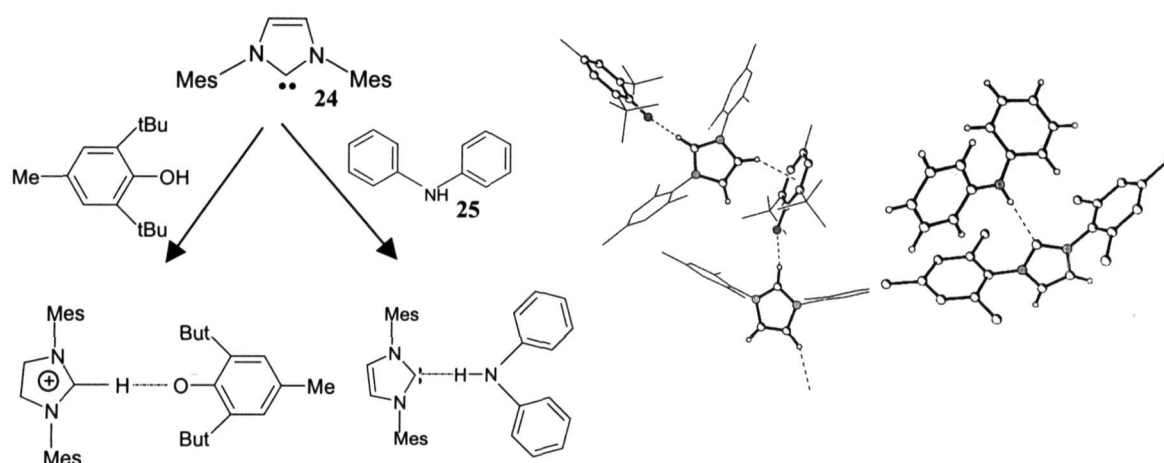
Figure 1.18: *Reaction of **24** with a phenol derivative and diphenylamine (**25**) (left). X-ray crystal structures of the resulting products (on the right).*[80]

N-H···I and C-H···I bonds dominate the crystal packing pattern in the structure of 4,4'-bipyridinium diiodide.[82] The N···I distance of 3.47 Å lies just within the sum of the van der Waals radii of 1.55 Å for N and 1.98 Å for I. The C···I distance of 3.74 to 3.77 Å lies outside the range for C (1.70 Å) and I. It has been pointed out that these types of interactions should not be thought of as van der Waals, but as weakly directional, electrostatic attractions.[83]

1.4.3 Co-existence of strong and weak hydrogen bonds

Many crystal structures result from a balance between strong and weak hydrogen bonds. Both types of hydrogen bonds are structure-directing in the formation of such a supramolecular assembly. For precise supramolecular construction, a subtle and simultaneous manipulation of the strong and weak interactions becomes necessary. There are varied examples of weak hydrogen bonds being organizing forces even in the presence of strong hydrogen bonds. Some examples are discussed below.

The co-crystal of formic acid with hydrogen fluoride (**26**) (Figure 1.19) consists of strong O-H···O and F-H···O bonds, in addition to C-H···O and C-H···F bonds.[84a] The C-H···F bonds[84b-d] are much stronger and may have a greater structure directing effect in comparison to C-H···O bonds due to the presence of the more electronegative F atom.
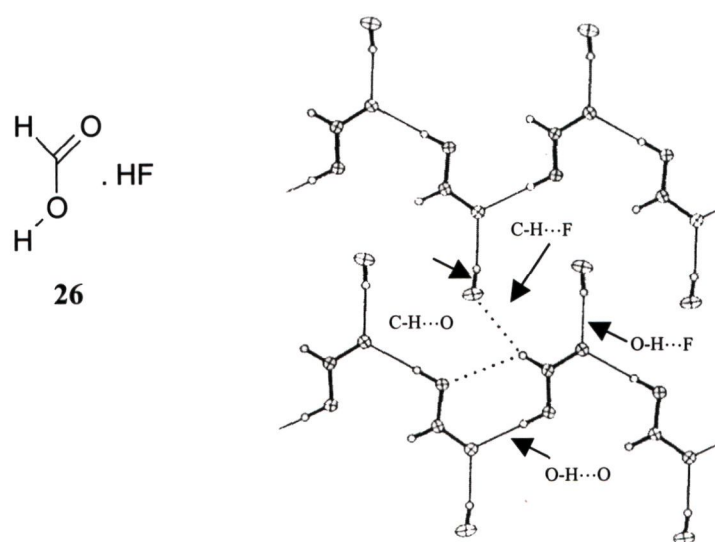
Figure 1.19: *Structure of the adduct HCOOH●HF. A bifurcated interaction (C-H···O and C-H···F) is shown. Formic acid molecules are O-H···O hydrogen-bonded in the main chain. The molecules of HF are attached to the chains through the rare F-H···O bonds.[84a]*

Both O-H···O and C-H···O hydrogen bonds dominate the crystal packing of the 2:1 complex of trimesic acid (**4**) with phloroglucinol (1,3,5-trihydroxyphenol), **27**.[85] All the donors and acceptors are utilized for hydrogen bond formation in phloroglucinol, as illustrated in the crystal structure, depicted in Figure 1.20. Rosette-shaped repeating units with many hydrogen bonds are formed.
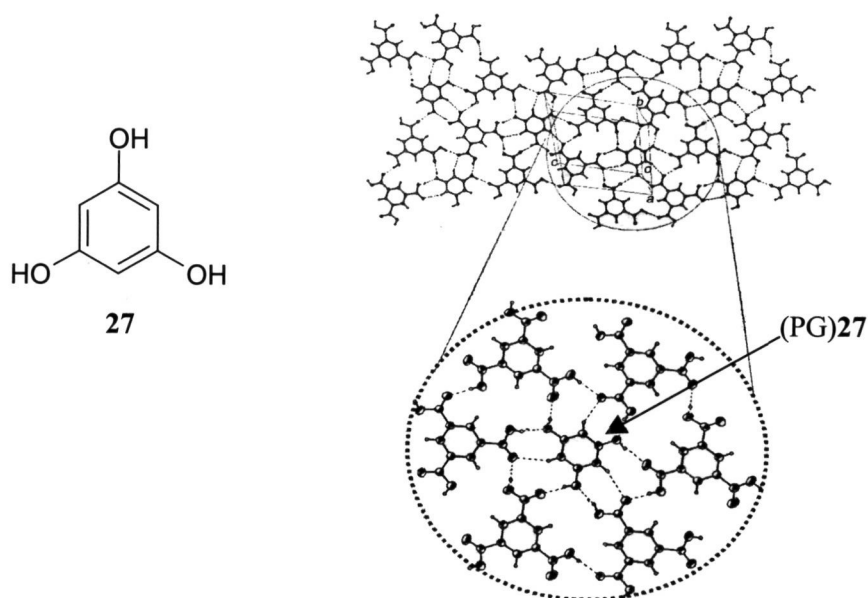
Figure 1.20: *Structure of the adduct TMA(4)•(PG)27. One planar lamella (top right) and an enlarged rosette (bottom right) are depicted: Note the utilization of all the O-H donor and acceptor groups on molecule 27.*[85]

Gem-alkynols are a class of compounds that exhibit a high degree of interaction interference between their different functional groups. Molecules **28** and **29** assemble with the aid of O-H···O, C-H···O and C-H···π bonds.[86] The crystal structures of the two molecules are indicated in Figure 1.21. Molecule **28** exhibits infinite cooperative O-H···O-H···O-H···O-H··· chains while C-H···O and C-H···π

bonds are formed in a different plane. Molecule **29** exhibits an elaborate cooperative network of both strong and weak hydrogen bonds.

(a)

(b)
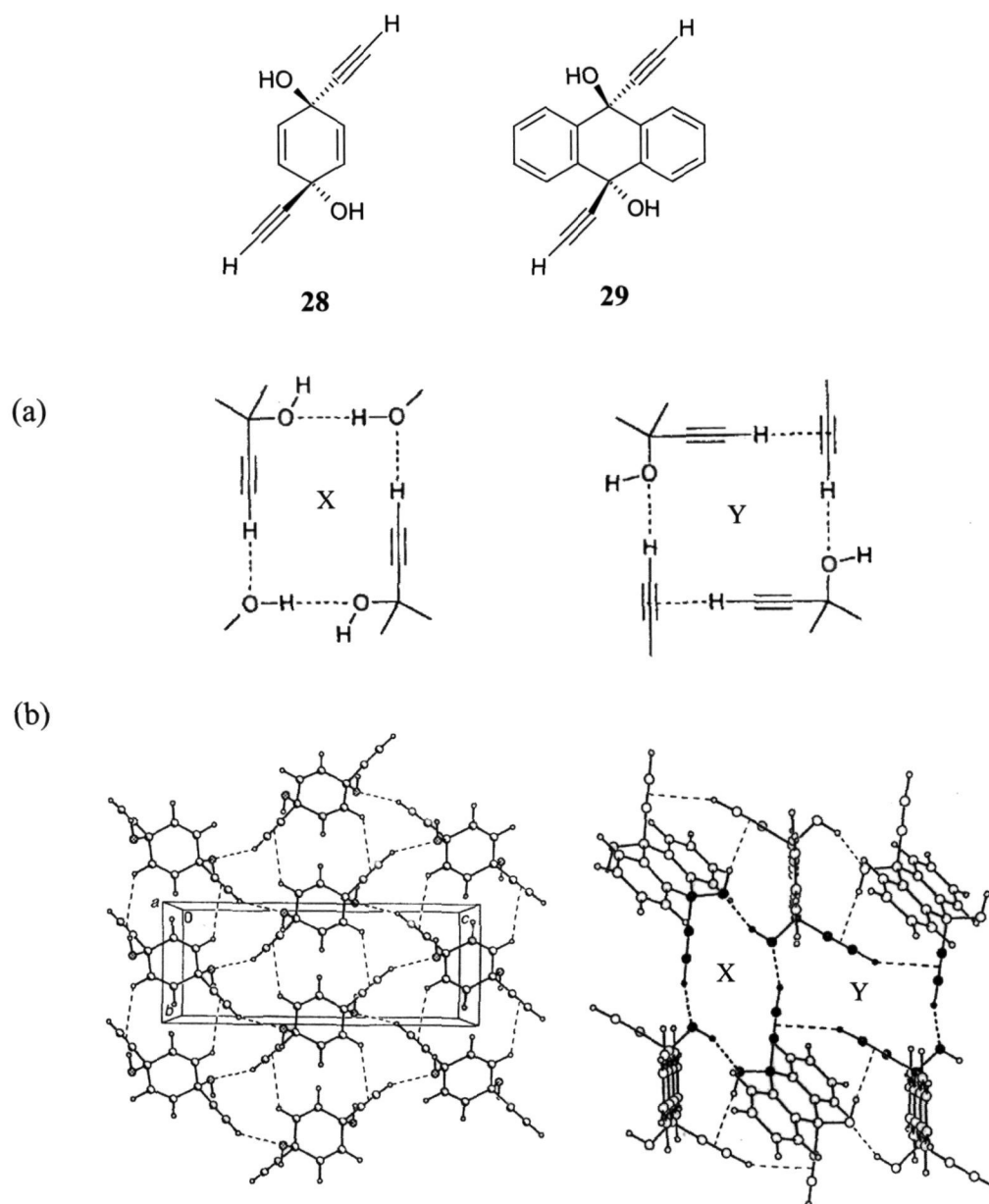
Figure 1.21: *(a) O-H⋯O, C-H⋯O and C-H⋯π interactions, represented as hydrogen-bonded couplings, X and Y. (b) Left: crystal structure of alkynol **28**, the O-H⋯O bonds are not shown, the C-H⋯O and C-H⋯π bonds are indicated by the dotted lines. Replacement of any of the alkynic H atoms with a substituent may change the structure. Right: Crystal structure of alkynol **29**, showing the couplings X and Y.[86]*

1.4.4 Other types of intermolecular interactions

In addition to hydrogen bonds, there are other weak intermolecular interactions which play a structure-directing role. Some of these interactions include halogen-halogen, halogen-nitro, nitro-nitro, aromatic (π-π) and even gold(I)-gold(I) interactions. Halogen-halogen contacts have been used in the design strategies by Schmidt as early as the 1970s.[2] A crystallographic analysis by Pedireddi *et al*[87] has confirmed their undoubted directionality. 1-iodo-4-nitrobenzene (**30**) and the 1:2 complex of 1,4-dinitrobenzene (**31**) and 4-iodobenzoic acid (**32**) exhibit halogen-nitro interactions (synthon **M**), while the latter also exhibits centrosymmetric O-H$\cdots$O dimers. A retrosynthestic analysis (the task of working backward from the target structure to the precursors) is illustrated in Figure 1.22.[88]
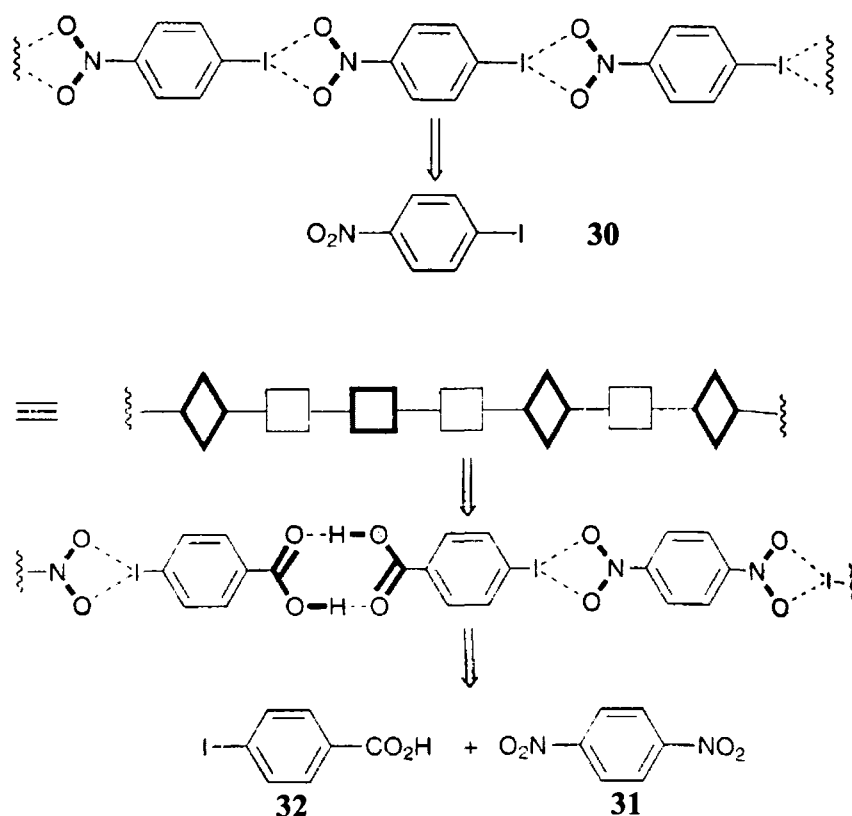
Figure 1.22: Retrosynthetic analysis for the linear ribbon patterns.[88]

Aurophilicity or aurophilic bonding is the attractive interaction that exists between closed-shell gold(I) centres. This interaction has been estimated to have a strength similar to hydrogen bonding (29 - 46 kJmol^{-1}).[89] It is also distinctly directional like hydrogen bonding.[90] The use of aurophilic bonds (Figure 1.23) to control the supramolecular structure of n-alkylisonitrile complexes of AuCl (**33**) has been determined and its phase behaviour has been analyzed by Bachman *et al.*[91]
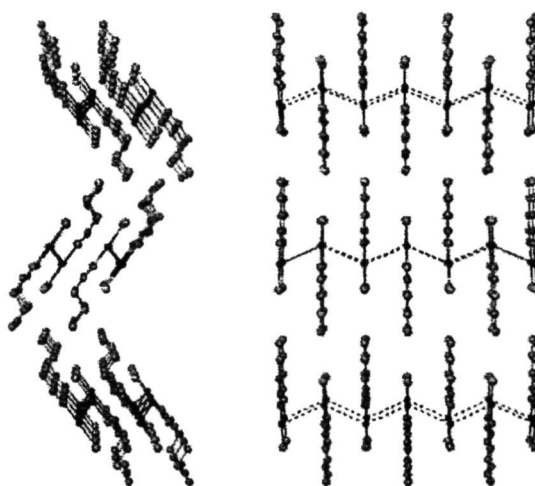
Figure 1.23: *Two views of the packing of C$_3$H$_7$NCAuCl (33)*[91]

1.4.5. Hydrogen bonds as steering forces for the supramolecular assembly of organometallic and coordination complexes

Organometallic systems show a great structural diversity arising from the variability of the ligands and from the ligand-metal(s) bonding. As the metal atom is completely encased by organic ligands such as CO, CN$^-$, NCS$^-$, etc, it is usually unable to participate directly in intermolecular interactions. As a result, the entirely organic molecular peripheries have considerable flexibility to form intermolecular contacts, which may be comparable to those found in purely organic systems. Braga *et*

al[92] have examined the transferability of synthons or couplings adopted by organic molecules to organometallic systems, and have found a certain degree of similarity. (η^2-fumaric acid)Fe(CO)$_4$ (**34**) exists in two forms, one containing chains mediated by synthon **A** (Figure 1.24a), and the other in which synthon **A** coexists with a catemer pattern similar to synthon **C**[93] (Figure 1.24b). See Scheme 1.3 for an illustration of the synthons.
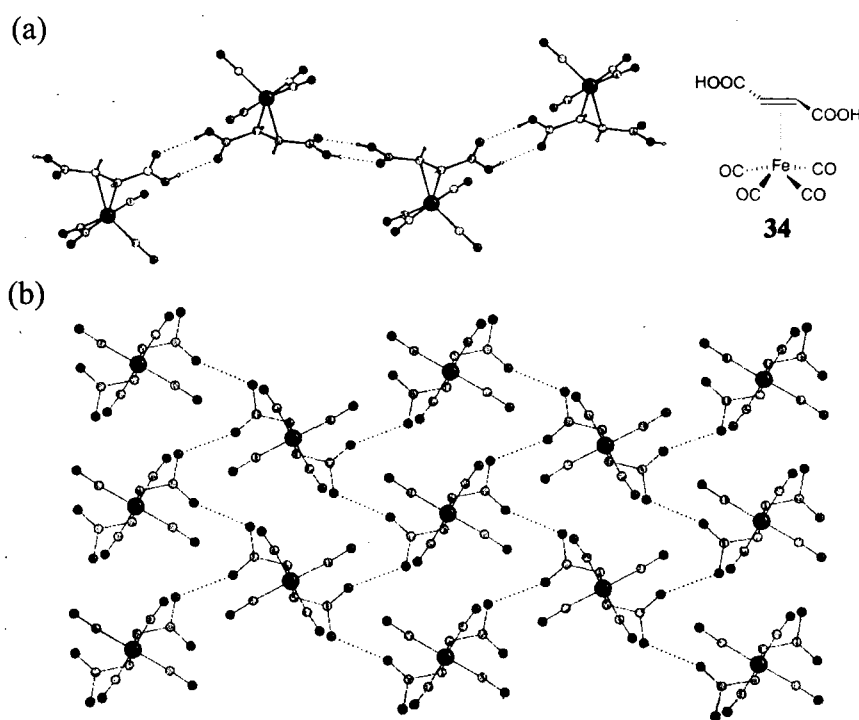
Figure 1.24: Polymorphs of 34. (a) Chains mediated by synthon A (b) catemer patterns resembling synthon D.[93]

The cyclic synthon **B** (in Scheme 1.3) is observed in the crystal structures of primary amide complexes[94] (For an example, see [(η^2-C$_5$H$_5$)Mn(CO)(NO)(CONH$_2$)], in Figure 1.25).

34
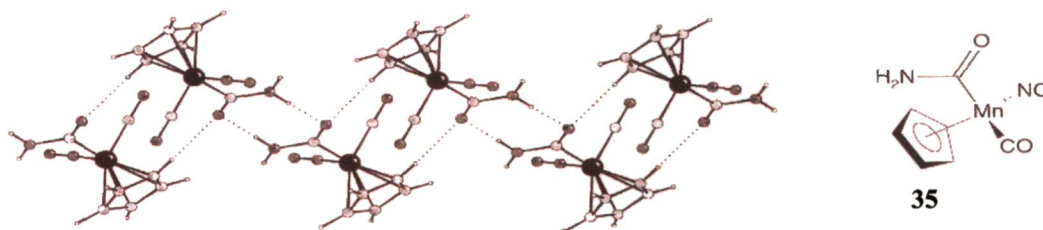
Figure 1.25: *Synthon **B** observed in the crystal structure of 35.*[94]

Mingos and co-workers[95] have employed triple hydrogen bond patterns for the design of supramolecular aggregates of metal complexes and organic moieties. For instance, co-crystals of the metal complex Ni(dithiobiuret)$_2$ (**36**) with 1,8-naphthalimide (Figure 1.26) linked by N-H⋯O and N-H⋯N bonds, display self-assembly through triple complementary hydrogen bond interactions (synthon **F** in Scheme 1.3).
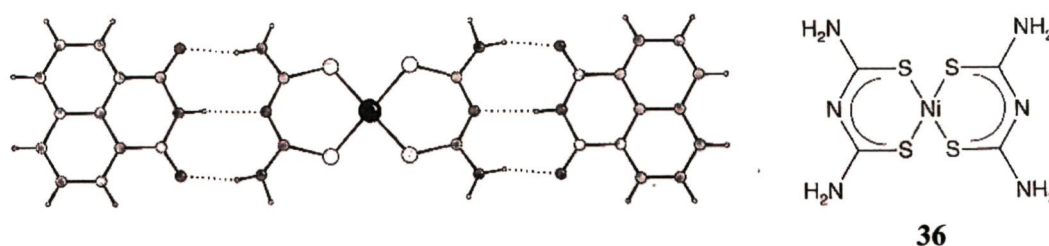
Figure 1.26: *Supramolecular assemblies based on synthon **F**.*[95]

Beatty has reviewed the significance of strong hydrogen bonding interactions on the intermolecular assembly of coordination complexes.[96] Some notable examples of coordination complexes are those which contain heterocyclic molecules as ligands.

Supramolecular hydrogen-bonded networks usually extend in directions dictated by the coordination geometry of the metal centre.

The cyclic synthon **B** (in Scheme 1.3) is observed in the 1D architectures formed by [Ag(nicotinamide)$_2$][O$_3$SCF$_3$], **37**, in which the dimeric N-H$\cdots$O bonds, formed by the -CONH$_2$ group give rise to a ladder type structure.[97] There are many unusual examples of metal-melamine coordination. N-H$\cdots$N bonds give rise to a linear assembly in some Ag(I) and Cu(II) complexes. Dimeric N-H$\cdots$N bonds are formed by melamine molecules coordinated to Cu(II) in the melamine-copper acetate complex.[98] The synthon **F** (in Scheme 1.3) is observed in some macrocyclic complexes that may contain melamine and cyanurates, which are capable of forming three-centered N-H$\cdots$O and N-H$\cdots$N hydrogen bonds.[99]

Halometallates are metal-bound halides that are shown to accept hydrogen bonds.[100] One such example is that of a tetrachloroplatinate with N-H$\cdots$Cl hydrogen bonds,[101] depicted in Figure 1.27.

Figure 1.27: *Infinite chains of 4,4'-bipyridinium tetrachloroplatinate.*[101]

The ligand, 2,2'-biimidazole (HBim) coordinates with Ni(II) in a bidentate fashion, forming N-H$\cdots$N hydrogen bonds.[102] A 2D honeycomb motif with encapsulated potassium counter-ions results, depicted in Figure 1.28.
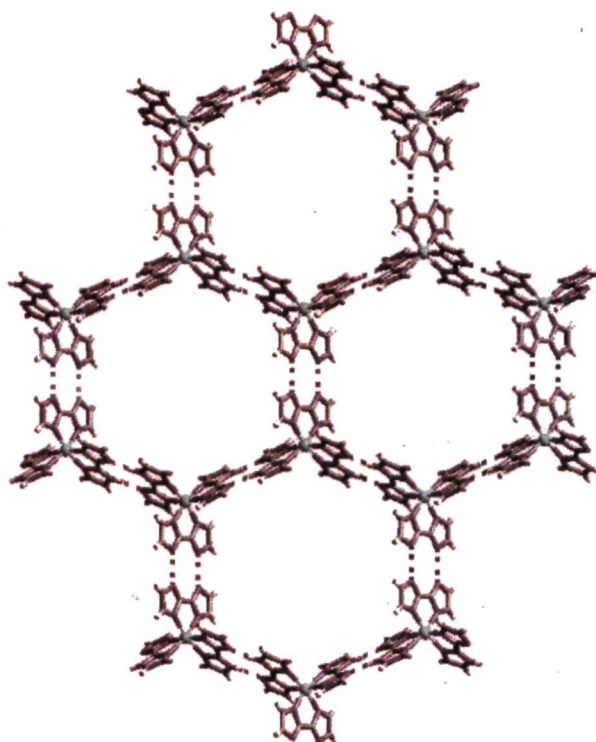
Figure 1.28: *Honey-comb motif of Ni(HBim)₃. The K⁺ counter-ions are not indicated.*[102]

Crystal engineering offers a largely unexplored opportunity to study the spectroscopic properties of molecules and geometry changes upon excitations in environments which can be engineered to have specific properties. Coppens *et al*[103] have highlighted the use of calixarene-based crystals in spectroscopy and time-resolved crystallography. This paper discusses the design of calixarene host-guest compounds with benzophenone, benzil, decamethylruthenocene and a binuclear Rh cationic complex (Figure 1.29). The authors have carried out photochemical and photophysical measurements, and demonstrate that photoactive molecules can be isolated from each other in supramolecular solids (or crystals) without sacrificing three-dimensional periodicity.
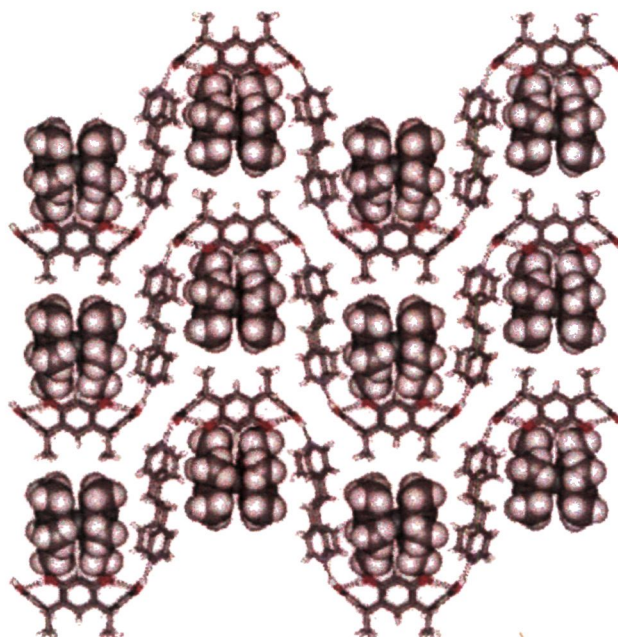
Figure 1.29: *Wavelike structure of [CMCR.2bpe].DMR [bpe = trans-1,2-bis(4-pyridyl)ethylene; DMR = decamethylruthenocene].*[103]

1.4.6 Organic porous solids

Principles of crystal engineering[104] can be used for the rational design and self-assembly of host lattices.[105] Such host lattices with included guest molecules have attracted considerable attention chiefly due to the diverse applications they offer: catalysis, separation, magnetic devices, optical lasers, improved pharmaceutical drugs, and so on.[106]

The natural and synthetic inorganic zeolites[107] with pore sizes of 10 to 20 Å are the classical examples of microporous materials with widespread industrial uses. Analogous microporous solids based on organic building blocks have the potential for a precise rational design, through control of the shape and size of the pores,[108-110] Host frameworks with an organic core offer some advantages: (1) The target network can

38

be controlled by suitable manipulation of the functional groups and supramolecular synthons; (2) the nature, size and shape of pores and cavities in organic three-dimensional host frameworks can be altered with hydrogen bonding and hydrophobic interactions; (3) Inclusion and release of guest species is much more facile in organic hosts than in inorganic zeolites.

Synthetic strategies employed in porosity tuning

Yaghi *et al*[108,110,111] have designed many metal-organic frameworks that bind aromatic guest molecules selectively. Most often, Yaghi's group has employed hydrothermal method as one of the synthetic routes. Moore and co-workers[112] have made porous materials from ring-shaped units that stack themselves by hydrogen bonding. Each ring is made up of six rigid rod-like units and six corner pieces to form a regular hexagon. Acetylenic groups, however, gave rods. The corner pieces were benzene rings with hydroxy groups that provide connections needed to make hexagons. The benzenes in neighbouring sheets interact in a way that encourages the rings to stack on top of one another, creating parallel channels about 9Å in diameter.

A slightly different approach has been developed by Wuest and co-workers.[113] They used building blocks that create channels as they assemble themselves into a network. Wuest, in fact introduced the concept of *tectons* into supramolecular chemistry. Tectons are the molecules with sticky ends that can participate in intermolecular interactions that are strong, specific and directional. The geometry of the tectons determines that of the network into which they assemble. A diamondoid network can be synthesized from tectons with four sticky hydrogen bonding sites in a

tetrahedral orientation. Such self-assembly often results in the formation of channel structures, which are being filled by solvent molecules.

Peptide nanotubes constructed from chiral amino acids[114] find applications as biological transport mimics, drug delivery systems and nanostructured biomaterials. Different ratios of L-cystine dimethyl ester and 1,ω-alkanedicarbonyl fragments have been coupled to prepare cyclobisamides. These molecules stack through N-H$\cdots$O=C hydrogen bonds at an inter-ring distance of $\sim$ 5.0 Å to produce nanotubes with 5-10 Å internal diameter.[115] The hydrophobic interior of these polymethylene-bridged cystine tubes has been used to solubilise highly lipophilic substances in water by selective host-guest complexation.

Host channel frameworks containing photoactive or photosensitive guest molecules

Ma and Coppens[116] have synthesized a solid based on C-methylcalix[4] resorcinarene and the linker molecule bis(4-pyridylmethylidyne) hydrazine, in which brick-wall sheets are linked in the third dimension to give networks with three intersecting perpendicular channels. Although these networks interpenetrate three-fold, they nevertheless leave cavities capable of including sizeable guest molecules. These three-dimensional interlinked channels have approximate dimensions of 16.6 $\times$ 16.0 Å, 16.6 $\times$ 16.5 Å and 16.5 $\times$ 10.0 Å. These cavities left after interpenetration, each accommodate two benzophenone guests. The phenyl rings from different benzophenones form strong π-π interactions (with center-center distances of 3.675 Å). The twist angles between two phenyl ring planes and the C(C=O)C plane of benzophenone are significantly different from those in neat benzophenone crystals and

benzophenone supramolecular compounds,[103] indicating the effect of the host framework on the conformation of the guest molecules.

Zaman *et al*[117] have synthesized supramolecular host-guest networks utilizing the 1,4-bis(x-pyridyl)butadiyne ligands where x=2 (L1), 3 (L2), 4 (L3). The different orientations of the nitrogen donors and the linear conformation of the spacer moiety (-$C\equiv C-C\equiv C-$) of these ligands have been used for constructing a large variety of new coordination polymers. Guest species with photo and catalytic activities have been used in the different channel frameworks. Photosensitive azobenzene (AZO) guest molecules occupy the cavities in the three-dimensional channel like network in $[Cu(L2)(NO_3)_2(H_2O)_2.AZO]_n$ and the rhombic-shaped channels in the two-dimensional interpenetrating square networks of $[Cu(L2)_2(NO_3)_2.AZO]_n$.

Channels formed by pharmaceutical hosts

An interesting example of the crystal engineering of a novel pharmaceutical composition containing channels has been reported by Walsh *et al*.[118] They have crystallized a series of pharmaceutical compounds like rac-ibuprofen, rac-flurbiprofen or aspirin in the presence of dipyridyls: (ibuprofen)$_2$(4,4'-bipyridine), (flurbiprofen)$_2$(4,4'-bipyridine), (flurbiprofen)$_2$(trans-1,2-bis(4-pyridyl)ethylene), (aspirin)$_2$(4,4'-bipyridine). These adducts exhibit supramolecular heterosynthons formed between the acid and the pyridyl unit. Of these, the supramolecular complex formed by aspirin with 4,4'-bipyridine results in the formation of hourglass channels, templated by the presence of hexane during crystallization. The authors state that

though these adducts should only be regarded as model compounds, the study could have broad implications for the formulation of pharmaceuticals.

1.4.7 Polymorphism

Polymorphism is defined as the phenomenon wherein the same chemical substance exists in different crystalline forms.[119] The best laid synthetic plans may become futile if the wrong polymorphic structure is obtained. Even though the discovery of polymorphs of molecular crystals or of their diverse solvate forms (pseudopolymorphs) is often serendipitous, crystal polymorphism can, to some extent, be controlled.[120] This phenomenon has brought into the forefront the litigation surrounding the widely used ulcer drug Zantac and the huge commercial interests involved.[121] Steed and co-workers[122] have reported structural, thermal and NMR studies on the long known polymorphic modification of $GeHPh_3$ and demonstrate the conversion of single crystals of the unstable β phase into the α form via a liquid phase thought to contain $(GeHPh_3)_2$ dimers, linked by a six-fold phenyl embrace. An analogous behaviour is found in the case of $SiHPh_3$, but not in $CHPh_3$. Davey and co-workers[123] have investigated the various aspects of crystal nucleation processes and the relationship between intermolecular interactions in solution and in the solid state. In the examples discussed in this highlight,[123] the molecular dimers are often common building blocks between solution and crystal and may act as a kind of 'structural messenger' between solution and crystal. Although controlled preparation and characterization of different crystal forms of the same substance could be achieved in some cases, our understanding of polymorphism remains scanty, and crystal engineers

face the same question: "Can we predict the crystal structure from any given chemical composition?". While there is some evidence of advancement in this direction with the development of new computational software, there are many limitations to these approaches yet to be overcome.[124]

2. SCOPE OF THE PRESENT INVESTIGATIONS

The basis of molecular recognition is the presence of information in the interacting components. Molecular recognition,[125] which was introduced in the chemical literature by Emil Fischer[126] in 1894 as the Schlüsset-Schloss-Prinzip (lock and key principle) has had a significant impact in the development of non-covalent synthesis.[127] In supramolecular assemblies, information is expressed by the potential of a component to enter into non-covalent bonding relationships with its partners and by its steric requirements. From a practical point of view, the large number of variables which have to be addressed, that is, the magnitude and direction of the non-covalent interactions involved, makes this a non-trivial task in multicomponent systems. Thus, most studies of molecular recognition directed self-assembly have been based on hydrogen bonding, metal-ligand, and/or aromatic stacking interactions, since the geometry of these interactions is often predictable. Hydrogen bonds like O-H$\cdots$O, N-H$\cdots$O, O-H$\cdots$N, N-H$\cdots$N (the classical hydrogen bonds) are being extensively used in the analysis and design of novel supramolecular assemblies which has opened up a new avenue in the synthesis of advanced materials with tailor-made properties that show promising industrial applications, such as in catalysis, separation science, optical activity (NLO, octupolar, switches), sensors, electronic materials, conducting and magnetic materials, nanotechnology, polymorphism, crystal growth, supramolecular devices, surfactants, and drug design, to name a few.

In order to explore the possible formation of two-dimensional layered and cavity structures as well as three-dimensional channel structures using hydrogen bond assemblies, we have carried out several co-crystallization experiments between many
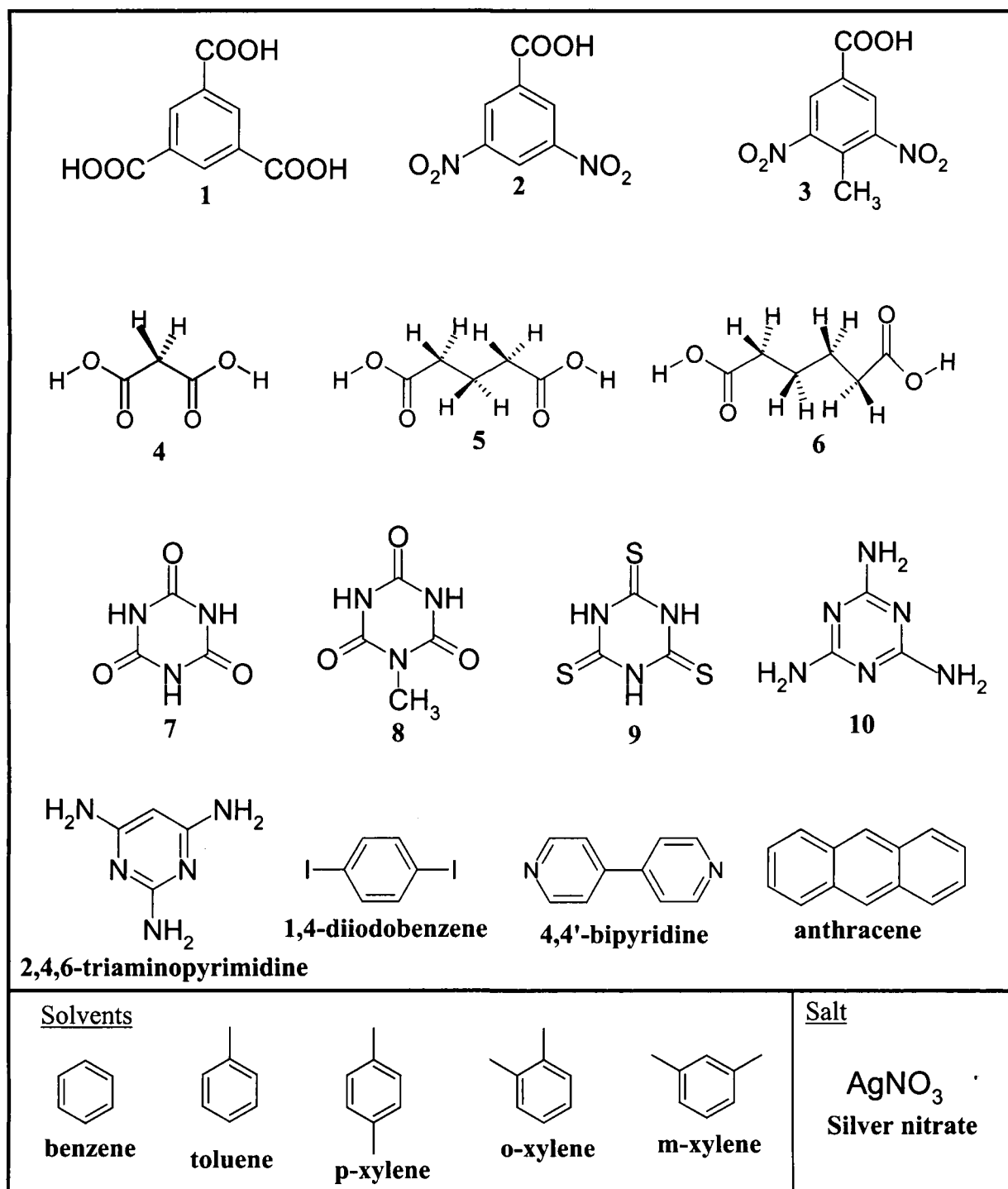
Figure 2.1: Molecules used for the co-crystallization experiments.

different molecules (Figure 2.1), possessing hydrogen bond donor and acceptor moieties. We have also synthesized co-crystals where weak bonds are the organizing forces, such as halogen···oxygen contacts that have a significant structure-directing effect and solely determine the crystal packing arrangement adopted by a molecule. We have synthesized a hydrogen-bonded coordination complex, where the hydrogen bonds act as steering forces in the formation of the complex, even in the presence of much stronger metal-ligand interactions.

In what follows, we intend to illustrate the structural and/or organizational characteristics of the interacting molecules necessary in order for molecular recognition to occur and also to present explicitly the supramolecular structures resulting from such interactions. The strategies employed in the synthesis of the assemblies are described.

2.1 Channel structures formed by self-assembled four-membered networks of trimesic acid

Carboxylic groups are among the best investigated hydrogen bond functionalities.[128] Since they possess a hydrogen bond donor as well as an acceptor site, carboxyl groups can readily form hydrogen bonds between each other as cyclic dimers. Scheme 2.1 depicts the commonly observed hydrogen bond couplings/synthons in carboxylic acids. The role of hydrogen bonding carboxyl groups in crystal packing has been analyzed in depth.[129]

(a) synthon **A**	(b) synthon **B**	(c) synthon **C**
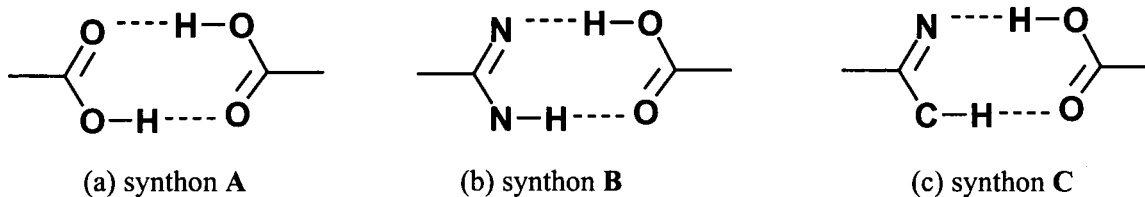
Scheme 2.1 *Commonly observed hydrogen bond couplings in carboxylic acid and in its co-crystals with other molecules – (a) centric carboxylic acid dimer coupling, (b) and (c) dimeric hydrogen bond coupling between carboxyl acid group and N(-H) or C(-H) functionality.*

Porous materials are crystalline or amorphous solids that permit the inclusion of small molecules through voids in their structures. The world on crystalline porous materials has long been dominated by aluminosilicate zeolites, which find wide use in catalysis, separation and ion exchange processes.[130] It is of interest to prepare channel structures of zeolite type using organic molecules alone.[131] The design of highly ordered and regular nanoporous architectures (< 15Å pore diameter) that have the added feature of 'tunability', that is, the ability to control the structure and function and modulate the nature and size of the aperture. In this respect, host frameworks with an organic core offer many advantages. Against this background, we reasoned that trimesic acid (**1**, TMA) that has a 14 × 14 Å cavity size in its two-dimensional arrangement would be a promising candidate for the design of porous solids, although in three dimensions, each hexagonal trimesic acid network interpenetrates into one another, forming a 4-fold inclined interpenetration. Herbstein and Marsh[132] determined the structures of molecular complexes formed by hydrates of trimesic acid and found that hydrogen-bonded layers of the composition TMA-H_2O gave rise to channels wherein picric acid molecules could reside. Further, Kolotuchin *et al*[56] have described

hexagonal channel structures of TMA containing ethanol, pyrene and tetrahydrofuran. In our investigation, surprisingly, simple crystallization of trimesic acid from methanol/benzene mixture or acetone resulted in the formation of a channel structure incorporating the solvent molecules within the channels. These results have been discussed in Section 4.1 along with the description of the crystal structure of the co-crystals formed by 1 with dimethylformamide.

2.2 Layered hydrogen-bonded structures formed by dinitrobenzoic acids

Although by intuition, one is tempted to take the carboxyl dimer as a very stable and robust hydrogen bond pattern, in reality, the formation of this motif is often displaced by other hydrogen bond configurations (see scheme 2.1).[133] We wanted to exploit these competitive effects and study and analyze a set of molecules that contain carboxyl groups and co-crystallize them with different donor/acceptor moieties.

Design strategies based on supramolecular synthons constructed from both strong and weak interactions are likely to provide a more complete understanding of crystal packing. Formation of such a coupling (see synthon **C** in Scheme 2.1) was reported to occur when carboxylic acid groups interact with hetero nitrogen atoms as was·described for the first time in the complexes of phenazine with 3,5-dinitrobenzoic acid, **2** and 3,5-dinitro-4-methylbenzoic acid, **3**.[134] The assemblies obtained consisted of linear tapes which are arranged in three dimensions to yield either a herringbone or crossed-ribbon networks. Further investigations of this synthon **C** have been reported by Batchelor *et al.*[135] The co-crystallization of phenazine with the *trans*-olefenic acids, fumaric and mesaconic, produced 1:1 supramolecular tapes, incorporating only the

synthon **C**. A complex between trimesic acid and 4,4'-bipyridine has been found to form a layered structure in which 4,4'-bipyridine expanded the two-dimensional cavities of trimesic acid by inserting in between the carboxyl group.[136] Hence, we have chosen to co-crystallize acids **2** and **3** in the presence of 4,4'-bipyridine to examine the perturbation of the hydrogen bonding networks present in the parent crystal structures and also the formation of the coupling **C**, to obtain layered structures. It has been noticed that 4,4'-bipyridine simply breaks the cyclic O-H···O hydrogen bond coupling between the adjacent acid moieties and forms single O-H···N and C-H···O hydrogen bonds. Also, the complex between 3,5-dinitro-4-methyl benzoic acid, **3**, 4,4'-bipyridine and anthracene, is stabilized by the formation of the pairwise O-H···N/C-H···O hydrogen bond coupling. The results are elaborated in Section 4.2.

2.3 Design of supramolecular assemblies using iodo···nitro interactions

In our continued interest to look at the variations in the hydrogen bond functionality of the carboxyl group upon co-crystallization with other molecules, we investigated the structure of 3,5-dinitrobenzoic acid (**2**) with 1,4-diiodobenzene. When nitro groups are present with iodine atoms in benzenoid compounds, the resulting intermolecular iodo···nitro interactions can play an important role in the supramolecular aggregation. One such example known in the literature is the 1:1 complex of 1,4-diiodobenzene with 1,4-dinitrobenzene which forms tapes via I···O interactions.[30] There are also other known examples from the literature.[137] In our study, the crystal structure of the complex of **2** with 1,4-diiodobenzene consists of

bifurcated I···O interactions, that helps to bring in two molecules of the acid, each of which is hydrogen-bonded to one another. The results are discussed in section 4.3.

2.4 Layered hydrogen-bonded structures formed by aliphatic carboxylic acids with azaaromatics

The carboxylic group can form stable cyclic hydrogen-bonded systems with a donor molecule as shown in Scheme 2.1[138-140] in which the coupling **B** is very robust.[138] A study of the assemblage of acylaminopyrimidine and aliphatic carboxylic acids has shown the design of novel assemblies using the coupling **B**.[138]

We wanted to explore supramolecular hydrogen-bonded assemblies formed by aliphatic dicarboxylic acids with a donor molecule such as 2,4,6-triaminopyrimidine involving the coupling **B**. As each of the supramolecular species of the reacting precursor molecules has characteristic features, it was therefore of interest to study the interaction between such components in the solid state. In this regard, crystal structures of hydrogen-bonded molecular complexes of malonic, **4**, glutaric, **5** and adipic, **6** acids with 2,4,6-triaminopyrimidine have been studied in order to examine the hydrogen-bonded structures formed in a system where the nitrogens of the heterocyclic ring as well as of the amino side chain of an azaaromatic compound can interact simultaneously with the carboxyl group. The results are discussed in section 4.4. Interestingly, we have found that the complexes differ among themselves depending upon the number of $-CH_2$ groups present in a given carboxylic acid.

2.5 Solvent-directed supramolecular assembly of the adducts of 4,4'-bipyridine with cyanuric acid and *N*-methylcyanuric acid

Apart from the carboxyl group, the other potential functional groups to form hydrogen-bonded networks are the amide groups. In particular, cyclic amide groups, present in molecules like cyanuric acid are of special interest with the availability of symmetrically substituted amide groups to form cyclic hydrogen bond networks.[127b] Such networks may yield cavities or channel type structures like in trimesic acid.[132] For this purpose, we wished to co-crystallize cyanuric acid, **7**, with 2,4,6-triaminopyrimidine and 4,4'-bipyridyl. We were not successful to get co-crystals with 2,4,6-triaminopyrimidine, but interesting crystal structures were obtained with 4,4'-bipyridine. 4,4'-bipyridine is a rather rigid weak bidentate base, popular in other crystal engineering studies because of its bridging ability.[141] Cyanuric acid, **7** and 4,4'-bipyridyl form two different crystals depending upon the solvent of crystallization and such solvent dependence on the formation of co-crystals is hitherto unknown. The feature is related to the formation of different hydrogen-bonded networks by the cyanuric acid upon crystallization from different solvents.

The N-methylated form of cyanuric acid, *N*-methylcyanuric acid, **8**, was co-crystallized with 4,4'-bipyridine using different solvents for crystallization, to check if there were any differences in the hydrogen bond packing arrangements compared to the cyanuric acid-bipyridine co-crystal. It was found that only one type of hydrogen bond network resulted for the adduct of *N*-methylcyanuric acid and 4,4'-bipyridine, irrespective of the solvent of crystallization. This can be explained because **8** forms only one type of hydrogen bond pattern in its pure crystal structure, and it is not

dependent on the solvent of crystallization. The results are discussed in detail in section 4.5.

2.6 Cyanurate mimics of hydrogen bonding patterns of nucleic bases: A 1:1 molecular complex formed by 9-ethyladenine with *N*-methylcyanuric acid

The specific base pair recognition of adenine (A) by thymine (T) and thymine (T) by adenine (A) as well as guanine (G) by cytosine (C) and cytosine (C) by guanine (G) through hydrogen bond formation is the key factor in the formation of the DNA duplex structure.[142] The unnatural or nonstandard nucleobases have gained importance in mimicking DNA structures and play a dominant role in the synthesis of novel molecular architectures. For instance, cyanuric acid and *N*-methylcyanuric acid have a close structural resemblance to uracil and form a variety of hydrogen-bonded base pairs in their pure[143] as well as mixed crystals. One such example is the ability of cyanurate-derivatized PNA monomer, ethyl *N*-(2-Boc-aminoethyl)-*N*-(cyanuric-1-yl acetate)glycinate to form a hydrogen-bonded supramolecular helicate structure.[144]

We chose to study the complexation of cyanuric acid **7** and *N*-methyl cyanuric acid **8** with 9-ethyladenine. In this context, ethyladenine has been shown to form interesting hydrogen bonding networks[145] in its molecular complex with 5,5-diethylbarbituric acid. We were not able to obtain the co-crystals of **7** and ethyladenine. But ethyladenine forms crystals readily with **8**. The crystal structure exhibits novel features that are unique among the hydrogen bonding patterns so far realized in the related structures formed by ethyladenine with various barbiturates.[145] The complex consists of homomeric and heteromeric hydrogen bonding patterns. The

homomeric hydrogen bond pattern is different than that observed in the pure crystal structure of 9-ethyladenine. The results are elaborated in section 4.6.

2.7 Hydrothermal synthesis of organic channel structures formed by the hydrogen bonding interaction of melamine with cyanuric and trithiocyanuric acids

Cyanuric acid-melamine adduct is expected to form a hexagonal network through the formation of hydrogen bonds as shown in Scheme 2.2. Such a network was referred to as a rosette by Whitesides.[27]
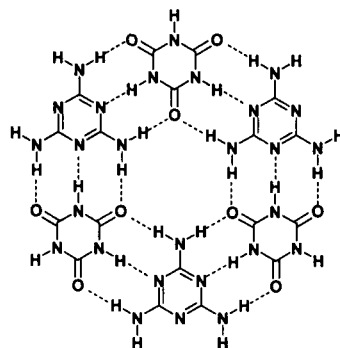
Scheme 2.2

Whitesides and coworkers synthesized a family of self-assembled hydrogen-bonded aggregates, stable in solution, based on this template.[146,147] However, the structure of the parent lattice, formed between pure cyanuric acid, **7** and melamine, **10**, has not been established by single crystal X-ray crystallography as single crystals of suitable quality could not be prepared by the generally known crystallization methods such as slow evaporation, sublimation etc. The difficulty in growing crystals of the adduct is partly because both the reactants **7** and **10** are hydrogen-bonded solids melting at very high temperatures, with limited solubility in most organic solvents. We have therefore,

made use of hydrothermal conditions,[148] commonly employed in the synthesis of quartz, zeolites and inorganic open-framework structures, to obtain the crystals of the 1:1 adduct. Crystals of the 1:1 adduct of trithiocyanuric acid, **9** and **10** could also not be obtained by any other crystallization methods, but have been prepared by employing this procedure. The structure determination reveals that the rosette arrangement forms channels of ~ 4 Å in dimension. The results are discussed in Section 4.7. These examples highlight the application of the hydrothermal technique for the synthesis of organic supramolecular assemblies, which is well known for the synthesis of inorganic or organometallic assemblies.

2.8 Organic porous solids formed by the hydrogen-bonded self-assembly of trithiocyanuric acid and 4,4'-bipyridyl

As mentioned in Section 2.5, cyanuric acid forms interesting co-crystals with other substrates. This is partly because of the formation of strong N-H$\cdots$O hydrogen bonds between cyanuric acid molecules. It was of interest to prepare channel structures of zeolite type using organic molecules alone.[131a] Such structures are very few in the literature, the noted examples being the self-assembly of three-dimensional networks with large chambers by using a pyridone as the tecton[131b] and complexes of urea and thiourea with channels as well as the quinol clathrates with cages. We were interested to synthesize materials of that kind by noncovalent synthesis, as they can be easily used in the industry for the purification of various chemicals or in catalysis, etc. Also, the efforts toward noncovalent synthesis based on hydrogen bonds employing sulfur donors have been quite limited. In this connection, we have chosen

trithiocyanuric acid, **9**, as a model compound as it can form N-H⋯S hydrogen bonds which are weaker molecular recognition forces, leading to greater flexibility.

We have investigated the hydrogen-bonded adduct formed between **9** and 4,4'-bipyridyl that has nice three-dimensional channels accommodating benzene. We have carried out detailed study to explore whether other aromatic compounds can be introduced in these channels and if so, there is any shape selectivity as in zeolites. We find that supramolecular hydrogen-bonded porous structures formed by **9** and 4,4'-bipyridyl is not only thermally stable but also accommodates several aromatic molecules like toluene, *o*-, *m*-, *p*-xylenes and anthracene, with some shape selectivity. The results are explained in Section 4.8.

2.9 A hybrid layered compound formed by silver sheets with cyanuric acid as the spacer molecule

Design of infinite two- and three-dimensional arrays of metal-ligand networks has attracted considerable attention in the last few years not only because of the structural and topological novelty of such engineered solids but also due to their potentially interesting electrical and magnetic properties.[149,150] Interesting structures containing polymeric Ag(I) species and heterocyclic as well as aromatic compounds have been described.[150-152] For example, Ag(I)-benzenesulfonate has a layered structure containing a planar hexagonal array of Ag(I) ions incorporating the anion.[152] A coordination network of dicyanodiphenylacetylene comprising Ag(I) sheets with an Ag⋯Ag separation of 3.39 Å has also been reported.[153] Equally interesting are the supramolecular Ag(I) complexes constructed with several polycyclic aromatic

hydrocarbons (PAHs) exhibiting the herringbone packing pattern.[154] Many of these compounds have Ag$\cdots$Ag separation significantly shorter than the van der Waals contact distance, with Ag(I) having linear, trigonal, tetrahedral or hexagonal coordination,[155] however the materials are generally either insulators or semiconductors.

During the course of our investigations of supramolecular assemblies of cyanuric acid, involving both hydrogen bonding and metal-ion coordination, we isolated a novel silver compound possessing two-dimensional silver sheets with the cyanuric acid (CA, 7) molecules in the interlayer space, forming linear hydrogen-bonded chains. This compound of composition, Ag$_2$.CA, is a unique organic-inorganic hybrid with electrical properties. The structure and properties of this Ag(I) compound are described in the Section 4.9.

3. EXPERIMENTAL

All the chemicals used in the present studies, except *N*-methylcyanuric acid, were obtained from commercial sources. *N*-methylcyanuric acid was prepared in the National Chemical Laboratory (courtesy of Dr. K. N. Ganesh). Preparation of *N*-methylcyanuric acid: melamine (5gm) and dimethyl sulphate (5gm) were refluxed in dioxane (20mL) for 4 hours in an atmosphere of argon. The reaction was stripped of the solvent and subjected to exhaustive hydrolysis by refluxing in a mixture of glacial acetic acid, concentrated hydrochloric acid and water for 24 hours. The solid residue obtained by evaporating the solvents under reduced pressure, was triturated with 20mL chilled water and filtered and the solid obtained was characterized by ^{1}H NMR and chemical analysis.

3.1 Preparation of the various adducts and complexes

Crystallization of trimesic acid adducts with various organic solvents

The adduct of trimesic acid and methanol was prepared by the crystallization of the acid (21.0 mg) from a mixture of 1:1 solution of methanol and benzene. However, the adduct of the acid and acetone, was obtained from the crystallization of trimesic acid (21.0 mg) from a solution of acetone. Crystals of trimesic acid and dimethylformamide (DMF), were obtained by crystallization of trimesic acid (21.0 mg) from a 1:1 solution of DMF and benzene. Single crystals obtained in all the cases were of good quality, suitable for crystal structure analysis to characterize by single crystal diffraction method.

Layered hydrogen-bonded complexes formed by dinitrobenzoic acids

Co-crystals, of 3,5-dinitrobenzoic acid (21.2 mg) and 3,5-dinitro-4-methylbenzoic acid (22.6 mg) respectively with 4,4'-bipyridine (15.6 mg), were prepared from a methanol solution. In both the cases, complexes were obtained in a 2:1 stoichiometry. Further, co-crystallization of the adducts with anthracene was carried out. 3,5-dinitrobenzoic acid did not yield any co-crystals with anthracene, but 3,5-dinitro-4-methylbenzoic acid gave crystals of good quality with anthracene (17.8 mg) in a 1:1 molar ratio that were suitable for single crystal X-ray diffraction studies.

Supramolecular assembly of 3,5-dinitrobenzoic acid and 1,4-diiodobenzene

A 2:1 ratio of 3,5-dinitrobenoic acid (42.4 mg) and 1,4-diiodobenzene (33.0 mg) were dissolved in methanol by heating. Slow evaporation of the hot methanol solution afforded good quality single crystals after a week's time. The same 2:1 complex is obtained even when the ratio of the precursor components that are mixed is 1:1.

Hydrogen-bonded complexes formed by aliphatic dicarboxylic acids and dinitrobenzoic acids with azaaromatic donors

Co-crystals of the azaaromatic donor, 2,4,6-triaminopyrimidine (12.5mg) with aliphatic dicarboxylic acids, malonic (10.4 mg), glutaric (13.2 mg) and adipic (14.6 mg) acids were prepared in a 1:1 molar ratio from a methanol solution by slow evaporation method. Good quality single crystals were obtained in all the cases.

Molecular complexes of cyanuric acid and N-methylcyanuric acid with 4,4'-bipyridine

Co-crystals formed between 4,4'-bipyridine (15.6 mg) and cyanuric acid (12.9 mg) were prepared from a methanol solution and from water. Crystals of *N*-methylcyanuric acid (15.0 mg) with 4,4'-bipyridine (15.6 mg) were obtained from a methanol solution.

Molecular complex of 9-ethyladenine and N-methylcyanuric acid

9-ethyladenine was crystallized from ethyl acetate by slow evaporation at room temperature. A 1:1 mixture of 9-ethyladenine (16.3 mg) and *N*-methylcyanuric acid (15.0 mg) were warmed in methanol and good quality crystals of the complex were obtained by slow evaporation from the methanol solution.

Hydrothermal synthesis of molecular complexes of melamine with cyanuric acid and trithiocyanuric acid

Single crystals of melamine with cyanuric acid could not be obtained by the usual crystallization methods from organic solvents. There was however evidence for the formation of an adduct from the powder X-ray diffraction patterns of the polycrystalline precipitates obtained on mixing the two in methanol. Since cyanuric acid, trithiocyanuric acid and melamine are solids with high melting points (>300°C), we made use of hydrothermal conditions, commonly employed in the synthesis of quartz, zeolites and inorganic framework structures, to obtain the crystals.

Aqueous solutions of cyanuric acid (129 mg) and melamine (126 mg) were mixed in a teflon flask and the mixture (15mL) was kept in a stainless steel bomb. The bomb was sealed and maintained in a furnace at 180°C. Rectangular plate-like

crystals of good quality separated from the solution, upon cooling the bomb to room temperature over a period of 4 hours. Crystals of the trithiocyanuric acid and melamine adduct were also obtained by a similar procedure except that the temperature of the furnace was maintained at 100°C (trithiocyanuric acid decomposed when the temperature was maintained at 180°C).

Adduct of trithiocyanuric acid and 4,4'-bipyridine formed in the presence of aromatic hydrocarbons

The adduct of trithiocyanuric acid with 4,4'-bipyridine was prepared by the co-crystallization of the two components from a methanol solution, but the crystals were not very stable. In the presence of benzene, toluene, *o*-, *m*- or *p*-xylene or anthracene, however, stable crystals, were obtained accommodating the respective aromatic guest molecules. In a typical preparation, 354 mg of trithiocyanuric acid and 156 mg of 4,4'-bipyridine were taken in 15mL of methanol in the presence of one of the above mentioned aromatic solvents (5mL). After slow evaporation, crystals of the adduct of trithiocyanuric acid-4,4'-bipyridine, containing the aromatic compound were obtained. In all these cases, good quality single crystals were obtained and these were employed for the determination of molecular and crystal structures, by single crystal X-ray diffraction. The ratio of trithiocyanuric acid, 4,4'-bipyridine and the aromatic molecule in the adducts containing benzene, toluene, *o*- and *m*-xylene was 2:1:1. The ratio was 2:1:0.5 in the adducts containing *p*-xylene and anthracene.

A hybrid layer compound containing silver sheets and cyanuric acid spacer molecules

A 10 mL solution consisting of a mixture of $AgNO_3$ (170 mg) and cyanuric acid (129 mg) in water in a Teflon flask was placed in a steel bomb. The bomb was placed in an oven maintained at 180°C for 24 h and then cooled to room temperature (298 K) over a period of 3 h. Good quality off-white plate-like single crystals were obtained. There were no other products in the reaction mixture.

3.2 Methods of characterization

3.2.1 Single crystal X-ray diffraction

All data sets have been collected using a SIEMENS 3-circle X-ray diffractometer with χ-axis fixed at 54.74° in which the positive and the negative limits for 2θ and $(\omega\text{-}2\theta)$ axes are 30° and -85°; 26° and -208°, respectively. The ϕ-axis on the other hand could be moved in the whole range of 0 to 360°. A photograph of the X-ray diffractometer is shown in Figure 3.1. The MoK_α radiation generated from a sealed X-ray tube (50 kV, 40 mA) is monochromatised using a graphite monochromator held at 6°. The beam is the passed through a 0.5-mm collimator before falling on the crystal. The direct beam from the collimator is stopped using a beam-stop, which is placed beyond the crystal. A charge coupled device (CCD) serves as the detector. It has a 1024 × 1024 pixeled phosphor screen protected by a beryllium window. At each pixel point on the screen, the X-ray photons are converted to optical photons, which are then carried to the CCD chip. The charge build-up is a measure of the diffracted intensity. Before a data collection, dark current measurement is done without opening the shutter. The dark frames (16 frames) are collected for the same exposure time as the data and are

averaged to obtain the background. The components of the SMART system are indicated in Figure 3.2.

The copper pip with a crystal on top is mounted on the goniometer-head and the sleds on the goniometer head are adjusted to center the crystal with respect to the cross-hairs of the optical microscope attached to the diffractometer. The data collection/reduction is done on a Pentium-DOS machine connected to the diffractometer using the SMART software.[156] Initially, the orientation of the crystal with respect to the diffractometer is determined by collecting over a range of ~ 7° in ω in ~ 45 frames, each frame being read for about 10 seconds. The width of each frame was 0.3°. By this method, the cell parameters and the orientation of the crystal could be obtained. For extended data, a separate SGI workstation connected to the Pentium PC over the Local Area Network (100 Mbps) is used. A room temperature hemisphere data is usually recorded to check the quality of the data at various resolution levels. Depending upon the intensity of diffraction, the data is collected for 20 to 40 seconds per frame. The data reduction is carried out using the SAINT software in the SGI workstation. This computer also houses SHELXTL[157] for structure solution and other programs like PLATON.[158]
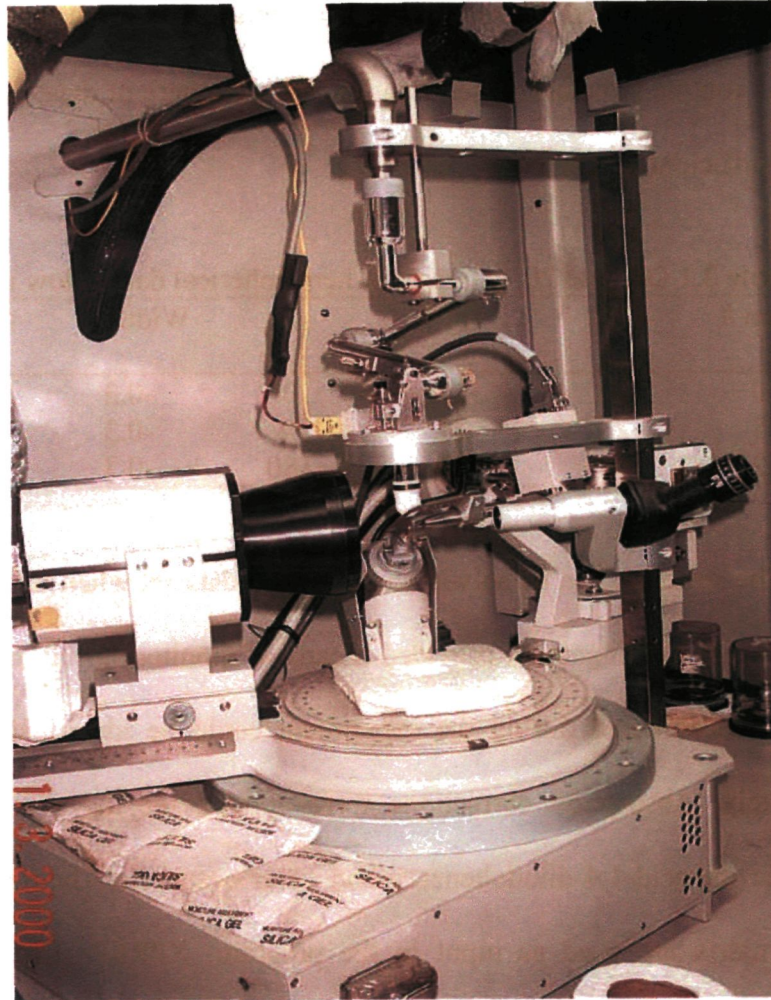
Figure 3.1: *Single crystal X-ray diffractometer*
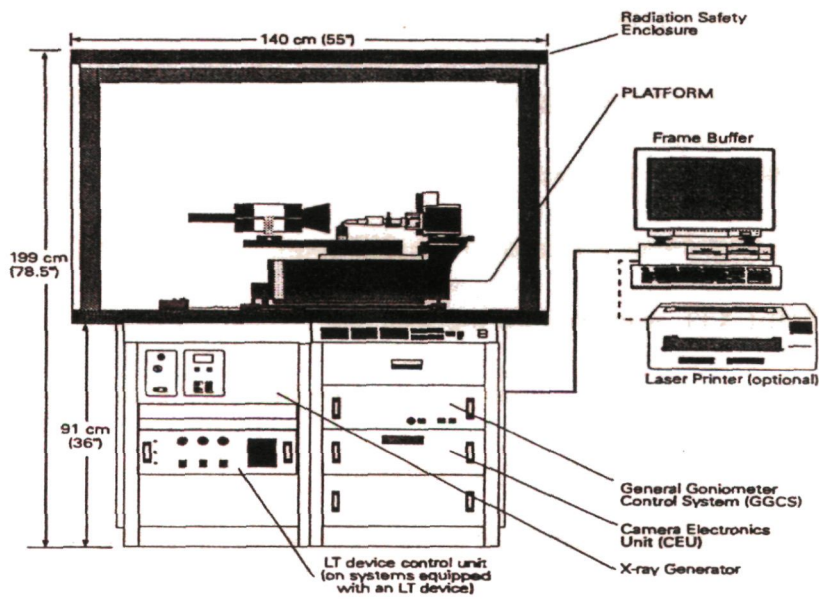
Figure 3.2: *Components of the Siemens SMART/CCD system.*

The values of 2θ, φ and ω used for the hemisphere data are listed below in Table 3.1. For a routine structural determination, a hemisphere of data, collected at low-angle is sufficient.

Table 3.1 Optimal 2θ, ω and φ for hemispherical data at low resolution

Run #	2θ	ω	φ	Width	# of frames
0	-28	-26	0	-0.3	606
1	-28	-21	88	-0.3	435
2	-28	-23	180	-0.3	230

The structure can be solved with a partial data set when the data collection is still on. This arrangement provided means of monitoring the data, so that any problems encountered during the experiment could be identified and corrected immediately. Absorption corrections were applied for the complexes of 3,5-dinitrobenzoic acid-1,4-diiodobenzene and silver cyanurate. The total data and the refined matrix are used as input in the program, XPREP. The centric or the noncentric nature of the crystal is determined based on the normalized structure factor, E; Mean $|E^2 - 1|$ being 0.968 (for centric) and 0.736 for non-centric crystal structures.[159] The exact space group is determined from the systematic absences. The graphic routine XP was used for the visualization purposes. All the structures were solved using direct methods of the XS routine of SHELXTL.[157] The XL routine of SHELXTL was used for the structure refinement over F^2. All the non-hydrogen atoms were refined anisotropically. The fractional atomic coordinates of the various molecular crystals investigated are given in Appendix A1. Intermolecular bonds were calculated using the program PLATON.[158]

3.2.2 *Thermogravimetric analysis*

Thermogravimetric analysis (TGA) has been carried out to study the porous nature of the host-guest complexes formed by the adduct trithiocyanuric acid and 4,4'-bipyridine using a Mettler-Toledo TG850 instrument. Initially, the complexes as-prepared were heated in the furnace attached to the instrument over the temperature range 25-200°C. This led to the removal of the aromatic guest molecules as confirmed by the weight loss noted in process. The host material obtained after removing the aromatic molecule was immersed in the aromatic liquid for several hours. The crystals were then taken out, and TGA repeated. This procedure was repeated more than once to find out whether the inclusion of the guest molecule was reversible and also whether there was any change in the temperature of decomposition or in the proportion of the aromatic compound in the adduct, with such cycling.

4. RESULTS AND DISCUSSION

4.1 Channel structures formed by self-assembled four-membered networks of trimesic acid

Trimesic acid generally forms hexagonal networks, by the formation of O-H···O hydrogen bond couplings between the adjacent carboxylic groups.[42] However, in our exploration, we have found that a rectangular network of the type reported by Herbstein[132] in the complex of trimesic acid with picric acid forms novel assemblies, giving channel structures. Our investigation originated with our attempt to crystallize trimesic acid, **1**, with dimethylformamide (DMF). It is known in the literature that **1** forms an adduct with dimethylamine rather than with DMF upon crystallization of the acid from DMF.[160] The amine results from the decomposition of DMF during crystallization with TMA. This prompted us to explore the possible methods to incorporate DMF itself into the crystal structure of the acid, **1**. We therefore attempted to crystallize **1** from a mixture of DMF and benzene, with the expectation that **1** while crystallizing from benzene, may trap DMF molecules into the lattice. Similar experiments were carried out with other solvent mixtures.

4.1.1 Hydrogen-bonded adduct of trimesic acid with dimethylformamide, 1a

The asymmetric unit of **1a**, which consists of one trimesic acid (**1**, TMA) molecule and two DMF molecules, is shown in Figure 4.1. The TMA.DMF adduct crystallizes in a monoclinic, $P2_1/c$ space group. The crystallographic data and experimental details are given in Table 4.1. The atomic coordinates and isotropic displacement parameters are listed in Table A1.1 (see Appendix A1).

Crystallization of **1** with DMF in the presence of benzene yields **1a**, which comprises

of two-dimensional molecular tapes formed between the molecules of TMA and DMF

through hydrogen bonds.
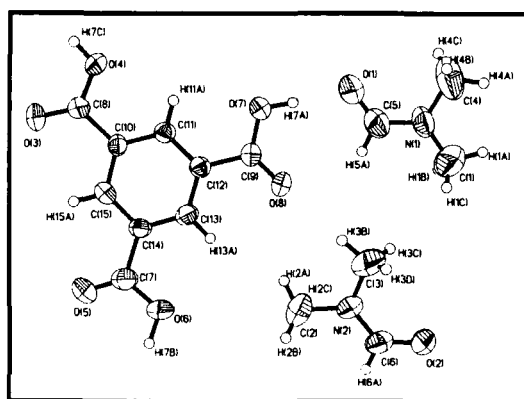
Figure 4.1: *ORTEP plot of trimesic acid-DMF, 1a. Thermal ellipsoids are given at 50% probability.*

Table 4.1 Crystal structure data of molecular complexes of trimesic acid + dimethylformamide (**1a**)

Chemical formula	$C_{15}H_{20}N_2O_8$
Formula weight	356.33
Cell setting	Monoclinic
Space group	$P2_1/c$
A (Å)	16.912(6)
B (Å)	14.475(5)
C (Å)	7.390(2)
α (°)	90
β (°)	90.55(3)
γ (°)	90
Cell volume (Å³)	1809.0(10)
Z	4
F(000)	752
ρ (Mg/m³)	1.308
μ, mm⁻¹	0.107
λ (Å)	0.7107
Crystal size (mm)	0.40 × 0.30 × 0.25
Diffractometer	Smart, CCD area detector
Radiation type	MoKα
Crystal-detector distance(cm)	5.0
Temperature (K)	293(2)
No. of measured reflections	3513

Table 4.1 (*continued*)

No. of independent reflections	2100
θ_{max} (°)	2 - 24
Range of *h, k, l*	-12 to 15
	-16 to 6
	-8 to 8
R_1	0.0587
wR_2	0.1161
S	1.419
No. of parameters refined	239
Max. eÅ^{-3}	0.239

The interatomic bond distances and angles for **1a** are listed below in Table 4.2.

Table 4.2. Bond lengths and angles **1a**

Moiety	Distance (Å)	Moiety	Angle (°)
O(6)-C(7)	1.328(5)	C(15)-C(10)-C(11)	119.1(3)
O(8)-C(9)	1.206(4)	C(15)-C(10)-C(8)	119.4(4)
C(10)-C(15)	1.390(5)	C(11)-C(10)-C(8)	121.5(4)
C(10)-C(11)	1.391(5)	C(13)-C(12)-C(11)	119.0(4)
C(10)-C(8)	1.491(5)	C(13)-C(12)-C(9)	119.0(4)
O(4)-C(8)	1.311(5)	C(11)-C(12)-C(9)	122.1(4)
O(7)-C(9)	1.324(4)	C(13)-C(14)-C(15)	119.5(4)
O(5)-C(7)	1.197(5)	C(13)-C(14)-C(7)	122.7(4)
C(12)-C(13)	1.392(5)	C(15)-C(14)-C(7)	117.8(4)
C(12)-C(11)	1.393(5)	O(8)-C(9)-O(7)	122.9(4)
C(12)-C(9)	1.489(5)	O(8)-C(9)-C(12)	122.7(4)
C(14)-C(13)	1.378(5)	O(7)-C(9)-C(12)	114.4(4)
C(14)-C(15)	1.392(5)	C(14)-C(13)-C(12)	121.0(4)
C(14)-C(7)	1.507(5)	C(10)-C(15)-C(14)	120.7(4)
O(3)-C(8)	1.210(4)	C(10)-C(11)-C(12)	120.8(4)
N(2)-C(6)	1.302(5)	O(3)-C(8)-O(4)	123.6(4)
N(2)-C(3)	1.439(5)	O(3)-C(8)-C(10)	124.0(4)
N(2)-C(2)	1.449(5)	O(4)-C(8)-C(10)	112.4(4)
O(2)-C(6)	1.239(5)	C(6)-N(2)-C(3)	119.8(4)
O(1)-C(5)	1.244(5)	C(6)-N(2)-C(2)	123.5(4)
N(1)-C(5)	1.312(5)	C(3)-N(2)-C(2)	116.7(4)
N(1)-C(1)	1.433(6)	O(5)-C(7)-O(6)	123.9(4)
N(1)-C(4)	1.435(6)	O(5)-C(7)-C(14)	123.2(4)
Moiety	**Angle (°)**	O(6)-C(7)-C(14)	112.9(4)
C(1)-N(1)-C(4)	116.8(4)	C(5)-N(1)-C(1)	123.3(5)
O(2)-C(6)-N(2)	124.8(5)	C(5)-N(1)-C(4)	119.9(5)
		O(1)-C(5)-N(1)	125.8(5)

The C-C distances of the phenyl ring in **1** are ~ 1.4 Å. The C-O and C=O distances of the carboxyl groups are ~ 1.3 and 1.2 Å, respectively. The C-N distances in DMF are in the range of 1.3 - 1.45 Å (see Table 4.2).

The two-dimensional arrangement of the molecules in a sheet is shown in Figure 4.2. Out of the three carboxyl groups, two of them interact with DMF molecules forming a cyclic coupling consisting of O-H···O and C-H···O hydrogen bonds. The corresponding H···O distances are 1.67, 1.68 and 2.53, 2.94 Å respectively. The third carboxyl group forms O-H···O (H···O, 1.77Å) and C-H···O (H···O, 2.43Å) hydrogen bonds. The unique hydrogen bonding distances of **1a** are given in Table 4.3.
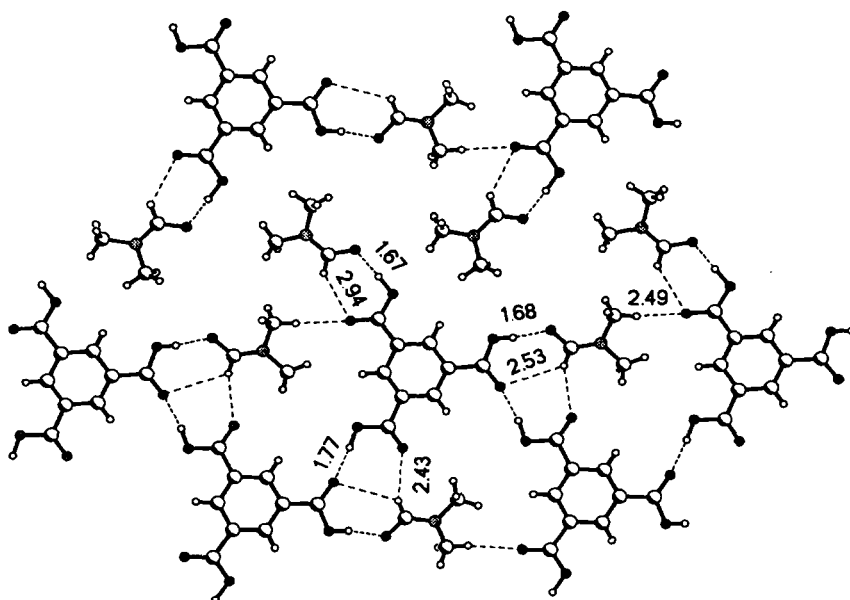
Figure 4.2: Two-dimensional molecular tapes formed between trimesic acid and DMF in the crystal structure of **1a**. Unique hydrogen bonding distances are only indicated.

Table 4.3. Unique hydrogen bond parameters **1a**

H-bond	D-H (Å)	H···A (Å)	D···A (Å)	D-H···A (°)
O(7)-H(7A)···O(1)	0.95(5)	1.67(5)	2.611(5)	167(5)
O(6)-H(7B)···O(3)	0.98(5)	1.77(5)	2.747(5)	179(5)
O(4)-H(7C)···O(2)	0.86(4)	1.67(4)	2.517(4)	171(5)
C(3)-H(3B)···O(8)	0.960(6)	2.491(6)	3.371(6)	152.4(7)
C(5)-H(5A)···O(8)	0.930(7)	2.524(6)	3.207(6)	130.5(6)
C(6)-H(6A)···O(5)	0.929(7)	2.431(6)	3.212(6)	141.7(5)

4.1.2 Trimesic acid with methanol, 1b

Interestingly, trimesic acid **1** forms crystals upon crystallization from a methanol/benzene mixture. The asymmetric unit of the compound resulting from the crystallization, **1b**, is shown in Figure 4.3. The asymmetric unit consists of one TMA molecule, one methanol and one water molecule. The hydrogen atoms are not indicated in the figure. The adduct **1b** crystallizes in a triclinic, P-1 space group. The crystal structure data are listed in Table 4.4. There are four adjacent trimesic acid molecules, connected to each other through regular centrosymmetric O-H···O hydrogen bonds as well as by single O-H···O hydrogen bonds leading to the formation of a four-membered network rather than the usual hexagonal network.
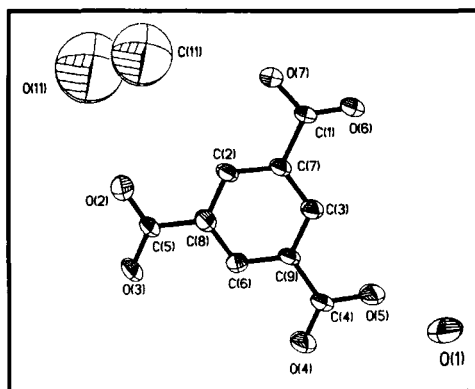
Figure 4.3: ORTEP plot of trimesic acid-methanol, **1b**. Thermal ellipsoids at 50% probability.

Table 4.4 Crystal structure data of the adduct of trimesic acid + methanol **1b**

Chemical formula	$C_{10}H_{12}O_8$
Formula weight	260.20
Cell setting	Triclinic
Space group	P-1
A (Å)	3.679(1)
B (Å)	8.971(2)
C (Å)	18.038(3)
α (°)	77.76(1)
β (°)	86.86(1)
γ (°)	88.04(1)
Cell volume (Å³)	580.8(2)
Z	2
F(000)	272
ρ (Mg/m³)	1.488
μ, mm⁻¹	0.132
λ (Å)	0.7107
Crystal size (mm)	0.35 × 0.22 × 0.38
Diffractometer	Smart, CCD area detector
Radiation type	MoKα
Crystal-detector distance(cm)	5.0
Temperature (K)	293(2)
No. of measured reflections	2426
No. of independent reflections	1630
θmax (°)	2 – 24
Range of h, k, l	-4 to 4
	-8 to 9
	-19 to 18
R₁	0.1328
wR₂	0.3082
S	1.657
No. of parameters refined	153
Max. eÅ⁻³	0.967

The atomic coordinates and isotropic displacement parameters are listed in Table A1.2. The interatomic bond lengths and valence angles are given in Table 4.5. The bond distances of the C-C bonds in the phenyl ring of TMA are ~ 1.4 Å and the C-C-C angles of the phenyl ring are nearly 120°. The C-O distance in methanol is ~ 1.5 Å.

Table 4.5 Bond lengths and angles **1b**

Moiety	Distance (Å)	Moiety	Angle (°)
C(9)-C(3)	1.384(12)	C(3)-C(9)-C(6)	121.7(8)
C(9)-C(6)	1.388(12)	C(3)-C(9)-C(4)	120.4(8)
C(9)-C(4)	1.511(12)	C(6)-C(9)-C(4)	117.9(7)
C(8)-C(2)	1.398(12)	C(2)-C(8)-C(6)	120.3(8)
C(8)-C(6)	1.402(12)	C(2)-C(8)-C(5)	120.0(8)
C(8)-C(5)	1.481(12)	C(6)-C(8)-C(5)	119.7(8)
O(7)-C(1)	1.301(11)	C(2)-C(7)-C(3)	120.8(8)
O(5)-C(4)	1.308(11)	C(2)-C(7)-C(1)	120.3(7)
O(6)-C(1)	1.214(11)	C(3)-C(7)-C(1)	119.0(7)
O(4)-C(4)	1.206(11)	C(9)-C(6)-C(8)	119.1(8)
O(3)-C(5)	1.281(11)	O(2)-C(5)-O(3)	123.0(8)
C(7)-C(2)	1.391(12)	O(2)-C(5)-C(8)	118.2(8)
C(7)-C(3)	1.406(12)	O(3)-C(5)-C(8)	118.7(8)
C(7)-C(1)	1.519(12)	O(4)-C(4)-O(5)	123.0(9)
O(2)-C(5)	1.275(11)	O(4)-C(4)-C(9)	122.0(8)
O(11)-C(11)	1.52(4)	O(5)-C(4)-C(9)	114.9(7)
Moiety	**Angle (°)**	C(9)-C(3)-C(7)	118.7(8)
O(6)-C(1)-C(7)	122.8(8)	C(7)-C(2)-C(8)	119.4(8)
O(7)-C(1)-C(7)	112.3(8)	O(6)-C(1)-O(7)	124.8(8)

In the four-membered network formed by the TMA molecules, two sides are made up of dimeric hydrogen bonds between the trimesic acid molecules (O⋯O, 2.61 and 2.64 Å) and these sides are connected to each other through H_2O molecules, giving rise to singly bridged dimers formed by O-H⋯O bonds (O⋯O, 2.61 and 2.87 Å), to yield planar sheets. The hydrogen atoms were not included in the refinement. This structure is similar to the one described by Herbstein and Marsh.[132] These sheets are stacked in a three-dimensional arrangement yielding channels occupied by methanol molecules as shown in Figure 4.4. The methanol molecules are hydrogen-bonded to one another (as shown in the inset of Figure 4.4). Such a polymeric chain of methanol molecules with O-H⋯O hydrogen bonds (O⋯O, 2.43Å) has not been

isolated or characterized hitherto and this has been possible in the present study since

the methanol molecules are present in the channel.
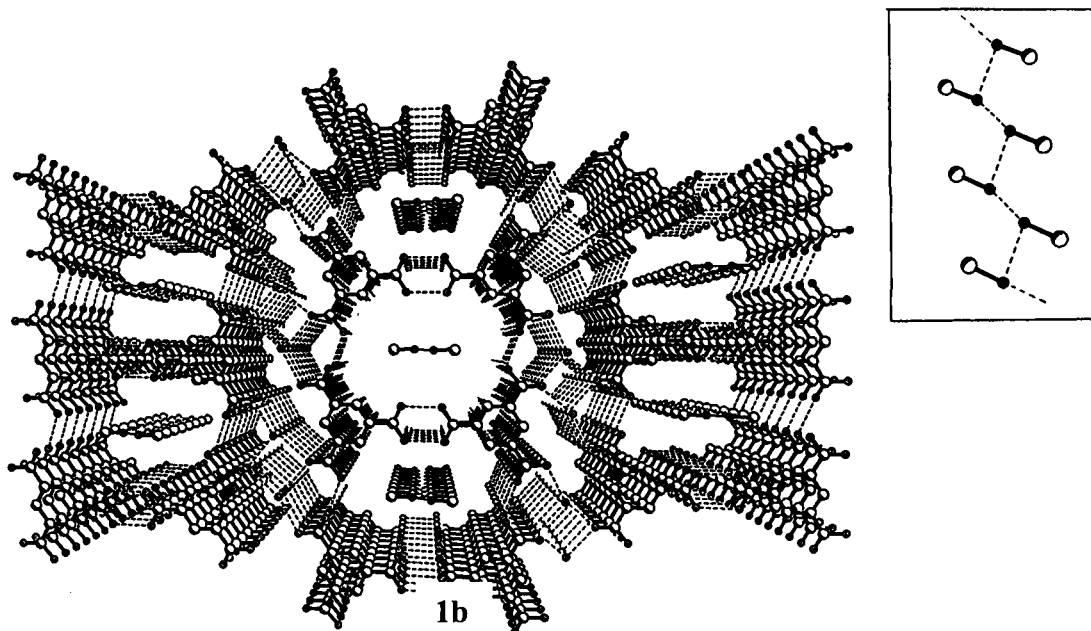
Figure 4.4: Three-dimensional arrangement in the crystal structure of trimesic acid, obtained from the crystallizaton from methanol/benzene *(1b)*. In the inset, a polymeric chain of methanol molecules present in the channels are shown.

4.1.3 Trimesic acid with acetone

A structure slightly similar to the one shown in Figure 4.4 is obtained upon crystallization of trimesic acid from acetone, the latter contains only one singly-bridged dimer with water molecule, and a linear O-H···O bond with another trimesic acid molecule, within a four-membered network. This is in contrast to the presence of two singly bridged dimers in the methanol adduct. There are molecules of acetone occupying the channels in Figure 4.5. However, the positions of the atoms corresponding to the acetone molecules could not be refined to a satisfactory level.
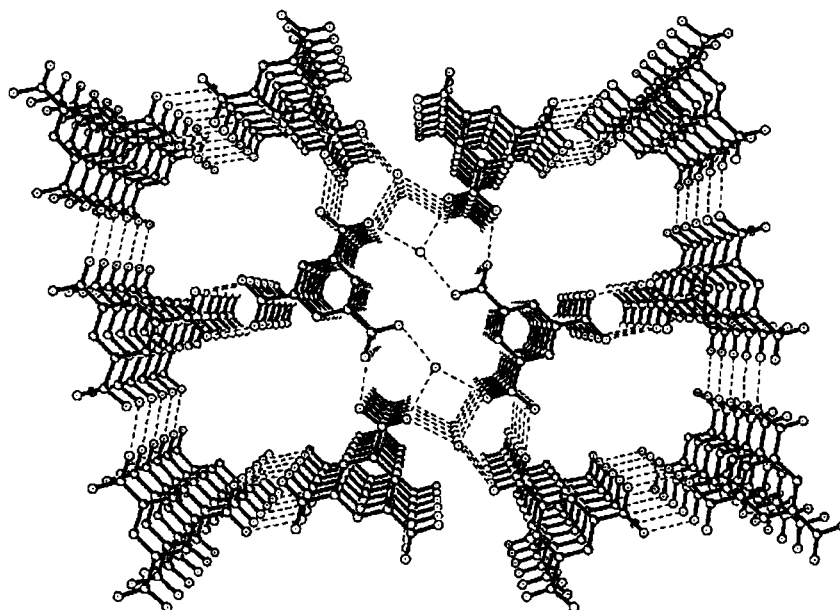
Figure 4.5: *Three-dimensional arrangement in the crystal structure of trimesic acid, obtained by crystallization from acetone. Acetone molecules are not shown in the channels.*

4.2 Layered structures formed by 3,5-dinitrobenzoic acid and 3,5-dinitro-4-methylbenzoic acid with 4,4'-bipyridine

3,5-dinitrobenzoic acid, **2**, is known to form a structure with cavities when crystallized from benzene solution, the cavities accommodating anthracene.[161] In the absence of benzene, however, it does not form a layered structure. Crystallization of 3,5-dinitro-4-methylbenzoic acid, **3**, from most solvents yields structures with cavities in a two-dimensional arrangement, which can accommodate anthracene.[161a] We have investigated whether the cavities formed by **2** and **3** could be modified by incorporating an azaaromatic donor molecule such as 4,4'-bipyridyl. Crystallization of **2** and **3** in the presence of bipyridine gave complexes **2a** and **3a** respectively in the 2:1 stoichiometry. The asymmetric units of the two co-crystals are shown in Figure 4.6. Crystal structure data of **2a** and **3a** are given in Table 4.6. The atomic coordinates and

isotropic displacement values for **2a** and **3a** are listed in Tables A1.3 and A1.4 respectively. **2a** crystallizes in a monoclinic, P2₁/n space group, and **3a** in P-1 space group (triclinic crystal system). Intramolecular bond lengths and angles for **2a** and **3a** are given in Tables 4.7 and 4.8 respectively.
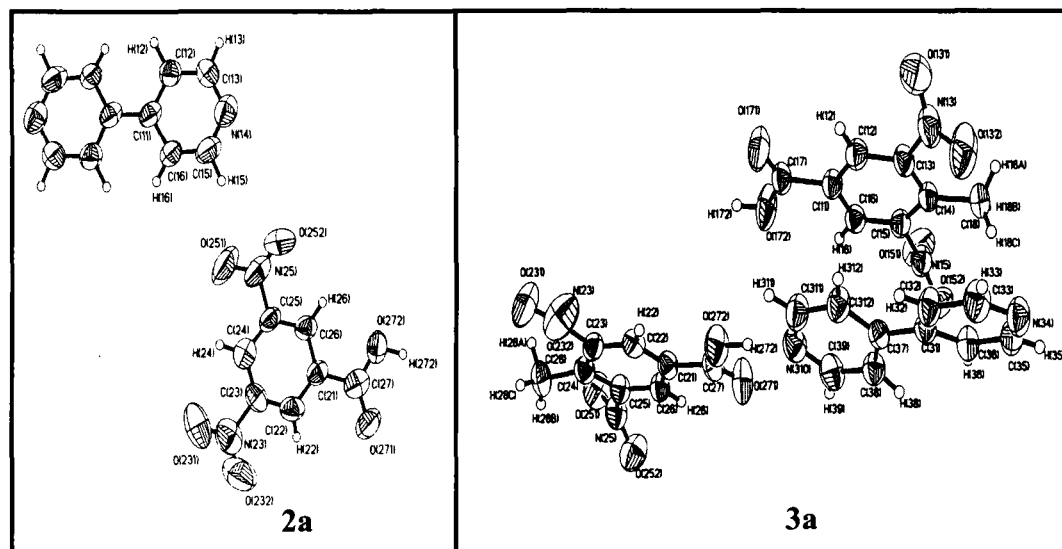
Figure 4.6: *ORTEP plots of 3,5-dinitrobenzoic acid-4,4'-bipyridyl, 2a, and 3,5-dinitro-4-methyl benzoic acid-4, 4'-bipyridyl, 3a.*

Table 4.6 Crystal structure data of molecular complexes of 3,5-dinitrobenzoic acid + 4,4'-bipyridyl (**2a**), 3,5-dinitro-4-methylbenzoic acid + 4,4'-bipyridyl (**3a**) and 3,5-dinitro-4-methylbenzoic acid + 4,4'-bipyridyl + anthracene (**3b**).

	2a	**3a**	**3b**
Chemical formula	$C_7H_4N_2O_6{:}C_{10}H_8N_2$	$C_8H_6N_2O_6{:}C_{10}H_8N_2$	$C_{16}H_{12}N_4O_{12}{:}C_{14}H_{10}$ $O_1{:}C_{10}H_8O_1$
Formula weight	580.43	608.48	786.70
Cell setting	monoclinic	triclinic	triclinic
Space group	P2₁/n	P-1	P-1
a (Å)	6.226(1)	9.852(1)	9.121(1)
b (Å)	22.150(2)	11.297(1)	9.260(1)
c (Å)	9.417(1)	14.827(1)	11.199(2)
α (°)	90	67.72(1)	73.83(1)
β (°)	99.17(1)	89.77(2)	89.58(1)
γ (°)	90	64.85(1)	81.78(1)
Cell volume (Å³)	1282.1(3)	1357.7(2)	898.6(2)
Z	2	2	1
F(000)	596	628	408
ρ (Mg/m³)	1.504	1.488	1.454

Table 4.6 (*continued*)

μ, mm^{-1}	0.124	0.121	0.110
λ (Å)	0.7107	0.7107	0.7107
Crystal size (mm)	0.25 × 0.25 × 0.25	0.35 × 0.30 × 0.20	0.25 × 0.30 × 0.30
Diffractometer	Smart, CCD area detector	Smart, CCD area detector	Smart, CCD area detector
Radiation type	MoKα	MoKα	MoKα
Crystal-detector distance(cm)	5.0	5.0	5.0
Temperature (K)	293(2)	293(2)	293(2)
No. of measured reflections	4885	5368	3537
No. of independent reflections	1831	3811	2528
θ_{max} (°)	2 - 24	2 - 24	2 - 24
Range of h, k, l	-6 to 6	-6 to 10	-10 to 9
	-17 to 24	-11 to 12	-8 to 10
	-10 to 8	-16 to 14	-12 to 12
R_1	0.0654	0.0487	0.0547
wR_2	0.0865	0.0980	0.0848
S	0.906	1.30	1.294
No. of parameters refined	223	478	322
Max. eÅ^{-3}	0.131	0.179	0.162

Table 4.7 Bond lengths and angles **2a**

Moiety	Distance (Å)	Moiety	Angle (°)
C(11)-C(12)	1.405(6)	C(16)-C(11)-C(12)	115.6(5)
C(11)-C(11)#1	1.460(8)	C(16)-C(11)-C(11)#1	123.1(7)
C(12)-C(13)	1.383(7)	C(12)-C(11)-C(11)#1	121.3(6)
C(12)-H(12)	1.07(4)	C(11)-C(12)-H(12)	116(3)
C(13)-N(14)	1.318(6)	N(14)-C(13)-C(12)	122.5(6)
C(13)-H(13)	0.99(5)	N(14)-C(13)-H(13)	122(3)
N(14)-C(15)	1.309(6)	C(12)-C(13)-H(13)	115(3)
C(15)-C(16)	1.376(7)	C(15)-N(14)-C(13)	118.5(6)
C(15)-H(15)	1.02(4)	N(14)-C(15)-C(16)	123.2(6)
C(16)-H(16)	0.97(4)	N(14)-C(15)-H(15)	121(2)
C(21)-C(26)	1.388(6)	C(16)-C(15)-H(15)	116(2)
C(21)-C(22)	1.401(6)	C(15)-C(16)-C(11)	120.3(6)
C(21)-C(27)	1.494(7)	C(15)-C(16)-H(16)	125(3)
C(22)-C(23)	1.366(7)	C(11)-C(16)-H(16)	115(3)
C(22)-H(22)	0.90(5)	C(26)-C(21)-C(22)	119.6(5)
C(23)-C(24)	1.355(6)	C(26)-C(21)-C(27)	120.6(6)
C(23)-N(23)	1.507(7)	C(22)-C(21)-C(27)	119.7(6)
N(23)-O(232)	1.194(6)	C(23)-C(22)-C(21)	117.9(6)
N(23)-O(231)	1.219(6)	C(23)-C(22)-H(22)	116(3)

Table 4.7 (*continued*)

Moiety	Distance	Moiety	Angle (°)
C(24)-C(25)	1.357(6)	C(21)-C(22)-H(22)	124(3)
C(24)-H(24)	0.99(4)	C(24)-C(23)-C(22)	123.1(6)
C(25)-C(26)	1.364(7)	C(24)-C(23)-N(23)	118.7(7)
C(25)-N(25)	1.485(7)	C(22)-C(23)-N(23)	118.2(6)
N(25)-O(252)	1.203(5)	O(232)-N(23)-O(231)	125.8(8)
N(25)-O(251)	1.213(5)	O(232)-N(23)-C(23)	117.7(7)
C(26)-H(26)	0.97(3)	O(231)-N(23)-C(23)	116.5(7)
C(27)-O(271)	1.229(5)	C(23)-C(24)-C(25)	118.0(6)
C(27)-O(272)	1.292(6)	C(23)-C(24)-H(24)	124(3)
O(272)-H(272)	0.98(4)	C(25)-C(24)-H(24)	117(2)
Moiety	**Angle (°)**	C(24)-C(25)-C(26)	122.5(6)
C(21)-C(26)-H(26)	122(2)	C(24)-C(25)-N(25)	118.7(6)
O(271)-C(27)-O(272)	124.2(6)	C(26)-C(25)-N(25)	118.7(6)
O(271)-C(27)-C(21)	122.6(6)	O(251)-N(25)-C(25)	116.4(6)
O(272)-C(27)-C(21)	113.2(6)	C(25)-C(26)-C(21)	118.8(6)
C(27)-O(272)-H(272)	113(2)	C(25)-C(26)-H(26)	118(2)

Table 4.8 Bond lengths and angles **3a**

Moiety	Distance (Å)	Moiety	Angle (°)
C(11)-C(12)	1.377(4)	C(12)-C(11)-C(16)	119.0(3)
C(11)-C(16)	1.388(4)	C(12)-C(11)-C(17)	120.3(3)
C(11)-C(17)	1.507(4)	C(16)-C(11)-C(17)	120.6(3)
C(12)-C(13)	1.375(4)	C(13)-C(12)-C(11)	120.3(3)
C(12)-H(12)	0.94(2)	C(13)-C(12)-H(12)	120(2)
C(13)-C(14)	1.401(4)	C(11)-C(12)-H(12)	119(2)
C(13)-N(13)	1.480(3)	C(12)-C(13)-C(14)	123.5(3)
C(14)-C(15)	1.392(4)	C(12)-C(13)-N(13)	117.0(3)
C(14)-C(18)	1.511(4)	C(14)-C(13)-N(13)	119.5(3)
C(15)-C(16)	1.372(4)	C(15)-C(14)-C(13)	113.1(2)
C(15)-N(15)	1.487(3)	C(15)-C(14)-C(18)	122.4(3)
C(16)-H(16)	1.00(2)	C(13)-C(14)-C(18)	124.4(3)
C(17)-O(171)	1.204(3)	C(16)-C(15)-C(14)	125.6(3)
C(17)-O(172)	1.283(3)	C(16)-C(15)-N(15)	116.0(2)
C(18)-H(18A)	0.93(4)	C(14)-C(15)-N(15)	118.3(2)
C(18)-H(18B)	0.91(4)	C(15)-C(16)-C(11)	118.4(3)
C(18)-H(18C)	1.00(4)	C(15)-C(16)-H(16)	120.8(14)
N(13)-O(132)	1.217(3)	C(11)-C(16)-H(16)	120.7(14)
N(13)-O(131)	1.220(3)	O(171)-C(17)-O(172)	124.9(3)
N(15)-O(151)	1.207(3)	O(171)-C(17)-C(11)	122.7(3)
N(15)-O(152)	1.217(3)	O(172)-C(17)-C(11)	112.4(3)
O(172)-H(172)	0.95(4)	C(14)-C(18)-H(18A)	113(2)
C(21)-C(26)	1.379(4)	C(14)-C(18)-H(18B)	106(3)
C(21)-C(22)	1.382(4)	H(18A)-C(18)-H(18B)	106(4)
C(21)-C(27)	1.503(4)	C(14)-C(18)-H(18C)	111(3)
C(22)-C(23)	1.382(4)	H(18A)-C(18)-H(18C)	106(3)
C(22)-H(22)	0.94(2)	H(18B)-C(18)-H(18C)	115(4)

Table 4.8 (*continued*)

C(23)-C(24)	1.395(4)	O(132)-N(13)-O(131)	124.6(3)
C(23)-N(23)	1.494(4)	O(132)-N(13)-C(13)	118.0(3)
C(24)-C(25)	1.397(4)	O(131)-N(13)-C(13)	117.4(3)
C(24)-C(28)	1.518(4)	O(151)-N(15)-O(152)	124.2(3)
C(25)-C(26)	1.377(4)	O(151)-N(15)-C(15)	118.2(3)
C(25)-N(25)	1.475(3)	O(152)-N(15)-C(15)	117.5(3)
C(26)-H(26)	0.93(3)	C(17)-O(172)-H(172)	119(2)
C(27)-O(271)	1.212(3)	C(26)-C(21)-C(22)	118.8(3)
C(27)-O(272)	1.299(3)	C(26)-C(21)-C(27)	119.5(3)
C(28)-H(28A)	1.08(5)	C(22)-C(21)-C(27)	121.7(3)
C(28)-H(28B)	0.97(4)	C(23)-C(22)-C(21)	119.3(3)
C(28)-H(28C)	0.94(3)	C(23)-C(22)-H(22)	123(2)
N(23)-O(232)	1.208(3)	C(21)-C(22)-H(22)	117(2)
N(23)-O(231)	1.216(3)	C(22)-C(23)-C(24)	124.7(3)
N(25)-O(252)	1.223(3)	C(22)-C(23)-N(23)	114.8(3)
N(25)-O(251)	1.224(3)	C(24)-C(23)-N(23)	120.5(3)
O(272)-H(272)	1.00(4)	C(23)-C(24)-C(25)	112.8(2)
C(31)-C(32)	1.391(4)	C(23)-C(24)-C(28)	125.1(3)
C(31)-C(36)	1.393(4)	C(25)-C(24)-C(28)	121.8(3)
C(31)-C(37)	1.484(4)	C(26)-C(25)-C(24)	124.6(3)
C(32)-C(33)	1.383(4)	C(26)-C(25)-N(25)	115.8(3)
C(32)-H(32)	0.96(3)	C(24)-C(25)-N(25)	119.6(2)
C(33)-N(34)	1.330(4)	C(25)-C(26)-C(21)	119.7(3)
C(33)-H(33)	0.93(3)	C(25)-C(26)-H(26)	120(2)
N(34)-C(35)	1.324(4)	C(21)-C(26)-H(26)	120(2)
C(35)-C(36)	1.374(4)	O(271)-C(27)-O(272)	125.4(3)
C(35)-H(35)	0.93(3)	O(271)-C(27)-C(21)	122.3(3)
C(36)-H(36)	0.93(3)	O(272)-C(27)-C(21)	112.2(3)
C(37)-C(312)	1.387(4)	C(24)-C(28)-H(28A)	110(3)
C(37)-C(38)	1.390(4)	C(24)-C(28)-H(28B)	114(3)
C(38)-C(39)	1.387(4)	H(28A)-C(28)-H(28B)	104(3)
C(38)-H(38)	0.97(3)	C(24)-C(28)-H(28C)	111(2)
C(39)-N(310)	1.330(4)	H(28A)-C(28)-H(28C)	104(3)
C(39)-H(39)	0.97(3)	H(28B)-C(28)-H(28C)	114(3)
N(310)-C(311)	1.325(4)	O(232)-N(23)-O(231)	124.3(3)
C(311)-C(312)	1.377(4)	O(232)-N(23)-C(23)	117.4(3)
C(311)-H(311)	0.94(4)	O(231)-N(23)-C(23)	118.3(3)
C(312)-H(312)	0.94(3)	O(252)-N(25)-O(251)	123.8(3)

Moiety	**Angle (°)**		
C(31)-C(36)-H(36)	123(2)	O(252)-N(25)-C(25)	117.5(3)
C(312)-C(37)-C(38)	116.9(3)	O(251)-N(25)-C(25)	118.6(3)
C(312)-C(37)-C(31)	121.2(2)	C(27)-O(272)-H(272)	116(2)
C(38)-C(37)-C(31)	122.0(3)	C(32)-C(31)-C(36)	116.8(3)
C(39)-C(38)-C(37)	119.7(3)	C(32)-C(31)-C(37)	121.2(3)
C(39)-C(38)-H(38)	120(2)	C(36)-C(31)-C(37)	122.0(2)
C(37)-C(38)-H(38)	120(2)	C(33)-C(32)-C(31)	119.6(3)
N(310)-C(39)-C(38)	122.7(3)	C(33)-C(32)-H(32)	120(2)
		C(31)-C(32)-H(32)	120(2)

Table 4.8 (*continued*)

N(310)-C(39)-H(39)	117(2)	N(34)-C(33)-C(32)	123.2(3)
C(38)-C(39)-H(39)	120(2)	N(34)-C(33)-H(33)	115(2)
C(311)-N(310)-C(39)	117.8(3)	C(32)-C(33)-H(33)	121(2)
N(310)-C(311)-C(312)	123.4(3)	C(35)-N(34)-C(33)	117.0(3)
N(310)-C(311)-H(311)	116(2)	N(34)-C(35)-C(36)	124.3(3)
C(312)-C(311)-H(311)	121(2)	N(34)-C(35)-H(35)	116(2)
C(311)-C(312)-C(37)	119.6(3)	C(36)-C(35)-H(35)	119(2)
C(311)-C(312)-H(312)	117(2)	C(35)-C(36)-C(31)	119.1(3)
C(37)-C(312)-H(312)	123(2)	C(35)-C(36)-H(36)	118(2)

In both **2a** and **3a**, bipyridyl molecules break up the hydrogen bonds between the carboxyl groups as shown in Figure 4.7. The hydrogen bond geometries for complexes, **2a** and **3a** are listed in Tables 4.9 and 4.10, respectively.

Table 4.9 Unique hydrogen bond parameters **2a**

H-bond	D-H (Å)	H⋯A (Å)	D⋯A (Å)	D-H⋯A (°)
O(272)-H(272)⋯N(14)	0.97(4)	1.61(4)	2.577(7)	172(3)
C(12)-H(12)⋯O(231)	1.06(5)	2.57(4)	3.296(8)	125(3)
C(15)-H(15)⋯O(251)	1.02(4)	2.53(4)	3.439(8)	148(3)
C(22)- H(22)⋯O(232)	0.90(5)	2.39(5)	2.722(9)	102(4)
C(26)- H(26)⋯O(252)	0.97(4)	2.37(4)	2.702(8)	100(3)

Table 4.10 Unique hydrogen bond parameters **3a**

H-bond	D-H (Å)	H⋯A (Å)	D⋯A (Å)	D-H⋯A (°)
O(172)-H(172)⋯N(34)	0.95(4)	1.64(4)	2.579(5)	167(3)
O(272)-H(272)⋯N(310)	1.01(5)	1.58(5)	2.581(5)	171(4)
C(16)-H(16)⋯O(252)	0.99(3)	2.51(3)	3.489(4)	169(3)
C(18)-H(18B)⋯N(15)	0.91(4)	2.52(5)	2.910(5)	106(4)
C(22)-H(22)⋯O(272)	0.94(3)	2.37(3)	2.724(5)	101.8(19)
C(28)-H(28B)⋯O(251)	0.98(4)	2.37(5)	2.872(6)	111(4)
C(28)-H(28B)⋯N(25)	0.98(4)	2.55(5)	2.929(6)	103(3)
C(28)-H(28C)⋯O(231)	0.94(4)	2.41(4)	2.768(6)	102(3)
C(33)-H(33)⋯O(132)	0.94(3)	2.53(3)	3.453(5)	167(3)
C(312)-H(312)⋯O(232)	0.94(3)	2.53(3)	3.240(4)	132(3)

2a

3a
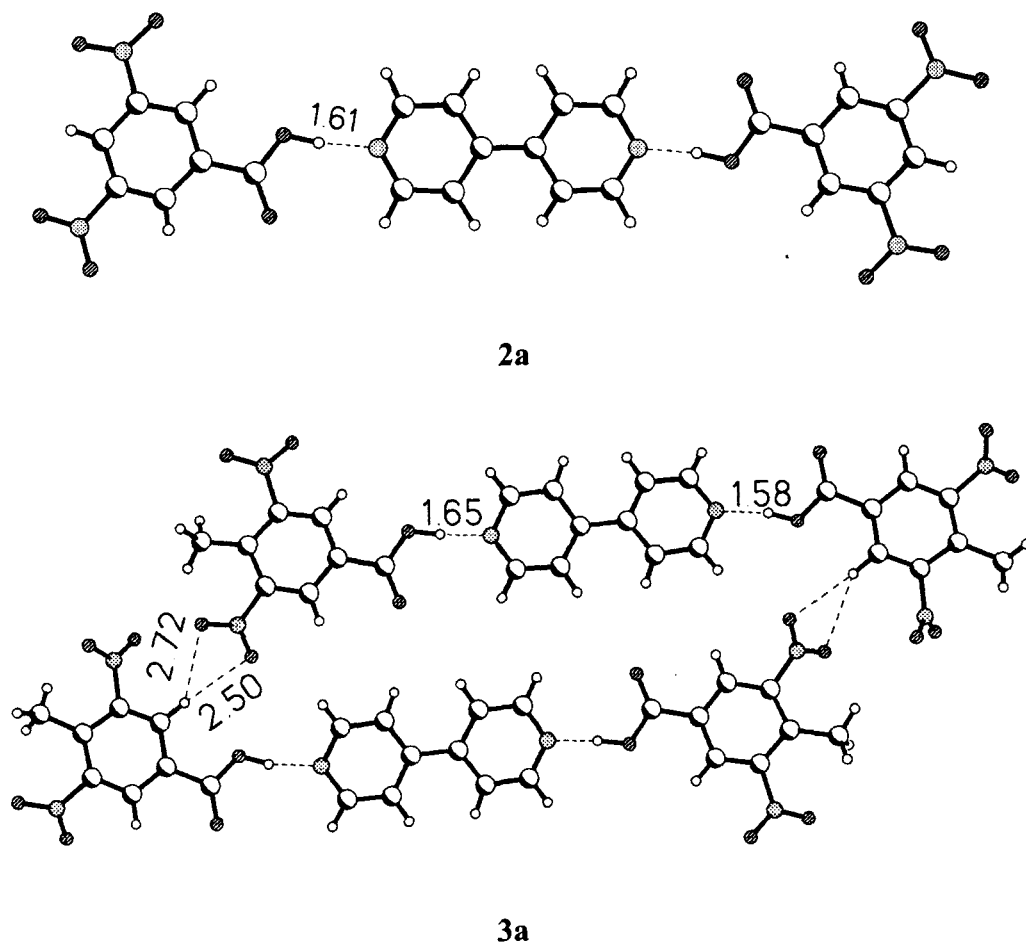
Figure 4.7: Top: Recognition pattern between 3,5-dinitrobenzoic acid, **2**, and 4,4'-bipyridine in the molecular complex, **2a**. Bottom: Two-dimensional arrangement of supermolecules of 3,5-dinitro-4-methylbenzoic acid, **3**, and 4,4'-bipyridyl in the complex, **3a**. The dashed lines represent hydrogen bonds.

Interestingly, interaction between the carboxylic acid and the bipyridyl molecule in these complexes occur through the formation of a single O-H⋯N hydrogen bond (Figure 4.7), unlike the pair-wise hydrogen bond coupling observed in other related systems. The H⋯N distances in **2a** and **3a** are 1.61 and 1.65 Å respectively. There are also C-H⋯O hydrogen bonds between the acid molecules in both **2a** and **3a** (H⋯O ~ 2.4 to 2.5 Å, ∠C-H⋯O, 100° - 170°). Furthermore, molecules of **3a** are arranged in

two dimensions to yield planar sheets (Figure 4.7, bottom) which in turn are stacked in the three-dimensional packing while molecules of **2a** adopt a herringbone-packing pattern.

Although both **2a** and **3a** do not possess cavities, the two-dimensional arrangement in **3a** (Figure 4.7, bottom), which is similar to that of the structures of the pure acid, **3**, encouraged us to investigate the co-crystallization of **2a** and **3a** in the presence of anthracene. **2a** did not yield any co-crystals with anthracene, but **3a** gave crystals of good quality suitable for single crystal X-ray diffraction studies. The asymmetric unit of the **3a**-anthracene system consists of one dinitrobenzoic acid molecule, half a molecule of bipyridine, and half a molecule of anthracene as shown in Figure 4.8. The crystal structure data of this co-crystal, **3b**, is given in Table 4.6.
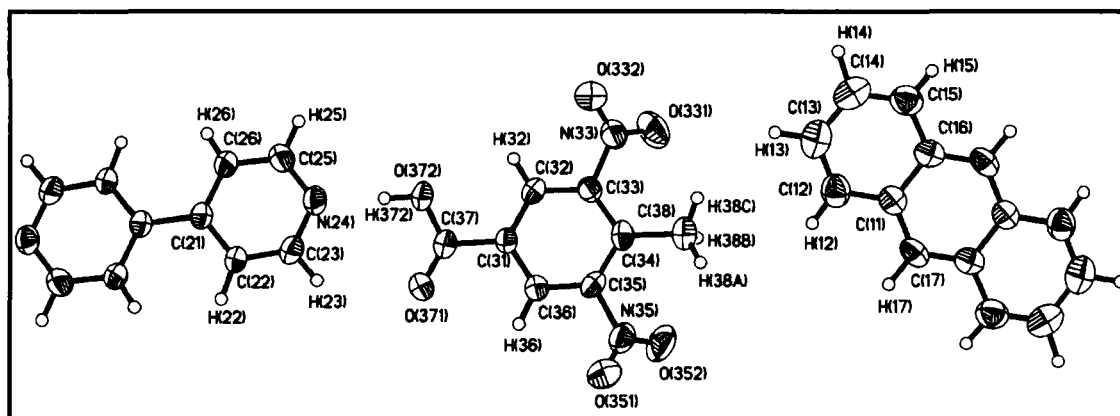
Figure 4.8: *ORTEP plot of the complex of 3,5-dinitro-4-methylbenzoic acid + 4, 4'-bipyridyl + anthracene, 3b. Thermal ellipsoids shown at 50% probability.*

The atomic coordinates and isotropic displacement parameters of **3b** are listed in Table A1.5. The intramolecular bond lengths and angles of **3b** are given in Table 4.11.

Table 4.11 Bond lengths and angles **3b**

Moiety	Distance (Å)	Moiety	Angle (°)
O(372)-C(37)	1.308(3)	C(33)-C(34)-C(35)	113.1(3)
C(34)-C(33)	1.389(4)	C(33)-C(34)-C(38)	124.2(3)
C(34)-C(35)	1.397(4)	C(35)-C(34)-C(38)	122.5(3)
C(34)-C(38)	1.510(4)	C(22)-C(21)-C(26)	116.5(3)
C(21)-C(22)	1.384(4)	C(22)-C(21)-C(21)#1	122.2(3)
C(21)-C(26)	1.389(4)	C(26)-C(21)-C(21)#1	121.3(3)
C(21)-C(21)#1	1.488(5)	C(32)-C(33)-C(34)	124.3(3)
C(33)-C(32)	1.378(4)	C(32)-C(33)-N(33)	114.9(3)
C(33)-N(33)	1.481(4)	C(34)-C(33)-N(33)	120.8(3)
N(24)-C(23)	1.327(4)	C(23)-N(24)-C(25)	117.0(3)
N(24)-C(25)	1.337(4)	C(23)-C(22)-C(21)	119.9(3)
C(22)-C(23)	1.381(4)	O(331)-N(33)-O(332)	124.5(3)
N(33)-O(331)	1.218(3)	O(331)-N(33)-C(33)	118.8(3)
N(33)-O(332)	1.223(3)	O(332)-N(33)-C(33)	116.7(3)
C(31)-C(36)	1.379(4)	C(36)-C(31)-C(32)	118.9(3)
C(31)-C(32)	1.376(4)	C(36)-C(31)-C(37)	119.4(3)
C(31)-C(37)	1.505(4)	C(32)-C(31)-C(37)	121.7(3)
C(26)-C(25)	1.379(4)	C(25)-C(26)-C(21)	120.0(3)
O(371)-C(37)	1.202(3)	C(31)-C(32)-C(33)	120.0(3)
N(35)-O(352)	1.218(3)	O(352)-N(35)-O(351)	125.1(3)
N(35)-O(351)	1.225(3)	O(352)-N(35)-C(35)	117.8(3)
N(35)-C(35)	1.480(4)	O(351)-N(35)-C(35)	117.1(3)
C(36)-C(35)	1.383(4)	C(31)-C(36)-C(35)	119.2(3)
C(11)-C(17)	1.393(4)	O(371)-C(37)-O(372)	125.9(3)
C(11)-C(12)	1.427(4)	O(371)-C(37)-C(31)	122.2(3)
C(11)-C(16)	1.434(4)	O(372)-C(37)-C(31)	111.9(3)
C(17)-C(16)#2	1.388(4)	N(24)-C(25)-C(26)	123.1(3)
C(16)-C(17)#2	1.388(4)	C(36)-C(35)-C(34)	124.5(3)
C(16)-C(15)	1.424(4)	C(36)-C(35)-N(35)	115.7(3)
C(12)-C(13)	1.341(5)	C(34)-C(35)-N(35)	119.8(3)
C(13)-C(14)	1.412(5)	N(24)-C(23)-C(22)	123.5(3)
C(15)-C(14)	1.354(5)	C(17)-C(11)-C(12)	122.5(3)

Moiety	Angle (°)		
		C(17)-C(11)-C(16)	118.3(3)
C(31)-C(36)-C(35)	119.2(3)	C(12)-C(11)-C(16)	119.2(3)
O(371)-C(37)-O(372)	125.9(3)	C(16)#2-C(17)-C(11)	122.4(3)
O(371)-C(37)-C(31)	122.2(3)	C(17)#2-C(16)-C(15)	123.6(3)
O(372)-C(37)-C(31)	111.9(3)	C(17)#2-C(16)-C(11)	119.3(3)
N(24)-C(25)-C(26)	123.1(3)	C(15)-C(16)-C(11)	117.1(3)
C(36)-C(35)-C(34)	124.5(3)	C(13)-C(12)-C(11)	121.2(4)
C(36)-C(35)-N(35)	115.7(3)	C(12)-C(13)-C(14)	120.0(4)
C(34)-C(35)-N(35)	119.8(3)	C(14)-C(15)-C(16)	121.4(4)
N(24)-C(23)-C(22)	123.5(3)	C(15)-C(14)-C(13)	121.0(4)
C(17)-C(11)-C(12)	122.5(3)	C(33)-C(34)-C(35)	113.1(3)
C(17)-C(11)-C(16)	118.3(3)	C(33)-C(34)-C(38)	124.2(3)
C(12)-C(11)-C(16)	119.2(3)	C(35)-C(34)-C(38)	122.5(3)
C(16)#2-C(17)-C(11)	122.4(3)	C(22)-C(21)-C(26)	116.5(3)

Table 4.11 (*continued*)

C(17)#2-C(16)-C(15)	123.6(3)	C(22)-C(21)-C(21)#1	122.2(3)
C(17)#2-C(16)-C(11)	119.3(3)	C(26)-C(21)-C(21)#1	121.3(3)
C(15)-C(16)-C(11)	117.1(3)	C(32)-C(33)-C(34)	124.3(3)
C(13)-C(12)-C(11)	121.2(4)	C(32)-C(33)-N(33)	114.9(3)
C(12)-C(13)-C(14)	120.0(4)	C(34)-C(33)-N(33)	120.8(3)
C(14)-C(15)-C(16)	121.4(4)	C(23)-N(24)-C(25)	117.0(3)
C(15)-C(14)-C(13)	121.0(4)	C(23)-C(22)-C(21)	119.9(3)
C(32)-C(31)-C(37)	121.7(3)	O(331)-N(33)-O(332)	124.5(3)
C(25)-C(26)-C(21)	120.0(3)	O(331)-N(33)-C(33)	118.8(3)
C(31)-C(32)-C(33)	120.0(3)	O(332)-N(33)-C(33)	116.7(3)
O(352)-N(35)-O(351)	125.1(3)	C(36)-C(31)-C(32)	118.9(3)
O(352)-N(35)-C(35)	117.8(3)	C(36)-C(31)-C(37)	119.4(3)
		O(351)-N(35)-C(35)	117.1(3)

Symmetry transformations used to generate equivalent atoms:
#1 -x+1,-y,-z-1
#2 -x,-y+1,-z+2
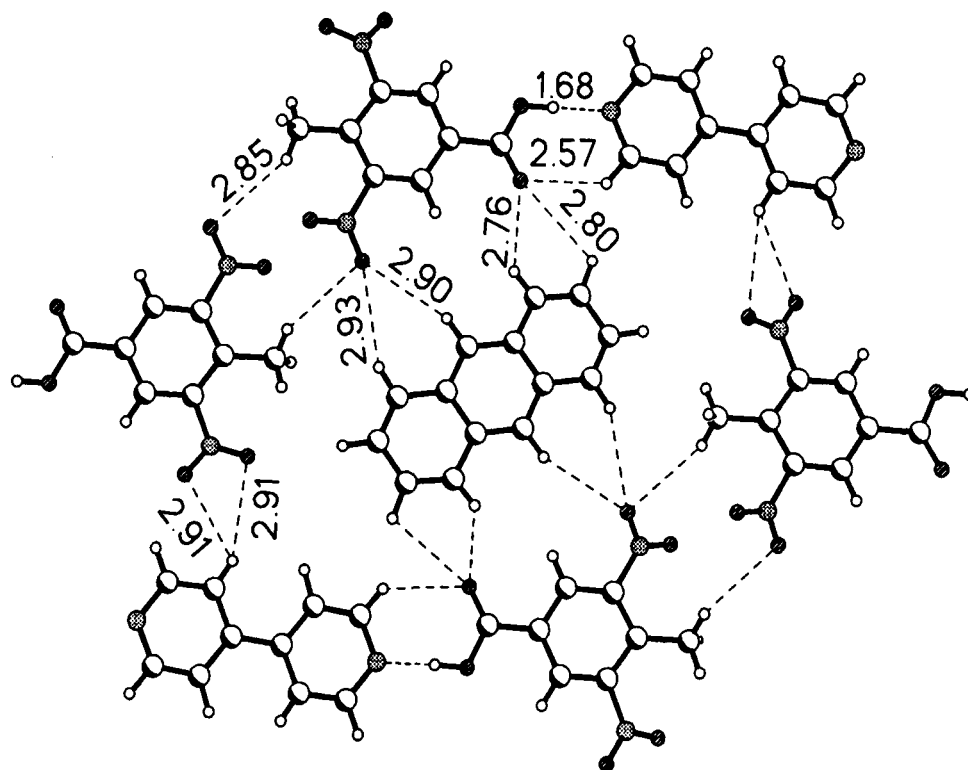
Figure 4.9. *Two-dimensional arrangement of hexagonal cavity, formed by acid, 3 and 4,4'-bipyridyl which is filled by molecules of anthracene in the complex, 3b.*

The complex, **3b** formed between **3a** and anthracene is stabilized by the formation of

O-H···N and C-H···O hydrogen bond couplings, not found either in **2a** or **3a**, as

shown in Figure 4.9. The hydrogen bond geometries in **3b** are given in Table 4.12.

The H···N and H···O distances between the acid and 4,4'-bipyridine in the anthracene

adduct, **3b** are 1.68 and 2.57 Å, respectively. Figure 4.9 shows that the supermolecules

are arranged in two dimensions in a hexagonal mode through the formation of C-

H···O hydrogen bonds between anthracene and the neighbouring molecules of

carboxylic acid, **3** such that a cavity of dimension 10×12 Å results. The anthracene

molecules are accommodated in these cavities through the formation of C-H···O

hydrogen bonds. The H···O distances are in the range of 2.76 - 2.93 Å. A comparison

of the structure of **3b** (Figure 4.9) with the anthracene adduct formed by the parent

carboxylic acid alone indicates that the recognition pattern between anthracene and the

acid **3** is not perturbed in the presence of bipyridine in **3b**.

Table 4.12 Unique hydrogen bond parameters **3b**

H-bond	D-H (Å)	H···A (Å)	D···A (Å)	D-H···A (°)
N(32)-H(32A)···S(33)	0.860(13)	2.561(10)	3.410(10)	169.6(9)
N(34)-H(34A)···S(45)	0.860(12)	2.476(10)	3.306(10)	162.6(10)
N(36)-H(36A)···N(24)	0.860(13)	1.969(13)	2.829(13)	177.4(12)
N(42)-H(42A)···N(29)	0.860(12)	1.939(12)	2.798(12)	178.7(12)
N(44)-H(44A)···S(43)	0.860(14)	2.566(10)	3.408(10)	166.5(9)
N(46)-H(46A)···S(33)	0.860(14)	2.776(10)	3.634(10)	174.6(11)

4.3 A 2:1 supramolecular assembly of 3,5-dinitrobenzoic acid and 1,4-diiodobenzene

3,5-dinitrobenzoic acid, **2**, forms a 2:1 molecular complex with 1,4-diiodobenzene. The asymmetric unit consists of one molecule of 3,5-dinitrobenzoic

acid and a half molecule of 1,4-diiodobenzene, as shown in Figure 4.10. This complex

crystallizes in a monoclinic crystal system and I2/a space group. Crystal structure

determination of the complex reveals that the interacting molecules recognize each

other through the formation of a three-centered iodo-nitro coupling consisting of two

I···O interactions as shown in Figure 4.11. The I···O distances are within the

acceptable limits described in the literature and conform to $\mathbf{Q}$ type contacts.[162] Tables

4.13 and 4.14 give the crystallographic data and interatomic bond distances and

angles, respectively. The atomic coordinates and isotropic displacement parameters

are listed in Table A1.6.
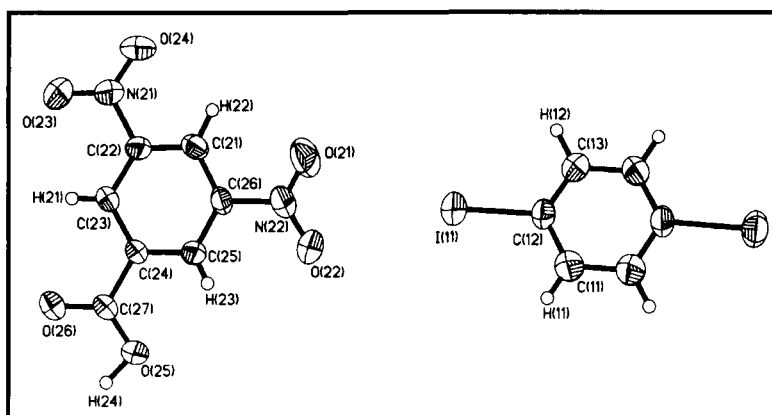
Figure 4.10: *ORTEP plot of the 3,5-dinitrobenzoic acid - 1,4-diiodobenzene complex.*

Table 4.13 Crystal structure data for 3,5-dinitrobenzoic acid - 1,4-diiodobenzene complex.

Chemical formula	$(C_7H_4N_2O_6){:}(C_6H_4I_2)$
Formula weight	754.14
Cell setting	Monoclinic
Space group	I2/a
a (Å)	9.647(1)
b (Å)	8.978(1)
c (Å)	28.263(2)
α (°)	90
β (°)	93.36(1)
γ (°)	90
Cell volume (Å^3)	2443.7(3)

Table 4.13 (*continued*)

Z	4
F(000)	1448
ρ (Mg/m^3)	2.05
μ, mm^{-1}	2.646
λ (Å)	0.7107
Crystal size (mm)	0.35 × 0.25 × 0.30
Diffractometer	Smart, CCD area detector
Radiation type	MoKα
Crystal-detector distance(cm)	5.0
Temperature (K)	293(2)
No. of measured reflections	4613
No. of independent reflections	1748
θ_{max} (°)	2 - 24
Range of *h, k, l*	-9 to 10
	-9 to 9
	-31 to 28
R$_1$	0.0424
wR$_2$	0.1141
S	1.093
No. of parameters refined	196
Max. eÅ^{-3}	1.203

The carboxylic group of the acid joins the adjacent supramolecular assemblages through the formation of a centrosymmetric dimeric unit of O-H$\cdots$O hydrogen bonds (H$\cdots$O, 1.79 Å, Figure 4.11). This arrangement ultimately leads to a helical type structure in the three-dimensional network (not shown in the figure).

Table 4.14 Bond lengths and angles of 3,5-dinitrobenzoic acid-1,4-diiodobenzene complex

Moiety	Distance (Å)	Moiety	Angle (°)
I(11)-C(12)	2.108(6)	C(12)-C(11)-C(11)#1	119.1(3)
C(11)-C(12)	1.377(8)	C(12)-C(11)-H(11)	121(4)
C(11)-C(11)#1	1.399(12)	C(11)#1-C(11)-H(11)	119(4)
C(11)-H(11)	0.94(8)	C(13)-C(12)-C(11)	121.5(6)
C(12)-C(13)	1.370(8)	C(13)-C(12)-I(11)	120.0(4)
C(13)-C(13)#1	1.397(11)	C(11)-C(12)-I(11)	118.4(4)
C(13)-H(12)	1.02(8)	C(12)-C(13)-C(13)#1	119.3(3)
N(21)-O(24)	1.212(6)	C(12)-C(13)-H(12)	122(4)
N(21)-O(23)	1.216(5)	C(13)#1-C(13)-H(12)	119(4)
N(21)-C(22)	1.468(6)	O(24)-N(21)-O(23)	124.4(5)

Table 4.14 (*continued*)

Moiety		Moiety	Angle (°)
N(22)-O(22)	1.219(6)	O(24)-N(21)-C(22)	117.1(4)
N(22)-O(21)	1.219(6)	O(23)-N(21)-C(22)	118.5(4)
N(22)-C(26)	1.462(6)	O(22)-N(22)-O(21)	123.4(5)
O(25)-C(27)	1.265(6)	O(22)-N(22)-C(26)	117.8(4)
O(25)-H(24)	0.96(10)	O(21)-N(22)-C(26)	118.8(5)
O(26)-C(27)	1.255(6)	C(27)-O(25)-H(24)	103(6)
C(21)-C(22)	1.374(7)	C(22)-C(21)-C(26)	116.6(5)
C(21)-C(26)	1.387(8)	C(22)-C(21)-H(22)	118(3)
C(21)-H(22)	0.93(5)	C(26)-C(21)-H(22)	125(3)
C(22)-C(23)	1.387(8)	C(21)-C(22)-C(23)	123.3(5)
C(23)-C(24)	1.389(7)	C(21)-C(22)-N(21)	118.4(4)
C(23)-H(21)	0.90(5)	C(23)-C(22)-N(21)	118.3(5)
C(24)-C(25)	1.382(6)	C(22)-C(23)-C(24)	117.7(5)
C(24)-C(27)	1.498(6)	C(22)-C(23)-H(21)	121(3)
C(25)-C(26)	1.368(7)	C(24)-C(23)-H(21)	121(3)
C(25)-H(23)	0.77(5)	C(25)-C(24)-C(23)	120.6(4)
Moiety	**Angle (°)**	C(25)-C(24)-C(27)	119.6(4)
C(25)-C(26)-C(21)	122.5(5)	C(23)-C(24)-C(27)	119.8(4)
C(25)-C(26)-N(22)	119.1(5)	C(26)-C(25)-C(24)	119.3(5)
C(21)-C(26)-N(22)	118.4(5)	C(26)-C(25)-H(23)	125(4)
O(26)-C(27)-O(25)	124.4(4)	C(24)-C(25)-H(23)	116(4)
O(25)-C(27)-C(24)	116.7(4)	O(26)-C(27)-C(24)	118.9(4)

Symmetry transformations used to generate equivalent atoms:
#1 -x-1/2,y,-z+1

In accordance with the previous reports of designing supramolecular assemblies using iodo-nitro interactions,[163] formation of a molecular complex between **2** and 1,4-diiodobenzene is expected to be in the ratio of 1:1 as the acid **2** possesses two nitro groups. Such a 1:1 complex is described by Scheme 4.1. However, a 2:1 complex is only obtained exclusively even when we start with a 1:1 mixture of the acid and diiodobenzene. The hydrogen bond geometries are indicated in Table 4.15.
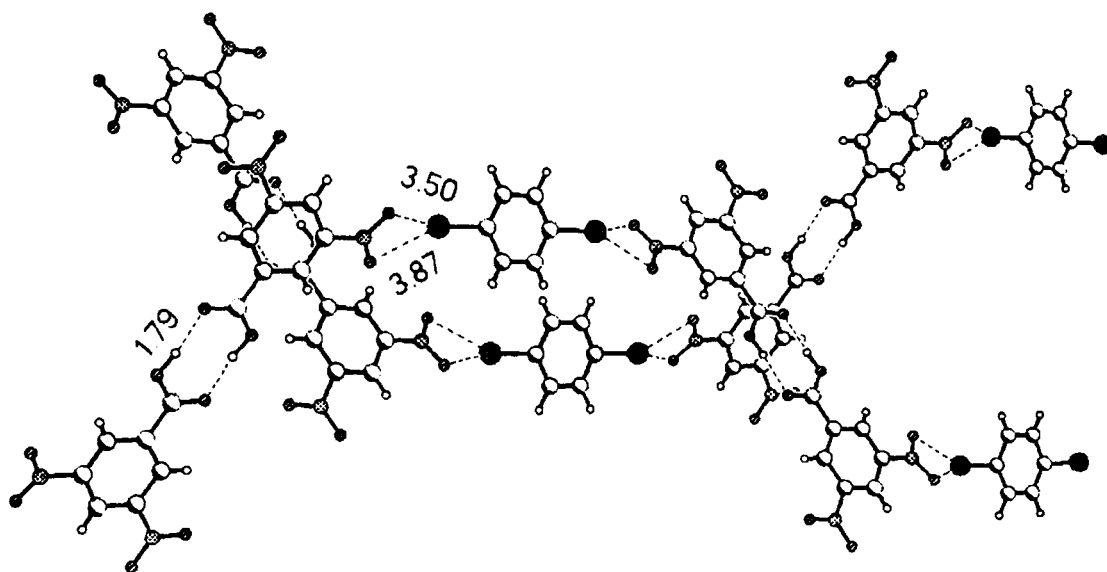
Figure 4.11: *Packing arrangement of 3,5-dinitrobenzoic acid and 1,4-diiodobenzene, in the complex.*
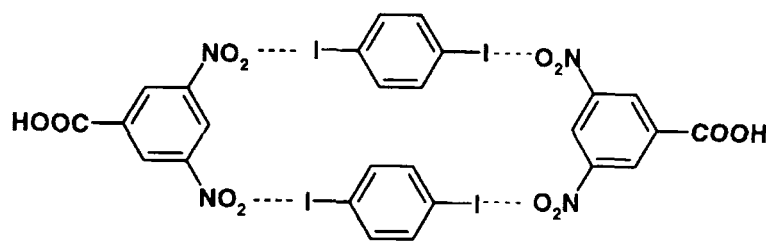
Scheme 4.1

Table 4.15 Unique hydrogen bond parameters of the complex of 3,5-dinitrobenzoic acid and 1,4-diiodobenzene

H-bond	D-H (Å)	H···A (Å)	D···A (Å)	D-H···A (°)
O(25)-H(24)···O(26)	0.96(10)	1.78(9)	2.693(6)	157(10)
C(13)-H(12)···O(21)	1.02(8)	2.54(7)	3.530(8)	162(5)
C(21)-H(22)···O(24)	0.93(5)	2.35(5)	2.678(7)	101(4)
C(25)-H(23)···O(25)	0.77(5)	2.42(5)	2.752(7)	107(4)

In addition, we have found that 3,5-dinitro-4-methylbenzoic acid, **3**, which is analogous to **2** does not form any complex with 1,4-diiodobenzene. Formation of a 2:1

complex (Figure 4.11) between **2** and 1,4-diiodobenzene could be rationalized on the basis of the following considerations. In the crystal structure of the acid **2**,[164] one of the nitro groups is involved in the formation of a centrosymmetric dimer through C-H···O hydrogen bonds as shown in Scheme 4.2a while the other nitro group is essentially free. It would therefore, be natural for **2** to form only a 2:1 complex with diiodobenzene through the free nitro group. This effect is seen more vividly in the structure of the acid[165] **3** where both the nitro groups are involved in the formation of centrosymmetric couplings with the adjacent molecules through C-H···O hydrogen bonds (Scheme 4.2b), thereby preventing **3** from forming a complex with 1,4-diiodobenzene. Thus, the interactions present in the parent molecules can be used as a basis to rationalize the nature of the intermolecular interactions present in the target structure.

(a)   (b)
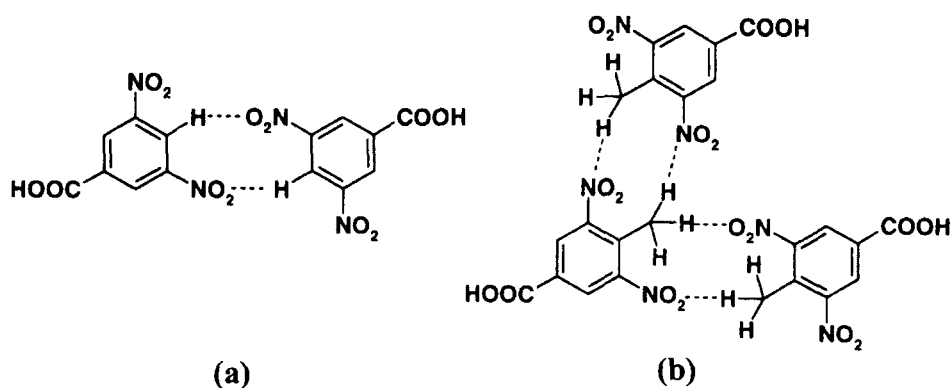
Scheme 4.2

4.4 Layered hydrogen-bonded structures formed by aliphatic dicarboxylic acids with azaaromatics

Co-crystallization of 2,4,6-triaminopyrimidine with malonic (4), glutaric (5), and adipic (6) acids resulted in the formation of molecular complexes, which are designated as 4a, 5a and 6a respectively. The asymmetric units for 4a and 5a are shown in Figure 4.12. The crystal structure data for the three co-crystals are given in Table 4.16. The atomic coordinates and isotropic displacement parameters for the three complexes 4a, 5a and 6a are given in Tables A1.7, A1.8 and A1.9, respectively.
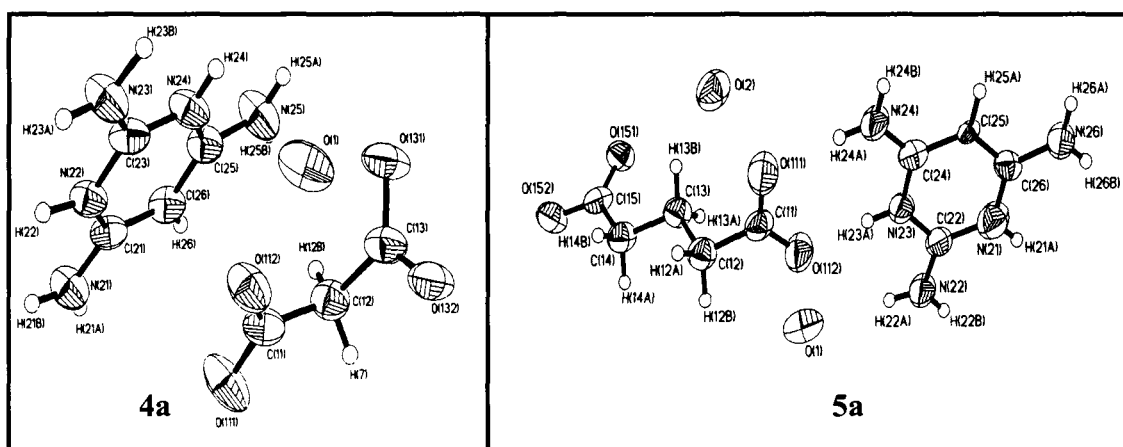
Figure 4.12: ORTEP plots of the complexes of 2,4,6-triaminopyrimidine with malonic acid, 4a and glutaric acid, 5a.

Table 4.16 Crystal structure data of molecular complexes of 2,4,6-triaminopyrimidine with malonic (4a), glutaric (5a) and adipic acids (6a)

	4a	5a	6a
Chemical formula	$C_4H_7N_5:C_3H_4O_4$:0.5(H_2O)	$C_4H_7N_5:C_5H_8O_4$:1.5(H_2O)	2($C_4H_7N_5$):3($C_6H_{10}O_4$)
Formula weight	237.21	281.26	688.71
Cell setting	Monoclinic	monoclinic	Monoclinic
Space group	C2/c	C2/c	P2$_1$/c
a (Å)	12.060(2)	11.929(3)	9.808(1)
b (Å)	10.748(2)	10.883(3)	16.104(1)
c (Å)	16.501(2)	20.559(5)	10.182(1)
α (°)	90	90	90
β (°)	107.22(9)	98.77(3)	93.07(2)

Table 4.16 (*continued*)

γ (°)	90	90	90
Cell volume (Å^3)	2043.0(6)	2638.1(2)	1605.9(1)
Z	8	8	2
F(000)	992	1184	732
ρ (Mg/m^3)	1.542	1.416	1.424
μ, mm^{-1}	0.130	0.118	0.114
λ (Å)	0.7107	0.7107	0.7107
Crystal size (mm)	0.30 × 0.25 × 0.25	0.20 × 0.25 × 0.15	0.40 × 0.35 × 0.25
Diffractometer	Smart, CCD area detector	Smart, CCD area detector	Smart, CCD area detector
Radiation type	MoKα	MoKα	MoKα
Crystal-detector distance (cm)	5.0	5.0	5.0
Temperature (K)	298	298	298
No. of measured reflections	3788	2359	2246
No. of independent reflections	1477	1609	2323
θ_{max} (°)	2 - 24	2 - 24	2 - 24
Range of *h, k, l*	-13 to 13	-13 to 9	-7 to 10
	-11 to 7	-6 to 12	-16 to 17
	-14 to 18	-20 to 21	-8 to 11
R_1	0.074	0.056	0.044
wR_2	0.120	0.105	0.083
S	1.097	1.02	1.377
No. of parameters refined	175	178	230
Max. eÅ^{-3}	0.572	0.422	0.373

The crystal structures of these complexes reveal a new structural feature related to the hydrogen bonds involving the carboxylic group and the heterocyclic nitrogen. The basic recognition between the pyrimidine and the acids occurs between the carboxylic group and the pyridyl nitrogen. Figure 4.13 depicts the molecular tapes formed by the adducts of 2,4,6-triaminopyrimidine with malonic (**4a**) and glutaric (**5a**) acids. Note that there are water molecules in both the crystal structures, forming N-H$\cdots$O

hydrogen bonds with the pyrimidines and O-H⋯O hydrogen bonds with the carboxylic acid molecules.

4a   **5a**
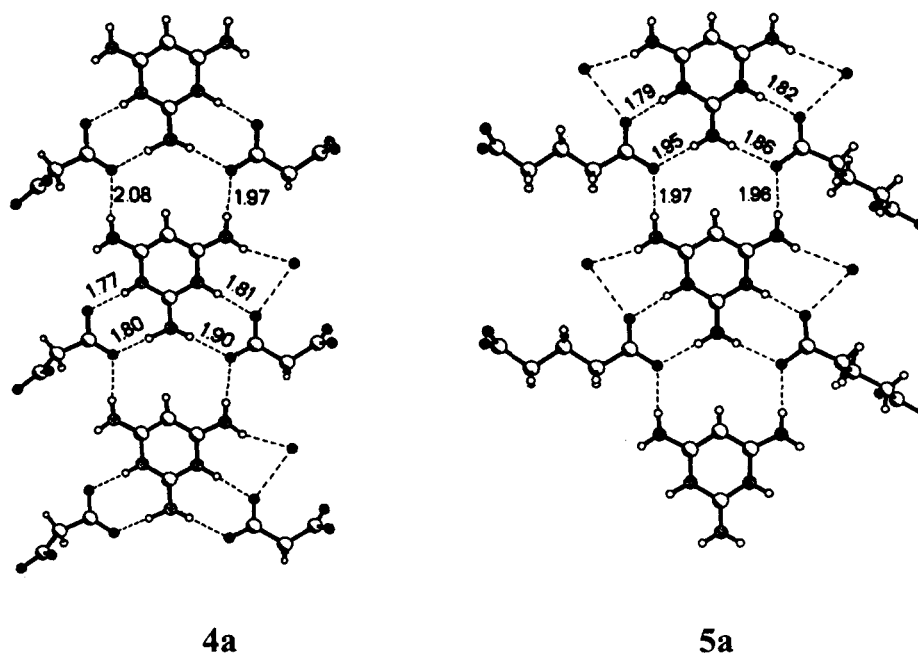
Figure 4.13: *Molecular tapes formed by 2,4,6-triaminopyrimidine in the adducts* **4a** *(left) and* **5a** *(right).*

The asymmetric unit of the triaminopyrimidine-adipic acid complex, **6a**, is depicted in Figure 4.14. The complex **6a** crystallizes in a P2₁/c space group. The interatomic bond distances and angles for the three complexes, **4a**, **5a** and **6a** are listed in Tables 4.17, 4.18 and 4.19, respectively. The bond lengths of the C-C and C-N bonds in the pyrimidine ring ~ 1.40 and 1.33 Å, respectively. The C-C bonds in the aliphatic acids have bond lengths in the range of ~ 1.50 to 1.54 Å. The C-C-C angles in the acids is 109.5°. The hydrogen bond pattern in **6a** is depicted in Figure 4.15.
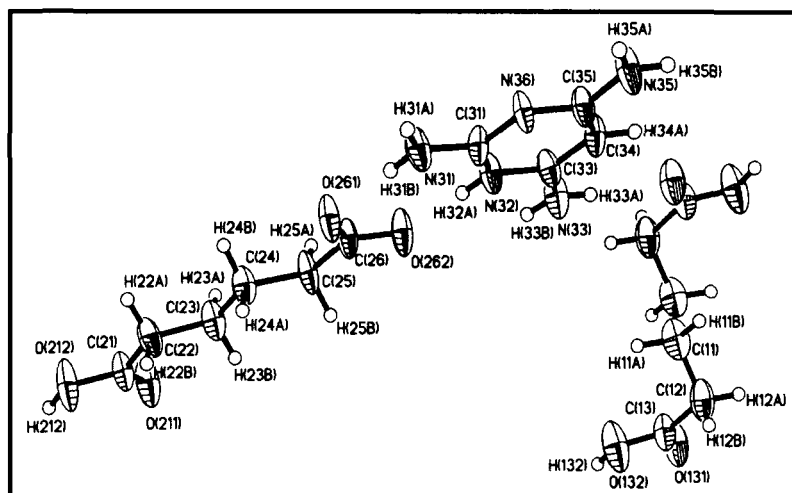
Figure 4.14: *ORTEP plot of the triaminopyrimidine-adipic acid crystal,* **6a**. *Thermal ellipsoids are given at 50% probability.*
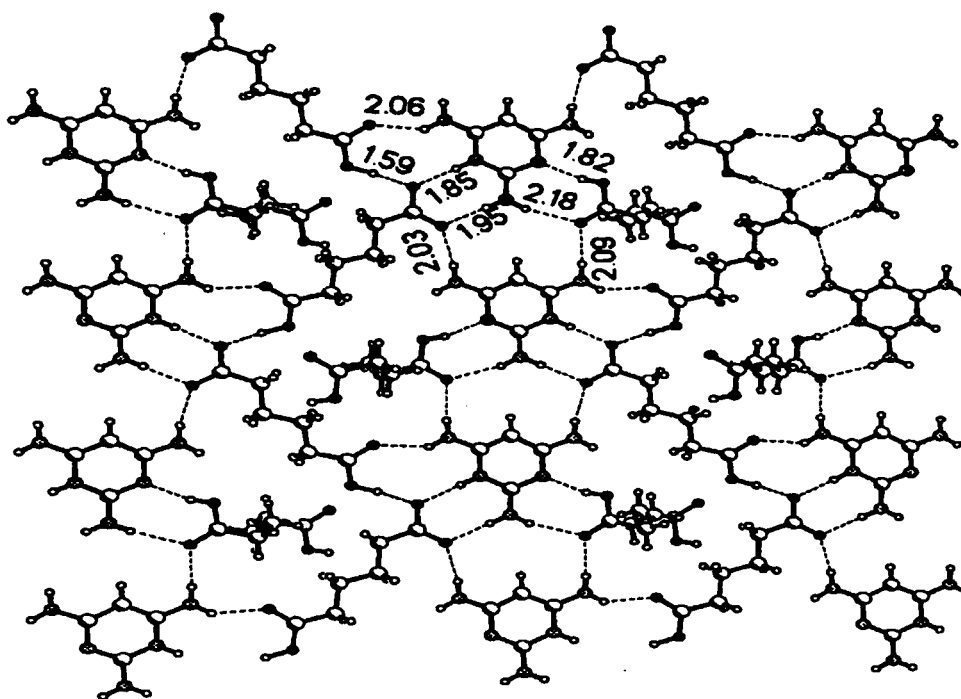
Figure 4.15: *Arrangement of molecules of adipic acid and 2,4,6-triaminopyrimidine in a two-dimensional planar sheet of the complex,* **6a**

Table 4.17 Bond lengths and angles **4a**

Moiety	Distance (Å)	Moiety	Angle (°)
N(22)-C(23)	1.353(6)	C(23)-N(22)-C(21)	120.5(4)
N(22)-C(21)	1.378(5)	C(21)-C(26)-C(25)	119.4(4)
N(23)-C(23)	1.328(5)	C(23)-N(24)-C(25)	118.9(4)
N(25)-C(25)	1.330(6)	N(25)-C(25)-N(24)	116.0(4)
C(26)-C(21)	1.374(7)	N(25)-C(25)-C(26)	122.9(4)
C(26)-C(25)	1.375(6)	N(24)-C(25)-C(26)	121.1(4)
N(24)-C(23)	1.323(6)	N(24)-C(23)-N(23)	120.1(4)
N(24)-C(25)	1.363(5)	N(21)-C(21)-C(26)	125.2(3)
N(21)-C(21)	1.319(6)	N(21)-C(21)-N(22)	116.6(4)
O(112)-C(11)	1.254(4)	C(26)-C(21)-N(22)	118.1(4)
O(132)-C(13)	1.218(6)	C(13)-C(12)-C(11)	114.3(3)
O(111)-C(11)	1.233(5)	O(132)-C(13)-O(131)	123.4(4)
C(12)-C(13)	1.500(7)	O(132)-C(13)-C(12)	120.6(4)
C(12)-C(11)	1.515(7)	O(131)-C(13)-C(12)	116.0(5)
O(131)-C(13)	1.294(5)	O(112)-C(11)-C(12)	119.1(4)

Table 4.18 Bond lengths and angles **5a**

Moiety	Distance (Å)	Moiety	Angle (°)
C(11)-O(112)	1.243(7)	O(112)-C(11)-O(111)	123.6(5)
C(11)-O(111)	1.248(6)	O(112)-C(11)-C(12)	118.6(5)
C(11)-C(12)	1.527(8)	O(111)-C(11)-C(12)	117.9(5)
C(12)-C(13)	1.526(7)	C(11)-C(12)-C(13)	109.8(5)
C(12)-H(12A)	0.97	C(11)-C(12)-H(12A)	109.7(3)
C(12)-H(12B)	0.97	C(13)-C(12)-H(12A)	109.7(3)
C(13)-C(14)	1.538(8)	C(11)-C(12)-H(12B)	109.7(3)
C(13)-H(13A)	0.97	C(13)-C(12)-H(12B)	109.7(3)
C(13)-H(13B)	0.97	H(12A)-C(12)-H(12B)	108.2
C(14)-C(15)	1.512(7)	C(12)-C(13)-C(14)	110.6(5)
C(14)-H(14A)	0.97	C(12)-C(13)-H(13A)	109.5(3)
C(14)-H(14B)	0.97	C(14)-C(13)-H(13A)	109.5(4)
C(15)-O(151)	1.243(7)	C(12)-C(13)-H(13B)	109.5(3)
C(15)-O(152)	1.289(7)	C(14)-C(13)-H(13B)	109.5(3)
C(21)-C(26)	1.388(7)	H(13A)-C(13)-H(13B)	108.1
C(21)-C(22)	1.399(8)	C(15)-C(14)-C(13)	114.0(5)
C(21)-H(21A)	0.93	C(15)-C(14)-H(14A)	108.8(3)
N(22)-C(22)	1.329(6)	C(13)-C(14)-H(14A)	108.8(3)
N(22)-H(22A)	0.86	C(15)-C(14)-H(14B)	108.8(3)
N(22)-H(22B)	0.86	C(13)-C(14)-H(14B)	108.8(4)
C(22)-N(23)	1.360(7)	H(14A)-C(14)-H(14B)	107.6
N(23)-C(24)	1.343(6)	O(151)-C(15)-O(152)	122.9(5)
N(23)-H(23A)	0.86	O(151)-C(15)-C(14)	121.4(5)
N(24)-H(24B)	0.86	O(152)-C(15)-C(14)	115.7(5)
C(24)-N(25)	1.379(7)	C(26)-C(21)-C(22)	117.5(5)
N(25)-C(26)	1.353(7)	C(26)-C(21)-H(21A)	121.3(3)
N(25)-H(25A)	0.86	C(22)-C(21)-H(21A)	121.3(3)
N(26)-C(26)	1.339(7)	C(22)-N(22)-H(22A)	120.0(3)

Table 4.18 (*continued*)

Moiety	Distance (Å)	Moiety	Angle (°)
N(26)-H(26A)	0.86	C(22)-N(22)-H(22B)	120.0(3)
N(26)-H(26B)	0.86	H(22A)-N(22)-H(22B)	120
Moiety	**Angle (°)**	N(22)-C(22)-N(23)	117.6(5)
N(24)-C(24)-N(25)	120.6(4)	N(22)-C(22)-C(21)	123.2(5)
N(23)-C(24)-N(25)	117.3(5)	N(23)-C(22)-C(21)	119.1(4)
C(26)-N(25)-C(24)	121.4(4)	C(24)-N(23)-C(22)	123.6(5)
C(26)-N(25)-H(25A)	119.3(3)	C(24)-N(23)-H(23A)	118.2(3)
C(24)-N(25)-H(25A)	119.3(3)	C(22)-N(23)-H(23A)	118.2(3)
C(26)-N(26)-H(26A)	120.0(3)	C(24)-N(24)-H(24A)	120.0(3)
C(26)-N(26)-H(26B)	120.0(3)	C(24)-N(24)-H(24B)	120.0(3)
H(26A)-N(26)-H(26B)	120	H(24A)-N(24)-H(24B)	120
N(25)-C(26)-N(26)	117.6(4)	N(24)-C(24)-N(23)	122.1(5)
N(26)-C(26)-C(21)	121.4(5)	N(25)-C(26)-C(21)	121.0(5)

Table 4.19 Bond lengths and angles **6a**

Moiety	Distance (Å)	Moiety	Angle (°)
C(11)-C(11)#1	1.508(12)	C(11)#1-C(11)-C(12)	113.5(6)
C(11)-C(12)	1.526(10)	C(13)-C(12)-C(11)	111.1(5)
C(12)-C(13)	1.469(8)	O(131)-C(13)-O(132)	121.0(5)
C(13)-O(131)	1.218(6)	O(131)-C(13)-C(12)	125.2(6)
C(13)-O(132)	1.312(7)	O(132)-C(13)-C(12)	113.8(5)
C(21)-O(211)	1.194(6)	O(211)-C(21)-O(212)	122.1(5)
C(21)-O(212)	1.307(6)	O(211)-C(21)-C(22)	124.7(5)
C(21)-C(22)	1.496(7)	O(212)-C(21)-C(22)	113.2(4)
C(22)-C(23)	1.506(8)	C(23)-C(22)-C(21)	113.6(5)
C(23)-C(24)	1.511(8)	C(22)-C(23)-C(24)	114.2(5)
C(24)-C(25)	1.527(7)	C(23)-C(24)-C(25)	110.5(4)
C(25)-C(26)	1.509(7)	C(26)-C(25)-C(24)	116.7(4)
C(26)-O(261)	1.227(6)	O(261)-C(26)-O(262)	123.0(5)
C(26)-O(262)	1.282(6)	O(261)-C(26)-C(25)	122.3(4)
C(31)-N(31)	1.327(7)	O(262)-C(26)-C(25)	114.6(5)
C(31)-N(36)	1.325(6)	N(31)-C(31)-N(36)	118.6(5)
C(31)-N(32)	1.339(6)	N(31)-C(31)-N(32)	118.0(5)
N(32)-C(33)	1.370(7)	N(36)-C(31)-N(32)	123.4(4)
C(33)-N(33)	1.328(7)	C(31)-N(32)-C(33)	119.4(4)
C(33)-C(34)	1.359(7)	N(33)-C(33)-C(34)	123.8(5)
C(34)-C(35)	1.372(7)	N(33)-C(33)-N(32)	116.8(5)
C(35)-N(35)	1.330(6)	C(34)-C(33)-N(32)	119.4(5)
C(35)-N(36)	1.357(6)	C(33)-C(34)-C(35)	118.4(5)
		N(35)-C(35)-N(36)	115.5(5)
		N(35)-C(35)-C(34)	122.4(5)
		N(36)-C(35)-C(34)	122.2(5)
		C(31)-N(36)-C(35)	117.2(4)

The complexes **4a-6a** differ from one another in some aspects, the common feature being that the pyrimidine and the acid molecules are held together by the couplings consisting of $O^-\cdots H^+$-N / N-H$\cdots$O bonds as shown in Figures 4.13 and 4.15. While **4a** and **5a** are formed in a 1:1 ratio, with each pyrimidine attached to an acid molecule through $O^-\cdots H^+$-N / N-H$\cdots$O hydrogen bonds (Figure 4.13), the complex **6a** between adipic acid and the pyrimidine is formed in the 3:2 ratio (Figure 4.15). On comparison with the literature data on aminopyrimidines,[166] we would expect the hydrogen-bond coupling in **4a-6a** to be O-H$\cdots$N and N-H$\cdots$O. However the couplings actually observed by us in **4a-6a** involve proton transfer from the carboxylic group to the heterocyclic nitrogen as shown below in Scheme 4.3.
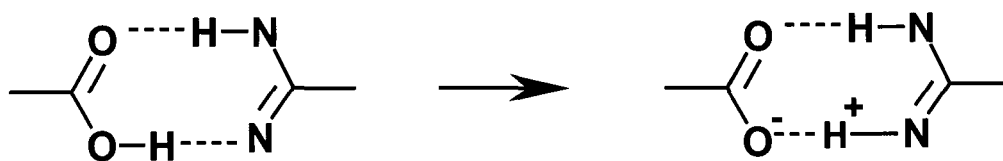
Scheme 4.3

Such proton transfer occurs because of strong hydrogen bonds initially formed between the carboxyl and the pyridyl nitrogen atoms. The H$\cdots$O distances in the cyclic hydrogen bond structures also supports the occurrence of proton transfer as the $H^+\cdots O^-$ and H$\cdots$O distances in the $O\cdots H^+$-N and O$\cdots$H-N bonds are comparable (~1.80Å). The complexes **4a-5a** are stabilized by the incorporation of guest molecules. In the case of **4a** and **5a**, water molecules are the guest molecules. The interaction of the water molecules with the acids and the pyrimidine is shown in Figure 4.13. However in **6a**, additional acid molecule has been incorporated as the guest molecule.

It appears that the large chain length of adipic acid, **6** facilitates the formation of larger voids as shown in Figure 4.16 (right) which are filled by the additional acid molecules. Furthermore, the three-dimensional arrangement resembles a typical inorganic pillared type structure as depicted in Figure 4.16 (left).

6a
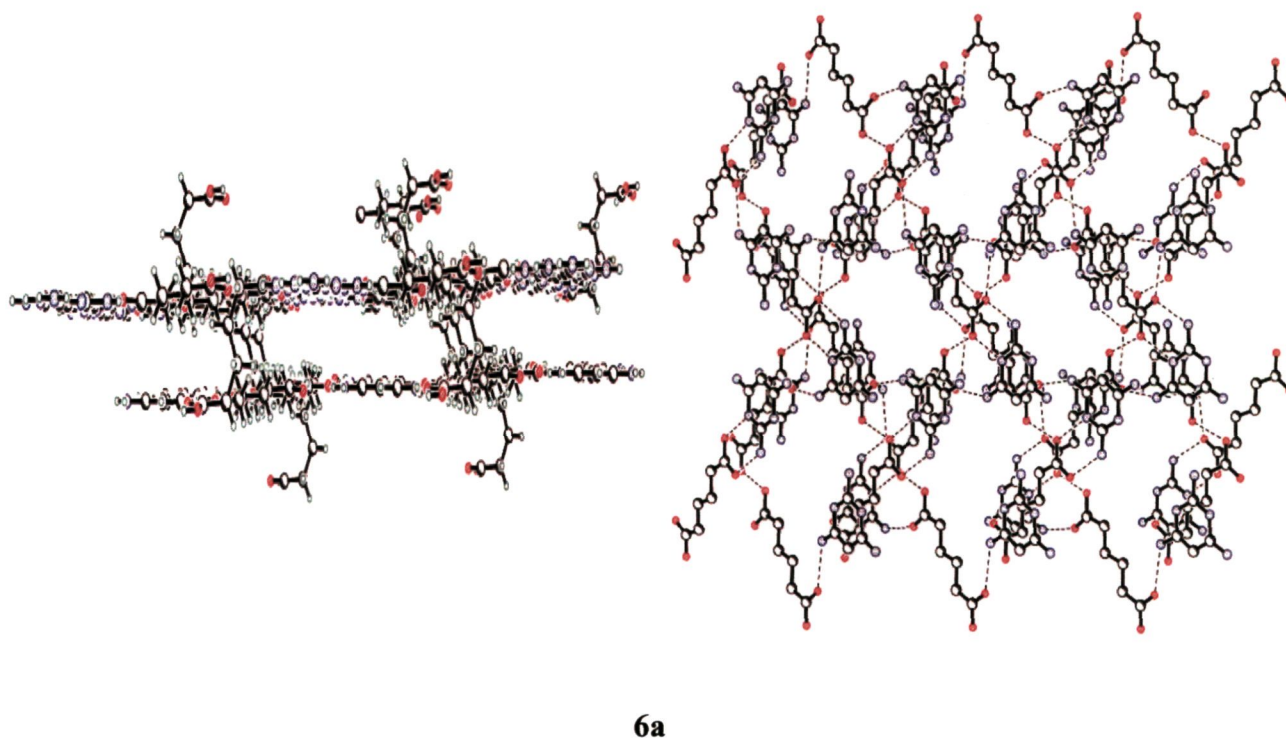
Figure 4.16: *Three-dimensional arrangement of the planar sheets formed in the co-crystals, **6a** formed by 2,4,6-triaminopyrimidine and adipic acid. Left: the additional adipic acid molecules are shown as pillaring the sheets. Right: Another orientation of the planar sheets, after removal of the guest adipic acid molecules, to depict the porosity in the structure.*

In addition, a comparison of the crystal packing of the complexes **4a-6a** reveals another noteworthy feature that the number of -CH$_2$ groups in the constituent acid plays an important role in the pattern of crystallization. This becomes evident as **6a**

consisting of an acid with even number -CH$_2$ groups yields two-dimensional network (Figure 4.15) whereas complexes **4a** and **5a** with acids possessing an odd number of CH$_2$ groups constitute three-dimensional crossed networks. Such a network corresponding to **4a** is shown in Figure 4.17. The hydrogen bond geometries in **4a- 6a** are given in Tables 4.20 to 4.22.
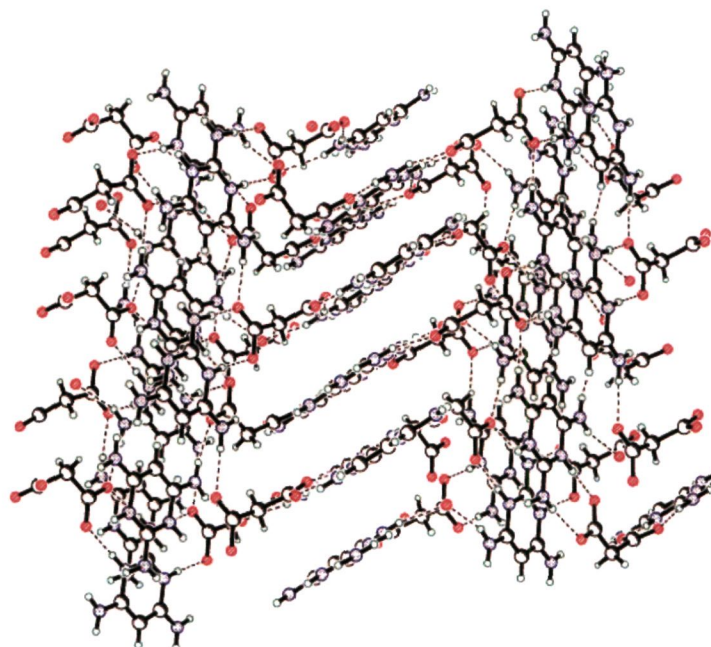
4a

Figure 4.17: *Three-dimensional arrangement of molecular tapes observed in the crystal structure of the complex between 2,4,6-triaminopyrimidine and malonic acid, 4a. A crossed ribbon network is shown.*

Table 4.20 Unique hydrogen bond parameters **4a**

H-bond	D-H (Å)	H···A (Å)	D···A (Å)	D-H···A (°)
N(21)-H(21A)···O(111)	0.859(5)	1.968(5)	2.818(5)	169.7(5)
N(21)-H(21B)··· O(1)	0.861(6)	2.124(5)	2.950(5)	160.9(5)
N(22)-H(22)···O(112)	0.95(6)	1.81(6)	2.754(5)	179(5)
N(23)-H(23A)···O(111)	0.86(5)	1.91(5)	2.741(6)	164(4)
N(23)-H(23B)···O(132)	1.03(6)	1.81(6)	2.840(5)	174(5)
N(24)-H(24)···O(131)	0.860(5)	1.767(6)	2.624(6)	173.5(5)
N(25)-H(25B)···O(132)	0.860(6)	2.083(5)	2.934(5)	170.3(5)

Table 4.21 Unique hydrogen bond parameters **5a**

H-bond	D-H (Å)	H···A (Å)	D···A (Å)	D-H···A (°)
N(22)-H(22A)···O(1)	0.860(6)	2.475(4)	3.305(5)	162.6(5)
N(22)-H(22B)···O(111)	0.860(6)	1.977(7)	2.834(7)	174.8(5)
N(23)-H(23A)···O(112)	0.860(6)	1.791(6)	2.649(7)	174.5(5)
N(24)-H(24A)···O(111)	0.860(6)	1.950(6)	2.808(6)	176.8(5)
N(24)-H(24B)···O(152)	0.860(6)	1.864(6)	2.722(6)	175.3(5)
N(25)-H(25A)···O(151)	0.860(5)	1.816(5)	2.671(5)	172.5(5)
N(26)-H(26A)···O(2)	0.859(6)	2.126(6)	2.958(6)	162.8(6)
N(26)-H(26B)···O(152)	0.860(7)	1.956(6)	2.812(6)	173.1(5)

Table 4.22 Unique hydrogen bond parameters **6a**

H-bond	D-H (Å)	H···A (Å)	D···A (Å)	D-H···A (°)
N(31)-H(31A)···O(131)	0.860(6)	2.178(6)	3.023(6)	167.0(5)
N(31)-H(31B)···O(261)	0.860(6)	1.952(6)	2.811(6)	178.0(5)
N(32)-H(32A)···O(262)	0.860(6)	1.849(6)	2.709(6)	178.8(5)
N(33)-H(33A)···O(131)	0.860(7)	2.093(6)	2.949(6)	174.1(7)
N(33)-H(33B)···O(211)	0.860(7)	2.061(7)	2.797(7)	143.2(6)
N(35)-H(35A)···O(132)	0.860(7)	2.518(7)	3.191(7)	135.8(5)
N(35)-H(35B)···O(261)	0.860(7)	2.038(6)	2.891(6)	171.5(6)
O(132)-H(132)···N(36)	0.820(6)	1.820(6)	2.613(6)	162.1(6)
O(212)-H(212)···O(262)	1.03(8)	1.58(8)	2.607(6)	172(8)
C(11)-H(11A)···O(132)	0.971(9)	2.569(8)	2.900(8)	100.0(6)
C(25)-H(25B)···O(212)	1.12(7)	2.51(6)	3.048(6)	108(4)

4.5 Solvent-directed supramolecular assembly in the adducts formed by 4,4'-bipyridine with cyanuric acid and *N*-methylcyanuric acid

Cyanuric acid crystallized from methanol has a planar sheet structure wherein adjacent molecules are held together by symmetrical cyclic N-H···O hydrogen bonds (H···O, 1.90Å), as shown in Figure 4.18a.[143] This bonding gives rise to molecular tapes connected to each other by single N-H···O hydrogen bonds (H···O, 1.80 Å). Cyanuric acid crystallized from water, however, incorporates the solvent of crystallization into the structure giving the composition cyanuric acid.H_2O. This has a chain structure where adjacent molecules are connected together by single N-H···O

bonds (H⋯O, 2.01Å) rather than by the cyclic hydrogen-bonded dimers[167] (Figure 4.18b). The chains are held together by O-H⋯O and N-H⋯O hydrogen bonds with the water molecules (H⋯O, 2.00-2.15Å). The N-H⋯O bonds forming the chains in cyanuric acid.H_2O (Figure 4.18b) are considerably longer than those in cyanuric acid crystallized from methanol.
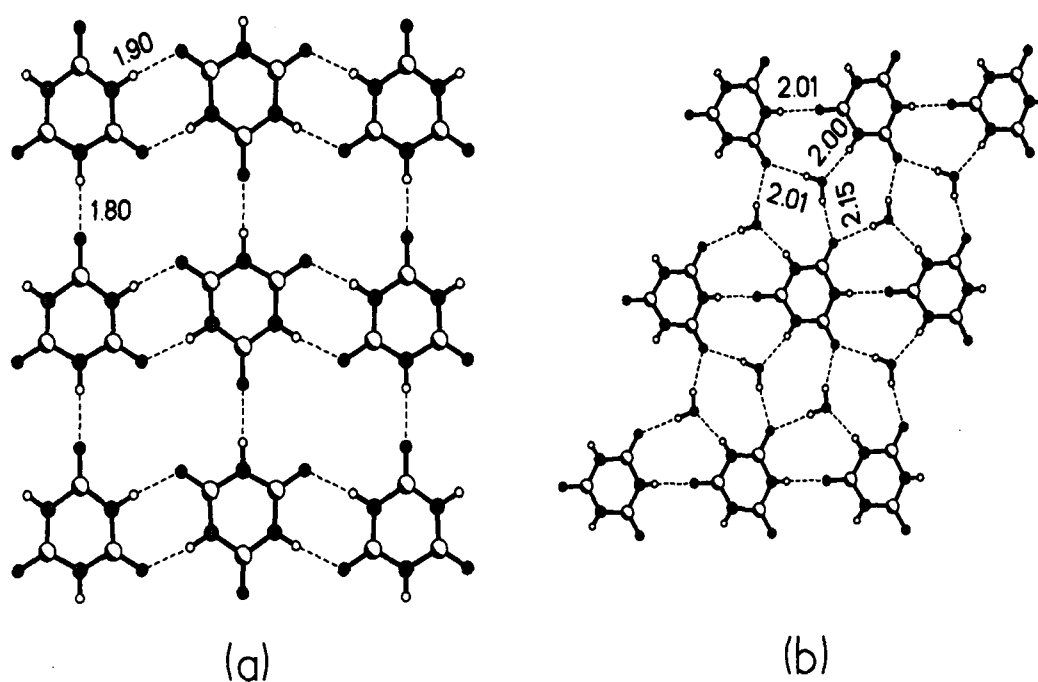
Figure 4.18: (a) *Arrangement of molecules forming tapes in cyanuric acid, crystallized from methanol in its crystal structure* (b) *Interaction of water molecules with cyanuric acid forming a planar sheet structure in a two-dimensional arrangement*

Co-crystallization of cyanuric acid, 7, with 4,4'-bipyridine results in two different types of molecular complexes depending upon the solvent of crystallization. From methanol, a complex, 7a, in a ratio of 2:1 results while co-crystallization from water gives a 1:1 adduct, 7b. The asymmetric units of 7a and 7b are shown in Figure

4.19. In both cases, the solvent molecule does not get incorporated into the crystal structure. For the adduct from methanol, **7a**, the asymmetric unit contains one cyanuric acid molecule and half a molecule of 4,4'-bipyridine. **7a** crystallizes in a triclinic, P-1 space group. **7b** crystallizes in a monoclinic $P2_1/n$ space group. The crystallographic data for the two complexes are given in Table 4.23. The atomic coordinates and isotropic displacement parameters for **7a** and **7b** are listed in Tables A1.10 and A1.11, respectively.
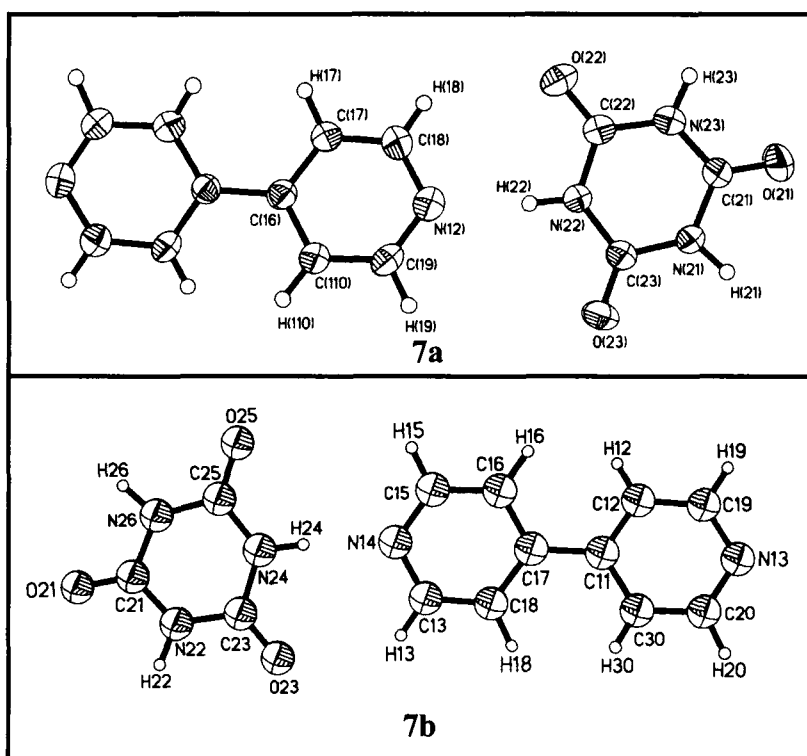
Figure 4.19: ORTEP plots of the cyanuric acid-4,4'-bipyridine complex crystallized from methanol, **7a** and water, **7b**.

Table 4.23 Crystal structure data of molecular complexes of cyanuric acid + 4,4'-bipyridyl + methanol (**7a**) and cyanuric acid + 4,4'-bipyridyl + water (**7b**)

	7a	7b
Chemical formula	$(C_{10}H_8N_2):2(C_3H_3N_3O_3)$	$C_{10}H_8N_2: C_3H_3N_3O_3$
Formula weight	414.35	285.27

Table 4.23 (*continued*)

	Triclinic	Monoclinic
Cell setting	Triclinic	Monoclinic
Space group	P-1	P2$_1$/n
a (Å)	4.320(1)	6.845(1)
b (Å)	9.202(1)	28.779(3)
c (Å)	11.70(2)	7.139(1)
α (°)	78.75(1)	90
β (°)	82.64(2)	115.47(1)
γ (°)	86.36(1)	90
Cell volume (Å^3)	452.1(1)	1269.6(3)
Z	1	4
F(000)	214	592
ρ (Mg/m^3)	1.522	1.492
μ, mm^{-1}	0.120	0.111
λ (Å)	0.7107	0.7107
Crystal size (mm)	0.25 × 0.15 × 0.30	0.25 × 0.35 × 0.20
Diffractometer	Smart, CCD area detector	Smart, CCD area detector
Radiation type	MoKα	MoKα
Crystal-detector distance (cm)	5.0	5.0
Temperature (K)	293(2)	293(2)
No. of measured reflections	1767	5266
No. of independent reflections	1259	1820
θ_{max} (°)	2 - 24	2 - 24
Range of h, k, l	-4 to 4	-7 to 7
	-9 to 10	-31 to 31
	-12 to 11	-7 to 7
R$_1$	0.0325	0.0577
wR$_2$	0.0869	0.1251
S	1.037	1.240
No. of parameters refined	165	235
Max. eÅ^{-3}	0.129	0.319

The interatomic bond distances and angles for the two complexes **7a** and **7b** are given in Tables 4.24 and 4.25, respectively. The distances of the C-N bonds in cyanuric acid in the two complexes are in the range of 1.36 - 1.37 Å.

Table 4.24 Bond lengths and angles **7a**

Moiety	Distance (Å)	Moiety	Angle (°)
N(23)-C(21)	1.364(4)	C(21)-N(23)-C(22)	124.9(3)
N(23)-C(22)	1.379(5)	C(21)-N(23)-H(23)	114(3)
N(23)-H(23)	0.91(5)	C(22)-N(23)-H(23)	120(3)
N(22)-C(22)	1.368(4)	C(22)-N(22)-C(23)	124.7(3)
N(22)-C(23)	1.376(4)	C(22)-N(22)-H(22)	113(3)
N(22)-H(22)	0.93(4)	C(23)-N(22)-H(22)	122(3)
N(21)-C(23)	1.360(4)	C(23)-N(21)-C(21)	125.5(3)
N(21)-C(21)	1.372(4)	C(23)-N(21)-H(21)	125(2)
N(21)-H(21)	0.94(4)	C(21)-N(21)-H(21)	110(2)
O(23)-C(23)	1.216(4)	C(19)-N(12)-C(18)	116.5(3)
N(12)-C(19)	1.329(5)	O(23)-C(23)-N(21)	122.5(3)
N(12)-C(18)	1.339(5)	O(23)-C(23)-N(22)	122.5(3)
O(22)-C(22)	1.211(4)	N(21)-C(23)-N(22)	115.0(3)
O(21)-C(21)	1.216(4)	C(110)-C(16)-C(17)	115.9(3)
C(16)-C(110)	1.392(5)	C(110)-C(16)-C(14)	122.4(3)
C(16)-C(17)	1.392(5)	C(17)-C(16)-C(14)	121.7(3)
C(110)-C(19)	1.382(5)	O(22)-C(22)-N(22)	122.6(3)
C(110)-H(110)	0.97(4)	O(22)-C(22)-N(23)	122.4(3)
C(19)-H(19)	0.94(3)	N(22)-C(22)-N(23)	115.0(3)
C(17)-C(18)	1.372(5)	C(15)-C(14)-C(16)	122.0(3)
C(17)-H(17)	1.00(3)	O(21)-C(21)-N(23)	123.1(3)
C(18)-H(18)	0.93(3)	O(21)-C(21)-N(21)	122.1(3)
		N(23)-C(21)-N(21)	114.8(3)
Moiety	**Angle (°)**	C(19)-C(110)-C(16)	119.9(4)
N(11)-C(12)-H(12)	123(2)	C(19)-C(110)-H(110)	124(2)
C(13)-C(12)-H(12)	114(2)	C(16)-C(110)-H(110)	116(2)
N(12)-C(18)-C(17)	123.4(4)	N(12)-C(19)-C(110)	123.8(4)
N(12)-C(18)-H(18)	118(2)	N(12)-C(19)-H(19)	118(2)
C(17)-C(18)-H(18)	118(2)	C(110)-C(19)-H(19)	118(2)
N(11)-C(11)-C(15)	123.3(4)	C(18)-C(17)-C(16)	120.5(4)
N(11)-C(11)-H(11)	116(2)	C(18)-C(17)-H(17)	121(2)
C(15)-C(11)-H(11)	120(2)	C(16)-C(17)-H(17)	119(2)

Table 4.25 Bond lengths and angles **7b**

Moiety	Distance (Å)	Moiety	Angle (°)
N(26)-C(21)	1.370(2)	C(21)-N(26)-C(25)	124.42(14)
N(26)-C(25)	1.370(2)	C(21)-N(22)-C(23)	124.07(14)
O(25)-C(25)	1.218(2)	C(16)-C(11)-C(11)#1	122.3(2)
O(23)-C(23)	1.213(2)	C(15)-N(14)-C(13)	116.3(2)
N(24)-C(25)	1.364(2)	O(25)-C(25)-N(26)	121.87(14)
N(24)-C(23)	1.375(2)	C(13)-C(12)-C(11)	119.9(2)

Table 4.25 (*continued*)

Moiety		Moiety	Angle (°)
O(21)-C(21)	1.227(2)	N(14)-C(15)-C(16)	123.9(2)
N(22)-C(21)	1.359(2)	O(23)-C(23)-N(24)	122.2(2)
N(22)-C(23)	1.373(2)	O(21)-C(21)-N(22)	122.29(14)
C(11)-C(16)	1.383(2)	N(22)-C(21)-N(26)	116.21(14)
C(11)-C(12)	1.384(2)	C(25)-N(24)-C(23)	125.23(14)
C(11)-C(11)#1	1.491(3)	C(16)-C(11)-C(12)	116.0(2)
N(14)-C(15)	1.325(2)	C(12)-C(11)-C(11)#1	121.7(2)
N(14)-C(13)	1.326(2)	O(25)-C(25)-N(24)	123.36(14)
C(12)-C(13)	1.376(3)	N(24)-C(25)-N(26)	114.77(14)
C(16)-C(15)	1.374(3)	C(15)-C(16)-C(11)	120.0(2)
Moiety	**Angle (°)**	O(23)-C(23)-N(22)	122.7(2)
O(21)-C(21)-N(26)	121.50(14)	N(22)-C(23)-N(24)	115.13(14)
N(14)-C(13)-C(12)	123.8(2)		

Symmetry transformations used to generate equivalent atoms:
#1 –x, -y+1, -z-1

In **7a**, adjacent molecules of **7** are held together by two different cyclic N-H···O hydrogen-bonded dimers (H···O, 1.94 and 1.96Å) as shown in Figure 4.20. The hydrogen bond geometries are listed in Tables 4.26 and 4.27. The bipyridyl molecules interact with **7** through a N-H···N hydrogen bond (H···N, 1.77Å). There is also a C-H···O interaction between bipyridyl and **7** (H···O, 2.40Å). The structure of the 1:1 hydrogen-bonded adduct, **7b**, crystallized from water is altogether different from that of the 2:1 hydrogen-bonded adduct **7a**, crystallized from methanol. We show the structure of **7b** in Figure 4.20. In this structure, molecules of **7** form a chain held together by single N-H···O hydrogen bonds (H···O, 2.02Å). The bipyridyl molecules hold the chains together through N-H...N bonds (H···N, 1.92, 1.94Å). The N-H···O bonds forming the chains in **7b** are very much longer than those in **7a**. The N-H···N hydrogen bond between bipyridyl and **7** is also considerably longer in **7b**.

Table 4.26 Unique hydrogen bond parameters **7a**

H-bond	D-H (Å)	H···A (Å)	D···A (Å)	D-H···A (°)
N(22)-H(22)···N(12)	0.93(4)	1.92(4)	2.843(4)	174(5)
N(23)-H(23)···O(23)	0.91(6)	2.02(6)	2.928(5)	173(4)
C(19)-H(19)···O(22)	0.94(4)	2.38(4)	3.221(5)	149(3)

Table4.27 Unique hydrogen bond parameters **7b**

H-bond	D-H (Å)	H···A (Å)	D···A (Å)	D-H···A (°)
N(22)-H(22)···N(14)	0.93(4)	1.92(3)	2.84(3)	174(1)
N(22)-H(22)···N(14)	0.91(5)	2.02(4)	2.93(4)	172(1)
C(12)-H(12)···O(23)	0.95(3)	2.37(4)	3.22(4)	149(3)
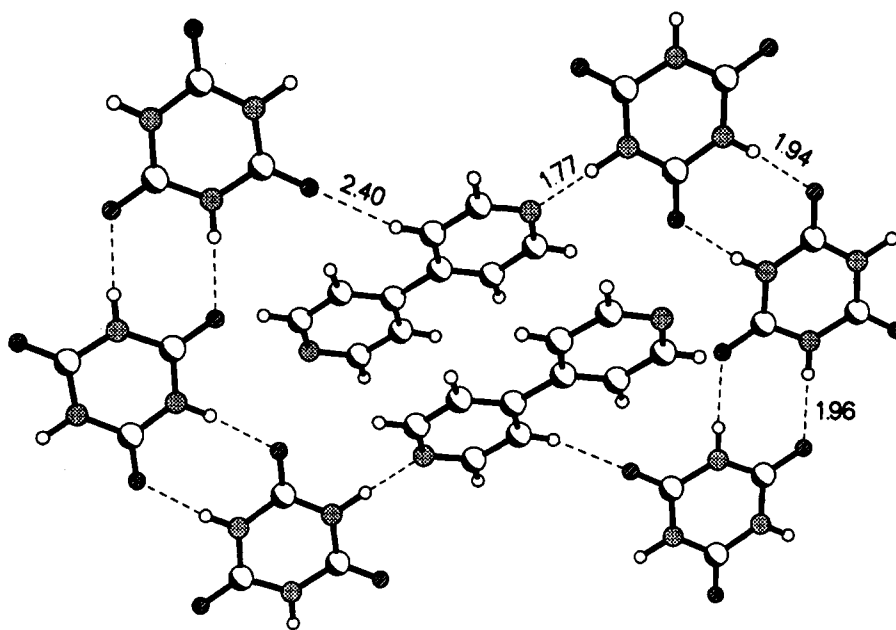
7a

Figure 4.20: Arrangement of molecules of cyanuric acid, and 4,4'-bipyridyl in the crystal structure of the complex, 7a. Dashed lines represent hydrogen bonds. Unique hydrogen bond distances are quoted.

The chain structure of the 1:1 adduct between bipyridyl and cyanuric acid, **7b**,

(Figure 4.21) is comparable to that of the crystal structure of **7** obtained from

crystallization from water (Figure 4.18b), the water being replaced by bipyridyl

forming N-H···N bonds (instead of the O-H···O or N-H···O bonds). Interestingly, the

N-H···O bonds forming the chains are of comparable length. Similarly, the structure

of the 2:1 adduct between cyanuric acid and bipyridyl (Figure 4.20) crystallized from

methanol (**7a**) bears resemblance to the structure of **7** crystallized from the same

solvent (Figure 4.18a) both having cyclic hydrogen bond couplings between adjacent

molecules of **7**. The N-H···O hydrogen bonds in the dimers have comparable

dimensions.
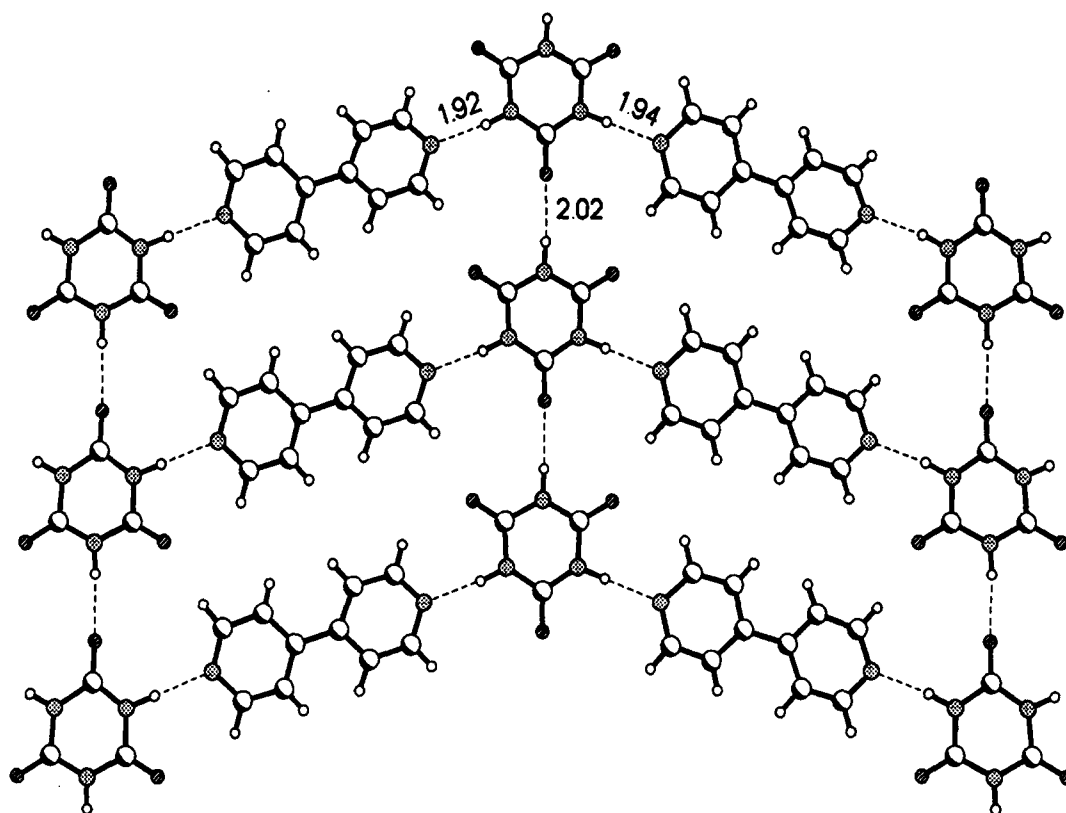
Figure 4.21: *Two-dimensional arrangement of molecules of cyanuric acid and 4,4'-bipyridyl in a planar sheet of complex,* **7b**.

Thus, the formation of two different hydrogen-bonded adducts between **7** and bipyridyl from methanol and water solvents can be attributed to the presence of different hydrogen bonding networks in the parent structures of **7** crystallized from these solvents.

When one of the N-H groups in **7** is methylated to form *N*-methylcyanuric acid, **8**, we would expect differences in the nature of the hydrogen-bonded structures formed by them. For example, the formation of the cyclic (dimeric) hydrogen bonds between the amide groups would not be as favoured in **8** compared to **7**. A search on the Cambridge Crystallographic Database (CSD) showed that there was no structural information on **8** in the literature. We have, therefore, carried out a structural study of **8** crystallized from methanol and water. The asymmetric unit of *N*-methylcyanuric acid is shown in Figure 4.22. The structural data of **8** crystallized from methanol and water are given in Table 4.28.
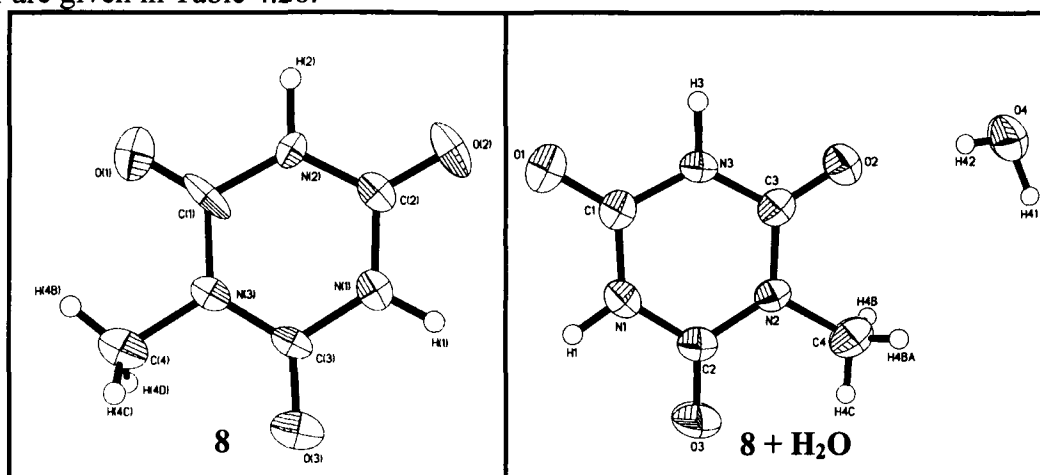
Figure 4.22: ORTEP plots of N-methylcyanuric acid, 8 and 8 + H₂O. Thermal ellipsoids are given at 50% probability.

Table 4.28 Crystal structure data of molecular complexes of *N*-methylcyanuric acid (**8**), its adduct with water (**8 + H₂O**) and *N*-methylcyanuric acid + 4,4'-bipyridyl (**8a**).

	8	**8 + H₂O**	**8a**
Chemical formula	$C_4H_5N_3O_3$	$C_4H_5N_3O_3 \colon H_2O$	$C_{14}H_{13}N_5O_3$
Formula weight	143.11	161.13	299.29
Cell setting	Orthorhombic	Monoclinic	Monoclinic
Space group	Pnma	P2₁/m	P2₁/n
a (Å)	6.743(2)	6.695(2)	3.878(1)
b (Å)	6.306(2)	6.275(2)	16.943(1)
c (Å)	13.612(4)	8.375(2)	20.830(2)
α (°)	90	90	90
β (°)	90	105.06(4)	90.75(1)
γ (°)	90	90	90
Cell volume (Å³)	578.8(3)	339.8(2)	1368.5(4)
Z	4	2	4
F(000)	296	168	624
ρ (Mg/m³)	1.642	1.575	1.453
μ, mm⁻¹	0.142	0.141	0.107
λ (Å)	0.7107	0.7107	0.7107
Crystal size (mm)	0.10 × 0.10 × 0.15	0.25 × 0.10 × 0.20	0.15 × 0.25 × 0.30
Crystal color			
Diffractometer	Smart, CCD area detector	Smart, CCD area detector	Smart, CCD area detector
Radiation type	MoKα	MoKα	MoKα
Crystal-detector distance (cm)	5.0	5.0	5.0
Temperature (K)	293(2)	293(2)	293(2)
No. of measured reflections	2184	1263	5640
No. of independent reflections	459	531	1977
θ_max (°)	2 – 24	2 – 24	2 – 24
Range of *h, k, l*	-7 to 6	-7 to 7	-4 to 4
	-5 to 7	-6 to 5	-14 to 18
	-15 to 14	-9 to 8	-23 to 22
R₁	0.0501	0.057	0.0633
wR₂	0.1072	0.088	0.1105
S	1.16	1.805	0.69
No. of parameters refined	68	87	240
Max. eÅ⁻³	0.38	0.243	0.48

The atomic coordinates and isotropic displacement parameters for *N*-methylcyanuric acid crystallized from methanol (**8**) and water (**8 + H₂O**) are listed in Table A1.12.

The bond distances and angles for **8** crystallized from methanol and water are given in

Tables 4.29 and 4.30.

Table 4.29 Bond lengths and angles **8**

Moiety	Distance (Å)	Moiety	Angle (°)
N(3)-C(3)	1.36(2)	C(3)-N(3)-C(1)	123.2(11)
N(3)-C(1)	1.39(2)	C(3)-N(3)-C(4)	117.1(11)
N(3)-C(4)	1.456(12)	C(1)-N(3)-C(4)	119.7(13)
N(2)-C(2)	1.36(2)	C(2)-N(2)-C(1)	125.8(11)
N(2)-C(1)	1.36(2)	C(3)-N(1)-C(2)	122.9(13)
N(1)-C(3)	1.388(12)	O(2)-C(2)-N(2)	124.6(12)
N(1)-C(2)	1.395(14)	O(2)-C(2)-N(1)	120(2)
O(3)-C(3)	1.235(12)	N(2)-C(2)-N(1)	115.1(11)
O(1)-C(1)	1.20(2)	O(3)-C(3)-N(3)	124.2(11)
C(2)-O(2)	1.216(12)	O(3)-C(3)-N(1)	118.6(14)
Moiety	**Angle (°)**	N(3)-C(3)-N(1)	117.2(10)
N(2)-C(1)-N(3)	115.9(14)	O(1)-C(1)-N(2)	121.7(13)
		O(1)-C(1)-N(3)	122.4(12)

Table 4.30 Bond lengths and angles **8 + H$_2$O**

Moiety	Distance (Å)	Moiety	Angle (°)
N(3)-C(3)	1.369(5)	C(3)-N(3)-C(1)	125.5(4)
N(3)-C(1)	1.370(5)	C(3)-N(3)-H(3)	118(2)
N(3)-H(3)	0.96(4)	C(1)-N(3)-H(3)	117(2)
N(2)-C(3)	1.373(5)	C(3)-N(2)-C(2)	123.1(3)
N(2)-C(2)	1.383(5)	C(3)-N(2)-C(4)	117.8(4)
N(2)-C(4)	1.483(6)	C(2)-N(2)-C(4)	119.1(4)
O(2)-C(3)	1.217(5)	C(1)-N(1)-C(2)	125.6(4)
N(1)-C(1)	1.356(4)	C(1)-N(1)-H(1)	122(2)
N(1)-C(2)	1.371(5)	C(2)-N(1)-H(1)	113(2)
N(1)-H(1)	0.91(5)	O(2)-C(3)-N(3)	121.1(4)
O(1)-C(1)	1.216(4)	O(2)-C(3)-N(2)	123.2(3)
C(4)-H(4C)	0.92(5)	N(3)-C(3)-N(2)	115.7(4)
C(4)-H(4B)	1.00(5)	N(2)-C(4)-H(4C)	114(3)
C(2)-O(3)	1.201(4)	N(2)-C(4)-H(4B)	112(3)
O(4)-H(42)	0.73(5)	H(4C)-C(4)-H(4B)	101(3)
O(4)-H(41)	1.02(6)	O(3)-C(2)-N(1)	121.9(4)
Moiety	**Angle (°)**	O(3)-C(2)-N(2)	122.4(4)
N(1)-C(1)-N(3)	114.4(4)	N(1)-C(2)-N(2)	115.7(4)
H(42)-O(4)-H(41)	107(5)	O(1)-C(1)-N(1)	123.7(4)

N-methylcyanuric acid, **8** yields different hydrogen-bonded assemblies when crystallized from methanol and water, incorporating the solvent of crystallization in the latter case. The structure of **8** crystallized from methanol solution has linear chains formed by N-H$\cdots$O hydrogen bonds (H$\cdots$O, 1.87Å). These chains are held together through N-H$\cdots$O (H$\cdots$O, 1.78Å) bonds on one side and by weak C-H$\cdots$O interaction (H$\cdots$O, 2.87Å) on the other. This results in a hexagonal network involving molecules of **8** as shown in Figure 4.23a. The unique hydrogen bond distances are listed in Table 4.31.

Table 4.31 Important hydrogen bond parameters **8**

H-bond	D-H (Å)	H$\cdots$A (Å)	D$\cdots$A (Å)	D-H$\cdots$A (°)
N(1)-H(1)$\cdots$O(1)	0.96(3)	1.86(2)	2.808(3)	165.2(5)
N(2)-H(2)$\cdots$O(2)	1.00(3)	1.77(3)	2.781(4)	177.2(5)
C(4)-H(4B)$\cdots$O(1)	0.96(4)	2.34(3)	2.762(4)	106.0(6)

N-methylcyanuric acid obtained by crystallization from water has a structure similar to that of cyanuric acid obtained from water (see Figure 4.18b). The unique hydrogen bond parameters are given in Table 4.32.

Table 4.32 Important hydrogen bond parameters **8+H$_2$O**

H-bond	D-H (Å)	H$\cdots$A (Å)	D$\cdots$A (Å)	D-H$\cdots$A (°)
N(1)-H(1)$\cdots$O(4)	0.91(4)	1.92(5)	2.811(5)	167(4)
N(3)-H(3)$\cdots$O(3)	0.96(4)	1.81(4)	2.772(5)	175(3)
O(4)-H(41)$\cdots$O(1)	1.02(7)	1.88(7)	2.885(5)	166(5)
O(4)-H(42)$\cdots$O(2)	0.73(6)	2.05(6)	2.776(5)	179(7)
C(4)-H(4C)$\cdots$O(3)	0.92(6)	2.43(5)	2.763(6)	102(4)

The structure involves chains of molecules of **8** formed by N-H$\cdots$O hydrogen bonds (H$\cdots$O, 1.82Å). These chains are, in turn, connected together by water molecules forming O-H$\cdots$O and N-H$\cdots$O hydrogen bonds (H$\cdots$O 1.88 - 2.05Å) as shown in

Figure 4.23b. It is evident from Figure 4.23 that unlike cyanuric acid, *N*-methylcyanuric acid crystallizes in chain structures involving single hydrogen bonds from both the solvents, the cyclic hydrogen-bonded dimers being disfavored by the presence of the methyl group.

(a) **8**   (b) **8 + H₂O**
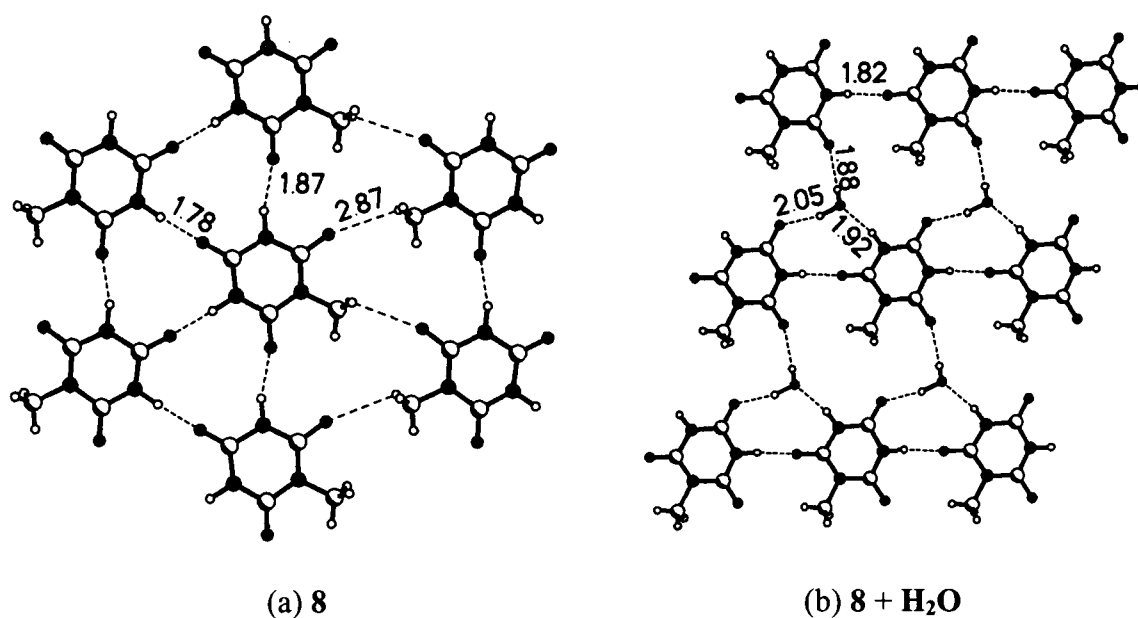
Figure 4.23: (a) Hexagonal arrangement of molecules of N-methylcyanuric acid, **8**, crystallized from methanol. (b) Interaction of water molecules with N-methylcyanuric acid in a two-dimensional planar sheet **8** + H₂O.

The 1:1 adduct **8a** formed between *N*-methylcyanuric acid and 4,4'-bipyridyl crystallized from either methanol and water has the same structure. The asymmetric unit is shown in Figure 4.24. The crystallographic information for *N*-methylcyanuric acid-4,4'-bipyridine complex (**8a**) are listed in Table 4.28. The atomic coordinates and isotropic displacement parameters are given in Table A1.13. The two-dimensional

arrangement of molecules in **8a** is shown in Figure 4.25. Amazingly, the linear chains

of molecules of **8** only involve weak C-H···O interaction (H···O, 2.73Å).
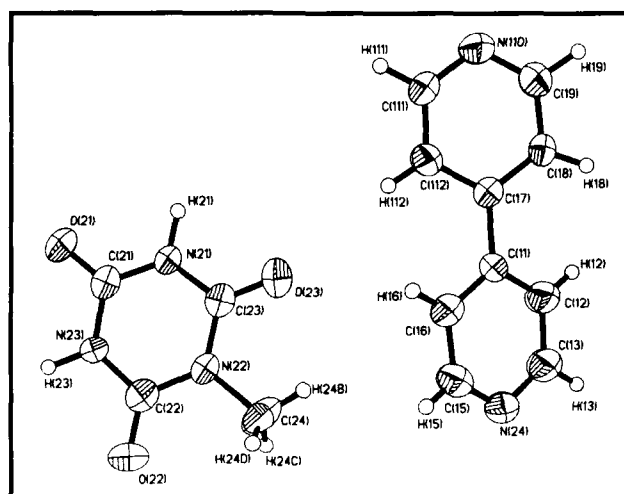
Figure 4.24: *ORTEP plot of the adduct of N-methylcyanuric acid with 4,4'-bipyridine 8a. Thermal ellipsoids are given at 50% probability.*
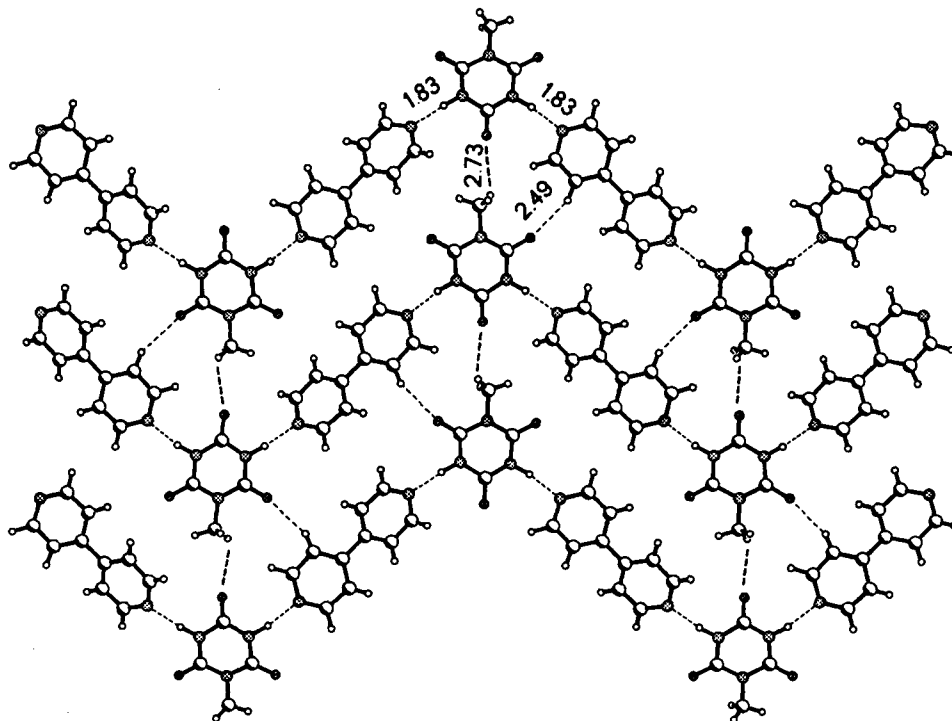
Figure 4.25: *Arrangement of molecules of N-methylcyanuric acid and 4,4'-bipyridyl in the crystal structure of the complex, 8a.*

The bond distances and angles are given in Table 4.33 and the unique hydrogen bond

geometries are given in Table 4.34.

Table 4.33 Bond lengths and angles **8a**

Moiety	Distance (Å)	Moiety	Angle (°)
O(21)-C(21)	1.225(5)	C(15)-N(24)-C(13)	115.7(4)
O(23)-C(23)	1.214(5)	C(22)-N(23)-C(21)	124.2(4)
O(22)-C(22)	1.225(5)	C(22)-N(22)-C(23)	123.7(4)
N(24)-C(15)	1.322(6)	C(22)-N(22)-C(24)	119.0(4)
N(24)-C(13)	1.324(5)	C(23)-N(22)-C(24)	117.3(4)
N(23)-C(22)	1.374(5)	C(16)-C(11)-C(12)	116.8(4)
N(23)-C(21)	1.374(5)	C(16)-C(11)-C(17)	121.6(4)
N(22)-C(22)	1.371(5)	C(12)-C(11)-C(17)	121.5(4)
N(22)-C(23)	1.385(5)	C(21)-N(21)-C(23)	124.6(4)
N(22)-C(24)	1.476(5)	C(18)-C(17)-C(112)	116.0(4)
C(11)-C(16)	1.375(5)	C(18)-C(17)-C(11)	122.5(4)
C(11)-C(12)	1.395(6)	C(112)-C(17)-C(11)	121.5(4)
C(11)-C(17)	1.485(5)	C(11)-C(16)-C(15)	119.1(5)
N(21)-C(21)	1.356(5)	O(21)-C(21)-N(21)	122.7(4)
N(21)-C(23)	1.377(5)	O(21)-C(21)-N(23)	121.3(4)
C(17)-C(18)	1.373(5)	N(21)-C(21)-N(23)	116.0(4)
C(17)-C(112)	1.398(5)	C(19)-C(18)-C(17)	120.7(4)
C(16)-C(15)	1.382(6)	C(111)-N(110)-C(19)	116.6(4)
C(18)-C(19)	1.372(5)	O(22)-C(22)-N(22)	123.1(4)
N(110)-C(111)	1.321(5)	O(22)-C(22)-N(23)	121.0(4)
N(110)-C(19)	1.327(5)	N(22)-C(22)-N(23)	115.9(4)
C(112)-C(111)	1.377(6)	O(23)-C(23)-N(21)	121.7(4)
C(13)-C(12)	1.383(6)	O(23)-C(23)-N(22)	122.7(4)

Moiety	Angle (°)		
		N(21)-C(23)-N(22)	115.5(4)
N(24)-C(15)-C(16)	125.0(5)	C(111)-C(112)-C(17)	119.2(4)
N(110)-C(19)-C(18)	123.3(4)	N(24)-C(13)-C(12)	124.2(5)
C(13)-C(12)-C(11)	119.1(5)	N(110)-C(111)-C(112)	124.2(5)

Table 4.34 Important hydrogen bond parameters **8a**

H-bond	D-H (Å)	H···A (Å)	D···A (Å)	D-H···A (°)
N(21)-H(21)···N(110)	1.00(3)	1.83(3)	2.819(5)	169.6(6)
N(23)-H(23)···N(24)	1.01(3)	1.83(5)	2.828(7)	173.1(7)
C(12)-H(12)···O(22)	0.92(5)	2.72(5)	3.563(7)	150.0(4)
C(15)-H(15)···O(21)	0.86(5)	2.83(5)	3.395(6)	124.1(4)
C(16)-H(16)···O(23)	0.98(3)	2.83(6)	3.455(5)	121.6(5)
C(18)-H(18)···O(22)	0.93(4)	2.48(4)	3.365(6)	155.3(5)
C(19)-H(19)···O(21)	1.03(4)	2.61(4)	3.389(6)	131.4(6)

Table 4.34 (*continued*)

C(24)-H(24B)···O(23)	0.95(4)	2.28(3)	2.732(4)	107(7)
C(24)-H(24C)···O(21)	0.95(5)	2.72(6)	3.208(5)	111(3)
C(24)-H(24D)···O(22)	0.96(4)	2.79(5)	3.515(4)	133(4)
C(112)-H(112)···O(23)	0.90(4)	2.86(5)	3.760(4)	171.1(5)

The chains are actually the consequence of the positioning of the molecules of

8 along the chain, through strong N-H···N bonds (H···N, 1.83Å) with bipyridyl,

besides the strong C-H···O interaction (H···O, 2.49Å) between the two molecules.

This C-H···O interaction is considerably stronger than that between the molecules of **8**

in the linear chain or in the parent **8** crystals (Figure 4.23a). In Table 4.35, the

hydrogen-bonded distances in cyanuric acid and *N*-methylcyanuric acid structures are

listed for comparison.

The above co-crystallization experiments form a basis for the rationalization of

structural comparisons between the formed co-crystals and the crystal structure of one

of the pure phases.

Table 4.35 Hydrogen bond distances [in Å] in cyanuric acid, N-methylcyanuric acid and their adducts with 4,4'-bipyridine

H-bond	CA	CA.BP(H_2O)	Cyanuric acid.H_2O	CA.BP(MeOH)	8	8+H_2O	8a
H···O(N-H···O)[a]	1.80	-	2.01	2.02	1.87[f]	1.82	-
H···O(N-H···O)[b]	1.90	1.94, 1.96	-	-	-	-	-
H···N(N-H···N)[c]	-	1.77	-	1.92, 1.94	-	-	1.83
H···O(C-H···O)[d]	-	2.40	-	-	2.87	-	2.49, 2.73
H···O(O-H···O)[e]	-	-	2.01, 2.15	-	-	1.88, 2.05	-

[a]single N-H···O bond forming chains between cyanuric acid molecules.
[b]cyclic dimer formed between two cyanuric acid molecules
[c]N-H···N bond between 4,4'-bipyridine and cyanuric acid (N-methylcyanuric acid)
[d]C-H···O interaction
[e]O-H···O bonds formed by water molecules; water molecules also form N-H···O bonds using the lone pair on the oxygen atom, the H···O distances being 2.00 and 1.92 Å respectively in cyanuric acid.H_2O and *N*-methylcyanuric acid

114

For **Table 4.35**:

ᶠThere is an additional N-H···O bond (H···O, 1.78 Å) between the *N*-methylcyanuric acid molecules

4.6 Cyanurate mimics of hydrogen bonding patterns of nucleic bases: A 1:1 molecular complex formed by 9-ethyladenine with *N*-methylcyanuric acid

A 1:1 adduct of *N*-methylcyanuric acid, **8** (**MCA**) with 9-ethyladenine was obtained upon co-crystallization from a methanol solution. Crystal structure determination of the adduct, **8b**, gave an asymmetric unit of the co-crystals in a triclinic, P-1 space group, as shown in Figure 4.26. The crystal structure data on **8b** and 9-ethyladenine are given in Table 4.36. In this structure of the adduct **8b**, both *N*-methylcyanuric acid **8** and 9-ethyladenine molecules are quite planar and the crystal structure involves two-dimensional sheets that are in turn stacked in three dimensions. In each sheet (see Figure 4.27), the molecules are held together to form molecular strips as in the crystal structure of 9-ethyladenine with 5,5'-diethylbarbituric acid or other uracil derivatives.[168]
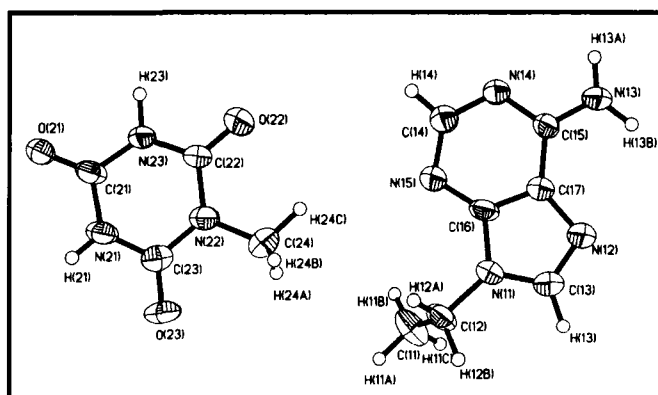
Figure 4.26: *ORTEP drawing of the molecular complex of N-methycyanuric acid and 9-ethyladenine (8b).*

Table 4.36 Crystal structure data of molecular complexes of 9-ethyladenine (**EA**) and the molecular complex of 9-ethyladenine + *N*-methylcyanuric acid (**8b**)

	9-ethyladenine (EA)	8b
Chemical formula	$C_7H_9N_5$	$(C_4H_5N_3O_3){:}(C_7H_9N_5)$
Formula weight	163.19	306.3
Cell setting	Monoclinic	Triclinic
Space group	$P2_1/c$	P-1
a (Å)	8.712(1)	7.334(3)
b (Å)	12.524(2)	8.164(2)
c (Å)	8.438(1)	12.640(5)
α (°)	90	75.12(3)
β (°)	117.2(1)	82.59(3)
γ (°)	90	70.78(3)
Cell volume ($Å^3$)	818.9(2)	689.8(4)
Z	4	2
F(000)	344	320
ρ (Mg/m^3)	1.324	1.475
μ, mm^{-1}	0.09	0.113
λ (Å)	0.7107	0.7107
Crystal size (mm)	0.35 × 0.30 × 0.30	0.30 × 0.25 × 0.30
Diffractometer	Smart, CCD area detector	Smart, CCD area detector
Radiation type	MoKα	MoKα
Crystal-detector distance(cm)	5.0	5.0
Temperature (K)	293(2)	293(2)
No. of measured reflections	3310	2904
No. of independent reflections	1175	1944
θ_{max} (°)	2 - 24	2 - 24
Range of h, k, l	-9 to 9	-8 to 6
	-13 to 13	-7 to 9
	-9 to 9	-10 to 14
R_1	0.0665	0.0783
wR_2	0.1423	0.138
S	1.136	1.942
No. of parameters refined	146	256
Max. $eÅ^{-3}$	0.274	0.417

The arrangement of the molecular strips in two-dimensional sheets is however unique with each strip containing molecules of both ethyladenine and *N*-methylcyanuric acid existing as pairs (cyanuric acid and ethyladenine did not yield a complex perhaps due to the fact that cyanuric acid forms an infinite chain of molecular

network rather than simple dimers to yield a molecular strip). There are two distinct

types of hydrogen-bonded interactions in this complex – homomeric (**MCA···MCA**

and **EA···EA**) and heteromeric (**MCA···EA**).
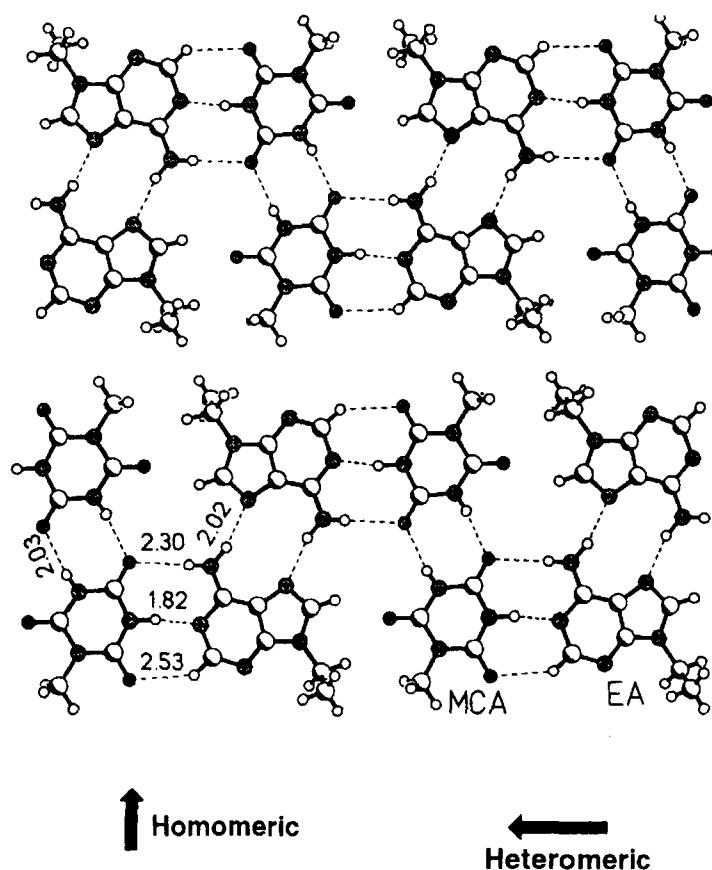
Figure 4.27: Molecular strips showing homomeric and heteromeric arrangement of the molecules of MCA and 9-ethyladenine (EA) in the complex MCA:EA (8b)

Each strip consists of a polymeric chain made up of continuous hydrogen-bonded

networks of alternating homo- and hetero-dimers, **MCA···MCA···EA···EA···**

MCA···MCA···. In both cases, the N-H···O and N-H···N hydrogen bonds form

distinct cyclic rings. The geometries of the intra- and intermolecular interactions of 9-

ethyladenine and the complex, **8b**, are given in Tables 4.37 to 4.40. The atomic

coordinates and isotropic displacement parameters of 9-ethyladenine and the complex,

8b are listed in Tables A1.14 and A1.15, respectively.

Table 4.37 Bond lengths and angles 9-ethyladenine (**EA**).

Moiety	Distance (Å)	Moiety	Angle (°)
N(19)-C(19)	1.325(5)	C(19)-N(19)-H(19B)	122(2)
N(19)-H(19B)	0.90(4)	C(19)-N(19)-H(19A)	121(2)
N(19)-H(19A)	0.99(4)	H(19B)-N(19)-H(19A)	116(3)
C(19)-N(18)	1.348(4)	N(19)-C(19)-N(18)	118.5(3)
C(19)-C(13)	1.414(5)	N(19)-C(19)-C(13)	124.6(3)
N(16)-C(17)	1.325(5)	N(18)-C(19)-C(13)	116.9(3)
N(16)-C(14)	1.344(5)	C(17)-N(16)-C(14)	109.9(3)
C(13)-C(14)	1.380(5)	C(14)-C(13)-N(12)	110.4(3)
C(13)-N(12)	1.388(4)	C(14)-C(13)-C(19)	117.1(3)
N(15)-C(11)	1.355(5)	N(12)-C(13)-C(19)	132.4(3)
N(15)-C(14)	1.375(4)	C(11)-N(15)-C(14)	105.4(3)
N(15)-C(12)	1.475(5)	C(11)-N(15)-C(12)	128.5(4)
N(12)-C(11)	1.313(5)	C(14)-N(15)-C(12)	126.1(4)
N(18)-C(17)	1.334(5)	C(11)-N(12)-C(13)	103.3(3)
C(12)-C(22)	1.496(8)	N(16)-C(14)-N(15)	126.6(3)
C(12)-H(12B)	1.12(4)	N(16)-C(14)-C(13)	127.2(3)
C(12)-H(12A)	1.05(5)	N(15)-C(14)-C(13)	106.1(3)
C(17)-H(17)	0.93(4)	C(17)-N(18)-C(19)	118.8(3)
C(11)-H(11)	1.01(4)	N(15)-C(12)-C(22)	110.7(5)
C(22)-H(22B)	0.90(5)	N(15)-C(12)-H(12B)	110(2)
C(22)-H(22B)	0.94(6)	C(22)-C(12)-H(12B)	112(2)
C(22)-H(22A)	0.90(8)	N(15)-C(12)-H(12A)	113(2)

Moiety	Angle (°)		
		C(22)-C(12)-H(12A)	102(3)
N(15)-C(11)-H(11)	120(2)	H(12B)-C(12)-H(12A)	108(3)
C(12)-C(22)-H(22B)	114(3)	N(16)-C(17)-N(18)	130.1(4)
C(12)-C(22)-H(22B)	98(4)	N(16)-C(17)-H(17)	113(2)
H(22B)-C(22)-H(22B)	108(5)	N(18)-C(17)-H(17)	117(2)
C(12)-C(22)-H(22A)	108(5)	N(12)-C(11)-N(15)	114.7(4)
H(22B)-C(22)-H(22A)	110(6)	N(12)-C(11)-H(11)	125(2)
		H(22B)-C(22)-H(22A)	119(7)

Table 4.38 Important hydrogen bond parameters 9-ethyladenine (**EA**)

H-bond	D-H (Å)	H⋯A (Å)	D⋯A (Å)	D-H⋯A (°)
N(19)-H(19A)⋯N(12)	0.99(4)	2.08(4)	3.069(5)	176(3)
N(19)-H(19B)⋯N(18)	0.90(4)	2.12(4)	2.983(5)	161(4)

118

Table 4.39 Bond lengths and angles **8b** (MCA:EA)

Moiety	Distance (Å)	Moiety	Angle (°)
O(21)-C(21)	1.222(6)	C(22)-N(23)-C(21)	125.7(4)
O(23)-C(23)	1.218(5)	C(22)-N(23)-H(23)	114(3)
O(22)-C(22)	1.210(6)	C(21)-N(23)-H(23)	120(3)
N(23)-C(22)	1.363(6)	C(23)-N(22)-C(22)	122.5(4)
N(23)-C(21)	1.369(6)	C(23)-N(22)-C(24)	118.0(4)
N(23)-H(23)	0.97(5)	C(22)-N(22)-C(24)	119.4(4)
N(22)-C(23)	1.386(7)	C(23)-N(21)-C(21)	125.8(5)
N(22)-C(22)	1.388(5)	C(23)-N(21)-H(21)	113(3)
N(22)-C(24)	1.465(7)	C(21)-N(21)-H(21)	120(3)
N(21)-C(23)	1.378(7)	O(23)-C(23)-N(21)	121.8(5)
N(21)-C(21)	1.378(6)	O(23)-C(23)-N(22)	122.6(5)
N(21)-H(21)	0.86(5)	N(21)-C(23)-N(22)	115.6(4)
C(24)-H(24C)	1.10(9)	O(22)-C(22)-N(23)	122.1(4)
C(24)-H(24A)	0.91(7)	O(22)-C(22)-N(22)	121.7(5)
C(24)-H(24B)	0.95(9)	N(23)-C(22)-N(22)	116.3(4)
N(15)-C(14)	1.338(5)	O(21)-C(21)-N(23)	123.3(4)
N(15)-C(16)	1.343(6)	O(21)-C(21)-N(21)	123.1(4)
N(11)-C(13)	1.359(7)	N(23)-C(21)-N(21)	113.6(5)
N(11)-C(16)	1.381(5)	N(22)-C(24)-H(24C)	114(4)
N(11)-C(12)	1.464(6)	N(22)-C(24)-H(24A)	119(4)
N(14)-C(15)	1.350(6)	H(24C)-C(24)-H(24A)	105(6)
N(14)-C(14)	1.351(6)	N(22)-C(24)-H(24B)	120(6)
C(17)-C(16)	1.376(7)	H(24C)-C(24)-H(24B)	97(6)
C(17)-N(12)	1.395(6)	H(24A)-C(24)-H(24B)	98(6)
C(17)-C(15)	1.410(6)	C(14)-N(15)-C(16)	110.1(4)
N(13)-C(15)	1.337(6)	C(13)-N(11)-C(16)	105.7(4)
N(13)-H(13B)	0.99(5)	C(13)-N(11)-C(12)	126.9(4)
N(13)-H(13A)	0.92(5)	C(16)-N(11)-C(12)	127.2(4)
C(14)-H(14)	0.97(4)	C(15)-N(14)-C(14)	119.9(4)
N(12)-C(13)	1.320(6)	C(16)-C(17)-N(12)	111.1(4)
C(12)-C(11)	1.497(8)	C(16)-C(17)-C(15)	116.9(4)
C(12)-H(12B)	1.06(4)	N(12)-C(17)-C(15)	132.0(4)
C(12)-H(12A)	0.95(5)	C(15)-N(13)-H(13B)	118(3)
C(13)-H(13)	0.99(5)	C(15)-N(13)-H(13A)	114(3)
C(11)-H(11C)	1.01(8)	H(13B)-N(13)-H(13A)	128(4)
C(11)-H(11B)	0.98(7)	N(15)-C(16)-C(17)	128.3(4)
C(11)-H(11A)	1.04(6)	N(15)-C(16)-N(11)	125.9(4)

Moiety	Angle (°)	C(17)-C(16)-N(11)	105.8(4)
H(12B)-C(12)-H(12A)	108(4)	N(13)-C(15)-N(14)	119.1(4)
N(12)-C(13)-N(11)	114.6(4)	N(13)-C(15)-C(17)	124.1(5)
N(12)-C(13)-H(13)	126(3)	N(14)-C(15)-C(17)	116.8(4)
N(11)-C(13)-H(13)	119(3)	N(15)-C(14)-N(14)	128.1(5)
C(12)-C(11)-H(11C)	110(4)	N(15)-C(14)-H(14)	121(3)
C(12)-C(11)-H(11B)	115(4)	N(14)-C(14)-H(14)	110(3)
H(11C)-C(11)-H(11B)	109(6)	C(13)-N(12)-C(17)	102.8(4)
C(12)-C(11)-H(11A)	116(3)	N(11)-C(12)-C(11)	111.9(5)

Table 4.39 *(continued)*

H(11C)-C(11)-H(11A)	102(5)	N(11)-C(12)-H(12B)	111(3)
H(11B)-C(11)-H(11A)	105(5)	C(11)-C(12)-H(12B)	109(3)
C(11)-C(12)-H(12A)	111(3)	N(11)-C(12)-H(12A)	105(3)

Table 4.40 Important hydrogen bond parameters **8b** (MCA:EA)

H-bond	D-H (Å)	H···A (Å)	D···A (Å)	D-H···A (°)
N(13)-H(13A)···O(21)	0.92(6)	2.30(6)	3.220(6)	177(5)
N(13)-H(13B)···N(12)	0.99(5)	2.02(5)	2.969(7)	162(4)
N(21)-H(21)···O(21)	0.86(5)	2.03(5)	2.886(6)	171(5)
N(23)-H(23)···N(14)	0.97(6)	1.82(6)	2.793(6)	178(5)
C(11)-H(11C)···O(22)	1.02(8)	2.56(7)	3.461(10)	148(5)
C(13)-H(13)···O(23)	0.99(6)	2.25(5)	3.165(7)	154(4)
C(14)-H(14)···O(22)	0.99(5)	2.53(5)	3.362(7)	144(4)

While in both **MCA···MCA** and **EA···EA** homomeric units, the H···O and H···N distances 2.03 and 2.02 Å, respectively, the corresponding distances in the heteromeric unit are 2.30 and 1.82 Å. Thus heterodimer formation involves lengthening of the H···O distance by 0.28 Å but shortening of the H···N distance by 0.2 Å compared to the homodimers (see Table 4.40). The strips are aligned in a two-dimensional arrangement in an *anti*-parallel manner, stabilized by hydrophobic interaction between the ethyl groups located in the adjacent strips, leading to a molecular zip as shown in Figure 4.27.

The observed complementary hydrogen bonding interaction between **8** and ethyladenine is similar to that between thymine and adenine with respect to Watson-Crick base pairing of hydrogen bonds as shown in Scheme 4.4. However, the helical arrangement of units in a chain or a sheet is absent and only a σ-planar arrangement is seen.
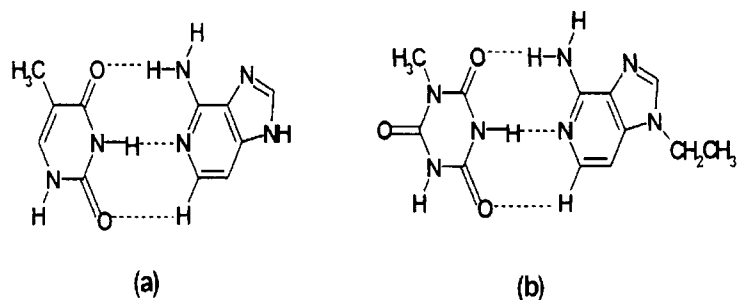
Scheme 4.4 *(a) Thymine···adenine (b) MCA···adenine*

It is interesting to note the unusual features of hydrogen bonding patterns in the homo-

and heteromeric pairs, particularly the nature of N-H···O hydrogen bonds. The N-

H···O hydrogen bond in the heteromeric pattern is unusually longer and appears to be

the resultant of a strong C-H···O hydrogen bond with an H···O distance of 2.53 Å.

Such a correlation is in agreement with the statistical analysis of Leonard *et al* from a

series of crystal structures found in the literature.[169] Further, in the homomeric pattern,

the N-H···O bond between the **MCA** molecules is longer than the corresponding

distance in the parent crystal structure of **MCA**. The N-H···N hydrogen bond pattern

between dimeric **EA** molecules adopts a 10-membered homodimeric structure in a

centrosymmetric pattern. A comparison of the structural patterns exhibited by this

complex with that of pure ethyladenine: 9-ethyladenine crystallizes in a monoclinic

space group, P2$_1$/c from an ethylacetate solution. The molecules are packed in a two-

dimensional arrangement to yield the layer structure shown in Figure 4.28. In each

layer, adjacent molecules are held together, yielding one-dimensional molecular tapes

through the formation of unsymmetrical N-H···N hydrogen bonds, with H···N

distances of 2.08 and 2.12 Å. These distances are similar to that noted in the complex

with *N*-methylcyanuric acid. For a given pair of molecules, both the acceptor and the donor moieties of a pyrimidine moiety interact with both the imadazole and pyrimidine moieties of the adjacent molecules to give a 9-membered dimer ring. The adjacent molecular tapes are then aligned to form layers in a two-dimensional arrangement in which the hydrocarbon groups are always oriented on one side and interlocked (Figure 4.27) as in the DNA-recognizing leucine zipper protein.[170]
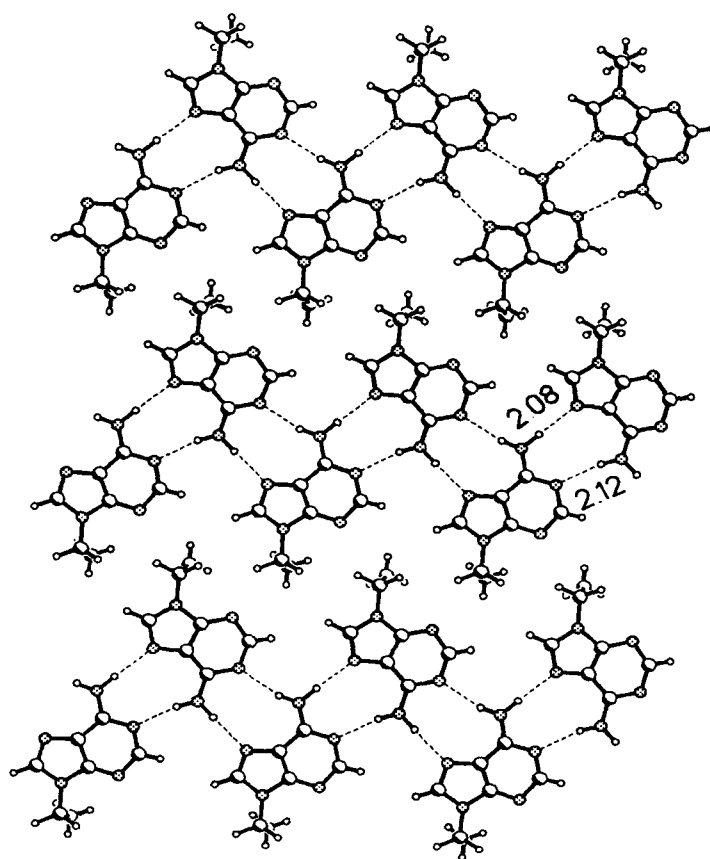
Figure 4.28: *Two-dimensional arrangement of the adjacent molecules connected together by hydrogen bonds in the crystal structure of 9-ethyladenine (EA).*

(a)

(b)
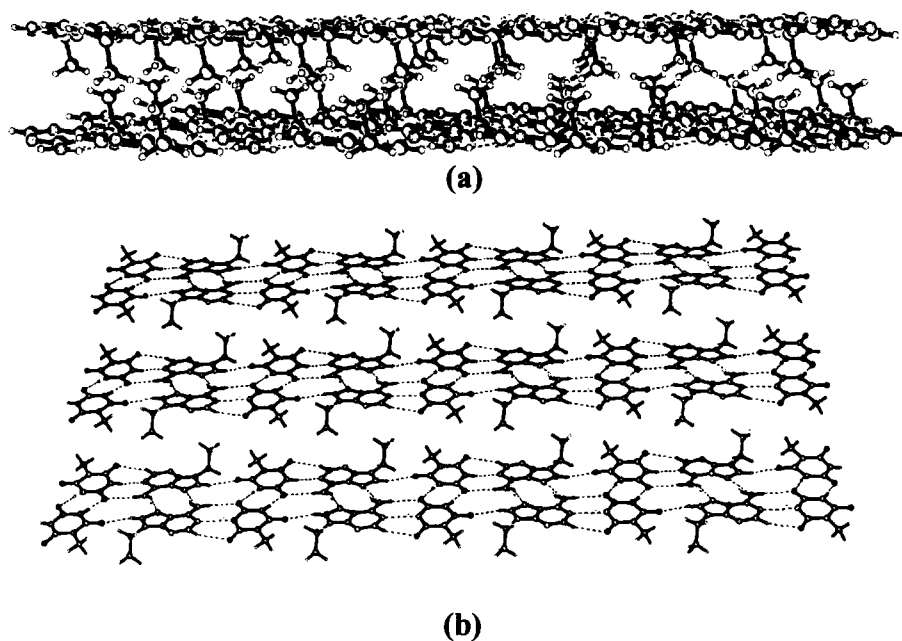
Figure 4.29: (a) Three-dimensional packing of the sheets in the crystal structure of EA. (b) Three-dimensional arrangement of stacking of the sheets in the crystal structure of the MCA:EA complex, **8b**.

The three-dimensional arrangement shown in Figure 4.29a is unusual and unique. The layers arranged in a three-dimensional stack exhibit two types of interactions between them, one due to π-π stacking and the other resulting from the packing of the nonpolar ethyl side chain. In contrast, in the crystal structure of the molecular complex of 9-ethyladenine and N-methylcyanuric acid, although the sheets stack to yield a three-dimensional structure, generally π-π interactions are only involved in the stabilization of sheets. The role of the nucleobases T or U in complementary base pairing with A can be mimicked by N-methylcyanuric acid in its complexation with 9-ethyladenine. This study highlights the intriguing feature of cyanurate-adenine molecular

123

recognition, with implications for development of different bio-relevant experimental and computational structural models.

4.7 Hydrothermal synthesis of organic channel structures formed by melamine with cyanuric and trithiocyanuric acids

Whitesides and co-workers have studied the 1:1 complex of cyanuric acid and melamine as a model two-component hydrogen-bonded system.[27] As a result of the geometrical disposition of the supramolecular functionality in the two components, a sheet structure was proposed for the cyanuric acid-melamine complex containing hexagonal rosettes. Melamine combines with cyanuric acid in water to form a fine, insoluble white precipitate. Difficulty in obtaining single crystals suitable for X-ray analysis was due to the limited solubility in most organic solvents and extensive hydrogen bonding of both cyanuric acid and melamine. Hence, verification of the crystal structure of the complex was hindered for a number of years. We therefore attempted to crystallize the cyanuric acid-melamine complex with the utilization of the hydrothermal synthesis method.[148]

Cyanuric acid, 7, forms a 1:1 adduct with melamine, 9. Crystals of the adduct are however obtained only by the hydrothermal method. The adduct, 9a, has an asymmetric unit consisting of the molecules of 7 and 9 with 50% occupancy of each. An ORTEP drawing of the superimposed asymmetric unit is shown in Figure 4.30. The adduct (9a) crystallizes in a C2/m space group. The crystal structure data of the adduct 9a are given in Table 4.41. The atomic coordinates and isotropic displacement parameters are given in Table A1.16.
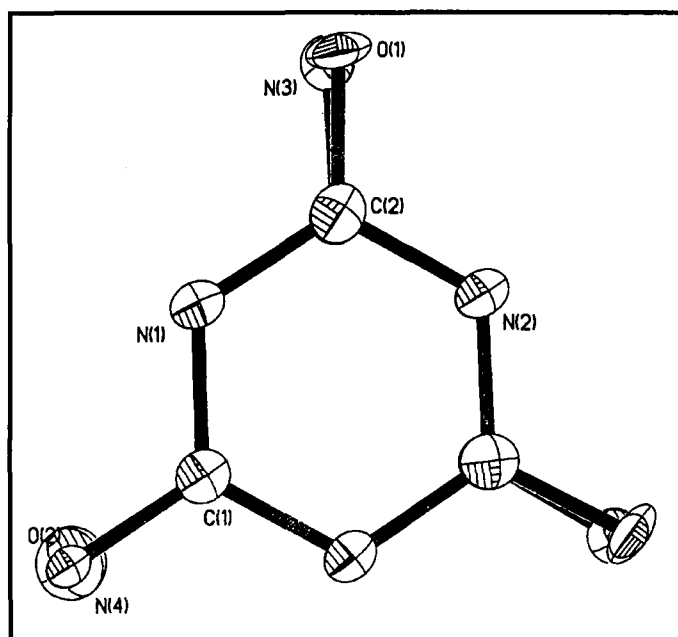
Figure 4.30: *An ORTEP drawing showing the asymmetric unit in the 1:1 adduct of cyanuric acid with melamine, 9a.*

Table 4.41 Crystal structure data of molecular complexes of cyanuric acid + melamine (**9a**) and trithiocyanuric acid + melamine (**9b**)

	9a	9b
Chemical formula	$(C_3H_3N_3O_3):(C_3H_6N_6)$	$(C_3H_3N_3S_3):(C_3H_6N_6)$
Formula weight	255.22	303.39
Cell setting	Monoclinic	Monoclinic
Space group	C2/m	C2/m
a (Å)	14.853(2)	14.862(3)
b (Å)	9.641(2)	9.650(2)
c (Å)	3.851(1)	3.588(1)
α (°)	90	90
β (°)	92.26(1)	92.32(1)
γ (°)	90	90
Cell volume (Å³)	512.4(2)	514.2(2)
Z	2	2
F(000)	264	294
ρ (Mg/m³)	1.654	1.901
μ, mm⁻¹	0.136	0.716
λ (Å)	0.7107	0.7107
Crystal size (mm)	0.25 × 0.30 × 0.30	0.25 × 0.35 × 0.35
Crystal color	Colorless	Yellow
Diffractometer	Smart, CCD area detector	Smart, CCD area detector
Radiation type	MoKα	MoKα
Crystal-detector distance(cm)	5.0	5.0
Temperature (K)	293(2)	293(2)

Table 4.41 (*continued*)

No. of measured reflections	1095	1091
No. of independent reflections	395	397
θ_{max} (°)	2 - 24	2 - 24
Range of *h, k, l*	-16 to 14	-13 to 16
	-8 to 10	-10 to 10
	-3 to 3	-3 to 3
R_1	0.0557	0.0622
wR_2	0.1413	0.1341
S	1.766	1.936
No. of parameters refined	56	47
Max. $e\text{Å}^{-3}$	0.393	0.474

Packing analysis shows that **7** and **9** are held together by antiparallel, triple, N-H$\cdots$O and N-H$\cdots$N hydrogen bonds yielding the hexameric unit (rosette). Such a rosette is shown in Figure 4.31. The hydrogen atoms were not included in the refinement. The bond distances and angles are given below in Table 4.42.

Table 4.42 Bond lengths and angles **9a**

Moiety	Distance (Å)	Moiety	Angle (°)
N(2)-C(2)#1	1.364(4)	C(2)#1-N(2)-C(2)	118.7(4)
N(2)-C(2)	1.364(4)	C(2)-N(1)-C(1)	119.4(3)
N(1)-C(2)	1.354(5)	N(3)-C(2)-O(1)	17.3(6)
N(1)-C(1)	1.365(4)	N(3)-C(2)-N(1)	118.3(6)
C(2)-N(3)	1.300(14)	O(1)-C(2)-N(1)	120.6(5)
C(2)-O(1)	1.299(9)	N(3)-C(2)-N(2)	119.7(6)
C(1)-N(4)	1.29(3)	O(1)-C(2)-N(2)	117.8(5)
C(1)-O(2)	1.27(2)	N(1)-C(2)-N(2)	121.1(3)
C(1)-N(1)#1	1.365(4)	N(4)-C(1)-O(2)	16(2)

Moiety	Angle (°)	N(4)-C(1)-N(1)#1	119.6(2)
O(2)-C(1)-N(1)	119.6(2)	O(2)-C(1)-N(1)#1	119.6(2)
N(1)#1-C(1)-N(1)	120.3(4)	N(4)-C(1)-N(1)	119.6(2)

Symmetry transformations used to generate equivalent atoms:
#1 x,-y,z
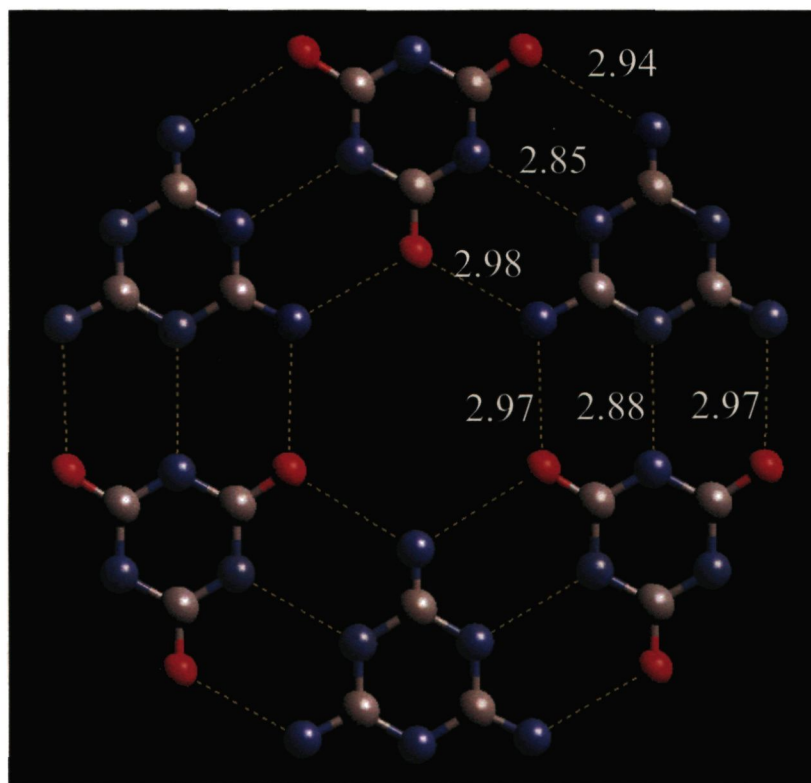
9a

Figure 4.31: *Hexagonal arrangement of the molecules of **7** and **9** forming a rosette structure in the adduct, **9a**. Only the donor⋯acceptor distances are indicated.*

The intermolecular N⋯O and N⋯N distances corresponding to N-H⋯O and N-H⋯N bonds are in the range of 2.94 - 2.98Å and 2.85 - 2.88 Å, respectively. The hexamers are arranged in two dimensions to form planar sheets, the structure being exactly as predicted by Whitesides (refer Scheme 2.2). A significant feature is that the planar sheets are stacked in three dimensions to give channels with a diameter of 4Å (Figure 4.32). These channels are comparable to the cavities in cryptands.

The best stacking arrangement was one with alternating cyanuric acid and melamine molecules (with 50% occupation each), as established by the low R-factor (R_1) and also by energy calculations using the MOPAC program.
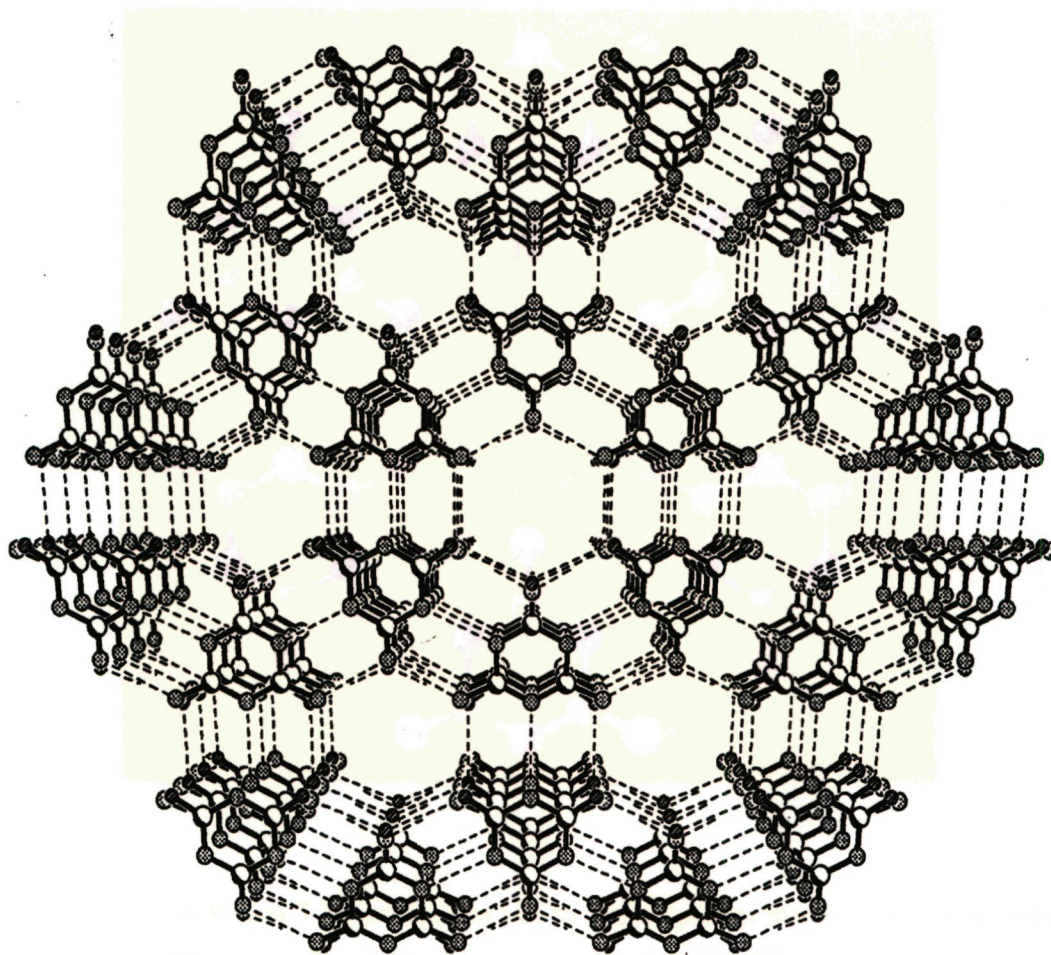
Figure 4.32*: Three-dimensional arrangement of the sheets in the adduct **9a** forming channels.*

The least stable arrangement is the one with cyanuric acid on top of another cyanuric acid molecule. Cyanuric acid on top of melamine is more stable by 37 kcal mol^{-1} relative to cyanuric acid on cyanuric acid. The packing coefficient of the cyanuric acid (**7**): melamine (**9**) adduct calculated using Cerius is 67.5 %.

Crystal structure of the adduct, **9b**, found in trithiocyanuric acid, **10** and melamine, **9** reveals that it also has features similar to those of **9a** with a superimposed asymmetric unit (Figure 4.33), except that the N-H$\cdots$O hydrogen bonds are replaced

by the N-H···S hydrogen bonds as shown in Figure 4.34. The crystal structure data of **9b** are given in Table 4.41. The atomic coordinates and isotropic displacement parameters are listed in Table A1.17.
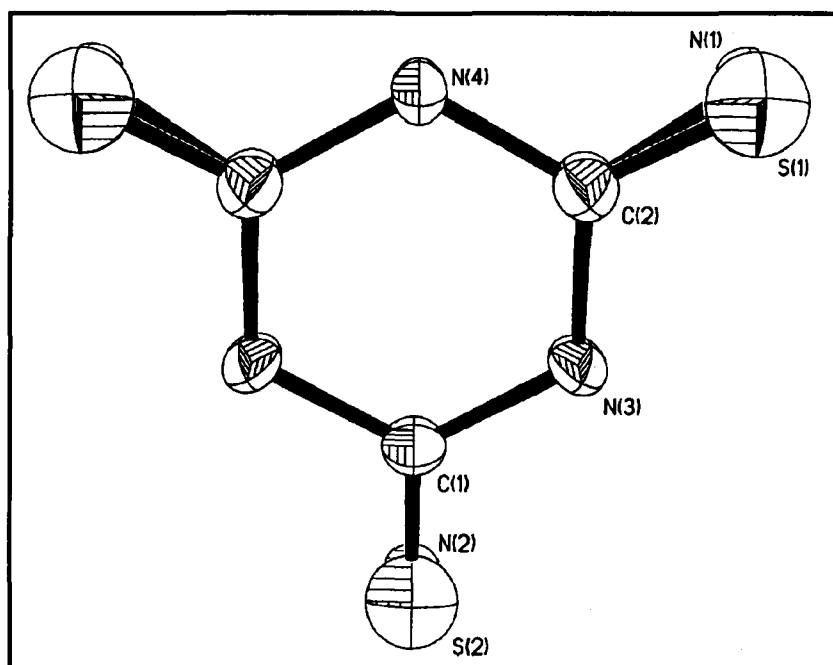
Figure 4.33: An ORTEP drawing showing the asymmetric unit in the 1:1 adduct of trithiocyanuric acid with melamine, **9b**.

The bond lengths and angles are listed below in Table 4.43.

Table 4.43 Bond lengths and angles **9b**

Moiety	Distance (Å)	Moiety	Angle (°)
N(4)-C(2)	1.358(5)	C(2)-N(4)-C(2)#1	119.0(5)
N(4)-C(2)#1	1.358(5)	C(1)-N(3)-C(2)	118.8(4)
N(3)-C(1)	1.358(4)	N(1)-C(2)-S(1)	17.8(8)
N(3)-C(2)	1.363(5)	N(1)-C(2)-N(4)	118.0(8)
C(2)-N(1)	1.32(2)	S(1)-C(2)-N(4)	119.8(4)
C(2)-S(1)	1.288(7)	N(1)-C(2)-N(3)	119.4(8)
C(1)-S(2)	1.287(9)	S(1)-C(2)-N(3)	118.9(4)
C(1)-N(2)	1.32(2)	N(4)-C(2)-N(3)	121.0(4)
C(1)-N(3)#1	1.358(4)	S(2)-C(1)-N(2)	18.0(9)
Moiety	**Angle (°)**	S(2)-C(1)-N(3)#1	119.3(3)
N(2)-C(1)-N(3)#1	118.4(3)	N(2)-C(1)-N(3)	118.4(3)
S(2)-C(1)-N(3)	119.3(3)	N(3)#1-C(1)-N(3)	121.2(5)

Symmetry transformations used to generate equivalent atoms: #1 x,-y,z

The N···S and N···N distances corresponding to N-H···S and N-H···N bonds are in the range of 2.96 - 2.98Å and 2.86 - 2.88 Å, respectively. The sheets are stacked in a three-dimensional channel arrangement as depicted in Figure 4.35. The diameter of the channel (in Figure 4.35) is approximately 4Å here as well.

The best stacking arrangement is trithiocyanuric acid on top of melamine. The packing coefficient of the adduct is 74.6 % as calculated from Cerius.

9b
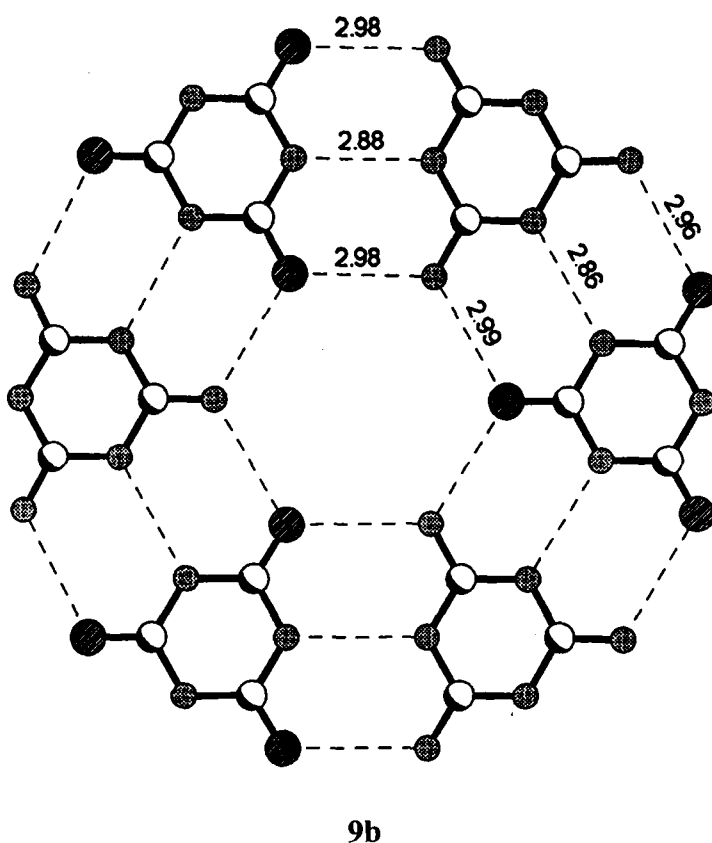
Figure 4.34: *Rosette structure noticed in the adduct,* ***9b.***

The powder X-ray diffraction pattern of the cyanuric acid:melamine adduct simulated on the basis of structure found by us agrees with the experimental powder pattern of the polycrystalline sample.

130
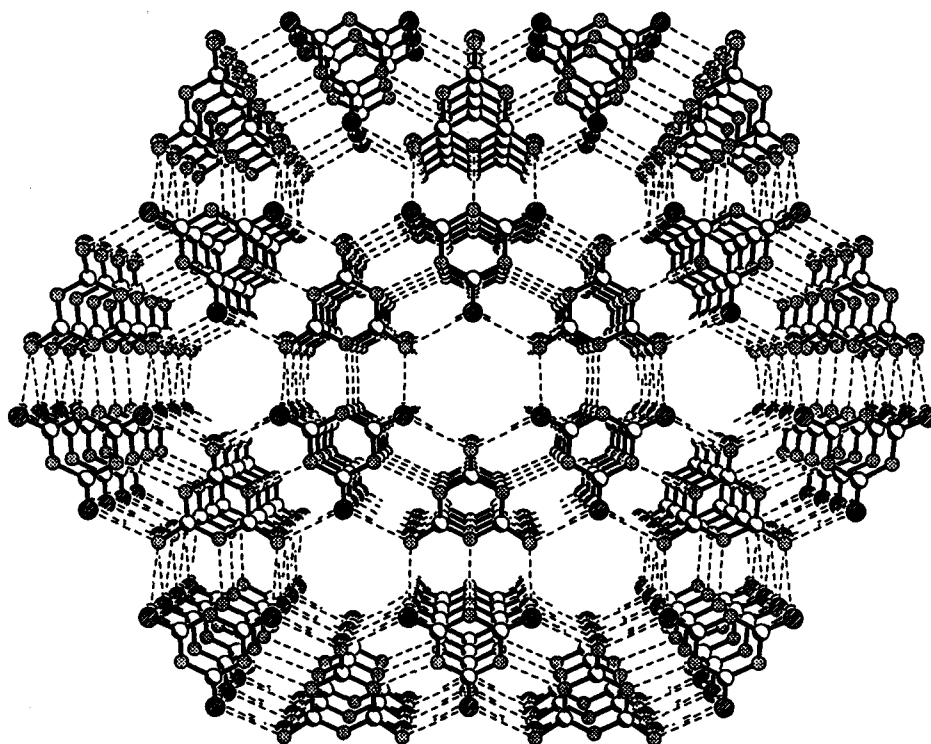
Figure 4.35: *Three-dimensional arrangement of the sheets in the crystal structure of* **9b**.

It is evident that the two crystal structures of the adducts **9a** and **9b** suggest an equivalent structure-directing role for N-H···O and N-H···S hydrogen bonds. The main difference in structure between **9a** and **9b** arises largely from the differences in the strengths and directionality of the N-H···O and N-H···S hydrogen bond interactions.

131

4.8 Organic porous solids formed by the hydrogen-bonded self-assembly of trithiocyanuric acid and 4,4'-bipyridine

We have carried out a systematic study of the supramolecular hydrogen-bonded assemblages obtained from the crystallization of trithiocyanuric acid, **10**, with 4,4'-bipyridine in a variety of solvents. While the adduct of **10** with 4,4'-bipyridine was not stable, the adducts of these molecules obtained along with benzene, toluene, *o*-, *m*- and p-xylenes and anthracene gave good crystals, whose structures we have investigated. In Table 4.44, the crystal structure data of these hydrogen-bonded adducts are given. All these adducts crystallize in a triclinic, P-1 space group. The fractional atomic coordinates and isotropic displacement parameters of these adducts are listed in Tables A1.18 to A1.23.

Table 4.44 Crystal structure data for molecular complexes of trithiocyanuric acid and 4, 4'-bipyridine with benzene **(10a)**, toluene **(10b)**, *p*-xylene **(10c)**, *o*-xylene **(10d)**, *m*-xylene **(10e)** and anthracene **(10f)**

	10a	10b	10c
Chemical formula	$C_{11}H_{10}N_4S_3$	$C_{23}H_{22}N_{12}S_6$	$C_{24}H_{24}N_8S_6$
Formula weight	294.41	658.89	616.87
Cell setting	Triclinic	Triclinic	Triclinic
Space group	P-1	P-1	P-1
a (Å)	7.019(1)	7.112(1)	7.282(1)
b (Å)	10.336(1)	10.489(1)	10.621(1)
c (Å)	10.748(1)	10.681(1)	10.648(1)
α (°)	63.79(1)	65.40(1)	66.30(1)
β (°)	75.77(1)	76.58(1)	76.53(1)
γ (°)	73.80(1)	73.05(1)	70.42(1)
Cell volume (Å³)	665.04(13)	687.35(13)	705.86(13)
Z	2	1	1
F(000)	304	340	320
ρ (Mg/m³)	1.47	1.592	1.451
μ, mm⁻¹	0.543	0.539	0.516
λ (Å)	0.7107	0.7107	0.7107
Crystal size (mm)	$0.26 \times 0.18 \times 0.31$	$0.25 \times 0.35 \times 0.30$	$0.20 \times 0.15 \times 0.15$
Diffractometer	Smart, CCD area detector	Smart, CCD area detector	Smart, CCD area detector
Radiation type	MoKα	MoKα	MoKα

Table 4.44 (*continued*)

Crystal-detector distance (cm)	5.0	5.0	5.0
Temperature (K)	293(2)	293(2)	293(2)
No. of measured reflections	2603	2887	2781
No. of independent reflections	1857	1928	1970
θ_{max} (°)	2 - 24	2 - 24	2 - 24
Range of *h, k, l*	-5 to 7	-7 to 7	-7 to 8
	-11 to 11	-11 to 9	-11 to 11
	-11 to 11	-11 to 5	-11 to 11
R_1	0.0350	0.0698	0.0555
wR_2, Goodness-of-fit (S)	0.0778, 1.181	0.1538, 1.253	0.1489, 1.163
No. of parameters refined	203	188	219
Max. $e\text{\AA}^{-3}$	0.193	0.535	0.253

Table 4.44 (*continued*)

	10d	10e	10f
Chemical formula	$C_{24}H_{24}N_8S_6$	$(C_3H_3N_3S_3){:}1.5(C_{10}H_8N_2){:}(C_8H_{10})$	$C_{23}H_{19}N_8S_6$
Formula weight	616.87	872.23	599.82
Cell setting	Triclinic	Triclinic	Triclinic
Space group	P-1	P-1	P-1
a (Å)	10.324(1)	10.359(1)	10.472(1)
b (Å)	11.615(1)	11.467(1)	11.419(1)
c (Å)	12.319(1)	18.412(1)	12.932(1)
α (°)	102.16(1)	83.65(1)	100.46(2)
β (°)	93.46(1)	75.00(1)	107.69(2)
γ (°)	90.68(1)	67.94(1)	111.28(2)
Cell volume ($\text{\AA}^3$)	1441.0(2)	1957.7(3)	1296.5(2)
Z	2	2	2
F(000)	640	902	618
ρ (Mg/m^3)	1.422	1.48	1.536
μ, mm^{-1}	0.505	0.553	0.559
λ (Å)	0.7107	0.7107	0.7107
Crystal size (mm)	0.30 × 0.25 × 0.20	0.25 × 0.35 × 0.20	0.10 × 0.25 × 0.10
Diffractometer	Smart, CCD area detector	Smart, CCD area detector	Smart, CCD area detector
Radiation type	MoKα	MoKα	MoKα
Crystal-detector distance (cm)	5.0	5.0	5.0
Temperature (K)	293(2)	293(2)	293(2)
No. of measured reflections	6134	7548	4996
No. of independent reflections	4109	5489	3556
θ_{max} (°)	2 - 24	2 - 24	2 - 24
Range of *h, k, l*	-11 to 9	-10 to 11	-11 to 9

Table 4.44 (*continued*)

	-12 to 12	-12 to 12	-11 to 12
	-10 to 13	-12 to 20	-13 to 14
R_1	0.0829	0.0575	0.0487
wR_2, Goodness-of-fit (S)	0.1929, 1.315	0.1315, 0.436	0.0983, 1.263
No. of parameters refined	344	478	334
Max. e$Å^{-3}$	0.985	0.561	0.422

4.8.1 Adduct of trithiocyanuric acid and 4,4'-bipyridyl from methanol solution

Co-crystallization of trithiocyanuric acid with 4,4'-bipyridyl from methanol solution gives a 2:1 hydrogen-bonded adduct containing the solvent of crystallization. The crystal structure of the adduct reveals the presence of intermolecular N-H···N hydrogen bonds between trithiocyanuric acid and the bipyridyl as shown in Figure 4.36.
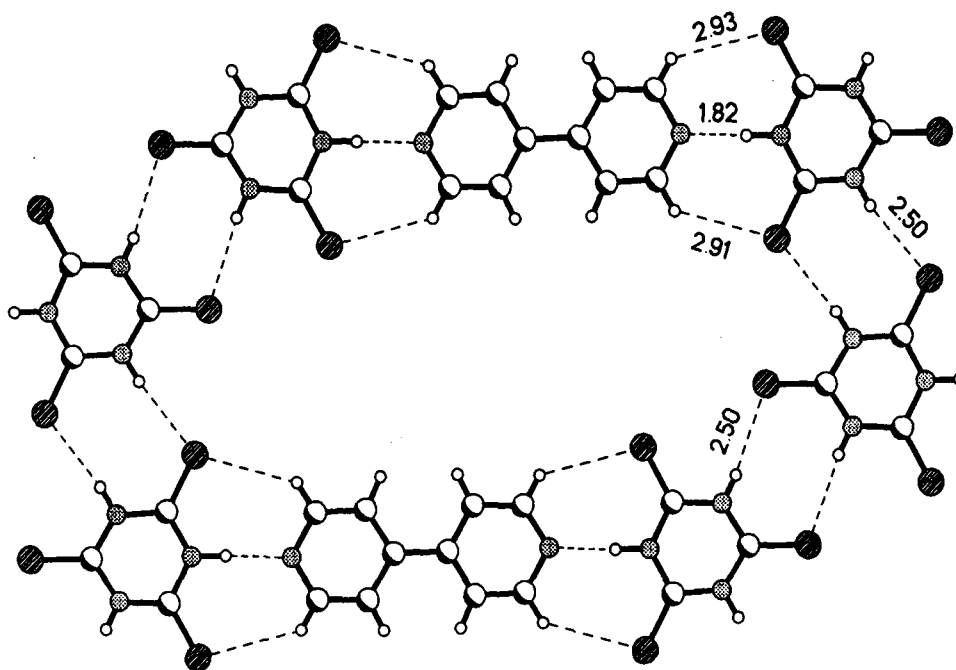
Figure 4.36: *Self-assembly of trithiocyanuric acid, 10 and 4,4'-bipyridyl forming a layered network with a cavity.*

This hydrogen-bonded structure has a cavity of 10Å in dimension, occupied by methanol molecules. These crystals were unstable under ambient conditions because of the evaporation of methanol.

4.8.2 Adduct of trithiocyanuric acid with 4,4'-bipyridyl and benzene

The 2:1 adduct of **10** with 4,4'-bipyridyl incorporating benzene was highly stable (**10a**). The molar ratio of benzene and bipyridyl was 1:1. These crystals also gave the same two-dimensional hydrogen-bonded structure as in Figure 4.36. The asymmetric unit of this adduct, **10a**, which consists of trithiocyanuric acid, 4,4'-bipyridyl and benzene is depicted in Figure 4.37.
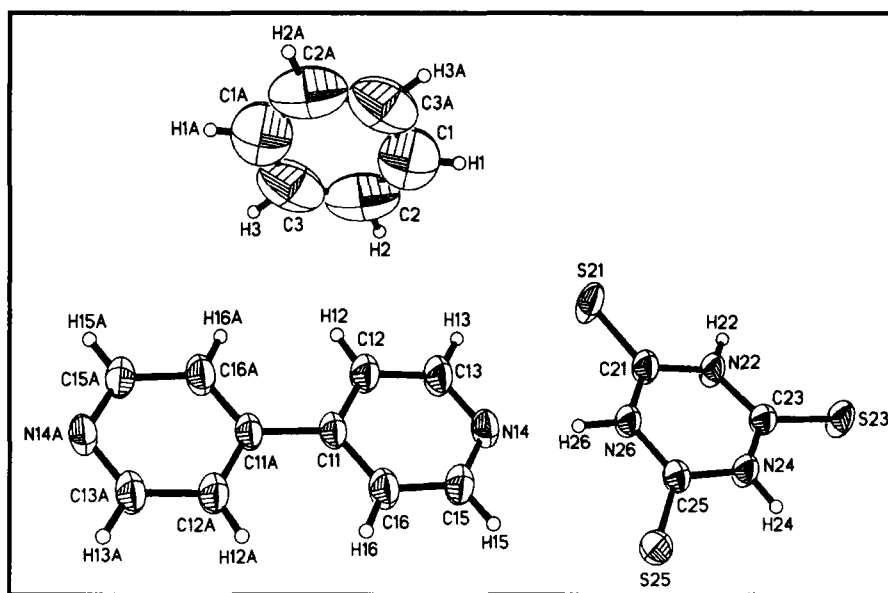
Figure 4.37: *An ORTEP drawing showing the asymmetric unit in the 2:1:1 adduct of trithiocyanuric acid, 4,4'-bipyridine and benzene, 10a.*

The intramolecular bond distances and angles of the adduct **10a** are given in Table 4.45 and the intermolecular, hydrogen bond interactions are given in Table 4.46.

135

Table 4.45 Bond lengths and angles for the benzene adduct, 10a

Moiety	Distance (Å)	Moiety	Angle (°)
S(25)-C(25)	1.644(3)	C(21)-N(26)-C(25)	123.7(2)
S(23)-C(23)	1.658(3)	C(12)-C(11)-C(16)	116.5(3)
S(21)-C(21)	1.661(3)	C(12)-C(11)-C(11)#1	121.7(3)
N(26)-C(21)	1.354(3)	C(16)-C(11)-C(11)#1	121.7(3)
N(26)-C(25)	1.365(3)	N(14)-C(15)-C(16)	123.4(3)
C(11)-C(12)	1.391(4)	C(13)-C(12)-C(11)	119.8(3)
C(11)-C(16)	1.394(4)	C(23)-N(24)-C(25)	125.3(2)
C(11)-C(11)#1	1.494(5)	C(15)-C(16)-C(11)	119.6(3)
C(15)-N(14)	1.330(4)	C(23)-N(22)-C(21)	125.1(2)
C(15)-C(16)	1.385(4)	C(15)-N(14)-C(13)	117.0(2)
C(12)-C(13)	1.375(4)	N(26)-C(25)-N(24)	115.4(2)
N(24)-C(23)	1.354(3)	N(26)-C(25)-S(25)	123.7(2)
N(24)-C(25)	1.380(3)	N(24)-C(25)-S(25)	120.9(2)
N(22)-C(23)	1.362(3)	N(24)-C(23)-N(22)	114.3(2)
N(22)-C(21)	1.373(3)	N(24)-C(23)-S(23)	123.6(2)
N(14)-C(13)	1.330(4)	N(22)-C(23)-S(23)	122.1(2)
C(2)-C(3)	1.351(10)	N(26)-C(21)-N(22)	116.1(2)
C(2)-C(1)	1.362(11)	N(26)-C(21)-S(21)	122.9(2)
C(1)-C(3)#2	1.372(11)	N(22)-C(21)-S(21)	121.0(2)
C(3)-C(1)#2	1.372(11)	N(14)-C(13)-C(12)	123.7(3)
Moiety	**Angle (°)**	C(3)-C(2)-C(1)	120.9(7)
C(2)-C(3)-C(1)#2	119.6(8)	C(2)-C(1)-C(3)#2	119.5(8)

Symmetry transformations used to generate equivalent atoms:
#1 −x+2,−y+1,−z
#2 −x+2,−y+1,−z−1

Table 4.46 Important hydrogen bond parameters for the benzene adduct, 10a

H-bond	D-H (Å)	H···A (Å)	D···A (Å)	D-H···A (°)
N(22)-H(22)···S(21)	0.84(3)	2.50(3)	3.324(2)	167(3)
N(24)-H(24)···S(23)	0.88(4)	2.44(4)	3.316(2)	175(4)
N(26)-H(26)···N(14)	0.97(5)	1.80(5)	2.769(4)	176(4)

The lengths of the C-N and C-S bonds of trithiocyanuric acid in 10a are ~ 1.4 and 1.6 Å, respectively. The C-C and C-N distances of the bipyridyl ring are ~ 1.4 and ~ 1.3 Å, respectively. The crystal structure of the adduct, 10a, is stabilized by the three-point recognition synthon (C-H···S− N-H···N− C-H···S) a centrosymmetric N-H···S hydrogen bonded dimeric coupling. The N-H···N bonds have hydrogen bond (H···N) distances of the order of ~2.77 Å. The weak C-H···S bonds (H···S, 2.91, 2.93Å)

between **10** and 4,4'-bipyridyl also stabilize the structure. The N-H···S hydrogen bonds between the trithiocyanuric acid molecules have H···S distances of ~ 2.5 Å. The donor···acceptor (D···A) distances are of the order of 3 Å. The N-H···S and N-H···N hydrogen bond angles are in the range of ~167 – 175° (see Table 4.46).

The three-dimensional structure of the 2:1 adduct of trithiocyanuric acid, **10** and 4,4'-bipyridyl with benzene is shown in Figure 4.38. The structure clearly reveals the presence of channels formed by the stacking of the layers with cavities. The channels accommodate benzene molecules as can be seen in Figure 4.38.
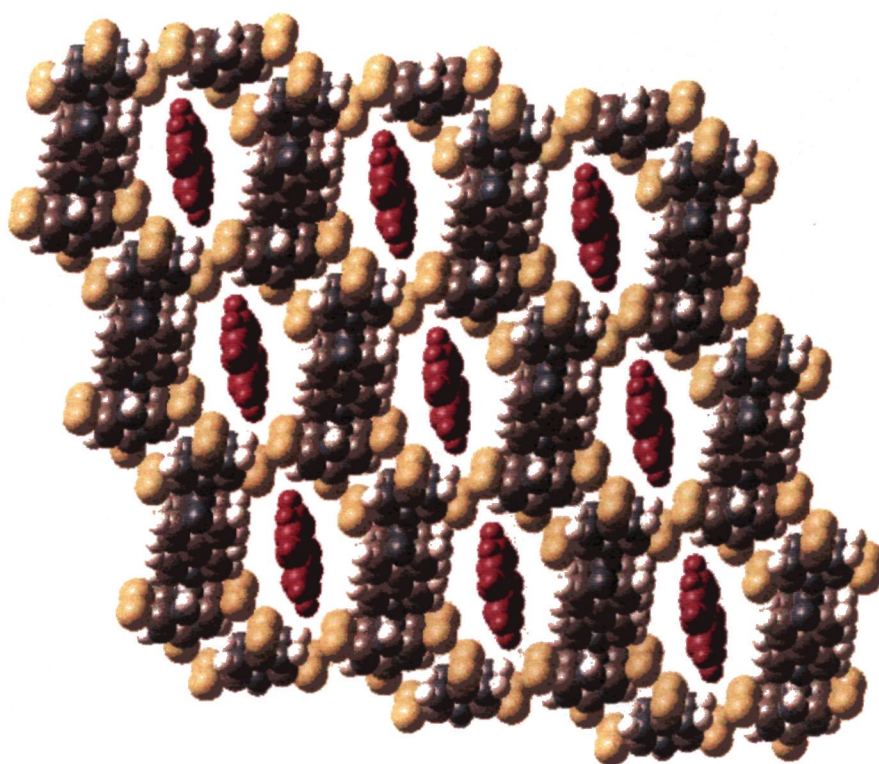
10a

Figure 4.38: *Three-dimensional structure of the 2:1 trithiocyanuric acid-4,4'-bipyridyl adduct, **10a** containing benzene in the channels*

An interesting feature is that the crystals were stable and heating up to 180°C or slightly higher did not destroy the crystals. Hence, we were interested to see whether the channel structure will remain intact even after the removal of benzene molecules to have a zeolite-type structure. In this connection, thermogravimetric analysis was carried out on the crystals of the adduct, **10a**.
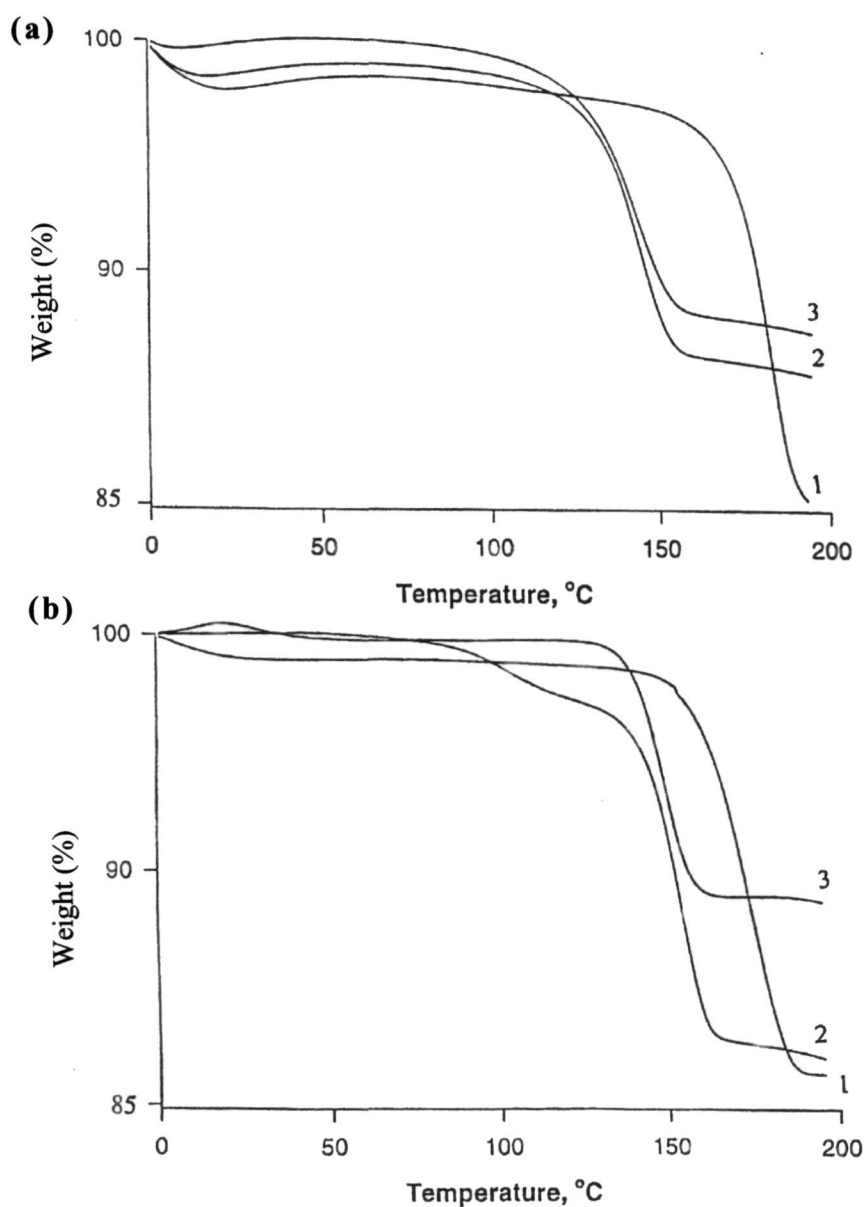
***Figure 4.39**: Thermogravimetric analysis of the adducts, (a) **10a** and (b) **10b**.*

The TGA curves are shown in Figure 4.39. In Figure 4.39(a), the TGA curve of the benzene adduct is shown, recorded at a heating rate of 2°C min⁻¹. We see that all the benzene (mass loss, 13%) is removed around 190°C, which is well above the boiling point of benzene (shown in curve 1). After the removal of benzene, the host crystals soaked in benzene for several hours were again subjected for TGA. These crystals showed a loss of benzene at a lower temperature (158°C). Furthermore, the amount of benzene in the channels is less by about 4% as can be seen from curve 2 in Figure 4.39a (see Table 4.47 for results of the TGA experiments). A repetition of this procedure showed that the removal of benzene continued to occur around the same temperature (158°C) with the same mass loss (curve 3 in Figure 4.39a). It thus appears that after the benzene in the channels of the initial adduct is removed, the empty channel can accommodate benzene which is removed around 158°C.

Table 4.47 Summary if the results of thermogravimetric analyses (TGA)						
Complex	First heating		Second heating		Third heating	
	Weight loss (%)	Temp (°C)	Weight loss (%)	Temp (°C)	Weight loss (%)	Temp (°C)
benzene	13.86(13.26)	192	9.70	158	9.24	157
toluene	14.81(15.26)	183	9.23	166	9.26	162
o-xyelne	16.16(17.18)	172	-	-	-	-
m-xylene	17.67(17.18)	131	-	-	-	-
p-xylene	12.24(12.15)	167	6.84	139	7.96	143

The crystal structure of the adduct, **10a** heated to 200°C (to remove all the benzene) gave a single crystal X-ray diffraction pattern, although the data were not sufficiently good to obtain the detailed structure. The dimensions of the unit cell remained essentially the same as those of the parent adduct. The unit cell parameters of the adduct with empty channels were: a=7.181, b=10.455, c=10.956Å, α=63.80°, β=77.70° and γ=75.82°. Encouraged by the findings, we were interested to see

whether the solvent molecules, benzene, in the channels can be exchangeable with other molecules and also the prevalence of shape selectivity. So, **10** and 4,4'-bipyridyl were co-crystallized in various solvents like toluene, different isomers of xylenes and anthracene.

4.8.3 Adduct of trithiocyanuric acid, 4,4'-bipyridyl and toluene

Thioimide, **10** and 4,4'-bipyridyl indeed formed a structure, **10b**, with toluene, identical to that of **10a**, with a three-dimensional channel structure (refer Figure 4.38) except that benzene molecules are replaced by the toluene molecules. The asymmetric unit of this adduct **10b** is depicted in Figure 4.40.
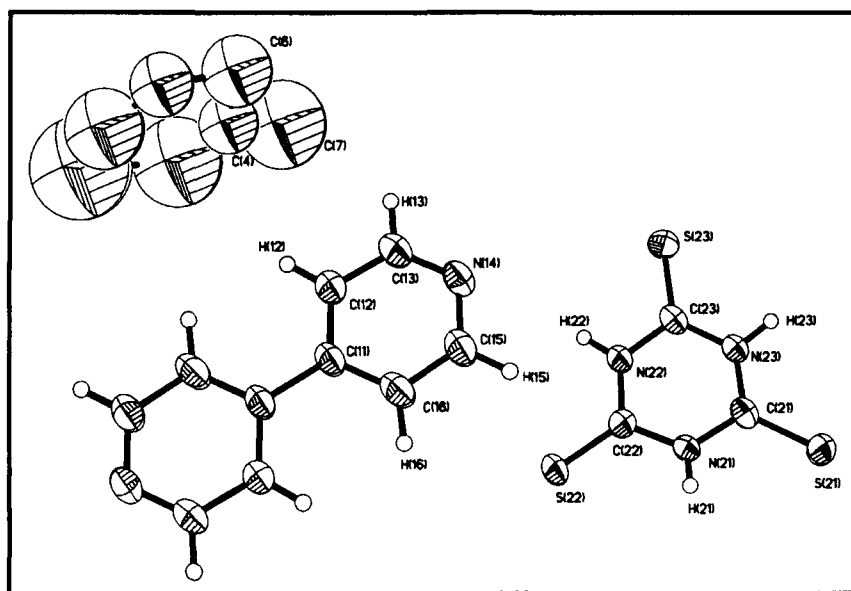
Figure 4.40: *An ORTEP drawing showing the asymmetric unit in the 2:1:1 adduct of trithiocyanuric acid, 4,4'-bipyridine and toluene, 10b.*

The geometries of the intra- and intermolecular (hydrogen bonding) interactions are listed in Tables 4.48 and 4.49, respectively.

Table 4.48 Bond lengths and angles for the toluene adduct, **10b**

Moiety	Distance (Å)	Moiety	Angle (°)
S(23)-C(23)	1.654(6)	C(21)-N(23)-C(23)	123.3(5)
S(22)-C(22)	1.651(6)	C(16)-C(11)-C(12)	116.5(6)
S(21)-C(21)	1.662(6)	C(16)-C(11)-C(11)#1	122.4(7)
N(23)-C(21)	1.357(8)	C(12)-C(11)-C(11)#1	121.1(7)
N(23)-C(23)	1.369(8)	N(14)-C(15)-C(16)	122.4(7)
C(11)-C(16)	1.387(9)	C(22)-N(22)-C(23)	125.4(5)
C(11)-C(12)	1.393(9)	C(13)-C(12)-C(11)	119.6(6)
C(11)-C(11)#1	1.493(11)	N(23)-C(23)-N(22)	115.8(5)
C(15)-N(14)	1.339(8)	N(23)-C(23)-S(23)	123.4(4)
C(15)-C(16)	1.393(9)	N(22)-C(23)-S(23)	120.9(5)
N(22)-C(22)	1.363(7)	C(11)-C(16)-C(15)	120.5(6)
N(22)-C(23)	1.378(7)	C(22)-N(21)-C(21)	126.1(5)
C(12)-C(13)	1.392(9)	N(21)-C(22)-N(22)	113.4(5)
N(21)-C(22)	1.361(8)	N(21)-C(22)-S(22)	122.8(5)
N(21)-C(21)	1.369(7)	N(22)-C(22)-S(22)	123.7(5)
N(14)-C(13)	1.327(9)	C(13)-N(14)-C(15)	117.5(6)
C(4)-C(7)	1.26(3)	N(23)-C(21)-N(21)	115.9(6)
C(4)-C(2)#2	1.39(3)	N(23)-C(21)-S(21)	122.6(4)
C(4)-C(6)#2	1.41(2)	N(21)-C(21)-S(21)	121.5(5)
C(4)-C(5)	1.47(3)	N(14)-C(13)-C(12)	123.5(7)
C(4)-C(6)	1.78(3)	C(7)-C(4)-C(2)#2	107(3)
C(3)-C(5)	1.35(4)	C(7)-C(4)-C(6)#2	158(2)
C(3)-C(6)	1.53(4)	C(2)#2-C(4)-C(6)#2	51(2)
C(3)-C(2)	1.97(5)	C(7)-C(4)-C(5)	71(2)
C(5)-C(6)	1.23(3)	C(2)#2-C(4)-C(5)	178(3)
C(5)-C(7)	1.60(3)	C(6)#2-C(4)-C(5)	131(2)
C(2)-C(6)	1.20(3)	C(7)-C(4)-C(6)	115(2)
C(2)-C(4)#2	1.39(3)	C(2)#2-C(4)-C(6)	138(2)
C(6)-C(4)#2	1.41(2)	C(6)#2-C(4)-C(6)	87(2)
Moiety	**Angle (°)**	C(5)-C(4)-C(6)	43.3(11)
C(2)-C(6)-C(4)#2	64(2)	C(5)-C(3)-C(6)	50(2)
C(5)-C(6)-C(4)#2	148(3)	C(5)-C(3)-C(2)	88(3)
C(2)-C(6)-C(3)	91(3)	C(6)-C(3)-C(2)	38(2)
C(5)-C(6)-C(3)	57(2)	C(6)-C(5)-C(3)	72(3)
C(4)#2-C(6)-C(3)	155(3)	C(6)-C(5)-C(4)	82(2)
C(2)-C(6)-C(4)	157(3)	C(3)-C(5)-C(4)	154(4)
C(5)-C(6)-C(4)	55(2)	C(6)-C(5)-C(7)	130(3)
C(4)#2-C(6)-C(4)	93(2)	C(3)-C(5)-C(7)	158(4)
C(3)-C(6)-C(4)	112(3)	C(4)-C(5)-C(7)	48.1(14)
C(4)-C(7)-C(5)	61(2)	C(6)-C(2)-C(4)#2	65(2)
C(2)-C(6)-C(5)	148(3)	C(6)-C(2)-C(3)	51(2)
		C(4)#2-C(2)-C(3)	116(3)

Symmetry transformations used to generate equivalent atoms:
#1 -x+2,-y,-z
#2 -x+2,-y,-z-1

Table 4.49 Important hydrogen bond parameters for the toluene adduct, **10b**

H-bond	D-H (Å)	H···A (Å)	D···A (Å)	D-H···A (°)
N(21)-H(21)···S(21)	0.79(7)	2.60(7)	3.370(6)	167(7)
N(22)-H(22)···S(22)	0.87(8)	2.47(8)	3.336(5)	180(8)
N(23)-H(23)···N(14)	0.91(11)	1.88(11)	2.788(8)	171(10)

The H···S and H···N bond distances in the hydrogen-bonded adduct **10b** are of the order of ~ 2.5 and ~ 1.9 Å. The N-H···S and N-H···N hydrogen bond angles vary between 170° - 180°. TG analysis on the crystals of this adduct reveals that the channel structure remains intact even in the absence of the toluene molecules. TGA of the toluene adduct (Figure 4.41b) shows a mass loss of 14.8% at 183°C (curve 1). The host crystal with the empty channels soaked in toluene and then subjected to TGA, gives a mass loss of 9.2% at 166°C (curve 2). A repetition of the procedure shows that the same mass loss occurs at 162°C (curve 3). The behaviour is similar to that of the benzene adduct (Table 4.47).

4.8.4. Adduct of trithiocyanuric acid, 4,4'-bipyridyl and p-xylene

Co-crystallization of **10** with 4,4'-bipyridyl from *p*-xylene yields a complex, **10c**, in a 2:1:1 ratio similar to that of **10a** and **10b**. The asymmetric unit of the adduct **10c** is depicted in Figure 4.41. The bond distances and angles of the adduct **10c** are given in Table 4.50. The unique hydrogen bond parameters are given in Table 4.51.

Table 4.50 Bond lengths and angles for the *p*-xylene adduct, **10c**

Moiety	Distance (Å)	Moiety	Angle (°)
C(11)-C(12)	1.54(2)	C(12)-C(11)-H(11C)	109.5(8)
C(11)-H(11C)	0.96	C(12)-C(11)-H(11B)	109.5(8)
C(11)-H(11B)	0.96	H(11C)-C(11)-H(11B)	109.5
C(11)-H(11A)	0.96	C(12)-C(11)-H(11A)	109.5(6)
C(12)-C(13)	1.35(2)	H(11C)-C(11)-H(11A)	109.5
C(12)-C(14)#1	1.42(2)	H(11B)-C(11)-H(11A)	109.5
C(13)-C(14)	1.39(2)	C(13)-C(12)-C(14)#1	115(2)
C(13)-H(13)	0.93	C(13)-C(12)-C(11)	124(2)

Table 4.50 (*continued*)

C(14)-C(12)#1	1.42(2)	C(14)#1-C(12)-C(11)	121(2)
C(14)-H(14)	0.93	C(12)-C(13)-C(14)	125(2)
C(21)-C(22)	1.48(2)	C(12)-C(13)-H(13)	117.5(10)
C(21)-H(21C)	0.96	C(14)-C(13)-H(13)	117.5(10)
C(21)-H(21B)	0.96	C(13)-C(14)-C(12)#1	120.0(14)
C(21)-H(21A)	0.96	C(13)-C(14)-H(14)	120.0(10)
C(22)-C(24)#2	1.36(2)	C(12)#1-C(14)-H(14)	120.0(12)
C(22)-C(23)	1.37(2)	C(22)-C(21)-H(21C)	109.5(12)
C(23)-C(24)	1.40(2)	C(22)-C(21)-H(21B)	109.5(9)
C(23)-H(223)	0.93	H(21C)-C(21)-H(21B)	109.5
C(24)-C(22)#2	1.36(2)	C(22)-C(21)-H(21A)	109.5(9)
C(24)-H(24)	0.93	H(21C)-C(21)-H(21A)	109.5
N(31)-C(31)	1.368(11)	H(21B)-C(21)-H(21A)	109.5
N(31)-C(32)	1.406(11)	C(24)#2-C(22)-C(23)	115(2)
N(31)-H(31)	0.86	C(24)#2-C(22)-C(21)	120(2)
S(31)-C(31)	1.634(10)	C(23)-C(22)-C(21)	126(2)
C(31)-N(33)	1.375(10)	C(22)-C(23)-C(24)	122(2)
S(32)-C(32)	1.624(9)	C(22)-C(23)-H(223)	119(2)
N(32)-C(32)	1.359(11)	C(24)-C(23)-H(223)	118.9(14)
N(32)-C(33)	1.373(11)	C(22)#2-C(24)-C(23)	123(2)
N(32)-H(32)	0.86	C(22)#2-C(24)-H(24)	118.6(14)
S(33)-C(33)	1.610(9)	C(23)-C(24)-H(24)	118.6(14)
N(33)-C(33)	1.414(11)	C(31)-N(31)-C(32)	127.0(8)
N(33)-H(33)	0.86	C(31)-N(31)-H(31)	116.5(5)
C(41)-C(46)	1.382(12)	C(32)-N(31)-H(31)	116.5(5)
C(41)-C(42)	1.397(13)	N(31)-C(31)-N(33)	114.4(8)
C(41)-C(41)#3	1.50(2)	N(31)-C(31)-S(31)	121.9(7)
C(42)-C(43)	1.373(12)	N(33)-C(31)-S(31)	123.6(7)
C(42)-H(42)	0.93	C(32)-N(32)-C(33)	128.5(9)
C(43)-N(44)	1.321(11)	C(32)-N(32)-H(32)	115.7(5)
C(43)-H(43)	0.93	C(33)-N(32)-H(32)	115.7(6)
N(44)-C(45)	1.343(12)	N(32)-C(32)-N(31)	111.8(8)
C(45)-C(46)	1.383(12)	N(32)-C(32)-S(32)	124.8(8)
C(45)-H(45)	0.93	N(31)-C(32)-S(32)	123.4(7)
C(46)-H(46)	0.93	C(31)-N(33)-C(33)	124.7(8)
C(51)-C(52)	1.340(12)	C(31)-N(33)-H(33)	117.7(5)
C(51)-C(56)	1.390(13)	C(33)-N(33)-H(33)	117.6(5)
C(51)-C(57)	1.504(12)	N(32)-C(33)-N(33)	113.1(8)
C(52)-C(53)	1.374(13)	N(32)-C(33)-S(33)	123.5(8)
C(52)-H(52)	0.93	N(33)-C(33)-S(33)	123.2(7)
C(53)-N(54)	1.342(12)	C(46)-C(41)-C(42)	116.3(8)
C(53)-H(53)	0.93	C(46)-C(41)-C(41)#3	122.0(12)
N(54)-C(55)	1.308(11)	C(42)-C(41)-C(41)#3	121.8(11)
C(55)-C(56)	1.372(12)	C(43)-C(42)-C(41)	119.2(9)
C(55)-H(55)	0.93	C(43)-C(42)-H(42)	120.4(6)
C(56)-H(56)	0.93	C(41)-C(42)-H(42)	120.4(6)
C(57)-C(512)	1.363(12)	N(44)-C(43)-C(42)	125.1(10)

143

Table 4.50 (*continued*)

C(57)-C(58)	1.409(12)	N(44)-C(43)-H(43)	117.4(6)
C(58)-C(59)	1.381(12)	C(42)-C(43)-H(43)	117.5(6)
C(58)-H(58)	0.93	C(43)-N(44)-C(45)	115.9(9)
C(59)-N(510)	1.307(11)	N(44)-C(45)-C(46)	123.1(10)
C(59)-H(59)	0.93	N(44)-C(45)-H(45)	118.4(6)
S(61)-C(61)	1.668(9)	C(46)-C(45)-H(45)	118.4(6)
C(61)-N(62)	1.360(11)	C(41)-C(46)-C(45)	120.4(10)
C(61)-N(63)	1.379(11)	C(41)-C(46)-H(46)	119.8(6)
N(61)-C(63)	1.365(10)	C(45)-C(46)-H(46)	119.8(6)
N(61)-C(62)	1.398(11)	C(52)-C(51)-C(56)	116.0(10)
N(61)-H(61)	0.86	C(52)-C(51)-C(57)	121.7(9)
S(62)-C(62)	1.623(9)	C(56)-C(51)-C(57)	122.3(9)
N(62)-C(63)	1.357(10)	C(51)-C(52)-C(53)	120.8(11)
N(62)-H(62)	0.86	C(51)-C(52)-H(52)	119.6(6)
C(62)-N(63)	1.366(10)	C(53)-C(52)-H(52)	119.6(7)
S(63)-C(63)	1.640(10)	N(54)-C(53)-C(52)	123.7(10)
N(63)-H(63)	0.86	N(54)-C(53)-H(53)	118.1(6)
S(71)-C(71)	1.662(10)	C(52)-C(53)-H(53)	118.1(7)
N(71)-C(73)	1.352(10)	C(55)-N(54)-C(53)	115.2(9)
N(71)-C(72)	1.373(10)	N(54)-C(55)-C(56)	124.3(10)
N(71)-H(71)	0.86	N(54)-C(55)-H(55)	117.9(6)
C(71)-N(73)	1.352(11)	C(56)-C(55)-H(55)	117.9(7)
C(71)-N(72)	1.372(10)	C(55)-C(56)-C(51)	120.0(10)
S(72)-C(72)	1.642(9)	C(55)-C(56)-H(56)	120.0(7)
C(72)-N(72)	1.380(11)	C(51)-C(56)-H(56)	120.0(6)
N(72)-H(72)	0.86	C(512)-C(57)-C(58)	115.5(9)
S(73)-C(73)	1.649(9)	C(512)-C(57)-C(51)	124.1(10)
N(73)-C(73)	1.357(11)	C(58)-C(57)-C(51)	120.3(9)
N(73)-H(73)	0.86	C(59)-C(58)-C(57)	118.7(10)
N(510)-C(511)	1.316(11)	C(59)-C(58)-H(58)	120.6(6)
C(511)-C(512)	1.384(13)	C(57)-C(58)-H(58)	120.6(6)
C(511)-H(511)	0.93	N(510)-C(59)-C(58)	124.1(10)
C(512)-H(512)	0.93	N(510)-C(59)-H(59)	117.9(6)
Moiety	**Angle (°)**	N(72)-C(71)-S(71)	122.0(7)
C(58)-C(59)-H(59)	117.9(6)	N(71)-C(72)-N(72)	114.3(8)
N(62)-C(61)-N(63)	114.0(8)	N(71)-C(72)-S(72)	122.5(7)
N(62)-C(61)-S(61)	123.1(8)	N(72)-C(72)-S(72)	123.2(7)
N(63)-C(61)-S(61)	122.9(7)	C(71)-N(72)-C(72)	124.1(8)
C(63)-N(61)-C(62)	125.0(8)	C(71)-N(72)-H(72)	118.0(5)
C(63)-N(61)-H(61)	117.5(5)	C(72)-N(72)-H(72)	118.0(5)
C(62)-N(61)-H(61)	117.5(5)	C(71)-N(73)-C(73)	126.0(8)
C(63)-N(62)-C(61)	127.2(8)	C(71)-N(73)-H(73)	117.0(5)
C(63)-N(62)-H(62)	116.4(5)	C(73)-N(73)-H(73)	117.0(5)
C(61)-N(62)-H(62)	116.4(5)	N(71)-C(73)-N(73)	114.5(8)
N(63)-C(62)-N(61)	114.4(8)	N(71)-C(73)-S(73)	122.8(8)
N(63)-C(62)-S(62)	120.8(7)	N(73)-C(73)-S(73)	122.7(8)
N(61)-C(62)-S(62)	124.8(7)	C(511)-N(510)-C(59)	118.0(9)

Table 4.50 (*continued*)

C(62)-N(63)-C(61)	125.2(8)	N(510)-C(511)-C(512)	121.9(10)
C(62)-N(63)-H(63)	117.4(5)	N(510)-C(511)-H(511)	119.0(6)
C(61)-N(63)-H(63)	117.4(5)	C(512)-C(511)-H(511)	119.0(6)
N(62)-C(63)-N(61)	114.2(9)	C(57)-C(512)-C(511)	121.7(10)
N(62)-C(63)-S(63)	122.6(7)	C(57)-C(512)-H(512)	119.2(6)
N(61)-C(63)-S(63)	123.2(7)	C(511)-C(512)-H(512)	119.2(7)
C(73)-N(71)-C(72)	125.9(8)	C(72)-N(71)-H(71)	117.0(5)
C(73)-N(71)-H(71)	117.1(5)	N(73)-C(71)-N(72)	115.1(9)
		N(73)-C(71)-S(71)	122.8(8)

Symmetry transformations used to generate equivalent atoms:
#1 -x,-y+1,-z+1   #2 -x+1,-y+1,-z   #3 -x+1,-y+1,-z+1
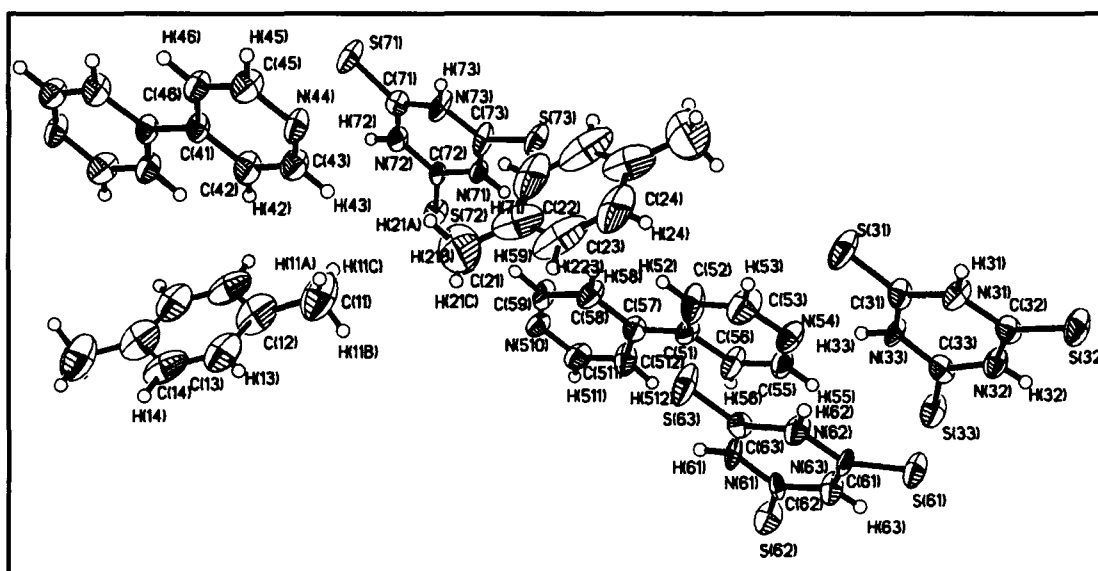
Figure 4.41: *An ORTEP drawing showing the asymmetric unit in the 2:1:1 adduct of trithiocyanuric acid, 4,4'-bipyridine and p-xylene, 10c.*

Table 4.51 Important hydrogen bond parameters for the *p*-xylene adduct, **10c**

H-bond	D-H (Å)	H···A (Å)	D···A (Å)	D-H···A (°)
N(31)-H(31)···S(32)	0.860(12)	2.541(10)	3.389(10)	169.0(8)
N(32)-H(32)···S(61)	0.861(11)	2.471(9)	3.310(9)	164.8(9)
N(33)-H(33)···N(54)	0.860(11)	1.928(12)	2.787(12)	177.6(11)
N(61)-H(61)···N(510)	0.860(10)	1.934(11)	2.793(11)	177.6(9)
N(62)-H(62)···S(71)	0.861(13)	2.551(10)	3.403(10)	170.5(8)
N(63)-H(63)···S(32)	0.860(11)	2.749(8)	3.596(8)	168.6(8)
N(71)-H(71)···S(73)	0.860(11)	2.475(9)	3.325(9)	169.9(9)
N(72)-H(72)···N(44)	0.860(10)	1.939(11)	2.799(11)	177.9(11)
N(73)-H(73)···S(63)	0.860(12)	2.479(9)	3.308(9)	162.4(8)
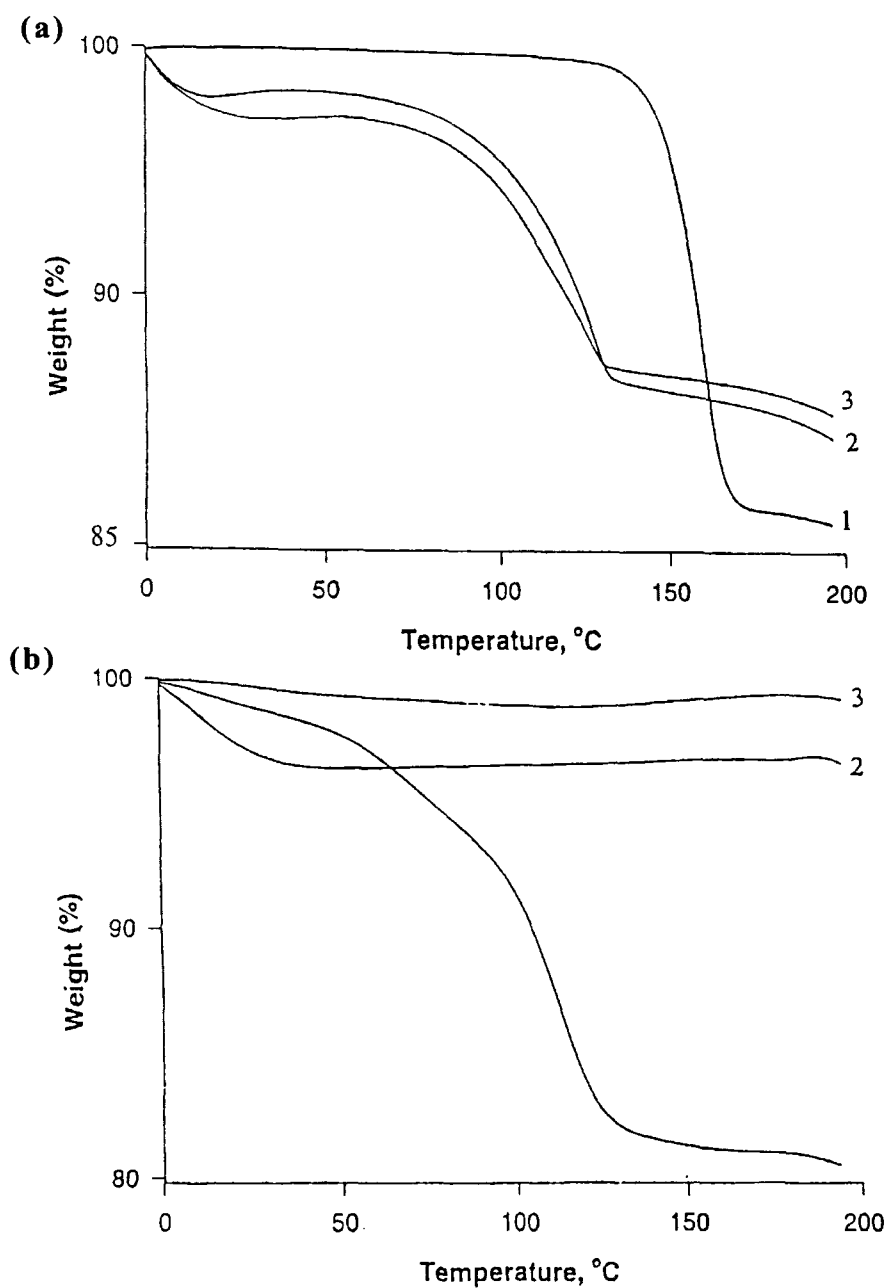
Figure 4.42: *Thermogravimetric analysis curves of the adducts (a) 10c and (b) 10e.*

TGA of the p-xylene adduct shows a mass loss (12.2%) due to the removal of p-xylene around 167°C (curve 1 in Figure 4.42a). After re-incorporation of p-xylene in the channels, the mass loss occurs around 139°C, but the magnitude of mass loss is

146

smaller (7%) as can be seen from curve 2 in Figure 4.42a. The temperature of decomposition and the mass loss remain the same in further cycling (curve 3 of Figure 4.42a).

4.8.5 Adduct of trithiocyanuric acid and 4,4'-bipyridyl with o- and m-xylenes

Unlike **10a-10c**, co-crystallization of 4,4'-bipyrdiyl from o- and m-xylenes

Figure 4.43: ORTEP diagrams showing the asymmetric units in the adducts of trithiocyanuric acid and 4,4'-bipyridine with (a) o-xylene, **10d** and (b) m-xylene, **10e**.

formed slightly different lattices (see unit cell dimensions in Table 4.44). These

adducts are labeled as **10d** and **10e**. The asymmetric unit of the adducts **10d** and **10e**

are depicted in Figure 4.43. The geometries of the intra- and intermolecular bonds for

the adducts **10d** and **10e** are listed in Tables 4.52 to 4.55.

Table 4.52 Bond lengths and angles for the *o*-xylene adduct, **10d**

Moiety	Distance (Å)	Moiety	Angle (°)
S(13)-C(13)	1.643(4)	C(12)-N(13)-C(13)	124.1(4)
S(11)-C(11)	1.647(4)	C(12)-N(13)-H(13)	118(4)
S(12)-C(12)	1.657(4)	C(13)-N(13)-H(13)	118(4)
N(13)-C(12)	1.358(5)	C(23)-C(21)-C(22)	115.4(4)
N(13)-C(13)	1.363(5)	C(23)-C(21)-C(21)#1	122.7(5)
N(13)-H(13)	0.84(6)	C(22)-C(21)-C(21)#1	121.9(5)
C(21)-C(23)	1.372(7)	C(11)-N(12)-C(13)	126.5(4)
C(21)-C(22)	1.391(7)	C(11)-N(12)-H(12)	119(3)
C(21)-C(21)#1	1.489(8)	C(13)-N(12)-H(12)	114(3)
N(12)-C(11)	1.346(5)	N(24)-C(25)-C(22)	123.5(5)
N(12)-C(13)	1.372(5)	N(24)-C(25)-H(25)	115(3)
N(12)-H(12)	0.78(4)	C(22)-C(25)-H(25)	122(3)
C(25)-N(24)	1.330(6)	N(13)-C(13)-N(12)	114.7(4)
C(25)-C(22)	1.381(7)	N(13)-C(13)-S(13)	123.6(3)
C(25)-H(25)	0.94(6)	N(12)-C(13)-S(13)	121.6(3)
N(11)-C(12)	1.368(5)	C(12)-N(11)-C(11)	125.8(4)
N(11)-C(11)	1.364(6)	C(12)-N(11)-H(11)	118(3)
N(11)-H(11)	0.74(4)	C(11)-N(11)-H(11)	116(3)
N(24)-C(21)	1.316(6)	N(13)-C(12)-N(11)	115.4(4)
C(23)-C(21)	1.372(7)	N(13)-C(12)-S(12)	123.1(3)
C(23)-H(23)	0.85(6)	N(11)-C(12)-S(12)	121.6(3)
C(22)-H(22)	0.88(6)	C(21)-N(24)-C(25)	116.4(4)
C(21)-H(21)	0.86(8)	C(21)-C(23)-C(21)	121.0(5)
C(4)-C(1)#2	1.39(3)	C(21)-C(23)-H(23)	118(4)
C(4)-C(5)	1.95(5)	C(21)-C(23)-H(23)	122(4)
C(4)-C(3)	1.91(5)	N(12)-C(11)-N(11)	113.4(4)
C(3)-C(2)	1.27(3)	N(12)-C(11)-S(11)	124.4(3)
C(3)-C(1)#2	1.38(4)	N(11)-C(11)-S(11)	122.1(3)
C(3)-C(7)	1.96(10)	C(25)-C(22)-C(21)	120.0(5)
C(5)-C(7)#2	1.04(13)	C(25)-C(22)-H(22)	117(4)
C(5)-C(2)#2	1.22(2)	C(21)-C(22)-H(22)	123(4)
C(5)-C(1)#2	1.85(5)	N(24)-C(21)-C(23)	123.7(5)
C(1)-C(3)#2	1.38(4)	N(24)-C(21)-H(21)	119(5)
C(1)-C(2)#2	1.41(2)	C(23)-C(21)-H(21)	117(5)
C(1)-C(4)#2	1.39(3)	C(1)#2-C(4)-C(5)	65(2)
C(1)-C(2)	1.61(2)	C(1)#2-C(4)-C(3)	45.9(13)
C(1)-C(5)#2	1.85(5)	C(5)-C(4)-C(3)	111(2)
C(1)-C(1)#2	1.83(3)	C(2)-C(3)-C(1)#2	64.1(11)

148

Table 4.52 (*continued*)

Moiety	Distance	Moiety	Angle (°)
C(2)-C(5)#2	1.22(2)	C(2)-C(3)-C(4)	111(3)
C(2)-C(7)	1.36(6)	C(1)#2-C(3)-C(4)	46(2)
C(2)-C(1)#2	1.41(2)	C(2)-C(3)-C(7)	44(3)
C(7)-C(5)#2	1.04(13)	C(1)#2-C(3)-C(7)	107(3)

Moiety	Angle (°)	Moiety	Angle (°)
		C(4)-C(3)-C(7)	153(3)
C(4)#2-C(1)-C(1)#2	160(3)	C(7)#2-C(5)-C(2)#2	74(5)
C(2)-C(1)-C(1)#2	47.6(11)	C(7)#2-C(5)-C(1)#2	131(5)
C(5)#2-C(1)-C(1)#2	88(2)	C(2)#2-C(5)-C(1)#2	59(2)
C(5)#2-C(2)-C(7)	47(6)	C(7)#2-C(5)-C(4)	166(6)
C(5)#2-C(2)-C(3)	144(3)	C(2)#2-C(5)-C(4)	102(3)
C(7)-C(2)-C(3)	96(6)	C(1)#2-C(5)-C(4)	43(2)
C(5)#2-C(2)-C(1)#2	155(3)	C(3)#2-C(1)-C(2)#2	54(2)
C(7)-C(2)-C(1)#2	156(6)	C(3)#2-C(1)-C(4)#2	88(3)
C(3)-C(2)-C(1)#2	62(3)	C(2)#2-C(1)-C(4)#2	142(3)
C(5)#2-C(2)-C(1)	80(3)	C(3)#2-C(1)-C(2)	160(3)
C(7)-C(2)-C(1)	126(6)	C(2)#2-C(1)-C(2)	105.6(13)
C(3)-C(2)-C(1)	136(3)	C(4)#2-C(1)-C(2)	112(3)
C(1)#2-C(2)-C(1)	74.4(13)	C(3)#2-C(1)-C(5)#2	160(2)
C(5)#2-C(7)-C(2)	59(4)	C(2)#2-C(1)-C(5)#2	146(2)
C(5)#2-C(7)-C(3)	99(4)	C(4)#2-C(1)-C(5)#2	72(2)
C(2)-C(7)-C(3)	40(3)	C(2)-C(1)-C(5)#2	40.4(14)
C(2)#2-C(1)-C(1)#2	58.0(12)	C(3)#2-C(1)-C(1)#2	112(3)

Symmetry transformations used to generate equivalent atoms:
#1 -x+2,-y,-z
#2 -x,-y,-z+1

Table 4.53 Bond lengths and angles for the *m*-xylene adduct, **10e**

Moiety	Distance (Å)	Moiety	Angle (°)
S(33)-C(33)	1.651(10)	C(33)-N(33)-C(31)	122.8(8)
S(22)-C(22)	1.656(10)	C(22)-N(23)-C(23)	126.2(9)
S(31)-C(31)	1.651(10)	C(32)-N(32)-C(33)	125.5(8)
S(32)-C(32)	1.620(10)	C(21)-N(22)-C(23)	126.7(8)
S(21)-C(21)	1.646(10)	N(33)-C(33)-N(32)	117.0(8)
S(23)-C(23)	1.626(10)	N(33)-C(33)-S(33)	122.5(7)
N(33)-C(33)	1.360(11)	N(32)-C(33)-S(33)	120.5(7)
N(33)-C(31)	1.365(12)	C(19)-N(110)-C(111)	117.1(9)
N(23)-C(22)	1.363(11)	N(22)-C(23)-N(23)	112.5(8)
N(23)-C(23)	1.378(12)	N(22)-C(23)-S(23)	124.0(7)
N(32)-C(32)	1.366(11)	N(23)-C(23)-S(23)	123.5(8)
N(32)-C(33)	1.375(11)	C(22)-N(21)-C(21)	124.6(8)
N(22)-C(21)	1.357(12)	N(32)-C(32)-N(31)	112.6(8)
N(22)-C(23)	1.371(11)	N(32)-C(32)-S(32)	124.6(8)
N(110)-C(19)	1.313(12)	N(31)-C(32)-S(32)	122.7(7)
N(110)-C(111)	1.327(13)	N(14)-C(15)-C(16)	123.2(10)
N(21)-C(22)	1.353(11)	C(15)-C(16)-C(11)	120.8(10)
N(21)-C(21)	1.371(11)	C(13)-N(14)-C(15)	116.5(9)
C(32)-N(31)	1.388(11)	C(111)-C(112)-C(17)	119.8(10)

Table 4.53 (*continued*)

C(15)-N(14)	1.339(13)	N(21)-C(22)-N(23)	115.2(9)
C(15)-C(16)	1.362(13)	N(21)-C(22)-S(22)	123.2(7)
C(16)-C(11)	1.378(13)	N(23)-C(22)-S(22)	121.6(7)
N(14)-C(13)	1.331(12)	C(16)-C(11)-C(12)	116.4(9)
C(112)-C(111)	1.347(14)	C(16)-C(11)-C(17)	122.8(9)
C(112)-C(17)	1.374(14)	C(12)-C(11)-C(17)	120.7(9)
C(11)-C(12)	1.381(13)	C(31)-N(31)-C(32)	126.0(8)
C(11)-C(17)	1.498(13)	C(11)-C(12)-C(13)	119.7(10)
N(31)-C(31)	1.375(11)	C(19)-C(18)-C(17)	119.3(10)
C(12)-C(13)	1.386(14)	C(112)-C(17)-C(18)	116.7(9)
C(18)-C(19)	1.365(14)	C(112)-C(17)-C(11)	123.0(9)
C(18)-C(17)	1.387(13)	C(18)-C(17)-C(11)	120.3(10)
C(7)-C(1)	1.58(3)	N(33)-C(31)-N(31)	115.9(8)
C(4)-C(3)	1.15(4)	N(33)-C(31)-S(31)	123.3(7)
C(4)-C(5)	1.18(4)	N(31)-C(31)-S(31)	120.9(8)
C(2)-C(1)	1.43(3)	N(110)-C(111)-C(112)	123.7(11)
C(2)-C(3)	1.88(5)	N(22)-C(21)-N(21)	114.8(9)
C(1)-C(6)	1.43(4)	N(22)-C(21)-S(21)	123.0(8)
C(5)-C(8)	1.21(6)	N(21)-C(21)-S(21)	122.2(8)
C(5)-C(6)	1.91(6)	N(110)-C(19)-C(18)	123.4(10)

Moiety	**Angle (°)**	N(14)-C(13)-C(12)	123.3(10)
C(4)-C(3)-C(2)	81(5)	C(3)-C(4)-C(5)	163(8)
C(4)-C(5)-C(8)	156(8)	C(1)-C(2)-C(3)	139(2)
C(4)-C(5)-C(6)	120(4)	C(6)-C(1)-C(2)	117(3)
C(8)-C(5)-C(6)	84(6)	C(6)-C(1)-C(7)	131(4)
C(1)-C(6)-C(5)	100(3)	C(2)-C(1)-C(7)	112(2)

Table 4.54 Important hydrogen bond parameters for the *o*-xylene adduct, **10d**

H-bond	D-H (Å)	H···A (Å)	D···A (Å)	D-H···A (°)
N(11)-H(11)···S(12)	0.75(5)	2.66(5)	3.397(4)	173(5)
N(12)-H(12)···S(11)	0.78(4)	2.58(4)	3.360(4)	173(4)
N(13)-H(13)···N(24)	0.84(7)	1.96(7)	2.796(6)	177(6)

Table 4.55 Important hydrogen bond parameters for the *m*-xylene adduct, **10e**

H-bond	D-H (Å)	H···A (Å)	D···A (Å)	D-H···A (°)
N(21)-H(21A)···N(14)	0.859(12)	1.983(13)	2.842(13)	178.9(10)
N(22)-H(22A)···S(31)	0.860(12)	2.528(9)	3.381(9)	171.8(9)
N(23)-H(23A)···S(22)	0.859(12)	2.482(9)	3.330(9)	169.1(9)
N(31)-H(31A)···S(21)	0.860(12)	2.511(9)	3.346(9)	163.9(9)
N(32)-H(32A)···S(32)	0.860(11)	2.430(8)	3.284(8)	172.0(9)
N(33)-H(33A)···N(110)	0.860(12)	1.885(12)	2.745(12)	177.8(10)

Although, the basic recognition pattern and cavity structure is similar to **10a-10c**, the two-dimensional network shows expanded cavity as shown in Figure 4.44 for the

adduct of **10e** obtained from *m*-xylene. The corresponding three-dimensional channel structure is given in Figure 4.45.

In addition, an interesting feature is that the crystals of **10d** and **10e** appear to be unstable with the removal of the corresponding solvent molecules as they could not be re-incorporated after their removal from the as-prepared crystals.
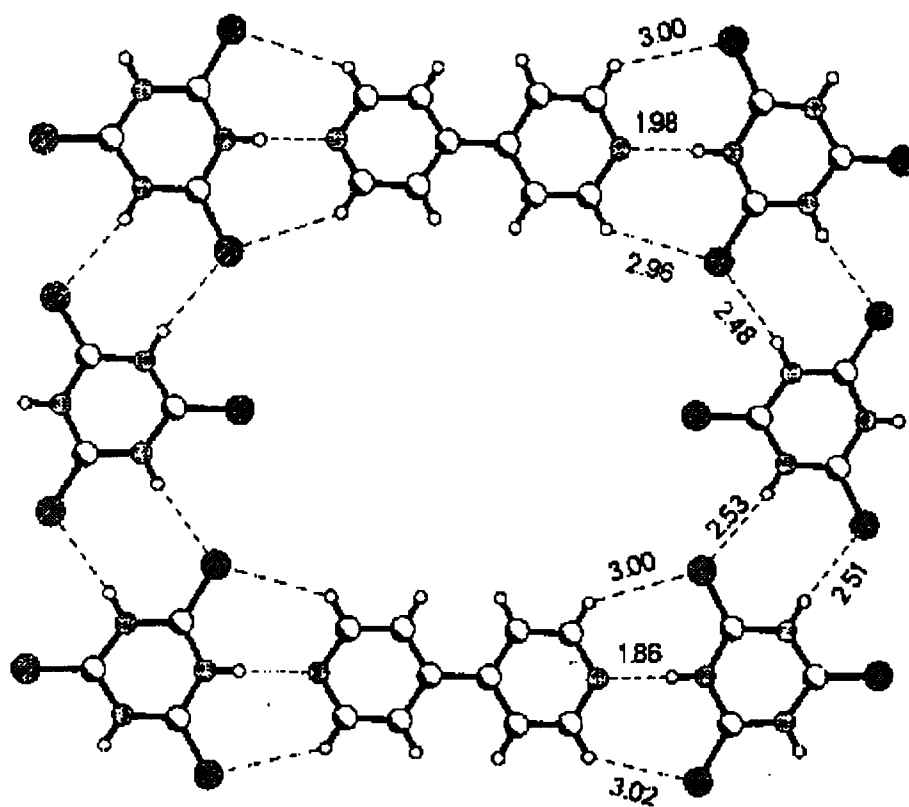
10e

Figure 4.44: *Two-dimensional arrangement of the molecules of 10 and 4,4'-bipyridyl in the complex, 10e, with m-xylene.*
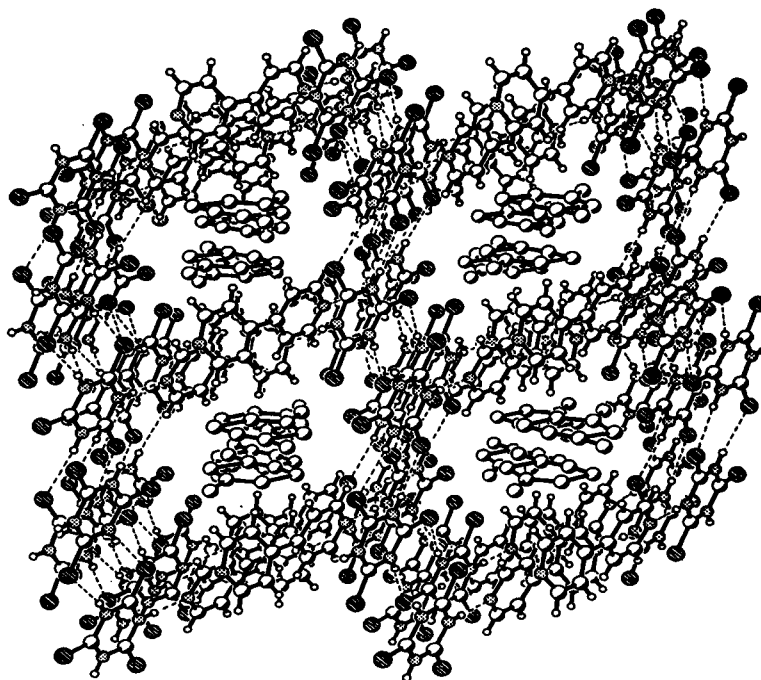
10e

Figure 4.45: *Three-dimensional arrangement of molecules in the crystal structure of 10e shown channels occupied by m-xylene molecules.*

Typical TGA data is shown for the *m*-xylene adduct in Figure 4.42b. The as-prepared adduct of *m*-xylene undergoes a mass loss (17%) at 131°C (curve 1). However *m*-xylene could not be put back in the channels even after soaking the host crystals with empty channels in *m*-xylene for long periods. This is confirmed by the TGA curves 2 and 3 in Figure 4.42b which shows no mass loss corresponding to m-xylene (Table 4.47). The behaviour of the *o*-xylene adduct was similar to that of the *m*-xylene adduct, in that *o*-xylene could not be reintroduced into the channels once it was removed at 172°C from the as-prepared adduct. Clearly, there is some selectivity in the channels of the trithiocyanuric acid-4,4'-bipyridyl adduct. This can be understood from

the obvious differences in the shapes of *p*-, *o*- and *m*-xylenes. In *p*-xylene, the two

methyl groups are symmetrically positioned and favour the ready re-incorporation into

the channels of the host crystal. This is not the case in the other two isomers.

Accordingly, the empty channels of the trithiocyanuric acid-4,4'-bipyridyl adduct only

take in *p*-xylene from a mixture of the three xylene isomers. Furthermore, no crystals

were obtained when mesitylene is the solvent of crystallization to form an adduct

between **10** and 4,4'-bipyridyl and supports the shape selectivity of the channels

towards guest molecules.

4.8.6 Adduct of trithiocyanuric acid and 4,4'-bipyridyl with anthracene

In further continuation of the work, we intended to accommodate larger

molecules like naphthalene and anthracene in the channels of the adduct of **10** and

4,4'-bipyridyl. We present here, the results obtained with anthracene. **10** and 4,4'-

bipyridyl upon co-crystallization with anthracene from methanol solution yields a

structure, **10f**, the asymmetric unit of which is depicted in Figure 4.46.
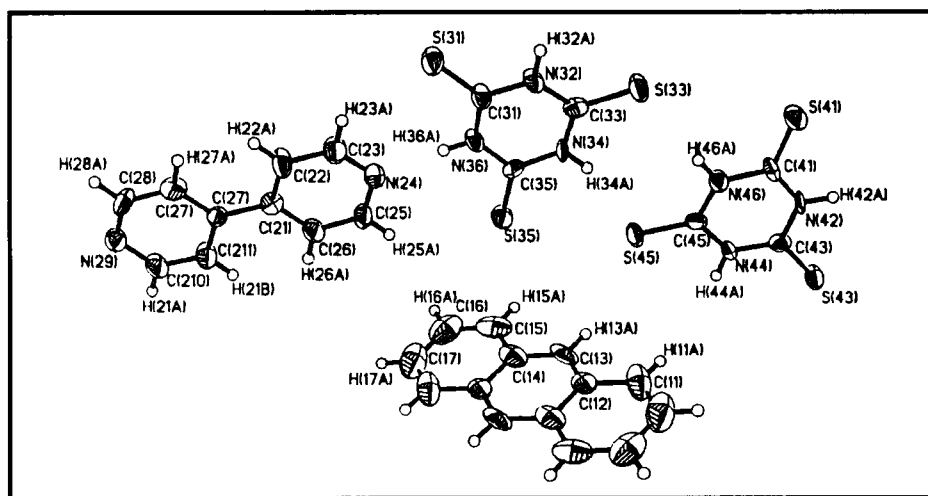
Figure 4.46: ORTEP diagram showing the asymmetric unit in the adducts of trithiocyanuric acid, 4,4'-bipyridine and anthracene, 10f.

The molecules of **10** and bipyridyl form a hexagonal network with channels in three-dimensional arrangement, which are being occupied by anthracene molecules (see Figure 4.47). The three-dimensional structure of the adduct of trithiocyanuric acid and 4,4'-bipyridyl with anthracene is shown in Figure 4.47. It is seen that trithiocyanuric acid and bipyridyl form channels that accommodate anthracene. The bond lengths and angles are listed in Table 4.56. The unique hydrogen bond parameters are listed in Table 4.57.
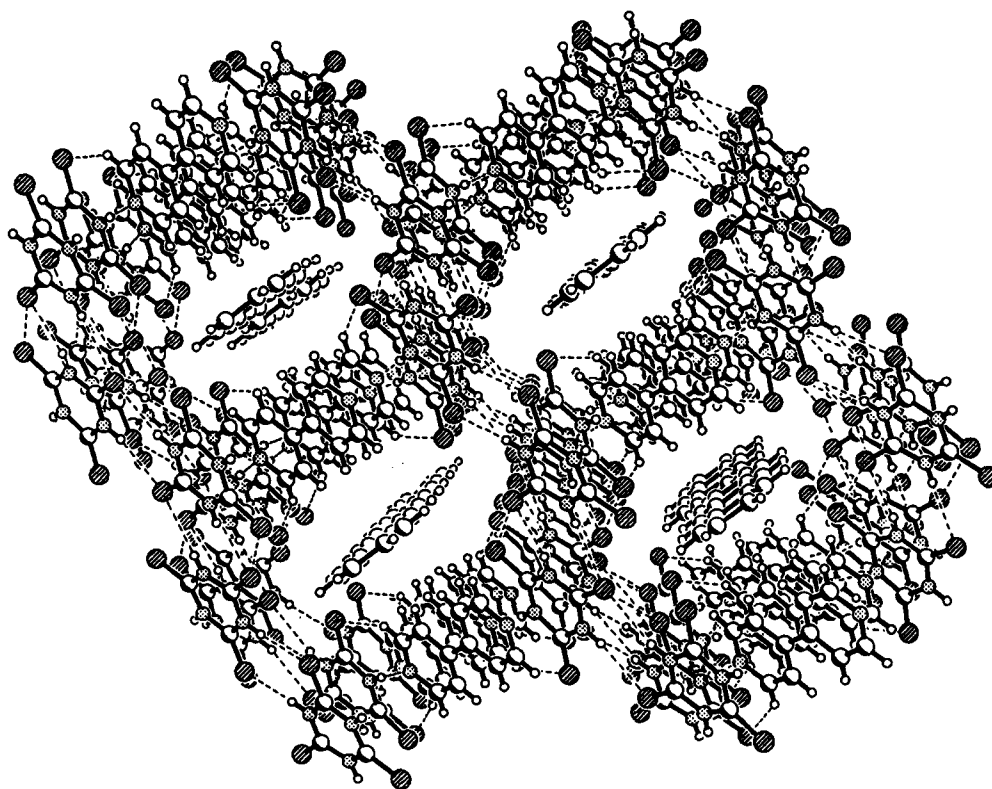
10f

Figure 4.47: Three-dimensional structure of adduct of trithiocyanuric acid and 4,4'-bipyridine with anthracene (10f) in the channels.

Table 4.56 Bond lengths and angles for the anthracene adduct, **10f**

Moiety	Distance (Å)	Moiety	Angle (°)
S(43)-C(43)	1.661(10)	C(45)-N(44)-C(43)	125.1(8)
S(41)-C(41)	1.648(10)	C(43)-N(42)-C(41)	124.1(8)
S(35)-C(35)	1.642(9)	C(31)-N(36)-C(35)	125.3(8)
S(45)-C(45)	1.655(10)	C(45)-N(46)-C(41)	126.0(9)
S(31)-C(31)	1.632(10)	C(33)-N(34)-C(35)	126.5(8)
S(33)-C(33)	1.663(10)	C(33)-N(32)-C(31)	126.7(8)
N(44)-C(45)	1.360(12)	C(26)-C(21)-C(22)	116.5(9)
N(44)-C(43)	1.368(12)	C(26)-C(21)-C(27)	123.2(9)
N(42)-C(43)	1.365(12)	C(22)-C(21)-C(27)	120.3(9)
N(42)-C(41)	1.367(12)	N(34)-C(35)-N(36)	114.0(8)
N(36)-C(31)	1.371(12)	N(34)-C(35)-S(35)	123.4(7)
N(36)-C(35)	1.377(12)	N(36)-C(35)-S(35)	122.6(7)
N(46)-C(45)	1.352(12)	C(211)-C(27)-C(27)	115.6(9)
N(46)-C(41)	1.377(12)	C(211)-C(27)-C(21)	122.5(9)
N(34)-C(33)	1.348(11)	C(27)-C(27)-C(21)	121.8(9)
N(34)-C(35)	1.376(12)	N(34)-C(33)-N(32)	113.7(8)
N(32)-C(33)	1.366(12)	N(34)-C(33)-S(33)	122.0(7)
N(32)-C(31)	1.370(12)	N(32)-C(33)-S(33)	124.2(7)
C(21)-C(26)	1.378(14)	N(46)-C(45)-N(44)	114.4(8)
C(21)-C(22)	1.382(13)	N(46)-C(45)-S(45)	123.8(7)
C(21)-C(27)	1.495(13)	N(44)-C(45)-S(45)	121.8(7)
C(27)-C(211)	1.377(13)	C(210)-N(29)-C(28)	116.6(9)
C(27)-C(27)	1.389(14)	N(29)-C(210)-C(211)	122.2(10)
N(29)-C(210)	1.328(13)	N(29)-C(28)-C(27)	124.3(10)
N(29)-C(28)	1.333(13)	N(42)-C(43)-N(44)	115.7(8)
C(210)-C(211)	1.379(14)	N(42)-C(43)-S(43)	122.5(8)
C(28)-C(27)	1.385(14)	N(44)-C(43)-S(43)	121.8(7)
C(26)-C(25)	1.386(14)	C(21)-C(26)-C(25)	120.2(10)
N(24)-C(23)	1.308(13)	C(23)-N(24)-C(25)	116.7(9)
N(24)-C(25)	1.338(12)	C(210)-C(211)-C(27)	122.0(10)
C(22)-C(23)	1.403(14)	N(24)-C(25)-C(26)	123.2(10)
C(13)-C(12)	1.39(2)	N(42)-C(41)-N(46)	114.6(8)
C(13)-C(14)	1.41(2)	N(42)-C(41)-S(41)	124.6(7)
C(15)-C(16)	1.38(2)	N(46)-C(41)-S(41)	120.8(8)
C(15)-C(14)	1.44(2)	C(21)-C(22)-C(23)	119.3(10)
C(14)-C(12)#1	1.43(2)	C(28)-C(27)-C(27)	119.2(9)
C(12)-C(14)#1	1.43(2)	N(36)-C(31)-N(32)	113.7(8)
C(12)-C(11)	1.44(2)	N(36)-C(31)-S(31)	124.6(7)
C(17)-C(11)#1	1.34(2)	N(32)-C(31)-S(31)	121.7(8)
C(17)-C(16)	1.41(2)	N(24)-C(23)-C(22)	123.9(10)
C(11)-C(17)#1	1.34(2)	C(12)-C(13)-C(14)	121.1(11)

Moiety	Angle (°)		
		C(16)-C(15)-C(14)	119.8(13)
C(14)#1-C(12)-C(11)	118.4(14)	C(13)-C(14)-C(12)#1	119.3(12)
C(11)#1-C(17)-C(16)	120(2)	C(13)-C(14)-C(15)	122.1(12)
C(15)-C(16)-C(17)	121(2)	C(12)#1-C(14)-C(15)	118.5(12)
C(17)#1-C(11)-C(12)	122(2)	C(13)-C(12)-C(14)#1	119.5(11)

Table 4.56 (*continued*)   C(13)-C(12)-C(11)   121.9(12)

Symmetry transformations used to generate equivalent atoms:
#1: -x+2,-y+2,-z+2

Table 4.57 Important hydrogen bond parameters for the anthracene adduct, **10f**

H-bond	D-H (Å)	H···A (Å)	D···A (Å)	D-H···A (°)
N(32)-H(32A)···S(33)	0.860(13)	2.561(10)	3.410(10)	169.6(9)
N(34)-H(34A)···S(45)	0.860(12)	2.476(10)	3.306(10)	162.6(10)
N(36)-H(36A)···N(24)	0.860(13)	1.969(13)	2.829(13)	177.4(12)
N(42)-H(42A)···N(29)	0.860(12)	1.939(12)	2.798(12)	178.7(12)
N(44)-H(44A)···S(43)	0.860(14)	2.566(10)	3.408(10)	166.5(9)
N(46)-H(46A)···S(33)	0.860(14)	2.776(10)	3.634(10)	174.6(11)

The three-dimensional channels of the organic porous solid formed by the supramolecular hydrogen-bonded assembly of trithiocyanuric acid and 4,4'-bipyridyl can accommodate aromatic molecules like benzene, toluene, p-xylene and anthracene. This porous solid is thermally stable up to 200°C and exhibits selectivity with respect to the xylene isomers. The channels do not accommodate mesitylene.

4.9 A hybrid layered compound formed by silver sheets with cyanuric acid as the spacer molecule

During the course of our investigations of supramolecular assemblies of cyanuric acid, we have studied the role of hydrogen bonding interactions as steering forces in the presence of strong metal-ligand interactions. We have isolated a novel silver compound possessing two-dimensional silver sheets with the cyanuric acid molecules in the interlayer space, forming linear hydrogen-bonded chains. This compound of composition $Ag_2.CA$ (CA: cyanuric acid), is a unique organic-inorganic hybrid with novel electrical properties. The asymmetric unit of the compound is shown in Figure 4.48.
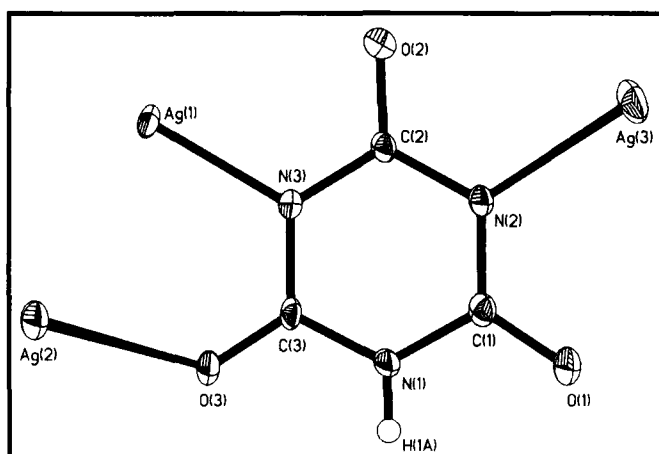
Figure 4.48: *ORTEP drawing of silver-cyanurate complex*

This silver-cyanurate complex crystallizes in a C2/c space group. Crystal structure data are given in Table 4.58. The fractional atomic coordinates and isotropic displacement parameters are listed in Table A1.24.

Table 4.58 Crystal structure data for silver-cyanurate, Ag_2CA

Chemical formula	$C_3H_1N_3O_3Ag_2$
Formula weight	342.81
Cell setting	monoclinic
Space group	C2/c
a (Å)	12.726(1)
b (Å)	13.064(1)
c (Å)	6.623(1)
α (°)	90
β (°)	97.350(1)
γ (°)	90
Cell volume (Å^3)	1092.0(2)
Z	8
F(000)	1264
ρ (Mg/m^3)	4.17
μ, mm^{-1}	7.114
λ (Å)	0.7107
Crystal size (mm)	0.35 × 0.25 × 0.20
Crystal color	Colorless
Diffractometer	Smart, CCD area detector
Radiation type	$MoK\alpha$
Crystal-detector distance(cm)	5.0

Table 4.58 (*continued*)

Temperature (K)	293(2)
No. of measured reflections	2266
No. of independent reflections	785
θ_{max} (°)	2 - 24
Range of *h, k, l*	-13 to 14
	-11 to 14
	-6 to 7
R	0.0351
R_w	0.0831
S	1.201
No. of parameters refined	103
Max. $eÅ^{-3}$	1.602

The structure viewed down the *b*-axis (Figure 4.49) reveals the presence of two-dimensional sheets of Ag atoms separated by cyanuric acid molecules, the intersheet separation being ~ 6 Å. The average Ag···Ag distance in the sheets is 2.95 Å, slightly longer than the Ag-Ag distance in metallic silver (2.89 Å). The dative Ag-O and Ag-N bond distances are in the range 2.22 - 2.76 and 2.09 - 2.21 Å, respectively, and the cyanuric acid molecules are linked by relatively short N-H···O hydrogen bonds (H···O, 1.90 Å, N···O, 2.75 Å), giving rise to a linear chain (Figure 4.49). The arrangement of the cyanuric acid molecules in the layers perpendicular to the silver sheets is illustrated in Figure 4.50.

Another notable feature of Ag_2.CA is that the organic spacer itself is the anion. Ag_2.CA can also be compared with Ag_3O with an *anti*-BiI_3 structure with the O atoms occupying 2/3 of the octahedral holes.[171] The Ag···Ag and Ag-O distances in Ag_2.CA are slightly longer than in Ag_3O, except for one Ag-O bond of 2.22 Å.
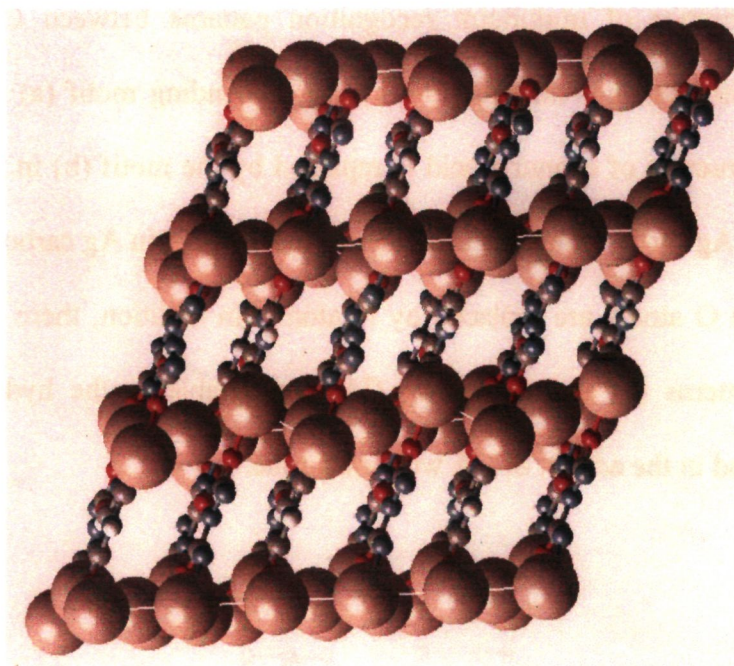
Figure 4.49: *Structure of Ag₂.CA showing Ag sheets and linear cyanuric acid chains.*
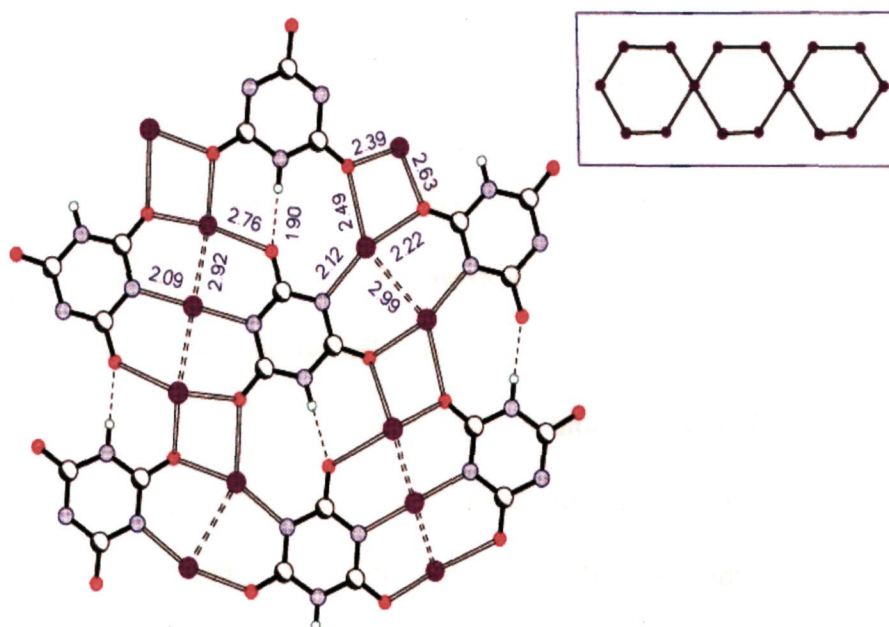
Figure 4.50: *Structure of a layer perpendicular to the Ag sheets: solid line, covalent bonds; double lines, dative bonds; dashed lines, hydrogen bonds; double dashed lines, Ag-Ag bonds. A hexameric unit of silver atoms is shown in the inset.*

159

The presence of multipoint recognition patterns between CA and Ag in Ag$_2$.CA is of interest. For instance, the hydrogen bonding motif (a) in Scheme 4.5 found in the structure of cyanuric acid is replaced by the motif (b) in Ag$_2$.CA by the substitution of Ag for H. Motif (b) is similar to that present in Ag carboxylates, except that two of the O atoms are replaced by N atoms. In addition, there are three-point recognition patterns (c) and (d) in Ag$_2$.CA, comparable to the hydrogen bonding pattern (e) found in the adduct of CA with melamine.

(a)   (b)

(c)   (d)   (e)
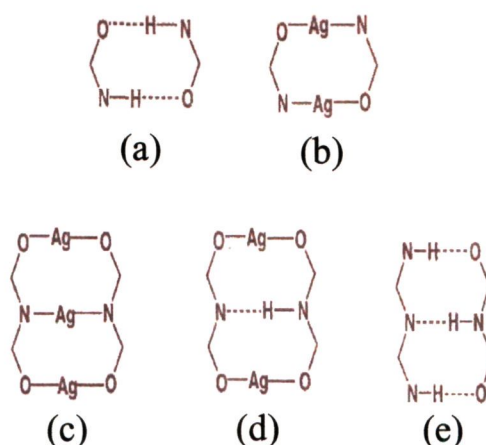
Scheme 4.5

Ag$_2$.CA crystals are mica-like and are readily cleaved because of the layer structure and the presence of weakly bound Ag sheets. The presence of two-dimensional Ag sheets is expected to give rise to conductivity. Accordingly, the values of the dc conductivity are of the order of 10^{-3} S cm^{-1}, at 300 K. The conductivity along the sheets is temperature-independent down to 15 K. Ag$_2$.CA, in which the conducting Ag sheets are separated by the organic spacer molecules, can be considered as an infinite capacitor with the organic cyanuric acid spacer molecules acting as the dielectric

medium. In accord with this, the crystals possess a high static dielectric constant of ~ 22000 at 300 K, a phenomenally high value which promises potential applications. This value of the dielectric constant is comparable with that of barium titanate (of the order of 12000 at 300 K). Bond lengths and angles of the Ag_2CA complex are given below in Table 4.59.

Table 4.59 Bond lengths and angles Ag_2CA

Moiety	Distance (Å)	Moiety	Angle (°)
Ag(1)-N(3)	2.085(5)	N(3)-Ag(1)-N(3)#1	180
Ag(1)-N(3)#1	2.085(5)	N(3)-Ag(1)-Ag(2)#1	94.49(14)
Ag(1)-Ag(2)#1	2.9231(6)	N(3)#1-Ag(1)-Ag(2)#1	85.51(14)
Ag(1)-Ag(2)	2.9231(6)	N(3)-Ag(1)-Ag(2)	85.51(14)
Ag(1)-Ag(1)#2	3.3115(5)	N(3)#1-Ag(1)-Ag(2)	94.49(14)
Ag(1)-Ag(1)#3	3.3115(5)	Ag(2)#1-Ag(1)-Ag(2)	180
Ag(2)-O(3)#3	2.388(4)	N(3)-Ag(1)-Ag(1)#2	68.17(13)
Ag(2)-O(3)	2.388(4)	N(3)#1-Ag(1)-Ag(1)#2	111.83(13)
Ag(2)-Ag(1)#3	2.9231(6)	Ag(2)#1-Ag(1)-Ag(1)#2	55.498(9)
O(3)-C(3)	1.246(7)	Ag(2)-Ag(1)-Ag(1)#2	124.501(9)
O(3)-Ag(3)#4	2.490(4)	N(3)-Ag(1)-Ag(1)#3	111.83(13)
N(3)-C(3)	1.355(8)	N(3)#1-Ag(1)-Ag(1)#3	68.17(13)
N(3)-C(2)	1.365(8)	Ag(2)#1-Ag(1)-Ag(1)#3	124.503(9)
C(3)-N(1)	1.364(8)	Ag(2)-Ag(1)-Ag(1)#3	55.498(9)
Ag(3)-N(2)	2.156(5)	Ag(1)#2-Ag(1)-Ag(1)#3	180
Ag(3)-O(1)#5	2.217(4)	O(3)#3-Ag(2)-O(3)	156.5(2)
Ag(3)-O(3)#6	2.490(4)	O(3)#3-Ag(2)-Ag(1)#3	72.32(10)
Ag(3)-Ag(3)#5	2.9938(10)	O(3)-Ag(2)-Ag(1)#3	129.77(10)
Ag(3)-Ag(3)#7	3.0083(10)	O(3)#3-Ag(2)-Ag(1)	129.77(10)
O(2)-C(2)	1.252(6)	O(3)-Ag(2)-Ag(1)	72.32(10)
N(2)-C(1)	1.341(8)	Ag(1)#3-Ag(2)-Ag(1)	69.00(2)
N(2)-C(2)	1.377(8)	C(3)-O(3)-Ag(2)	120.6(4)
N(1)-C(1)	1.369(8)	C(3)-O(3)-Ag(3)#4	138.7(4)
N(1)-H(1A)	0.86	Ag(2)-O(3)-Ag(3)#4	98.1(2)
C(1)-O(1)	1.252(8)	C(3)-N(3)-C(2)	120.5(5)
O(1)-Ag(3)#5	2.217(4)	C(3)-N(3)-Ag(1)	120.2(4)
Moiety	**Angle (°)**	C(2)-N(3)-Ag(1)	119.2(4)
Ag(3)#5-Ag(3)-Ag(3)#7	85.29(2)	O(3)-C(3)-N(3)	122.4(5)
C(1)-N(2)-C(2)	119.3(5)	O(3)-C(3)-N(1)	120.5(5)
C(1)-N(2)-Ag(3)	122.4(4)	N(3)-C(3)-N(1)	117.1(5)
C(2)-N(2)-Ag(3)	118.2(4)	N(2)-Ag(3)-O(1)#5	161.3(2)
C(1)-N(1)-C(3)	123.3(5)	N(2)-Ag(3)-O(3)#6	124.4(2)
C(1)-N(1)-H(1A)	118.3(3)	O(1)#5-Ag(3)-O(3)#6	73.42(14)
C(3)-N(1)-H(1A)	118.3(3)	N(2)-Ag(3)-Ag(3)#5	84.71(13)

Table 4.59 (*continued*)

O(2)-C(2)-N(2)	120.5(6)	O(1)#5-Ag(3)-Ag(3)#5	76.78(12)
O(2)-C(2)-N(3)	118.6(6)	O(3)#6-Ag(3)-Ag(3)#5	149.23(10)
N(2)-C(2)-N(3)	120.9(5)	N(2)-Ag(3)-Ag(3)#7	102.11(13)
O(1)-C(1)-N(2)	124.0(6)	O(1)#5-Ag(3)-Ag(3)#7	79.23(11)
O(1)-C(1)-N(1)	117.3(5)	O(3)#6-Ag(3)-Ag(3)#7	96.40(10)
C(1)-O(1)-Ag(3)#5	131.9(4)	N(2)-C(1)-N(1)	118.6(5)

Symmetry transformations used to generate equivalent atoms:

#1 -x,-y,-z-1
#2 -x,y,-z-1/2
#3 -x,y,-z-3/2
#4 -x+1/2,y+1/2,-z-1/2
#5 -x+1,-y,-z
#6 -x+1/2,y-1/2,-z-1/2
#7 -x+1,y,-z-1/2

REFERENCES

1. M. D. Cohen, G. M. J. Schmidt, *J. Chem. Soc.* (1964), and the three succeeding papers.

2. G. M. J. Schmidt, *Pure Appl. Chem.* (1971), **27**, 647.

3. (a) A. I. Kitaigorodskii, *Molecular Crystals and Molecules*, Academic Press, New York, (1973). (b) A. I. Kitaigorodskii, *Organic Chemical Crystallography*, (1961), Consultants Bureau.

4. (a) W. M. Latimer, W. H. Rodebush, *J. Am. Chem. Soc.* (1920), **42**, 1419. (b) G. C. Pimentel, A. L. McClellan, *The Hydrogen Bond*, W. H. Freeman, San Francisco, Calif., (1960). (c) W. C. Hamilton; J. A. Ibers, *Hydrogen Bonding In Solids*, W. A. Benjamin, Inc. N.Y., (1968).

5. (a) P. Schuster, G. Zundel, C. Sandorfy, *The Hydrogen Bond, Recent Developments in Theory and Experiments*, North-Holland, New York, (1976). (b) G. A. Jeffrey, W. Saenger, *Hydrogen Bonding in Biological Structures*, Springer, Berlin, (1991). (c) T. Steiner, *Angew. Chem. Int. Ed. Engl.* (2002), **41**, 48.

6. F. H. Allen, J. A. K. Howard, V. J. Hoy, G. R. Desiraju, D. S. Reddy, C. C. Wilson, *J. Am. Chem. Soc.*, (1996), **118**, 4081.

7. N. N. Laxmi Madhavi, A. K. Katz, H. L. Carrell, A. Nangia, G. R. Desiraju, *Chem. Commun.* (1997), 1953.

8. O. A. Mikhno, Z. I. Ezhkova, G. S. Zhdanov, *Krist.* (1973), **18**, 99. (b) S. C. Nyburg, C. H. Faerman, *Acta Cryst.* (1985), **B41**, 274.

9. (a) H. Adams, K. D. M. Harris, G. A. Hembury, C. A. Hunter, D. Ivingstone, J. F. McCabe, *Chem. Commun.* (1996), 2531. (b) H. Adams, F. J. Carver, C. A. Hunter,

N. J. Osborne, *Chem. Commun.* (1996), 2529. (c) U. Samanta, P. Chakrabarti, J. Chandrasekhar, *J. Phys. Chem.* A. (1998), **102**, 8964.

10. G. R. Desiraju, T. Steiner, *The Weak Hydrogen bond*, Oxford University Press: Oxford, (1999).

11. (a) D. Hadzi, *Pure Appl. Chem.* (1965), **11**, 435. (b) S. J. Barlow, G. V. Bondarenko, Y. E. Gorbaty, T. Yamaguchi, M. Poliakoff, *J. Phys. Chem. A* (2002), **106**, 10452.

12. D. F. Brougham, R. Caciuffo, A. J. Horsewill, *Nature* (1999), **397**, 241.

13. J. M. Robertson, A. R. Ubbelohde, *Proc. Roy. Soc. London* (1939), **A170**, 222.

14. (a) T. Steiner, E. B. Starikov, A. M. Amado, J. J. C. Teixera-Dias, *J. Chem. Soc. Perkin Trans.* (1995), **2**, 1321. (b) T. Steiner, *J. Phys. Chem. A*, (1998), **102**, 7041.

15. F. H. Allen, *Acta Crystallogr.* (2002), **B58**, 380.

16. For a survey, see: F. H. Allen, W. D. S. Motherwell, *Acta Crystallogr.*, (2002), **B58**, 407.

17. (a) D. Ranganathan, C. Lakshmi, I. L. Karle, *J. Am. Chem. Soc.* (1999), **121**, 6103. (b) N. Patel, D. K. Jones, E. L. Raven, *Eur. J. Biochem.* (2000), **267**, 2581. (c) G. Gemmecker, *Angew. Chem. Int. Ed. Engl.* (2000), **39**, 1224. (d) E. T. Kool, J. C. Morales, J. C. K. M. Guckian, *Angew. Chem. Int. Ed. Engl.* (2000), **39**, 991.

18. M. C. Etter, *Acc. Chem. Res.* (1990), **23**, 120.

19. (a) L. Pauling, *Proc. Nat. Acad. Sci.* (1928), **14**, 359. (b) S. Bratoz, *Advan. Quantum. Chem.* (1967), **3**, 209. (c) J. Lennard-Jones, J. A. Pople, *Proc. Roy. Soc., Ser. A* (1951), **205**, 155. (d) J. A. Pople, *Proc. Roy. Soc., Ser. A* (1951), **205**, 163.

20. L. Pauling, *The Nature of the Chemical Bond*, Cornell University Press, (1944).

21. (a) H. Tsubomura, *Bull. Chem. Soc.*, (1954), **27**, 445. (b) C. A. Coulson, *Research (London)* (1957), **10**, 149.

22. R. F. W. Bader, *Can. J. Chem.* (1964), **42**, 1822.

23. (a) A. S. N. Murthy, C. N. R. Rao, *J. Mol. Struc.* (1970), **6**, 253. (b) C. N. R. Rao, In *Water*, Ed: F. Franks, Plenum Press, New York, (1972), **1**, 93. (c) P. A. Kollman L. C. Allen, *Chem. Rev.* (1972), **72**, 283.

24. H. Umeyama, K. Morokuma, *J. Am. Chem. Soc.* (1977), **99**, 1316.

25. C. N. R. Rao, B. S. Sudhindra, H. Ratajczak, W. J. Orville-Thomas, *Molecular Interactions*, (1980), ch.3, 67.

26. (a) J. -M. Lehn *Supramolecular Chemistry – Concepts and Perspectives* VCH, Weinheim. (b) J. -M. Lehn, *Angew. Chem. Int. Ed. Engl.* (1988), **27**, 89. (c) J. M. Lehn, *Pure Appl. Chem.* (1978), **50**, 871.

27. G. M. Whitesides, E. E. Simanek, J. P. Mathias, C. T. Seto, D. N. Chin, M. M. Mammen, D. M. Gordon., *Acc. Chem. Res.* (1995), **28**, 37.

28. *Supramolecular Organization and Materials Design*. Eds: W. Jones, C. N. R. Rao, Cambridge University Press, (2002).

29. (a) J. D. Dunitz, *Pure Appl. Chem.* (1991), **63**, 177 (b) G. R. Desiraju in *Comprehensive Supramolecular Chemistry* Vol. 6. Eds: D. D. MacNicol, F. Toda, R. Bishop), Pergamon, Oxford, (1996).

30. F. H. Allen, B. S. Goud, V. J. Hoy, J. A. K. Howard, G. R. Desiraju., *J. Chem. Soc. Chem. Commun.* (1994), 2729.

31. E. J. Corey, *Pure Appl. Chem.* (1967), **14**, 19.

32. E. J. Corey, *Chem. Soc. Rev.* (1988), **17**, 111.

33. J. Bernstein, M. C. Etter, L. Leiserowitz, in *The Role of Hydrogen Bonding in Molecular Assemblies*, Eds. H. –B. Burgi, J. D. Dunitz, VCH, Weinheim (1994).

34. M. C. T. Fyfe, J. F. Stoddart, *Synthetic Supramolecular Chemistry*, (1997), **30**, 393.

35. C. B. Aakeröy, K. R. Seddon, *Chem. Soc. Rev.* (1993), **22**, 397.

36. C. B. Aakeröy, *Acta Cryst.* (1997), **B53**, 569.

37. A. Nangia, G. R. Desiraju, *Acta Cryst.* (1998), **A54**, 934.

38. R. Taylor, O. Kennard, *Acc. Chem. Res.* (1984), **17**, 320.

39. G. A. Sim, J. M. Robertson, T. H. Goodwin, *Acta Cryst.* (1955), **8**, 157.

40. M. Bailey, C. J. Brown, *Acta Cryst.* (1967), **22**, 387.

41. R. Alcala, S. M. Carrera, *Acta Cryst.* (1972), **B28**, 1671.

42. D. J. Duchamp, R. E. Marsh, *Acta Cryst.* (1969), **B25**, 5.

43. O. Ermer, *J. Am. Chem. Soc.* (1988), **110**, 3747.

44. L. Leiserowitz, *Acta Cryst.* (1976), **B32**, 775.

45. D. Braga, L. Maini, F. Grepioni, *CrystEngComm* (2001), **6**, 1

46. Y. Wangs, G. D. Stucky, J. M. Williams, *J. Chem. Soc. Perkin Trans.* 2 (1974), **35**, 2.

47. (a) D. J. Cram, J. M. Cram, *Container Molecules and their Guests*, Royal Society of Chemistry, Cambridge, (1994). (b) M. M. Conn, J. Rebek, Jr., *Chem. Rev.* (1997), **97**, 1647. (c) J. de Mendoza, *Chem. Eur. J.* (1998), **4**, 1373.

48. (a) D. J. Cram, *Science*, (1983), **219**, 1177. (b) D. M. Rudkevich, J. Rebek, Jr., *Eur. J. Org. Chem.* (1999), 1991.

49. (a) A. Jasat, J. C. Sherma, *Chem. Rev.* (1999), **99**, 931. (b) A. Collet, J. -P. Dutasta, B. Lozach, J. Canceill, *Top. Curr. Chem.* (1993), **165**, 103.

50. (a) K. D. Shimizu, J. Rebek, Jr., *Proc. Natl. Acad. Sci. U.S.A.* (1995), **92**, 12403. (b) O. Mogck, V. Böhmer, W. Vogt, *Tetrahedron* (1996), **52**, 8489. (c) T. Heinz, D. M. Rudkevich, J. Rebek, Jr., *Nature* (1998), **394**, 764.

51. (a) C. D. Gutsche, *Calixarenes*, Royal Society of Chemistry, Cambridge, (1989). (b) C. D. Gutsche, *Calixarenes Revisited*, Royal Society of Chemistry, Cambridge, (1998). Review articles: (c) S. Shinkai, *Tetrahedron* (1993), **49**, 8933. (d) V. Böhmer, *Angew. Chem.* (1995), **107**, 785. (e) A. Pochini, R. Ungaro in *Comprehensive Supramolecular Chemistry*, Volume 2, Eds. J. L. Atwood, J. E. D. Davies, D. D. MacNicol, F. Vögtle, Pergamon, (1996), 103.

52. D. M. Rudkevich, *Chem. Eur. J.* (2000), **6**, 2679.

53. *Calixarenes. A Versatile Class of Macrocyclic Compounds.* Eds: J. Vicens, V. Böhmer, Kluwer, Dordrecht, (1991).

54. L. R. MacGillivray, J. L. Atwood, *Nature* (1997), **389**, 69.

55. F. H. Herbstein, M. Kapon, *Acta Cryst.* **B34** (1978), 1608.

56. S. V. Kolotuchin, E. E. Fenlon, R. W. Wilson, C. J. Loweth, S. C. Zimmerman, *Angew. Chem. Int. Ed. Engl.* **34**, (1995), 2654.

57. J. Narasimha Moorthy, R. Natarajan, P. Venugopalan, *Angew. Chem. Int. Ed. Engl.* (2002), **41**, 3417.

58. M. Currie, J. C. Speakman, *J. Chem. Soc. A.* (1970), 1923.

59. P. Gilli, V. Bertolasi, V. Ferretti, G. Gilli, *J. Am. Chem. Soc.* (1994), **116**, 909.

60. P. Vishweshwar, A. Nangia, V. M. Lynch, *Chem. Commun.* (2001), 179.

61. B. R. Penfold, J. C. B. White, *Acta Cryst.* (1959), **12**, 130.

62. T. L. Nguyen, A. Scott, B. Dinkelmeyer, F. W. Fowler, J. W. Lauher, *New. J. Chem.* (1998), **22**, 129.

63. (a) G. R. Desiraju, *Angew. Chem.* (1995), **107**, 2541. (b) J. D. Dunitz, *Pure Appl. Chem.* (1991), **63**, 177. (c) M. C. Etter, *J. Phys. Chem.* (1991), **95**, 4601.

64. R. F. M. Lange, F. H. Beijer, R. P. Sijbesma, R. W. W. Hooft, H. Kooijman, A. L. Spek, J. Kroon, E. W. Meijer, *Angew. Chem. Int. Ed. Engl.* (1997), **36**, 969.

65. B. Gong, C. Zheng, E. S-Jankun, Y. Yan, J. Zhang, *J. Am. Chem. Soc.* (1998), **120**, 11194.

66. (a) J. A. Zerkowski, C. T. Seto, G. M. Whitesides, *J. Am. Chem. Soc.* (1992), **114**, 5473. (b) J. A. Zerkowski, J. C. MacDonald, C. T. Seto, D. A. Wierda, G. M. Whitesides, *J. Am. Chem. Soc.* (1994), **116**, 2382.

67. J. R. Ferrer, P. M. Lahti, C. George, P. Oliete, M. Julier, F. Palacio, *Chem. Mater.* (2001), **13**, 2447.

68. (a) J. Donohue, in *Selected Topics in Hydrogen Bonding*, Eds. A. Rich, N. Davidson, Freeman, San Francisco, (1968). (b) F. A. Cotton, L. M. Daniels, G. T. Jordan, C. A. Murillo, *J. Chem. Soc. Chem. Commun.* (1997), 1673.

69. T. Steiner, G. R. Desiraju, *Chem. Commun.* (1998), 891.

70. R. Taylor, O. Kennard, *J. Am. Chem. Soc.* (1982), **104**, 5063.

71. V. R. Thalladi, H. C. Weiss, D. Blaser, R. Boese, A. Nangia, G. R. Desiraju, *J. Am. Chem. Soc.* (1998), **120**, 8702.

72. C. Glidewell, W. T. A. Harrison, J. N. Low, J. G. Sime, J. L. Wardell, *Acta Cryst.* (2001), **B57**, 190.

73. J. M. A. Robinson, D. Philip, K. D. M. Harris, B. M. Kariuki, *New J. Chem.* (2000), **24**, 799.

74. M. Ohkita, T. Suzuki, K. Nakatani, T. Tsuji, *Chem. Commun.* (2001), 1454.

75. *Nonlinear Optical Properties of Organic Molecules and Crystals*, Eds: D. S. Chemla, J. Zyss, Academic Press, Boston, (1987).

76. M. Nishio, M. Hirota, Y. Umezawa, *The CH/π Interaction. Evidence, Nature, and Consequences.* Wiley-VCH, New York, (1998).

77. V. R. Thalladi, R. Boese, S. Brasselet, I. Ledoux, J. Zyss, R. K. R. Jetti, G. R. Desiraju, *Chem. Commun.* (1999), 1639.

78. H. Adams, F. J. Carver, C. A. Hunter, N. J. Osborne, *Chem. Commun.* (1996), 2529.

79. (a) M. Levitt, M. F. Perutz, *J. Mol. Biol.* (1988), **201**, 751. (b) M. F. Perutz, *Phil. Trans. R. Soc. Lond. A.* (1993), 105. (c) J. B. O. Mitchell, C. L. Nandi, I. K. McDonald, J. M. Thornton, S. L. Price, *J. Mol. Biol.* (1994), **239**, 315.

80. J. A. Cowan, J. A. C. Clyburne, M. G. Davidson, R. L. W. Harris, J. A. K. Howard, P. Küpper, M. A. Leech, S. P. Richards, *Angew. Chem. Int. Ed. Engl.* (2002), **41**, 1432.

81. (a) M. A. Viswamitra, R. Radhakrishnan, J. Bandekar, G. R. Desiraju, *J. Am. Chem. Soc.* (1993), **115**, 4868. (b) H. S. Rzepa, M. H. Smith, M. L. Webb, *J. Chem. Soc. Perkin Trans. 2* (1994), 703. (c) T. Steiner, E. B. Starikov, M. Tamm, *J. Chem. Soc. Perkin Trans. 2* (1995), 67.

82. P. A. Iyere, L. J. Kayren, A. W. Cordes, C. T. Eagle, T. A. Nile, G. L. Schimek, W. T. Pennington, *Cryst. Engg.* (1998), **1**, 159.

83. G. R. Desiraju, *Angew. Chem. Int. Ed. Engl.* (1995), **34**, 2311.

84. (a) D. Wiechert, D. Mootz, T. Dahlems, *J. Am. Chem. Soc.* (1997), **119**, 12665. (b) F. Grepioni, C. Cojazzi, S. M. Draper, N. Scully, D. Braga, *Organometallics* (1998), **17**, 296. (c) D. Britton, W. E. Noland, T. K. Henke, *Acta Cryst.* (2002), **E58**, o185. (d) G. Ompraba, Z. A. Rafi, M. Yogavel, D. Velmurugan, K. Sekar, E. Karthikeyan, S. Perumal, A. R. Choudhry, T. N. Guru Row, *Cryst. Res. Technol.* (2003), **38**, 822.

85. R. Liu, K. –F. Mok, S. Valiyaveetil, *New J. Chem.* (2001), **25**, 890.

86. N. N. Laxmi Madhavi, C. Bilton, J. A. K. Howard, F. H. Allen, A. Nangia, G. R. Desiraju, *New J. Chem.* (2000), **24**, 1.

87. V. R. Pedireddi, D. S. Reddy, B. S. Goud, D. C. Craig, A. D. Rae, G. R. Desiraju, *J. Chem. Soc. Perkin Trans. 2* (1994), 2353.

88. V. R. Thalladi, B. S. Goud, V. J. Hoy, F. H. Allen, J. A. K. Howard, G. R. Desiraju, *Chem. Commun.* (1996), 401.

89. (a) H. Schmidbaur, W. Graf, G. Müller, *Angew. Chem. Int. Ed. Engl.* (1988), **27**, 417. (b) J. Zank, A. Schier, H. Schmidbaur, *J. Chem. Soc. Dalton Trans.* (1998), 323. (c) C. B. Aakeroy, D. S. Leinen in *Crystal Engineering: From Molecules and Crystals to Materials.* Eds. D. Braga, F. Grepioni, A. G. Orpen, Kluwer, Academic, Dordrect, The Netherlands, (1999), pp 89 - 106.

90. S. S. Pathaneni, G. R. Desiraju, *J. Chem. Soc. Dalton Trans.* (1993), 319.

91. R. E. Bachman, M. S. Fioritto, S. K. Fetics, T. M. Cocker, *J. Am. Chem. Soc.* (2001), **123**, 5376.

92. (a) D. Braga, F. Grepioni, P. Sabatino, G. R. Desiraju, *Organometallics*, (1994), **13**, 3532. (b) K. Biradha, G. R. Desiraju, D. Braga, F. Grepioni, *Organometallics*, (1996), **15**, 1284.

93. (a) Y. Hsiou, Y. Wang, L. -K. Liu, *Acta Cryst.* (1989), **C45**, 721. (b) C. Pedone, A. Sirigu, *Inorg. Chem.* (1968), **7**, 2614.

94. D. Messer, G. Landgraf, H. Behrens, *J. Organometallic Chem.* (1979), **172**, 349.

95. A. D. Burrows, C. -W. Chan, M. M. Chowdry, J. E. McGrady, D. M. P. Mingos. *Chem. Soc. Rev.* (1995), **24**, 329.

96. A. M. Beatty, *CrystEngComm*, (2001), **51**, 1.

97. C. B. Aakeroy and A. M. Beatty, *Chem. Commun.* (1998), 1067.

98. D. M. L. Goodgame, I. Hussain, A. J. P. White and D. J. Williams, *J. Chem. Soc. Dalton Trans.* (1999), 2899.

99. P. V. Bernhardt, *Inorg. Chem.* (1999), **38**, 3481.

100. G. Aullón, D. Bellamy, L. Brammer, E. E. Bruton, A. G. Orpen, *Chem. Commun.* (1998), 653.

101. (a) J. C. Mareque Rivas, L. Brammer, *Inorg. Chem.* (1998), **37**, 4756. (b) A. L. Gillon, G. R. Lewis, A. G. Orpen, S. Rotter, J. Starbuck, X. -M. Wang, Y. Rodriguez-Martin, C. Ruiiz-Perez, *J. Chem. Soc. Dalton Trans.* (2000), 3897. (c) A. Angeloni, A. G. Orpen, *Chem. Commun.* (2001), 343.

102. (a) M. Tadokoro, K. Nakasuji, *Coord. Chem. Rev.* (2000), **198**, 205. (b) M. Tadokoro, K. Isobe, H. Uekusa, Y. Ohashi, J. Toyoda, K. Tashiro, K. Nakasuji, *Angew. Chem. Int. Ed. Engl.* (1999), **38**, 95.

103. P. Coppens, B. Ma, O. Gerlits, Y. Zhang, P. Kulshrestha, *CrystEngComm* (2002), **4**, 302.

104. G. R. Desiraju, *Curr. Opin. Solid State Mater. Sci.* (1997), **2**, 451.

105. (a) D. D. MacNicol, F. Toda, R. Bishop, Eds. *Comprehensive Supramolecular Chemistry* Vol.6, Oxford: Pergamon, (1996). (b) L. R. MacGillivray, J. L. atwood, *Angew. Chem. Int. Ed. Engl.* (1999), **38**, 1018. (c) A. Nangia, *Curr. Opin. Solid State Mater. Sci.* (1997), **2**, 451.

106. (a) P. L. Langley, J. Hulliger, *Chem. Soc. Rev.* (1999), **28**, 279. (b) T. J. Barton, L. M. Bull, W. G. Klemperer, D. A. Loy, B. McEnaney, M. Misono, P. A. monson, G. Pez, G. W. Scherer, J. C. Vartuli, O. M. Yaghi, *Chem. Mater.* (1999), **11**, 2633.

107. (a) J. C. Scaiano, H. Garciá, *Acc. Chem. Res.* (1999), **32**, 783. (b) G. A. Ozin, A. Kuperman, A. Stein, *Angew. Chem. Int. Ed. Engl.* (1989), **28**, 359. (c) D. R. Robinson, *Chem. Rev.* (1990), **90**, 867.

108. O. M. Yaghi, G. Li, *Angew. Chem. Int. Ed. Engl.* (1995), **90**, 867.

109. G. B. Gardner, D. Venkataraman, J. S. Moore, S. Lee, *Nature* (1995), **374**, 792.

110. L. R. MacGillivray, S. Subramanian, M. J. Zaworotko, *J. Chem. Soc. Chem. Commun.* (1994), 1325.

111. O. M. Yaghi and H. Li, *J. Am. Chem. Soc.* (1996), **118**, 295.

112. D. Venkataraman, S. Lee, J. Zhang, J. S. Moore, *Nature* (1994), **371**, 591.

113. X. Wang, M. Simard, J. D. Wuest, *J. Am. Chem. Soc.* (1994), **371**, 591.

114. D. Ranganathan, C. lakshmi, I. L. Karle, *J. Am. Chem. Soc.* (1999), **121**, 6103.

115. D. Ranganathan, V. Haridas, C. S. Sundari, D. BalaSubramanian, K. P. Madhusudanan, R. Roy, I. L. Karle, *J. Org. Chem.* (1999), **64**, 9230.

116. B. Q. Ma, P. Coppens, *Chem. Commun.* (2003), 412.

117. Md. B. Zaman, K. Udachin, Md. Akhtaruzzaman, Y. Yamashita, J. A. Ripmeester, *Chem. Commun.* (2002), 2322.

118. R. D. B. Walsh, M. W. Bradner, S. Fleischman, L. A. Morales, B. Moulton, N. R. Hornedo, M. J. Zaworotko, *Chem. Commun.* (2003), 186.

119. C. N. R. Rao and K. J. Rao, *Phase transitions in solids*, McGraw-Hill, New York, (1978).

120. (a) D. Braga, F. Grepioni, *Chem. Soc. Rev.* (2000), **4**, 229. (b) N. Bladgen, R. J. Davey, *Chem. Br.* (1999), **35**, 44.

121. G. R. Desiraju, *Science* (1997), **278**, 404.

122. G. S. McGrady, M. Odlyha, P. D. Prince, J. W. Steed, *CrystEngComm* (2002), **4**, 271.

123. R. J. Davey, K. Allen, N. Bladgen, W. I. Cross, H. F. Lieberman, M. J. Quayle, S. Righini, L. Seton, G. J. T. Tiddy, *CrystEngComm* (2002), 4(47), 257.

124. Polymorph Predictor, *Cerius²* Module (Molecular Simulations, San Diego, CA, and Cambridge, UK).

125. (a) F. W. Lichtenthaler, *Angew. Chem. Int. Ed. Engl.* (1994), **33**, 2364. (b) D. E. Kashland, Jr., *Angew. Chem. Int. Ed. Engl.* (1994), **33**, 2375.

126. E. Fischer, *Ber. Dtsch. Chem. Ges.* (1894), **27**, 2985.

127. (a) G. M. Whitesides, E. E. Simanek, J. P. Mathias, C. T. Seto, D. N. Chin, M. Mammen, D. M. Gordon, *Acc. Chem. Res.* (1995), **28**, 37. (b) J. C. MacDonald, G. M. Whitesides, *Chem. Rev.* (1994), **94**, 2383.

128. G. A. Jeffrey, *An Introduction to Hydrogen Bonding*, Oxford University Press (1997).

129. M. C. Etter, L. Leiserowitz, in *Structure Correlation*, Eds. H. -B. Bürgi, J. D. Dunitz, (1994), Vol. 2, 431, Weinheim: VCH.

130. M. E. Davis, *Chem. Eur. J.* (1997), **3**, 1745, and references therein.

131. (a) O. M. Yaghi, H. Li, C. Davis, D. Richardson, T. L. Groy, *Acc. Chem. Res.* (1998), **31**, 474. (b) S. C. Zimmerman, *Science* (1997), **276**, 544.

132. F. H. Herbstein, R. E. Marsh, *Acta Cryst.* (1997), **B34**, 2358.

133. F. H. Allen, W. D. S. Motherwell, P. R. Raithby, G. P. Shields, R. Taylor, *New J. Chem.* (1999), **23**, 25.

134. V. R. Pedireddi, W. Jones, A. Chorlton, R. Docherty, *J. Chem. Soc. Chem. Commun.* (1996), 997.

135. E. Batchelor, J. Klinowski, W. Jones, *J. Mater. Chem.* (2000), **10**, 839.

136. C. V. K. Sharma, M. J. Zaworotko, *Chem. Commun.* (1996), 2655.

137. (a) N. Masciocchi, M. Bergamo, A. Sironi, *Chem. Commun.* (1998), 1347. (b) S. A. McWilliam, J. M. S. Skakle, J. N. Low, J. L. Wardell, S. J. Garden, A. C. Pinto,

J. C. Torres, C. Glidewell, *Acta Cryst.* (2001), **C57**, 942. (c) C. J. Kelly, J. M. S. Skakle, J. L. Wardell, S. M. S. V. Wardell, J. N. Low, C. Glidewell, *Acta Cryst.* (2002), **B58**, 94. (d) S. J. Garden, S. P. Fontes, J. L. Wardell, J. M. S. Skakle, J. N. Low, C. Glidewell, *Acta Cryst.* (2002), **B58**, 701.

138. F. Garcia-Tellado, S. Goswami, S. K. Chang, S. J. Geib, A. D. Hamilton, *J. Am. Chem. Soc.* (1990), **112**, 7393.

139. K. R. Adam, I. M. Atkinson, R. L. Davis, L. F. Lindoy, M. S. Mahinay, B. J. McCool, B. W. Skelton, a. H. White, *Chem. Commun.* (1997), 467.

140. C. Meiners, S. Valiyaveetil, V. Enkelmann, K. Mullen, *J. Mater. Chem.* (1997), 7(12), 2367.

141. (a) M. B. Zaman, M. Tomura, Y. yamashita, *Chem. Commun.* (1999), 999. (b) P. I. Coupar, G. Ferguson, C. Glidewell, *Acta Cryst.* (1996), **C52**, 2524. (c) E. J. MacLean, P. S. Wheatley, G. Ferguson, C. Glidewell, *Acta Cryst.* (1999), **C55**, 1892.

142. (a) J. D. Watson, F. H. Crick, *Nature* (1953), **171**, 737. (b) W. Saenger, in *Principles of Nucleic Acid Structure*, Springer-Verlag: New York, (1984).

143. P. Coppens, A. Vos, *Acta Cryst.* (1971), **B27**, 146.

144. G. J. Sanjayan, V. R. Pedireddi, K. N. Ganesh, *Org. Lett.* (2000), **2**, 2825.

145. (a) H. Shieh, D. Voet, *Acta Crystallogr.* (1975), **B31**, 2192. (b) H. Shieh, D. Voet, *Acta Crystallogr.* (1976), **B32**, 2361. (c) D. Voet, A. Rich, *J. Am. Chem. Soc.*

(1972), **94**, 5888. (d) D. Voet, *J. Am. Chem. Soc.* (1972), **94**, 8213. (e) J. Matsui, M. Higashi, T. Takeuchi, *J. Am. Chem. Soc.* (2000), **122**, 5218.

146. C. T. Seto, G. M. Whitesides, *J. Am. Chem. Soc.* (1993), **115**, 4696.

147. (a) J. P. Mathias, E. E. Simanek, J. A. Zerkowski, C. T. Seto, G. M. Whitesides, *J. Am. Chem. Soc.* (1994), **116**, 4316. (b) J. A. Zerkowski, C. T. Seto, D. A. Wierda, G. M. Whitesides, *J. Am. Chem. Soc.* (1990), **112**, 9025.

148. C. N. R. Rao, *Chemical Approaches to the Synthesis of Inorganic Materials*, John Wiley, New York, (1993).

149. R. Robson, B. F. Abrahams, S. R. Batten, R. W. Gable, B. F. Hoskins, J. Liu, *Supramolecular Architecture*, ACS Symp. Ser., Washington, D. C. vol. 449, ch. 19, (1992).

150. L. Carlucci, G. Ciani, D. M. Proserpio, A. Sironi, *Angew. Chem. Int. Ed. Engl.* (1995), **34**, 1895.

151. G. K. H. Shimizu, G. D. Enright, C. I. Ratcliffe, J. A. Ripmeester, D. D. M. Wayner, *Angew. Chem. Int. Ed. Engl.* (1998), **37**, 1407.

152. G. K. H. Shimizu, G. D. Enright, C. I. Ratcliffe, K. F. Preston, J. L. Reid, J. A. Ripmeester, *Chem. Commun.* (1999), 1485.

153. K. A. Hirsch, S. R. Wilson, J. S. Moore, *Inorg. Chem.* (1997), **36**, 2960.

154. (a) M. Munakata, L. P. Wu, T. Kuroda-Sowa, M. Maekawa, Y. Suenaga, G. L. Ning, T. Kojima, *J. Am. Chem. Soc.* (1998), **120**, 8610. (b) G. L. Ning, L. P. Wu, K. Sugimoto, M. Munakata, T. Kuroda-Sowa, M. Maekawa, *J. Chem. Soc. Dalton Trans.* (1999), 2529.

155. D. Venkataraman, Y. Du, S. R. Wilson, P. Zhang, K. Hirsch, J. S. Moore, *J. Chem. Edu.* (1997), **74**, 915.

156. Siemens Analytical X-ray Instruments Inc., Madison, Wisconsin, USA (1995).

157. SHELXTL (SGI version) Siemens Analytical X-ray Instruments Inc., Madison, Wisconsin, USA (1995).

158. A. L. Spek, Acta Cryst (1990), **A46**, C34.

159. G. H. Stout and L. H. Jensen, *X-ray Structure Determination -- A practical guide*, John Wiley & sons, NY, (1989).

160. R. E. Melendez, C. V. K. Sharma, M. J. Zaworotko, Bauer, R. D. Rogers, *Angew. Chem. Int. Ed. Engl.* (1996), **35**, 2213.

161. (a) V. R. Pedireddi, W. Jones, A. P. Chorlton, R. Docherty, *Chem. Commun.* (1996), 987. (b) V. R. Pedireddi, W. Jones, A. P. Chorlton, R. Docherty, *Tet. Lett.* (1998), **39**, 5409.

162. G. R. Desiraju, V. R. Pedireddi, J. A. R. P. Sharma, D. E. Zacharias, *Acta Chim. Hung.* (1993), 130, 451.

163. V. R. Thalladi, B. S. Goud, V. J. Hoy, F. H. Allen, J. A. K. Howard, G. R. Desiraju, *Chem. Commun.* (1996), 401.

164. P. Prince, F. R. Fronczek, R. D. Gandour, *Acta Cryst.* (1991), **C47**, 895.

165. D. F. Grant, J. P. G. Richards, *Acta Cryst.* (1969), **B25**, 564.

166. M. C. Etter, D. A. Adsmond, *J. Chem. Soc. Chem. Commun.* (1990), 589.

167. C. Chang-Zhang, S. Jian-qiu, L. Zhou-Bin, G. Dong-Shou, H. X. L. Ding, *J. Struct. Chem.* (1995), **14**, 241.

168. L. Katz, K. Tomita, A. Rich, *J. Mol. Biol.* (1965), **13**, 340.

169. G. A. Leonard, K. H. McAuley, T. Brown, W. N. Hunter, *Acta Crystallogr.* (1995), **D51**, 136.

170. W. H. Landschulz, P. F. Johnson, S. L. McKnight, *Science*, (1988), **240**, 1759.

171. W. Beesk, P. G. Jones, H. Rumpel, E. Schwarzmann, G. M. Sheldrick, *J. Chem. Soc. Chem. Commun.* (1981), 664.

PART 2

INVESTIGATIONS OF HYDROGEN-BONDED ORGANIC SOLIDS BY EXPERIMENTAL CHARGE DENSITIES[*]

SUMMARY

The charge or electron density $\rho(r)$, a physical observable, can be obtained experimentally from high-resolution X-ray diffraction experiments at low temperatures. In contrast to theoretical results, which usually refer to isolated molecules, the X-ray experiment yields a charge density in the crystalline state. The electron density distribution thus obtained can be used as a powerful and independent source of information for characterizing hydrogen bonds. Since the topology of $\rho(r)$ allows a partitioning of chemical structures into sub-molecular regions like atoms or functional groups, comparative studies can be performed on entirely different classes of hydrogen bonds.

We have examined the charge density and topological properties of various types of hydrogen bonding interactions, such as O-H$\cdots$O, N-H$\cdots$O, C-H$\cdots$O, O-H$\cdots$N, N-H$\cdots$N, N-H$\cdots$S and C-H$\cdots$S bonds, present in different molecular crystals, such as the disodium croconate trihydrate, disodium squarate trihydrate, piperazinium-

---

180

oxalate, thiodiglycollic acid-4,4'-bipyridine, melamine, thionicotinamide and thioacetamide. The H···A distances in these systems lie in the range of ~ 1.4 to ~ 3.0 Å, with densities and Laplacians evaluated at the (3, -1) hydrogen bond critical points varying between ~ 0.01 - 0.45 eÅ^{-3} and ~ 0.05 - 6.0 eÅ^{-5}, respectively. Static deformation density maps reveal depletion of electron density in the hydrogen-acceptor (H···A) regions. While the total density and the Laplacian at the H···A critical points exhibit an exponential dependence on the H···A distance, the positive curvature of the electron density, λ_3, closely follows the exponential relation with a considerably better correlation factor. The λ_3 values vary between 0.4 to 12 eÅ^{-5}. As the hydrogen bond is a closed-shell interaction, the charge is predominantly depleted between the two participating hydrogen and acceptor nuclei, λ_3 becomes the dominant curvature and hence gives a good exponential fit. A number of charge density studies on hydrogen bonds gathered from the literature, have delivered additional 178 data points to corroborate our findings. It was found that for all the hydrogen bonds, irrespective of the nature or type of the donor and the acceptor atoms, the total electron density, the Laplacian and the positive curvature of the density vary exponentially with the H···A distance. The variation of the positive curvature (λ_3), considered as a universal parameter, is particularly exact. Besides these charge density descriptors, an analysis of the polarizations of the hydrogen-acceptor regions shows that the bonds fall into different sets depending on the strength of the hydrogen bond. Thus, O-H···O, N-H···O, O-H···N and such strong hydrogen bonds form one set while the weak hydrogen bonds such as C-H···O form another set.

The experimental charge density method has been employed to provide a more detailed description of the hydrogen bond in terms of the location of the bond critical point and the geometry of the lone-pair of electrons. Based on a study of five different molecular systems (disodium salts of croconic and squaric acids, piperazine-oxalate, *o*-ethoxy cinnamic acid and adipic acid), which exhibit nineteen O-H$\cdots$O type hydrogen bonds and cover a wide range of hydrogen bond distances and angles, it has been possible to arrive at a generalization of the topological descriptors. In all the hydrogen bonds studied, the electron density at the bond critical point (BCP) and its Laplacian fall in the range of 0.03 - 0.39 eÅ^{-3} and 0.7 - 6.0 eÅ^{-5}, respectively. The non-bonded charge concentrations (lone-pairs of electrons) in the deformation density have been studied. A thorough analysis of the bond paths indicate that they deviate, in some instances widely, from the H$\cdots$O bond axis and the resulting d_{CP} values (vertical displacement of the bond critical point from the internuclear line) range from 0.036 to 0.418 Å. The origin of such high d_{CP} values has been related to the constellation of the various interaction centers - the lone-pairs and the atom cores of the donor and the acceptor oxygens and the hydrogen atom. This study provides a useful classification of the hydrogen bonds in terms of a new interaction line, L_{i-j}, connecting the various centers, i and j. A nearness parameter, d_L, that represents the perpendicular distance of the critical point from the interaction line, L_{i-j}, justifies the classification. The d_L values are found to be much smaller than the corresponding d_{CP}.

1. CHARGE DENSITY IN CRYSTALS – THE CHARGE DISTRIBUTION AND ITS TOPOLOGY – AN OVERVIEW

1.1 Introduction

Most X-ray crystallographic studies are aimed at structural information and pay little attention, if any, to the details of the electron distribution. But the two are, in practice, inseparably linked. It is only when we are content with a routinely approximate structure that we can afford to disregard the electron density. The description of charge distribution in crystalline lattices has come a long way since the first quantum model of the atom. It was known from early days that a quantitative account of the chemical bonds in molecules and crystals would require the calculation of the probability density of the electron cloud between atoms. The possibility of measuring the charge density in a crystal from its X-ray diffraction pattern was envisioned many years ago when Debye and Scherrer discussed the possibility that the halos on a powder photograph were images of the electron orbits around the atoms.[1] This is evident from Debye's statement in 1915.

"It seems to me that experimental study of scattered radiation, in particular from light atoms, should get more attention, since along this way it should be possible to determine the arrangement of electrons in the atoms."

Convinced that X-rays were scattered by electrons, Debye joined by Scherrer, turned his attention to chemical bonding and thereby initiated the field of X-ray charge density studies. Debye and Scherrer wondered how the valency dashes, used by chemists to describe the bond between atoms, could be replaced by an electron model that was consistent with their results with the newly discovered powder diffraction method and with Bragg's ionization counter measurements.

Present day techniques[2] for studying charge density distributions by diffraction methods originated in the 1960s with theoretical chemists' interest in calculating charge distributions to reproduce observed diffraction intensities for certain covalent crystals such as those of diamond and silicon. For these crystals, so-called space group-forbidden reflections are observed. Dawson[3] studied diamond (see Figure 1.1) in 1967.
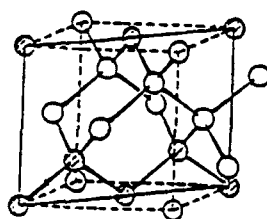
Figure 1.1: *The diamond structure*

The space group is Fd-3m. Carbon atoms are linked tetrahedrally to four equivalent neighbours, each having point symmetry 4-3m (T_d), lacking a centre of symmetry. The space group allowed reflections are h+k+l=4n. However, the (222) reflection is observed for which h+k+l=4n+2. In the conventional representation of X-ray structure factors, atoms are taken to be spherically

symmetrical. Dawson generalized the treatment to recognize non-centrosymmetry in the electron charge distribution about each nuclear position. Dawson's "generalized structure factor formulation" reproduces the observed diffraction intensities, in particular the space group-forbidden (222) reflection. The formalism showed, for the first time, that it was possible to measure experimentally the aspherical features in covalent charge distributions arising from chemical bond formation.

1.2 The charge density

Electron or charge density in a N-electron system is the probability density of finding any of the N electrons in an infinitesimally small volume of space, the phase space, $d\tau$.

$$\rho(r) = N \int \psi^* \psi \, d\tau \qquad \qquad ...(1)$$

where ψ is the stationary state function; τ denotes the spin coordinates of all the electrons and the cartesian coordinates of all electrons but one. It is expressed in $e\text{Å}^{-3}$ or atomic units, au (1 au = 6.7483 $e\text{Å}^{-3}$). The description of electronic structure of a molecule in real space therefore relates to the charge density distribution around the constituent atoms.

1.3 Charge density from theoretical calculations

Charge density distribution in a molecule or a crystal may be obtained by *ab initio* Hartree-Fock calculations.[4] In this method, the electrons are assumed to move in a symmetric field generated by the nuclei and the other electrons. Since

the wave function and the potential are correlated, one obtains the wave function using an iterative procedure till a change in the potential does not produce any significant change in the wave function. Once the wave function is obtained, the electron density distribution can be readily determined. Commercial programs such as Gaussian[5] and Gamess[6] are used regularly for this purpose. Calculations for crystals can be performed using the periodic Hartree-Fock method employing the density functional theory. Both of these options have been incorporated in the CRYSTAL program of Dovesi and co-workers.[7] The Kohn-Sham Density Functional approach has also been used for crystals. Within the density functional formalism, calculations can be done either at local density approximation (LDA) or using Generalized Gradient Approximation (GGA). Either of the methods is known to yield good results. R. F. W. Bader has initiated and made significant contributions in the last four decades to the understanding of the topology of charge density distribution in molecular crystals. In his 'Quantum Theory of Atoms in Molecules' (AIM),[8] information well beyond classical atomic connectivity has been obtained from analysis of the charge distribution. By the AIM approach, Bader has defined bond properties in terms of various topological entities. The theory of Atoms in Molecules is an interpretative theory that uses the electron density ρ as the information source. Transferability of the topological properties derived from an electron density distribution, between molecules containing different functional groups, is one of the important features of AIM. Bader has also defined the reactivity and stability of bonds in terms of the charge distribution.

1.4 Charge density from experiment

Experimental determination of charge density mostly relies on X-ray diffraction. Owing to the periodical nature of the atomic distribution in crystals and the interaction of the X-ray radiation with the electrons in it, it is possible to deduce the distribution of electron density in crystals from the intensities of the diffracted beams. What we actually measure in a crystallographic experiment are the structure factors F(H) where H are indices denoting a particular scattering direction corresponding to a crystal plane. The fundamental equations are:

$$I(H) \propto |F(H)|^2$$

$$\propto |\sum_i f_i(H)\exp(2\pi iH.r)|^2 \qquad \qquad ...(2)$$

$$F(H) = \int_V \rho(r)\exp(2\pi iH.r)dr \qquad \qquad ...(3)$$

where r is a position vector in direct space, H is a reciprocal lattice vector, I the intensity of the diffracted beam, F the structure factor, $f_i(H)$ is the atomic scattering factor of the ith atom in the unit cell, $\rho(r)$ is the electron density and V is the unit cell volume. The electron density is obtained from these structure factors via the following equation,

$$\rho(r) = \frac{1}{V} \sum_H F(H)\exp(-2\pi iH.r) \qquad \qquad ...(4)$$

In the final stage of data processing, non-linear least-square refinements are used to fit a model electron density to the measured one. This is equivalent to minimizing the difference density $\Delta\rho$, which is defined as $\rho_{observed} - \rho_{calculated}$. In routine molecular geometry determinations, $\rho_{calculated}$ is just a superposition of

spherically symmetrical atomic densities. The density in a molecule can be conveniently modeled by partitioning it into core, spherical valence and deformation valence around each atom (the deformation being caused by the interatomic bonding).[9]

$$\rho_{atom}(r) = \rho_{core}(r) + \rho_{valence}(r) + \rho_{deformation}(r,\theta,\phi) \qquad ...(5)$$

For a complete description of bonding, accurate modeling of $f_i(H)$ becomes necessary. In parallel to $\rho(r)$ (see equation 5),

$$f(H) = f_{core}(H) + f_{valence}(H) + f_{deformation}(H) \qquad ...(6)$$

Such a partitioning of $f(H)$ is justifiable in X-ray diffraction since one can select regions of reciprocal space where core scattering is predominant. In Figure 1.2, we show the variation of $f(H)$ with scattering angle θ for various elements.
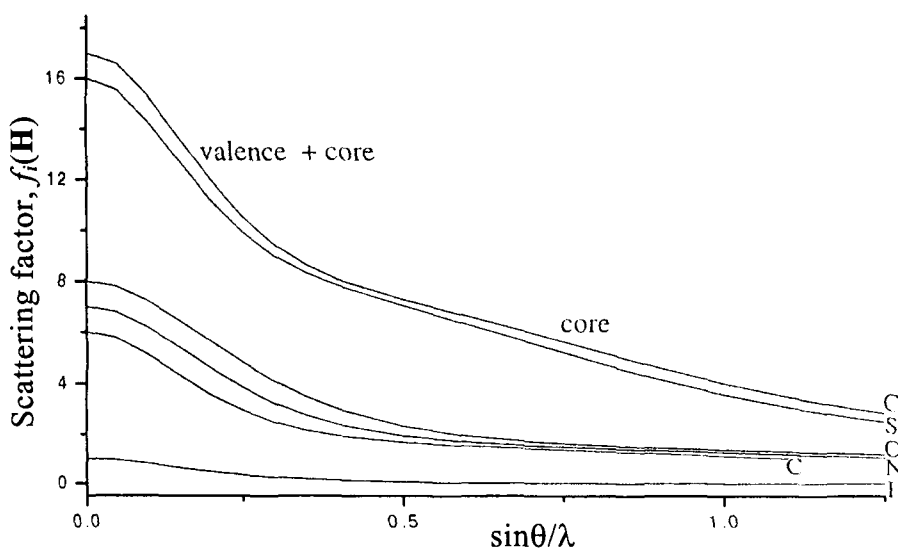
Figure 1.2: *Variations of the scattering factor with $\sin\theta/\lambda$ for different atoms. Above 0.5 $Å^{-1}$, the scattering due to valence electrons decreases gradually and the atom-core becomes visible. The scattering factors were obtained from the International Tables for Crystallography, Vol. IV, page 71 (1974).*

Each curve is composed of two regions. At low angles or Bragg vector ($H=2\sin\theta/\lambda$), $f(H)$ decreases sharply and above ~ 0.5Å^{-1}, the fall is gradual. The first part has contributions from both the atom-core and the valence density, while the second arises mainly due to the core.

One major requirement for an experimental charge density data is to have a resolution better than 0.5 Å. For small unit cells with dimensions ~ 30 Å, data collection up to moderately high resolution (1.25 Å^{-1}) can be achieved using short wavelength radiation such as MoK_α (0.7107Å). Moreover, data collection strategy typically depends on the type of the diffractometer. Fortunately, an increasing number of affordable and high-quality diffraction apparatus are now available, such as a low temperature rotating anode or even a dedicated synchrotron facility with state-of-the-art area detector. These powerful devices yield an experimental electron density ($\rho_{observed}$) which contains much more information than required merely to find nuclear positions. In 1998, it was reported that a very high resolution picture of an amino acid could be obtained within one day,[10] whereas in the past this could be a matter of several months. The Atoms in Molecules (AIM) analysis is equally valid for ρ retrieved from an X-ray diffraction experiment.

1.5 Representation of the charge density and deformation densities

The charge density can be represented either as a two-dimensional contour map, a three-dimensional contour map or as a relief map. Figure 1.3a shows the 2D contour map of ρ evaluated in the symmetry plane of

formaldehyde. The outer contour line (corresponding to ρ = 0.001 au or 0.0067

eÅ^{-3}) can be taken as the boundary of the molecule. Inside this contour line, lies

a set of non-intersecting contour lines of higher electron density, each

completely enclosing the next one (of higher ρ value). Figure 1.3b is termed a

relief map, which utilizes the third dimension to depict the value of ρ. From

these figures, it looks as if ρ is quite featureless except for indicating the

positions of the nuclei.

(a)   (b)
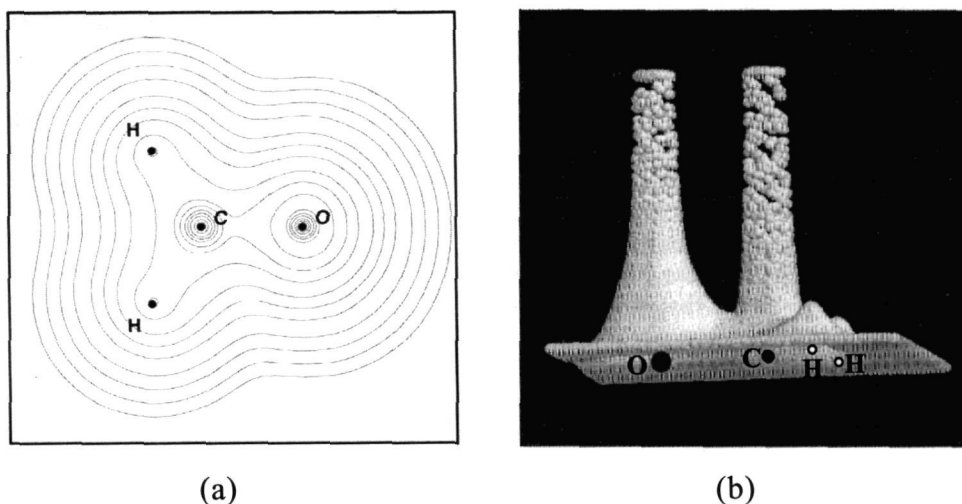
Figure 1.3: *(a) A contour plot of the electron density in the symmetry plane of formaldehyde. The outer contour line corresponds to 0.0067 eÅ^{-3}, and the electron density increases exponentially toward the innermost contours.[11] (b) A relief map of the electron density in the symmetry plane of formaldehyde. The nuclei are marked under the relief map, oxygen (left), carbon (middle) and hydrogen atoms (right).[11]*

In the relief map in Figure 1.3b, the electron density appears as being

dominated by a handful of huge peaks. In order to see the chemistry hidden in ρ,

we have to eliminate the enormous contributions of the nuclear core regions. For

this purpose, the experimental deformation density was introduced, where the

promolecule density is subtracted from the total electron density (or observed electron density). The promolecule is a superposition of spherical atoms, centered at the nuclear positions. An example of such a deformation density map for the oxalic acid molecule is shown in Figure 1.4. It can be seen that the deformation density reveals chemically relevant features such as bond regions and lone-pair regions.
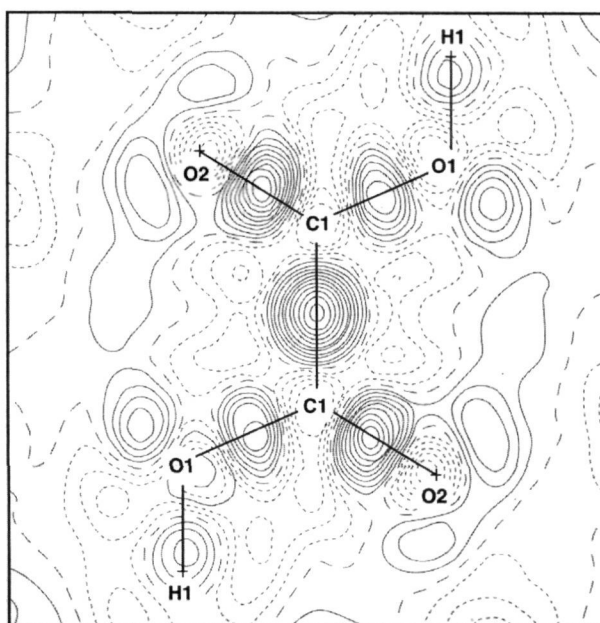
Figure 1.4: *Standard deformation denity in the molecular plane of the oxalic acid molecule at 15 K. Zero and negative lines are dashed.*[12]

Thus, X-ray diffraction facilitates extraction of the bonding or the deformation density,

$$\rho_{deformation} = \rho_{total} - \rho_{promolecule} \qquad ...(7)$$

The $\rho_{deformation}$ reveals the asphericity of the valence electron density due to chemical bonding and intra/intermolecular interactions in the crystal. The above method is called the (X-X) method. In the (X-N) method, the core positions

along with the thermal parameters are obtained from a neutron diffraction experiment. The latter is particularly useful while dealing with hydrogen atom positions though it requires two data sets, which can be expensive besides having to grow larger crystals. In the recent years, the (X-X) method has become more popular. In this part of the thesis, only the (X-X) method has been employed.

1.6 The multipole model and use of computer codes

In parallel with the early experimental studies came developments in the theory of modeling charge densities in crystals. R. F. Stewart[13] formulated a general analytical description of the atomic density distribution, which is the basis for present-day models. The implementation by Hansen and Coppens,[14] consists of a core contribution, a valence contribution, and a deformation term representing the deviation of the valence density from spherical symmetry:

$$\rho_{atom}(r) = \rho_{core}(r) + P_V\kappa^3 \, \rho_{valence}(\kappa r) + \sum_l \kappa'^3 \, R_l(\kappa'\xi r) \sum_{m=-l}^{l} P_{lmp}Y_{lmp}(\theta,\varphi) \quad ...(8)$$
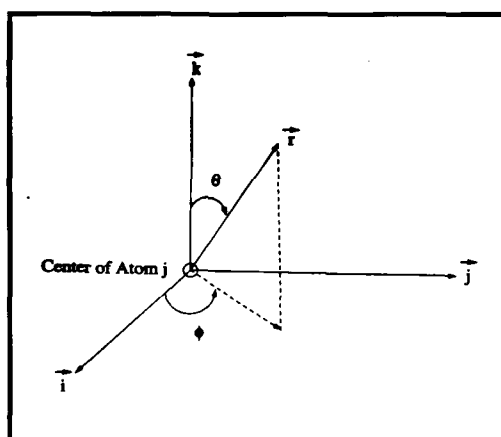
Figure 1.5: Local coordination system.

Figure 1.5 depicts the definition of local axes centered on an atom. The deformation is expressed in terms of a radial function $R_l(r)$ modulated by angular functions $Y_{lm}(\theta, \phi)$, defined on local axes centered on the atoms. The angular functions are the same spherical harmonic functions, which are used to describe atomic orbitals, but normalized for charge density rather than for wavefunctions. Their graphical representations are given in Figure 1.6. The functions with $l = 1$ are called dipoles, $l = 2$ quadrupoles, $l = 3$ octopoles, $l = 4$ hexadecapoles. The population parameters P_v, P_{lm} and expansion-contraction coefficients κ and κ' are refinable parameters, together with the coordinates and temperature factors.
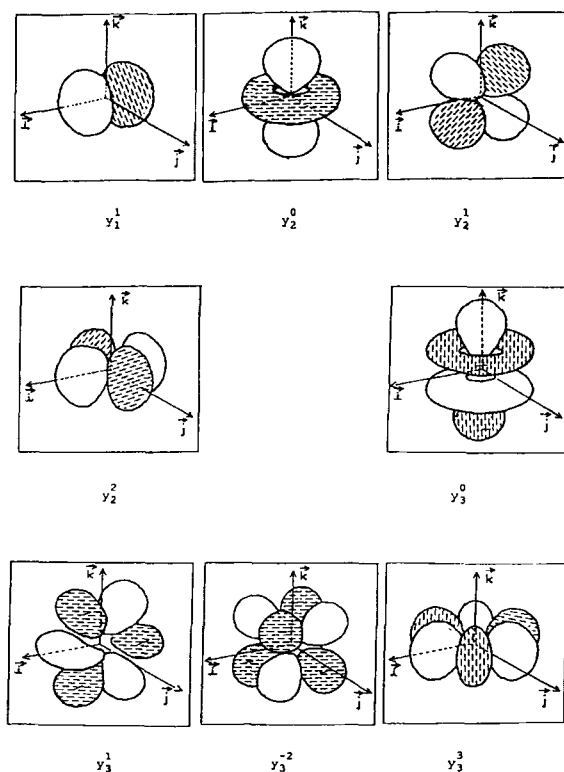
Figure 1.6: Spherical harmonic functions used to describe atomic orbitals.

For a stable least-squares refinement the number of observations to parameters ratio should be atleast seven, with $\sin\theta/\lambda$ up to atleast 1.1 $Å^{-1}$. The multipoles on the first row atoms are generally refined up to octopole moments, while for the heavier ones, moments up to hexadecapole are used. Hydrogen atoms are restricted to dipole. Kappa values greater than unity indicate contraction while lesser than unity indicate expansion. As the core is not affected by chemical bonding, there is no kappa on core, while on the valence shell, various types of kappa's namely, spherical, deformation, monopole, dipole, quadrupole, octopole and hexadecapoles are applied. As hydrogen has only one electron, the kappa value for hydrogen is quite high (close to being 1.2) compared to other atoms, which are close to 1. The above formalism is well adopted in the recently developed user-friendly program package – XD.[15a] Older codes such as MOLLY,[14a] VALRAY,[15b] LSEXP,[15c] POP[15d] are also still in use. The quality of a refined model can be monitored based on the residuals and the goodness-of-fit parameter, besides closely inspecting the deformation density maps.

$$R_1 = \Sigma \, (\,|F_o| - |F_c|\,)/\Sigma \, |F_o| \qquad \ldots(9)$$

$$wR_2 = [\Sigma w(F_o^2 - F_c^2)^2]/\,\Sigma \, w(F_o^2)^2]^{1/2} \qquad \ldots(10)$$

$$S = ([\Sigma w(F_o^2 - F_c^2)^2]/(n\text{-}p))^{1/2} \qquad \ldots(11)$$

where n refers to the number of reflections and p is the total number of parameters refined.

1.7 Some important experimental aspects of charge density determination

1.7.1 The temperature factor

Qualitatively, the effect of atomic vibrations is that X-ray structure factors decrease in magnitude with increasing scattering angle, because of the individual scattering factors and the temperature factors. In the isotropic approximation the temperature factor is

$$T_j(\mathbf{H}) = \exp(-8\pi^2 \bar{u}_j{}^2 \sin^2\theta/\lambda^2) \qquad \ldots(12)$$

Where $\bar{u}_j{}^2$ is the mean-square displacement of atom j. The factor T_j multiplies the scattering factor for atom j. The factor $8\pi^2\bar{u}_j{}^2$ is the Debye-Waller factor, B, referred to as the temperature parameter. To obtain enough data for a multipolar refinement, it is necessary to lower the temperature of the crystal. There have been a few studies at temperatures close to liquid helium,[16] but mostly the experiments are carried out at liquid nitrogen temperatures.

1.7.2 High angle refinements and the multipole model

The valence electrons are affected by chemical bonding, and refinement of this aspherical density within a spherical atom model gives errors in positions and thermal parameters. The core density near the atomic nuclei can be taken to represent the atom in a refinement using only the high-order data. Following this, an X-X_{high} deformation density can be obtained. The use of the high angle data is critical to define the thermal motion of the atoms properly and is a more satisfactory way of obtaining positional parameters unbiased by the electron re-distribution associated with bond formation.

1.7.3 Criteria for the use of the multipole model

Electron density distribution studies are usually undertaken with the aim of analyzing finer details of the charge distribution by way of comparing chemically related molecules. In this context, a test for the rigidity of the molecule is important since anisotropic displacement parameters are known to compensate both for systematic errors in the data and for inadequacies of the model. Hirshfeld[17] reasoned that the relative vibrational motion of a pair of bonded atoms has an effectively vanishing component in the direction of the bond. If $z^2_{A,B}$ denotes the mean square displacement amplitude of atom A in the direction of atom B, then for every covalently bonded pair of atoms A and B,

$$\Delta_{A,B} = z_{A,B}{}^2 - z_{B,A}{}^2 = 0 \qquad \qquad ...(13)$$

If parts of the molecule fail the *rigid bond postulate*, one may deduce that the structural model is insufficient. Hirshfeld estimated that for atoms at least as heavy as carbon, $\Delta_{A,B}$ should normally be smaller than 0.001 Å^2. Verification of the model and the anisotropic displacement parameters by this test strengthens confidence in the experimentally determined electron density distribution. In addition, for a precise multipolar modeling of the fitted data, very accurate intensity measurements, chemical suitability (sufficiently small molecules, composed of atoms with $Z < 35$, with minimal hydrogen content) and crystal suitability such as ordered structure, appropriate size and a well-characterized morphology are essential.

1.8 Topography of charge distributions

1.8.1 Critical points

Irrespective of whether an experimental or theoretical method is used to obtain the charge distribution of a molecular system, various chemical and physical properties that depend on the distribution can be derived. The topology of a charge distribution has many rich features – maxima, minima, saddles and nodes that help characterize elements like atom-cores, bonds, lone-pair of electrons etc. These are analyzed in terms of critical points, the points where the electron density exhibits an extremum. As an example, the charge density distribution in water molecule[18] is depicted in Figure 1.7 in the form of contour as well as deformation density maps. The density is maximum at the oxygen core position and decreases steeply toward the mid-region between oxygen and hydrogen reaching the minimum value at the 'critical point' (CP at which $\nabla\rho = 0$). This point carries maximum densities from the other two perpendicular directions. For example, the density in the xy plane (normal to the O-H bond) appears as a local maximum at the critical point lying between the oxygen and the hydrogen nuclei, while in the other dimension, it appears as a saddle. In other words, by moving along the x or y axes towards the critical point (CP) we reach a maximum in $\rho(r)$ [$\partial^2\rho(r_c)/ \partial x^2 < 0$ *and* $\partial^2\rho(r_c)/ \partial y^2 < 0$]. But if we move along the z-axis towards the CP, then a minimum in $\rho(r)$ is reached [$\partial^2\rho(r_c)/ \partial z^2 > 0$].

A quantitative description of the charge density thus boils down to examining the number and the nature of such critical points in and around the molecule.

(a)

(b)
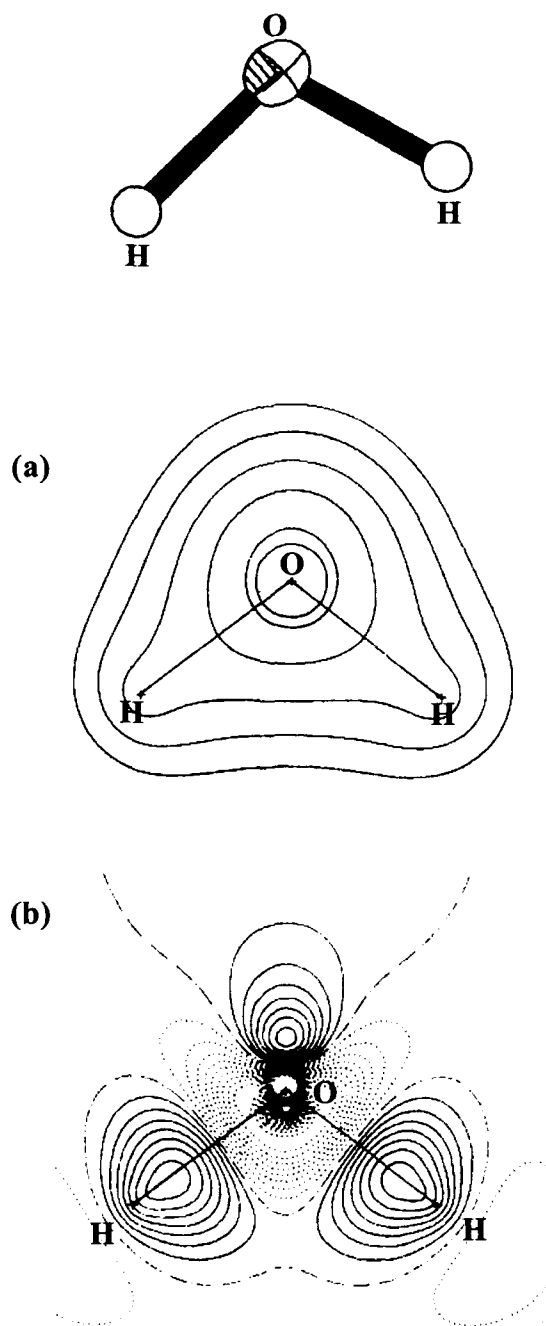
Figure 1.7: Water: Charge density in the symmetry plane, (a) the contour map. The outermost contour line has the value 0.0067 e$Å^{-3}$. The density increases exponentially for inner contours. (b) The deformation density map where the bond-regions and one of the lone-pair lobes on the oxygen atom are seen.[18]

A critical point is characterized not only by its electron density, but also by the curvatures and the associated signs.

For an arbitrary choice of coordinate axes, one encounters nine second derivatives of the form $\partial^2\rho/\partial x\partial y$ in the determination of the curvatures of ρ at a point in space. Their ordered 3×3 array is called the Hessian matrix of the charge density. Thus,

$$\text{Hessian, H} = \begin{bmatrix} \partial^2\rho/\partial x^2 & \partial^2\rho/\partial x\partial y & \partial^2\rho/\partial x\partial z \\ \partial^2\rho/\partial y\partial x & \partial^2\rho/\partial y^2 & \partial^2\rho/\partial y\partial z \\ \partial^2\rho/\partial z\partial x & \partial^2\rho/\partial z\partial y & \partial^2\rho/\partial z^2 \end{bmatrix}$$

is a real, symmetric matrix and can be diagonalized. The new axes about which the Hessian is diagonalized is called the principal axes of curvature, so termed because the magnitude of the three second derivatives of ρ calculated with respect to these axes are extremized.

$$\begin{bmatrix} \partial^2\rho/\partial x^2 & \partial^2\rho/\partial x\partial y & \partial^2\rho/\partial x\partial z \\ \partial^2\rho/\partial y\partial x & \partial^2\rho/\partial y^2 & \partial^2\rho/\partial y\partial z \\ \partial^2\rho/\partial z\partial x & \partial^2\rho/\partial z\partial y & \partial^2\rho/\partial z^2 \end{bmatrix} \Longrightarrow \begin{bmatrix} \lambda_1 & 0 & 0 \\ 0 & \lambda_2 & 0 \\ 0 & 0 & \lambda_3 \end{bmatrix}$$

The trace of the Hessian matrix, that is, the sum of the diagonal elements, is invariant to the rotation of the coordinate system. Thus, the curvature of charge density $\nabla^2\rho$, called the Laplacian, obtained as the sum of eigenvalues - λ_1, λ_2, λ_3 of the Hessian matrix, is invariant to the choice of the coordinate system.

$$\text{Trace} = \lambda_1 + \lambda_2 + \lambda_3 = \text{Laplacian of the charge density}$$

The nature of the critical points is uniquely defined by the set (rank, signature). The rank (r) of the critical point refers to the number of non-zero eigenvalues of the Hessian matrix, while the signature (s) refers to the sum of their signs (refer Tables 1.1 and 1.2). The critical points can be characterized in a quantitative way by evaluating properties at them.

Table 1.1

Critical point	Meaning
(3, -3)	All curvatures are negative and ρ is a local maximum at r_c.
(3, -1)	Two curvatures are negative and ρ is a maximum at r_c in the plane defined by their corresponding axes. ρ is a minimum at r_c along the third axis, perpendicular to this plane.
(3, +1)	Two curvatures are positive and ρ is a minimum at r_c in the plane defined by their corresponding axes. ρ is a maximum at r_c along the third axis, perpendicular to this plane.
(3, +3)	All curvatures are positive and ρ is a local minimum at r_c.

Table 1.2 Chemical entity defined in terms of critical points

Chemical entity	Property	Critical point	Acronym
Atom-cores (or nuclear attractors)	ρ (local maximum)	(3, -3)	NA
Bonds	ρ (first order saddle)	(3, -1)	BCP
Rings	ρ (second order saddle)	(3, +1)	RCP
Cages	ρ (local minimum)	(3, +3)	CCP
Lone-pair	$\nabla^2\rho$	(3, +3)	LP

Covalent bonds are usually associated with high charge densities (1.5 to 3 $e\text{Å}^{-3}$) and negative Laplacians, while ionic bonds are characterized by small densities and positive Laplacians. Table 1.3 lists some typical values of ρ and $\nabla^2\rho$ at the bond critical point for covalent bonds. Thus, a typical C-C bond carries a density of ~ 1.7 $e\text{Å}^{-3}$ and a Laplacian of ~ -16.0 $e\text{Å}^{-5}$ at the critical point, while a KF bond carries a density of 0.37 $e\text{Å}^{-3}$ and a Laplacian of 7.47 $e\text{Å}^{-5}$. Hydrogen

bonds are associated with even smaller densities and Laplacians. The hydrogen

bond in water carries a density of 0.133 e$Å^{-3}$ and a Laplacian of 1.50 e$Å^{-5}$.

Table 1.3 Typical values of charge density parameters at the BCP for covalent bonds[19]

Type of covalent bond	ρ (e$Å^{-3}$)	$\nabla^2\rho$ (e$Å^{-5}$)
C-C in CH_3CH_3	1.707	-15.953
C=C in CH_2CH_2	2.467	-29.495
C-O in CH_3OH	1.775	-3.493
N-O in NH_2OH	2.155	-13.522
N≡N in N_2	4.801	-66.490
C-N in CH_3NH_2	1.866	-22.762
O-H in H_2O	2.475	-50.155
N-H in NH_3	2.312	-41.737
C-H in CH_4	1.846	-22.977

In addition to the charge density maps, sometimes it is necessary to draw

Laplacian maps to unravel the nature of interaction in the intramolecular and

intermolecular regions as well as the shape of the lone-pairs. Figure 1.8 shows

Laplacian maps of tetrasulfur tetranitride (experimentally and theoretically

derived),[20] in the plane formed by the sulfur and nitrogen atoms. The lone pairs on

the sulfur and nitrogen atoms are clearly seen as lobes. We observe that there

exists shared (covalent) interaction between the intramolecular sulphur and

nitrogen atoms (S-N bond: ρ=1.54(1) e$Å^{-3}$, $\nabla^2\rho$= -10.60(3) e$Å^{-5}$), while there is a

weak, closed-shell (ionic) interaction between the two sulphur atoms (S-S bond:

ρ=0.37(1) e$Å^{-3}$, $\nabla^2\rho$=1.61(1) e$Å^{-5}$), as evident from the positive value of the

Laplacian.

(a)

(b)

$$\nabla^2 \rho_{exp} \qquad \nabla^2 \rho_{exp} \qquad \nabla^2 \rho_{calc}$$
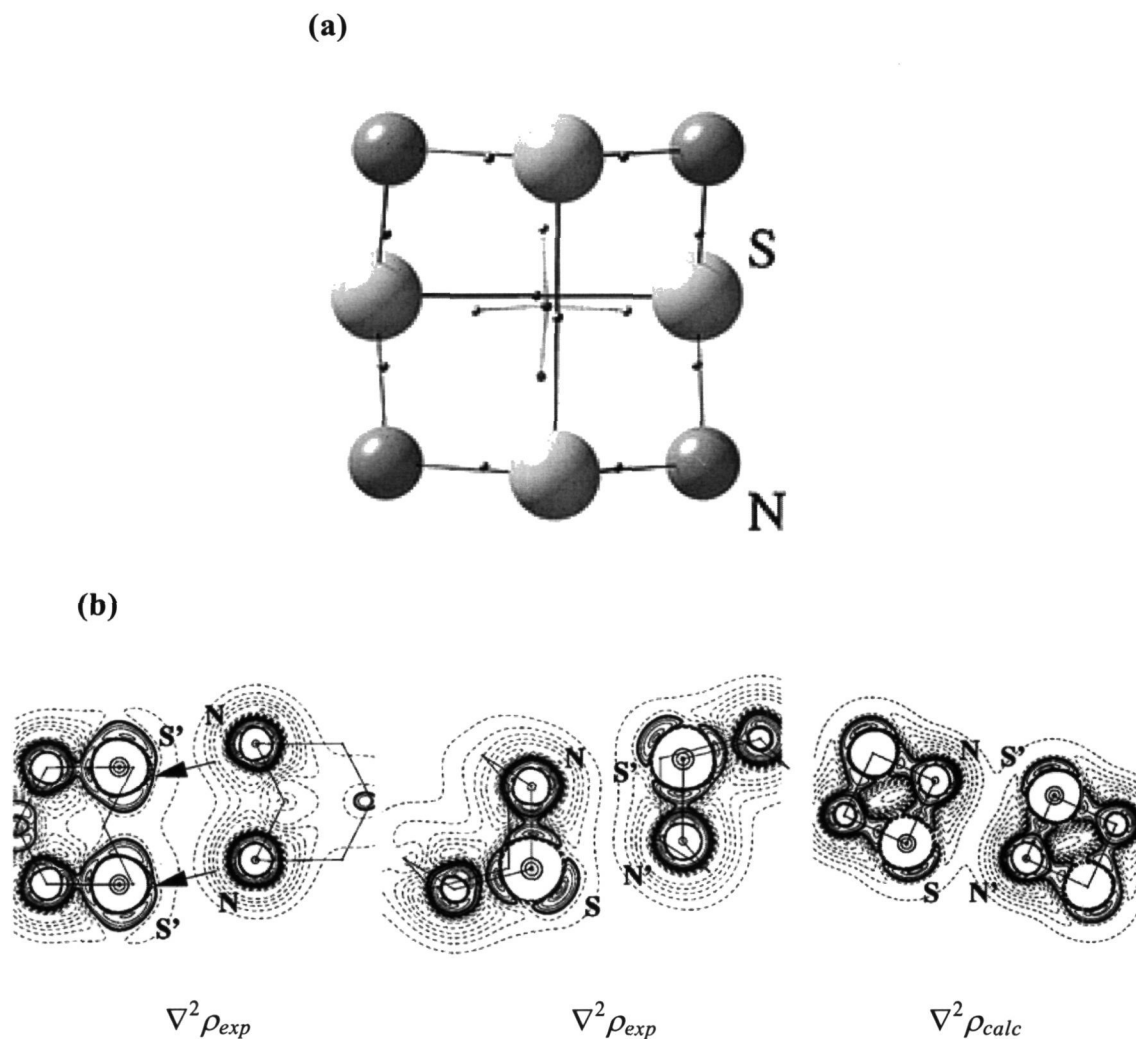
Figure 1.8: *(a) Location of the critical points denoted by closed circles in the tetrasulphur tetranitride (S_4N_4) skeleton. The bond critical points along the S-N bonds are shifted towards the more electropositive sulfur atoms. (b) Contour maps of the Laplacian derived experimentally and by ab initio calculation, using Gaussian. From left: $\nabla^2\rho_{exp}$ in the NNS'S' plane; $\nabla^2\rho_{exp}$ in the SNN'S' plane; $\nabla^2\rho_{calc}$ in the SNN'S' plane of the $(S_2N_2)_2$ dimer. Note the charge concentrations in the intramolecular regions and charge depletions in the intermolecular regions.[20]*

1.8.2 Bond properties

Bond path

A gradient vector is a vector that points in the direction of greatest increase in the scalar function (the electron density, ρ). A gradient path is a succession of tiny segments of gradient vectors, which gives rise to a trajectory. The pairs of gradient paths which originate at each (3, -1) critical point and terminate at the nuclei define a line through the charge distribution linking the neighbouring nuclei, along which $\rho(r)$ is a maximum with respect to any neighbouring line. This line (the atomic interaction line) is called a bond path (BP). The bond critical point (BCP) lies on the bond path. This is the topological definition of a chemical bond, formalising the theoretically predicted and experimentally observed (from deformation maps) accumulation of charge between bonded nuclei. Figure 1.9 shows the collection of bond paths in [1.1.1] propellane.[21]

It is clear from the figure that the bond paths are not always straight lines. Note, for example, the considerable curvature in the cyclopropane carbon-carbon bond paths. These curved bond paths are consistent with the concept of bond strain. The deviation of bond paths from straight lines can be quantified by measuring the bond path length R_b, the distance between two nuclei measured along the bond path. The bond path length is always greater than or equal to the bond length, R_e, which is simply the distance between the bonded nuclei, measured along a straight line.
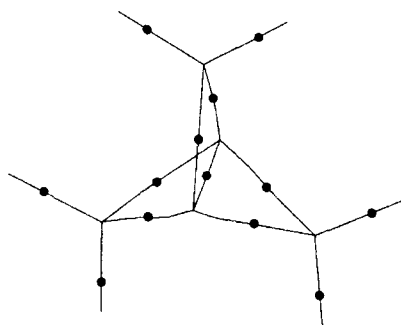
Figure 1.9: Planar projection of the molecular graph of [1.1.1] propellane generated from a theoretical electron density. The small black dots denote the bond critical points.[21]

A molecular graph is a representation of a molecule containing the bond paths and the bond critical points (see Figure 1.9).

Bond order

The value of the electron density at the bond critical point, ρ_{BCP} is a measure of the extent of charge accumulation along the bond path and can be related to bond order. Cremer and Kraka have obtained an exponential relationship[19] between bond order and the electron density, ρ_{BCP}. The exponential relation is given by

$$n\ (A,B) = \exp\{a \cdot [\ \rho_{BCP}\text{-}b]\} \qquad \qquad ...(14)$$

where $n\ (A,B)$ is the bond order, A and B are the atoms forming the bond, ρ_{BCP} is the electron density at BCP and a and b are constants for the bond order relation. For the single bond in ethane, ρ_{BCP} is ~ 2 eÅ^{-3}. Correspondingly higher values of ρ_{BCP} are found for benzene (bond order 1.6), ethylene (2.0), and acetylene (3.0).

Bond ellipticity

The bond critical point is a minimum of ρ along the bond path. The associated curvature of ρ (λ_3) is therefore positive in this direction. But in the plane normal to the bond path, ρ has a maximum value at the BCP and the two curvatures are negative. If the bond is not cylindrically symmetric (as for a bond with π character) then charge is preferentially accumulated in a particular plane along the bond path. A quantitative measure of this cylindrical asymmetry is the bond ellipticity (ε). Values of ε provide a measure of the extent to which the charge density is asymmetrically concentrated perpendicular to the bond path.

$$\varepsilon = \frac{\lambda_1}{\lambda_2} - 1 \qquad \qquad ...(15)$$

λ_1 and λ_2 are the two negative Hessian eigenvalues, λ_2 being the curvature of smaller magnitude. The corresponding eigenvector is the major axis of curvature, defining the orientation of the plane in which charge is smeared. For example, the ellipticity value obtained for ethane and acetylene is 0.0, while for benzene it is 0.23 and for ethylene 0.45. In these last two cases, the major axis is normal to the plane of the nuclei. In cyclopropane, by contrast, charge is concentrated over the ring surface and the major axis of curvature lies in the ring plane, with an ellipticity value of 0.45.

Bond polarization

An estimate of bond polarization[19] can be obtained from the location of the bond CP with respect to the internuclear vector,
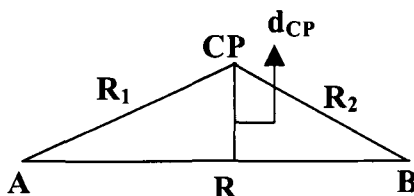
$$\Delta_{BCP} \% = 100 \times (R_m - R_1) / R_m \qquad \ldots(16)$$

where $R_m = (R_1 + R_2)/2$. The Δ value is used to describe relative electronegativities of atoms forming the bond. The strain involved in a bond can be estimated[21] in terms of the vertical displacement, d_{CP} of the bond path from the internuclear vector

$$d_{CP} = 2 \times [(s \times (s - R_1) \times (s - R_2) \times (s - R))^{1/2}]/R \qquad \ldots(17)$$

where $s = (R_1 + R_2 + R)/2$.

The above topological and charge density properties in combination with pseudoatomic charges describe a bond quantitatively.

The other quantity of interest is the kinetic energy density at the critical point, G_{CP}[22] which is obtained by

$$G_{CP} = \left(\frac{3}{10}\right)(3\pi^2)^{2/3} \rho_{CP}^{\frac{5}{3}} + \frac{\nabla^2 \rho_{CP}}{6} \qquad \ldots(18)$$

It has been used in some cases for the calculation of hydrogen bond energies[23] and their classification.[24]

1.8.3 Ring properties

When nuclei are topologically connected to form a ring structure such as in benzene, a ring critical point (RCP) arises, which lies somewhere close to the

geometric centroid of the ring. In the case of benzene, the ring consists of a set of six C-C bond paths. The spectrum of curvatures (λ_1, λ_2 and λ_3) give rise to a (3, +1) critical point. This is because, along the ring surface, in two dimensions, the electron density is a minimum at the RCP and the associated curvatures are positive (λ_2 and λ_3). And perpendicular to the ring surface, the electron density is a maximum at the RCP with the associated curvature (λ_1) being negative.
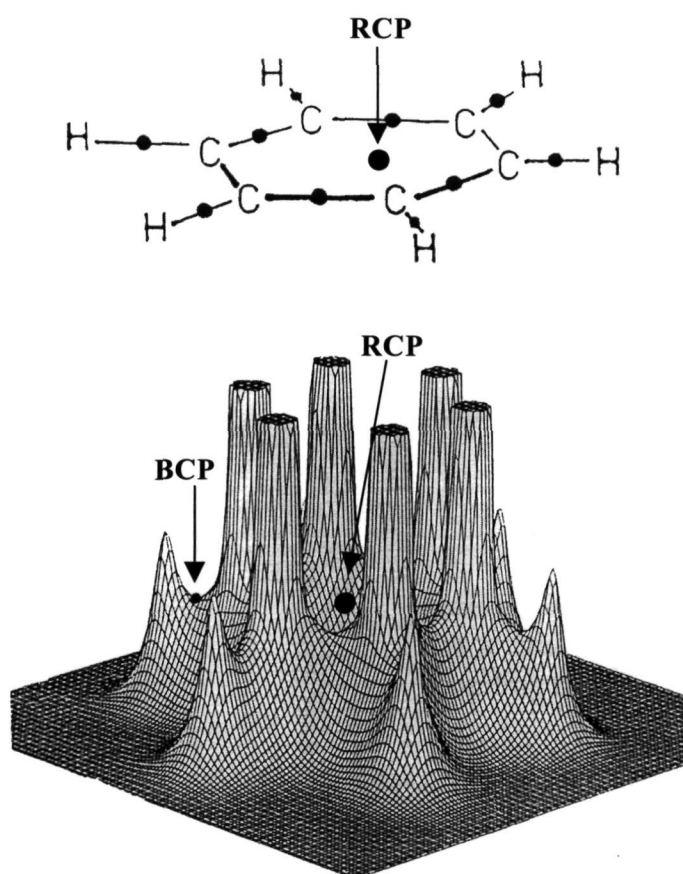
Figure 1.10: *The upper half of the figure illustrates the molecular graph of benzene with BPs and BCPs. The lower half is a perspective diagram of the calculated electron density of benzene with respect to the plane containing the 12 nuclei. The position of the bond (BCP) and the ring critical point (RCP) are marked by black circles and arrows.*[25]

Therefore, at the RCP, the Hessian possesses two positive and one negative eigenvalues and the signature equals (+1) + (+1) + (-1) = +1. Figure 1.10 shows the position of the RCP in the charge density distribution of benzene.[25]

1.8.4 Intermolecular regions - hydrogen bonds

The electron distribution can be used as a powerful and independent source of information for characterizing the hydrogen bond (D-H$\cdots$A: D-donor and A-acceptor). Koch and Popelier[26] proposed a set of "necessary and sufficient" criteria, based on the AIM theory, for recognizing an H$\cdots$A interaction as a hydrogen bond. These criteria are listed in Table 1.4.

Table 1.4 Some important criteria by Koch and Popelier for hydrogen bonding.[26]

A well defined topology (bond critical point BCP and bond path BP) for each hydrogen bond

A ρ value at the BCP within the range [0.013, 0.27 eÅ^{-3}][a]

A Laplacian value at the BCP within the range [0.5, 3.5 eÅ^{-5}][a]

Loss of charge of the hydrogen atom

Decrease of the hydrogen atom's volume

[a]*Compare these values with those for covalent bonds given in Table 1.3.*

The characterization of intra- and intermolecular hydrogen bonds on the basis of charge density distribution has attracted considerable attention over the past decade. Early topological analyses of theoretical electron densities of hydrogen-bonded complexes between nitriles and hydrogen halides[27] have shown a linear correlation between the bond energy and ρ_{BCP} of the H$\cdots$N bonds for internuclear separation greater then 2 Å. The Atoms in Molecules (AIM) theory is the ideal tool to detect and classify hydrogen bonds.

An example to illustrate the calculated electron density distribution in hydrogen bonds: Vorobyov *et al*[28] have carried out *ab initio* calculations on complexes of water with ethene, propene and allyl alcohol. The molecular graphs of these πH-bonded complexes are illustrated in Figure 1.11. The authors have analyzed the energetics and electron density redistribution associated with hydrogen bonding interactions in these clusters. Topological analysis of the electron density performed using Bader's AIM theory confirms the closed-shell, hydrogen bonding nature of O-H⋯O ($\rho \sim 0.13$ eÅ^{-3}, $\nabla^2\rho \sim 2.30$ eÅ^{-5}) and O-H⋯π interactions ($\rho \sim 0.13$ eÅ^{-3}, $\nabla^2\rho \sim 0.92$ eÅ^{-5}).
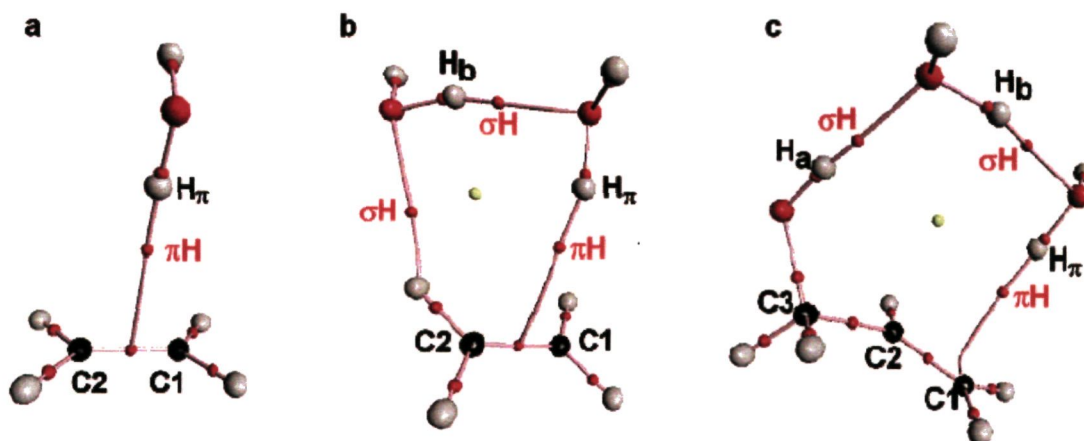
Figure 1.11: *Molecular graphs for some πH-bonded complexes: (a) water⋯ethene, (b) water dimer⋯ethene, (c) water dimer⋯allyl alcohol. Bond paths are denoted by pink cable like connections, nuclei are indicated by large spheres, and BCPs and RCPs are indicated by red and yellow small spheres, respectively.[28]*

High ellipticity values (~0.6) at the H⋯π BCPs of these complexes indicates their additional floppiness compared to the classical type of hydrogen bonds.

Properties of the H···π BCPs place O-H···π interactions within the spectrum of values proposed by Koch and Popelier for hydrogen bonds. The Laplacian maps are depicted in Figure 1.12.

(a)   **(b)**
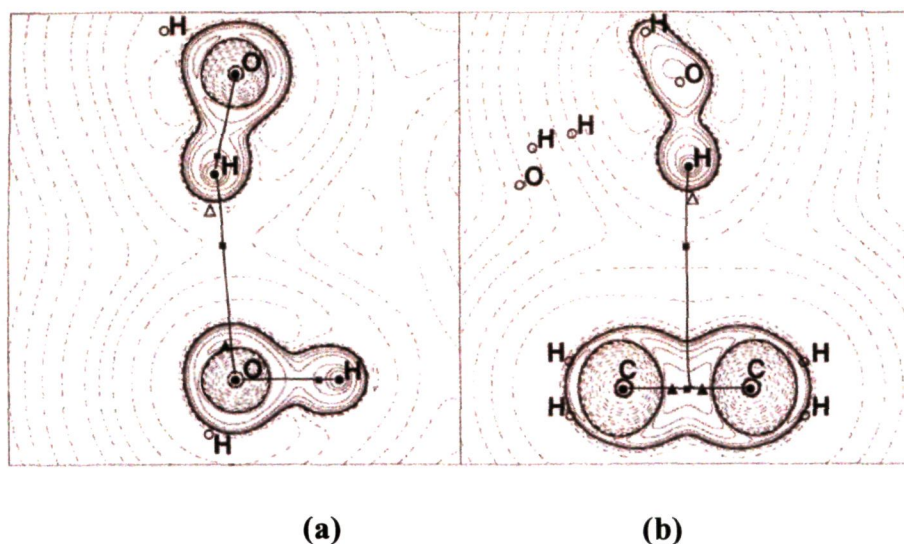
Figure 1.12: *Contour plots of the negative of the Laplacian (-$\nabla^2\rho$) for the complex of ethene with the water dimer in the plane of (a) O-H···O and (b) O-H···π bonded atoms. Solid contours denote positive values of -$\nabla^2\rho$, regions of charge concentration, and dashed contours denote -$\nabla^2\rho$ < 0, regions of charge depletion. BCPs are shown as solid squares. Bond paths: solid lines connecting nuclei. Maxima and minima in -$\nabla^2\rho$ are denoted by solid and open triangles, respectively.*[28]

Hydrogen bonds can be classified on the basis of charge density. Alkorta and co-workers studied various types of hydrogen bonds including dihydrogen bonds,[29] bifurcated hydrogen bonds,[30] H···π interactions,[31] inverse hydrogen bonds[32] and hydrogen bonds involving carbenes and silylenes as acceptors.[33] Charge density studies on some systems that exhibit dihydrogen bonds (H···H) have also been studied. Zhang *et al*[34] carried out theoretical studies on hydrogen-

bonded complexes, with strained organic systems like tetrahedrane acting as pseudo π-acceptors.

Experimental charge density studies have been performed on a variety of hydrogen-bonded systems, most pertaining to O-H⋯O[35] and N-H⋯O[36] hydrogen bonds although weak C-H⋯O,[37] N-H⋯π[38] and C-H⋯π[39] interactions have also been explored. As an example for O-H⋯O type of hydrogen bond, Figure 1.13 shows methylammonium hydrogen succinate monohydrate, which is a dicarboxylic acid salt.[40] Very strong H⋯O type hydrogen bonds, with O⋯O distances less than 2.5 Å, are usually found in the crystal structures of acid salts of dicarboxylic acids. The O-H⋯O hydrogen bond is symmetric, with the proton situated near the midpoint of the O⋯O internuclear line. Usually, the proton occupies a special position, being shared by two symmetry related carboxyl groups.[41] In the crystal structure of methylammonium hydrogen succinate monohydrate,[40] the hydrogen succinate anion and the proton are located on inversion centres while the methylammonium cation and the water molecules are situated on a mirror plane of space group P2$_1$/m. A symmetric O-H-O hydrogen bond is formed, with the proton occupying an inversion centre, with an H⋯O distance of 1.221 Å. The negative Laplacian values for these bonds (-6.8(10) eÅ^{-5}) indicate considerable covalent character.
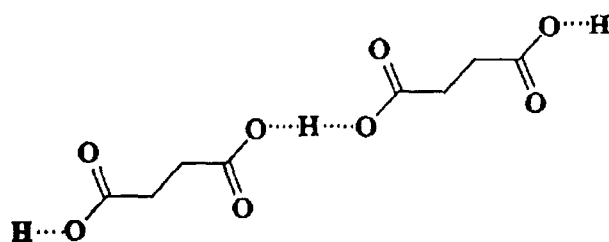
Figure 1.13: *The symmetric O-H-O hydrogen bond in methylammonium hydrogen succinate monohydrate.*[40]

The covalent nature of the strong H···O bond is also supported by the non-equivalence of the carbonyl bonds in the carboxylate group (R_{C-O} = 1.286 Å, ρ_{BCP} = 2.52(2) eÅ^{-3} and $\nabla^2\rho$ = -29.7(1.2) eÅ^{-5}, relative to the second C-O bond - R_{C-O} = 1.245 Å, ρ_{BCP} = 2.86(2) eÅ^{-3} and $\nabla^2\rho$ = -35.4(1.3) eÅ^{-5}).

Similarly, experimental charge density investigations have been carried out to probe O-H···O hydrogen bonds in benzoylacetone,[42] urea-phosphoric acid,[43] potassium hydrogenoxalate,[44] *p*-nitrophenol,[45] to cite a few.

An example of a charge density study on N-H···O hydrogen bonds is the co-crystallized complex of betaine, imidazole and picric acid. Low temperature (28 K) X-ray and neutron diffraction data were carried out by Overgaard *et al*[46] on this complex that exhibits three different short N-H···O hydrogen bonds (see Figure 1.14). The H···O distances of the N-H···O bonds in the betaine, imidazole and picric acid complex lie in the range of 1.6 - 1.7 Å (well within the van der Waals cut-off) and the N-H···O angles vary from 155 to 171°. The electron densities and Laplacians at the hydrogen bond critical points are in the range 0.3 - 0.4 eÅ^{-3} and 1.8 - 3.2 eÅ^{-5}, respectively.
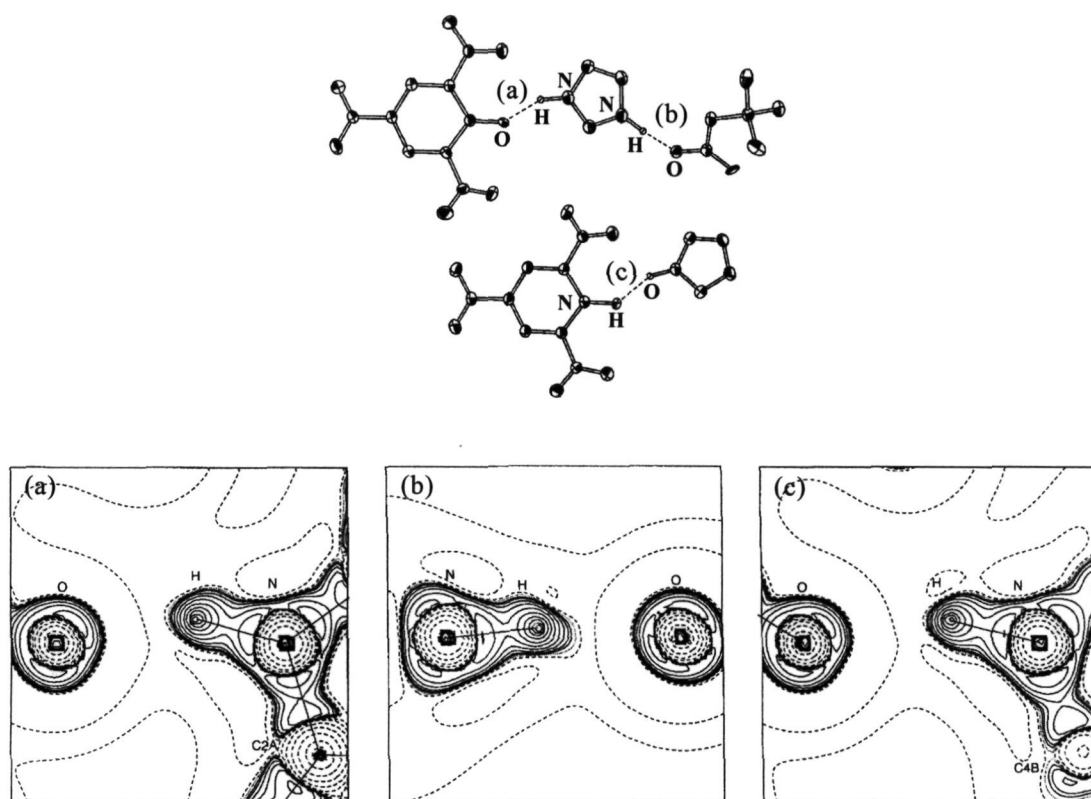
Figure 1.14: *Top- ORTEP plot of the co-crystal of betaine, imidazole and picric acid. The N-H···O hydrogen bonds are depicted. Bottom- Contour plot of -$\nabla^2\rho$ in the planes of three strong N-H···O hydrogen bonds in the co-crystal.*[46]

A few other examples of molecular crystals exhibiting N-H···O hydrogen bonds for which experimental charge densities have been determined are cyanuric acid,[47] 5-nitrouracil,[48] 2-methyl-5-nitroaniline,[49] to name a few.

Charge density analyses of N-H···N hydrogen bonds are few. An important study is by Mallinson *et al*[50] who have characterized the intramolecular N-H···N hydrogen bonds in a proton sponge, 1,8-bis(dimethylamino)naphthalene, and in its ionic complex with 1,2-dichloromaleic acid. Owing to its extremely high proton affinity, 1,8-bis(dimethylamino)naphthalene ("proton sponge"),[50a] forms very stable ionic complexes with acids. The proton is captured in an N-

H⋯N intramolecular hydrogen bond (see Figure 1.15), the strength of which alone would not explain the unusually high basicity of the acceptor molecule. In the ionic complex of bis(dimethylamino)naphthalene with 1,2-dichloromaleic acid,[50b] the N-H and H⋯N distances in the N-H⋯N hydrogen bond (1.106(5) and 1.608(6) Å) indicate that the proton in the cation is more strongly bonded to one of the N atoms. Also, it does not lie on the N-N internuclear axis. The analysis of the experimental electron density and its Laplacian (Figure 1.15) obtained from X + N data give information on the nature of the hydrogen bonds and provide evidence for the charge redistribution upon protonation.
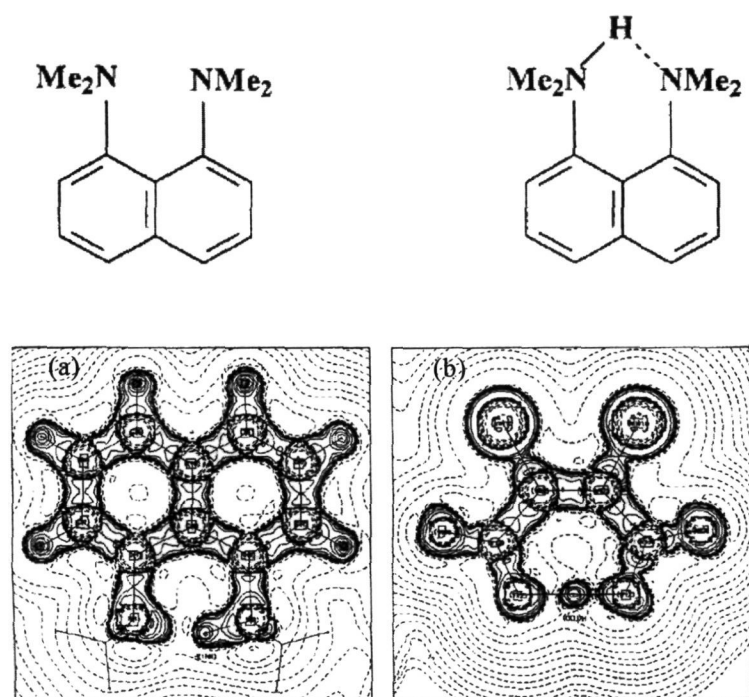
Figure 1.15: *Top- A schematic diagram of capture of the proton in 1,8-bis-(dimethylamino)naphthalene. Bottom- Experimental Laplacian maps in the molecular plane of (a) 1,8-bis-(dimethylamino)naphthalene and (b) 1, 2-dichloromaleic acid.[50]*

The proton in the cation is covalently bonded to the nearest N atom, but the CP of the second H$\cdots$N interaction in the cation is in a region of positive Laplacian (ρ_{BCP} = 0.53(2) eÅ^{-3}, $\nabla^2\rho_{BCP}$ = 4.3(1) eÅ^{-5}). The trajectory of the bond path along the N-H$\cdots$N bond is not linear, that is, the N-H and H$\cdots$N bond paths (R_b) are longer than the corresponding internuclear distances (note that the bond paths are not indicated in Figure 1.15).

There have also been many charge density investigations on C-H$\cdots$O hydrogen bonds, such as those found in 3,4-bis(dimethylamino)-3-cyclobutene-1,2-dione.[51] There have been charge density studies on crystals hosting both O-H$\cdots$O and N-H$\cdots$O bonds as in 1-methyuracil,[52a] p-nitrobenzene derivatives,[52b] 2-amino-5-nitropyridinium dihydrogen phosphate,[52c] and N-acetyl-L-tyrosine ethyl ester monohydrate.[52d] Compounds containing both O-H$\cdots$O and C-H$\cdots$O bonds such as the polymorphs of cinnamic acid and its photodimer[53a] and aliphatic dicarboxylic acids[53b] have been analyzed. DL-histidine which exhibits a variety of intermolecular (N-H$\cdots$O, N-H$\cdots$N, C-H$\cdots$O, C-H$\cdots$N, O-H$\cdots$C, N-H$\cdots$C and C-H$\cdots$C) bonds has also been investigated.[54] In general, the total density at the bond critical points of the hydrogen bonds in all such systems is generally in the range- 0.01 - 0.6 eÅ^{-3} while the Laplacians are positive and fall in the range, 0.3 - 6.0 eÅ^{-5}.

2. SCOPE OF THE PRESENT INVESTIGATIONS

The family of hydrogen bonds includes the strongest, the moderate as well as the weakest species, and inter- as well as intramolecular interactions (O-H$\cdots$O, O-H$\cdots$N, N-H$\cdots$O, N-H$\cdots$N, N-H$\cdots$S, C-H$\cdots$O, C-H$\cdots$N, O-H$\cdots\pi$, N-H$\cdots\pi$, C-H$\cdots\pi$, etc). A technical or quantitative definition of the hydrogen bond essentially includes a series of threshold values. The "van der Waals cut-off" definition[55] for identifying hydrogen bonds on a structural basis (requiring that the H$\cdots$A distance is substantially shorter than the sum of the van der Waals radii of the hydrogen (H) and acceptor (A) atoms) has been considered to be too restrictive and has not been applied very frequently.[55,56] If distance cut-off limits must be used, D-H$\cdots$A interactions with H$\cdots$A distances up to 3.0 or even 3.2 Å are considered as potentially hydrogen bonding. An angular cut-off can be set as $> 90°$ or $> 110°$. A necessary geometric criterion for hydrogen bonding is a positive directionality preference, that is, linear D-H$\cdots$A angles must be statistically favoured over bent ones. There are also spectroscopic criteria that give a specialized characterization of the hydrogen bond, like certain effects in infra-red absorption spectra (red-shift and intensification of v_{D-H}, etc). All these criteria with the respective threshold values provide the structural quantifiers for the hydrogen bond. But a complete quantification of the hydrogen bond still entails an intensive study. Against this background, we reasoned that the experimental charge density method might provide an absolute quantification of the hydrogen bond, based on the electron density and topological parameters obtained from such studies.
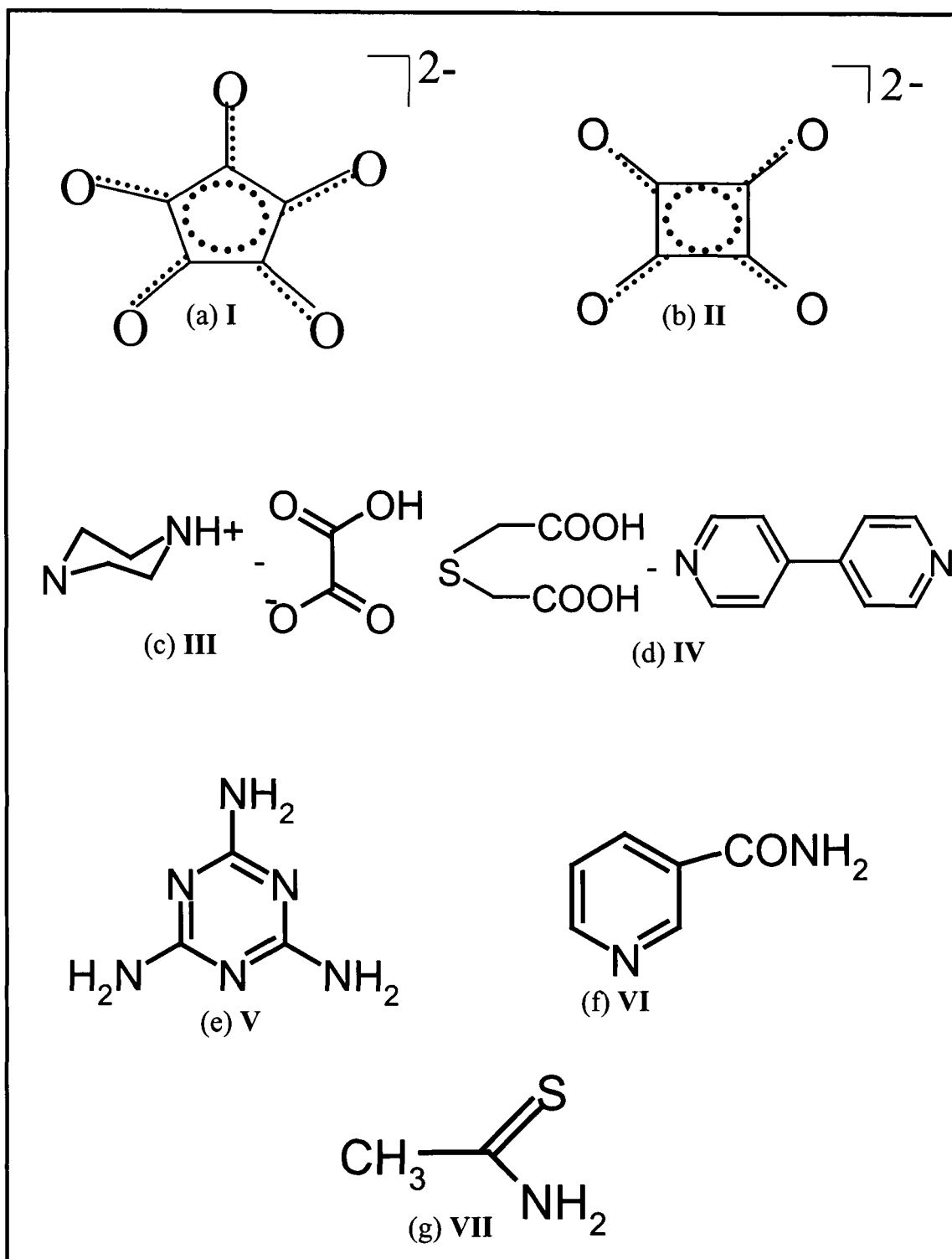
Figure 2.1: *Structural diagrams of the molecules chosen for the experimental charge density studies - (a) croconate dianion,* **I** *(b) squarate dianion,* **II** *(c) piperazine-oxalate,* **III** *(d) thiodiglycolloic acid-4,4'-bipyridine,* **IV** *(e) melamine,* **V** *(f) thionicotinamide,* **VI** *(g) thioacetamide,* **VII**.

217

As a total electron redistribution occurs upon hydrogen bond formation, an electron density analysis would provide the key to many unanswered questions. We have carried out structural and charge density investigations of various molecular crystals, in addition to several other aspects of interest (see Figure 2.1 for the structural diagrams of the molecules under study).

2.1 Trends in experimental charge density parameters of hydrogen bonds

Several reviews and monographs in the literature have highlighted the trends in the nature and geometry of the hydrogen bond.[57,58] In this context, the Cambridge Structural Database (CSD) containing more than a quarter of a million crystal structures[59] has proved to be a great resource for searching hydrogen bond patterns and possible correlations. Figure 2.2 depicts some results of statistical analyses obtained from the vast amount of literature on the structural aspects of hydrogen bonds. Deformation densities and electrostatic potential maps derived from experimental densities reveal vital characteristics of the hydrogen bond and there have been attempts to relate the charge density descriptors with the geometric parameters of the hydrogen bond. Thus, Espinosa *et al*,[60] based on an analysis of a number of D-H$\cdots$O bonds (D: donor), have proposed possible relationships between the topological properties at the critical points (CPs) and geometrical parameters such as the H$\cdots$O distance. These authors observed an exponential dependence of the positive curvature of the electron density (λ_3) with the H$\cdots$O distance. Figure 2.3 illustrates the variation of parameters obtained from charge density studies (experimental and theoretical) with the hydrogen$\cdots$acceptor distance for D-H$\cdots$O bonds. A similar relation has been

reported by Slouf *et al*[61] for O-H⋯O and N-H⋯O bonds in a nucleoside phosphonate.

However, these studies were restricted to only those hydrogen bonds with oxygen as

an acceptor atom.
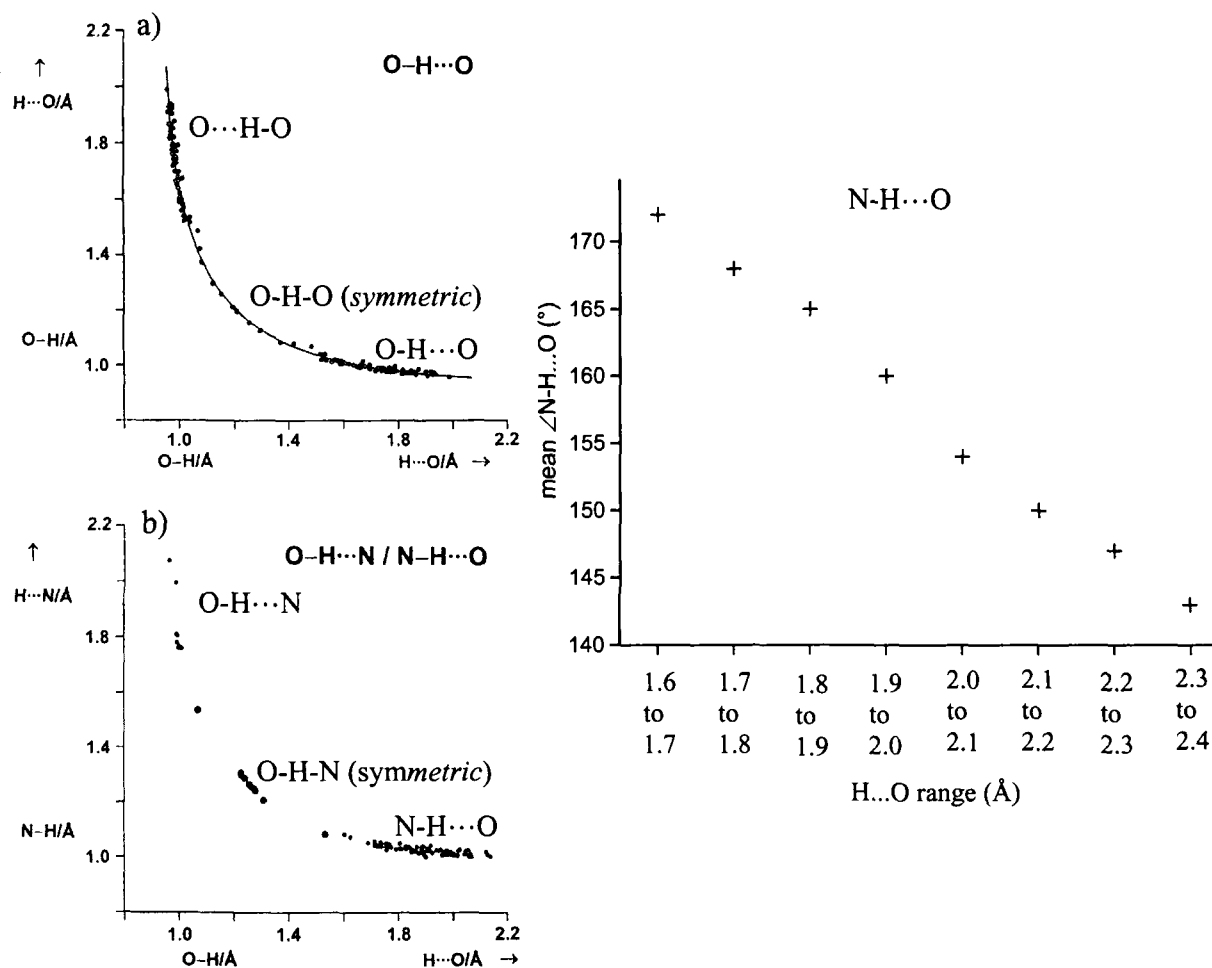
Figure 2.2: *Lengthening of the X-H bond in X-H⋯A hydrogen bonds. a) Correlation of O-H and H⋯O distances in O-H⋯O hydrogen bonds.*[63] *The plot is symmetrized with respect to the two O atoms.*[64] *(b) Correlation of N-H with H⋯O bond lengths and O-H with H⋯N bond lengths.*[65] *The right branch shows N-H⋯O, and the left branch O-H⋯N hydrogen bonds. The symmetric hydrogen bonds are indicated by solid lines (O-H-O and O-H-N). Both plots are based on neutron diffraction data. (c) Variation of the N-H⋯O hydrogen bond angle with the hydrogen bond H⋯O distance. Short distances are associated with high hydrogen bond angles, close to 180°.*[66]
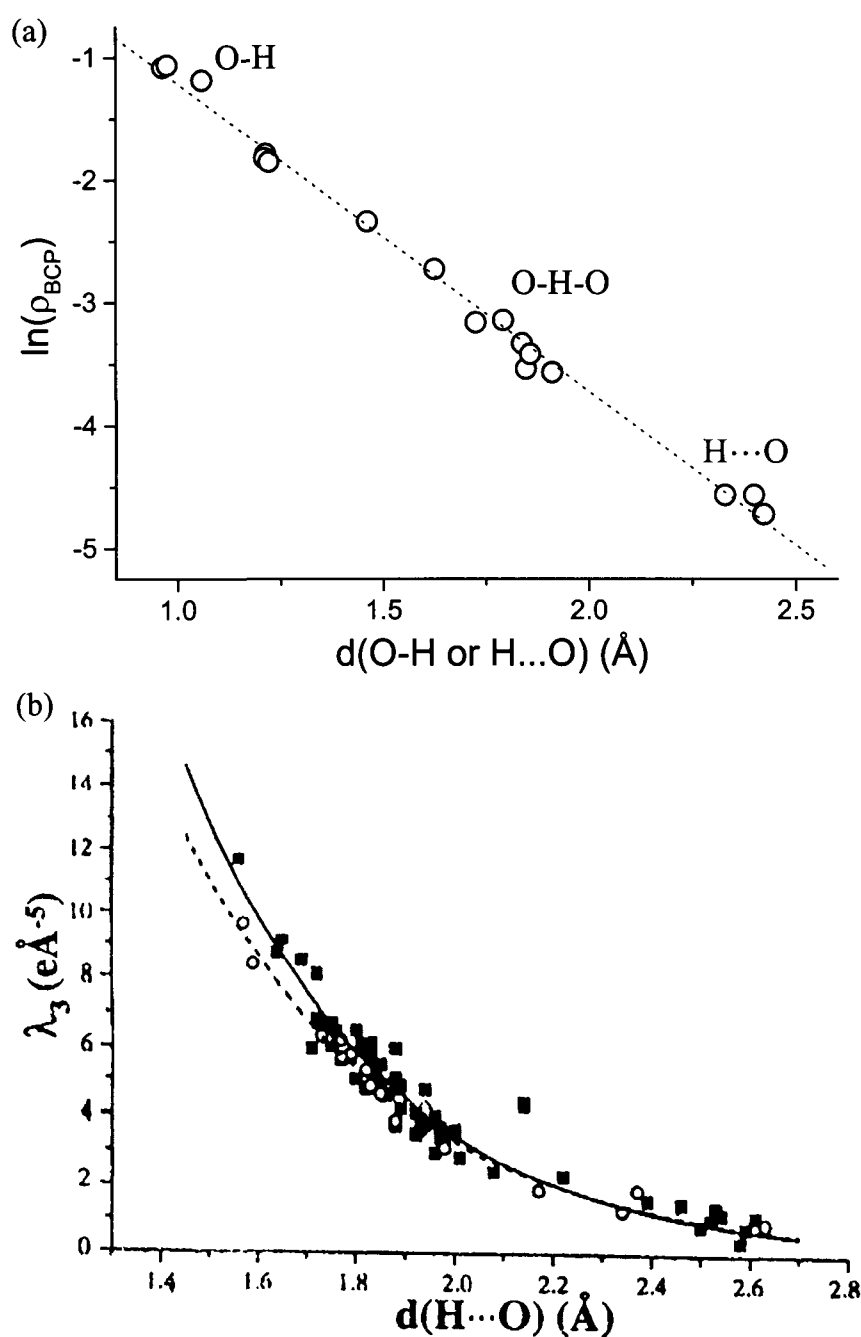
Figure 2.3: *(a) Variation of the electron density at the bond critical points, ρ_{BCP}, with the O-H and H···O distances, for a set of O-H···O hydrogen bonds. The fitted logarithmic relationship for the experimental data is displayed by the dotted line. Data points corresponding to the covalent bond O-H, symmetric O-H-O bond and the H···O bonds are marked.[67] (b) Variation of the positive curvature of the electron density with the H···O distance. The solid exponential fit indicates combined X-ray and neutron data for O-H···O, N-H···O and C-H···O hydrogen bonds, and the dotted exponential line indicates the fit corresponding to only X-ray data.[60] The above correlation plots consist of only those hydrogen bonds with oxygen as the acceptor.*

220

Woźniak *et al*[62] analyzed the charge density distribution in the N-H$\cdots$O and C-H$\cdots$O

bonds of dipicrylamine and showed a linear relationship between the charge density at

the CPs and the N$\cdots$O contact distance. Besides, the kinetic and potential energy

densities are also found to show some systematics with the H$\cdots$O distance in several

D-H$\cdots$O bonds.[68,69] There have been theoretical efforts to relate distances and the

electron density parameters at the bond critical point.[70]

We have been interested in employing charge densities to understand the

hydrogen bond and have carried out a systematic analysis of the densities in a variety

of hydrogen-bonded systems, ranging from the strong O-H$\cdots$O and N-H$\cdots$O

interactions to the weak interaction, involving carbon and sulphur atoms. The

hydrogen-bonded systems studied by us experimentally, include disodium salts of

croconic and squaric acids, thiodiglycolic acid-4,4'-bipyridine complex, piperazine-

oxalate complex, melamine, thionicotinamide and thioacetamide (see Figure 2.1). A

complete discussion on the geometrical and charge density results obtained from the

experimental X-ray data is given in Section 4.1. We have carried out a correlation

analysis of the electron densities, bond polarizations, Laplacians and their principle

curvatures with respect to the hydrogen bond distance. For this purpose, we have also

made use of the charge density data from other hydrogen bond systems reported in the

literature. This study, contrary to those in literature, employs a large variety of donor

and acceptor atoms, and has shown that among the various charge density parameters,

the positive curvature of the electron density exhibits a strict exponential dependence

on the hydrogen bond distance. The results of the correlation analyses are discussed in

detail in Section 4.2.

2.2 Investigations of the bond paths of O-H$\cdots$O hydrogen bonds

It is well known from a large number of purely structural studies that the hydrogen bond is predominantly a three atom - two center interaction. The directionality of the hydrogen bond has been the subject of much study and controversy.[71] To quote J. D. Bernal: "The strength of the hydrogen bond does not seem as sensitive to the orientation of the acceptor electron pair as it is to the collinearity of the hydrogen with the two atoms that it links." In a molecular orbital study, Del Bene and Marchese,[72] computed various possible structures of HF-HCN dimer. It was shown that only in one case the bond is formed through the nitrogen lone-pair of electrons while for the rest, the formation is through the C$\equiv$N π-electron system. A comparison of the energies revealed that the lone pair on the nitrogen provides a better site for hydrogen bonding than the π electrons. In a statistical study of N-H$\cdots$O bonds from 84 amino acids and peptide structures,[73] it was found that the N-H bond was directed either towards one of the carbonyl oxygen lone pairs or midway between the two, depending on whether the donor shared the proton between two oxygen acceptors or bonded directly with one. Similarly, a survey of O-H$\cdots$O bonds in structures of amino acids, peptides and oligosaccharides[74] showed that the O-H bonds tend to align along the carbonyl oxygen lone pair. The directional preference of an O-H or an N-H group towards the lone pair on the acceptor atom is found to depend on the nature of hybridization of the acceptor's lone pair of electrons. Corroborating this finding are several statistical surveys of X-ray and neutron structures by Taylor and Kennard[66] and many other workers.[75] Kroon *et al*[76] showed that there is a preference for hydrogen bonding in the plane defined by the lone pairs

on the acceptor. There are many surveys, solely based on structural or geometrical data, that demonstrate the directionality of hydrogen bonds.[77-82] These statistical and structural analyses do not throw much light on what effect lone-pairs of electrons have on the hydrogen bond formation. Also, from a charge density point of view, not much is known on the influence and directionality of the lone-pairs on the nature and formation of the hydrogen bond. Most charge density studies have dealt with the type of hybridization of the lone-pairs, and their polarization. For instance, a charge density study of symmetric and asymmetric O-H···O bonds in dimethylammonium hydrobis(squarate) by Lin *et al*[83] has revealed that the electron density of the carbonyl oxygen lone-pairs has a mixed nature between the sp^3 and sp^2 hybrids.

We were interested in understanding the topological properties of the experimental charge densities in hydrogen bonds, especially with respect to the nature of bond paths and the geometry of the lone-pairs on the donor and the acceptor atoms. We have analyzed as to how the orientation or directionality of the lone-pairs would affect the topological behaviour of the hydrogen bond. We have carried out a careful analysis of the experimental charge densities of O-H···O bonds of different geometries present in the following hydrogen bond systems: piperazine-oxalate complex, the α-form of ethoxy cinnamic acid, adipic acid, disodium salts of croconic and squaric acids. These systems possess linear, bifurcated and trifurcated hydrogen bonds with a range of hydrogen bond angles and H···O distances. Besides enabling a complete charge density description of the hydrogen bond, this study provides new and important insights with respect to the location of the critical point and its relation to the lone-pairs involved in the formation of the hydrogen bonds, and is therefore useful

for a better understanding of the hydrogen bond, in general. Being entirely based on an

experimental charge density analysis, the results (discussed extensively in Section 4.3)

are of considerable significance.

3. EXPERIMENTAL AND RELATED ASPECTS

3.1 Crystals

The crystals were grown by the slow evaporation of the solvent. Typical growth periods were about five to seven days. The compounds were commercially available and procured from ALDRICH and FLUKA.

Disodium croconate trihydrate: A saturated solution of the compound was prepared in distilled water and kept for crystallization by slow evaporation. Yellow-colored crystals of the croconate salt were obtained.

Disodium squarate trihydrate: The disodium salt of squaric acid was prepared by the addition of 10 mL of 1M NaOH to a saturated solution of 0.114g (1mmol) of squaric acid in water. Colorless crystals grown from the aqueous solution by slow evaporation at room temperature were separated and washed with water.

Piperazine-oxalate: Separate saturated solutions of piperazine (0.1mmol, 0.019 g) and oxalic acid (0.1mmol, 0.009 g) in water were prepared. The two solutions were mixed, which resulted in a clear mixture, and kept for crystallization. Colorless, transparent crystals were formed. Alternatively, the crystals were also prepared by the hydrothermal method by keeping the mixture in a polypropylene bottle, maintained at 70° C in an oven.

Thiodiglycollic acid-4,4'-bipyridine: Separate saturated solutions (using distilled methanol) of thiodiglycollic acid (0.1mmol, 0.015 g) and 4,4'-bipyridine (0.1mmol,

0.016 g) were prepared. The thiodiglycollic acid solution was slowly mixed with bipyridine solution, stirred, which resulted in a clear solution of the mixture. This was then kept for crystallization. Colorless crystals of the complex were obtained.

Melamine: Colorless crystals were obtained by slow evaporation from a saturated methanol (distilled methanol was used) solution.

Thionicotinamide: Yellow colored crystals were obtained from a saturated methanol solution.

Thioacetamide: Transparent colorless crystals were obtained by slow evaporation from a saturated methanol solution.

A polarizing microscope, LEICA MZ8 was used to examine the crystals. Crystals with dimensions in the range of ~ 0.1 to 0.3 mm were chosen for the investigations. For low temperature, charge density studies, the cold nitrogen gas from the dewar is made to shower on the crystal. The temperature of the stream could be recorded using a Chromel-Alumel (K-type) thermocouple. The temperature of the crystal could be maintained within ± 1° using the thermocontroller. The temperature was chosen such that the consumption of liquid nitrogen was optimal (~ 5 L/h). In order to circumvent ice formation on the crystal, copper pips specially designed for this purpose were used. A thin glass fibre at the end of the pip carried the crystal under measurement. With this kind of an arrangement, the data collection could be carried out without any interruption for a period of two to three days. All the charge density

experiments presented in this thesis were carried out at 130 K. A diagram of the low

temperature setup, on the SMART 3-circle goniometer is shown in Figure 3.1. For

details on the single crystal X-ray diffractometer, see the experimental section on

Methods of characterization (page 61) in Part 1 of the thesis.
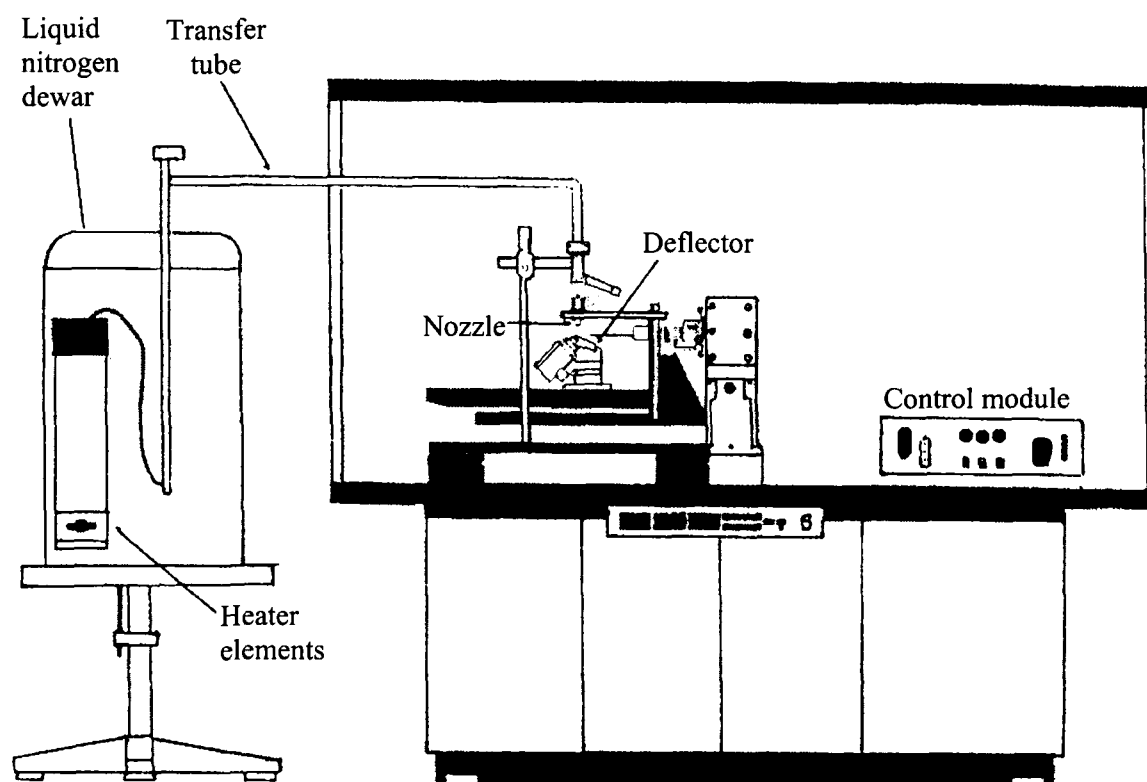
Figure 3.1: *Diagram of the low temperature setup on the SMART 3-circle goniometer.*

3.2 Data collection strategy

The crystal is cooled to 130 K and a hemisphere (for centric crystals) or a full sphere (for non-centric or triclinic crystals) data is collected, both at low and high resolution ($2\theta = 28°$, $75°$), the maximum resolution achievable being ~ 0.45 Å. The values of 2θ, ϕ and ω used for the hemisphere and the full sphere data are listed in Table 3.1 and Table 3.2, respectively.

During the data reduction, the original orientation matrix along with the lattice parameters is refined every 40 frames and the orientation matrix and lattice parameters obtained using the total data is used for structure refinement and charge density.

Table 3.1 Optimal 2θ, ω and ϕ for hemispherical data at low and high resolutions[a]

Run #	2θ	ω	ϕ	Width	# of frames
0	-28	-26	0	-0.3	606
1	-28	-21	88	-0.3	435
2	-28	-23	180	-0.3	230
3	-75	-75	0	-0.3	606
4	-75	-75	88	-0.3	435
5	-75	-75	180	-0.3	230

[a]Note that two complete hemisphere of data are collected, in comparison to only a low order data for a routine structure determination

Table 3.2 Optimal 2θ, ω and ϕ for full-spherical data at low and high resolutions

Run #	2θ	ω	ϕ	Width	# of frames
0	-28	-26	0	-0.3	636
1	-28	-21	88	-0.3	465
2	-28	-23	180	-0.3	636
3	-75	-75	270	-0.3	465
4	-75	-75	0	-0.3	636
5	-75	-75	88	-0.3	465
6	-75	-75	180	-0.3	636
7	-75	-75	270	-0.3	465

3.3 Structure and multipole refinement

The crystal structure determination is carried out by routine structure solution and refinement (for a complete description, see the experimental section, page 64 in Part 1 of the thesis). Absorption correction was applied using the SADABS program (Siemens, USA, 1995) for the systems: disodium salts of croconic (**I**) and squaric acids (**II**), thiodiglycolic acid-4,4-bipyridine (**IV**), thionicotinamide (**VI**) and thioacetamide (**VII**). In all the cases, the non-hydrogen atoms were first located and refined anisotropically. The hydrogen atoms were located using the difference Fourier technique and refined isotropically. In some instances, extinction corrections were needed. The weights w_1 and w_2 were adjusted in order to obtain the goodness-of-fit close to unity. A high order refinement was performed on the structure so obtained, using the high-resolution reflections, $\sin\theta/\lambda > 0.6$ Å^{-1}. During this refinement, the hydrogens were moved to average neutron diffraction distances (C(ar)-H, 1.085; C(sp^3)-H, 1.06; C(sp^2)-H, 1.075; O-H, 0.96; N-H, 1.01 Å).[84] The positional and thermal parameters of hydrogen atoms were kept fixed thereafter. The resultant file of the high order refinement served as the initial input to the charge density analysis.

The multipole refinement is done using a full-matrix least squares refinement routine, XDLSM of XD.[15] The flowchart shown on page 232 illustrates the various steps involved in the structure and charge density refinements. Additional details of the multipole refinement are listed below.

1. Coordinates and thermal parameters from high angle refinement ($\sin\theta/\lambda > 0.6$ Å^{-1}) is taken as the input to charge density analysis.

2. Scaling refinement.

3. P_{00} refined.

4. P_{lm} (l, m > 0) refined.

5. Spherical kappa (κ) refined on all atoms.

6. P_{00} refined.

7. P_{lm} (l, m > 0).

8. Deformation kappa (κ') refined on all non-hydrogen atoms.

9. P_{00} refined.

10. P_{lm} (l, m > 0).

11. Atom positions of non-hydrogen atoms refined.

12. P_{00} refined.

13. P_{lm} (l, m > 0) refined.

14. P_{00} and P_{lm} refined.

Each step is repeated till the shift/esd values become small. The quality of the refinement is constantly monitored through goodness-of-fit (S), R_1 and wR_2. For a reliable electron density calculation, caution is exercised to maintain N_{ref}/N_V greater than ten.

The electronic properties like dipole, electron density, Laplacian etc are calculated using XDPROP.[15] The experimental deformation map is obtained using the calculated multipole phases with the observed structure factors F_o.

$$\delta\rho^{exp}(r) = \frac{1}{V}\sum_{H}\left[\left|F_o(H)\right|e^{i\phi_{mul}} - \left|F_{sph}(H)\right|e^{i\phi_{sph}}\right]e^{-2\pi iH.r} \qquad ...(18)$$

$F_{sph}(H)$ is computed with atomic positions and thermal parameters obtained from the multipole refinement. The dynamic model map is obtained from the calculated multipole factors, that is, the Fourier coefficients are the difference of the two values of F_c.

$$\delta\rho^{dyn}(r) = \frac{1}{V}\sum_H \left[\left|F_{mul}(H)\right|e^{i\phi_{mul}} - \left|F_{sph}(H)\right|e^{i\phi_{sph}}\right]e^{-2\pi i H \cdot r} \qquad \ldots(19)$$

The use of multipole phases makes the maps slightly model dependent. To check that all the significant density features of the experimental data are included in the model, one computes the residual density. This is defined as the difference between the total electron density and that obtained by the multipole model.

$$\delta\rho^{res}(r) = \frac{1}{V}\sum_H \left[\left|F_o(H)\right| - \left|F_{mul}(H)\right|\right]e^{i\phi_{mul}}e^{-2\pi i H \cdot r} \qquad \ldots(20)$$

This is obtained using the XDFOUR routine and plotted using XDGRAPH. A featureless, flat residual density means a good modeling of the electron density by the multipole model.

Flowchart

Top branch (XD software pathway):

Intra and intermolecular properties ← XDPROP ←(Yes)— Is the residual density featureless?

xd.hkl

XDINI → xd.mas

xd.inp

XDLSM → Multipole, Kappa refinement → XDFOUR

Is the residual density featureless? —(No)→ XDLSM

High angle refinement ← Hydrogens fixed to average neutron distances ← Structure ← Locate hydrogens by difference Fourier

Rigid bond test ← PLATON ← Hydrogens fixed to average neutron distances

Hydrogen bonding ← PLATON and XP ← Hydrogens fixed to average neutron distances

Change TREF, PHAN ←(No)— Is the structure reasonable? —(Yes)→ Refinement ← Locate other atoms by difference Fourier

Change TREF, PHAN ← Direct methods

Locate hydrogens by difference Fourier ← Refinement

Bottom branch (crystal preparation pathway):

Crystals → Regular, clear good crystals? —(No)→ Regrow crystals

Regular, clear good crystals? —(Yes)→ Mounted on a copper pip using adhesive → Orientation matrix → Reasonable cell?

Reasonable cell? —(No)→ Choose better crystal

Reasonable cell? —(Yes)→ Cool crystal → Data up to 0.4 Å → Any heavy atoms expected?

Any heavy atoms expected? —(Yes)→ Patterson method

Any heavy atoms expected? —(No)→ Direct methods

Patterson method → Locate other atoms by difference Fourier

4. RESULTS AND DISCUSSION

We have investigated seven molecular crystals (**I** - **VII**, see Figure 2.1 in Section 2, Part 2), with special emphasis on the various types of hydrogen bonds formed by them. A complete description of the structural and charge density parameters obtained for the intra- and intermolecular interaction is given in the following sections. The charge density studies on these seven molecular crystals are reported by us for the first time.

4.1 Structural aspects and charge density analysis

4.1.1 *Disodium croconate trihydrate and disodium squarate trihydrate*

The asymmetric units of the two compounds, disodium croconate trihydrate (**I**) and disodium squarate trihydrate (**II**) with atom labeling are shown in Figure 4.1. The crystal data and other experimental details are listed in Table 4.1. The asymmetric unit in both the cases consists of an anion ring, two sodium cations and three water molecules.
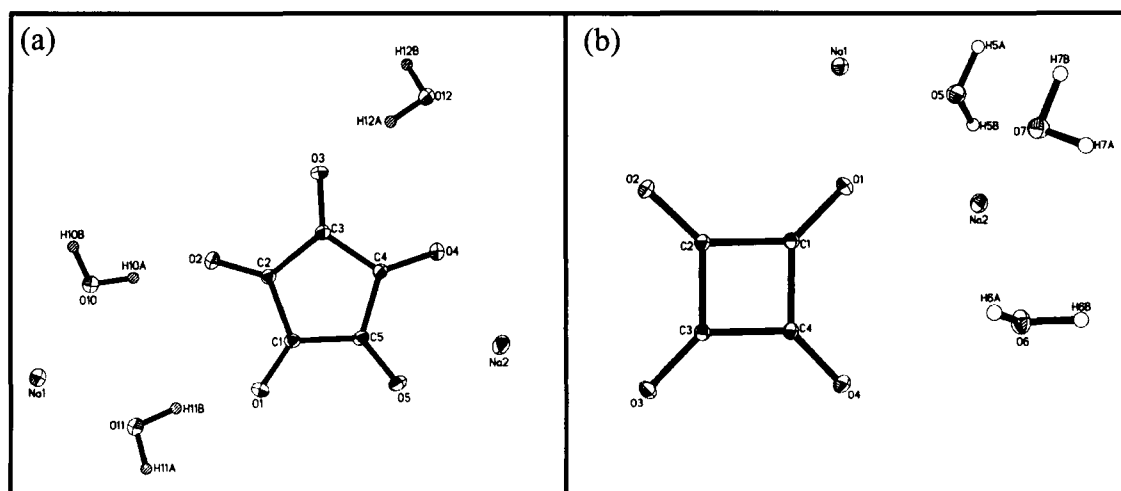
Figure 4.1: The ORTEP plots for (a) disodium croconate trihydrate and (b) disodium squarate trihydrate. Thermal ellipsoids are given at 50% probability.

The disodium salt of croconic acid crystallizes in a monoclinic crystal system (space group $P2_1/c$). The structure of the squarate salt belongs to a triclinic, P-1 space group, as distinct from the reported monoclinic form.[85]

Table 4.1 Crystal Structure data for disodium salts of croconic (**I**) and squaric acids (**II**)

	$Na_2C_5O_5.3H_2O$	$Na_2C_4O_4.3H_2O$
Chemical formula	$Na_2C_5O_5.3H_2O$	$Na_2C_4O_4.3H_2O$
Formula weight	240.08	212.07
Cell setting	Monoclinic	Triclinic
Space group	$P2_1/c$	P-1
a (Å)	6.3444 (10)	6.9879 (10)
b (Å)	13.099 (3)	8.0949 (10)
c (Å)	10.662 (3)	8.2286 (10)
α (°)	90	113.12
β (°)	105.87 (2)	100.04
γ (°)	90	111.62
ρ (Mg/m³)	1.871	1.907
μ, mm⁻¹	0.260	0.276
Cell volume (Å³)	852.3 (3)	369.24 (8)
Crystal size (mm)	$0.22 \times 0.33 \times 0.33$	$0.50 \times 0.13 \times 0.30$
Z	4	2
F(000)	488	216
Diffractometer	Siemens CCD 3 circle diffractometer	Siemens CCD 3 circle diffractometer
Radiation type	MoK_α (0.71073 Å)	MoK_α (0.71073 Å)
Crystal-detector distance (cm)	5.0	5.0
Temperature (K)	130 (2)	130 (2)
No. of measured reflections	12439	11165
No. of independent reflections	6915	6254
R_{merge}	0.08	0.0683
R_{int}	0.043	0.0392
θ_{max} (°), $sin\theta/\lambda$ (Å⁻¹)	49.17, 1.06	49.45, 1.07
Range of h, k, l	$-12 \le h \le 12$	$-13 \le h \le 14$
	$-26 \le k \le 22$	$-17 \le k \le 17$
	$-21 \le l \le 13$	$-17 \le l \le 16$
Refinement		
Refinement on F^2		
R_1	0.048	0.040
WR_2	0.113	0.100
S	0.940	0.960
No. of reflections used in the refinement	6915	6254
No. of parameters refined	160	142
After multipole refinement		
Weighting scheme	0.057, 0.114	0.047, 0.094
R{F}	0.039	0.037

Table 4.1 (*continued*)

$R\{F^2\}$	0.064	0.070
S	1.196	1.0496
No. of variables	263	245
N_{ref}/N_v	23.0	25.8
Cambridge Crystallographic Database Deposition No.	CCDC 171699	CCDC 171698

The Cambridge Structural database (CSD) deposition numbers are also given in Table 4.1. The geometrical features, such as the bond lengths and the valence angles are listed in Table 4.2 for the croconate and in Table 4.3 for the squarate dianion. The C-C and C-O bonds constituting the anion rings have nearly equal bond lengths. The mean C-C distances for the croconate and squarate rings are 1.468(2) and 1.471(9) Å, respectively, whereas the mean C-O distances are 1.248(4) and 1.259(6) Å, respectively. The C-C-C angles for the croconate and squarate rings are 108° and 90°, respectively. The C-C-O valence angle is smaller (125°) for the croconate than for the squarate ring (135°). The Na-O distances in the two salts are in the range of 2.3 to 2.5 Å. The triclinic form of disodium squarate trihydrate and the monoclinic form of disodium croconate trihydrate are being reported by us for the first time. In addition, a triclinic form of the croconate was also obtained, but the high resolution data was not collected for this polymorph. The charge density analysis of the croconate dianion is also reported by us for the first time.

Table 4.2 Bond lengths and angles for disodium salt of croconic acid I

Moiety	Distance (Å)	Moiety	Angle (°)
C(1)-C(2)	1.4681(11)	O(3)-C(3)-C(4)	127.09(7)
C(2)-C(3)	1.4665(11)	O(3)-C(3)-C(2)	125.15(7)
C(3)-C(4)	1.4657(11)	C(4)-C(3)-C(2)	107.76(6)
C(4)-C(5)	1.4712(11)	O(1)-C(1)-C(2)	126.07(7)
C(5)-C(1)	1.4686(11)	O(1)-C(1)-C(5)	126.16(7)
O(1)-C(1)	1.2452(10)	C(2)-C(1)-C(5)	107.77(6)
O(2)-C(2)	1.2464(10)	O(2)-C(2)-C(3)	125.66(7)
O(3)-C(3)	1.2497(10)	O(2)-C(2)-C(1)	125.99(7)
O(4)-C(4)	1.2555(10)	C(3)-C(2)-C(1)	108.35(6)

Table 4.2 (*continued*)

Moiety	Length	Moiety	Angle (°)
O(5)-C(5)	1.2446(10)	O(4)-C(4)-C(3)	127.21(7)
Na(1)-O(12)#1	2.3093(8)	O(4)-C(4)-C(5)	124.60(7)
Na(1)-O(11)	2.3718(8)	C(3)-C(4)-C(5)	108.19(7)
Na(1)-O(10)	2.4247(9)	O(5)-C(5)-C(1)	126.66(7)
Na(1)-O(11)#2	2.4289(9)	O(5)-C(5)-C(4)	125.48(7)
Na(1)-O(4)#1	2.4371(9)	C(1)-C(5)-C(4)	107.86(7)
Na(1)-O(4)#3	2.5545(9)	O(12)#1-Na(1)-O(11)	167.43(3)
Na(2)-O(1)#5	2.3189(8)	O(12)#1-Na(1)-O(10)	86.61(3)
Na(2)-O(12)#6	2.3212(9)	O(11)-Na(1)-O(10)	84.84(3)
Na(2)-O(5)	2.3773(10)	O(12)#1-Na(1)-O(11)#2	95.65(3)
Na(2)-O(10)#7	2.4432(9)	O(11)-Na(1)-O(11)#2	91.76(3)
Na(2)-O(4)	2.4817(8)	O(10)-Na(1)-O(11)#2	79.11(3)
O(4)-Na(1)#8	2.4370(9)	O(12)#1-Na(1)-O(4)#1	85.96(3)
O(4)-Na(1)#3	2.5545(9)	O(11)-Na(1)-O(4)#1	103.79(3)
O(1)-Na(2)#9	2.3189(8)	O(10)-Na(1)-O(4)#1	168.68(3)
O(12)-Na(1)#8	2.3093(8)	O(11)#2-Na(1)-O(4)#1	93.14(3)
O(12)-Na(2)#6	2.3212(9)	O(12)#1-Na(1)-O(4)#3	79.45(3)
O(11)-Na(1)#2	2.4289(9)	O(11)-Na(1)-O(4)#3	92.69(3)
O(10)-Na(2)#7	2.4432(9)	O(10)-Na(1)-O(4)#3	98.33(3)
Na(2)-C(5)	3.0291(11)	O(11)#2-Na(1)-O(4)#3	174.64(3)
Na(2)-C(4)	3.0791(10)	O(4)#1-Na(1)-O(4)#3	88.68(3)
Na(2)-Na(1)#3	3.6301(7)	O(12)#1-Na(1)-Na(1)#2	139.83(3)
Na(2)-Na(1)#8	3.7952(8)	O(11)-Na(1)-Na(1)#2	46.58(2)
Na(1)-Na(1)#2	3.3423(9)	O(10)-Na(1)-Na(1)#2	78.40(2)
Na(1)-Na(1)#4	3.5709(9)	O(11)#2-Na(1)-Na(1)#2	45.18(2)
Na(1)-Na(2)#3	3.6302(7)	O(4)#1-Na(1)-Na(1)#2	102.06(3)
Na(1)-Na(2)#1	3.7952(8)	O(4)#3-Na(1)-Na(1)#2	139.19(3)
Moiety	**Angle (°)**	O(12)#1-Na(1)-Na(1)#4	79.68(2)
Na(1)#8-O(4)-Na(2)	100.99(3)	O(11)-Na(1)-Na(1)#4	101.32(3)
C(4)-O(4)-Na(1)#3	121.42(6)	O(10)-Na(1)-Na(1)#4	140.61(3)
Na(1)#8-O(4)-Na(1)#3	91.32(3)	O(11)#2-Na(1)-Na(1)#4	138.56(3)
Na(2)-O(4)-Na(1)#3	92.23(2)	O(4)#1-Na(1)-Na(1)#4	45.66(2)
C(5)-O(5)-Na(2)	109.50(5)	O(4)#3-Na(1)-Na(1)#4	43.02(2)
O(5)-C(5)-Na(2)	47.71(4)	Na(1)#2-Na(1)-Na(1)#4	133.17(2)
C(1)-C(5)-Na(2)	172.77(5)	O(12)#1-Na(1)-Na(2)#3	38.49(2)
C(4)-C(5)-Na(2)	77.96(5)	O(11)-Na(1)-Na(2)#3	130.83(2)
O(4)-C(4)-Na(2)	50.69(4)	O(10)-Na(1)-Na(2)#3	82.81(2)
C(3)-C(4)-Na(2)	174.07(5)	O(11)#2-Na(1)-Na(2)#3	131.61(2)
C(5)-C(4)-Na(2)	74.18(5)	O(4)#1-Na(1)-Na(2)#3	96.55(2)
C(1)-O(1)-Na(2)#9	122.73(5)	O(4)#3-Na(1)-Na(2)#3	43.09(2)
Na(1)#8-O(12)-Na(2)#6	103.25(3)	Na(1)#2-Na(1)-Na(2)#3	161.19(2)
Na(1)-O(11)-Na(1)#2	88.24(3)	Na(1)#4-Na(1)-Na(2)#3	63.61(2)
Na(1)-O(10)-Na(2)#7	126.73(3)	O(12)#1-Na(1)-Na(2)#1	125.46(3)
O(5)-Na(2)-Na(1)#8	107.97(2)	O(11)-Na(1)-Na(2)#1	63.85(2)
O(10)#7-Na(2)-Na(1)#8	69.21(2)	O(10)-Na(1)-Na(2)#1	147.86(2)
O(4)-Na(2)-Na(1)#8	39.08(2)	O(11)#2-Na(1)-Na(2)#1	94.02(2)
C(5)-Na(2)-Na(1)#8	85.66(2)	O(4)#1-Na(1)-Na(2)#1	39.94(2)
C(4)-Na(2)-Na(1)#8	59.11(2)	O(4)#3-Na(1)-Na(2)#1	90.61(2)
Na(1)#3-Na(2)-Na(1)#8	57.44(2)	Na(1)#2-Na(1)-Na(2)#1	74.83(2)

236

Table 4.2 (*continued*)

C(4)-O(4)-Na(1)#8	135.56(6)	Na(1)#4-Na(1)-Na(2)#1	58.959(14)
C(4)-O(4)-Na(2)	106.27(5)	Na(2)#3-Na(1)-Na(2)#1	122.564(14)
O(4)-Na(2)-C(5)	50.83(2)	O(1)#5-Na(2)-O(12)#6	103.92(3)
O(1)#5-Na(2)-C(4)	150.46(3)	O(1)#5-Na(2)-O(5)	100.08(3)
O(12)#6-Na(2)-C(4)	98.13(3)	O(12)#6-Na(2)-O(5)	125.75(3)
O(5)-Na(2)-C(4)	50.60(2)	O(1)#5-Na(2)-O(10)#7	92.37(3)
O(10)#7-Na(2)-C(4)	85.45(3)	O(12)#6-Na(2)-O(10)#7	135.22(3)
O(4)-Na(2)-C(4)	23.04(2)	O(5)-Na(2)-O(10)#7	90.70(3)
C(5)-Na(2)-C(4)	27.86(2)	O(1)#5-Na(2)-O(4)	173.50(3)
O(1)#5-Na(2)-Na(1)#3	138.45(2)	O(12)#6-Na(2)-O(4)	80.76(2)
O(12)#6-Na(2)-Na(1)#3	38.26(2)	O(5)-Na(2)-O(4)	73.45(2)
O(5)-Na(2)-Na(1)#3	95.92(3)	O(10)#7-Na(2)-O(4)	87.25(3)
O(10)#7-Na(2)-Na(1)#3	125.66(2)	O(1)#5-Na(2)-C(5)	122.67(3)
O(4)-Na(2)-Na(1)#3	44.68(2)	O(12)#6-Na(2)-C(5)	116.06(3)
C(5)-Na(2)-Na(1)#3	79.92(2)	O(5)-Na(2)-C(5)	22.79(2)
C(4)-Na(2)-Na(1)#3	59.89(2)	O(10)#7-Na(2)-C(5)	86.97(3)
O(1)#5-Na(2)-Na(1)#8	146.18(3)	O(12)#6-Na(2)-Na(1)#8	74.66(2)

Symmetry transformations used to generate equivalent atoms:
#1 x,y,z-1; #2 -x,-y+1,-z; #3 -x+1,-y+1,-z+1; #4 -x+1,-y+1,-z; #5 x,-y+3/2,z+1/2; #6 -x+1,-y+1,-z+2; #7 -x,-y+1,-z+1; #8 x,y,z+1; #9 x,-y+3/2,z-1/2.

Table 4.3 Bond lengths and angles for disodium salt of squaric acid **II**

Moiety	Distance (Å)	Moiety	Angle (°)
C(1)-C(2)	1.4695(8)	O(3)-C(3)-C(2)	134.73(5)
C(2)-C(3)	1.4596(8)	O(3)-C(3)-C(4)	134.86(5)
C(3)-C(4)	1.4693(8)	C(2)-C(3)-C(4)	90.39(4)
C(4)-C(1)	1.4843(8)	O(4)-C(4)-C(3)	134.13(5)
O(1)-C(1)	1.2605(7)	O(4)-C(4)-C(1)	136.25(5)
O(2)-C(2)	1.2668(7)	C(3)-C(4)-C(1)	89.61(4)
O(3)-C(3)	1.2601(7)	O(2)-C(2)-C(3)	134.11(5)
O(4)-C(4)	1.2488(7)	O(2)-C(2)-C(1)	135.33(5)
O(1)-Na(1)#1	2.5271(6)	C(3)-C(2)-C(1)	90.57(4)
Na(1)-O(7)#1	2.3575(6)	O(1)-C(1)-C(2)	135.20(5)
Na(1)-O(5)	2.3586(5)	O(1)-C(1)-C(4)	135.36(5)
Na(1)-O(3)#2	2.4073(5)	C(2)-C(1)-C(4)	89.42(4)
Na(1)-O(3)#3	2.4247(5)	O(7)#1-Na(1)-O(3)#2	86.39(2)
Na(1)-O(1)	2.4259(6)	O(5)-Na(1)-O(3)#2	97.91(2)
Na(1)-O(1)#1	2.5271(6)	O(7)#1-Na(1)-O(3)#3	86.32(2)
Na(1)-Na(2)#1	3.4207(4)	O(5)-Na(1)-O(3)#3	90.70(2)
Na(1)-Na(1)#4	3.4267(6)	O(3)#2-Na(1)-O(3)#3	89.67(2)
Na(1)-Na(2)	3.4279(4)	O(7)#1-Na(1)-O(1)	85.43(2)
Na(1)-Na(1)#1	3.6052(6)	O(5)-Na(1)-O(1)	90.79(2)
Na(2)-O(4)#5	2.3080(5)	O(3)#2-Na(1)-O(1)	167.72(2)
Na(2)-O(6)#5	2.3246(6)	O(3)#3-Na(1)-O(1)	98.92(2)
Na(2)-O(7)	2.3468(6)	O(7)#1-Na(1)-O(1)#1	88.07(2)
Na(2)-O(1)	2.4218(5)	O(5)-Na(1)-O(1)#1	95.33(2)
Na(2)-O(6)	2.4550(6)	O(3)#2-Na(1)-O(1)#1	83.98(2)
Na(2)-O(5)	2.4809(6)	O(3)#3-Na(1)-O(1)#1	171.78(2)
Na(2)-Na(2)#5	3.1993(6)	O(1)-Na(1)-O(1)#1	86.60(2)

237

Table 4.3 (*continued*)

Na(2)-Na(1)#1	3.4207(4)	O(7)#1-Na(1)-Na(2)#1	43.229(14)
O(4)-Na(2)#5	2.3080(5)	O(5)-Na(1)-Na(2)#1	140.34(2)
O(3)-Na(1)#6	2.4073(5)	O(3)#2-Na(1)-Na(2)#1	80.28(2)
O(3)-Na(1)#3	2.4247(5)	O(3)#3-Na(1)-Na(2)#1	128.71(2)
O(7)-Na(1)#1	2.3575(6)	O(1)-Na(1)-Na(2)#1	87.49(2)
O(6)-Na(2)#5	2.3246(6)	O(1)#1-Na(1)-Na(2)#1	45.011(12)
Moiety	**Angle (°)**	O(7)#1-Na(1)-Na(1)#4	84.86(2)
Na(2)-O(7)-Na(1)#1	93.30(2)	O(5)-Na(1)-Na(1)#4	96.05(2)
Na(2)#5-O(6)-Na(2)	83.99(2)	O(3)#2-Na(1)-Na(1)#4	45.038(14)
Na(1)-O(5)-Na(2)	90.16(2)	O(3)#3-Na(1)-Na(1)#4	44.628(13)
Na(2)#5-Na(2)-Na(1)#1	116.642(14)	O(1)-Na(1)-Na(1)#4	142.77(2)
O(4)#5-Na(2)-Na(1)	129.68(2)	O(1)#1-Na(1)-Na(1)#4	128.81(2)
O(6)#5-Na(2)-Na(1)	92.21(2)	Na(2)#1-Na(1)-Na(1)#4	108.896(13)
O(7)-Na(2)-Na(1)	89.95(2)	O(7)#1-Na(1)-Na(2)	130.24(2)
O(1)-Na(2)-Na(1)	45.047(13)	O(5)-Na(1)-Na(2)	46.36(2)
O(6)-Na(2)-Na(1)	141.33(2)	O(3)#2-Na(1)-Na(2)	141.51(2)
O(5)-Na(2)-Na(1)	43.477(13)	O(3)#3-Na(1)-Na(2)	102.44(2)
Na(2)#5-Na(2)-Na(1)	128.835(14)	O(1)-Na(1)-Na(2)	44.950(13)
Na(1)#1-Na(2)-Na(1)	63.527(10)	O(1)#1-Na(1)-Na(2)	85.776(14)
C(1)-O(1)-Na(2)	127.22(4)	Na(2)#1-Na(1)-Na(2)	116.473(10)
C(1)-O(1)-Na(1)	129.35(4)	Na(1)#4-Na(1)-Na(2)	134.610(14)
Na(2)-O(1)-Na(1)	90.00(2)	O(7)#1-Na(1)-Na(1)#1	85.57(2)
C(1)-O(1)-Na(1)#1	118.03(4)	O(5)-Na(1)-Na(1)#1	94.26(2)
Na(2)-O(1)-Na(1)#1	87.43(2)	O(3)#2-Na(1)-Na(1)#1	125.73(2)
Na(1)-O(1)-Na(1)#1	93.40(2)	O(3)#3-Na(1)-Na(1)#1	142.95(2)
C(4)-O(4)-Na(2)#5	137.27(4)	O(1)-Na(1)-Na(1)#1	44.405(13)
C(3)-O(3)-Na(1)#6	129.53(4)	O(1)#1-Na(1)-Na(1)#1	42.199(12)
C(3)-O(3)-Na(1)#3	114.00(4)	Na(2)#1-Na(1)-Na(1)#1	58.333(9)
Na(1)#6-O(3)-Na(1)#3	90.34(2)	Na(1)#4-Na(1)-Na(1)#1	167.16(2)
O(1)-Na(2)-O(6)	97.38(2)	Na(2)-Na(1)-Na(1)#1	58.140(9)
O(4)#5-Na(2)-O(5)	86.33(2)	O(4)#5-Na(2)-O(6)#5	87.53(2)
O(6)#5-Na(2)-O(5)	87.16(2)	O(4)#5-Na(2)-O(7)	93.52(2)
O(7)-Na(2)-O(5)	96.57(2)	O(6)#5-Na(2)-O(7)	176.18(2)
O(1)-Na(2)-O(5)	88.02(2)	O(4)#5-Na(2)-O(1)	173.21(2)
O(6)-Na(2)-O(5)	173.79(2)	O(6)#5-Na(2)-O(1)	88.43(2)
O(4)#5-Na(2)-Na(2)#5	87.03(2)	O(7)-Na(2)-O(1)	90.86(2)
O(6)#5-Na(2)-Na(2)#5	49.74(2)	O(4)#5-Na(2)-O(6)	88.47(2)
O(7)-Na(2)-Na(2)#5	126.61(2)	O(6)#5-Na(2)-O(6)	96.01(2)
O(1)-Na(2)-Na(2)#5	94.51(2)	O(7)-Na(2)-O(6)	80.35(2)
O(6)-Na(2)-Na(2)#5	46.271(14)	O(7)-Na(2)-Na(1)#1	43.476(14)
O(5)-Na(2)-Na(2)#5	136.62(2)	O(1)-Na(2)-Na(1)#1	47.562(14)
O(4)#5-Na(2)-Na(1)#1	137.00(2)	O(6)-Na(2)-Na(1)#1	84.85(2)
O(6)#5-Na(2)-Na(1)#1	135.39(2)	O(5)-Na(2)-Na(1)#1	96.66(2)

Symmetry operations used to generate equivalent atoms:

1 -x+1,-y+1,-z; #2 x+1,y+1,z; #3 -x+1,-y,-z; #4 -x+2,-y+1,-z; # 5 -x+1,-y+1,-z+1; #6 x+1,y-1,z.

In Figure 4.2, the static deformation densities in the ring planes are shown. Concentric contours typify the various bonding regions in the molecule between the atom-cores. In the squarate ring, the C-C bonding density appears spread out of the square frame, implying that the ring is considerably strained (Figure 4.2a). On the other hand, the C-C bonding density in the croconate ring (Figure 4.2b) appears more uniform across the internuclear axes. The bonding density in the C-O bond regions is more toward the electropositive carbon atom. The lone pair lobes on the oxygens are also clearly seen in the figure. The critical point analysis in the bonding regions of the squarate and the croconate anions reveals (3, -1) CPs (Table 4.4 and Table 4.5).

(a)   (b)
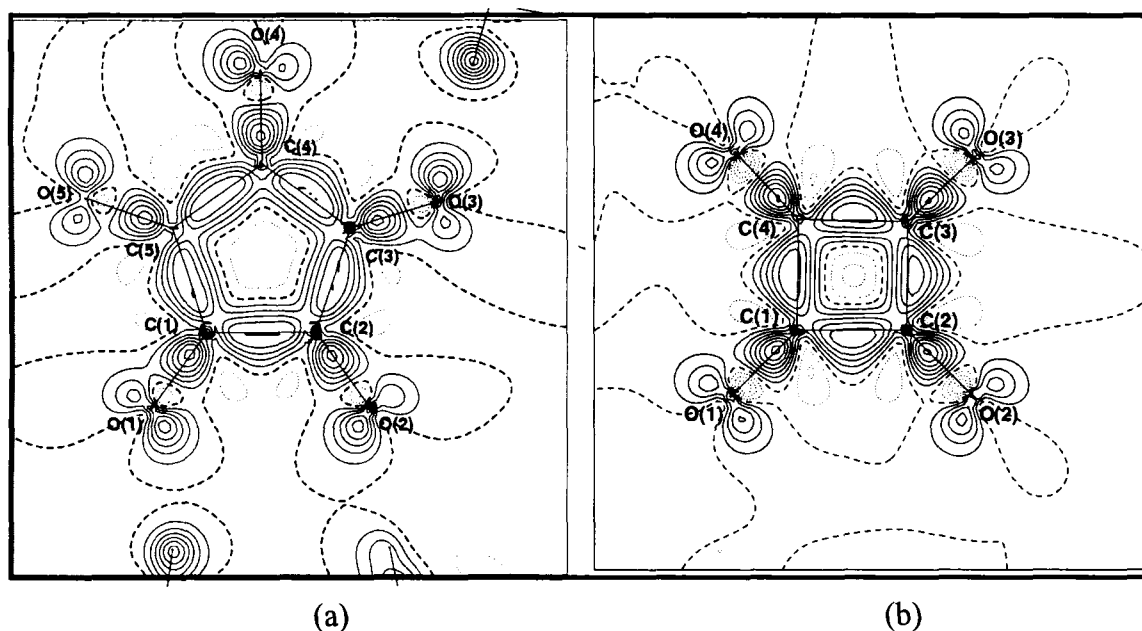
Figure 4.2: *Static deformation density in the symmetry plane of (a) croconate dianion, (b) squarate dianion. Contour levels are given at 0.1 e$\AA^{-3}$.*

The ρ_{BCP} values for the C-C bonds of the squarate ion fall in a narrow range of 1.85(1) to 1.87(1) e$\AA^{-3}$. Those of the croconate ion are slightly lower with a mean value of 1.81(1) e$\AA^{-3}$ but their spread is similar (~0.01 e$\AA^{-3}$). The Laplacians also behave in a

likewise manner. The magnitude of the Laplacians are somewhat higher (of the order of

-13.4(3) eÅ^{-5}) in the squarate than in the croconate (~ -12.2(3) eÅ^{-5}).[33] The ellipticity (ε)

values in squarate vary between 0.23 and 0.27, with a mean value of 0.25 and those in

croconate, are somewhat lower, between 0.18 and 0.25 with the mean value at 0.22

(Table 4.4). The mean d$_{CP}$ value for the C-C bonds in the squarate ring is 0.058 Å while

for the croconate the value is much smaller, 0.015 Å in accordance with the observed

strain in the rings (see Figure 4.2). The mean C-O bond density of the squarate ion is

2.72(3) eÅ^{-3} as compared to 2.66(2) eÅ^{-3} in the croconate ion. The pseudoatomic charges

on the carbonyl oxygens are -0.15 e in the squarate and –0.13 e in the croconate ion. The

charge on the squarate ring carbon is -0.14 e, and in the croconate, the carbon atom

carries a smaller charge (-0.07 e). Accordingly, the C-O bond appears to be less

polarized in squarate (Δ ~ 18 %) compared to croconate (Δ ~ 25 %).

Table 4.4 Charge density parameters for intramolecular bonds in disodium salt of croconic acid **I** - Bond critical point properties:

Bond	ρ_{BCP} (eÅ^{-3})	$\nabla^2\rho_{BCP}$ eÅ^{-5}	λ_1 (eÅ^{-5})	λ_2 (eÅ^{-5})	λ_3 (eÅ^{-5})	ε
C(1)-C(2)	1.82(1)	-12.27(1)	-13.55	-11.08	12.36	0.22
C(2)-C(3)	1.82(1)	-12.31(1)	-13.57	-11.09	12.35	0.22
C(3)-C(4)	1.82(1)	-12.53(1)	-13.42	-11.37	12.27	0.18
C(4)-C(5)	1.80(1)	-11.78(3)	-13.47	-10.78	12.47	0.25
C(1)-C(5)	1.81(1)	-12.18(3)	-13.50	-11.06	12.38	0.22
O(1)-C(1)	2.67(1)	-28.35(2)	-23.52	-20.58	15.75	0.14
O(2)-C(2)	2.67(1)	-28.15(1)	-23.48	-20.48	15.80	0.15
O(3)-C(3)	2.66(1)	-27.68(1)	-23.24	-20.40	15.95	0.14
O(4)-C(4)	2.64(1)	-27.01(1)	-23.03	-20.17	16.20	0.14
O(5)-C(5)	2.68(2)	-28.49(10)	-23.58	-20.61	15.70	0.14
O(10)-H(10A)	2.70(9)	-25.5(6)	-43.83	-42.19	60.54	0.04
O(10)-H(10B)	2.90(9)	-23.2(5)	-42.82	-42.60	55.17	0.01
O(11)-H(11A)	2.55(10)	-32.1(6)	-40.09	-38.43	46.41	0.04
O(11)-H(11B)	2.77(9)	-29.5(7)	-45.09	-44.04	59.60	0.02
O(12)-H(12A)	2.93(9)	-26.4(6)	-45.05	-42.77	61.44	0.05
O(12)-H(12B)	2.92(9)	-42.2(7)	-52.45	-49.54	59.75	0.06

Ring critical point properties: ρ_{RCP} = 0.30(2) eÅ^{-3}, $\nabla^2\rho_{RCP}$ = 5.4(4) eÅ^{-5}.

Table 4.5 Charge density parameters for intramolecular bonds in disodium salt of squaric acid **II** - Bond critical point properties:

Bond	ρ_{BCP} $(e\text{Å}^{-3})$	$\nabla^2\rho_{BCP}$ $(e\text{Å}^{-5})$	λ_1 $(e\text{Å}^{-5})$	λ_2 $(e\text{Å}^{-5})$	λ_3 $(e\text{Å}^{-5})$	ε
C(1)-C(2)	1.87(1)	-13.38(2)	-13.90	-11.12	11.64	0.25
C(2)-C(3)	1.87(1)	-13.57(1)	-14.03	-11.06	11.52	0.27
C(3)-C(4)	1.87(1)	-13.54(1)	-13.99	-11.16	11.62	0.25
C(4)-C(1)	1.85(1)	-12.96(2)	-13.65	-11.12	11.81	0.23
O(1)-C(1)	2.73(2)	-32.75(8)	-25.52	-21.37	14.13	0.19
O(2)-C(2)	2.68(1)	-30.64(1)	-24.95	-20.92	15.23	0.19
O(3)-C(3)	2.71(1)	-32.35(1)	-25.44	-21.30	14.39	0.19
O(4)-C(4)	2.75(1)	-35.02(1)	-26.28	-21.96	13.22	0.20
O(5)-H(5A)	2.64(8)	-39.6(5)	-39.19	-38.11	37.75	0.03
O(5)-H(5B)	2.36(7)	-23.3(4)	-32.37	-31.27	40.39	0.04
O(6)-H(6A)	2.62(9)	-41.2(5)	-38.15	-37.33	34.33	0.02
O(6)-H(6B)	2.35(7)	-36.0(5)	-36.28	-35.12	35.41	0.03
O(7)-H(7A)	2.65(8)	-32.7(4)	-36.60	-35.86	39.78	0.02
O(7)-H(7B)	2.40(7)	-33.5(4)	-36.11	-34.81	37.38	0.04

Ring critical point properties: $\rho_{RCP} = 0.59(1)$ $e\text{Å}^{-3}$, $\nabla^2\rho_{RCP} = 11.8(1)$ $e\text{Å}^{-5}$

Hydrogen bonds

The croconate anion **I** forms four O-H···O hydrogen bonds with the surrounding water molecules grouped into two bifurcated systems (designated as *b* in Figure 4.3).[86] In each case, an acceptor oxygen atom makes contact with two hydrogen atoms from two different water donor groups. Many other systems with such bifurcated hydrogen bonds are known.[87] The remaining hydrogen on each water donor is involved in a bifurcated bond originating from a neighboring croconate ion (not shown in the Figure 4.3). Thus, b_{11} and b_{21} bonds share a common donor and so does the b_{12} and b_{22} pair. As shown in Table 4.6, the H···O bond lengths are spread between 1.8 to 1.9 Å, with O-H···O angles ranging between 170° and 176°. The bifurcation angles (angle between the two O-H···O bonds) are 88.6° and 85.1° for b_1 and b_2, respectively. The croconate ion also forms two linear bonds (l_1 and l_2) with the water
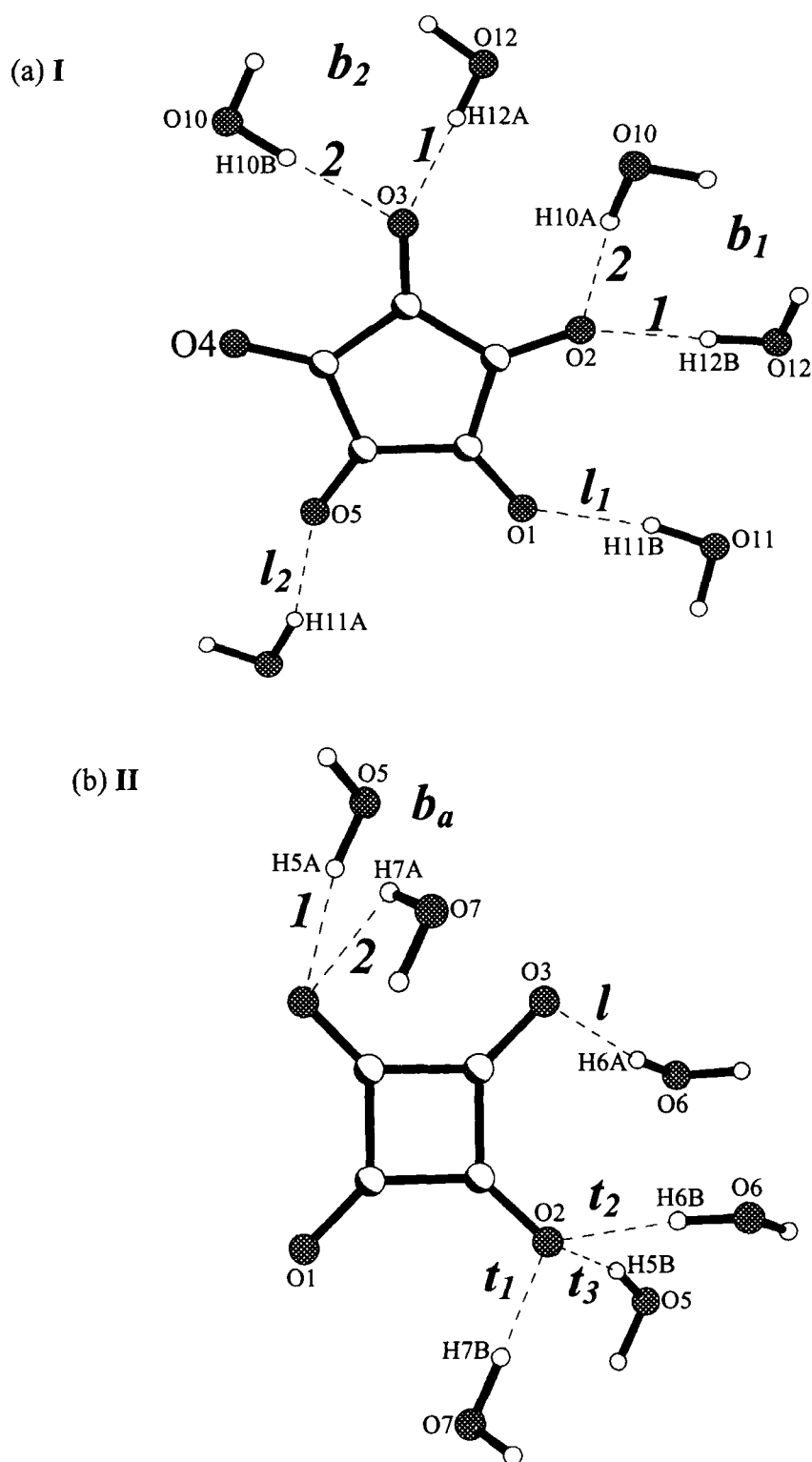
Figure 4.3: Unique hydrogen bonds in (a) croconate **I**, (b) squarate**II** . Symbols l, b and t designate linear, bifurcated and trifurcated hydrogen bonds.

molecules, the H···O bond distances being 1.841(5) and 1.998(7) Å with the corresponding angles of 166.9(17)° and 164.5(15)°, respectively. The water molecule engaged in l_1 forms a l_2 hydrogen bond with a neighboring croconate ion. This results in a network of croconate ions linked by bifurcated and linear hydrogen bonds with the surrounding water molecules. A unique feature of the squarate ion **II** (see Table 4.7 for hydrogen bond parameters) is the presence of the trifurcated hydrogen bond (designated as *t*), where the acceptor oxygen atom makes contact with three water donor groups. The squarate ion also exhibits a bifurcated bond, b_a, which is highly asymmetrical in that one bond is much longer (b_{a2}, 2.495(17) Å) than the other (b_{a1}, 1.871(19) Å). The hydrogen bond angles are correspondingly very different, 131.0(13)° and 163.8(19)°, respectively. The bifurcation angle is also small (63.1°). As in the case of the croconate ion, here too, the water donor groups are shared between neighboring squarate ions.

Table 4.6 Hydrogen bond parameters for disodium croconate trihydrate I

H-Bond		H···A (Å)	D···A (Å)	D-H···A (°)	ρ_{BCP} (eÅ^{-3})	$\nabla^2\rho_{BCP}$ (eÅ^{-5})
O(11)-H(11B)···O(1)	(l_1)	1.841(5)	2.784(1)	166.9(17)	0.21(3)	3.02(1)
O(11)-H(11A)···O(5)	(l_2)	1.998(7)	2.934(1)	164.5(15)	0.09(3)	1.94(1)
O(10)-H(10A)···O(2)	(b_{11})	1.829(7)	2.782(1)	171.9(17)	0.21(3)	3.00(1)
O(12)-H(12B)···O(2)	(b_{12})	1.797(8)	2.751(1)	171.1(14)	0.18(3)	2.97(1)
O(10)-H(10B)···O(3)	(b_{21})	1.889(14)	2.849(1)	176.2(16)	0.09(3)	2.52(1)
O(12)-H(12A)···O(3)	(b_{22})	1.817(6)	2.770(1)	170.9(17)	0.20(3)	3.32(1)

Table 4.7 Hydrogen bond parameters for disodium squarate trihydrate II

H-Bond		H···A (Å)	D···A (Å)	D-H···A (°)	ρ_{BCP} (eÅ^{-3})	$\nabla^2\rho_{BCP}$ (eÅ^{-5})
O(6)-H(6A)···O(3)	(*l*)	1.912(8)	2.853(1)	166.4(12)	0.07(3)	2.31(1)
O(5)-H(5A)···O(4)	(b_{a1})	1.871(19)	2.806(1)	163.8(19)	0.14(3)	2.95(1)
O(7)-H(7A)···O(4)	(b_{a2})	2.495(17)	3.204(1)	131.0(13)	0.03(1)	0.647(3)
O(7)-H(7B)···O(2)	(t_1)	1.714(13)	2.664(1)	169.6(12)	0.23(3)	4.44(3)
O(6)-H(6B)···O(2)	(t_2)	1.873(12)	2.828(1)	172.5(10)	0.11(3)	3.56(3)
O(5)-H(5B)···O(2)	(t_3)	1.938(10)	2.872(1)	163.9(14)	0.14(3)	2.75(1)

The water donors involved in t_1, t_2 and t_3 also form b_{a2}, l and b_{a1} bonds respectively with the surrounding squarate ions.

The O-H$\cdots$O hydrogen bonds in croconate and squarate exhibit densities and Laplacians in the range of 0.1 - 0.2 eÅ^{-3} and 2 - 4 eÅ^{-5}, respectively. The two linear hydrogen bonds in croconate (l_1 and l_2) exhibit ρ_{BCP} values of 0.21(3) and 0.09(3) eÅ^{-3} and $\nabla^2\rho_{BCP}$ values of 3.02(1) and 1.94(1) eÅ^{-5} respectively. The linear bond in squarate (l) has a slightly lower electron density (0.07((3) eÅ^{-3}) and a Laplacian of 2.31(1) eÅ^{-5}. The two sets of symmetrical bifurcated hydrogen bonds in croconate (b_1 and b_2, see Table 4.6) have densities and Laplacians of the order of 0.2 and 3.0 eÅ^{-5}, respectively. On the other hand, the asymmetrical nature of the bifurcated hydrogen bond in squarate renders the two hydrogen bonds in the set with quite different ρ and $\nabla^2\rho$ values ($b_{a1} \rightarrow \rho = 0.14(3)$ eÅ^{-3}, $\nabla^2\rho = 2.95(1)$ eÅ^{-5} $b_{a2} \rightarrow \rho = 0.03(1)$ eÅ^{-3}, $\nabla^2\rho = 0.657(3)$ eÅ^{-5}). The longer b_{a2} hydrogen bond has much lower density and Laplacian at its BCP compared to the shorter b_{a1} hydrogen bond. The three O-H$\cdots$O bonds that form the trifurcated set (t_1, t_2 and t_3) in the squarate ion exhibit ρ and $\nabla^2\rho$ values in the range 0.1 to 0.2 eÅ^{-3} and 3 to 4 eÅ^{-5}, respectively. In the O-H$\cdots$O hydrogen bonds of both croconate and squarate, the two negative perpendicular curvatures (λ_1 and λ_2) are in the range, –0.1 to –1.5 eÅ^{-5} and the positive curvature of the electron density, λ_3 varies from ~3 to 7 eÅ^{-5}.

4.1.2 *Piperazine-oxalate*

Piperazine-oxalate (**III**) crystallizes in a monoclinic crystal system (space group C2/c).[88] The asymmetric unit (shown in Figure 4.4) consists of half a molecule of protonated, piperazinium cation and a full molecule of oxalate anion. The crystallographic data are listed in Table 4.8. The charge density study on this complex has not been reported before.
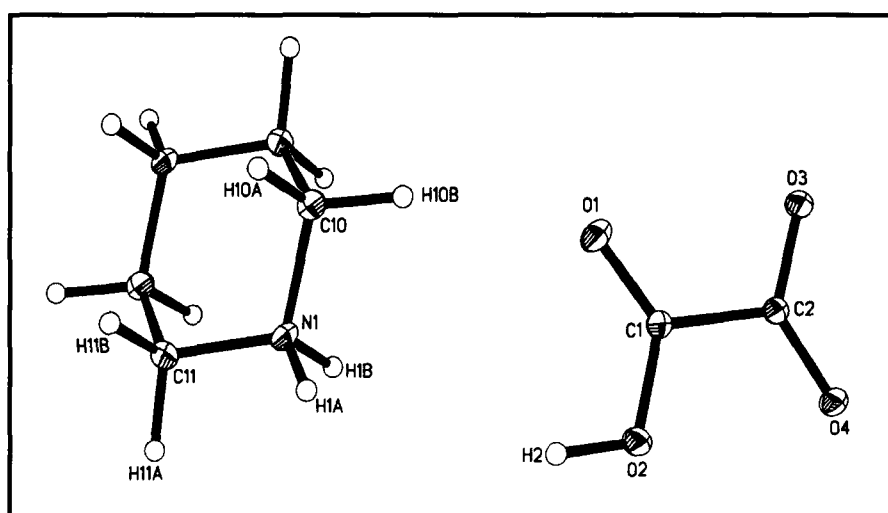
Figure 4.4: *The ORTEP diagram of piperazine-oxalate, with atom labeling. Thermal ellipsoids are given at 50% probability.*

Table 4.8 Crystal Structure data for piperazine oxalate **III**

Chemical formula	$C_4H_7N_1O_4$
Formula weight	133.11
Cell setting	Monoclinic
Space group	C2/c
a (Å)	15.8404 (1)
b (Å)	5.6866 (1)
c (Å)	12.1300 (1)
α (°)	90
β (°)	107.452(1)
γ (°)	90
ρ (Mg/m^3)	1.696
μ, mm^{-1}	0.153
Cell volume (Å^3)	1042.35(2)
Crystal size (mm)	0.35 × 0.25 × 0.23

Table 4.8 (*continued*)

Z	8
F(000)	560
Diffractometer	Siemens CCD 3 circle diffractometer
Radiation type	MoK_α (0.71073 Å)
Crystal-detector distance (cm)	5.0
Temperature (K)	130 (2)
No. of measured reflections	8538
No. of independent reflections	4631
R_{merge}	0.048
R_{int}	0.028
θ_{max} (°), $sin\theta/\lambda$ (Å^{-1})	49.38, 1.07
Range of h, k, l	$-15 \leq h \leq 33$
	$-10 \leq k \leq 11$
	$-25 \leq l \leq 24$

Refinement
Refinement on F^2

R_1	0.048
wR_2	0.128
S	1.083
No. of reflections used in the refinement	4631
No. of parameters refined	111

After multipole refinement

Weighting scheme	0.051, 0.095
$R\{F\}$	0.031
$R\{F^2\}$	0.050
S	1.024
No. of variables	253
N_{ref}/N_v	20.5
Cambridge Crystallographic Database Deposition No.	CCDC 203885

Piperazine is a non-planar, non-aromatic six-membered ring containing N-H groups in the para positions. On complex formation with oxalic acid, a proton transfer takes place from the O-H group of the acid to the N-H group of piperazine. This results in the formation of an NH_2^+ bond. The intramolecular bond distances and angles are given in Table 4.9. The C-C distances in the piperazine ring are ~ 1.52 - 1.56 Å. The C-N distances are ~ 1.50 Å. The two C-O bond distances of the deprotonated carboxyl

group in oxalic acid are nearly equal (~C2-O3 = 1.269(1) Å and C2-O4 = 1.242(1) Å).

The carboxylic acid group that retains the hydrogen atom on its O-H substituent has

varying C-O distances (C1-O1 = 1.216(1) Å and C1-O2 = 1.313(1) Å). The O-H, N-H

and C-H distances were fixed at neutron values, or what are better known as

normalized X-ray geometries (O-H ~ 1.02, N-H ~ 1.03 and C-H ~ 1.09 Å).

Table 4.9 Bond lengths and angles for piperazine oxalate III

Moiety	Distance (Å)	Moiety	Angle (°)
C(1)-O(1)	1.2159(8)	O(1)-C(1)-C(2)	121.27(5)
C(1)-O(2)	1.3132(7)	O(4)-C(2)-O(3)	127.08(5)
C(2)-O(3)	1.2692(7)	O(3)-C(2)-C(1)	114.31(5)
C(2)-O(4)	1.2415(7)	O(4)-C(2)-C(1)	118.61(5)
C(2)-C(1)	1.5545(8)	O(1)-C(1)-O(2)	126.19(6)
C(10)-N(1)	1.4922(8)	C(11)-N(1)-C(10)	111.33(5)
C(11)-N(1)	1.4910(8)	O(2)-C(1)-C(2)	112.54(5)
C(11)-C(10)#1	1.5169(9)	N(1)-C(11)-C(10)#1	109.84(5)
C(10)-C(11)#1	1.5169(9)	N(1)-C(10)-C(11)#1	109.53(5)

Symmetry transformations used to generate equivalent atoms:
#1 -x,-y+1,-z

Static deformation density maps are shown in Figure 4.5. There is an

accumulation of charge density in the bonding region, resulting in a shared interaction.
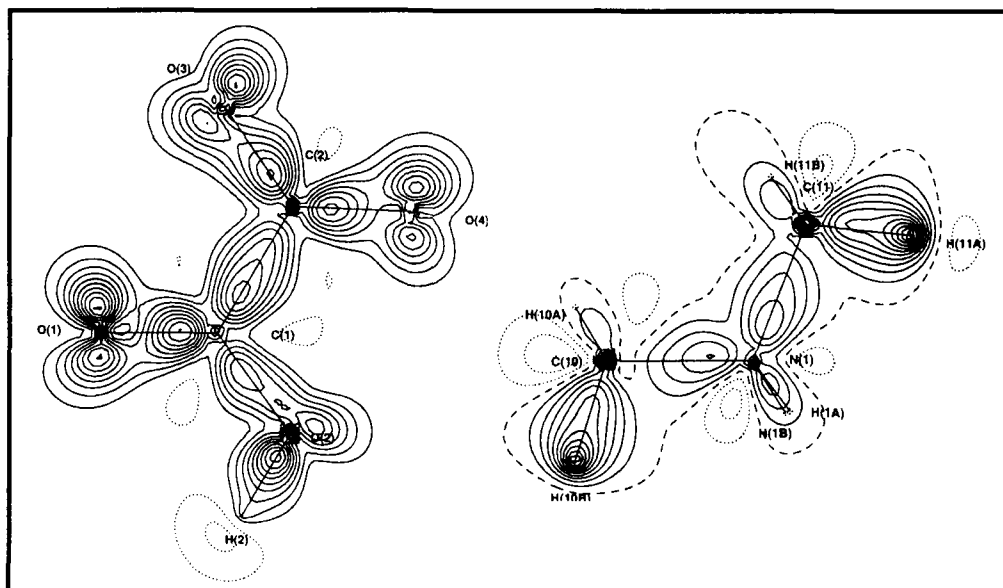
Figure 4.5: *Static deformation density in the symmetry plane of piperazine oxalate complex. Contour levels are given at 0.1 eÅ^{-3}.*

The two lone pair lobes on the oxygen atoms in the oxalate moiety and the single lone-pair lobe on the nitrogen atom of the piperazine ring are clearly visible. Only half the piperazine ring is shown, as in the asymmetric unit.

The bond and ring critical point (BCP and RCP) values of the complex are given in Table 4.10. The C-C and C-N bonds of the piperazine ring have densities and Laplacians in the range, 1.6 - 1.7 $e\text{Å}^{-3}$ and -7.2 to -7.6 $e\text{Å}^{-5}$, respectively. The C-O bonds of the deprotonated carboxyl group have nearly equal densities and Laplacians (C2-O3 ρ = 2.81(4) $e\text{Å}^{-3}$, $\nabla^2\rho$ = -34.7(2) $e\text{Å}^{-5}$ and C2-O4 ρ = 2.83(4) $e\text{Å}^{-3}$, $\nabla^2\rho$ = -35.6(2) $e\text{Å}^{-5}$). The C-O bonds of the non-deprotonated carboxylic acid group have markedly different ρ and $\nabla^2\rho$ values, the difference between the BCP values of the two bonds being ~ 0.6 $e\text{Å}^{-3}$ for ρ and ~ 1.0 $e\text{Å}^{-5}$ for $\nabla^2\rho$.

Table 4.10 Charge density parameters for intramolecular bonds in piperazine oxalate **III** Bond critical point properties:

Bond	ρ_{BCP} ($e\text{Å}^{-3}$)	$\nabla^2\rho_{BCP}$ ($e\text{Å}^{-5}$)	λ_1 ($e\text{Å}^{-5}$)	λ_2 ($e\text{Å}^{-5}$)	λ_3 ($e\text{Å}^{-5}$)	ε
O(2)-H(2)	1.88(6)	-23.2(4)	-29.17	-29.06	35.06	0.00
C(1)-O(1)	3.05(4)	-41.5(2)	-29.56	-26.72	14.82	0.11
C(1)-O(2)	2.46(3)	-31.4(2)	-22.97	-21.15	12.72	0.09
C(2)-O(3)	2.81(4)	-34.7(2)	-25.67	-23.61	14.54	0.09
C(2)-O(4)	2.83(4)	-35.6(2)	-26.42	-24.20	15.04	0.09
C(1)-C(2)	1.76(3)	-12.28(6)	-13.51	-11.43	12.66	0.18
N(1)-H(1A)	2.11(6)	-23.1(3)	-25.87	-25.10	27.86	0.03
N(1)-H(1B)	2.03(6)	-23.8(3)	-25.74	-25.50	27.47	0.01
C(10)-H(10A)	1.79(5)	-15.8(2)	-17.58	-16.73	18.55	0.05
C(10)-H(10B)	1.80(5)	-15.1(1)	-16.87	-16.07	17.81	0.05
C(11)-H(11A)	1.86(5)	-16.0(2)	-17.45	-16.61	18.10	0.05
C(11)-H(11B)	1.79(5)	-14.0(1)	-16.71	-15.77	18.51	0.06
N(1)-C(11)	1.72(3)	-7.23(8)	-11.95	-11.24	15.96	0.06
N(1)-C(10)	1.62(3)	-7.64(9)	-11.69	-10.15	14.20	0.15

Ring critical point properties: ρ_{RCP} = 0.18(1) $e\text{Å}^{-3}$, $\nabla^2\rho_{RCP}$ = 2.5(1) $e\text{Å}^{-5}$

Hydrogen bonds

Piperazine-oxalate **III** exhibits a variety of hydrogen bonds with oxygen as the acceptor (Figure 4.6). Table 4.11 lists the various types of hydrogen bonds formed by

the complex. The O-H$\cdots$O bond formed by the two oxalate moieties has an H$\cdots$O

distance of 1.532(9) Å and an angle of 174.1(16)°. Two sets of bifurcated N-H$\cdots$O

hydrogen bonds are formed by the protonated N-H group of the piperazine ring with

oxygen atoms of the oxalate moiety. The two N-H$\cdots$O bonds forming one bifurcated

set have markedly distinct geometries.
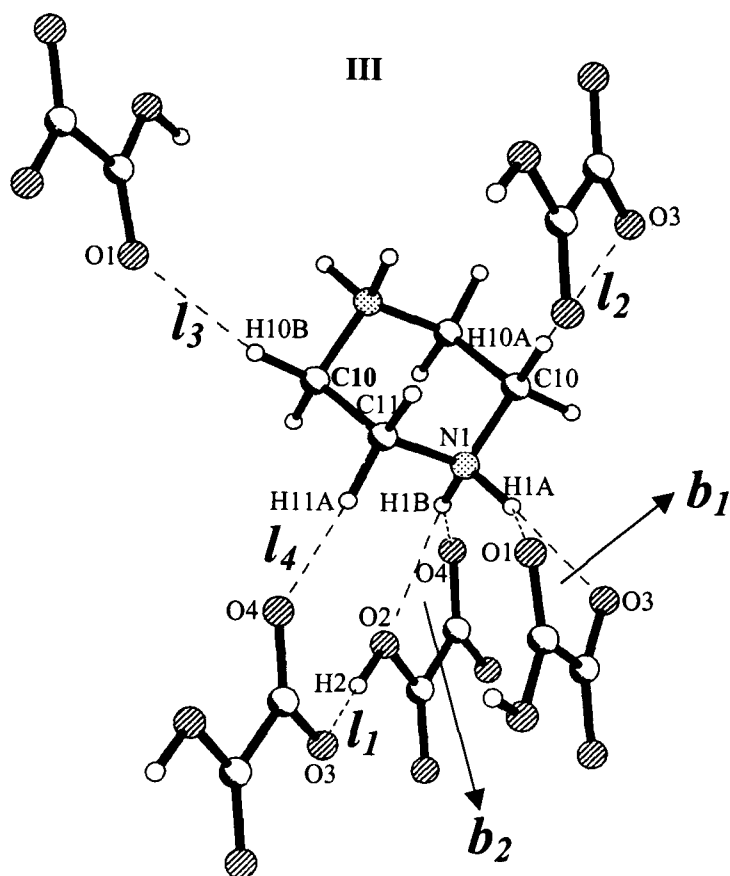
Figure 4.6: Unique hydrogen bonds in piperazine-oxalate III. Symbols l and b designate linear and bifurcated hydrogen bonds. The individual N-H$\cdots$O hydrogen bonds belonging to a bifurcated set are not labelled for the sake of clarity (see Table 4.11).

In each set, one N-H$\cdots$O bond is much longer than the other one. For example,

b_{II} (H$\cdots$O, 2.45(2) Å, N-H$\cdots$O, 134.8(11)°) does not have a very favourable geometry

when compared with b_{12} (H···O, 1.86(1) Å, N-H···O, 147.5(14)°). The three linear C-H···O hydrogen bonds (l_1, l_2 and l_3) have H···O distances of ~ 2.3 Å and a hydrogen bond angle of ~ 160°.

The bond critical point properties (given in Table 4.11) reveal that the O-H···O bond (l_1) is much stronger ($\rho_{H...O} = 0.39(4)$ eÅ^{-3} and $\nabla^2\rho_{H...O} = 5.95(8)$ eÅ^{-5}) compared to the N-H···O and C-H···O bonds formed by the complex. We could not find a bond critical point for the longer N-H···O bond in the bifurcated interaction. Thus b_{11} and b_{21} bonds showed no BCP values indicating that these bonds do not exist topologically, whereas the b_{12} and b_{22} bonds have a BCP, satisfying the criteria for hydrogen bonds formulated by Koch and Popelier (see Section 1, Table 1.4, page 208 in Part 2).

Table 4.11 Hydrogen bond parameters for piperazine oxalate III

H-Bond		H···A (Å)	D···A (Å)	D-H···A (°)	ρ_{BCP} (eÅ^{-3})	$\nabla^2\rho_{BCP}$ (eÅ^{-5})
O(2)-H(2)···O(3)	(l_1)	1.532(9)	2.544(1)	174.1(16)	0.385(44)	5.947(76)
N(1)-H(1A)···O(1)	(b_{11})	2.444(15)	3.255(1)	134.8(11)	-	-
N(1)-H(1A)···O(3)	(b_{12})	1.862(9)	2.789(1)	147.5(14)	0.123(22)	3.019(12)
N(1)-H(1B)···O(2)	(b_{21})	2.265(11)	2.912(1)	119.1(8)	-	-
N(1)-H(1B)···O(4)	(b_{22})	1.797(11)	2.763(1)	153.8(10)	0.148(28)	3.873(23)
C(10)-H(10A)···O(3)	(l_2)	2.317(11)	3.345(1)	156.3(9)	0.058(11)	1.192(2)
C(10)-H(10B)···O(1)	(l_3)	2.325(11)	3.389(1)	164.4(9)	0.056(10)	1.136(1)
C(11)-H(11A)···O(4)	(l_4)	2.251(11)	3.289(1)	158.1(9)	0.068(10)	1.246(1)

The electron densities and Laplacians of the C-H···O bonds are much smaller in magnitude (ρ ~ 0.06 eÅ^{-3} and $\nabla^2\rho$ ~ 1.2 eÅ^{-5}) in comparison to the O-H···O and N-H···O bonds. The positive curvature of the electron density is quite high for the O-

H···O (l_1) bond (λ_3 = 11.43 eÅ^{-5}), whereas for the C-H···O and N-H···O bonds, it is

quite small, in the range of 2 to 5 eÅ^{-5}.

4.1.3 Thiodiglycollic acid-4,4'-bipyridine

The asymmetric unit of thiodiglycollic acid-4,4'-bipyridine complex[89] (**IV**)

consists of one molecule of thiodiglycollic acid and one molecule of 4,4'-bipyridine

(shown in Figure 4.7). This complex crystallizes in a triclinic, P-1 space group. The

crystallographic data are given in Table 4.12. The bond distances and angles are listed

in Table 4.13. The atoms forming the pyridyl rings in 4,4'-bipyridine have bond

distances and angles as expected for any benzenoid heterocyclic ring (C-C ~ 1.40 Å,

C-N ~ 1.34Å and C-C-C, C-N-C angles ~ 120°).
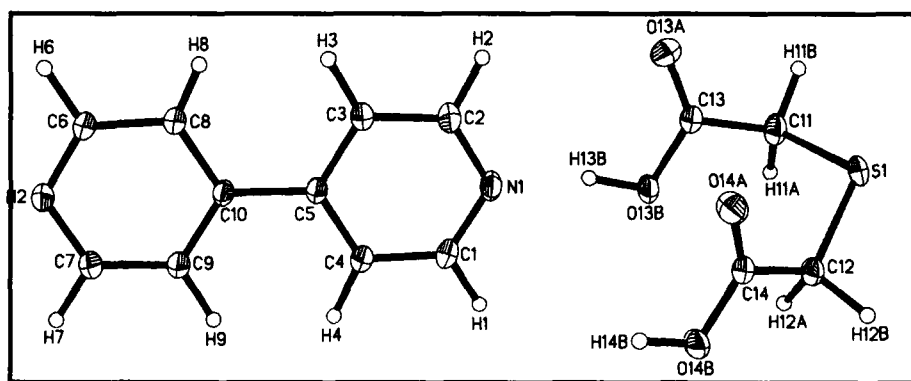
Figure 4.7: The ORTEP plot of thiodiglycollic acid:4,4'-bipyridine complex. Thermal ellipsoids are given at 50% probability.

Table 4.12 Crystal Structure data for thiodiglycollic acid:4,4'-bipyridine **IV**

Chemical formula	$C_{14}H_{14}N_2O_4S_1$
Formula weight	306.33
Cell setting	Triclinic
Space group	P-1
a (Å)	7.8034(1)
b (Å)	7.9444(1)
c (Å)	12.0714(1)
α (°)	79.030(1)

Table 4.12 (*continued*)

β (°)	81.940(1)
γ (°)	69.809(1)
ρ (Mγ/μ^3)	1.48
μ, mm^{-1}	0.253
Cell volume (Å^3)	678.27(1)
Crystal size (mm)	0.25 × 0.27 × 0.40
Z	2
F(000)	320
Diffractometer	Siemens CCD 3 circle diffractometer
Radiation type	MoK$_\alpha$ (0.71073 Å)
Crystal-detector distance (cm)	5.0
Temperature (K)	130 (2)
No. of measured reflections	17711
No. of independent reflections	10888
R$_{merge}$	0.056
R$_{int}$	0.031
θ_{max} (°), sinθ/λ (Å^{-1})	49.42, 1.069
Range of h, k, l	$-16 \leq h \leq 16$
	$-16 \leq k \leq 14$
	$-24 \leq l \leq 21$

Refinement
Refinement on F^2

R$_1$	0.059
wR$_2$	0.168
S	1.12
No. of reflections used in the refinement	10888
No. of parameters refined	246

After multipole refinement

Weighting scheme	0.057, 0.114
R{F}	0.037
R{F^2}	0.056
S	1.012
No. of variables	590
N_{ref}/N_v	17.3
Cambridge Crystallographic Database Deposition No.	CCDC 211329

Table 4.13 Bond lengths and angles for thiodiglycollic acid-4,4'-bipyridine **IV**

Moiety	Distance (Å)	Moiety	Angle (°)
S(1)-C(12)	1.799(10)	C(12)-S(1)-C(11)	102.4(5)
S(1)-C(11)	1.818(12)	C(8)-C(10)-C(9)	117.3(8)
C(10)-C(8)	1.396(14)	C(8)-C(10)-C(5)	121.0(8)
C(10)-C(9)	1.399(13)	C(9)-C(10)-C(5)	121.7(8)
C(10)-C(5)	1.485(13)	C(4)-C(5)-C(3)	117.4(8)

Table 4.13 (*continued*)

O(13B)-C(13)	1.314(12)	C(4)-C(5)-C(10)	121.2(8)
C(5)-C(4)	1.399(14)	C(3)-C(5)-C(10)	121.4(8)
C(5)-C(3)	1.400(13)	C(6)-N(2)-C(7)	117.8(8)
N(2)-C(6)	1.338(14)	C(1)-N(1)-C(2)	118.0(9)
N(2)-C(7)	1.340(14)	O(13A)-C(13)-O(13B)	124.6(9)
N(1)-C(1)	1.34(2)	O(13A)-C(13)-C(11)	123.7(10)
N(1)-C(2)	1.338(14)	O(13B)-C(13)-C(11)	111.7(9)
O(14B)-C(14)	1.317(12)	O(14A)-C(14)-O(14B)	124.5(9)
C(13)-O(13A)	1.220(13)	O(14A)-C(14)-C(12)	124.9(9)
C(13)-C(11)	1.511(14)	O(14B)-C(14)-C(12)	110.6(8)
C(14)-O(14A)	1.215(13)	C(7)-C(9)-C(10)	119.5(9)
C(14)-C(12)	1.522(13)	C(2)-C(3)-C(5)	119.1(9)
C(9)-C(7)	1.383(14)	C(6)-C(8)-C(10)	119.3(9)
C(3)-C(2)	1.386(14)	N(2)-C(7)-C(9)	123.0(9)
C(8)-C(6)	1.388(14)	C(14)-C(12)-S(1)	115.6(7)
C(4)-C(1)	1.387(14)	N(2)-C(6)-C(8)	123.1(9)
Moiety	**Angle (°)**	C(1)-C(4)-C(5)	119.5(9)
N(1)-C(1)-C(4)	122.8(10)	N(1)-C(2)-C(3)	123.2(10)
C(13)-C(11)-S(1)	113.2(7)		

The C-S and C-O bond distances in the acid are of the order of 1.8 and 1.2 Å, respectively.
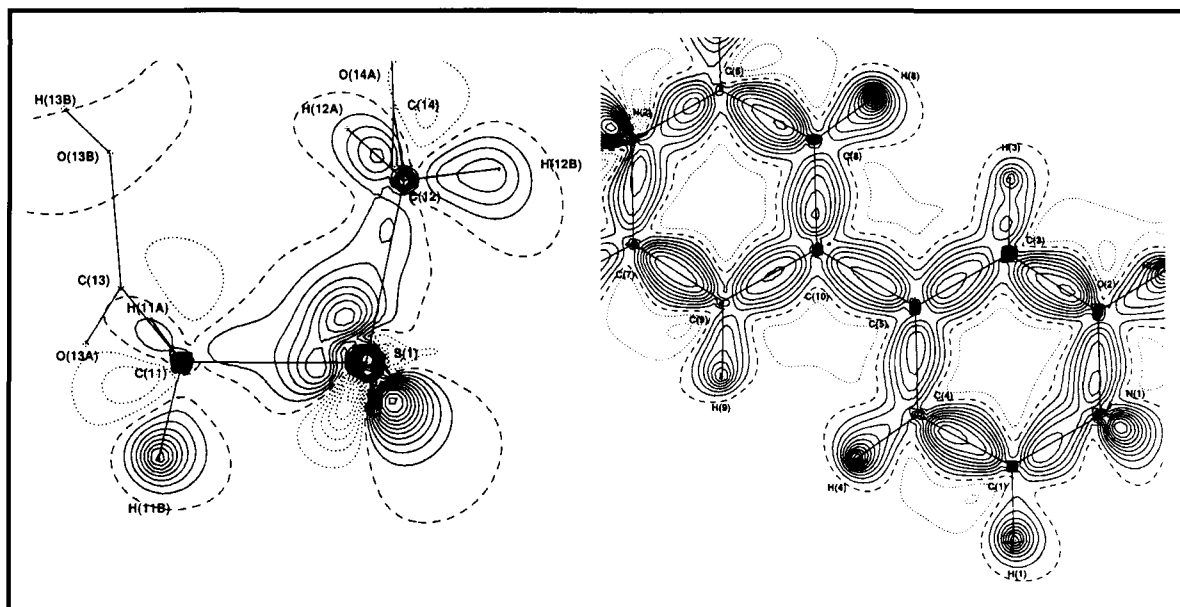
Figure 4.8: *Static deformation density in the symmetry plane of thiodiglycollic acid:4,4'-bipyridine complex. Contour levels are given at 0.1 eÅ^{-3}.*

A static deformation density map for the complex is depicted in Figure 4.8. Note the presence of a single lone-pair lobe on each N atom of bipyridine. Of the two lone-pair lobes on the S atom of the acid, only one is visible, as the other is below the symmetry plane of the molecule.

The BCP values for the complex are given in Table 4.14. Bipyridine exhibits a ring critical point (RCP). The ρ (0.16(1) eÅ^{-3}) and $\nabla^2\rho$ (3.5(1) eÅ^{-5}) at the RCP are comparable to those of benzene (0.16 eÅ^{-3} and 3.81 eÅ^{-5}).[34] The C-C and C-N bonds in bipyridine exhibit ρ values of ~ 2 eÅ^{-3} and $\nabla^2\rho$ of ~ -20 eÅ^{-5}. The C-S bonds in the acid have electron densities of ~ 1.1 to 1.2 eÅ^{-3} and very low $\nabla^2\rho$ of ~ -1 to -2 eÅ^{-5}.

Table 4.14 Charge density parameters for intramolecular bonds in thiodiglycollic acid:4,4'-bipyridine **IV** - Bond critical point properties:

Bond	ρ_{BCP} (eÅ^{-3})	$\nabla^2\rho_{BCP}$ (eÅ^{-5})	λ_1 (eÅ^{-5})	λ_2 (eÅ^{-5})	λ_3 (eÅ^{-5})	ε
C(1)-N(1)	2.36(4)	-20.5(2)	-19.86	-17.36	16.73	0.14
C(2)-N(1)	2.31(4)	-22.5(2)	-20.09	-14.98	12.56	0.34
C(2)-C(3)	2.35(4)	-23.1(1)	-20.17	-14.91	12.00	0.35
C(3)-C(5)	2.09(4)	-17.8(1)	-16.07	-13.32	11.64	0.21
C(5)-C(4)	2.01(4)	-17.4(1)	-15.25	-12.78	10.67	0.19
C(4)-C(1)	2.26(4)	-20.7(1)	-18.49	-14.27	12.08	0.30
C(5)-C(10)	1.89(3)	-13.35(9)	-14.42	-11.77	12.84	0.22
C(10)-C(8)	2.13(4)	-17.6(1)	-15.74	-13.71	11.88	0.15
C(8)-C(6)	2.30(4)	-23.0(1)	-19.24	-15.36	11.63	0.25
C(6)-N(2)	2.45(4)	-20.0(1)	-20.84	-17.22	18.11	0.21
N(2)-C(7)	2.18(5)	-21.4(2)	-18.81	-14.30	11.69	0.32
C(7)-C(9)	2.33(4)	-24.2(1)	-20.27	-15.30	11.39	0.32
C(9)-C(10)	2.11(4)	-18.6(1)	-16.68	-13.80	11.91	0.21
C(11)-C(13)	1.82(3)	-13.07(8)	-13.84	-11.73	12.50	0.18
C(12)-C(14)	1.95(3)	-14.66(8)	-14.55	-13.46	13.35	0.08
C(11)-H(11A)	1.65(7)	-11.6(2)	-16.04	-15.43	19.89	0.04
C(11)-H(11B)	1.77(6)	-15.5(2)	-16.19	-14.70	15.44	0.10
C(12)-H(12A)	1.75(6)	-13.6(2)	-16.96	-15.97	19.32	0.06
C(12)-H(12B)	1.74(7)	-15.0(2)	-16.43	-15.17	16.62	0.08
S(1)-C(11)	1.11(3)	-0.60(5)	-5.84	-5.15	11.59	0.13
S(1)-C(12)	1.17(4)	-1.93(5)	-7.17	-5.56	10.79	0.29
C(13)-O(13A)	2.84(5)	-29.0(2)	-25.10	-21.13	18.23	0.19
C(13)-O(13B)	2.29(4)	-20.5(2)	-19.50	-17.04	16.01	0.14
C(14)-O(14A)	2.85(5)	-31.8(3)	-26.93	-21.30	16.44	0.26
C(14)-O(14B)	2.34(4)	-22.7(2)	-20.75	-18.38	16.45	0.13
O(13B)-H(13B)	2.10(1)	-15.6(5)	-29.48	-28.62	42.48	0.03

Table 4.14 (*continued*)

O(14B)-H(14B)	2.1(1)	-14.0(5)	-29.19	-27.27	42.43	0.07
C(1)-H(1)	1.67(6)	-14.4(2)	-14.84	-13.90	14.37	0.07
C(2)-H(2)	1.74(6)	-17.0(2)	-17.50	-15.79	16.34	0.11
C(3)-H(3)	1.68(6)	-15.0(2)	-17.33	-15.28	17.66	0.13
C(4)-H(4)	1.77(6)	-14.7(2)	-16.84	-14.69	16.80	0.15
C(6)-H(6)	1.82(6)	-17.6(2)	-17.24	-14.69	14.35	0.17
C(7)-H(7)	1.74(6)	-16.7(2)	-16.66	-15.20	15.22	0.10
C(8)-H(8)	1.92(7)	-17.7(2)	-19.37	-15.55	17.25	0.25
C(9)-H(9)	1.76(6)	-17.5(2)	-17.85	-15.46	15.86	0.15

Ring critical point properties: $\rho_{RCP} = 0.16(1)$ eÅ^{-3}, $\nabla^2\rho_{RCP} = 3.5(1)$ eÅ^{-5}

Hydrogen bonds

The molecules of thiodiglycollic acid and 4,4'-bipyridine interact in a manner that a cyclic supermolecule is formed. The unique hydrogen bonds (O-H$\cdots$N and C-H$\cdots$O) formed by the complex are shown in Figure 4.9.
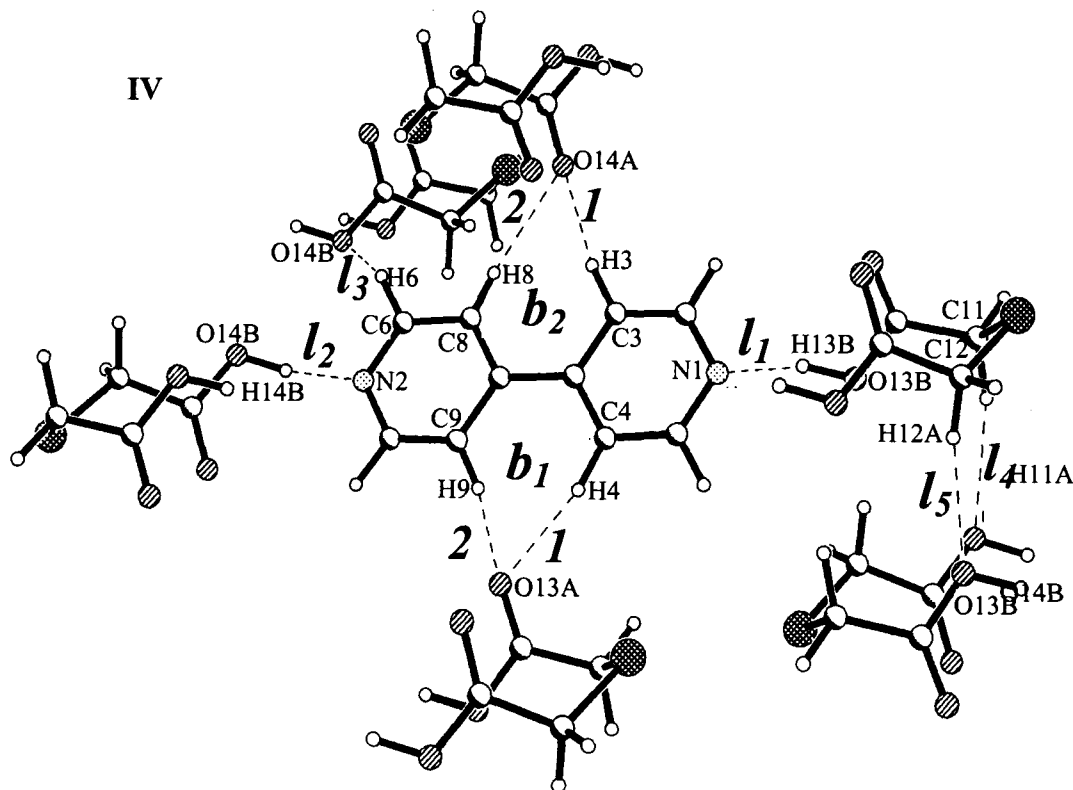
Figure 4.9: Unique hydrogen bonds in thiodiglycollic acid:4,4'-bipyridine **IV**. *Symbols l and b designate linear and bifurcated hydrogen bonds. Only the atoms involved in the formation of hydrogen bonds are labelled.*

255

The geometrical and charge density properties of the O-H⋯N and C-H⋯O

hydrogen bonds are listed in Table 4.15. The complex exhibits O-H⋯N bonds which

are formed by the N atom of bipyridine and the O-H group of the acid (H⋯N

distances of ~1.6 Å and angle of ~170°). Besides these, there are four C-H⋯O bonds

formed between the acid and bipyridine (two bifurcated sets – see Figure 4.9). The

two bifurcated C-H⋯O interactions have quite similar geometries. There are also two

C-H⋯O bonds formed by two acid molecules. The H⋯O distances of the C-H⋯O

bonds are in the range 2.2 - 2.6 Å, and angles ranging between 140° and 170°.

Table 4.15 Hydrogen bond parameters for thiodiglycollic acid-4,4'-bipyridine **IV**

H-Bond	H⋯A (Å)	D⋯A (Å)	D-H⋯A (°)	ρ_{BCP} (eÅ^{-3})	$\nabla^2\rho_{BCP}$ (eÅ^{-5})
O(13B)-H(13B)⋯N(1) (l_1)	1.60(2)	2.603(1)	164(2)	0.452(59)	4.958(80)
O(14B)-H(14B)⋯N(2) (l_2)	1.61(2)	2.592(1)	171(3)	0.461(66)	5.415(94)
C(4)-H(4)⋯O(13A) (b_{11})	2.38(1)	3.424(2)	161(1)	0.029(12)	0.837(2)
C(9)-H(9)⋯O(13A) (b_{12})	2.28(1)	3.339(1)	164(2)	0.035(14)	0.866(2)
C(3)-H(3)⋯O(14A) (b_{21})	2.46(8)	2.523(1)	167(1)	0.030(10)	0.637(3)
C(8)-H(8)⋯O(14A) (b_{22})	2.60(2)	3.541(2)	172(2)	0.035(7)	0.598(3)
C(6)-H(6)⋯O(14B) (l_3)	2.55(1)	3.467(1)	142(2)	0.029(7)	0.557(3)
C(11)-H(11A)⋯O(14B) (l_4)	2.48(2)	3.555(1)	164(2)	0.043(8)	0.692(3)
C(12)-H(12A)⋯O(13B) (l_5)	2.31(2)	3.248(1)	142(2)	0.043(15)	1.078(2)

The O-H⋯N hydrogen bonds exhibit high values of ρ and $\nabla^2\rho$ at the H⋯N critical

points ($\rho_{H...N} \sim 0.5$ eÅ^{-3} and $\nabla^2\rho_{H...N} \sim 5$ eÅ^{-5}). In comparison, the C-H⋯O hydrogen

bonds exhibit much lower ρ (~ 0.03 - 0.04 eÅ^{-3}) and $\nabla^2\rho$ (~ 0.5 - 1.0 eÅ^{-5}) values. The

positive curvature of $\rho_{H...N}$ (λ_3) is much higher (~11 - 12 eÅ^{-5}) for the O-H⋯N bonds

compared to the C-H···O bonds. The two negative perpendicular curvatures are also

smaller for the C-H···O bonds.

4.1.4 Melamine

Melamine (V) crystallizes in a monoclinic, $P2_1/c$ space group.[90] The

asymmetric unit, which consists of a single molecule, is shown in Figure 4.10. The

crystallographic information is given in Table 4.16.
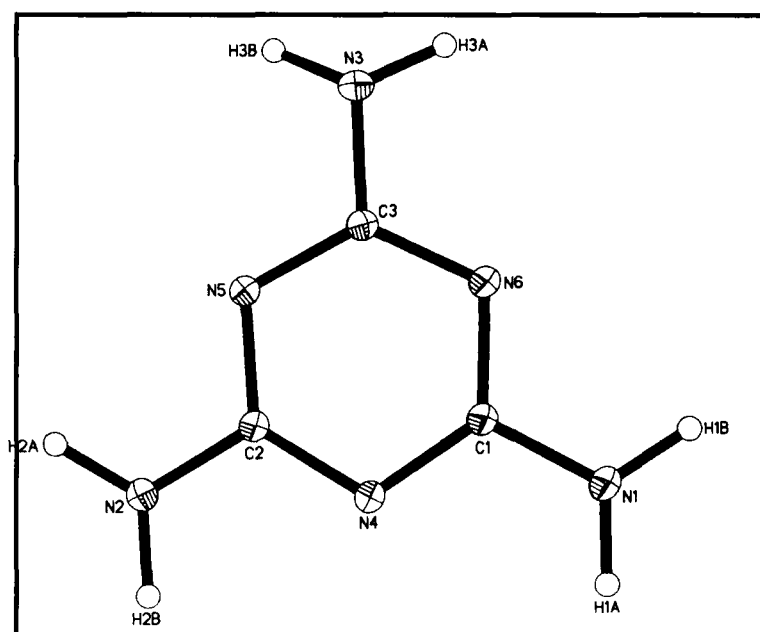
Figure 4.10: *The ORTEP plot of melamine. Thermal ellipsoids are given at 50%* *probability.*

Table 4.16 Crystal structure data for melamine (V)

Chemical formula	$C_3H_6N_6$
Formula weight	240.08
Cell setting	Monoclinic
Space group	$P2_1/c$
a (Å)	7.259(1)
b (Å)	7.4684(1)
c (Å)	10.1711(2)
α (°)	90
β (°)	108.094(1)

Table 4.16 (*continued*)

γ (°)	90
ρ (Mg/m^3)	1.599
μ, mm^{-1}	0.119
Cell volume (Å^3)	524.1(1)
Crystal size (mm)	0.32 × 0.39 × 0.43
Z	4
F(000)	264
Diffractometer	Siemens CCD 3 circle diffractometer
Radiation type	MoK$_\alpha$ (0.71073 Å)
Crystal-detector distance (cm)	5.0
Temperature (K)	130 (2)
No. of measured reflections	8651
No. of independent reflections	4227
R$_{merge}$	0.069
R$_{int}$	0.040
θ_{max} (°), sinθ/λ (Å^{-1})	49.43, 1.069
Range of *h, k, l*	$-15 \le h \le 14$
	$-15 \le k \le 13$
	$-21 \le l \le 20$

Refinement
Refinement on F^2

R$_1$	0.060
wR$_2$	0.105
S	0.972
No. of reflections used in the refinement	4227
No. of parameters refined	106

After multipole refinement

Weighting scheme	0.057, 0.114
R{F}	0.035
R{F^2}	0.079
S	1.025
No. of variables	153
N$_{ref}$/N$_v$	22.1
Cambridge Crystallographic Database Deposition No.	CCDC 211330

The data on bond lengths and angles are listed in Table 4.17. The C–C and C–N bond

distances are ~ 1.3 Å. The valence angles between the atoms forming the ring are of

the order of 116° to 120°.

Table 4.17 Bond lengths and angles for melamine V

Moiety	Distance (Å)	Moiety	Angle (°)
N(5)-C(3)	1.3425(10)	C(3)-N(5)-C(2)	114.72(6)
N(5)-C(2)	1.3542(10)	C(1)-N(4)-C(2)	114.78(7)
N(4)-C(1)	1.3468(11)	C(3)-N(6)-C(1)	114.29(7)
N(4)-C(2)	1.3498(10)	N(6)-C(3)-N(5)	125.91(7)
N(6)-C(3)	1.3414(10)	N(6)-C(3)-N(3)	117.58(7)
N(6)-C(1)	1.3527(10)	N(5)-C(3)-N(3)	116.48(7)
C(3)-N(3)	1.3625(10)	N(2)-C(2)-N(4)	118.16(7)
C(2)-N(2)	1.3377(11)	N(2)-C(2)-N(5)	117.07(7)
C(1)-N(1)	1.3414(10)	N(4)-C(2)-N(5)	124.77(7)
		N(1)-C(1)-N(4)	117.75(7)
		N(1)-C(1)-N(6)	116.83(7)
		N(4)-C(1)-N(6)	125.41(7)

A static deformation density map of melamine is depicted in Figure 4.11. The lone-pair lobes on the ring nitrogen atoms are distinctly seen.
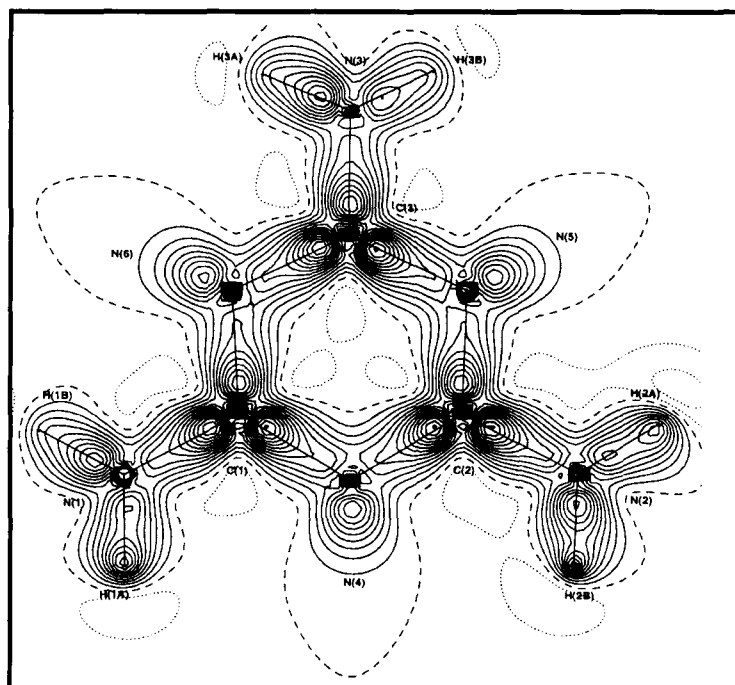
Figure 4.11: *Static deformation density in the symmetry plane of melamine. Contour levels are given at 0.1 eÅ⁻³.*

The charge density parameters for the ring bonds are given below in Table 4.18.

Table 4.18 Charge density parameters for intramolecular bonds in melamine V

Bond	ρ_{BCP} (eÅ^{-3})	$\nabla^2\rho_{BCP}$ (eÅ^{-5})	λ_1 (eÅ^{-5})	λ_2 (eÅ^{-5})	λ_3 (eÅ^{-5})	ε
C(1)-N(4)	2.55(3)	-23.35(8)	-22.19	-19.74	18.58	0.12
C(2)-N(4)	2.52(2)	-22.35(4)	-21.71	-19.45	18.81	0.12
C(2)-N(5)	2.42(1)	-21.09(2)	-20.60	-18.35	17.85	0.12
C(3)-N(5)	2.56(2)	-24.03(2)	-22.40	-19.99	18.36	0.12
C(3)-N(6)	2.58(3)	-25.46(1)	-22.68	-20.39	17.61	0.11
C(1)-N(6)	2.43(3)	-21.69(8)	-20.82	-18.53	17.66	0.12
C(1)-N(1)	2.58(3)	-25.22(9)	-23.57	-19.32	17.67	0.22
C(2)-N(2)	2.617(2)	-27.202(2)	-24.19	-20.05	17.03	0.21
C(3)-N(3)	2.401(2)	-20.364(2)	-21.12	-17.35	18.10	0.22
N(1)-H(1A)	2.32(6)	-25.1(3)	-29.56	-28.24	32.67	0.05
N(1)-H(1B)	2.12(6)	-28.1(4)	-30.58	-29.26	31.78	0.05
N(2)-H(2A)	2.32(7)	-28.2(3)	-30.35	-28.94	31.06	0.05
N(2)-H(2B)	2.12(7)	-26.9(4)	-30.18	-28.87	32.19	0.05
N(3)-H(3A)	2.23(7)	-27.2(4)	-30.86	-29.50	33.13	0.05
N(3)-H(3B)	2.27(6)	-24.1(3)	-29.14	-27.83	32.91	0.05

Ring critical point properties: ρ_{RCP} = 0.20 (2) eÅ^{-3}, $\nabla^2\rho_{RCP}$ = 4.2(1) eÅ^{-5}.

The electron densities of the C-C and C-N bonds are of the order of 2.4 - 2.6 eÅ^{-3}, while the Laplacians are ~ -20 to -27 eÅ^{-5}. The N-H bonds have slightly lower densities and lower ellipticities (Table 4.18).

Hydrogen bonds

Melamine V exhibits six unique N-H$\cdots$N hydrogen bonds (depicted in Figure 4.12), formed by the amino group of one molecule and the N atom of the hetero ring. Of the six hydrogen bonds, four have H$\cdots$N distances of ~ 2 Å, and N-H$\cdots$N angles of ~ 162° - 176°, while the other two have much longer H$\cdots$N distances (~2.6 Å) and lower hydrogen bond angles (~ 120°). The geometrical features and hydrogen bond critical points are given in Table 4.19.

Table 4.19 Hydrogen bond parameters for melamine V[a]

H-Bond		H···A (Å)	D···A (Å)	D-H···A (°)	ρ$_{BCP}$ (eÅ^{-3})	∇^{2}ρ$_{BCP}$ (eÅ^{-5})
N(1)-H(1A)···N(3)	(l_1)	2.553(13)	3.262(1)	126.9(13)	0.040(6)	0.682(2)
N(1)-H(1B)···N(6)	(l_2)	1.989(11)	2.997(1)	176.4(12)	0.135(27)	2.572(15)
N(2)-H(2A)···N(4)	(l_3)	2.066(12)	3.046(1)	162.7(16)	0.111(20)	2.150(6)
N(2)-H(2B)···N(5)	(l_4)	2.086(12)	3.094(1)	175.3(13)	0.111(21)	1.960(7)
N(3)-H(3A)···N(4)	(l_5)	2.623(14)	3.285(1)	123.1(8)	0.038(5)	0.605(2)
N(3)-H(3B)···N(5)	(l_6)	2.071(14)	3.060(1)	165.5(12)	0.112(19)	2.213(6)

[a]Refer Figure 4.12 for the hydrogen bond network
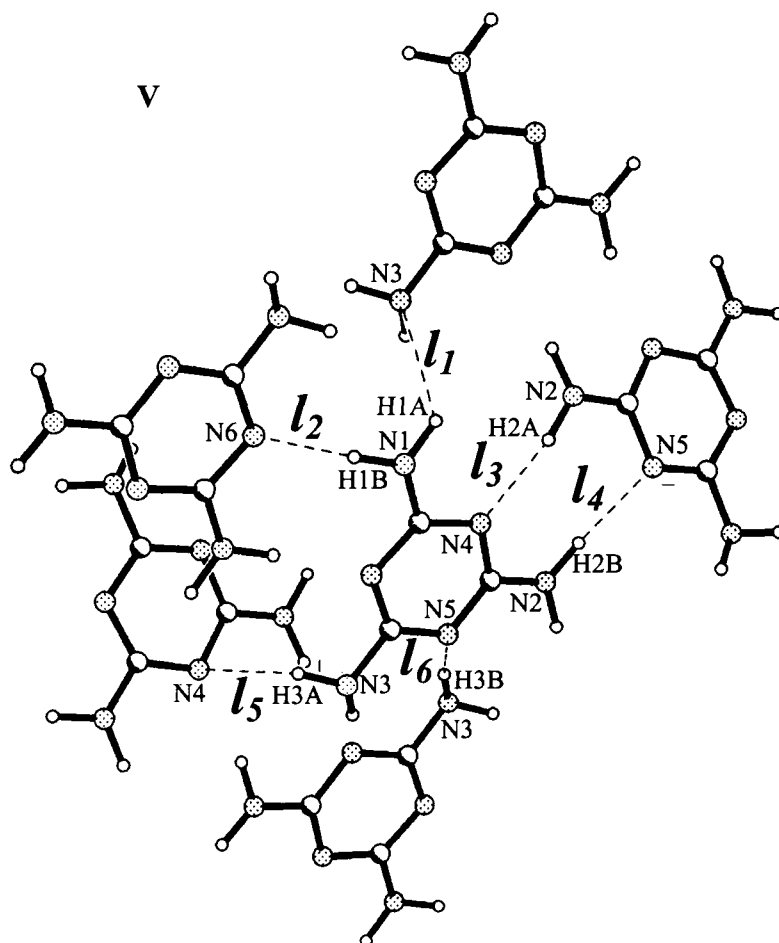
Figure 4.12: *Unique hydrogen bonds in melamine* (V). *Symbol l represents a linear hydrogen bond. Only the atoms involved in the formation of hydrogen bonds are labelled.*

261

The electron densities at the six H⋯N bond critical points vary between 0.04 - 0.14 $e\text{Å}^{-3}$, while the Laplacians are in the range of 0.6 to 2.6 $e\text{Å}^{-5}$. For N-H⋯N bonds with quite favourable geometry (l_2, l_3, l_4 and l_6), λ_3 values vary between 3.03 and 3.93 $e\text{Å}^{-5}$, whereas for l_1 and l_5, they are small, ~ 1 $e\text{Å}^{-5}$. The negative curvatures, λ_1 and λ_2 are of the order of ~ -0.5 to -0.7 $e\text{Å}^{-5}$ for l_2, l_3, l_4 and l_6 and ~ -0.1 $e\text{Å}^{-5}$ for l_1 and l_5.

4.1.5 Thionicotinamide

Thionicotinamide (**VI**) crystallizes in a monoclinic, P2$_1$/n space group.[91] The asymmetric unit, which consists of a single thionicotinamide molecule, is shown in Figure 4.13. Crystal structure data are given in Table 4.20. Bond lengths and valence angles are listed in Table 4.21.
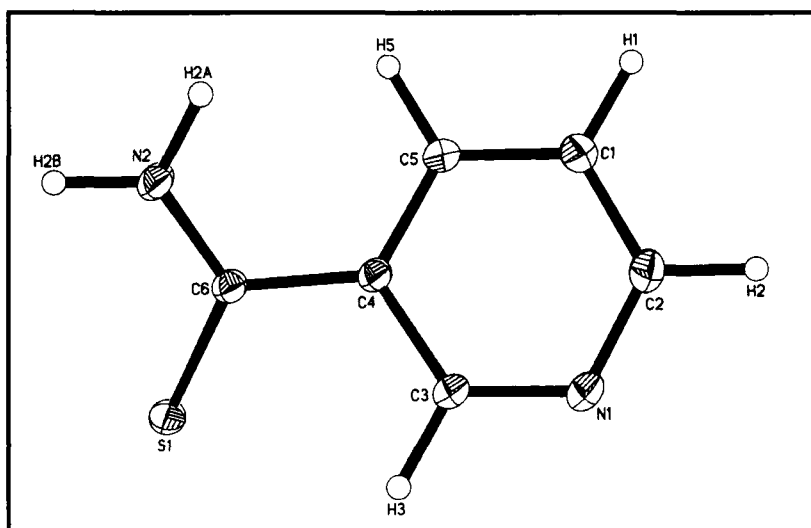
Figure 4.13: *The ORTEP plot of thionicotinamide. Thermal ellipsoids are given at 50% probability.*

Table 4.20 Crystal Structure data for thionicotinamide **VI**

Chemical formula	$C_6H_6N_2S_1$
Formula weight	138.19
Cell setting	Monoclinic
Space group	$P2_1/n$
a (Å)	3.9558(1)
b (Å)	10.5976(1)
c (Å)	15.2959(2)
α (°)	90
β (°)	95.087(1)
γ (°)	90
ρ (Mg/m³)	1.437
μ, mm⁻¹	0.403
Cell volume (Å³)	638.71(2)
Crystal size (mm)	0.30 × 0.41 × 0.33
Z	4
F(000)	288
Diffractometer	Siemens CCD 3 circle diffractometer
Radiation type	MoK_α (0.71073 Å)
Crystal-detector distance (cm)	5.0
Temperature (K)	130 (2)
No. of measured reflections	10829
No. of independent reflections	5549
R_{merge}	0.067
R_{int}	0.040
θ_{max} (°), sinθ/λ (Å⁻¹)	49.45, 1.069
Range of h, k, l	$-7 \leq h \leq 7$
	$-13 \leq k \leq 22$
	$-32 \leq l \leq 32$
Refinement	
Refinement on F²	
R_1	0.042
wR_2	0.107
S	1.02
No. of reflections used in the refinement	5549
No. of parameters refined	82
After multipole refinement	
Weighting scheme	0.045, 0.114
R{F}	0.0293
R{F²}	0.0474
S	0.8726
No. of variables	258
N_{ref}/N_v	23.1
Cambridge Crystallographic Database Deposition No.	CCDC 211331

Table 4.21 Bond lengths and angles for thionicotinamide **VI**

Moiety	Distance (Å)	Moiety	Angle (°)
C(1)-C(2)	1.3846(11)	C(3)-C(4)-C(6)	119.81(6)
C(2)-N(1)	1.3490(11)	C(3)-N(1)-C(2)	117.49(7)
N(1)-C(3)	1.3365(10)	C(4)-C(5)-H(5)	120.56(4)
C(3)-C(4)	1.3999(9)	C(5)-C(4)-C(3)	117.75(6)
C(5)-C(4)	1.3951(10)	C(1)-C(5)-C(4)	118.89(7)
C(5)-C(1)	1.3945(10)	H(2A)-N(2)-H(2B)	120
C(6)-C(4)	1.4888(9)	C(4)-C(6)-S(1)	120.57(5)
C(6)-N(2)	1.3211(9)	N(2)-C(6)-S(1)	123.09(5)
C(6)-S(1)	1.6791(7)	N(2)-C(6)-C(4)	116.33(6)
N(2)-H(2A)	1.01	C(6)-N(2)-H(2A)	120.00(4)
N(2)-H(2B)	1.01	C(6)-N(2)-H(2B)	120.00(4)
C(2)-H(2)	1.08	N(1)-C(3)-C(4)	123.86(7)
C(3)-H(3)	1.08	C(5)-C(4)-C(6)	122.44(6)
C(5)-H(5)	1.08	C(1)-C(5)-H(5)	120.56(4)
C(1)-H(1)	1.08	N(1)-C(3)-H(3)	118.07(4)
Moiety	**Angle (°)**	C(4)-C(3)-H(3)	118.07(4)
C(2)-C(1)-C(5)	118.98(7)	N(1)-C(2)-C(1)	123.03(7)
C(2)-C(1)-H(1)	120.51(4)	N(1)-C(2)-H(2)	118.48(4)
C(5)-C(1)-H(1)	120.51(4)	C(1)-C(2)-H(2)	118.48(4)

The bond distances of the C-C and C-N bonds forming the pyridyl ring in thionicotinamide are ~ 1.4 and ~ 1.3 Å, respectively, and the valence angles are nearly 120°. The C=S bond is ~ 1.7 Å. The N-H and C-H bonds were fixed at neutron values of 1.01 and 1.08 Å, respectively.

A static deformation density map is given for thionicotinamide in Figure 4.14. The sp^2 – hybridized lone-pair (lying in the same plane as that of the molecule) on the N atom of the pyridyl ring is visible. The planes in which the sulphur and amino nitrogen lone-pairs appear are not depicted in the figure. The properties evaluated at the intramolecular bond critical points and at the ring critical point of the pyridyl ring are listed in Table 4.22. The pyridyl ring bonds have ρ_{BCP} and $\nabla^2\rho_{BCP}$ values in the range of 2.1 to 2.5 eÅ^{-3} and -20 to -23 eÅ^{-5}. The C=S bond has a much lower value of ρ_{BCP} (1.42(3) eÅ^{-3}) and $\nabla^2\rho_{BCP}$ (-4.1(1) eÅ^{-5}). The ellipticity values of the pyridyl ring

bonds vary from 0.13 to 0.32 and the λ_3 values are in the range of 10 - 15 eÅ^{-5}. The N-

H and the C-H bonds of the thiocarbonyl fragment have higher values of λ_3 (see Table

4.22).
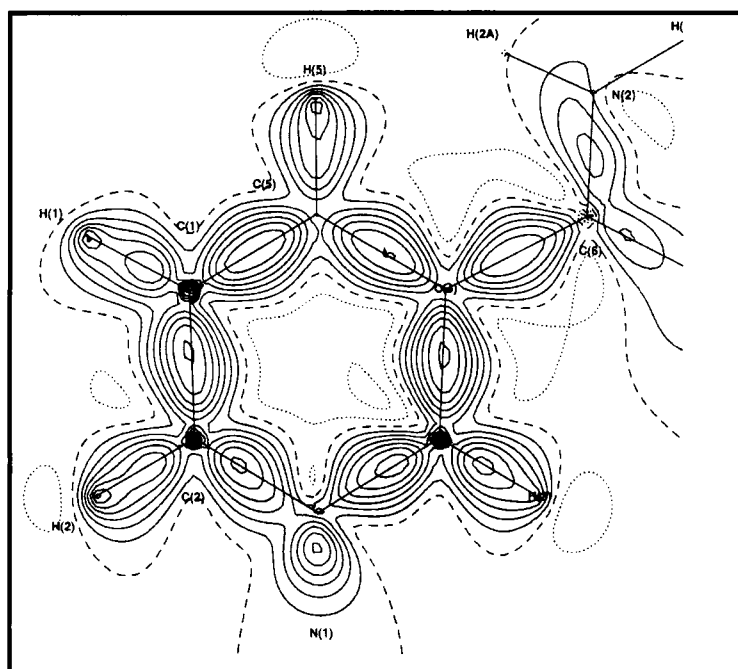
Figure 4.14: *Static deformation density in the symmetry plane of thionicotinamide. Contour levels are given at 0.1 eÅ^{-3}.*

Table 4.22 Charge density parameters for intramolecular bonds in thionicotinamide **VI**

Bond	ρ_{BCP} (eÅ^{-3})	$\nabla^2\rho_{BCP}$ (eÅ^{-5})	λ_1 (eÅ^{-5})	λ_2 (eÅ^{-5})	λ_3 (eÅ^{-5})	ε
C(1)-C(2)	2.20(3)	-20.71(8)	-17.51	-13.95	10.76	0.26
C(2)-N(1)	2.37(4)	-20.9(2)	-19.07	-16.85	15.06	0.13
N(1)-C(3)	2.45(4)	-23.2(1)	-21.18	-16.40	14.42	0.29
C(3)-C(4)	2.19(3)	-22.54(8)	-18.35	-14.24	10.05	0.29
C(4)-C(5)	2.09(3)	-18.73(8)	-16.67	-12.60	10.54	0.32
C(5)-C(1)	2.17(3)	-19.76(8)	-16.90	-13.89	11.02	0.22
C(4)-C(6)	1.87(3)	-16.02(7)	-14.50	-12.60	11.08	0.15
C(6)-N(2)	2.40(5)	-28.7(2)	-20.52	-17.22	9.04	0.19
C(6)-S(1)	1.42(3)	-4.1(1)	-6.54	-5.64	8.13	0.16
N(2)-H(2A)	2.10(6)	-28.6(3)	-27.99	-25.68	25.04	0.09
N(2)-H(2B)	2.04(6)	-25.7(4)	-29.02	-27.50	30.85	0.06
C(1)-H(1)	1.71(5)	-14.6(2)	-17.23	-16.11	18.80	0.07
C(3)-H(3)	1.76(5)	-19.0(2)	-18.44	-17.59	17.01	0.05
C(5)-H(5)	1.75(5)	-17.4(2)	-16.86	-16.31	15.80	0.03

Ring critical point properties: ρ_{RCP} = 0.20(2) eÅ^{-3}, $\nabla^2\rho_{RCP}$ = 4.2(1) eÅ^{-5}.

The two negative curvatures (λ_1 and λ_2) range between -6 eÅ^{-5} to -30 eÅ^{-5} for all the bonds in this system. The pyridyl ring exhibits an RCP (ρ_{RCP} = 0.20(2) eÅ^{-3}, $\nabla^2\rho_{RCP}$ = 4.2(1) eÅ^{-5}), which is comparable to that of benzene (0.16 eÅ^{-3} and 3.81 eÅ^{-5}).[92]

Hydrogen bonds

Thionicotinamide exhibits three unique hydrogen bonds in its crystal structure. The hydrogen bonding pattern is depicted in Figure 4.15. An intermolecular N-H$\cdots$N bond (H$\cdots$N, 2.950(1) Å, 159.15(7)°) is found in the crystal. In addition, it also has an N-H$\cdots$S bond (H$\cdots$S, 3.414(1) Å, 157.84(7)°). The presence of a C-H$\cdots$S bond (2.744(1) Å) can also be anticipated, although the hydrogen bonding angle is very small (101.23(6)°). Since the sulphur atom, S(1) hydrogen bonds to two different donor groups (N-H and C-H), the interaction could be termed as bifurcated, although the C-H$\cdots$S hydrogen bond has an extremely unfavourable geometry. The geometrical and charge density parameters of the hydrogen bond CPs are listed in Table 4.23.

The values of ρ and $\nabla^2\rho$ at the hydrogen bond CPs for the N-H$\cdots$N bond (*l*) is greater than for the N-H$\cdots$S bond (*b$_1$*). No BCP was located for the C-H$\cdots$S bond (*b$_2$*) indicating the absence of such a bond. The D$\cdots$A distances for the three types of hydrogen bonds (N-H$\cdots$N, N-H$\cdots$S and C-H$\cdots$S) are of the order of 3 Å (see Table 4.23).
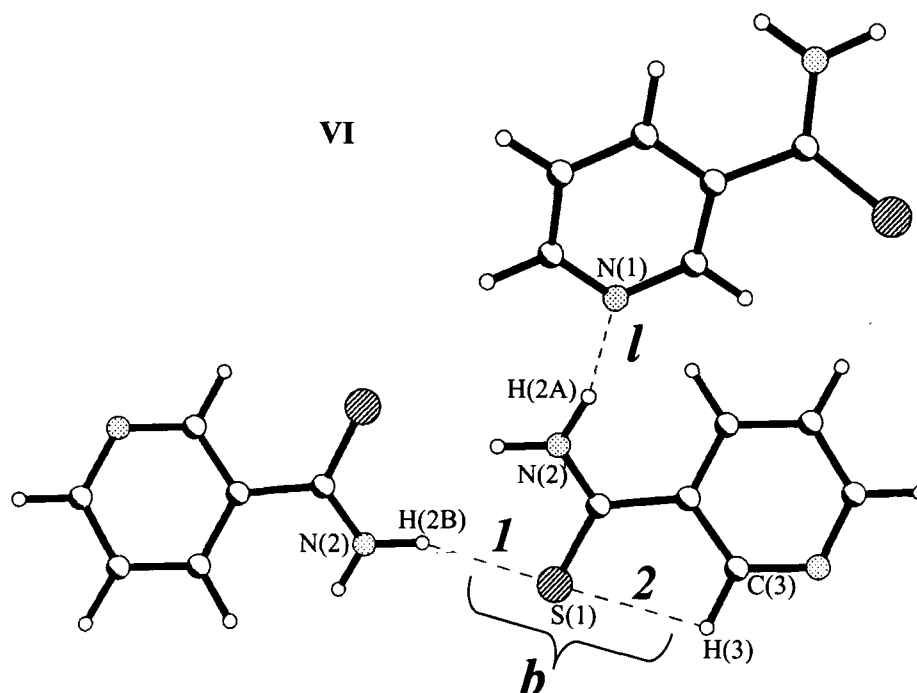
Figure 4.15: *Unique hydrogen bonds in thionicotinamide* (**VI**). *Symbols l and b represent linear and bifurcated hydrogen bonds. Only the atoms involved in the formation of hydrogen bonds are labelled.*

Table 4.23 Hydrogen bond parameters for thionicotinamide **VI**

H-Bond	H···A (Å)	D···A (Å)	D-H···A (°)	ρ_{BCP} (eÅ^{-3})	$\nabla^2\rho_{BCP}$ (eÅ^{-5})
N(2)-H(2A)···N(1) (*l*)	1.984(1)	2.950(1)	159.15(7)	0.140(22)	2.242(8)
N(2)-H(2B)···S(1) (*b₁*)	2.457(1)	3.414(1)	157.84(7)	0.112(15)	1.261(2)
C(3)-H(3)···S(1) (*b₂*)	2.744(1)	3.140(1)	101.23(6)	-	-

4.1.6 Thioacetamide

The asymmetric unit of thioacetamide (**VII**) consists of two symmetry-independent molecules.[93] These molecules are different rotamers as shown in Figure 4.16. The crystal structure occurs in a monoclinic, $P2_1/c$ space group. The crystal data and other experimental details are listed in Table 4.24.
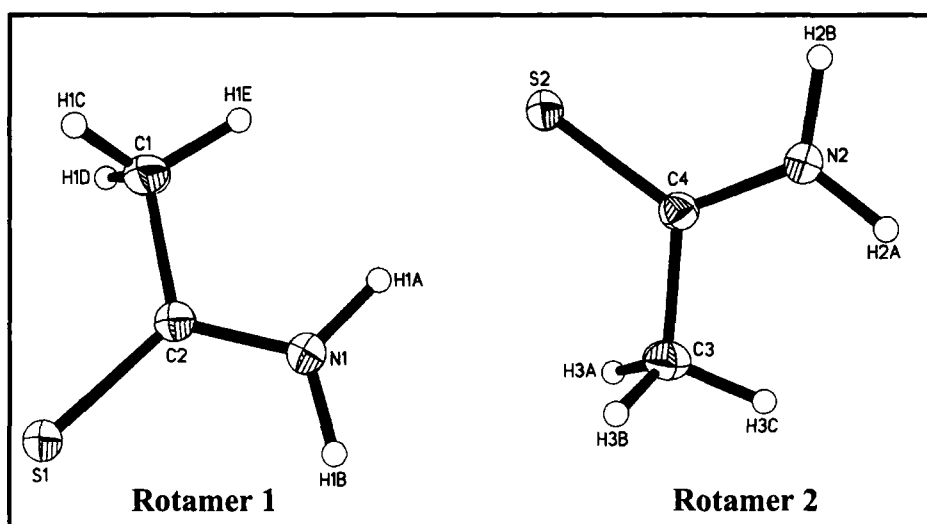
Figure 4.16: *The ORTEP plot of thioacetamide. Thermal ellipsoids are given at 50% probability. The two rotamers are indicated.*

The bond distances and angles are given in Table 4.25. The two rotamers do not show very significant differences in their bond lengths and angles ($C=S \approx 1.68$ Å, $N-C \approx 1.32$ Å, $C-C \approx 1.51$ Å).

Table 4.24 Crystal Structure data for thioacetamide **VII**

Chemical formula	$C_4H_{10}N_2S_2$
Formula weight	150.26
Cell setting	Monoclinic
Space group	$P2_1/c$
a (Å)	7.0377(1)
b (Å)	9.9202(1)
c (Å)	11.0268(2)
α (°)	90
β (°)	99.471(1)
γ (°)	90
ρ (Mg/m^3)	1.314
μ, mm^{-1}	0.609
Cell volume (Å^3)	759.35(2)
Crystal size (mm)	$0.30 \times 0.25 \times 0.28$
Z	4
F(000)	320
Diffractometer	Siemens CCD 3 circle diffractometer
Radiation type	MoK_α (0.71073 Å)
Crystal-detector distance (cm)	5.0
Temperature (K)	130 (2)

Table 4.24 (*continued*)

No. of measured reflections	12259
No. of independent reflections	6101
R_{merge}	0.0
R_{int}	0.043
θ_{max} (°), $\sin\theta/\lambda$ (Å^{-1})	49.45, 1.06
Range of h, k, l	$-14 \leq h \leq 13$
	$-20 \leq k \leq 19$
	$-20 \leq l \leq 22$

Refinement
Refinement on F^2

R_1	0.050
wR_2	0.122
S	0.984
No. of reflections used in the refinement	6101
No. of parameters refined	113

After multipole refinement

Weighting scheme	0.048, 0.091
R{F}	0.032
R{F^2}	0.046
S	0.9959
No. of variables	257
N_{ref}/N_v	18.6
Cambridge Crystallographic Database Deposition No.	CCDC 211332

But the most interesting experimental difference in the crystal structure is that in rotamer **1**, C(2) and its three sp^2 bonded atoms C(1), S(1) and N(1) are exactly planar. In addition, N1 and its sp^2 bonded atoms, C2, H1A and H1B are also planar. But in rotamer **2**, there are significant deviations from planarity with respect to both these four-atom groups.

Table 4.25 Bond lengths and angles for thioacetamide **VII**

Moiety	Distance (Å)	Moiety	Angle (°)
Rotamer 1			
C(1)-C(2)	1.509(2)	C(1)-C(2)-S(1)	120.91(9)
C(2)-N(1)	1.317(2)	N(1)-C(2)-S(1)	123.01(9)
C(2)-S(1)	1.6758(12)	N(2)-C(4)-C(3)	116.21(10)
Rotamer 2			
C(3)-C(4)	1.498(2)	N(1)-C(2)-C(1)	116.07(11)
C(4)-N(2)	1.317(2)	C(3)-C(4)-S(2)	121.56(9)
C(4)-S(2)	1.6853(11)	N(2)-C(4)-S(2)	122.23(8)

In both the rotamers, the N-C-S bond angle is above 120° (123.01(9) ° in **1** and

122.23(8)° in **2**). This is consistent with the repulsion between partially negative

nitrogen and sulphur atoms, causing the angle to increase above the expected value of

120°. The rotamer **1** is in the planar form, with the nitrogen atom being sp^2 hybridized.

On rotation of this rotamer about the C-N bond, it changes to form sp^3 hybridized

pyramidal nitrogen atom in rotamer **2**. The H-N-H angle is 118.5° in **1** and 121.1° in **2**.

Both the C-N-H angles decrease on going from **1** to **2**.

The non-planarity with respect to the sp^2 C atom arises due to the C(sp^2)

pyramidalization, which is believed to be an intrinsic property of the asymmetric

rotamers. This has been attributed to the presence of crystal - field forces like

hydrogen bonding, van der Waals or dipole interactions. G. A. Jeffrey *et al* have

studied the C sp^2 and N atom pyramidalization in thioacetamide by comparing the

results of a 15 K neutron diffraction experiment with *ab initio* molecular orbital

calculations.[93b] The two conformations arise due to the different orientations of the

methyl groups.

The static deformation density maps for the two rotamers are shown in Figure

4.17. We see that in rotamer **1**, there is a considerable mixing of the electron density

contours across the C sp^2 atom (the C(2) atom), but such a mixing is absent in the

deformation map of the unsymmetrical rotamer **2**.
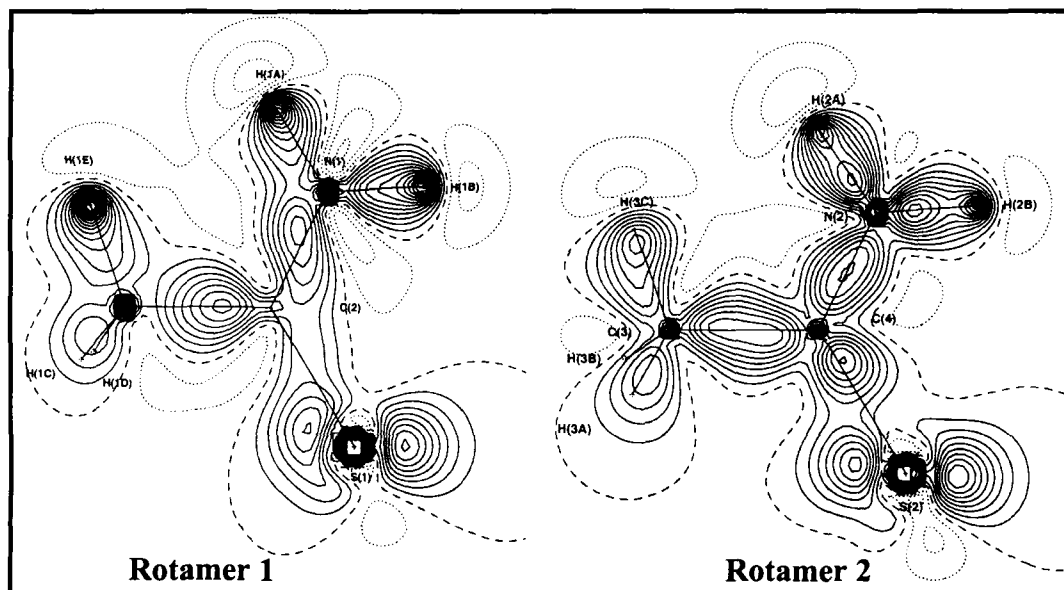
Figure 4.17: *Static deformation density in the symmetry plane of thioacetamide. Contour levels are given at 0.1 e$Å^{-3}$.*

Table 4.26 lists bond critical point properties of the intramolecular bonds of the two rotamers. The ρ_{BCP} values for the C-S bonds of the two rotamers, **1** and **2** are ~1.47 and 1.45 e$Å^{-3}$, respectively. The corresponding Laplacians are -4.2 and -1.4 e$Å^{-5}$ (we see that there is considerable difference in the Laplacian values of the C-S bonds of the two rotamers). This explains that greater is the charge concentration between the carbon and the sulphur atoms, greater is the amount of sp^2 character of the carbon atom of the C-S bond. The ρ_{BCP} values of the C-C bonds in the two rotamers differ by a value of ~ 0.18 e$Å^{-3}$. For the C-N bonds in **1** and **2**, the densities at the BCP are 2.35 and 2.42 e$Å^{-3}$, whereas the Laplacians are -25.0 and -24.7 e$Å^{-5}$, respectively. The C-N bonds are closer to the ρ_{BCP} values of C=N double bonds, which are ~2.74 e$Å^{-3}$, are

much higher compared to those of the C-N single bonds, ~1.87 eÅ^{-3}. The bond orders

for the C-N bonds in 1 and 2 are 0.96 and 1.02 eÅ^{-3}, respectively.

Table 4.26 Charge density parameters of the intramolecular bonds in the two rotamers (1 and 2) of thioacetamide, **VII**. Similar bonds in the two rotamers **1** and **2** are listed together.

Bond	ρ_{BCP} (eÅ^{-3})	$\nabla^2\rho_{BCP}$ (eÅ^{-5})	λ_1 (eÅ^{-5})	λ_2 (eÅ^{-5})	λ_3 (eÅ^{-5})	ε
1 C(1)-C(2)	1.78(4)	-12.14(9)	-11.48	-10.30	9.64	0.11
2 C(4)-C(3)	1.96(4)	-16.36(7)	-13.81	-12.32	9.77	0.12
1 C(2)-N(1)	2.35(5)	-25.0(2)	-17.66	-16.05	8.67	0.10
2 C(4)-N(2)	2.42(6)	-24.7(3)	-19.21	-16.25	10.72	0.18
1 C(2)-S(1)	1.47(4)	-4.18(9)	-8.64	-6.13	10.59	0.41
2 C(4)-S(2)	1.45(6)	-1.4(2)	-6.26	-5.50	10.34	0.14
1 N(1)-H(1A)	2.3(1)	-21.2(5)	-27.88	-24.98	31.71	0.12
2 N(2)-H(2A)	2.3(1)	-27.4(7)	-30.52	-28.20	31.33	0.08
1 N(1)-H(1B)	2.4(1)	-24.8(6)	-30.97	-27.66	33.87	0.12
2 N(2)-H(2B)	2.2(1)	-20.8(7)	-28.64	-27.06	34.92	0.06
1 C(1)-H(1C)	1.8(1)	-10.5(3)	-15.28	-13.98	18.75	0.09
2 C(3)-H(3A)	1.9(1)	-13.3(2)	-16.44	-13.29	16.46	0.24
1 C(1)-H(1D)	1.67(9)	-9.6(3)	-15.42	-13.97	19.78	0.10
2 C(3)-H(3B)	1.71(9)	-10.1(2)	-14.87	-10.67	15.44	0.39
1 C(1)-H(1E)	1.7(1)	-9.4(3)	-14.69	-12.91	18.20	0.14
2 C(3)-H(3C)	1.9(1)	-13.3(3)	-16.64	-13.45	16.67	0.24

The ellipticity values for the C-S and C-N bonds in the two rotamers are 0.41 {C(2)-S(1)}, 0.14 {C(4)-S(2)} and 0.10 {C(2)-N(1)}, 0.18 {C(4)-N(2)}.

The degree of the negative charge on the sulfur atoms in the two rotamers does not differ much, the pseudoatomic charges on the atoms, S(1) in **1** is -0.626e and S(2) in **2** is -0.551e. Also, there is a 0.01 Å difference in the C-S bond distances, 1.676(12) in **1** and 1.685(11) Å in **2**. But, there are changes in the C-N bonds in **1** and **2**. Although, their bond lengths, 1.317(2) Å in **1** and **2** are the same, we see that there is a

net electron transfer from the thiocarbonyl carbon to the nitrogen atom in **1** (the pseudoatomic charge on C(2) in **1** is –0.215e), whereas there is an electron transfer from the nitrogen to the carbon atom in **2** (pseudoatomic charge on C(4) in **2** is – 0.239e). The opposite electron transfer in **1** is attributed to the nitrogen atom being relatively electronegative, thus attracting electrons toward itself from the adjacent atoms. The Laplacian values of the C-N bond in rotamer **1** are -25.0 eÅ^{-5} and -24.7 eÅ^{-5} in **2**, showing that there is slightly a greater overlap in **1** than in **2**. Also, there is a greater charge difference between the C and N atoms in **2** than in **1** as is seen in the degree of polarization of the C-N bond, 27.45% in **1** and 30.58% in **2**. On the other hand, since sulphur has an electronegativity close to that of carbon, the C=S bond is not very strongly polarized (7.43% in **1** and 4.55% in **2**).

Hydrogen bonds

In the crystal structure, the two rotameric forms are involved in N-H⋯S hydrogen bonding interactions. Figure 4.18 depicts the hydrogen bond pattern. The two forms alternate, forming a strong hydrogen-bonded ring, consisting of N-H⋯S hydrogen bonds. There are five unique hydrogen bonds that are shown in Figure 4.25. The N-H⋯S bond formed by the amino group of rotamer **1** is more linear (H⋯S = 2.40 Å, N-H⋯S = 175.8°) than that formed by the amino group of rotamer **2** (H⋯S = 2.38 Å, N-H⋯S = 174.4°).

The geometrical data and charge density properties evaluated at the hydrogen bond critical points are given in Table 4.27.
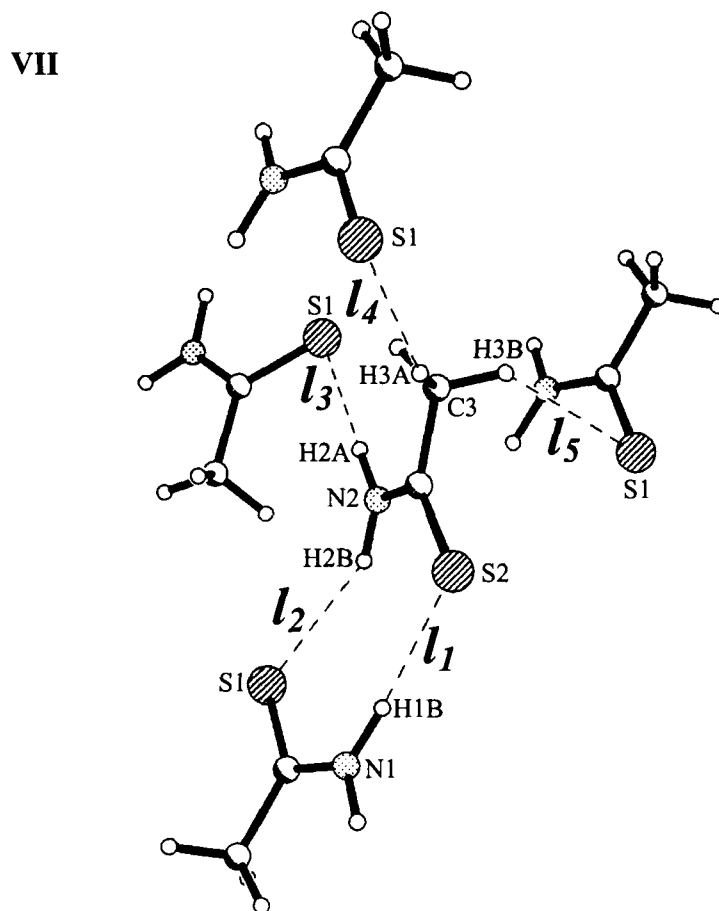
Figure 4.18: Unique hydrogen bonds in thioacetamide (VII). Symbols l and b represent linear and bifurcated hydrogen bonds. Only the atoms involved in the formation of hydrogen bonds are labelled.

Table 4.27 Hydrogen bond parameters for thioacetamide VII.

H-Bond		H···A (Å)	D···A (Å)	D-H···A (°)	ρ_{BCP} (eÅ^{-3})	$\nabla^2\rho_{BCP}$ (eÅ^{-5})
N(1)-H(1B)···S(2)	(l_1)	2.463(12)	3.434(1)	158.8(16)	0.076(32)	1.269(2)
N(2)-H(2A)···S(1)	(l_2)	2.381(15)	3.401(1)	174.3(17)	0.035(28)	0.951(2)
N(2)-H(2B)···S(1)	(l_3)	2.520(12)	3.472(1)	155.1(16)	0.093(26)	1.218(2)
C(3)-H(3A)···S(1)	(l_4)	2.792(12)	3.813(2)	154.3(15)	0.012(10)	0.276(5)
C(3)-H(3B)···S(1)	(l_5)	2.877(10)	3.700(1)	134.2(15)	0.034(9)	0.455(5)

The electron densities at the H$\cdots$S critical points for the N-H$\cdots$S hydrogen bonds (l_1, l_2 and l_3) lie in the range 0.01 to 0.1 eÅ^{-3} and the Laplacians are $\sim$ 0.3 to 1.0 eÅ^{-5}. Two C-H$\cdots$S hydrogen bonds are formed employing two different C-H donors belonging to the same methyl group (l_4 and l_5 in Figure 4.18).

In the preceding sections (Sections 4.1.1 to 4.1.6), we have seen that hydrogen bonding interactions can be adequately described and classified by the properties of the electron density, ρ at the bond (3, -1) critical points, where the gradients of ρ vanish. The next two sections 4.2 and 4.3 deal with systematic correlations between geometrical and charge density parameters as well as an accurate topological analysis of bond paths in the hydrogen$\cdots$acceptor regions.

4.2 Investigations of trends in the geometrical and charge density parameters of hydrogen bonds

For purposes of correlating charge density data with structural parameters, we have gathered the hydrogen bond parameters from the seven molecular systems studied by us (summarized in Table 4.28). From Table 4.28, we find that the hydrogen-acceptor distance in the O-H$\cdots$O bonds lie in the range of 1.5 - 2.5 Å, with angles between 131° and 176°. For N-H$\cdots$O bonds, the range shifts to $\sim$ 1.8 - 2.7 Å, and angles vary from $\sim$ 119° to 174°. This is primarily due to the less acidic nature of the N-H group compared to the O-H group. The C-H group, being even less acidic and hence a weak donor, exhibits much longer H$\cdots$O contacts in the range of 2.3 to 2.6 Å.

275

Table 4.28 Geometrical and charge density parameters of the types of hydrogen bonds from the present study.

Type of H-bond	H···A (Å)	D···A (Å)	D-H···A (°)	ρ_{BCP} (eÅ⁻³)	$\nabla^2\rho_{BCP}$ (eÅ⁻⁵)	λ_1 (eÅ⁻⁵)	λ_2 (eÅ⁻⁵)	λ_3 (eÅ⁻⁵)
			Disodium croconate trihydrate **I**					
O-H···O	1.817(6)	2.770(1)	170.9(17)	0.204(28)	3.32(1)	-1.07	-1.06	5.45
	1.89(1)	2.849(1)	176.2(16)	0.088(25)	2.52(1)	-0.49	-0.41	3.41
	1.797(8)	2.751(1)	171.1(14)	0.181(30)	2.97(1)	-0.96	-0.92	4.85
	1.829(7)	2.782(1)	171.9(17)	0.214(26)	3.00(1)	-1.14	-1.11	5.25
	1.841(5)	2.784(1)	166.9(17)	0.214(27)	3.02(1)	-1.12	-1.10	5.25
	1.998(7)	2.934(1)	164.5(15)	0.090(26)	1.94(1)	-0.46	-0.40	2.80
			Disodium squarate trihydrate **II**					
O-H···O	1.912(8)	2.853(1)	166.4(12)	0.068(25)	2.31(1)	-0.55	-0.25	3.11
	2.495(17)	3.204(1)	131.0(13)	0.031(7)	0.647(3)	-0.17	-0.09	0.91
	1.871(19)	2.806(1)	163.8(19)	0.141(29)	2.95(1)	-0.98	-0.69	4.62
	1.873(12)	2.828(1)	172.5(10)	0.105(33)	3.56(3)	-0.46	-0.44	4.46
	1.938(10)	2.872(1)	163.9(14)	0.142(25)	2.75(1)	-0.74	-0.64	4.12
	1.714(13)	2.664(1)	169.6(12)	0.233(34)	4.44(3)	-1.54	-1.34	7.31
			Piperazine oxalate **III**					
O-H···O	1.532(9)	2.544(1)	174.1(16)	0.385(44)	5.95(8)	-2.78	-2.71	11.43
N-H···O	2.444(15)	3.255(1)	134.8(11)	-	-	-		
	1.862(9)	2.789(1)	147.5(14)	0.123(22)	3.02(1)	-0.75	-0.52	4.28
	2.265(11)	2.912(1)	119.1(8)	-	-	-		
	1.797(11)	2.763(1)	153.8(10)	0.148(28)	3.87(2)	-0.80	-0.75	5.42
C-H···O	2.317(11)	3.345(1)	156.3(9)	0.058(11)	1.192(2)	-0.26	-0.23	1.68
	2.325(11)	3.389(1)	164.4(9)	0.056(10)	1.136(1)	-0.24	-0.21	1.59
	2.251(11)	3.289(1)	158.1(9)	0.068(10)	1.246(1)	-0.32	-0.27	1.83
			Thiodiglycollic acid-4,4'-bipyridyl **IV**					
C-H···O	2.55(1)	3.467(1)	142(2)	0.029(7)	0.557(3)	-0.13	-0.10	0.78
	2.60(2)	3.541(2)	172(2)	0.035(7)	0.598(3)	-0.12	-0.12	0.83
	2.46(8)	2.523(1)	167(1)	0.030(10)	0.637(3)	-0.10	-0.09	0.82
	2.28(1)	3.339(1)	164(2)	0.035(14)	0.866(2)	-0.17	-0.11	1.15
	2.38(1)	3.424(2)	161(1)	0.029(12)	0.837(2)	-0.12	-0.11	1.07
	2.48(2)	3.555(1)	164(2)	.043(8)	0.692(3)	-0.17	-0.16	1.02
	2.31(2)	3.248(1)	142(2)	0.043(15)	1.078(2)	-0.15	-0.13	1.36
O-H···N	1.60(2)	2.603(1)	164(2)	0.452(59)	4.96(8)	-3.08	-2.93	10.97
	1.61(2)	2.592(1)	171(3)	0.461(66)	5.42(9)	-3.34	-3.01	11.77
			Melamine **V**					
N-H···N	2.553(13)	3.262(1)	126.9(13)	0.040(6)	0.682(2)	-0.16	-0.12	0.96
	1.989(11)	2.997(1)	176.4(12)	0.135(27)	2.57(2)	-0.71	-0.64	3.92
	2.066(12)	3.046(1)	162.7(16)	0.111(20)	2.15(1)	-0.64	-0.50	3.29
	2.086(12)	3.094(1)	175.3(13)	0.111(21)	1.96(1)	-0.57	-0.50	3.03
	2.623(14)	3.285(1)	123.1(8)	0.038(5)	0.605(2)	-0.13	-0.11	0.84
	2.071(14)	3.060(1)	165.5(12)	0.112(19)	2.213(6)	-0.53	-0.51	3.24
			Thionicotinamide **VI**					
N-H···N	1.984(1)	2.950(1)	159.15(7)	0.140(22)	2.242(8)	-0.88	-0.64	3.76
N-H···S	2.457(1)	3.414(1)	157.84(7)	0.112(15)	1.261(2)	-0.41	-0.39	2.06
C-H···S	2.744(1)	3.140(1)	101.23(6)	-	-	-	-	-
			Thioacetamide **VII**					
N-H···S	2.463(12)	3.434(1)	158.8(16)	0.076(32)	1.269(2)	-0.40	-0.29,	1.96
	2.381(15)	3.401(1)	174.3(17)	0.035(28)	0.951(2)	-0.21	-0.09	1.25
	2.520(12)	3.472(1)	155.1(16)	0.093(26)	1.218(2)	-0.40	-0.37	1.99
C-H···S	2.792(12)	3.813(2)	154.3(15)	0.012(10)	0.276(5)	-0.10	-0.02	0.40
	2.877(10)	3.700(1)	134.2(15)	0.034(9)	0.455(5)	-0.13	-0.09	0.67

With N-H as a donor, and N or S atoms as acceptors, the H···A distances are longer (2 - 3 Å), with angles between 150° - 170°. For hydrogen bonds such as C-H···S, the H···S distances are very long, ~ 2.8 - 2.9 Å, with angles of ~ 130° - 150°. In general, hydrogen bonds with O(-H) and N(-H) as donor groups and acceptors (such as those found in the oxocarbon dianions, piperazine-oxalate, melamine, thionicotinamide) have a more favourable geometry, compared to those with C-H as a donor or sulphur atom as the acceptor (found in systems like thiodiglycollic acid-bipyridine, thionicotinamide and thioacetamide). Nevertheless, the latter hydrogen bonds may be sometimes useful in stabilizing the crystal packing of the molecules.

In Figure 4.19, typical deformation density maps are shown for the different types of hydrogen bonds. Concentric contours typify the various bonding regions in the molecule between the atom-cores. The maps clearly reveal significant features such as bond regions and lone-pair (non-bonding) regions. There is an accumulation of charge density in the bonding region between the donor atom and the hydrogen atom resulting in a shared interaction. On the other hand, in the hydrogen bond (H···A) region, there is depletion of charge density between the two nuclei. This is due to the closed-shell interaction. Accordingly, small densities and small and positive Laplacians are to be expected at the bond critical points.

For the thirteen O-H···O bonds examined experimentally in our study, the electron densities (ρ) and the Laplacians ($\nabla^2\rho$) at the bond critical point, are generally in the range of ~ 0.1 to 0.2 eÅ^{-3} and ~ 2 to 3 eÅ^{-5}, respectively (see Table

1.532 Å, 174.1°

(a) O-H···O

1.862 Å, 147.5°

(b) N-H···O

2.317 Å, 156.3°

(c) C-H···O

1.61 Å, 171°

(d) O-H···N

1.989 Å, 176.4°

(e) N-H···N

2.463 Å, 158.8°

(f) N-H···S

2.877 Å, 134.2°
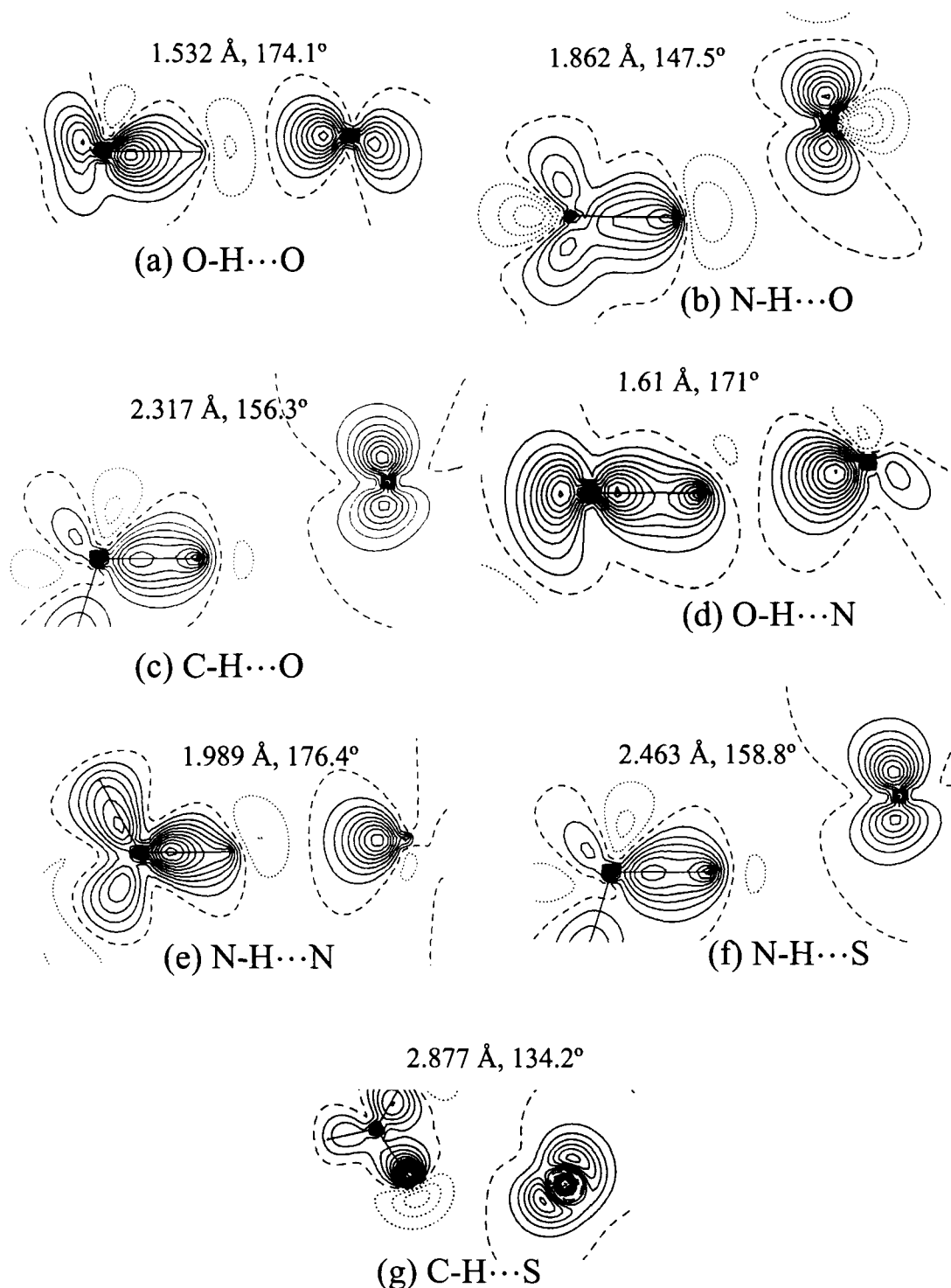
(g) C-H···S

Figure 4.19: Static deformation density maps in the hydrogen bond plane for (a) O-H···O, (b) N-H···O, (c) C-H···O, (d) O-H···N, (e) N-H···N, (f) N-H···S and (g) C-H···S (contours at intervals of 0.1 e$Å^{-3}$). The numbers on top of each map refer to the H···A distance and the D-H···A angle (see Table 4.28). The deformation density was obtained by subtracting the spherical atomic densities from the total charge density, $\delta\rho(r) = \rho^{total}(r) - \rho^{pro}(r)$. Solid lines indicate positive contours; dotted lines, negative contours and dashed lines, zero contours.

4.28). The two exceptions are the short bond (H···O, 1.532(9) Å) in piperazine oxalate for which ρ and $\nabla^2\rho$ are 0.39(4) eÅ^{-3} and 5.95(8) eÅ^{-5} respectively, and the long bond (H···O, 2.495(17) Å) formed by the squarate ion. The electron density and Laplacian value for the longer O-H···O bond (H···O, 2.495(17) Å) are 0.03(1) eÅ^{-3} and 0.647(3) eÅ^{-5}, respectively. The N-H···O bonds formed by piperazine oxalate exhibit H···O densities and Laplacians of ~ 0.1 eÅ^{-3} and 3 eÅ^{-5} respectively. We do not, however, find critical points for the longer N-H···O bonds in piperazine oxalate (H···O, 2.3 - 2.4 Å). The two O-H···N bonds in the thiodiglycolic acid-bipyridine complex exhibit higher electron densities and Laplacians (~ 0.5 eÅ^{-3} and ~ 5 eÅ^{-5}) at the H···N critical points. The H···N critical points of the N-H···N bonds in melamine have much lower values of ρ (0.04 - 0.14 eÅ^{-3}) and $\nabla^2\rho$ (0.6 - 2.6 eÅ^{-5}). The H···S regions of the N-H···S bonds in thioacetamide and thionicotinamide carry small densities of ~0.04 - 0.11 eÅ^{-3} and Laplacians of ~1.3 - 2.1 eÅ^{-5} at their critical points. The C-H···O bonds in the thiodiglycolic acid-bipyridine complex exhibit similar densities and Laplacians. Among the various hydrogen bonds studied, the C-H···S bonds in thioacetamide carry the smallest densities (0.01 - 0.03 eÅ^{-3}) and Laplacians (~0.3 - 0.5 eÅ^{-5}). Among the various charge density descriptors, the total density and Laplacian at the hydrogen bond CPs were chosen to be plotted to against the important geometric parameter, H···A distance, as shown in Figure 4.20. Both ρ and $\nabla^2\rho$ are observed to decrease exponentially with the H···A distance, although the latter shows a better trend. The fits are not as good as one would desire.
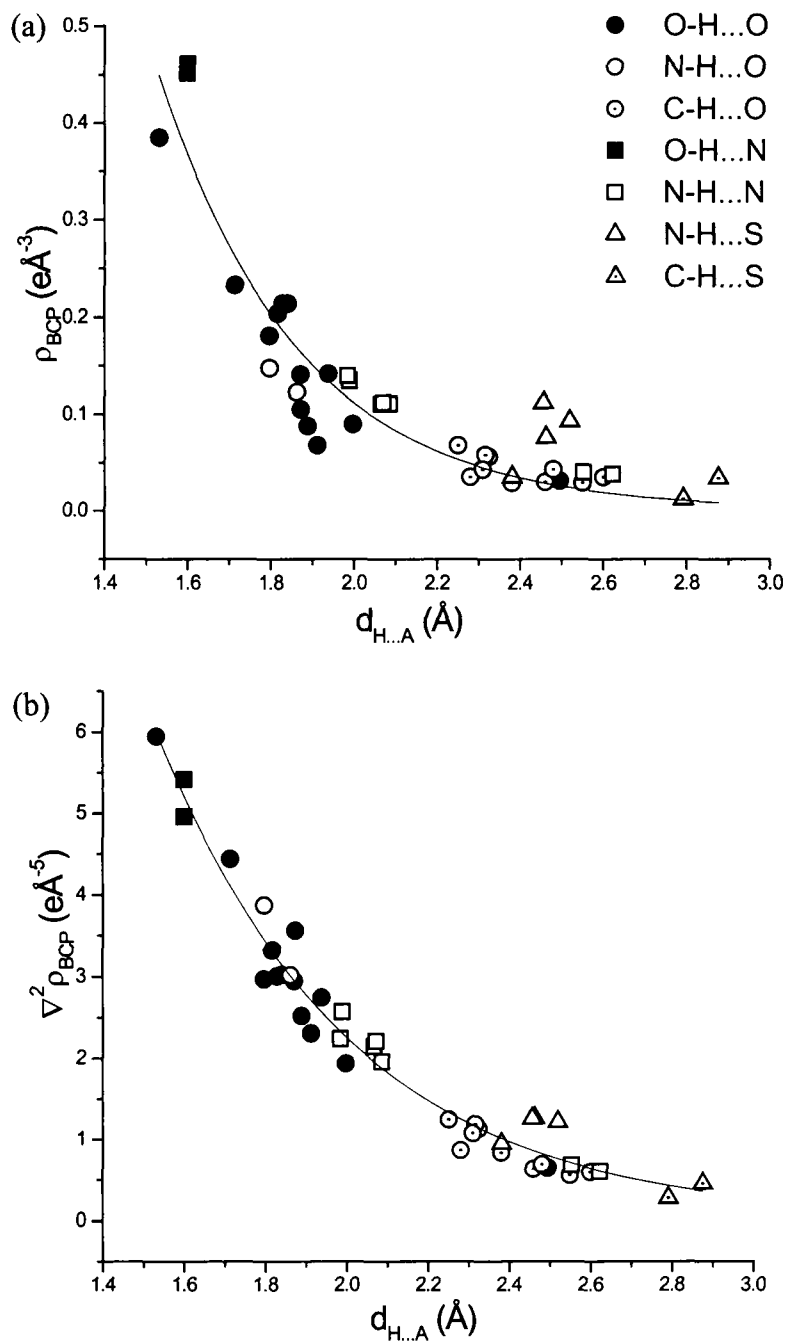
Figure 4.20: *(a) Plot of the total density ρ_{BCP} versus the hydrogen bond distance, $d_{H...A}$ for the hydrogen bonds (see Table 4.28). (b) Plot of the Laplacian of the electron density, $\nabla^2\rho_{BCP}$, versus the hydrogen bond distance, $d_{H...A}$, showing an approximate exponential dependence. The hydrogen bond depicting each symbol is shown in the top right-hand corner.*

The correlation factors, R, are 0.89 (standard deviation, 0.17) for the total electron density plot, and 0.97 (standard deviation, 0.16) for the Laplacian plot, respectively, quantifying that the spread in the data across the exponential fit is larger in the case of the total density than the Laplacian. The observed trends in Figure 4.20 can be confidently ascertained by increasing the number of data points. For this purpose, a variety of systems, such as aromatic alcohols, dicarboxylic acids, nitriles, heterocyclic compounds, amine complexes, amino acids and peptides, were chosen from the literature. The hydrogen bonds formed by these systems are listed in Tables 4.29 - 4.31. The numbers in the last column in each table indicate the reference numbers (see appropriate references).

The tables comprise 32 O-H$\cdots$O bonds (Table 4.29), 63 N-H$\cdots$O bonds (Table 4.30) as well as 71 C-H$\cdots$O, 10 C-H$\cdots$N and 2 C-H$\cdots$C bonds (Table 4.31). Taking all the available data from Tables 4.28 - 4.31, we find that the hydrogen-acceptor distance in the O-H$\cdots$O bonds lie in the range of 1.4 - 2.6 Å, with angles between 126° and 175°. For N-H$\cdots$O bonds, the range shifts to $\sim$ 1.7 - 2.7 Å, and angles vary from $\sim$ 90° to 178°. The C-H group exhibits much longer H$\cdots$O contacts in the range of 2.2 to 3.0 Å. Similarly, with N or C atoms as acceptors, the H$\cdots$A distances are longer (2 - 3 Å).

The H$\cdots$O densities and Laplacians of the O-H$\cdots$O bonds from the literature lie in the range 0.1 - 0.6 eÅ^{-3} and 0.3 to 6.0 eÅ^{-5} respectively (see Table 4.29). The N-H$\cdots$O bonds (Table 4.30) exhibit densities and Laplacians of the order of $\sim$ 0.1 - 0.3 eÅ^{-3} and $\sim$ 1 - 5 eÅ^{-5}. The C-H$\cdots$O bonds (Table 4.31) have slightly lower densities ($\sim$ 0.01 - 0.08 eÅ^{-3}) and Laplacian values (0.2 - 1.6 eÅ^{-5}).

On the other hand, the C-H···N and C-H···C bonds (Table 4.31) have much lower

values of $\rho_{H\cdots A}$ (0.03 to 0.06 eÅ^{-3}) and $\nabla^2\rho$ (0.4 - 2.2 eÅ^{-5}).

Table 4.29 Geometrical and charge density parameters of the O-H···O bonds from the literature

Type of H-bond	H···A (Å)	D···A (Å)	D-H···A (°)	ρ_{BCP} (eÅ^{-3})	$\nabla^2\rho_{BCP}$ (eÅ^{-5})	λ_1 (eÅ^{-5})	λ_2 (eÅ^{-5})	λ_3 (eÅ^{-5})	Ref. no.
O-H···O			L-Arginine phosphate monohydrate						94
	1.589	2.594	172.5	0.30	5.53	-1.46	-1.40	8.39	
	1.570	2.560	169.7	0.27	6.30	-1.76	-1.60	9.66	
	1.793	2.779	172.4	0.19	3.84	-1.02	-0.95	5.81	
	1.847	2.749	154.0	0.18	3.03	-0.83	-0.75	4.61	
			Leu-enkephaline trihydrate						95
	1.798	2.773	172.2	0.21	4.16	-1.25	-1.14	6.55	
	1.824	2.757	162.8	0.19	3.77	-1.11	-1.04	5.92	
	1.879	2.801	160.5	0.15	3.46	-0.81	-0.79	5.06	
	1.889	2.799	156.2	0.16	3.26	-0.81	-0.77	4.84	
	1.926	2.890	173.9	0.10	3.11	-0.39	-0.18	3.67	
			L-tyrosyl-glycyl-glycine monohydrate						96
	1.791	2.752	175.7	0.19	3.80	-0.97	-0.92	5.69	
	1.705	2.655	167.8	0.21	3.61	-1.19	-1.17	5.97	
	1.85	2.800	166.7	0.17	3.24	-0.83	-0.79	4.86	
			Glycyl L-aspartic acid dihydrate						96
	1.97	2.910	126.3	0.09	2.65	-0.43	-0.35	3.43	
	1.731	2.690	172.7	0.20	4.81	-0.92	-0.92	6.65	
	1.753	2.696	166.2	0.19	4.22	-0.97	-0.86	6.05	
	1.803	2.766	170.9	0.13	4.21	-0.64	-0.45	5.04	
	1.643	2.583	165.3	0.31	5.09	-1.88	-1.76	8.73	
			Citrinin						97
	1.691	2.532	152.2	0.35	4.44	-2.12	-1.94	8.51	
	1.561	2.473	154.7	0.54	4.74	-3.55	-3.39	11.68	
			L-Dopa						98
	1.760	2.717	166.3	0.22	3.90	-1.34	-1.28	6.52	
	1.880	2.816	160.9	0.20	3.50	-1.45	-1.05	6.00	
		Methyl ammonium hydrogen succinatemonohydrate							42
	1.848	2.796	167.5	0.20	2.23	-1.22	-1.15	4.61	
			Cinnamic acid and photodimer						53a
	1.40	2.617	162.4	0.6	1.9	-5.79	-5.33	13.05	
	1.67	2.627	174	0.19	5.31	-1.53	-1.02	7.86	
	1.68	2.633	172.1	0.28	5.13	-1.82	-1.80	8.75	
			Aliphatic dicarboxylic acids						99
	1.72	2.649	173	0.21	6.17	-1.34	-1.21	8.71	
	1.702	2.659	174	0.20	5.7	-1.04	-1.00	7.68	
	1.705	2.662	175	0.17	5.2	-0.83	-0.79	6.83	
	1.706	2.655	170	0.23	4.25	-1.39	-1.27	6.91	
			p-nitrophenol (β-form)						45
	1.909	2.832	160.6	0.11	4.66	-0.71	-0.45	5.82	
			p-nitrophenol (α-form)						45
	1.890	2.832	166.4	0.19	2.43	-1.35	-1.11	4.89	
	2.461	3.196	133.2	0.04	0.56	-0.13	-0.11	0.80	

Table 4.30 Geometrical and charge density parameters of the N-H$\cdots$O bonds from the literature.[a]

Type of H-bond	H...A (Å)	D...A (Å)	D-H...A (°)	ρ_{BCP} (eÅ^{-3})	$\nabla^2\rho_{BCP}$ (eÅ^{-5})	λ_1 (eÅ^{-5})	λ_2 (eÅ^{-5})	λ_3 (eÅ^{-5})	Ref .no.
N-H$\cdots$O	\multicolumn{8}{l}{L-Arginine phosphate monohydrate}	94
	1.739	2.772	167.2	0.19	4.24	-1.07	-0.97	6.28	
	1.767	2.795	168.8	0.15	4.55	-0.87	-0.82	6.24	
	1.815	2.824	161.2	0.17	3.75	-0.73	-0.82	5.30	
	1.831	2.845	171.9	0.15	3.56	-0.68	-0.59	4.83	
	1.883	2.879	166.7	0.14	2.57	-0.72	-0.58	3.87	
	1.982	2.922	151.7	0.10	2.26	-0.46	-0.42	3.14	
	2.172	3.062	144.0	0.06	1.39	-0.27	-0.22	1.88	
			Leu-enkephalin trihydrate						95
	1.653	2.660	160.9	0.31	5.27	-1.98	-1.90	9.15	
	1.826	2.871	171.1	0.13	4.69	-0.78	-0.71	6.18	
	1.941	2.839	140.3	0.13	2.69	-0.68	-0.64	4.01	
	1.941	2.925	156.4	0.09	2.91	-0.47	-0.41	3.79	
	1.987	2.977	154.7	0.11	2.53	-0.52	-0.51	3.56	
	2.079	3.064	155.9	0.06	1.92	-0.29	-0.23	2.44	
	2.385	3.020	118.0	0.08	1.12	-0.28	-0.22	1.62	
		L-Tyrosyl-glycyl-glycine monohydrate							96
	1.718	2.745	172.1	0.25	4.32	-1.30	-1.24	6.86	
	1.773	2.690	145.9	0.22	3.42	-1.21	-0.98	5.61	
	1.838	2.865	174.2	0.17	3.37	-0.86	-0.83	5.06	
	1.922	2.906	158.8	0.13	2.44	-0.59	-0.48	3.52	
	1.998	2.853	138.7	0.14	2.31	-0.67	-0.66	3.64	
		Glycyl – L- aspartic acid dihydrate							96
	1.881	2.885	168.4	0.12	2.93	-0.46	-0.41	3.80	
	1.957	2.987	169.7	0.05	2.60	-0.23	-0.17	3.00	
	1.890	2.811	145.1	0.18	2.58	-0.92	-0.73	4.23	
	1.822	2.759	149.3	0.17	3.12	-0.90	-0.75	4.77	
			L-Dopa						98
	1.960	2.964	168.9	0.15	2.65	-0.71	-0.64	4.01	
	1.940	2.854	149.8	0.19	2.91	-0.92	-0.89	4.72	
	1.830	2.811	162.4	0.24	3.64	-1.40	-1.30	4.56	
		Methyl ammonium hydrogen succinate monohydrate							42
	1.858	2.866	164.9	0.22	1.86	-1.40	-1.30	4.56	
	1.725	2.763	178.1	0.29	2.46	-1.99	-1.91	6.36	
		Deuterated methyl-ammonium hydrogen maleate							
	1.834	2.837	161.2	0.24	2.1	-1.6	-1.4	5.1	35a
	1.910	2.897	160.2	0.19	2.0	-1.1	-1.0	4.2	
	1.792	2.819	169.2	0.29	1.7	-2.0	-1.8	5.6	
			Triglycine						100
	1.832	2.731	143.4	0.18	3.63	-1.05	-0.91	5.59	
	1.875	2.899	171.6	0.09	3.96	-1.17	-1.17	4.80	
	1.941	2.902	153.7	0.12	2.73	-0.56	-0.54	3.83	
	1.965	2.909	150.6	0.11	2.73	-0.53	-0.48	3.74	
	2.005	2.960	101.0	0.07	2.20	-0.29	-0.25	2.86	
	2.136	3.075	150.5	0.08	1.69	-0.34	-0.33	4.37	
	2.608	2.731	140.2	0.05	0.84	-0.18	-0.14	1.16	
	1.745	2.724	156.7	0.21	4.17	-1.26	-1.15	6.57	
	1.883	2.909	171.5	0.25	2.44	-1.15	-1.13	4.72	
	1.750	2.776	173.1	0.24	4.01	-1.39	-1.35	6.75	
			L-Alanine						101
	1.827	2.835	161.0	0.19	3.50	-1.10	-1.10	5.70	
	1.832	2.814	161.2	0.20	3.60	-1.20	-1.20	6.00	
	1.722	2.792	169.5	0.27	4.70	-1.70	-1.70	8.10	

Table 4.30 (*continued*)

		(Z)-N-Acetyl-β-dihydro-phenylalanine						102
1.814	2.835	170.5	0.22	3.58	-1.32	-1.24	6.14	
1.849	2.869	170.3	0.19	3.33	-1.09	-1.06	5.48	
		N-Acetyl-L-Tryptophan methylamide						103
1.979	3.010	173.9	0.15	2.15	-0.68	-0.67	3.51	
1.918	2.880	155.0	0.21	2.06	-1.05	-0.99	4.11	
1.863	2.890	172.1	0.22	2.31	-1.20	-1.04	4.55	
		Ammonium dihydrogen phosphate						104
1.940	2.889	156.8	0.22	2.12	-1.10	-0.98	4.21	
2.634	3.172	89.2	0.04	0.69	-0.14	-0.12	0.95	
		Urea						18
2.067	2.960	147.6	0.08	1.54	-	-	-	
2.009	2.998	166.8	0.06	2.32	-	-	-	
		1-methyluracil						52a
1.770			0.23	2.10	-1.90	-1.70	5.70	
		L-Cystine						105
1.777	2.785	164.4	0.21	3.92	-0.99	-1.01	5.92	
1.910	2.827	146.3	0.16	2.47	-0.70	-0.77	3.94	
1.844	2.803	153.2	0.20	2.82	-0.93	-0.95	4.71	
		5-nitrouracil						48
1.82	2.82	174.1	0.181	3.321	-0.93	-0.90	5.15	
1.86	2.86	169.3	0.166	2.878	-0.87	-0.84	4.59	
1.84	2.80	155.9	0.158	2.993	-0.83	-0.81	4.64	
1.804	2.794	166.0	0.147	3.048	-0.84	-0.76	4.64	
		Urea-phosphoric acid						43
1.885	2.893	171.4	-	-	-	-	-	-
2.221	3.090	143.9	-	-	-	-	-	-
1.936	2.943	170.1	0.18	1.04	-1.16	-1.14	3.34	
2.180	3.064	146.2	-	-		-	-	-
		β-NTO						43
1.7233	-	-	0.290	4.06	-1.74	-1.55	7.36	
		2-methyl-5-nitroaniline						49
2.2228	-	153.83	0.065	1.07	-0.35	-0.27	1.69	
2.7436	-	142.28	-	-	-	-	-	
2.3180	-	145.48	0.066	0.66	-0.33	-0.29	1.28	

[a] '-' indicates non-availability of the data.

Table 4.31 Geometrical and charge density parameters of the C-H···O, C-H···N and C-H···C bonds from the literature.[a]

Type of H- bond	H...A (Å)	D...A (Å)	D-H...A (°)	ρ_{BCP} (eÅ^{-3})	$\nabla^2\rho_{BCP}$ (eÅ^{-5})	λ_1 (eÅ^{-5})	λ_2 (eÅ^{-5})	λ_3 (eÅ^{-5})	Ref no.
C-H···O	\multicolumn{8}{c}{Cinnamic acid and photodimer}	53a
	2.481	3.386	141.2	0.027	0.648	-0.14	-0.09	0.87	
	2.615	3.641	159.4	0.011	0.300	-0.04	-0.03	0.37	
	2.818	3.690	139.6	0.016	0.319	-0.05	-0.05	0.42	
	2.939	3.714	130.3	0.017	0.277	-0.05	-0.04	0.36	
	2.600	3.315	124.3	0.052	0.759	-0.17	-0.17	1.10	
	2.67	3.525	137	0.048	0.683	-0.18	-0.16	1.01	
	2.55	3.490	148	0.031	0.622	-0.14	-0.09	0.86	
	2.60	3.493	140	0.018	0.427	-0.10	-0.05	0.58	
	2.42	2.938	108	0.034	0.576	-0.15	-0.06	0.78	
	2.75	3.176	103	0.071	1.146	-0.27	-0.20	1.62	
	2.637	3.634	153.9	0.020	0.438	-0.09	-0.06	0.59	
	2.437	3.404	148.9	0.037	0.811	-0.13	-0.12	1.07	
	2.930	3.616	122.9	0.023	0.355	-0.07	-0.06	0.48	
	\multicolumn{8}{c}{Aliphatic dicarboxylic acids}	99
	2.97	3.883	145	0.023	0.338	-0.07	-0.06	0.47	
	2.69	3.180	108	0.047	0.681	-0.12	-0.11	0.91	
	2.74	3.421	120	0.043	0.636	-0.14	-0.11	0.88	
	2.89	3.512	119	0.026	0.397	-0.08	-0.07	0.54	
	3.02	3.860	127	0.021	0.344	-0.07	-0.03	0.44	
	2.779	3.574	132	0.039	0.516	-0.12	-0.11	0.75	
	2.803	3.717	145	0.030	0.419	-0.09	-0.08	0.59	
	2.937	3.775	137	0.029	0.393	-0.09	-0.08	0.56	
	2.710	3.228	110	0.057	0.750	-0.17	-0.13	1.05	
	2.623	3.294	121	0.053	0.727	-0.17	-0.10	1.00	
	2.832	3.724	142	0.033	0.424	-0.10	-0.09	0.61	
	2.988	3.930	137	0.019	0.289	-0.05	-0.05	0.39	
	2.761	3.421	120	0.040	0.536	-0.10	-0.01	0.65	
	2.765	3.194	104	0.048	0.638	-0.09	-0.07	0.80	
	2.986	3.878	142	0.026	0.327	-0.07	-0.07	0.47	
	2.716	3.278	113	0.044	0.591	-0.10	-0.04	0.73	
	2.978	4.016	168	0.019	0.252	-0.05	-0.05	0.35	
	2.765	3.453	123	0.036	0.523	-0.10	-0.08	0.70	
	2.958	3.605	122	0.030	0.410	-0.08	-0.04	0.53	
	\multicolumn{8}{c}{p-nitrophenol (β-form)}	45
	2.382	3.317	143.3	0.08	1.15	-0.44	-0.27	1.80	
	2.345	3.372	157.3	0.04	0.66	-0.25	-0.24	1.14	
	2.400	3.305	139.9	0.01	0.26	-0.08	-0.05	0.38	
	\multicolumn{8}{c}{p-nitrophenol (α-form)}	45
	2.509	3.336	132.1	0.03	0.81	-0.12	-0.06	0.99	
	2.406	3.359	145.7	0.04	0.89	-0.18	-0.12	1.19	
	\multicolumn{8}{c}{Triglycine}	100
	2.219	3.161	144.0	0.10	1.56	-0.40	-0.37	2.33	
	2.463	3.136	119.0	0.07	1.06	-0.24	-0.22	1.52	
	2.529	3.016	106.1	0.07	1.01	-0.25	-0.15	1.41	
	2.540	3.190	116.2	0.06	0.85	-0.20	-0.17	1.22	
	\multicolumn{8}{c}{1-methyluracil}	52a
	2.370	-	-	0.07	1.10	-0.40	-0.30	1.90	
	2.340	-	-	0.06	0.60	-0.40	-0.30	1.30	
	\multicolumn{8}{c}{2-methyl-5-nitroaniline}	49
	2.7521		128.6	0.030	0.444	-0.11	-0.08	0.63	
	2.3503	3.275	142.1	0.061	0.991	-0.26	-0.20	1.45	

285

Table 4.31 (*continued*)

	2.9573		154.3	0.024	0.284	-0.07	-0.04	0.40
	Lithium bis (tetramethylammonium) hexanitro cobalt (III)							106
	2.583	3.607	156.7	0.02	0.36	-0.04	-0.01	0.41
	2.519	3.251	124.4	0.05	0.77	-0.16	-0.15	1.08
	2.498	3.543	169.7	0.04	0.66	-0.21	-0.05	0.86
	2.591	3.476	140.9	0.03	0.59	-0.17	-0.08	0.84
	3,4-Bis(dimethylamino)-3-cyclobutene-1,2-dione							37a
	2.351	-	-	0.07	0.87	-	-	1.49
	2.453	-	-	0.06	0.75	-	-	1.23
	2.689	-	-	0.03	0.55	-	-	0.75
	2.727	-	-	0.02	0.49	-	-	0.60
	2.776	-	-	0.03	0.48	-	-	0.65
	2.907	-	-	0.03	0.35	-	-	0.48
	2.942	-	-	0.03	0.33	-	-	0.43
	2.574	-	-	0.04	0.61	-	-	0.84
	2.694	-	-	0.03	0.47	-	-	0.58
	2.787	-	-	0.02	0.33	-	-	0.41
	2.858	-	-	0.03	0.39	-	-	0.53
	2.875	-	-	0.03	0.31	-	-	0.41
	2.517	-	-	0.03	0.66	-	-	0.70
	2.543	-	-	0.04	0.75	-	-	0.94
	2.57	-	-	0.01	0.23	-	-	0.29
	2.594	-	-	0.04	0.67	-	-	0.82
	2.969	-	-	0.02	0.27	-	-	0.34
	2.219	-	-	0.11	1.51	-	-	2.29
	2.232	-	-	0.11	1.57	-	-	2.10
	2.211	-	-	0.11	1.50	-	-	2.27
	2.248	-	-	0.12	1.39	-	-	2.02
C-H···N	Monothionitrile							48
	2.594	3.617	162.0	0.032	0.522	-0.12	-0.10	0.74
	2.780	3.633	137.5	0.025	0.420	-0.08	-0.06	0.56
	2.443	3.463	161.2	0.05	0.691	-0.20	-0.17	1.06
	Dithionitrile							48
	2.564	3.541	152.8	0.035	0.653	-0.10	-0.09	0.85
	2.840	3.500	120.6	0.042	0.523	-0.14	-0.11	0.77
	2.586	3.631	168.6	0.04	0.619	-0.16	-0.13	0.91
	2.560	3.603	167.8	0.040	0.522	-0.09	-0.07	0.68
	2.886	3.554	121.3	0.048	0.566	-0.15	-0.07	0.78
	β-NTO							43
	2.0544	-	-	0.139	2.161	-0.63	-0.61	3.40
	2-methyl-5-nitroaniline							49
	2.7610	-	151.1	0.037	0.467	-0.16	-0.13	0.75
C-H···C	2-methyl-5-nitroaniline							49
	2.6473	-	160.3	0.062	0.597	-0.19	-0.09	0.87
	3.0109	-	142.5	0.026	0.382	-0.08	-0.02	0.48

[a] '-' indicates non-availability of the data.

In Figures 4.21a and b, the electron density and the Laplacian at the H···A

critical points from the literature and from our data points are plotted against the

H···A distance. These plots show that the ρ_{BCP} and $\nabla^2\rho_{BCP}$ of the H···A bonds

decrease exponentially with the H···A distance.
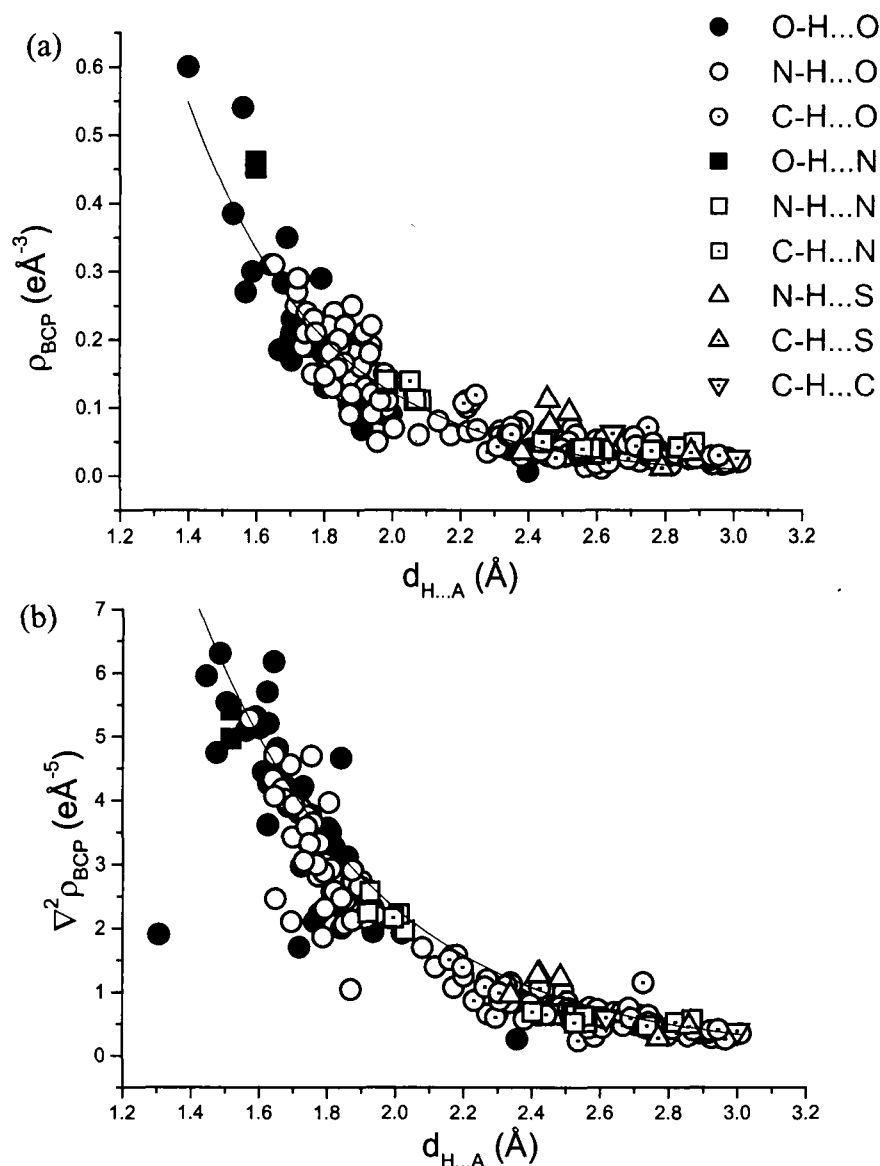
Figure 4.21: Data points from literature and inclusive of our data: (a) Plot of the total density ρ_{BCP} versus the hydrogen bond distance, $d_{H...A}$ for the hydrogen bond, (see Tables 4.29-4.31). (b) Plot of the Laplacian of the electron density, $\nabla^2\rho_{BCP}$, versus the hydrogen bond distance, $d_{H...A}$, showing an approximate exponential dependence. The hydrogen bond depicting each symbol is shown in the top right-hand corner.

It is indeed surprising that with increase in the number of data points, there is still a large dispersion of point across the fit for the total density plot (R-value 0.91), and the dispersion is only slightly lesser for the Laplacian plot (R-value 0.95).

The individual eigenvalues, λ_i, are of interest. For hydrogen bonds, the perpendicular curvatures, λ_1 and λ_2, are small in magnitude. The curvature along the internuclear vector (λ_3) can, however, be relatively large and positive. For hydrogen bonds from our study, we find that most of the O-H$\cdots$O bonds exhibit λ_3 values of ~3 to 7 eÅ^{-5}, with the exception of the longest bond (0.91 eÅ^{-5}) and the shortest bond (11.43 eÅ^{-5}). The values for O-H$\cdots$O bonds from the literature span between 0.4 and 13.0 eÅ^{-5}, the λ_1 and λ_2 values being nearly equal, in the range -0.1 to -6.0 eÅ^{-5}. Similar values for λ_i are found for the O-H$\cdots$N bonds. However, the N-H$\cdots$O bonds exhibit λ_i values over a narrower range (λ_3, 1 to 7 eÅ^{-5}; λ_1 and λ_2, -0.2 to -2.0 eÅ^{-5}). The other types of hydrogen bonds are associated with smaller curvatures. We see that for a hydrogen bond interaction (H$\cdots$A), the two perpendicular curvatures (λ_1 and λ_2) are small in magnitude, whereas the positive curvature of the electron density (λ_3 along the internuclear vector) is much larger in magnitude. This shows that λ_3 is the dominant curvature for such closed-shell interactions, as there is a depletion of electron density in the H$\cdots$A region.

In Figure 4.22a, we show the plot of λ_3 against the H$\cdots$A distance for the hydrogen bonds from our study. An exponential fit of the form, $\lambda_3 = A\exp(-B \times d_{H\cdots A})$ with a correlation factor, R, of 0.96 (standard deviation 0.11) is obtained. The A and B values are $0.8(2) \times 10^3$ and 2.8(1), respectively (R, 0.96 and standard

deviation, 0.11). A plot of λ_3 versus the H···A distance inclusive of all the

literature data is shown in Figure 4.22b.
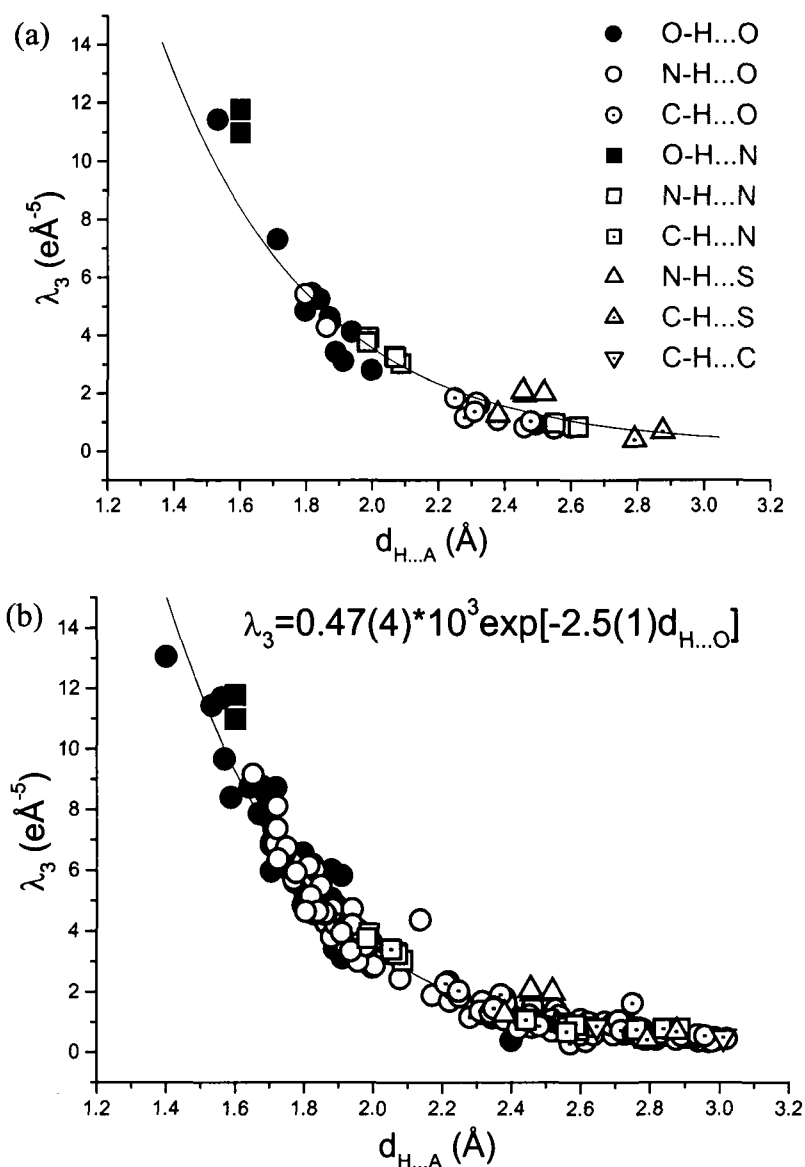
Figure 4.22: *Plot of the positive curvature of the electron density, λ_3, versus the hydrogen bond distance, $d_{H...A}$. (a) For data points corresponding to our study, (b) Plot inclusive of the literature data from Tables 4.29 - 4.31. The total number of data points in the curves is 218. The exponential curve follows the equation, λ_3 = $Aexp[-B \times d_{H...A}]$, written on top of figure (b). The hydrogen bond depicting each symbol is shown in the top right-hand corner.*

The exponential dependence is clearly seen. The R-value is 0.97 with a standard deviation of 0.11, the A and B constants being $0.47(4) \times 10^3$ and $2.5(1)$ respectively. These values of A and B are close to those reported by Espinosa *et al*,[60] who have described only O-H$\cdots$O, N-H$\cdots$O and C-H$\cdots$O bonds. We may therefore take the experimental relations obtained in the present study to be a general characteristic of all hydrogen bonds.

Besides the density and the Laplacian, we have looked for possible correlations between the topological polarization, Δ, and the H$\cdots$A distance for data points from this study. As shown in Figure 4.23, polarization generally decreases with increase in the H$\cdots$A distance. The O-H$\cdots$O bonds, with H$\cdots$O distances between 1.5 and 2.5 Å, exhibit polarization values between 15% and 37%. The Δ values of the N-H$\cdots$O and the N-H$\cdots$N bonds are nearly the same ($\sim$ 26 - 30 %), except in cases with long H$\cdots$N distances. The N-H$\cdots$S bonds exhibit higher polarization values ($\sim$ 30%). The C-H$\cdots$S bonds have higher polarization values than the C-H$\cdots$O bonds. In general, the polarization of the H$\cdots$A bond reflects the hydrogen bond distance or the strength of the hydrogen bond as can be seen from the different sets shown in Figure 4.23.
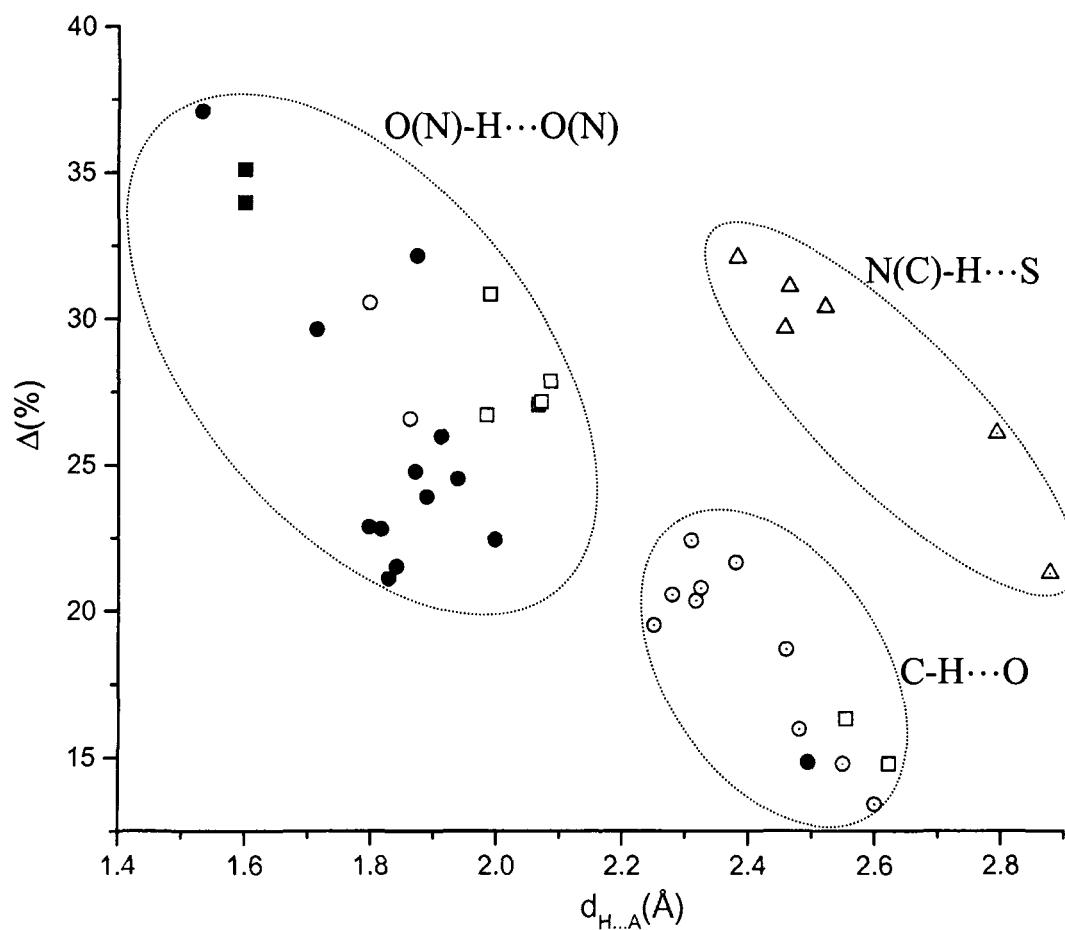
Figure 4.23: *Variation of polarization, Δ (in %) with the hydrogen bond distance, $d_{H...A}$. (Symbols as in Figure 4.20). The bonds are grouped based on the donor and (or) the acceptor.*

4.3 Topological analysis of bond paths of O-H···O hydrogen bonds

We were interested to study the nature and shape of bond paths (trajectories of gradient vectors) in a series of O-H···O hydrogen-bonded systems. For this purpose, we have gathered experimentally derived charge density properties of O-H···O bonds from our own study and a few from the literature. The hydrogen-bonded systems chosen from our study are piperazine-oxalate (**III**), disodium croconate trihydrate (**I**) and disodium squarate trihydrate (**II**).[107] In order to statistically improve the quantification analysis, we have also chosen systems whose charge density data were available in the laboratory. These are α-ethoxy cinnamic acid (**VIII**) and adipic acid (**IX**), for which the CSD deposition numbers and refinement parameters are listed in Table 4.32. Before discussing the results of the critical point analysis, a concise geometrical description of the hydrogen-bonded systems is provided. As shown in Figure 4.24, piperazine-oxalate (**III**) forms a linear O-H···O hydrogen bond (designated as *l*) with an H···O distance of 1.532(9) Å and an angle of 174.1(16)°. α-ethoxy cinnamic acid (**VIII**) and adipic acid (**IX**) form centrosymmetric dimers (*l*) of comparable geometries (see Figure 4.24 and Table 4.33). The croconate ion (**I**), in the monoclinic form of the disodium salt, forms four O-H···O bonds with the surrounding water molecules grouped into two bifurcated systems (designated as *b* in Figure 4.24). In each case, an acceptor oxygen atom makes contacts with two hydrogen atoms from different water donor groups. The other hydrogen atom on water is involved in a bifurcated bond originating from a neighboring croconate ion (not shown in the figure).

Thus, b_{11} and b_{21} bonds share a common donor and so does the b_{12} and b_{22} pair. As shown in Table 4.33, the H···O bond lengths are spread between 1.8 to 1.9 Å, with O-H···O angles between 170° and 176°.
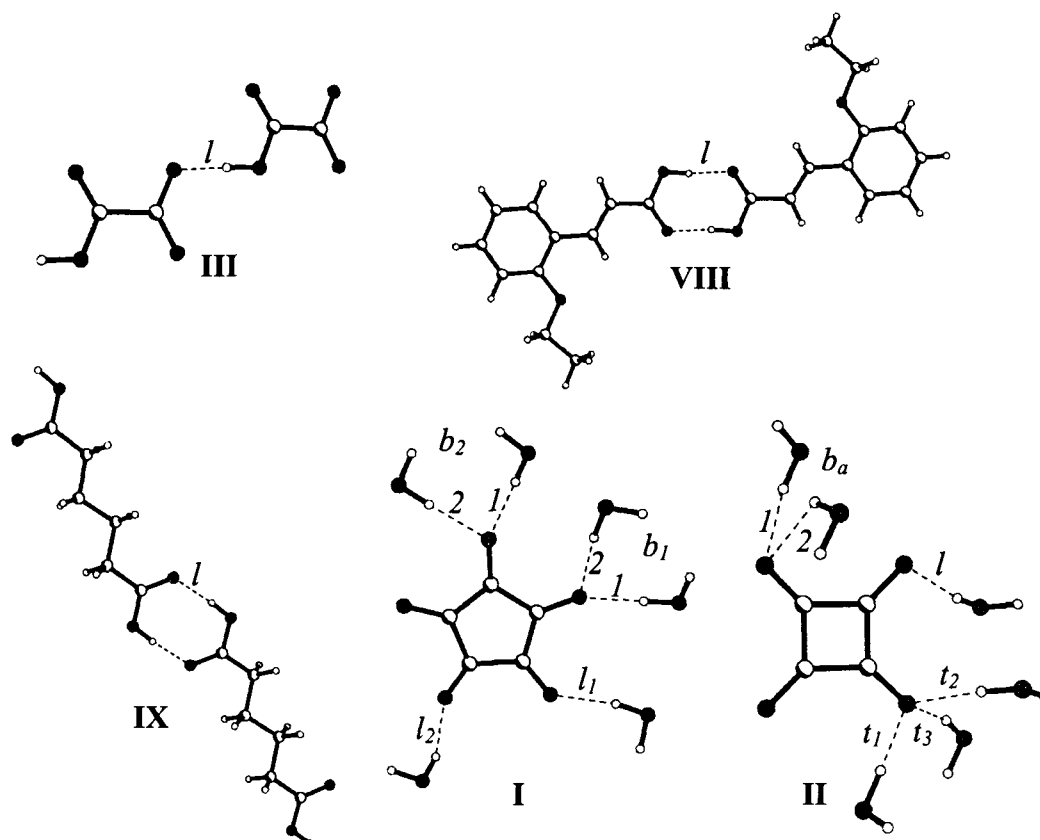
Figure 4.24: *A diagrammatic representation of the hydrogen bonds chosen for the study.* **III**, *the oxalate ion of the piperazine oxalate complex;* **VIII**,[#] *α-ethoxy cinnamic acid;* **IX**[#] *adipic acid;* **I**, *the croconate dianion;* **II**, *the squarate dianion.*

VIII[#] and **IX**[#]: Analyses carried out on data available in the laboratory.

Table 4.32 Refinement parameters for compounds **VIII** and **IX**.

	VIII	**IX**
CCDC number[a]	CCDC 205456	ADIPAC05
After multipole refinement		
Weighting scheme	0.070, 0.123	0.063, 0.113
$R\{F\}$	0.0426	0.0493
$R\{F^2\}$	0.0467	0.0868
S	0.9808	0.9685
No. of variables	272	100
N_{ref}/N_v	14.3382	24.5100

[a]*Crystallographic information may also be obtained from the deposition numbers in the Cambridge Crystallographic Data Centre (CCDC)*

Table 4.33 Bond distances and angles of the various hydrogen bonds

System	Type of H-bond	O-H (Å)	H⋯O (Å)	O-H⋯O (°)
III	Linear (l)	1.015(10)	1.532(9)	174.1(16)
VIII	Linear (l)	0.97(3)	1.68(2)	172.1(6)
IX	Linear (l)	0.958(19)	1.72(2)	173(3)
I	Linear (l_1)	0.960(3)	1.841(5)	166.9(17)
	Linear (l_2)	0.960(7)	1.998(7)	164.5(15)
	Bifurcated (b_{11})	0.959(7)	1.829(7)	171.9(17)
	Bifurcated (b_{12})	0.961(8)	1.797(8)	171.1(14)
	Bifurcated (b_{21})	0.961(13)	1.889(14)	176.2(16)
	Bifurcated (b_{22})	0.961(8)	1.817(6)	170.9(17)
II	Linear (l)	0.959(9)	1.912(8)	166.4(12)
	Bifurcated (b_{a1})	0.961(18)	1.871(19)	163.8(19)
	Bifurcated (b_{a2})	0.955(15)	2.495(17)	131.0(13)
	Trifurcated (t_1)	0.960(13)	1.714(13)	169.6(12)
	Trifurcated (t_2)	0.961(12)	1.873(12)	172.5(10)
	Trifurcated (t_3)	0.960(9)	1.938(10)	163.9(14)

The bifurcation angles (angle between the two O-H⋯O bonds) are 88.6° and 85.1° for

b_1 and b_2, respectively. The croconate ion also forms two linear bonds (l_1 and l_2) with

the water molecules (see Figure 4.24 and Table 4.33). The water molecule engaged in

l_1 forms a l_2 hydrogen bond with a neighboring croconate ion. This results in a network of croconate ions linked by bifurcated and linear bonds from the surrounding water molecules. A unique feature of the squarate ion (**II**) is the presence of the trifurcated hydrogen bond (designated as t) in the squarate ion, where the acceptor oxygen atom makes contact with three water donor groups. The squarate ion also exhibits a bifurcated bond, b_a, which is highly asymmetrical (see Table 4.33). Thus, the chosen set of hydrogen bonds is truly representative with the broad range of H$\cdots$O distances (1.53 to 2.50 Å) and angles (176° to 130°). The O-H distance is close to 0.96 Å in all the cases, except in two (**III** and **VIII**) where the bonds are slightly elongated while the corresponding H$\cdots$O distances are shorter (see Table 4.33).

In Figure 4.25, the static deformation density maps in the hydrogen bond (O-H$\cdots$O) plane are shown for four examples. The maps reveal chemically significant features such as bonding regions and lone-pair (non-bonding) regions. Concentric contours between the atom cores typify the bonding regions while localized lobes attached to the oxygen-core represent the lone-pairs. From Figures 4.25a-d, we see that there is an accumulation of charge density in the O-H regions, typical of shared interaction. On the other hand, there is a depletion of the charge density in the H$\cdots$O region. This is taken to represent a closed-shell interaction between the hydrogen and the acceptor. The distribution of the electron density is so varied among the different bonds that it brings out the diverse nature of the hydrogen bond.
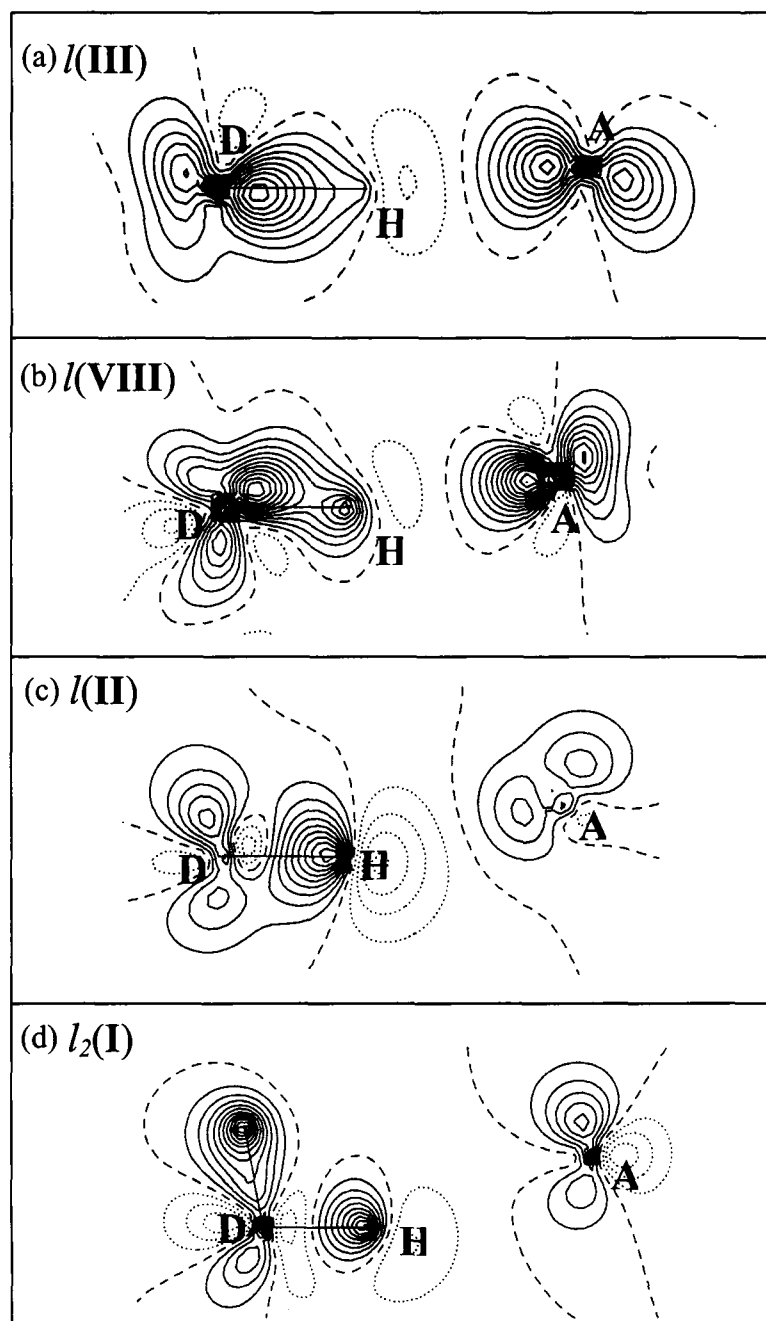
Figure 4.25: *Static deformation density plots (at contour intervals of 0.1 eÅ⁻³) in the hydrogen bond plane. D, H and A stand for the donor, hydrogen and the acceptor atoms. (a) l(III), (b) l(VIII), (c) l(I), (d) l₂(II).*

The positions of the lone-pair CPs relative to the donor and the acceptor cores are shown in Figure 4.26. The values of the total density at the lone-pair CPs are around 7 $e\text{Å}^{-3}$ with Laplacians of $\sim$ -115 $e\text{Å}^{-5}$, in agreement with those reported for oxygen lone-pairs.[18] Table 4.34 lists the geometrical parameters of the (3, -3) lone-pair CPs for all the hydrogen bonds obtained using the XDPROP routine. The distance from the eye of the lone-pair lobe (the CP) to the atomic (donor or acceptor) core is around 0.3 Å, except in a few cases where the distance extends to 0.5 Å. The distances agree well with the reported values in the literature.[45] The angles between the lone-pairs at the atom core (φ_D and φ_A), are usually in the range, 130° to 160°. Such high angles can be attributed to the lone-pair - lone-pair repulsion. We observe smaller angles (at 94° and 116°) in a few cases, especially with respect to the donors. We also estimated the angle subtended by the plane formed by the core of the donor and its lone-pairs with the hydrogen bond plane, ω_D, and the corresponding angle at the acceptor site, ω_A. The values are similar (134.3° and 135.1°) in the case of the linear hydrogen bond l(III). This is also the case in the l(VIII) and the t_3(II) bonds. For the rest of the hydrogen bonds, the two angles are different (Table 4.34).

The linear bond l(III), exhibits electron densities of 1.88(6) and 0.39(4) $e\text{Å}^{-3}$ respectively at the O-H and H$\cdots$O BCPs (see Figure 4.26a and Table 4.35). The corresponding Laplacian values are -23.2(4) and 5.95(8) $e\text{Å}^{-5}$, respectively. The small and positive Laplacian of the H$\cdots$O bond is typical of a closed-shell interaction while a highly negative Laplacian of the O-H bond is due to the shared interaction.
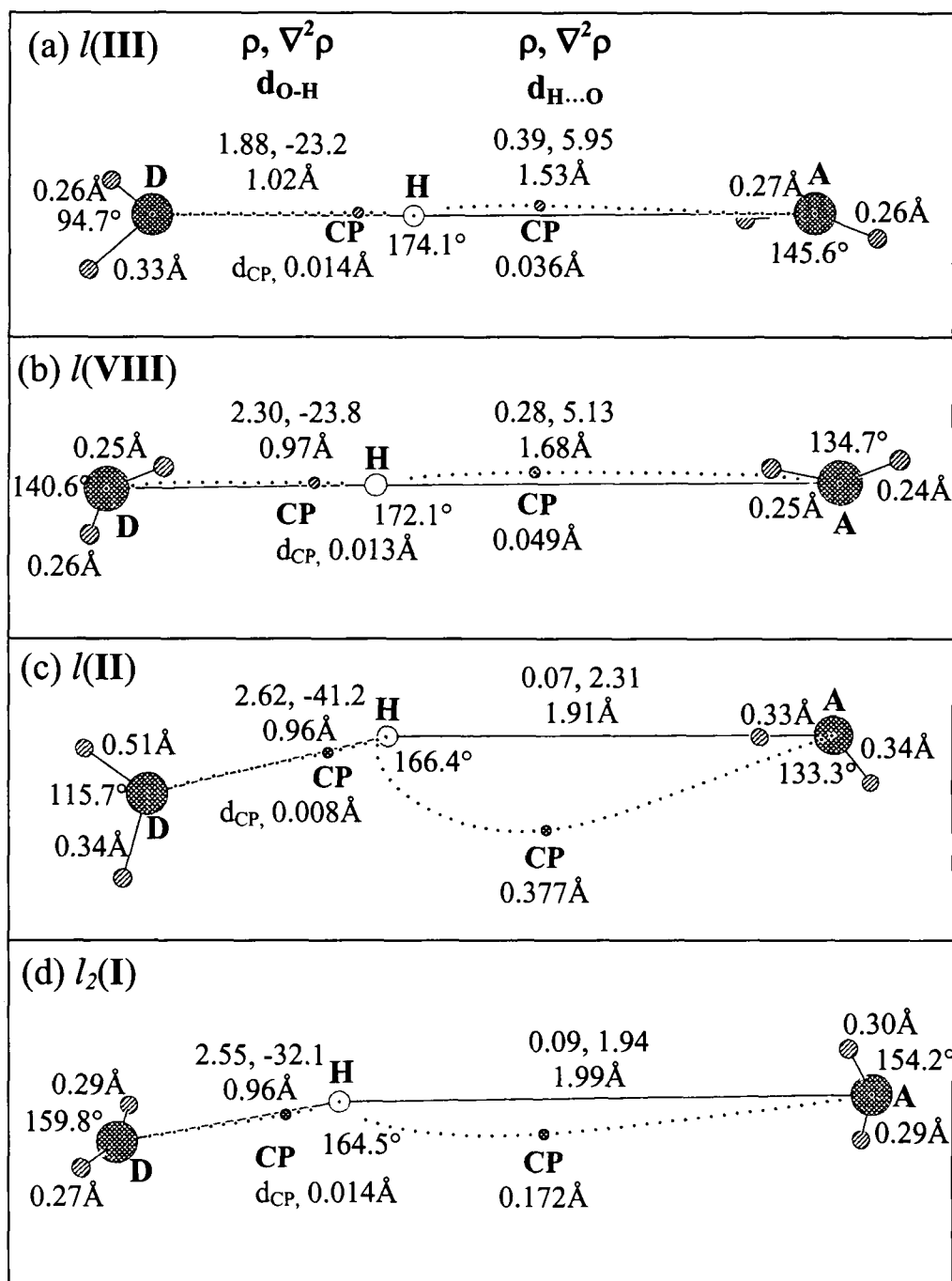
Figure 4.26: *Charge density parameters of the O-H⋯O bonds: large hatched circles, donor (D) and acceptor (A) cores; open circles, hydrogen (H); small hashed circles, lone-pair electrons; small filled circle, D-H and H⋯A critical points (CP). The values of ρ and ∇²ρ are given in eÅ⁻³ and eÅ⁻⁵ units, respectively. The O-H and H⋯O distances (d_{O-H} and d_{H⋯O}) are shown above the bonds. The value of d_{CP} is shown below the CP symbol. The distance of the lone-pair lobe to the donor or the acceptor atom-core is indicated adjacent to the lone-pair circles. Values of φ_D and φ_A, (see text) are shown close to the donor and the acceptor atoms.*

Table 4.34 The geometries of the lone-pairs on the donor and acceptor atoms of the O-H⋯O bonds[a]

System	Type of H-bond	d_{D-l} (Å)		d_{A-l} (Å)		φ_D, φ_A (°)		ω_D, ω_A (°)	
III	Linear (*l*)	0.261	0.332	0.265	0.263	94.7	145.6	134.3	135.1
VIII	Linear (*l*)	0.249	0.256	0.254	0.240	140.6	134.7	49.3	48.2
IX	Linear (*l*)	0.262	0.238	0.256	0.260	171.3	165.5	123.6	38.5
I	Linear (*l₁*)	0.268	0.290	0.279	0.280	159.8	159.2	55.8	176.3
	Linear (*l₂*)	0.268	0.290	0.290	0.295	159.8	154.2	107.6	168.8
	Bifurcated (*b₁₁*)	0.284	0.287	0.279	0.280	148.5	159.1	75.1	144.0
	Bifurcated (*b₁₂*)	0.287	0.276	0.279	0.280	162.4	159.1	124.1	70.2
	Bifurcated (b₂₁)	0.284	0.287	0.280	0.280	148.5	159.1	153.5	104.0
	Bifurcated (b₂₂)	0.287	0.276	0.280	0.280	162.4	159.1	70.2	80.4
II	Linear (*l*)	0.344	0.513	0.336	0.333	116.0	133.3	110.4	162.9
	Bifurcated (*b_{a1}*)	0.339	0.330	0.352	0.348	146.7	131.4	40.9	28.7
	Bifurcated (*b_{a2}*)	0.323	0.321	0.352	0.348	142.1	131.4	87.0	52.9
	Trifurcated (*t₁*)	0.323	0.321	0.337	0.333	142.1	133.2	55.9	142.3
	Trifurcated (*t₂*)	0.344	0.513	0.337	0.333	116.0	133.2	95.7	127.3
	Trifurcated (*t₃*)	0.339	0.330	0.337	0.333	146.7	133.2	80.2	82.1

[a]*Here, d_{D-l} and d_{A-l} are the distances from the eye of the lone-pair lobe to the donor and the acceptor core; φ_D and φ_A are the angles subtended at the donor and the acceptor atom by the two lone-pair lobes; ω_D represents the angle between the hydrogen bond plane and the donor-lone-pair plane (plane formed by the two lone-pair lobes and the donor core), and ω_A is the angle between the hydrogen bond plane and the acceptor-lone-pair plane (plane formed by the two lone-pair lobes and the acceptor core). Columns containing identical numbers originate from common donors or acceptors.*

The d_{CP} value for the H⋯O bond is slightly higher (0.036 Å) than that of the O-H bond (0.014 Å). Accordingly, the bond path (BP) in the H⋯O region is displaced slightly from the line joining the two atoms. This is also the case with the linear bond *l*(VIII) (Figure 4.26b). The *l*(II) bond (Figure 4.26c) carries much less density 0.07(3) eÅ⁻³ and Laplacian of 2.31(1) eÅ⁻⁵ and the BP is noticeably curved with a d_{CP} value of 0.377 Å. This is indeed surprising, for its geometry is not so unfavorable (H⋯O, 1.912(8)Å, 166.4(12)°). Similar values have been obtained for the *l₂*(I) bond (Figure 4.26d). As expected, hydrogen bonds with relatively short H⋯O distances and angles close to 180°, generally exhibit higher densities and Laplacians at the BCPs.[26] The BPs are less curved in such cases and are associated with small d_{CP} values. From Table 4.35, we notice that

the d_{CP} values of the H$\cdots$O bonds are often one order higher than the corresponding d_{CP}

values of the O-H bonds. Based on a study of a variety of hydrogen bonds, Lecomte and

co-workers have reported H$\cdots$O d_{CP} values of up to 0.12 Å for H$\cdots$O distances ranging

from 1.22 - 1.97 Å.[60]

Table 4.35 Charge density parameters for the O-H and H$\cdots$O bonds of the chosen hydrogen- bonded systems[a]

System	Type of H-bond	O-H			H$\cdots$O		
		ρ (eÅ^{-3})	$\nabla^2\rho$ (eÅ^{-5})	d_{CP} $\times 10^2$ (Å)	ρ (eÅ^{-3})	$\nabla^2\rho$ (eÅ^{-5})	d_{CP} $\times 10^2$ (Å)
III	Linear (l)	1.88(6)	-23.2(4)	1.4	0.39(4)	5.95(8)	3.6
VIII	Linear (l)	2.3(1)	-23.8(8)	1.3	0.28(7)	5.13(8)	4.9
IX	Linear (l)	2.6(1)	-54.0(9)	0.6	0.21(7)	6.17(9)	12.8
I	Linear (l_1)	2.77(9)	-29.5(7)	1.5	0.21(3)	3.02(1)	6.0
	Linear (l_2)	2.55(10)	-32.1(6)	1.4	0.09(3)	1.94(1)	17.2
	Bifurcated (b_{11})	2.70(9)	-25.5(6)	1.5	0.21(3)	3.00(1)	8.4
	Bifurcated (b_{12})	2.92(9)	-42.2(7)	0.7	0.18(3)	2.97(1)	5.4
	Bifurcated (b_{21})	2.90(9)	-30.2(5)	0.9	0.09(3)	2.52(1)	18.3
	Bifurcated (b_{22})	2.93(9)	-26.4(6)	0.9	0.20(3)	3.32(1)	4.3
II	Linear (l)	2.62(9)	-41.2(5)	0.8	0.07(3)	2.31(1)	37.7
	Bifurcated (b_{a1})	2.64(8)	-39.6(5)	2.4	0.14(3)	2.95(1)	24.0
	Bifurcated (b_{a2})	2.65(8)	-32.7(4)	1.8	0.03(1)	0.647(3)	41.8
	Trifurcated (t_1)	2.40(7)	-33.5(4)	2.1	0.23(3)	4.44(3)	14.6
	Trifurcated (t_2)	2.35(7)	-36.0(5)	1.3	0.11(3)	3.56(3)	10.1
	Trifurcated (t_3)	2.36(7)	-23.3(4)	1.5	0.14(3)	2.75(1)	9.7

[a]d_{CP} is the perpendicular distance of the critical point from the bond axis

The d_{CP} values of the H$\cdots$O bonds are indeed unusual and do not occur in

normal shared interactions. If a covalent bond has a slightly higher d_{CP} value, say ~ 0.05

Å, the bond is considered to be strained. One comes across such situations in strained

ring systems. For instance, the mean d_{CP} value of the C-C bonds in the squarate ring is

0.058 Å which is comparable to that in the cyclobutyl ring of α-truxillic acid (0.046

Å).[53a] A highly strained cyclopropyl ring exhibits a value of 0.06 Å.[108] The cage bonds

in a 1,2-difluorinated cubane derivative have an average d_{CP} value of 0.14 Å.[109] Since

the hydrogen bond interaction is mainly electrostatic (closed-shell), a simple 'bent bond' description would not be adequate, especially in situations where the d_{CP} values are high. We have therefore, attempted to relate d_{CP} values of the $H \cdots O$ bonds with the $H \cdots O$ distance, $O\text{-}H \cdots O$ angle, ρ_{BCP} and $\nabla^2 \rho_{BCP}$ (Figure 4.27).
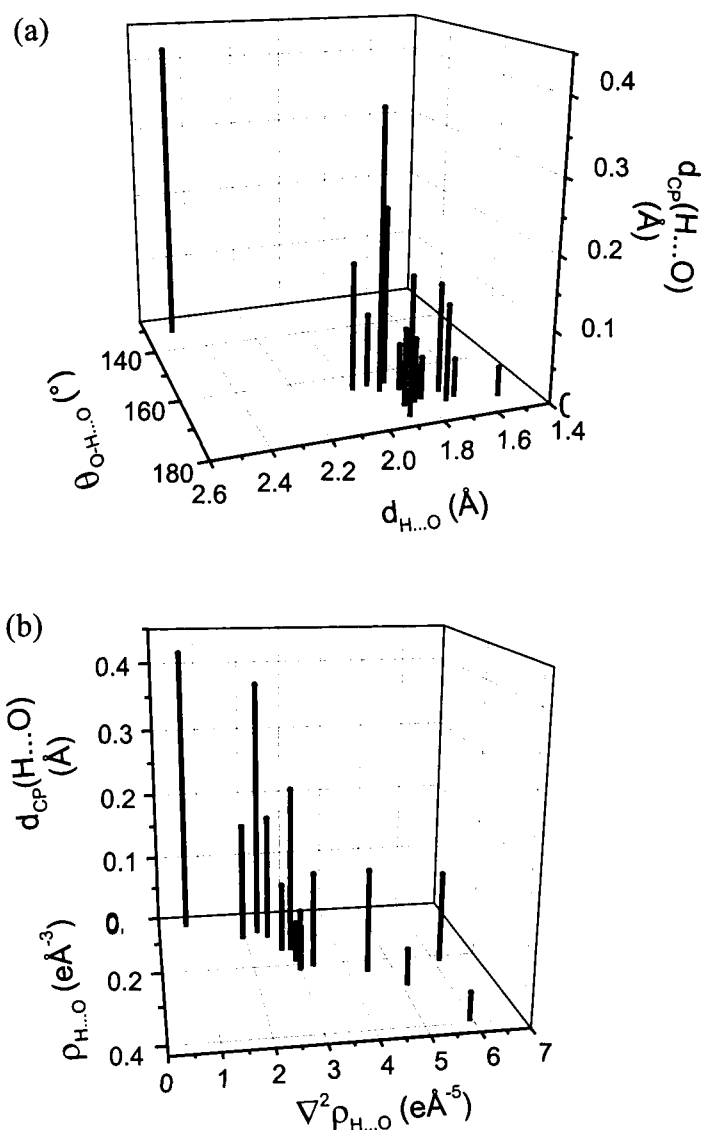
Figure 4.27: *Histograms depicting the d_{CP} against (a) the $O\text{-}H \cdots O$ angle and the hydrogen bond distance, $d_{H \cdots O}$ (b) total density and its Laplacian at the $H \cdots O$ CP.*

The plot in Figure 4.27a shows how short H···O distances and angles close to 180° are generally associated with small d_{CP} values. The l bond in **IX** and l_2 and b_{21} bonds of **I** seem to be exceptions. The data points in ρ_{BCP} and $\nabla^2\rho_{BCP}$ are somewhat spread (Figure 4.27b), but it appears that small d_{CP} values accompany high values of the density and the Laplacian.

We have found it instructive to examine the bond paths of the H···O bonds. The BP essentially lies in a plane, but different from the O-H···O plane. Small deviations of the BP from its mean plane are observed usually close to the atom cores. We have presented the BPs of the various H···O bonds in a single normalized plot in Figure 4.28. Each BP starts at the hydrogen core with a characteristic take-off, bends inwardly after covering nearly one-third of the H···O distance and then approaches the acceptor core with no appreciable curvature. The bond CP is located close to where the BP bends, giving rise to a high d_{CP} value (see Table 4.35). We find that the take-off angle is related to the d_{CP} value as shown in the inset of Figure 4.28. The figure reveals that high values of d_{CP} are associated with unusual BP take-off angles. An exact description of the bond path would, however, require an analysis of the various contributions to the hydrogen bond interaction, not only from the donor and acceptor cores and the hydrogen but also from the lone-pairs. Here, we resort to a simpler method to see how the lone-pairs on the donor and acceptor atoms, as distinct from their cores, participate in the formation of hydrogen bonds and influence the location of the CP in the H···O region.
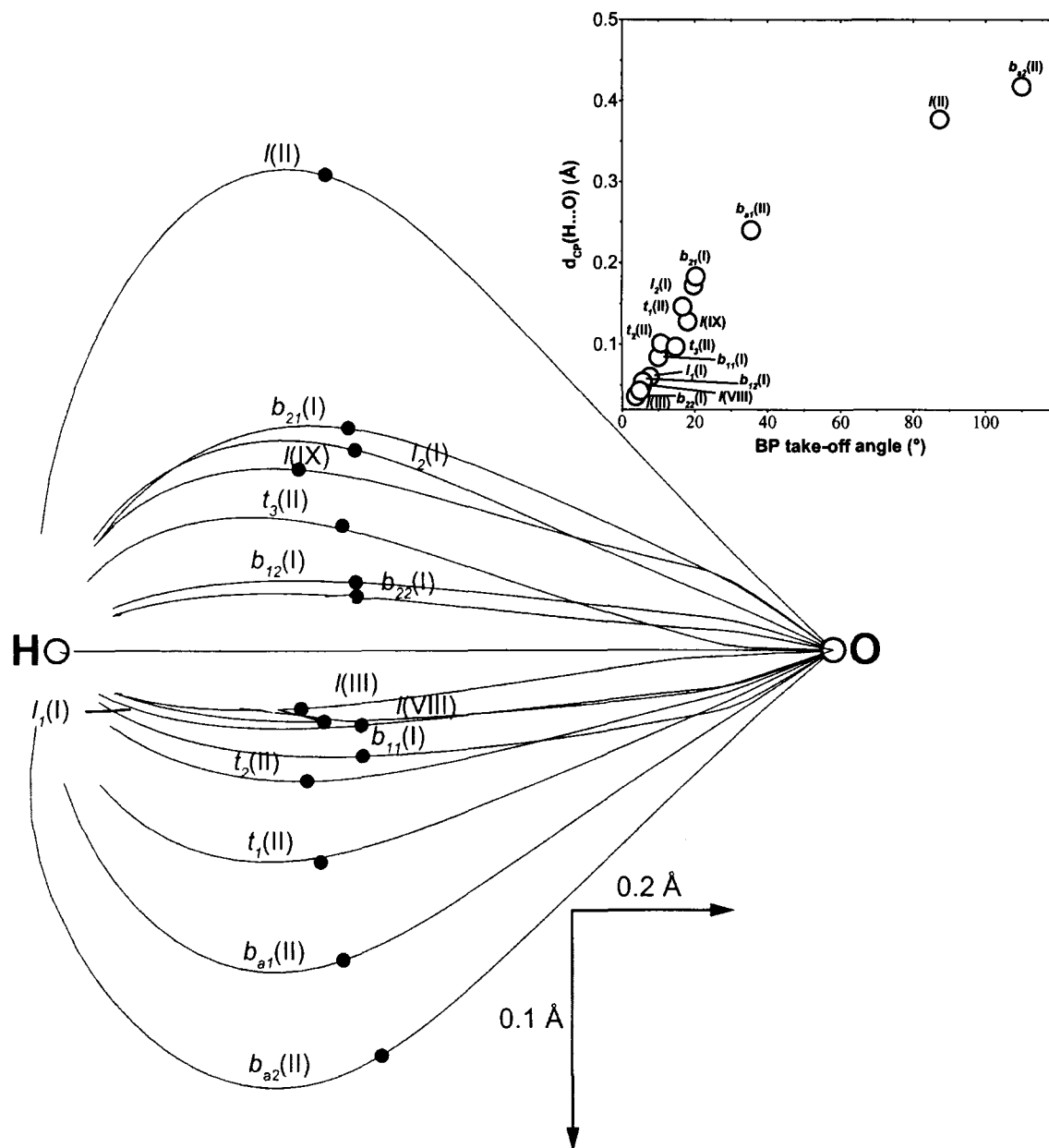
Figure 4.28: *The H···O bond paths normalized with respect to the H···O distance. The dark circles depict the H···O critical points. The type of the hydrogen bond is shown above the bond path. The inset shows the variation of the d_CP values of the H···O bond with the corresponding bond path take-off angle at the donor.*

Taking the example of a typical hydrogen bond, say l(**VIII**) (Figure 4.26b), we see

that one of its lone-pair lobes is inclined towards the hydrogen, the distance from its

CP to the hydrogen being shorter (1.43 Å) than the H$\cdots$O distance (1.68 Å). The lone-

pair under consideration would certainly affect the H$\cdots$O density. By considering the

lone-pairs distinctly (apart from the atom cores of the D and A), we are able to obtain

useful insights. We have paid attention to the location of the H$\cdots$O CP with respect to

a new interaction line (distinct from the atomic interaction line) connecting the

hydrogen and the CP of the lone-pair. Similar considerations involving the A and D

atom cores and the lone-pairs (A_ℓ and D_ℓ) on the donor and acceptor oxygens give rise

to a unique set of possibilities termed $L_{i\text{-}j}$, as depicted in Figure 4.29. In this figure, the

H$\cdots$O CP is shown to lie on the interaction line L joining i and j objects, the latter

corresponding to A, D, A_ℓ, D_ℓ or H. In the linear hydrogen bond shown in Figure

4.29a, the H$\cdots$O CP lies on the line joining the proton and the core of the acceptor.

Here, i and j correspond to H and A respectively and we assign the symbol, $L_{H\text{-}A}$ to

describe the line. The l(**III**) bond belongs to this category. Besides $L_{H\text{-}A}$, we find

another category involving the proton, $L_{H\text{-}A\ell}$ (Figure 4.29b) where the CP lies on the

line joining a lone-pair on the acceptor and the hydrogen. The b_{11} and b_{12} bonds of **I**

and l(**VIII**) belong to this category. Figures 4.29c to f depict other possibilities. Thus,

$L_{D\text{-}A}$ (Figure 4.29c) implies that the CP lies on the line joining the donor and the

acceptor. An example of this kind is the t_3 in system **II**. $L_{D\ell\text{-}A}$ (Figure 4.29d) is the line

joining a lone-pair on the donor with the acceptor core. The bonds, l of **IX** and b_{a1} of

II are examples of this category. Similarly, $L_{D-A\ell}$ (Figure 4.29e) stands for the line

connecting the donor core with a lone-pair on the acceptor, examples
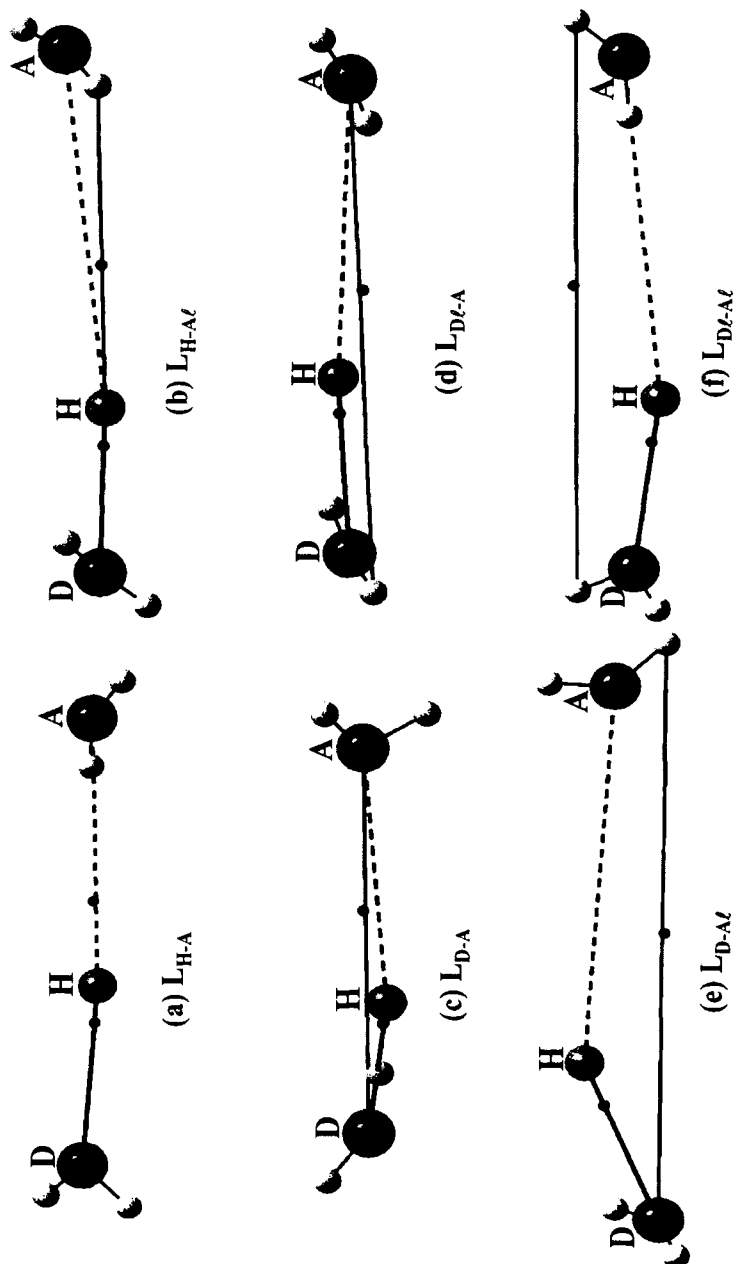
Figure 4.29: A schematic diagram showing connective relations. The open circles depict the hydrogen atoms. The O-H and H···O CPs are shown as tiny dark spheres. Six types of hydrogen bonds are depicted with different L_{i-j} relations, where L is the line joining i and j objects, the latter corresponding to the atom cores (A and D), their lone-pairs (A_ℓ and D_ℓ), or H. The L_{i-j} relation is established such that the H···O CP lies close to the line L. (a) L_{H-A}, (b) $L_{H-A\ell}$, (c) L_{D-A}, (d) $L_{D\ell-A}$, (e) $L_{D-A\ell}$, (f) $L_{D\ell-A\ell}$

of this kind being b_{a2} and t_1 of **II**. The $L_{D_{\ell}-A_{\ell}}$ category (Figure 4.29f) where the CP lies in the line of sight of the lone-pair on the donor and the lone-pair on the acceptor, finds many examples in the l_1, l_2, b_{21} and b_{22} hydrogen bonds of **I** as well as l and t_2 bonds of **II**.

Let us consider in detail, the simple case of the linear hydrogen bond l(**III**) shown in Figure 4.30a. Here, the O-H CP essentially lies on the internuclear axis (d_{CP}, 0.014 Å), while that in the H$\cdots$O region with a d_{CP} value of 0.036 Å, is well within that allowed for a bent bond. This hydrogen bond can be considered to belong to the class L_{H-A}. The lone-pairs on the donor are pointing in a direction opposite to that of the H$\cdots$O bond with an angle of 94.7°, while those on the acceptor are more spread out with an angle of 145.6°. Figure 4.30b contains the linear bond, l(**IX**). The O-H CP is on the internuclear line (d_{CP}, 0.006 Å), but the H$\cdots$O CP is significantly away from the respective line with a d_{CP} of 0.128 Å. It is striking, however, that the H$\cdots$O CP lies close to the line joining a lone-pair on the donor and the acceptor core. Thus, the l(**IX**) bond belongs to the class, $L_{D_{\ell}-A}$. It is convenient to define the perpendicular distance of the CP from the line L as 'the nearness parameter', d_L, to characterize the different hydrogen bonds. The value of d_L for l(**IX**) is 0.018 Å which is remarkably smaller than its d_{CP} value (0.128 Å).

In Figure 4.31, we show the new connective relations in the two bifurcated bonds of **I** where the same donor water molecules are shared by the two bonds. The b_{11} and b_{12} bonds of the bifurcated system b_1, exhibit $L_{H-A_{\ell}}$ relations engaging both the lone-pairs of the acceptor. The d_L values are similar (0.007 Å) and lower than the

corresponding H···O d_{CP} values (see Table 4.35). On the other hand, the b_{21} and b_{22}

bonds of b_2 exhibit $L_{D\ell\text{-}A\ell}$ relations involving both the lone-pairs of the acceptor with

d_L values of 0.042 and 0.014 Å, respectively.
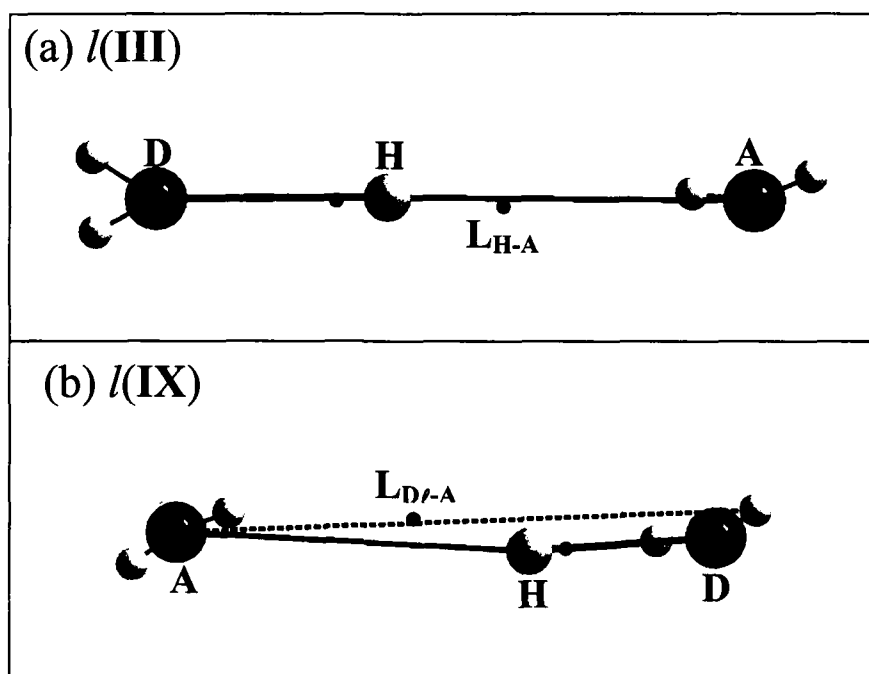
Figure 4.30: *Connective relations in linear hydrogen bonds. The small gray spheres depict the lone-pairs. The O-H and H···O CPs are shown as tiny dark spheres. (a) l(III) bond exhibiting relation $L_{H\text{-}A}$; (b) l(IX) bond of class $L_{D\ell\text{-}A}$.*

There seems to be some sort of cooperative effect in that the hydrogen bonds

belonging to a bifurcated system tend to exhibit similar relations due to the suitable

orientation of the acceptor lone-pairs. The lone-pair-core-lone-pair (A_ℓ-A-A_ℓ) angle in

both cases is 159.1°, which also reflects in similar bifurcation angles (88.6° and 85.1°)

of the hydrogen bonds. While one lone-pair from each donor water molecule is

involved in establishing a $L_{H\text{-}A\ell}$ or $L_{D\ell\text{-}A\ell}$ relation, the other lone-pair orients itself in a

manner that minimizes the lone-pair lone-pair repulsion. The corresponding φ_D angles

for b_1 and b_2 pair of bonds are 148.5° and 162.4°, respectively (Table 4.34).
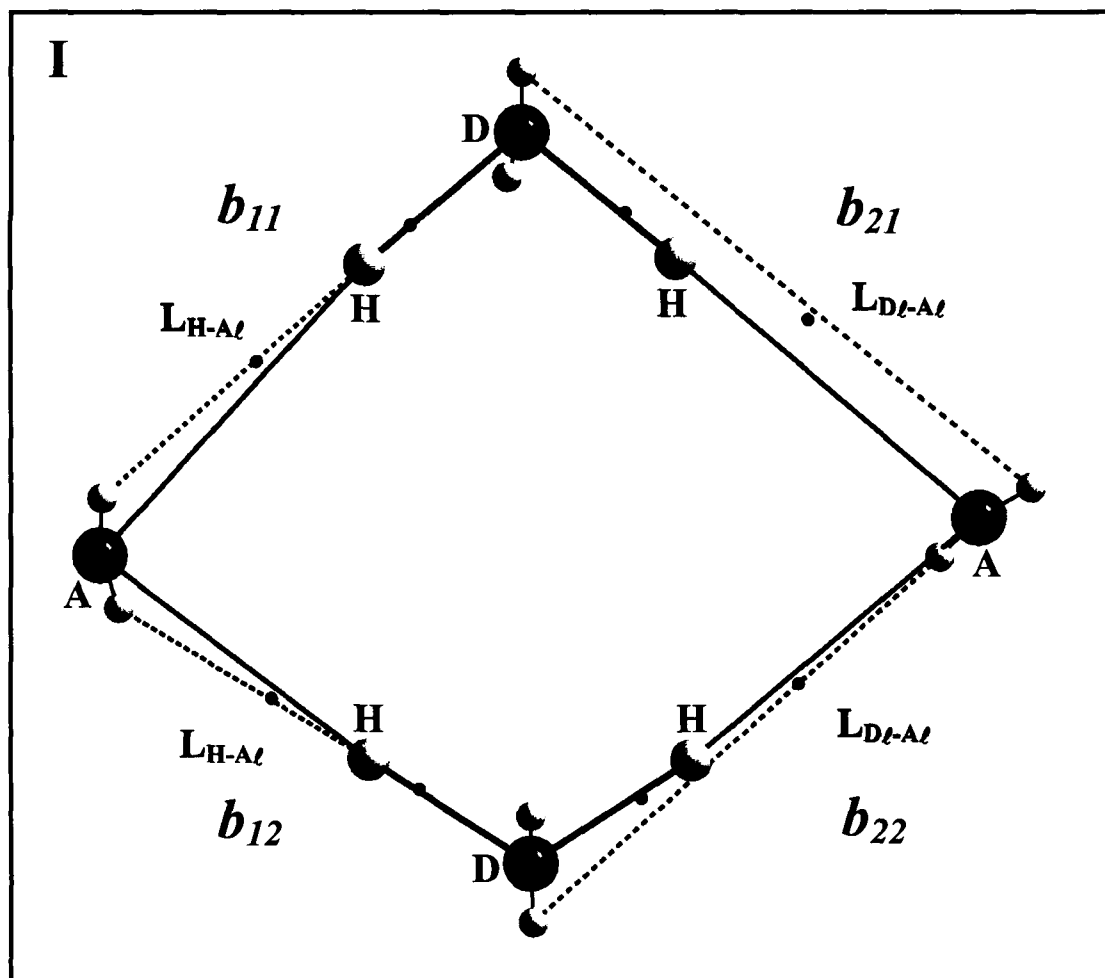
Figure 4.31: *Connective relations in bifurcated hydrogen bonds in I. The small gray spheres depict the lone-pairs. The O-H and H···O CPs are shown as tiny dark spheres. Note that both the lone-pairs on the acceptor (A) are involved in bonding while only one lone-pair on each water donor (D) is engaged. The bond symbol and its class are shown alongside each bond.*
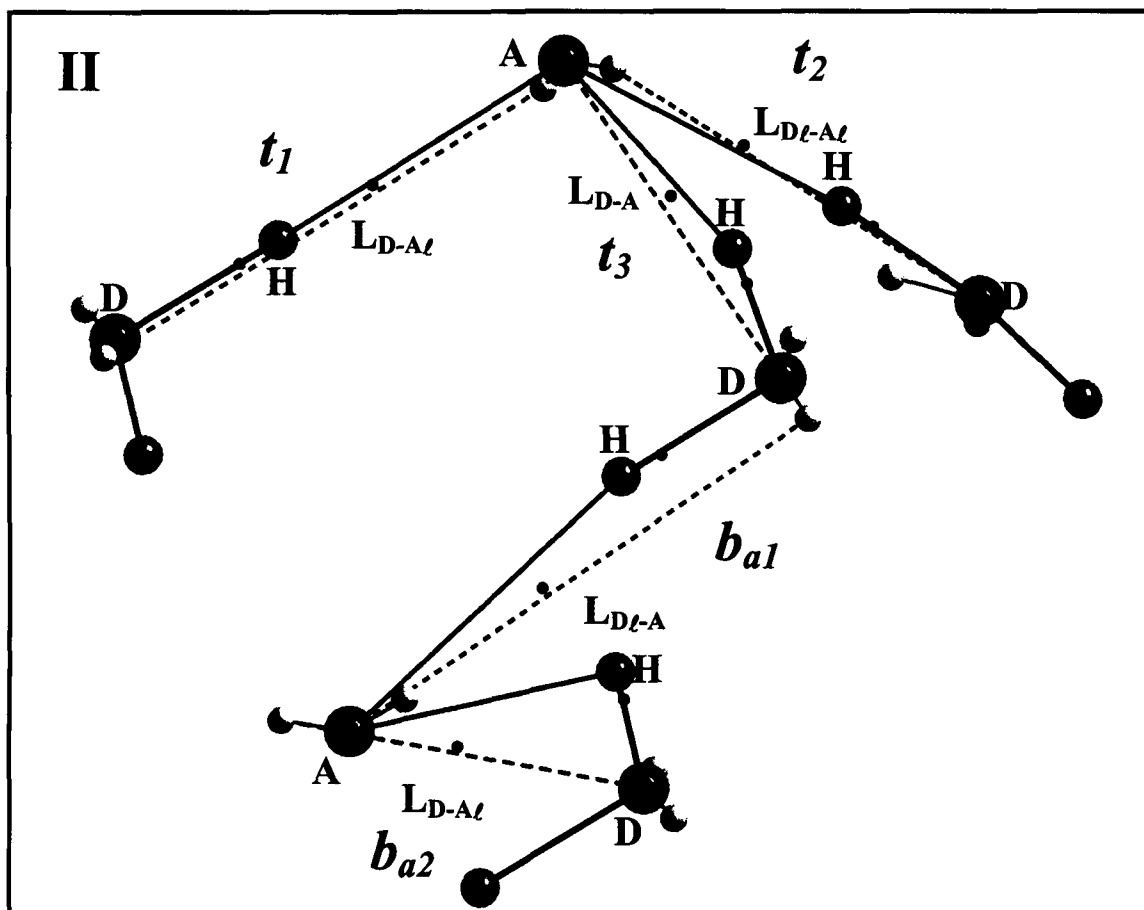
Figure 4.32: *Connective relations in trifurcated and bifurcated hydrogen bonds in V. The small gray spheres depict the lone-pairs. The O-H and H···O CPs are shown as tiny dark spheres. The bond symbol and its class are shown alongside each bond.*

Cooperative effects are not found in the bifurcated bond, b_a of **II**, shown in Figure 4.32. Here, the two bonds belong to two different relations perhaps due to the asymmetric nature of the bifurcation. The longer H···O bond (b_{a2}) follows a $L_{D-A\ell}$ relation, while the shorter bond (b_{a1}) obeys a $L_{D\ell-A}$ relation. The d_L values are small at 0.017 and 0.053 Å as against d_{CP} values of 0.418 and 0.240 Å, respectively. The trifurcated bonds provide examples of L_{D-A}, $L_{D-A\ell}$ and $L_{D\ell-A\ell}$ relations, where too, water molecules act as common donors.

In Table 4.36, we list the various hydrogen bonds studied by us along with their descriptions and the respective d_L values. Besides the examples discussed above, we have added some more examples to the list, three from a low temperature form of adipic acid[99] (**X**) and one from the γ polymorph of ethoxy cinnamic acid[53a] (**XI**). The d_L values for the listed L_{i-j} relations are below 0.04 Å while the corresponding d_{CP} were as high as 0.12 Å. From Tables 4.35 and 4.36, we notice that, whenever the d_{CP} value is higher than that is permissible (say, up to 0.04 Å), a new connective relation (L_{i-j}) is generally obtained with the smallest possible d_L value. For example, the l(**II**) bond belonging to the $L_{D\ell\text{-}A\ell}$ class, exhibits a d_L value of 0.043 Å as against a d_{CP} value of 0.377 Å. However, one can obtain a whole spectrum of values of d_L, which are considerably larger, by assuming this bond to belong to the other classes depicted in Figure 4.29. Thus, the next nearest d_L value for l(**II**) is 0.153 Å. Although most of the hydrogen bonds may permit a clear-cut assignment of the L_{i-j} type, it may prove difficult in certain situations. The b_{11} and b_{12} bonds of **I** with the smallest d_L values (0.007 Å) in $L_{H\text{-}A\ell}$, have the next nearest d_L values at 0.019 Å ($L_{D\text{-}A\ell}$) and 0.047 Å ($L_{D\ell\text{-}A\ell}$) with average values of 0.143 and 0.135 Å, respectively. The d_L values in $L_{H\text{-}A\ell}$ being so low, the original assignments are still justifiable.

Another example is the l_2(**I**) bond where the d_L values from the $L_{D\ell\text{-}A\ell}$, $L_{D\text{-}A\ell}$ and $L_{H\text{-}A\ell}$ relations are similar, (0.069, 0.073 and 0.070 Å respectively) but all of them being considerably lower than the d_{CP} value (0.172 Å). Such situations only reflect the complex nature of interactions in the hydrogen-bonded system and may require further analysis. Nevertheless, the above discussion should suffice to demonstrate how on the basis of charge density analysis, one is able to provide a better description of a

hydrogen bond in terms of the location of the CP, vis-à-vis the location of the lone-

pair of electrons on the donor and the acceptor atoms.

Table 4.36 A classification of the hydrogen bonds on the basis of the critical point position with their respective 'nearness' parameter[a]

System	Type of H-bond	Class	$d_L \times 10^2$ (Å)
III	Linear (l)	L_{H-A}	-
VIII	Linear (l)	$L_{H-A\ell}$	3.3
IX	Linear (l)	$L_{D\ell-A}$	1.8
I	Linear (l_1)	$L_{D\ell-A\ell}$	4.4
	Linear (l_2)	$L_{D\ell-A\ell}$	7.0
	Bifurcated (b_{11})	$L_{H-A\ell}$	0.7
	Bifurcated (b_{12})	$L_{H-A\ell}$	0.7
	Bifurcated (b_{21})	$L_{D\ell-A\ell}$	4.2
	Bifurcated (b_{22})	$L_{D\ell-A\ell}$	1.4
II	Linear (l)	$L_{D\ell-A\ell}$	4.3
	Bifurcated (b_{a1})	$L_{D\ell-A}$	5.3
	Bifurcated (b_{a2})	$L_{D-A\ell}$	1.7
	Trifurcated (t_1)	$L_{D-A\ell}$	3.0
	Trifurcated (t_2)	$L_{D\ell-A\ell}$	3.6
	Trifurcated (t_3)	L_{D-A}	8.5
X	Linear	L_{D-A}	3.9
	Linear	L_{H-A}	-
	Linear	L_{D-A}	3.7
XI	Linear	$L_{D\ell-A}$	1.0

[a] For a description of class, see Figure 4.36 and the text.
X: low temperature form of adipic acid; XI: γ form of ethoxy cinnamic acid.
L_{i-j} stands for the class, where the H···O BCP lies close to the line joining i and j objects. D and A stand for the donor and the acceptor atom cores; and D_ℓ and A_ℓ for the lone-pairs on the donor and the acceptor atom-cores, respectively. For L_{H-A}, $d_L = d_{CP}$.

This study brings out clearly the unusual nature of the bond paths and the

associated d_{CP} values in hydrogen bonds. In some sense, these situations are

comparable to bent bonds observed in shared interactions, but the shape of the bond

path as well as the magnitude of d_{CP} point to a more complex nature of the hydrogen

bond interaction. This unusual behavior of the hydrogen bond has been examined here

for the first time, taking examples from O-H$\cdots$O bonds. Significantly, this work demonstrates how using a simple rationale, apparently flexible unruly lone-pairs on the donor and acceptor atoms, can be linked to the hydrogen bond interaction in the vicinity, thereby providing an insight into the observed diverse geometries. Clearly, the hydrogen bond interaction is more than a simple H$\cdots$A interaction. Besides providing a useful classification, the study helps to understand the cooperative effects in hydrogen bonds, as illustrated in the case of bifurcated hydrogen bonds.

REFERENCES

1. (a) P. Debye, P. Scherrer, *Phys. Z.* (1918), **19**, 474. (b) P. Debye, Dispersion of Roentgen rays, *Ann. Phys.* (1915), **46**, 809.

2. For reviews, see: (a) *Electron Distributions and the Chemical Bond* Eds: P. Coppens, M. B. Hall, Plenum Press, New York, (1982). (b) P. Coppens, *J. Chem. Edu.* (1984), **61**, 761. (c) K. Angermund, K. H. Claus, R. Goddard, C. Krüger, *Angew. Chem. Int. Ed. Engl.* (1985), **24**, 237. (d) P. Coppens, *J. Phys. Chem.* (1989), **93**, 7979. (e) P. Coppens, *Ann. Rev. Phys. Chem.* (1992), **43**, 663. (f) *X-Ray Charge Densities and Chemical Bonding*, P. Coppens, Oxford University Press, IUCr Texts on Crystallography No. 4 (1997). (g) G. U. Kulkarni, R. S. Gopalan, C. N. R. Rao, *J. Mol. Struct. (Theochem)* (2000), **500**, 339.

3. B. Dawson, *Proc. Roy. Soc.* (1967), **A298**, 264.

4. W. J. Hehre, L. Radom, P. v. R. Schleyer, J. A. Pople, *Ab initio Molecular Orbital Theory*, Wiley, New York (1986).

5. M. J. Frisch, G. W. Trucks, H. B. Schlegel, P. M. W. Wong, J. B. Foresman, M. A. Robb, M. Head-Gordon, E. S. Replogle, R. Gomperts, J. L. Andres, K. Raghavachari, J. S. Binkley, C. Gonzales, R. L. Martin, D. J. Fox, D. J. Defrees, J. Baker, J. J. P. Stewart, J. A. Pople, GAUSSIAN 98/DFT, Rev. A.1.

6. GAMESS, M. W. Schmidt, K. K. Baldridge, J. A. Boatz, S. T. Elbert, M. S. Gordon, J. H. Jensen, S. Koseki, N. Matsunaga, K. A. Nguyen, S. J. Su, T. L. Windus, M. Dupuis, J. A. Montgomery, *J. Comput. Chem.* (1993), **14**, 1347.

7. R. Dovesi, V. R. Saunders, C. Roetti, M. Causa, N. M. Harrison, R. Orlando, R. Apra, CRYSTAL 95 User's Manual, University of Torino, Torino, Italy (1996).

8. R. F. W. Bader in *Atoms in Molecules – A Quantum Theory*, Clanderon press, Oxford, (1990).

9. N. K. Hansen, P. Coppens, *Acta Cryst.* (1978), **A34**, 909.

10. T. Koritsanszky, R. Flaig, D. Zobel, H. -G. Krane, W. Morgenroth, P. Luger, *Science* (1998), **279**, 356.

11. P. L. A. Popelier, *Atoms in Molecules – An Introduction*, Prentice Hall, (2000).

12. D. Zobel, P. Luger, W. Dreissig, T. Koritsanszky, *Acta Crystallogr.* (1992), **B48**, 837.

13. R. F. Stewart, *J. Chem. Phys.* (1973), **58**, 1668.

14. (a) N. K. Hansen and P. Coppens, *Acta Cryst.* (1978), **A34**, 909. (b) P. Coppens, T. N. Guru Row, P. Leung, E. D. Stevens, P. J. Becker and Y. W. Yang, *Acta Cryst.* (1979), **A35**, 63.

15. (a) T. Koritsanszky, S. T. Howard, T. Richter, P. R. Mallinson, Z. Su, N. K. Hansen, *XD, A computer program package for multipole refinement and analysis of charge densities from diffraction data*, Cardiff, Glasgow, Buffalo, Nancy, Berlin, (1995). (b) R. F. Stewart, *Acta Cryst.* **A32**, 565; R. F. Stewart, M. A. Spackman, VALRAY System, Department of Chemistry, Carnegie-Mellon University, Pittsburgh PA 15213, USA. (c) F. L. Hirshfeld, *Acta*

Cryst. (1971), **B27**, 769; F. L. Hirshfeld, *Isr. J. Chem.* (1977), **16**, 198. (d) J.

Epstein, J. R. Ruble, B. M. Craven, *Acta Cryst.* (1982), **B38**, 140.

16. (a) R. Destro, R. Bianchi, G. Morosi, *J. Phys. Chem.* (1989), **93**, 4447. (b) C.

Gatti, R. Bianchi, R. Destro, F. Merati, *J. Mol. Struct. (Theochem)* (1992)

255, 409.

17. F. L. Hirshfeld, *Acta Cryst.* (1976) **A32**, 239.

18. G. A. Jeffrey, J. F. Piniella, *The Application of Charge density Research to*

Chemistry and Drug Design. Plenum Publishing Corporation: New York and

London, (1991).

19. D. Cremer, E. Kraka, *Croat. Chem. Acta* (1984), **57**, 1259.

20. W. Scherer, M. Spiegler, B. Pedersen, M. Tafipolsky, W. Hieringer, B.

Reinhard, A. J. Downs, G. S. McGrady, *Chem. Commun.* (2000), 635.

21. R. F. W. Bader, T. Nguyen-Dang, Y. Tal, *Rep. Prog. Phys.* (1981), **44**, 893.

22. Y.Abramov, *Acta Cryst.* (1997), **A53**, 264.

23. P. Coppens, Y. Abramov, M. Carducci, B. Korjov, I. Novozhilova, C.

Alhambra, M. R. Pressprich, *J. Am. Chem. Soc.* (1999), **121**, 2585.

24. E. Espinosa, E. Mollins, C. Lecomte, *Chem. Phys. Lett.* (1998), **285**, 170.

25. E. Kraka, D. Cremer, *J. Mol. Struct. (Theochem)*, (1992), **255**, 189.

26. U. Koch and P. L. A. Popelier, *J. Chem. Phys.* (1995), **99**, 9747.

27. R. J. Boyd, S. C. Choi, *Chem. Phys. Lett.* (1986), **129**, 62.

28. I. Vorobyov, M. C. Yappert, D. B. DuPré, *J. Phys. Chem. A* (2002), **106**,

10691.

29. I. Alkorta, J. Elguero, C. Foces-Foces, *Chem. Commun.* (1996), 1633.

315

30. I. Rozas, I. Alkorta, J. Elguero, *J. Phys. Chem. A.* (1998), **102**, 9925.

31. I. Rozas, I. Alkorta, J. Elguero, *J. Phys. Chem. A.* (1997), **101**, 9457.

32. I. Rozas, I. Alkorta, J. Elguero, *J. Phys. Chem. A.* (1997), **101**, 4236.

33. I. Alkorta, J. Elguero, *J. Phys. Chem.* (1996), 100.

34. Y. H. Zhang, J. -K. Hao, X. Wang, W. Zhou, T. -H. Tang, *J. Mol. Struct. (Theochem)* (1998), **455**, 85.

35. (a) D. Madsen, C. Flensburg, S. Larsen, *J. Phys. Chem. A* (1998), **102**, 2177. (b) K. Hermansson, R. Tellgren, *Acta Crystallogr.* (1989), **B45**, 252. (c) M. P. C. M. Krijn, D. Feil, *J. Chem. Phys.* (1988), **89(7)**, 4199. (d) R. H. Blessing, *Acta Crystallogr.* (1988), **B44**, 334. (e) M. Gajhede, S. Larsen, S. Rettrup, *Acta Crystallogr.* (1986), **B42**, 545. (f) K. Hermansson, J. O. Thomas, *Acta Crystallogr.* (1982), **B38**, 2555.

36. (a) J. Overgaard, B. Schiott, F. K. Larsen, B. B. Iversen, *Chem. Eur. J.* (2001), **7**, 3756. (b) E. D. Stevens, J. Rys, P. Coppens, *J. Am. Chem. Soc.* (1978), **100**, 2324. (c) G. C. Verschoor, E. Keulen, *Acta Crystallogr.* (1971), **B27**, 134.

37. (a) C. Gatti, E. May, R. Destro, F. Cargnoni, *J. Phys. Chem. A* (2002), **106**, 2707. (b) P. Macchi, A. J. Schultz, F. K. Larsen, B. B. Iversen, *J. Phys. Chem. A* (2001), **105**, 9231.

38. (a) P. K. Bakshi, T. S. Cameron, O. Knop, *Can. J. Chem.* (1996), **74**, 201. (b) R. Bianchi, C. Gatti, V. Adovasio, M. Nardelli, *Acta Crystallogr.* (1996), **B52**, 471. (c) O. Knop, T. S. Cameron, P. K. Bakshi, W. Kwiatkowski, S. C. Choi, D. Adhikesavalu, *Can. J. Chem.* (1993), **71**, 1495.

39. T. S. Cameron, O. Knop, W. Kwiatkowski, K. N. Robertson, *ACA Annual meeting abstracts (St Louis)*, (1997).

40. C. Flensburg, S. Larsen, R. F. Stewart, *J. Phys. Chem.* (1995), **99**, 10130.

41. J. C. Speakman, *Struct. Bonding (Berlin)* (1972), **12**, 141.

42. G. K. H. Madsen, B. B. Iversen, F. K. Larsen, M. Kapon, G. M. Reisner, F. H. Herbstein, *J. Am. Chem. Soc.* (1998), **120**, 10040.

43. B. L. Rodrigues, R. Tellgren, N. G. Fernandes, *Acta Crystallogr. Structural Science* (2001), **B57**, 353.

44. P. Macchi, B. B. Iversen, A. Sironi, B. C. Chakoumakos, F. K. Larsen, *Angew. Chem. Int. Ed. Engl.* (2000), **39**, 2719.

45. G. U. Kulkarni, P. Kumaradhas, C. N. R. Rao, *Chem. Mater.* (1998), **10**, 3498.

46. J. Overgaard, B. Schiott, F. K. Larsen, A. J. Schultz, J. C. MacDonald, B. B. Iversen, *Angew. Chem. Int. Ed. Engl.* (1999), **38**, 1239.

47. P. Coppens, A. Vos, *Acta Crystallogr.* (1971), **B27**, 146.

48. R. S. Gopalan, G. U. Kulkarni, C. N. R. Rao, *Chem. Phys. Chem.* (2000), **1**, 127.

49. J. Ellena, A. E. Goeta, J. A. K. Howard, G. Punte, *J. Phys. Chem. A* (2001), **105**, 8696.

50. (a) P. R. Mallinson, K. Wozniak, C. C. Wilson, K. L. McCormack, D. S. Yufit, *J. Am. Chem. Soc.* (1999), **121**, 4640. (b) P. R. Mallinson, K. Wozniak, G. T. Smith, K. L. McCormack, D. S. Yufit, *J. Am. Chem. Soc.* (1997), **119**, 11502.

51. E. May, R. Destro, C. Gatti, *J. Am. Chem. Soc.* (2001), **123**, 12248.

52. (a) W. T. Klooster, S. Swaminathan, R. Nanni, B. M. Craven, *Acta Crystallogr.* (1992), **B48**, 217 (b) M. Tonogaki, T. Kawata, S. Ohba, *Acta Crystallogr.* (1993), **B49**, 1031. (c) A. Puig-Molina, A. Alvarez-Larena, J. F. Piniella, S. T. Howard, F. Baert, *Structural Chemistry* (1998), **9**, 395. (d) S. Dahaoui, C. Jelsch, J. A. K. Howard, C. Lecomte, *Acta Crystallogr.* (1999), **B55**, 226.

53. (a) R. S. Gopalan, G. U. Kulkarni, *Proc. Ind. Acad. Sci.* (2001), **113**, 307. (b) R. S. Gopalan, P. Kumaradhas, G. U. Kulkarni, C. N. R. Rao, *J. Mol. Struct.* (2000), **521**, 97.

54. P. Coppens, Yu Abramov, M. Carducci, B. Korjov, I. Novozhilova, C. Alhambra, M. R. Pressprich, *J. Am. Chem. Soc.* (1999), **121**, 2585.

55. G. R. Desiraju, T. Steiner in *The Weak Hydrogen Bond in Structural Chemistry and Biology*, Oxford University Press, Oxford, (1999).

56. G. A. Jeffrey, *An Introduction to Hydrogen Bonding*, Oxford University Press, Oxford, (1997).

57. (a) A. S. N. Murthy, C. N. R. Rao, *J. Mol. Struct.* (1970), **6**, 253. (b) C. N. R. Rao, in F. Franks Ed., *Water, A Comprehensive Treatise*, Vol. I, Plenum Press, New York, (1972), Chapter 3. (c) P. Schuster, G. Zundel, C. Sandorfy, Eds. *The Hydrogen Bond, Recent Developments in Theory and Experiments*, North-Holland, New York, (1976). (d) G. A. Jeffrey, W. Saenger, *Hydrogen Bonding in Biological Structures*, Springer, Berlin, (1991).

58. D. J. Millen, *Croat. Chem. Acta.* (1982), **55**, 133.

59. F. H. Allen, *Acta Crystallogr.* (2002), **B58**, 380.

60. E. Espinosa, M. Souhassou, H. Lachekar, C. Lecomte, *Acta Crystallogr.* (1999), **B55**, 563.

61. M. Slouf, A. Holy, V. Petricek, I. Cisarova, *Acta Crystallogr.* (2002), **B58**, 519.

62. K. Woźniak, P. R. Mallinson, C. C. Wilson, E. Hovestreydt, E. Grech, *J. Phys. Chem. A* (2002), **106**, 6897.

63. T. Steiner, W. Saenger, *Acta Crystallogr. Sect. B* (1994), **50**, 348.

64. H.-B. Bürgi, J. D. Dunitz, *Acc. Chem. Res.* (1983), **16**, 153.

65. T. Steiner, I. Majerz, C. C. Wilson, *Angew. Chem.* (2001), **113**, 2728. (b) T. Steiner, I. Majerz, C. C. Wilson, *Angew. Chem. Int. Ed.* (2001), **40**, 2651.

66. R. Taylor, O. Kennard, *Acc. Chem. Res.* (1984), **17**, 320.

67. I. Alkorta, J. Elguero, *J. Phys. Chem. A* (1999), **103**, 272.

68. E. Espinosa, E. Molins, C. Lecomte, *Chem. Phys. Lett.* (1998), **285**, 170.

69. M. A. Spackman, *Chem. Phys. Lett.* (1999), **301**, 425.

70. O. Knop, K. N. Rankin, R. J. Boyd, *J. Phys. Chem. A* (2001), **105**, 6552.

71. (a) J. Donohue, In *Strutural Chemistry and Molecular Biology*, Eds: A. Rich, N. Davidson, W. H. Freeman: San Francisco, (1968), 443. (b) A. C. Legon, D. J. Millen, *Acc. Chem. Res.* (1987), **20**, 39.

72. J. E. D. Bene, F. T. Marchese, *J. Chem. Phys.* (1973), **58**, 926.

73. C. Ramakrishnan, N. Prasad, *Int. J. Protein Res.* (1971), III, 209.

74. J. Mitra, C. Ramakrishnan, *Int. J. Peptide Protein res.* (1977), **9**, 27.

319

75. (a) R. Taylor, O. Kennard, *J. Am. Chem. Soc.* (1982), **104**, 5063. (b) R. Taylor, O. Kennard, W. Versichel, *Acta Cryst.* (1984), **B40**, 280. (c) P. Murray-Rust, J. P. Glusker, *J. Am. Chem. Soc.* (1984), **106**, 1018. (d) J. A. Platts, S. T. Howard, B. R. F. Bracke, *J. Am. Chem. Soc.* (1996), **118**, 2726. (e) T. Steiner, *Chem. Commun.* 1997, 727. (f) B. P. Hay, D. A. Dixon, J. C. Bryan, B. A. Moyer, *J. Am. Chem. Soc.* (2002), **124**, 182.

76. J. Kroon, J. A. Kanters, J. G. C. M. van Duijneveldt-van de Rijdt, J. Vliegenhardt, *J. Mol. Struct.* (1975), **24**, 109.

77. J. Kroon, J. A. Kanters, *Nature* (1974), **248**, 667.

78. T. Steiner, W. Saenger, *Acta Crystallogr. Sect. B* (1992), **48**, 819.

79. T. Steiner, W. Saenger, *J. Am. Chem. Soc.* (1992), **114**, 10146.

80. I. Olovsson, P. -G. Jönsson in *The Hydrogen Bond. Recent Developments in Theory and Experiment, Vol. 2* Eds. P. Schuster, G. Zundel, C. Sandorfy, North Holland, Amsterdam, (1976), 393.

81. F. H. Allen, C. M. Bird, R. S. Rowland, P. R. Raithby, *Acta Crystallogr. Sect. B* (1997), **53**, 680.

82. (a) P. K. Thallapally, A. Nangia, *CrystEngComm* (2001), 27. (b) C. B. Aakeröy, T. A. Evans, K. R. Seddon, I. Pálinko, *New J. Chem.* (1999), **23**, 145.

83. K. -J. Lin, M-C Cheng, Y. Wang, *J. Phys. Chem.* (1994), **98**, 11685.

84. F. H. Allen, O. Kennard, D. G. Watson, L. Brammer, A. G. Orpen, R. Taylor, *J. Chem. Soc. Perkin Trans. II.* S1 (1987).

85. V. Busetti, F. Marcuzzi, *Zeitschrift fur Kristallographie* (1997), **212(4)**, 302.

86. Throughout Part 2 of the thesis, linear, bifurcated and trifurcated hydrogen bonds are designated with symbols, *l*, *b* and *t*, respectively.

87. (a) Z. Berkovitch-Yellin, L. Leiserowitz, *Acta Crystallogr.* (1984), **B40**, 159. (b) C. J. Marsden, B. J. Smith, J. A. Pople, H. F. Schaefer, L. Radon, *J. Chem. Phys.* (1991), **95**, 1825. (c) O. Mó, M. Yáñez, J. Elguero, *J. Chem. Phys.* (1992), **97**, 6628. (d) G. Louit, A. Hocquet, M. Ghomi, M. Meyer, J. Sühnel, *Phys. Chem. Comm.* (2002), **5**, 94. Many examples of bifurcated hydrogen bonds are known where the hydrogen atom from a single donor group is bonded to two acceptor atoms. Such a configuration is also termed as a three-centered interaction. See: (e) G. Albrecht, R. B. Corey, *J. Am. Chem. Soc.* (1939), **61**, 1087. (f) R. E. Marsh, *Acta Crystallogr.* (1958), **11**, 654. (g) P. G. Jönsson, A. Kvick, *Acta Crystallogr.* (1972), **B28**, 1827. (h) G. A. Jeffrey, J. Mitra, *J. Am. Chem. Soc.* 1984, **106**, 5546. (i) I. Rozas, I. Alkorta, J. Elguero, *J. Phys. Chem.* A. (1998), **102**, 9925. (j) N. Goutev, H. Matsuura, *J. Phys. Chem. A* (2001), **105**, 4741.

88. R. Vaidhyanathan, S. Natarajan, C. N. R. Rao, *J. Mol. Struct.* (2001), **608**, 123.

89. V. R. Pedireddi, S. Chatterjee, A. Ranganathan, C. N. R. Rao, *Tetrahedron*, (1998), **54**, 9457.

90. A. C. Larson, D. T. Cromer, *J. Chem. Phys.* (1974), **60**, 185.

91. G. R. Form, E. S. Raper, T. C. Downie, *Acta Crystallogr.* (1973), **B29**, 776.

92. Y- H. Zhang, J- K. Hao, X. Wang, W. Zhou, and T- H. Tang, *J. Mol. Struct. (Theochem)* (1998), **455**, 85.

93. (a) M. R. Truter, *J. Chem. Soc.* (1960), 997. (b) G. A. Jeffrey, J. R. Ruble, J. H. Yates, *J. Am. Chem. Soc.* (1984), **106**, 1571.

94. E. Espinosa, C. Lecomte, E. Molins, S. Veintennillas, A. Cousson, W. Paulus, *Acta Crystallogr.* (1996), **B52**, 519.

95. R. Wiest, V. P. Pesme, M. Benard, C. Lecomte, *J. Phys. Chem.* (1994), **98**, 1351.

96. H. Lachekar, *These de I'Universite Henri Poincare*, Nancy 1, France, (1997).

97. R. Destro, F. Z. Merati, *Z. Naturforsch, Teil A* (1993), **48**, 99.

98. S. T. Howard, M. B. Hursthouse, C. W. Lehmann, E. A. Poyner, *Acta Crytsallogr.* (1995), **B51**, 328.

99. R. S. Gopalan, P. Kumaradhas, G. U. Kulkarni, *J. Solid State Chem.* (1999), **148**, 129.

100. V. P. Pesme, C. Lecomte, *Acta Crystallogr.* (1998), **B54**, 485.

101. R. Destro, R. Bianchi, C. Gatti, F. Merati, *Chem. Phys. Lett.* (1991), **186**, 47.

102. M. Souhassou, C. Lecomte, R. H. Blessing, A. Aubry, M. -M. Rohmer, R. Wiest, M. Benerd, M. Merraud, *Acta Crystallogr.* (1991), **B47**, 253.

103. M. Souhassou, C. Lecomte, M. E. Ghermani, M.-M. Rohmer, R. Wiest, M. Benard, R. H. Blessing, *J. Am. Chem. Soc.* (1992), **114**, 2371.

104. A. Boukhris, *These de Doctoral d'Etal*, Univ. of Agadir, Morocco and Henri Poincare, France.

105. S. Dahaoi, V. P. Pesme, J. A. K. Howard, C. Lecomte, *J. Phys. Chem. A* (1999), **103**, 6240.

106. R. Bianchi, C. Gatti, V. Adovasio, M. Nardelli, *Acta Crystallogr.* (1996), **B52**, 471.

107. For Section 4.3 - tables of geometrical and charge density data are borrowed from Section 4.1 for systems **I, II** and **III**. We resort to the usage of symbols, such as *l, b* and *t* to distinguish different types of O-H$\cdots$O hydrogen bonds.

108. D. Cremer, E. Kraka, *J. Am. Chem. Soc.* (1985), **107**, 3800.

109. H. Irngartinger, S. Strack, *J. Am. Chem. Soc.* (1998), **120**, 5818.

OTHER WORK DONE BY THE CANDIDATE

Ring critical point (RCP) as an index of delocalization in the squarate and croconate dianions

Aromaticity of cyclic molecules[1] is an aspect barely explored by experimental charge density analysis although a number of aromatic systems have been investigated during the last two decades by this method. Cameron *et al*[2] studied the topography of the electron density of benzene molecule trapped inside a phosphazene crystal, and provided evidence for the π-density above and below the ring planes. The charge density of a neat benzene crystal was examined by Spackman *et al*[3] who derived the quadrupolar moment. Electron delocalization in citrinin[4] and in an annulene derivative[5] has been analyzed in terms of the critical point parameters. There has been an effort to obtain information on the extent of conjugation in N-containing compounds such as imidazole,[6] triazole[7] and pyrimidine derivatives,[6] based on the bond properties. While the electron densities at the bond critical points were found to be intermediate to those of single and double bonds akin to aromatic rings, the Laplacian and the ellipticity values hardly showed any systematic trend. Koritsanszky and Coppens[8] point out that the bond properties obtained from the charge density alone may not provide a consistent description of aromaticity involving electron delocalization and should therefore be formulated in terms of the collective rather than the local parameters. Howard and Krygowski[9] in their theoretical study of benzenoid hydrocarbons, emphasize that the charge density descriptors evaluated at the ring

critical point (RCP) are more suitable for describing the aromatic character of a molecule.

We considered it interesting to examine the charge density distributions in oxocarbon rings, which have formed a subject of great interest ever since West et al[10] pointed out that these 2π electron ring dianions constitute a new aromatic system. West and Powell[11] calculated delocalization energies using the Hückel LCAO-MO method and predicted that the delocalization energy per π electron was substantial for all the oxocarbon dianion species, but falls sharply with increasing ring size. The use of delocalization energy as a measure of aromaticity is, however, questionable.[12] Based on the graph theory of aromaticity, Aihara[13] concluded that the degree of aromaticity in the oxocarbon dianions decreases with increasing ring size, as found by other workers as well.[14] Schleyer et al[15] have analyzed the degree of aromaticity in the oxocarbon dianions based on magnetic properties and found the deltate anion to be doubly aromatic (both σ and π aromatic), the squarate moderately aromatic and the croconate to be relatively less aromatic. Quiñonero et al[16] have used the Nucleus Independent Chemical Shifts (NICS), Wiberg bond indices and ^{17}O NMR calculated chemical shifts while dealing with the aromaticity of the oxocarbon anions.

In this section, we describe a comparative investigation of the squarate, $C_4O_4^{2-}$, and the croconate, $C_5O_5^{2-}$ anions by the experimental charge density method. We have analyzed the topography of the charge distribution in both the anion ring regions. We have also compared the charge density parameters at the ring critical points (RCP) of these two dianions with those of other cyclic systems reported in the literature. Our study provides some insight into the conjugation in the two anion rings, and also

shows how one may classify aromatic and non-aromatic rings based on the density and the Laplacian at RCP.

For crystallographic information and experimental details, refer Section 4.1.1 in Section 4 of Part 2. In both the salts, the anions are arranged in stacks, the spacing being 3.48 Å in the monoclinic form as compared to 3.37 Å in the triclinic form (both being close to the 3.40 Å separation expected for aromatic systems). The major difference between the two forms is in the octahedral coordination around the sodium ion. In the triclinic form reported here, four oxygens from water molecules and two from the squarate rings form the coordination shell while in the monoclinic form, water molecules and the squarate rings contribute equal number of oxygens to the coordination.

The structure of disodium croconate trihydrate is quite similar to that of potassium croconate dihydrate reported by Dunitz et al.[17] The interplanar spacing in the potassium salt is about 3.30 Å as compared to 3.20 Å in the present case. The potassium ion is surrounded by oxygen atoms of four separate anions and to the oxygen atom of a water molecule, which is somewhat different compared to the coordination of the sodium ion. In the sodium croconate trihydrate, the sodium ion is surrounded by three oxygen atoms from water molecules and a carbonyl oxygen from the neighboring croconate ring.

The C-C distances in each ring are quite similar, the mean values being 1.471(9) and 1.468(2) Å for the squarate and the croconate rings, respectively (see Tables 4.2 and 4.3, Section 4, Part 2). Likewise, the C-O bonds of the anions are nearly equal with mean values of 1.259(6) and 1.248(4) Å. The corresponding C-C-C

angles are 90° and 108° within 0.5°, but the O-C-C angles exhibit a larger spread especially for the croconate ion. Both the squarate and the croconate rings are essentially planar, the mean deviation of the atoms being ~0.007 and ~0.009Å respectively.

The critical point analysis in the bonding regions of the squarate and the croconate anions reveals (3, -1) CPs (see Tables 4.5 and 4.4, Section 4 in Part 2). The ρ_{BCP} values for the C-C bonds of the squarate ion fall in a narrow range of 1.85(1) to 1.87(1) eÅ^{-3}. Those of the croconate ion are slightly lower with a mean value of 1.81(1) eÅ^{-3} but their spread is similar (~0.01 eÅ^{-3}). The Laplacians also behave in a likewise manner. The magnitude of the Laplacian are somewhat higher (~ -13.4(3) eÅ^{-5}) in the squarate than in the croconate (~ -12.2(3) eÅ^{-5}). The ellipticity (ε) values in squarate vary between 0.23 and 0.27, with a mean value of 0.25 and those in croconate, are somewhat lower, between 0.18 and 0.25 with the mean value at 0.22. The mean d value for the C-C bonds in the squarate ring is 0.058 Å while for the croconate the value is much smaller, 0.015 Å in accordance with the observed strain in the rings. The mean C-O bond density of the squarate ion is 2.72(3) eÅ^{-3} as compared to 2.66(2) eÅ^{-3} in the croconate ion. The pseudoatomic charges on the carbonyl oxygens are -0.15 e in the squarate and –0.13 e in the croconate ion. The charge on the squarate ring carbon is -0.14 e, and in the croconate, the carbon atom carries a smaller charge (-0.07 e). Accordingly, the C-O bond appears to be less polarized in squarate (Δ ~ 18 %) compared to croconate (Δ ~ 25 %).

The ρ_{BCP} values in the C-C regions of the rings in the two dianions are considerably lower compared to those encountered in a benzenoid ring. Thus, the

naphthyl ring of 1,8-bis(dimethylamino) naphthalene exhibits a C-C bonding density of ~2.15 $eÅ^{-3}$.[18b] The values of the squarate and the croconate rings are rather close to the density in a typical single bond (ρ_{BCP}, 1.71 $eÅ^{-3}$). Following Cremer and Kraka,[19] the densities in the squarate and the croconate ions correspond to the bond order values of 1.19 and 1.12 respectively. These values may be contrasted with the bond orders of 1.62 in benzene[19] and 1.54 in the naphthyl ring of 1,8-bis(dimethylamino) naphthalene.[18b] This is probably because the π-acceptor carbonyl groups in the dianions withdraw the electron density away from the ring. Larger the number of carbonyl groups, greater is the charge separation between the carbonyl oxygens and the carbocyclic ring and lower is the C-C bond order. The ellipticity values, however, actually compare well with the value for benzene (0.23).[20] The group charges associated with the squarate and the croconate ions are −1.16 and −1.04 e, respectively. However, a comparison of our results with those obtained from theory[15] is not straightforward since the latter is based on isolated dianions.
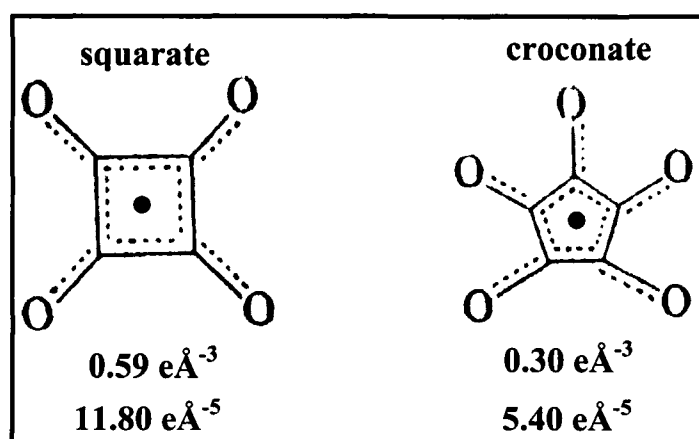
Figure 1: *The ring critical point (RCP) parameters of squarate and croconate dianions. ρ and $\nabla^2\rho$ at the RCP are indicated below each ring. The black circle close to the ring centre indicates the position of the RCP.*

We have analyzed the topological properties of the ring densities of the two

systems. Figure 1 illustrates the structural diagrams of the squarate and the croconate

rings, along with the RCP values. Figure 2 shows how ρ (normalized with respect to

ρ_{BCP}) varies along a perpendicular line passing through the BCP of a C-C bond in the

squarate and the croconate rings. Both the anion rings exhibit second-order saddles -

(3, +1) at the ring centers. The densities associated with the ring critical points (RCPs)

for the squarate and the croconate rings are 0.59(1) and 0.30(2) $e\text{Å}^{-3}$, respectively. As

shown in Figure 2, the density variation outside the rings is similar irrespective of the

ring size. This variation is extrapolated to inside the ring to represent the case of 'an

isolated bonding density'.
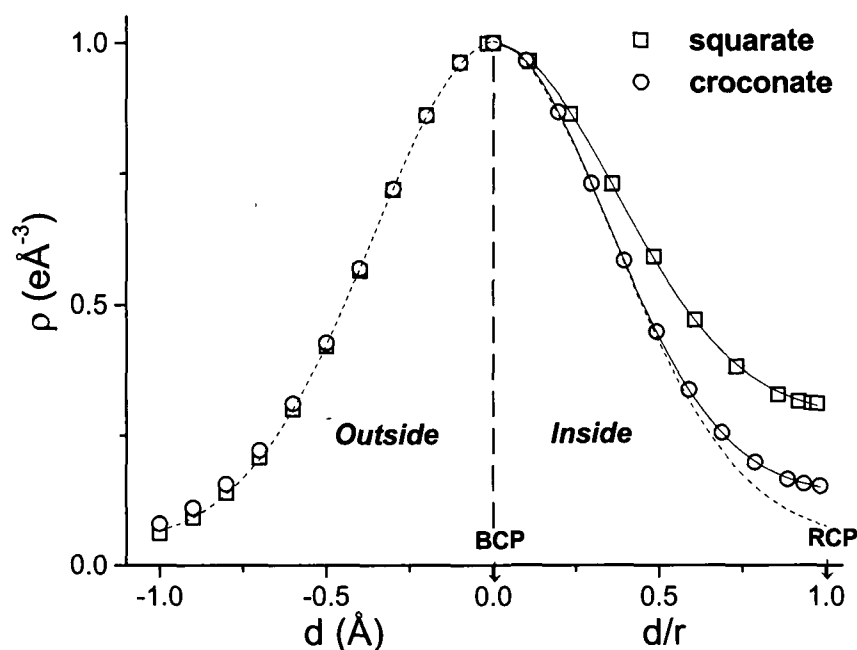
Figure 2: The total electron density profile in the squarate (squares) and the croconate (circles) rings along a line perpendicular to a C-C bond passing through its BCP. The density has been normalized with respect to the density at BCP. The distance from the BCP inside the ring region is normalized with respect to the distance, r, between BCP and RCP.

329

The variation of the charge density inside the ring, however, deviates significantly from the 'isolated bond density' due to contributions from the other bonds forming the ring. The deviation is more significant in the case of the squarate than the croconate due to the smaller ring size. Accordingly, the density at the squarate RCP is higher. This finding goes well with Bader's argument on charge densities at RCPs.[20] Interestingly, the Laplacians at the RCPs, $\nabla^2\rho_{RCP}$ also show a similar trend. The squarate and the croconate rings exhibit $\nabla^2\rho_{RCP}$ values of 11.8(1) and 5.4(4) eÅ^{-5} respectively.

It is instructive to examine whether the charge density descriptors at RCP may be useful in describing aromaticity of the rings. For this purpose, we compiled the RCP parameters of several examples of cyclic systems from the literature, aromatic as well as non-aromatic, investigated either experimentally or theoretically. These include benzene,[21] substituted phenyl rings,[22-25] naphthyl rings,[18] uracil,[26] quinoid,[27] and phosphazene rings,[28] besides the rings formed by intramolecular hydrogen bonds.[22,29] Examples of smaller ring systems from the literature are pyrrolidine,[27] bis-(thiodimethylene)tetrathiafulvalene rings,[30] cyclobutyl ring of a truxillic acid[24] and cyclopropyl rings.[21] We find that all the 6-membered rings,[27,28,21-25] irrespective of whether they are aromatic or non-aromatic, exhibit ρ_{RCP} values in the range 0.10 to 0.19 eÅ^{-3}. Similarly, the ρ_{RCP} values of the five-membered pyrrolidine and bis-(thiodimethylene)tetrathiafulvalene rings fall in the range 0.24 to 0.36 eÅ^{-3} while the 4-membered squarate from this study and the cyclobutyl ring carry a density of ~ 0.6 eÅ^{-3}. We have also examined the Laplacian values of the ring systems under consideration. Comparing the squarate dianion and the cyclobutyl ring, we found the

Laplacian values to be considerably different (11.8 $eÅ^{-5}$ and 5.8 $eÅ^{-5}$ respectively), unlike the densities. It is rather surprising that the Laplacian values can be so different in spite of the fact that the two rings possess similar geometries. The origin of this difference can be understood in terms of the variation of ρ within the two rings. In Figure 3, we show the variation of ρ across their RCP regions.
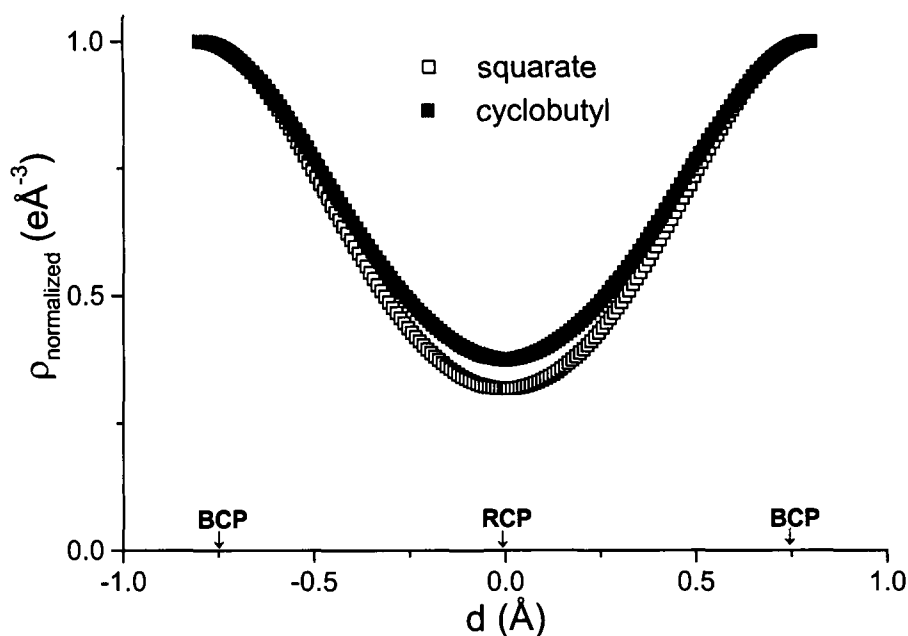
Figure 3: *The total electron density profile in the squarate (open squares) and the cyclobutyl ring (solid squares) regions along a line joining two opposite BCPs (passing through the RCP). The density has been normalized with respect to the density at BCP.*

The rate of fall of density towards RCP is higher in the squarate compared to the cyclobutyl ring, the latter showing a somewhat flat profile at the RCP. Accordingly, its $\nabla^2\rho_{RCP}$ value, which is a measure of curvature, is lesser than that of the squarate ring. The higher Laplacian of the squarate anion is clearly an outcome of the high degree of conjugation prevalent in it. A similar effect, though to a lesser

extent, is seen in the case of the croconate ion when compared with non-aromatic, five-membered rings. Laplacian of the croconate ring is 5.4 eÅ^{-5}, while the non-aromatic rings have $\nabla^2\rho_{RCP}$ values of approximately 4 eÅ^{-5}.

An examination of the variation of the Laplacian with ρ_{RCP} in ring systems yields useful insights. Thus, the plot presented in Figure 4 reveals the variation of $\nabla^2\rho_{RCP}$ to be markedly different for aromatic and nonaromatic systems. The aromatic systems seem to follow a trend where $\nabla^2\rho_{RCP}$ is roughly proportional to ρ_{RCP} and thus, fall into the hashed region in Figure 4. In non-aromatic systems, the $\nabla^2\rho_{RCP}$ values are much lower and do not exhibit any systematic trend. However, this distinction is not so clear in the case of the 6-membered rings. The ρ_{RCP} and $\nabla^2\rho_{RCP}$ values of benzene are 0.16 eÅ^{-3} and 3.81 eÅ^{-5}, respectively, which indeed do not differ much from the values exhibited by the non-aromatic 5-nitrouracil ring (0.19 eÅ^{-3}, 3.3 eÅ^{-5}). The quinoid ring in 7,7-di(S(+)-2-(methoxymethyl)pyrrolidino)-8,8-dicyanoquino dimethane with its partial benzenoid character induced by the donor and acceptor groups, carries a ρ_{RCP} value of 0.15 eÅ^{-3} and a Laplacian of 3.1 eÅ^{-5}. Interestingly, the non-aromatic ring formed by a strong intramolecular hydrogen bond in benzoyl acetone[22] lies quite close to benzene in Figure 4. The substituted phenyl rings[22-25] cluster below the benzene point in Figure 4. The ρ_{RCP} and Laplacian values corresponding to the non-aromatic cyclophosphazenes[28] are much lower compared to benzene and substituted phenyl rings. The hydrogen-bonded seven-membered maleate ring[29] lies below phosphazenes with ρ_{RCP} and $\nabla^2\rho_{RCP}$ as low as 0.08 eÅ^{-3} and 1.8 eÅ^{-5} respectively. The case of cyclopropane, however, deserves special mention. Besides carrying a relatively high density at RCP[21] (~1.28 eÅ^{-3}), the cyclopropyl ring exhibits

bond ellipticities which are actually comparable to those of double bonds, a property

which accounts for its ability to act like a π system.[20] However, the non-aromatic

nature of the cyclopropyl ring is clearly evident from Figure 4 where it falls

considerably below the aromatic regime.
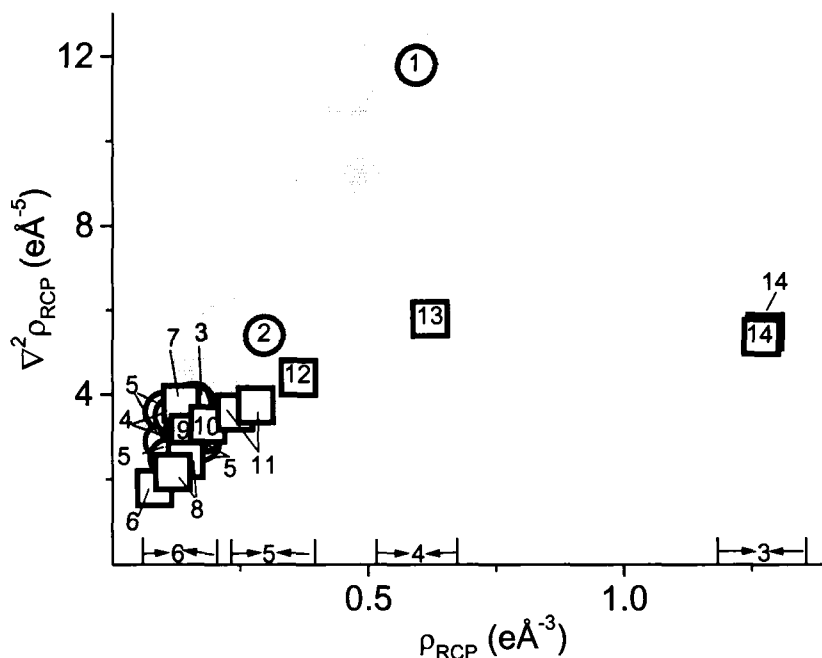
Figure 4: Plot of $\nabla^2 \rho_{RCP}$ versus ρ_{RCP} for the n-membered cyclic systems (n = 3, 4, 5, 6). The circles depict aromatic rings and the squares, the non-aromatic. The numbers inside the symbols, denote the type of ring. The numbers lying over the x-axis depict the size of the ring. The hashed region is where the Laplacian varies proportional to the density. 1-squarate, 2-croconate, 3,5-benzene and substituted benzene derivatives, 4-dimethylaminonaphthalene, 6,7-maleate ring, 8-phosphazene, 9-quinoid ring, 10-5-nitrouracil, 11- tetrathiafulvalene derivative, 12-pyrrolidine ring, 13-cyclobutyl ring of α-truxillic acid, 14-cyclopropane.

Thus, the plot of $\nabla^2 \rho_{RCP}$ versus ρ_{RCP} in Figure 4 appears to reflect the true

aromatic character of cyclic systems. This plot also shows how one can distinguish,

aromatic and nonaromatic systems. The aromatic rings fall in a region where the

Laplacian is roughly proportional to the density while the non-aromatics show no

definitive trend. The plot may be useful in the case of polycyclic systems where aromatic and nonaromatic rings coexist.

References

1. J. A. N. F. Gomes, R. B. Mallion, *Chem. Rev.* (2001), **101**, 1349.

2. T. S. Cameron, B. Borecks, W. Kwiatkowski, *J. Am. Chem. Soc.* (1994), **116**, 1211.

3. M. A. Spackman, A. E. Goeta, J. A. K. Howard, D. S. Yufit, private communication.

4. P. Roversi, M. Barzaghi, F. Merati, R. Destro, *Can. J. Chem.* (1996), **74**, 1145.

5. R. Destro, F. Merati, *Acta Crystallogr.* (1995), **B51**, 559.

6. R. F. Stewart, in *Applications of Charge Density Research to Chemistry and Drug Design;* G. A. Jeffrey, J. F. Piniella, Eds; Plenum: New York, (1991).

7. P. Fuhrmann, T. Koritsanszky, P. Luger, *Z. Kristallogr.* (1997), **212**, 213.

8. T. S. Koritsanszky, P. Coppens, *Chem. Rev.* (2001), **101**, 1583.

9. S. T. Howard, T. M. Krygowski, *Can. J. Chem.* (1997), **75**, 1174.

10. (a) R. West, H. -Y. Niu, D. L. Powell, M. V. Evans, *J. Am. Chem. Soc.* (1960), **82**, 6204. (b) R. West, H.- Y. Niu, *J. Am. Chem. Soc.* (1962), **81**, 1324.

11. R. West, D. L. Powell, *J. Am. Chem. Soc.* (1963), **85**, 2577.

12. B. A. Hess, Jr. L. J. Schaad, I. Agranat, *J. Am. Chem. Soc.* (1978), **100**, 5268.

13. (a) J. Aihara, *J. Am. Chem. Soc.* (1976), **98**, 2750. (b) Jun-ichi. Aihara, *J. Am. Chem. Soc.* (1981), **103**, 1633.

14. (a) F. Serratosa, *Acc. Chem. Res.* (1983), **16**, 170. (b) K. Jug, *J. Org. Chem.* (1983), **48**, 1344. (c) C. Puebla, T. K. Ha, THEOCHEM (1986), **137**, 171.

15. P v R. Schleyer, K. Najafian, B. Kiran, H. Jiao, *J. Org. Chem.* (2000), **65**, 426.

16. D. Quiñonero, C. Garau, A. Frontera, P. Ballester, A. Costa, P. M. Deya, *Chem. Eur. J.* (2002), **8**, 433.

17. J. D. Dunitz, P. Seiler, W. Czechtizky, *Angew. Chem. Int. Ed. Engl.* (2001), **40**, 1779.

18. (a) P. R. Mallinson, K. Wozniak, G. T. Smith, K. L. McCormack, D. S. Yufit, *J. Am. Chem. Soc.* (1997), **119**, 11502. (b) P. R. Mallinson, K. Wozniak, C. C. Wilson, K. L. McCormack, D. S. Yufit, *J. Am. Chem. Soc.* (1999), **121**, 4640.

19. D. Cremer, E. Kraka, *Croat. Chem. Acta* (1984), **57**, 1259.

20. R. F. W. Bader, *Atoms in Molecules – A quantum theory*, Clanderon Press, Oxford, (1990).

21. Y- H. Zhang, J- K. Hao, X. Wang, W. Zhou, T- H. Tang, *J. Mol. Struct. (Theochem)* (1998), **455**, 85.

22. G. K. H. Madsen, B. B. Iversen, F. K. Larsen, M. Kapon, G. M. Reisner, F. H. Herbstein, *J. Am. Chem. Soc.* (1998), **120**, 10040.

23. R. S. Gopalan, G. U. Kulkarni, E. Subramanian, S. Renganayaki, *J. Mol. Struct.* (2000), **524**, 169.

24. R. S. Gopalan, G. U. Kulkarni, *Proc. Ind. Acad. Sci.* (2001), **113**, 307.

25. A. Bach, D. Lentz, P. Luger, *J. Phys. Chem. A.* (2001), **105**, 7405.

26. R. S. Gopalan, G. U. Kulkarni, C. N. R. Rao, *Chem. Phys. Chem.* (2000), **1**, 127.

27. R. S. Gopalan, G. U. Kulkarni, C. N. R. Rao, *New J. Chem.* (2001), **25**, 1108.

28. V. Luana, A. M. Pendas, A. Costales, G. A. Carriedo, F. J. Garcia-Alonso, *J. Phys. Chem. A.* (2001), **105**, 5280.

29. D. Madsen, C. Flensburg, S. Larsen, *J. Phys. Chem. A.* (1998), **102**, 2177.

30. E. Espinosa, E. Molins, C. Lecomte, *Phys. Rev. B.* (1997), **56**, 1820.

APPENDIX

1. For PART 1 (A1)

Table A1.1 Fractional Coordinates and Equivalent Isotropic Displacement Parameters [Å^2] of Trimesic acid (dimethylformamide), **1a**

Atom	x/a	y/b	z/c	U_{eq} [a]
O(6)	0.4809(2)	0.4170(2)	0.2127(5)	0.074(1)
O(8)	0.2154(2)	0.4330(2)	-0.0668(4)	0.066(1)
C(10)	0.3359(2)	0.1421(2)	0.0736(5)	0.037(1)
O(4)	0.2650(2)	0.0076(2)	0.0109(5)	0.068(1)
O(7)	0.1464(2)	0.3035(2)	-0.1036(5)	0.066(1)
O(5)	0.5401(2)	0.2812(2)	0.2570(5)	0.087(1)
C(12)	0.2771(2)	0.2913(3)	0.0106(5)	0.037(1)
C(14)	0.4089(2)	0.2823(3)	0.1364(5)	0.039(1)
C(9)	0.2109(3)	0.3500(3)	-0.0572(6)	0.043(1)
C(13)	0.3458(2)	0.3338(3)	0.0745(5)	0.042(1)
C(15)	0.4039(2)	0.1863(3)	0.1357(5)	0.044(1)
C(11)	0.2726(2)	0.1953(2)	0.0117(5)	0.038(1)
O(3)	0.3825(2)	-0.0095(2)	0.1439(5)	0.071(1)
C(8)	0.3309(3)	0.0394(3)	0.0818(6)	0.046(1)
N(2)	0.2742(2)	0.6898(2)	0.0656(5)	0.063(1)
O(2)	0.2351(2)	0.8381(2)	0.0429(5)	0.087(1)
O(1)	0.0318(2)	0.4127(2)	-0.2076(5)	0.084(1)
C(7)	0.4843(3)	0.3254(3)	0.2067(6)	0.054(1)
N(1)	-0.0010(3)	0.5598(3)	-0.2869(5)	0.070(1)
C(6)	0.2873(3)	0.7783(3)	0.0578(7)	0.066(2)
C(5)	0.0491(3)	0.4945(4)	-0.2406(7)	0.078(2)
C(4)	-0.0840(4)	0.5400(4)	-0.2977(8)	0.108(2)
C(3)	0.1943(3)	0.6556(3)	0.0577(9)	0.117(2)
C(2)	0.3364(3)	0.6215(3)	0.0827(7)	0.085(2)
C(1)	0.0224(3)	0.6534(4)	-0.3203(9)	0.132(3)
H(15A)	0.4465(2)	0.1513(3)	0.1773(5)	0.053
H(11A)	0.2268(2)	0.1663(2)	-0.0295(5)	0.046
H(6A)	0.3395(3)	0.7982(3)	0.0637(7)	0.079
H(5A)	0.1022(3)	0.5107(4)	-0.2318(7)	0.093
H(4A)	-0.1122(4)	0.5947(4)	-0.3330(8)	0.162
H(4B)	-0.1022(4)	0.5197(4)	-0.1816(8)	0.162
H(4C)	-0.0932(4)	0.4923(4)	-0.3856(8)	0.162
H(3B)	0.1948(3)	0.5894(3)	0.0651(9)	0.175
H(3C)	0.1700(3)	0.6742(3)	-0.0543(9)	0.175
H(3D)	0.1649(3)	0.6803(3)	0.1571(9)	0.175
H(2A)	0.3135(3)	0.5608(3)	0.0860(7)	0.127
H(2B)	0.3658(3)	0.6322(3)	0.1924(7)	0.127
H(2C)	0.3711(3)	0.6261(3)	-0.0189(7)	0.127
H(1A)	-0.0234(3)	0.6895(4)	-0.3521(9)	0.198
H(1B)	0.0594(3)	0.6549(4)	-0.4179(9)	0.198
H(1C)	0.0467(3)	0.6786(4)	-0.2132(9)	0.198

Table A1.1 (*continued*)

H(7C)	0.2601(25)	-0.0512(32)	0.0220(61)	0.077(17)
H(7B)	0.5299(29)	0.4431(34)	0.2620(66)	0.116(20)
H(7A)	0.1084(29)	0.3433(33)	-0.1577(68)	0.111(20)

[a]U_{eq} is defined as one-third of the trace of the orthogonalized U_{ij} tensor.

Table A1.2 Fractional Coordinates and Equivalent Isotropic Displacement Parameters [Å^2] of Trimesic acid (methanol), **1b**

Atom	x/a	y/b	z/c	U_{eq}[a]
C(9)	0.2357(24)	-0.0030(9)	0.8047(9)	0.034(2)
C(8)	0.2261(26)	-0.0777(10)	0.6844(5)	0.039(2)
O(7)	0.6573(23)	-0.4979(7)	0.7820(4)	0.065(2)
O(5)	0.2405(22)	0.0784(7)	0.9219(4)	0.060(2)
O(6)	0.7049(20)	-0.4383(7)	0.8949(4)	0.054(2)
O(4)	-0.0146(22)	0.2336(8)	0.8259(4)	0.061(2)
O(3)	-0.0196(22)	0.0850(8)	0.5762(4)	0.064(2)
C(7)	0.4567(24)	-0.2522(9)	0.7930(5)	0.032(2)
O(2)	0.2220(23)	-1.0422(9)	0.5639(4)	0.071(2)
C(6)	0.0175(24)	0.0324(10)	0.7285(5)	0.035(2)
C(5)	0.1456(28)	-0.0414(10)	0.6029(5)	0.046(3)
C(4)	0.1452(26)	0.1158(9)	0.8515(5)	0.039(2)
C(3)	0.3848(25)	-0.1433(10)	0.8380(5)	0.037(2)
C(2)	0.3769(24)	-0.2202(9)	0.7167(5)	0.035(2)
C(1)	0.6172(26)	-0.4070(10)	0.8294(5)	0.040(2)
O(1)	0.0306(24)	0.2991(7)	-0.0108(4)	0.066(2)
O(11)	0.2026(86)	-0.5111(48)	0.5328(22)	0.365(19)
C(11)	0.4159(116)	-0.5440(54)	0.6045(26)	0.276(19)

[a]U_{eq} is defined as one-third of the trace of the orthogonalized U_{ij} tensor.

Table A1.3 Fractional Coordinates and Equivalent Isotropic Displacement Parameters [Å²] of 3,5-dinitrobenzoic acid + 4,4'-bipyridyl, **2a**

Atom	x/a	y/b	z/c	U_eq^a
C(11)	1.9105(8)	-0.0134(2)	-0.4693(5)	0.065(2)
C(12)	1.8224(10)	-0.0697(3)	-0.5161(6)	0.074(2)
C(13)	1.6518(10)	-0.0935(3)	-0.4564(7)	0.081(2)
N(14)	1.5696(8)	-0.0660(3)	-0.3531(6)	0.083(2)
C(15)	1.6518(11)	-0.0140(3)	-0.3064(6)	0.087(2)
C(16)	1.8187(11)	0.0139(3)	-0.3609(6)	0.082(2)
C(21)	1.0146(9)	0.1679(3)	0.1799(5)	0.061(1)
C(22)	1.1290(12)	0.2222(3)	0.2083(6)	0.075(2)
C(23)	1.3043(11)	0.2321(3)	0.1407(6)	0.072(2)
N(23)	1.4348(11)	0.2890(3)	0.1767(6)	0.106(2)
C(24)	1.3710(11)	0.1922(3)	0.0478(6)	0.074(2)
C(25)	1.2547(10)	0.1406(3)	0.0193(5)	0.068(2)
N(25)	1.3286(10)	0.0956(3)	-0.0794(5)	0.101(2)
C(26)	1.0783(10)	0.1272(3)	0.0827(5)	0.066(2)
C(27)	0.8314(10)	0.1533(3)	0.2590(6)	0.079(2)
O(231)	1.6072(9)	0.2923(2)	0.1313(6)	0.134(2)
O(232)	1.3597(10)	0.3270(2)	0.2442(6)	0.158(2)
O(251)	1.4769(8)	0.1110(2)	-0.1408(5)	0.146(2)
O(252)	1.2364(9)	0.0477(2)	-0.0923(5)	0.142(2)
O(271)	0.7749(6)	0.1873(2)	0.3494(4)	0.096(1)
O(272)	0.7404(7)	0.1020(2)	0.2222(4)	0.094(1)
H(12)	1.9042(80)	-0.0928(19)	-0.5913(47)	0.112(19)
H(16)	1.8864(75)	0.0514(21)	-0.3253(43)	0.092(20)
H(24)	1.5111(74)	0.1950(17)	0.0121(42)	0.071(17)
H(22)	1.0743(77)	0.2549(22)	0.2473(49)	0.107(23)
H(26)	1.0166(65)	0.0871(16)	0.0693(37)	0.064(16)
H(272)	0.6270(65)	0.0912(15)	0.2783(39)	0.045(13)
H(15)	1.5868(66)	0.0098(19)	-0.2312(39)	0.089(17)
H(13)	1.5983(79)	-0.1335(22)	-0.4948(45)	0.110(21)

^{a}U_eq is defined as one-third of the trace of the orthogonalized U_{ij} tensor.

Table A1.4 Fractional Coordinates and Equivalent Isotropic Displacement Parameters [Å^2] of 3,5-dinitro-4-methylbenzoic acid + 4,4'-bipyridyl, **3a**

Atom	x/a	y/b	Z/c	U$_{eq}$^{a}
C(11)	-0.0658(3)	0.5369(3)	0.3177(2)	0.046(1)
C(12)	-0.1651(3)	0.5615(3)	0.3817(2)	0.052(1)
C(13)	-0.3118(3)	0.6711(3)	0.3460(2)	0.050(1)
C(14)	-0.3697(3)	0.7631(3)	0.2453(2)	0.046(1)
C(15)	-0.2639(3)	0.7312(3)	0.1848(2)	0.046(1)
C(16)	-0.1162(3)	0.6239(3)	0.2169(2)	0.045(1)
C(17)	0.0960(3)	0.4188(3)	0.3571(2)	0.052(1)
C(18)	-0.5331(4)	0.8781(4)	0.2037(3)	0.063(1)
N(13)	-0.4103(3)	0.6925(4)	0.4198(2)	0.072(1)
N(15)	-0.3104(3)	0.8231(3)	0.0763(2)	0.056(1)
O(131)	-0.3984(3)	0.5852(3)	0.4898(2)	0.110(1)
O(132)	-0.4940(3)	0.8153(3)	0.4081(2)	0.104(1)
O(151)	-0.3135(3)	0.7680(3)	0.0212(2)	0.088(1)
O(152)	-0.3370(3)	0.9482(3)	0.0486(2)	0.081(1)
O(171)	0.1449(2)	0.3426(3)	0.4442(2)	0.086(1)
O(172)	0.1729(3)	0.4098(3)	0.2878(2)	0.086(1)
C(21)	0.6314(3)	0.4659(3)	0.1687(2)	0.046(1)
C(22)	0.7189(3)	0.3743(3)	0.2626(2)	0.048(1)
C(23)	0.8698(3)	0.2793(3)	0.2726(2)	0.049(1)
C(24)	0.9441(3)	0.2683(3)	0.1937(2)	0.050(1)
C(25)	0.8483(3)	0.3624(3)	0.1013(2)	0.049(1)
C(26)	0.6973(3)	0.4585(3)	0.0875(2)	0.050(1)
C(27)	0.4677(3)	0.5738(4)	0.1532(3)	0.057(1)
C(28)	1.1133(4)	0.1748(5)	0.2035(4)	0.069(1)
N(23)	0.9528(3)	0.1841(3)	0.3774(2)	0.068(1)
N(25)	0.9089(3)	0.3627(4)	0.0101(2)	0.065(1)
O(231)	1.0609(3)	0.0681(3)	0.3944(2)	0.106(1)
O(232)	0.9054(4)	0.2266(3)	0.4401(2)	0.104(1)
O(251)	0.9838(3)	0.2474(3)	0.0053(2)	0.083(1)
O(252)	0.8786(3)	0.4795(3)	-0.0573(2)	0.092(1)
O(271)	0.3883(3)	0.6512(3)	0.0714(2)	0.088(1)
O(272)	0.4264(3)	0.5772(3)	0.2358(2)	0.076(1)
C(31)	-0.2728(3)	1.0396(3)	0.2752(2)	0.044(1)
C(32)	-0.2952(4)	1.0341(3)	0.3691(2)	0.057(1)
C(33)	-0.4350(4)	1.1255(4)	0.3806(3)	0.065(1)
N(34)	-0.5522(3)	1.2195(3)	0.3057(2)	0.062(1)
C(35)	-0.5303(4)	1.2244(4)	0.2165(3)	0.059(1)
C(36)	-0.3956(3)	1.1395(3)	0.1970(2)	0.052(1)
C(37)	-0.1241(3)	0.9444(3)	0.2597(2)	0.043(1)
C(38)	-0.0837(3)	0.9740(4)	0.1667(2)	0.054(1)
C(39)	0.0570(4)	0.8818(4)	0.1563(3)	0.062(1)
N(310)	0.1574(3)	0.7647(3)	0.2325(2)	0.060(1)
C(311)	0.1199(4)	0.7371(4)	0.3214(3)	0.064(1)
C(312)	-0.0182(3)	0.8215(3)	0.3382(2)	0.056(1)
H(12)	0.1312(30)	0.5025(28)	0.4503(19)	0.052(8)
H(16)	-0.0477(29)	0.6068(25)	0.1687(17)	0.046(7)

Table A1.4 (*continued*)

H(18A)	-0.6019(46)	0.8540(39)	0.2393(27)	0.106(14)
H(18B)	-0.5556(51)	0.8843(46)	0.1424(32)	0.134(19)
H(18C)	-0.5462(48)	0.9696(48)	0.2053(27)	0.129(16)
H(172)	0.2737(43)	0.3343(38)	0.3038(23)	0.090(11)
H(22)	0.6739(28)	0.3872(26)	0.3166(18)	0.043(7)
H(26)	0.6409(31)	0.5199(29)	0.0240(19)	0.053(8)
H(28A)	1.1354(54)	0.0658(54)	0.2217(31)	0.149(18)
H(28B)	1.1517(49)	0.2023(44)	0.1424(30)	0.0127(17)
H(28C)	1.1697(40)	0.1675(36)	0.2580(25)	0.090(13)
H(272)	0.3181(46)	0.6480(41)	0.2298(25)	0.106(13)
H(32)	-0.2130(35)	0.9684(33)	0.4255(21)	0.070(10)
H(33)	-0.4521(35)	1.1263(32)	0.4425(21)	0.072(10)
H(35)	-0.6127(36)	1.2897(32)	0.1647(21)	0.068(10)
H(36)	-0.3897(31)	1.1540(29)	0.1312(20)	0.057(9)
H(38)	-0.1504(32)	1.0624(30)	0.1104(19)	0.057(9)
H(39)	0.0843(36)	0.8980(33)	0.0913(23)	0.080(10)
H(311)	0.1960(43)	0.6578(39)	0.3744(25)	0.097(12)
H(312)	-0.0346(34)	0.7935(31)	0.4037(21)	0.070(10)

[a]U_{eq} is defined as one-third of the trace of the orthogonalized U_{ij} tensor.

Table A1.5 Fractional coordinates and Equivalent Isotropic Displacement Parameters [Å^2] of 3,5-dinitro-4-methylbenzoic acid + 4,4'-bipyridyl+anthracene, 3b

Atom	x/a	y/b	z/c	U_{eq}[a]
O(372)	0.3112(3)	0.1179(3)	-0.0010(2)	0.051(1)
C(34)	0.2446(3)	0.3397(3)	0.3584(3)	0.039(1)
C(21)	0.4754(3)	0.0123(3)	-0.4397(2)	0.036(1)
C(33)	0.1705(3)	0.2494(3)	0.3066(3)	0.038(1)
N(24)	0.3803(3)	0.0581(3)	-0.2125(2)	0.045(1)
C(22)	0.5496(4)	0.0920(4)	-0.3780(3)	0.043(1)
N(33)	0.0377(3)	0.1883(4)	0.3650(2)	0.056(1)
C(31)	0.3293(3)	0.2658(3)	0.1347(3)	0.035(1)
C(26)	0.3503(4)	-0.0427(4)	-0.3838(3)	0.049(1)
O(371)	0.4641(3)	0.2924(3)	-0.0505(2)	0.062(1)
C(32)	0.2103(4)	0.2114(4)	0.1991(3)	0.039(1)
N(35)	0.4593(4)	0.4826(4)	0.3352(2)	0.059(1)
C(36)	0.4076(4)	0.3568(4)	0.1805(3)	0.042(1)
C(37)	0.3762(4)	0.2277(4)	0.0167(3)	0.043(1)
C(25)	0.03071(4)	-0.0179(4)	-0.2720(3)	0.052(1)
C(35)	0.3654(4)	0.3897(3)	0.2899(3)	0.042(1)
C(23)	0.4990(4)	0.1120(4)	-0.2663(3)	0.047(1)
O(352)	0.3975(3)	0.5833(3)	0.3762(2)	0.081(1)
O(351)	0.5935(3)	0.4533(3)	0.3266(2)	0.084(1)
O(332)	0.0218(3)	0.0612(3)	0.3599(2)	0.083(1)
C(38)	0.2076(5)	0.3718(6)	0.4810(4)	0.056(1)
O(331)	-0.0483(3)	0.2667(3)	0.4132(2)	0.083(1)
C(11)	0.0322(3)	0.4354(4)	0.9001(3)	0.045(1)
C(17)	0.1121(4)	0.5447(4)	0.9199(3)	0.049(1)
C(16)	-0.0834(4)	0.3896(4)	0.9836(3)	0.045(1)
C(12)	0.0605(5)	0.3689(5)	0.8001(3)	0.059(1)
C(13)	-0.0178(5)	0.2635(5)	0.7836(4)	0.071(1)
C(15)	-0.1636(4)	0.2782(4)	0.9610(4)	0.062(1)
C(14)	-0.1316(5)	0.2174(5)	0.8654(4)	0.072(1)
H(17)	0.1935(29)	0.5719(27)	0.8632(23)	0.036(8)
H(36)	0.4907(29)	0.3981(29)	0.1370(23)	0.041(9)
H(32)	0.1548(28)	0.1511(28)	0.1681(23)	0.038(8)
H(26)	0.2915(32)	-0.0926(32)	-0.4195(26)	0.056(10)
H(23)	0.5515(27)	0.1652(28)	-0.2202(23)	0.036(8)
H(25)	0.2144(34)	-0.0548(33)	-0.2355(27)	0.066(10)
H(22)	0.6444(33)	0.1329(33)	-0.4098(26)	0.068(11)
H(14)	-0.1986(36)	0.1373(37)	0.8555(29)	0.081(11)
H(38C)	0.1594(35)	0.2885(36)	0.5341(28)	0.068(11)
H(15)	-0.2398(31)	0.2536(31)	1.0185(25)	0.049(10)
H(38B)	0.1412(45)	0.4694(47)	0.4653(34)	0.108(16)
H(38A)	0.2916(38)	0.3813(36)	0.5252(29)	0.072(13)
H(12)	0.1437(39)	0.3979(39)	0.7480(31)	0.091(13)
H(372)	0.3325(42)	0.1032(42)	-0.0799(36)	0.110(15)
H(13)	-0.0048(38)	0.2240(39)	0.7082(33)	0.091(13)

[a]U_{eq} is defined as one-third of the trace of the orthogonalized U_{ij} tensor.

Table A1.6 Fractional Coordinates and Equivalent Isotropic Displacement Parameters [$Å^2$] of 3,5-dinitrobenzoic acid + 1,4-diiodobenzene

Atom	x/a	y/b	z/c	U_{eq}[a]
I(11)	0.0451(1)	0.2456(1)	0.4351(1)	0.063(1)
C(11)	-0.1916(7)	0.3766(7)	0.4865(2)	0.060(2)
C(12)	-0.1355(6)	0.2427(5)	0.4735(2)	0.046(1)
C(13)	-0.1913(6)	0.1097(7)	0.4866(2)	0.051(1)
N(21)	0.8325(5)	0.0504(5)	0.3296(2)	0.052(1)
N(22)	0.4428(5)	0.2989(6)	0.3995(2)	0.048(1)
O(21)	0.4442(5)	0.2063(6)	0.4311(2)	0.072(1)
O(22)	0.3508(4)	0.3909(5)	0.3930(2)	0.070(1)
O(23)	0.9300(4)	0.0583(5)	0.3043(2)	0.067(1)
O(24)	0.7996(5)	-0.0613(5)	0.3503(2)	0.081(1)
O(25)	0.6278(4)	0.6749(4)	0.2879(2)	0.062(1)
O(26)	0.8209(4)	0.5767(4)	0.2616(1)	0.058(1)
C(21)	0.6407(5)	0.1765(6)	0.3656(2)	0.040(1)
C(22)	0.7455(5)	0.1829(5)	0.3347(2)	0.040(1)
C(23)	0.7745(5)	0.3089(6)	0.3087(2)	0.038(1)
C(24)	0.6885(4)	0.4319(5)	0.3127(2)	0.035(1)
C(25)	0.5796(5)	0.4281(6)	0.3423(2)	0.039(1)
C(26)	0.5579(5)	0.3022(6)	0.3681(2)	0.037(1)
C(27)	0.7151(5)	0.5705(5)	0.2852(2)	0.041(1)
H(11)	-0.1488(70)	0.4671(88)	0.4799(23)	0.078(21)
H(12)	-0.1487(74)	0.0104(91)	0.4776(24)	0.089(23)
H(24)	0.6713(119)	0.7555(93)	0.2723(41)	0.130(41)
H(21)	0.8411(51)	0.3083(58)	0.2878(17)	0.035(12)
H(23)	0.5348(52)	0.4994(60)	0.3428(17)	0.038(15)
H(22)	0.6297(51)	0.0893(62)	0.3825(18)	0.047(14)

[a]U_{eq} is defined as one-third of the trace of the orthogonalized U_{ij} tensor.

343

Table A1.7 Fractional Coordinates and Equivalent Isotropic Displacement Parameters [Å^2] of 2,4,6-triaminopyrimidine + malonic acid, **4a**

Atom	x/a	y/b	z/c	U$_{eq}$^{a}
N(22)	0.7435(2)	0.0997(3)	0.5425(3)	0.040(1)
N(23)	0.5600(3)	0.1798(4)	0.4870(3)	0.051(1)
N(25)	0.6562(3)	-0.1750(4)	0.3694(3)	0.064(1)
C(26)	0.8000(3)	-0.0809(4)	0.4835(3)	0.044(1)
N(24)	0.6099(2)	0.0036(3)	0.4271(3)	0.045(1)
N(21)	0.9287(3)	0.0262(3)	0.6011(3)	0.053(1)
C(25)	0.6904(3)	-0.0854(4)	0.4270(3)	0.043(1)
C(23)	0.6376(3)	0.0934(4)	0.4845(3)	0.040(1)
C(21)	0.8275(3)	0.0127(4)	0.5429(3)	0.040(1)
O(112)	0.7209(2)	0.2235(3)	0.3316(2)	0.055(1)
O(132)	0.6606(2)	0.1476(3)	0.1347(2)	0.058(1)
O(111)	0.9034(2)	0.1632(3)	0.3767(3)	0.069(1)
C(12)	0.7832(3)	0.0566(5)	0.2598(4)	0.047(1)
O(131)	0.5886(2)	-0.0051(3)	0.1936(3)	0.063(1)
C(13)	0.6710(3)	0.0701(4)	0.1903(4)	0.047(1)
C(11)	0.8040(3)	0.1560(4)	0.3277(3)	0.044(1)
O(1)	0.5000	0.3079(4)	0.2500	0.059(1)
H(25A)	0.5869(3)	-0.1744(4)	0.3351(3)	0.076
H(25B)	0.7034(3)	-0.2336(4)	0.3665(3)	0.076
H(24)	0.5422(2)	0.0014(3)	0.3905(3)	0.054
H(21A)	0.9837(3)	-0.0260(3)	0.6040(3)	0.064
H(21B)	0.9396(3)	0.0873(3)	0.6363(3)	0.064
H(26)	0.8535(31)	-0.1433(39)	0.4797(30)	0.043(11)
H(23B)	0.4815(40)	0.1713(44)	0.4396(37)	0.069(15)
H(23A)	0.5818(33)	0.2350(40)	0.5260(34)	0.039(13)
H(7)	0.8467(41)	0.0691(47)	0.2371(36)	0.076(15)
H(22)	0.7561(36)	0.1597(50)	0.5856(38)	0.062(15)
H(25B)	0.7855(41)	-0.0201(54)	0.2854(41)	0.078(18)

^{a}U$_{eq}$ is defined as one-third of the trace of the orthogonalized U$_{ij}$ tensor.

Table A1.8 Fractional Coordinates and Equivalent Isotropic Displacement Parameters of 2,4,6-triaminopyrimidine + glutaric acid, **5a**.\

Atom	x/a	y/b	z/c	U_eq[a]
O(1)	1.0000	-0.1891(5)	0.7500	0.080(2)
O(2)	0.9729(5)	0.3159(4)	0.6765(2)	0.087(2)
C(11)	0.8649(5)	0.0423(5)	0.8431(3)	0.049(2)
C(12)	0.7608(5)	0.0272(5)	0.7904(3)	0.050(2)
C(13)	0.7710(5)	0.1111(5)	0.7322(3)	0.046(2)
C(14)	0.6640(5)	0.1022(5)	0.6802(3)	0.049(2)
C(15)	0.6660(5)	0.1849(4)	0.6213(3)	0.045(2)
C(21)	1.3108(5)	-0.1015(4)	0.9769(2)	0.045(2)
N(22)	1.1945(4)	-0.1899(4)	0.8830(2)	0.057(1)
C(22)	1.2121(5)	-0.1060(4)	0.9305(3)	0.044(1)
N(23)	1.1312(4)	-0.0185(3)	0.9320(2)	0.044(1)
N(24)	1.0591(4)	0.1492(4)	0.9786(2)	0.052(1)
C(24)	1.1380(5)	0.0707(4)	0.9775(2)	0.040(1)
N(25)	1.2358(4)	0.0762(3)	1.0229(2)	0.045(1)
N(26)	1.4108(4)	0.0032(4)	1.0697(2)	0.055(1)
C(26)	1.3193(5)	-0.0081(4)	1.0234(3)	0.041(1)
O(111)	0.8666(4)	0.1310(4)	0.8817(2)	0.074(2)
O(112)	0.9433(4)	-0.0335(4)	0.8452(2)	0.063(1)
O(151)	0.7482(3)	0.2531(3)	0.6171(2)	0.053(1)
O(152)	0.5763(4)	0.1824(3)	0.5775(2)	0.061(1)
H(13A)	0.8369(5)	0.0877(5)	0.7126(3)	0.055
H(13B)	0.7813(5)	0.1953(5)	0.7474(3)	0.055
H(14A)	0.6551(5)	0.0179(5)	0.6650(3)	0.058
H(14B)	0.5985(5)	0.1230(5)	0.7007(3)	0.058
H(21A)	1.3685(5)	-0.1589(4)	0.9767(2)	0.054
H(22A)	1.1335(4)	-0.1876(4)	0.8547(2)	0.069
H(22B)	1.2440(4)	-0.2465(4)	0.8806(2)	0.069
H(23A)	1.0723(4)	-0.0205(3)	0.9021(2)	0.053
H(24A)	0.9991(4)	0.1461(4)	0.9496(2)	0.062
H(24B)	1.0659(4)	0.2053(4)	1.0084(2)	0.062
H(25A)	1.2439(4)	0.1346(3)	1.0514(2)	0.054
H(26A)	1.4149(4)	0.0624(4)	1.0976(2)	0.066
H(26B)	1.4654(4)	-0.0489(4)	1.0714(2)	0.066

[a]U_{eq} is defined as one-third of the trace of the orthogonalized U_{ij} tensor.

Table A1.9 Fractional Coordinates and Isotropic Displacement Parameters [Å^2] of 2,4,6-triaminopyrimidine + adipic acid, **6a**

Atom	x/a	y/b	z/c	U_{eq}[a]
C(11)	0.4677(7)	0.4825(4)	-0.0629(5)	0.056(2)
C(12)	0.3269(8)	0.5185(4)	-0.0995(5)	0.057(2)
C(13)	0.2266(7)	0.4919(4)	-0.0060(5)	0.049(2)
O(131)	0.1646(5)	0.5381(2)	0.0644(4)	0.059(1)
O(132)	0.2061(5)	0.4114(3)	-0.0047(4)	0.074(2)
C(21)	0.4215(7)	-0.2880(3)	0.3089(5)	0.043(2)
C(22)	0.5214(7)	-0.2615(3)	0.2112(5)	0.048(2)
C(23)	0.5460(8)	-0.1691(3)	0.2096(5)	0.049(2)
C(24)	0.6450(7)	-0.1412(3)	0.1099(5)	0.043(2)
C(25)	0.6601(9)	-0.0468(3)	0.1127(6)	0.047(2)
C(26)	0.7515(6)	-0.0091(3)	0.0142(5)	0.040(2)
O(261)	0.8157(5)	-0.0515(2)	-0.0612(3)	0.052(1)
O(262)	0.7547(5)	0.0705(2)	0.0144(3)	0.056(1)
C(31)	0.9794(6)	0.1154(3)	-0.2405(5)	0.039(2)
N(32)	0.9043(5)	0.1564(2)	-0.1557(4)	0.043(1)
C(33)	0.9054(7)	0.2414(3)	-0.1553(5)	0.039(2)
C(34)	0.9835(6)	0.2826(3)	-0.2404(5)	0.043(2)
C(35)	1.0584(6)	0.2370(3)	-0.3245(5)	0.040(2)
N(36)	1.0561(5)	0.1527(2)	-0.3260(4)	0.038(1)
N(31)	0.9803(5)	0.0330(3)	- 0.2352(4)	0.048(2)
N(33)	0.8265(6)	0.2789(3)	-0.0713(4)	0.054(2)
N(35)	1.1393(6)	0.2722(3)	-0.4093(4)	0.055(2)
O(211)	0.3666(5)	-0.2422(2)	0.3816(4)	0.067(2)
O(212)	0.4017(6)	-0.3683(2)	0.3105(4)	0.066(2)
H(11A)	0.4596(7)	0.4227(4)	-0.0538(5)	0.068
H(11B)	0.5273(7)	0.4932(4)	-0.1339(5)	0.068
H(12A)	0.3323(8)	0.5787(4)	-0.1000(5)	0.069
H(12B)	0.2974(8)	0.5004(4)	-0.1873(5)	0.069
H(132)	0.1490(5)	0.4003(3)	0.0486(4)	0.112
H(22A)	0.6076(7)	-0.2895(3)	0.2310(5)	0.058
H(22B)	0.4879(7)	-0.2789(3)	0.1242(5)	0.058
H(23A)	0.5806(8)	-0.1519(3)	0.2964(5)	0.059
H(23B)	0.4594(8)	-0.1412(3)	0.1914(5)	0.059
H(24A)	0.6122(7)	-0.1588(3)	0.0227(5)	0.052
H(24B)	0.7332(7)	-0.1668(3)	0.1293(5)	0.052
H(32A)	0.8558(5)	0.1296(2)	-0.1020(4)	0.051
H(34A)	0.9860(6)	0.3403(3)	-0.2415(5)	0.052
H(31A)	1.0299(5)	0.0051(3)	-0.2866(4)	0.058
H(31B)	0.9312(5)	0.0076(3)	-0.1804(4)	0.058
H(33A)	0.8228(6)	0.3322(3)	-0.0687(4)	0.065
H(33B)	0.7791(6)	0.2498(3)	-0.0196(4)	0.065

[a] U_{eq} is defined as one-third of the trace of the orthogonalized U_{ij} tensor.

Table A1.10 Fractional coordinates and Equivalent Isotropic Displacement Parameters [$Å^2$] of cyanuric acid + 4,4'-bipyridyl (methanol), **7a**

Atom	x/a	y/b	z/c	U_{eq} [a]
N(26)	0.1952(3)	0.1613(1)	0.0346(1)	0.043(1)
O(25)	0.2527(3)	0.3985(1)	-0.0612(1)	0.056(1)
O(23)	0.7272(3)	0.2324(1)	0.2669(1)	0.061(1)
N(24)	0.4824(3)	0.3193(2)	0.1056(1)	0.047(1)
O(21)	0.1762(3)	-0.0805(1)	0.1235(1)	0.054(1)
N(22)	0.4440(3)	0.0738(1)	0.2001(1)	0.044(1)
C(11)	0.0758(4)	0.4303(2)	-0.4702(1)	0.042(1)
N(14)	0.3594(3)	0.1670(2)	-0.3584(1)	0.053(1)
C(25)	0.3075(4)	0.3004(2)	0.0208(1)	0.042(1)
C(12)	0.0867(5)	0.3002(2)	-0.5135(2)	0.060(1)
C(16)	0.2150(5)	0.4231(2)	-0.3691(2)	0.055(1)
C(15)	0.3517(5)	0.2919(2)	-0.3174(2)	0.059(1)
C(23)	0.5610(4)	0.2101(2)	0.1966(1)	0.044(1)
C(21)	0.2663(4)	0.0441(2)	0.1203(1)	0.041(1)
C(13)	0.2262(5)	0.1735(2)	-0.4553(2)	0.062(1)
H(26)	0.0853(45)	0.1410(19)	-0.0200(17)	0.054(5)
H(15)	0.4541(48)	0.2872(22)	-0.2509(19)	0.071(6)
H(24)	0.5606(48)	0.4072(25)	0.0967(17)	0.067(6)
H(16)	0.2206(49)	0.5078(24)	-0.3343(19)	0.076(6)
H(13)	0.2273(52)	0.0832(24)	-0.4838(19)	0.082(7)
H(12)	-0.0083(53)	0.2953(24)	-0.5829(20)	0.081(6)
H(22)	0.5036(47)	0.0100(24)	0.2629(18)	0.068(6)

[a]U_{eq} is defined as one-third of the trace of the orthogonalized U_{ij} tensor.

Table A1.11 Fractional coordinates and Equivalent Isotropic Displacement Parameters [Å^2] of Cyanuric acid + 4,4'-bipyridyl + water, **7b**

Atom	x/a	y/b	z/c	U_{eq}[a]
N(23)	0.6364(5)	0.0626(1)	0.2098(5)	0.042(1)
N(22)	0.9433(5)	0.0227(1)	0.2422(5)	0.041(1)
N(21)	0.9387(5)	0.1029(1)	0.2372(5)	0.040(1)
O(23)	1.2358(4)	0.0639(1)	0.2636(4)	0.053(1)
N(12)	1.1113(5)	-0.0686(1)	0.2699(5)	0.046(1)
O(22)	0.6529(4)	-0.0161(1)	0.2359(4)	0.060(1)
O(21)	0.6331(4)	0.1414(1)	0.1933(5)	0.063(1)
C(23)	1.0525(5)	0.0634(1)	0.2499(5)	0.036(1)
C(16)	1.2183(5)	-0.1623(1)	0.2474(5)	0.036(1)
N(11)	1.3805(5)	-0.3048(1)	0.2103(5)	0.046(1)
C(22)	0.7387(6)	0.0204(1)	0.2304(6)	0.041(1)
C(14)	1.2720(5)	-0.2114(1)	0.2317(5)	0.034(1)
C(21)	0.7286(6)	0.1048(1)	0.2124(6)	0.041(1)
C(110)	1.3722(6)	-0.1271(1)	0.3021(6)	0.042(1)
C(15)	1.4494(6)	-0.2241(1)	0.1966(6)	0.044(1)
C(19)	1.3119(7)	-0.0816(1)	0.3110(6)	0.045(1)
C(13)	1.1501(6)	-0.2476(1)	0.2521(6)	0.041(1)
C(17)	1.0091(6)	-0.1485(1)	0.2072(6)	0.043(1)
C(12)	1.2069(6)	-0.2931(1)	0.2390(6)	0.045(1)
C(18)	0.9635(7)	-0.1025(1)	0.2212(6)	0.048(1)
C(11)	1.4986(7)	-0.2700(1)	0.1894(6)	0.045(1)
H(11)	1.6256(58)	-0.2789(1)	0.1685(53)	0.053(11)
H(12)	1.1141(55)	-0.3152(15)	0.2562(52)	0.059(12)
H(13)	1.0373(52)	-0.2406(11)	0.2862(48)	0.033(9)
H(15)	1.5286(53)	-0.2020(11)	0.1712(49)	0.039(10)
H(17)	0.8935(54)	-0.1728(13)	0.1706(50)	0.055(11)
H(21)	0.9938(57)	0.1333(13)	0.2458(54)	0.052(11)
H(110)	1.5193(67)	-0.1370(13)	0.3359(58)	0.068(13)
H(22)	1.0075(68)	-0.0061(15)	0.2534(64)	0.074(14)
H(19)	1.4182(57)	-0.0583(11)	0.3397(52)	0.044(10)
H(18)	0.8222(57)	-0.0945(13)	0.1956(53)	0.057(12)
H(23)	0.5057(77)	0.0641(13)	0.2152(65)	0.071(13)

[a]U_{eq} is defined as one-third of the trace of the orthogonalized U_{ij} tensor.

Table A1.12 Fractional Coordinates and Equivalent Isotropic Displacement Parameters [Å^2] of N-methylcyanuric acid **(8)** and its adduct with water **(8 + H$_2$O)**

Atom	x/a	y/b	z/c	U$_{eq}$^{a}
N(3)	0.7346(21)	0.2500	0.5534(5)	0.034(3)
N(2)	0.7145(19)	0.2500	0.3824(5)	0.030(3)
N(1)	1.0237(20)	0.2500	0.4578(6)	0.036(3)
O(3)	1.0438(15)	0.2500	0.6233(4)	0.049(3)
O(1)	0.4389(17)	0.2500	0.4741(6)	0.054(3)
C(2)	0.9147(24)	0.2500	0.3708(7)	0.033(4)
C(3)	0.9359(25)	0.2500	0.5500(6)	0.029(3)
O(2)	0.9990(14)	0.2500	0.2917(4)	0.058(3)
C(1)	0.6163(26)	0.2500	0.4700(7)	0.041(4)
C(4)	0.6427(23)	0.2500	0.6502(5)	0.051(4)
H(4B)	0.50110(23)	0.2500	0.6432(5)	0.076
H(4C)	0.6832(23)	0.3743	0.6856(5)	0.076
H(4D)	0.6832(23)	0.1257	0.6856(5)	0.076
H(2)	0.6330(350)	0.2500	0.3208(109)	0.198(79)
H(1)	1.1653(179)	0.2500	0.4514(57)	0.015(28)
N-methylcyanuric acid + H$_2$O **(8 + H$_2$O)**				
N(3)	0.0183(5)	0.2500	0.8052(4)	0.040(1)
N(2)	0.2636(5)	0.2500	0.6537(4)	0.038(1)
N(1)	0.3626(5)	0.2500	0.9419(4)	0.044(1)
O(3)	0.6014(4)	0.2500	0.7961(3)	0.073(1)
O(1)	0.1176(4)	0.2500	1.0849(4)	0.063(1)
C(2)	0.4224(7)	0.2500	0.7973(5)	0.040(1)
C(3)	0.0583(6)	0.2500	0.6530(5)	0.038(1)
O(2)	-0.0816(4)	0.2500	0.5268(3)	0.053(1)
C(1)	0.1645(7)	0.2500	0.9540(5)	0.042(1)
C(4)	0.3150(9)	0.2500	0.4918(6)	0.057(2)
H(4B)	0.2716(73)	0.1160(77)	0.4284(59)	0.181(22)
H(4C)	0.4544(84)	0.2500	0.4987(57)	0.084(19)
H(4D)	0.2716	0.3839	0.4284	0.062(10)
H(2)	-0.1237(61)	0.2500	0.8087(42)	0.038(11)
H(1)	0.4722(70)	0.2500	1.0332(51)	0.060(14)
O(4)	-0.2612(5)	0.2500	0.1884(5)	0.061(1)
H(41)	-0.1419(108)	0.2500	0.1329(73)	0.148(26)
H(42)	0.2154(86)	0.2500	0.2773(67)	0.093(24)

^{a}U$_{eq}$ is defined as one-third of the trace of the orthogonalized U$_{ij}$ tensor.

Table A1.13 Fractional Coordinates and Equivalent Isotropic Displacement Parameters [Å^2] of N-methylcyanuric acid + 4,4'-bipyridyl, **8a**

Atom	x/a	y/b	Z/c	U_{eq}[a]
O(21)	0.1233(9)	0.6208(2)	0.7333(1)	0.065(1)
O(23)	0.6138(10)	0.3992(2)	0.6540(2)	0.075(1)
O(22)	0.1084(9)	0.3958(2)	0.8507(1)	0.072(1)
N(24)	0.7560(10)	0.0963(2)	0.6157(2)	0.057(1)
N(23)	0.1024(11)	0.5077(2)	0.7914(2)	0.049(1)
N(22)	0.3559(10)	0.3935(2)	0.7518(2)	0.049(1)
C(11)	1.0090(12)	0.2134(2)	0.5332(2)	0.043(1)
N(21)	0.3673(11)	0.5104(2)	0.6924(2)	0.052(1)
C(17)	1.1370(12)	0.2756(2)	0.4893(2)	0.045(1)
C(16)	0.9767(14)	0.2266(3)	0.5980(2)	0.055(2)
C(21)	0.1946(13)	0.5506(3)	0.7383(2)	0.053(1)
C(18)	1.2777(13)	0.2586(3)	0.4307(2)	0.053(2)
N(110)	1.3779(11)	0.3938(2)	0.4070(2)	0.057(1)
C(22)	0.1870(13)	0.4298(3)	0.8011(2)	0.053(1)
C(23)	0.4599(14)	0.4322(3)	0.6967(2)	0.055(2)
C(112)	1.1215(14)	0.3556(3)	0.5056(2)	0.057(2)
C(13)	0.7911(15)	0.0836(3)	0.5534(2)	0.062(2)
C(111)	1.2410(14)	0.4110(3)	0.4630(2)	0.061(2)
C(15)	0.8543(15)	0.1666(3)	0.6364(3)	0.062(2)
C(19)	1.3942(15)	0.3179(3)	0.3917(2)	0.064(2)
C(24)	0.4461(14)	0.3092(2)	0.7579(2)	0.072(2)
C(12)	0.9099(15)	0.1393(3)	0.5104(3)	0.062(2)
H(24B)	0.5625(14)	0.2921(2)	0.7199(2)	0.108
H(24C)	0.2397(14)	0.2787(2)	0.7631(2)	0.108
H(24D)	0.5949(14)	0.3018(2)	0.7946(2)	0.108
H(18)	1.3171(93)	0.2071(20)	0.4155(16)	0.036(12)
H(19)	1.5064(106)	0.3008(22)	0.3493(19)	0.063(13)
H(112)	1.0171(93)	0.3707(20)	0.5424(16)	0.030(11)
H(16)	1.0644(98)	0.2761(21)	0.6162(16)	0.046(12)
H(12)	0.9234(106)	0.1274(23)	0.4670(18)	0.056(14)
H(23)	0.0182(108)	0.5359(24)	0.8266(18)	0.069(15)
H(21)	0.4755(124)	0.5391(27)	0.6560(22)	0.090(17)
H(13)	0.7158(105)	0.0316(25)	0.5373(16)	0.057(14)
H(111)	1.2217(108)	0.4666(24)	0.4737(17)	0.057(13)
H(15)	0.8620(106)	0.1770(23)	0.6772(18)	0.050(14)

[a] U_{eq} is defined as one-third of the trace of the orthogonalized U_{ij} tensor.

Table A1.14 Fractional Coordinates and Equivalent Isotropic Displacement Parameters [Å²] of 9-ethyladenine

Atom	x/a	y/b	z/c	U$_{eq}$[a]
N(19)	0.6612(5)	0.7413(3)	0.1548(5)	0.052(1)
C(19)	0.6846(5)	0.8432(3)	0.1298(5)	0.045(1)
N(16)	0.7412(5)	1.0575(2)	0.0586(4)	0.060(1)
C(13)	0.6921(5)	0.9271(3)	0.2453(5)	0.046(1)
N(15)	0.7149(5)	1.0956(2)	0.3275(4)	0.055(1)
N(12)	0.6710(5)	0.9294(2)	0.3986(4)	0.058(1)
C(14)	0.7215(5)	1.0286(3)	0.2016(5)	0.048(1)
N(18)	0.7018(4)	0.8703(2)	-0.0159(4)	0.051(1)
C(12)	0.7339(7)	1.2127(3)	0.3333(7)	0.062(1)
C(17)	0.7298(6)	0.9724(3)	-0.0395(6)	0.061(1)
C(11)	0.6864(6)	1.0313(3)	0.4404(6)	0.064(1)
C(22)	0.9171(10)	1.2435(7)	0.3876(13)	0.097(2)

[a]U$_{eq}$ is defined as one-third of the trace of the orthogonalized U$_{ij}$ tensor.

Table A1.15 Fractional Coordinates and Equivalent Isotropic Displacement Parameters [Å²] of 9-ethyladenine + N-methylcyanuric acid, **8b**

Atom	x/a	y/b	z/c	U$_{eq}$[a]
O(21)	0.2554(4)	0.5820(5)	0.9559(3)	0.049(1)
O(23)	0.7827(4)	0.2371(5)	0.7954(3)	0.066(1)
O(22)	0.2082(5)	0.4702(6)	0.6295(3)	0.065(1)
N(23)	0.2265(5)	0.5116(6)	0.7968(3)	0.044(1)
N(22)	0.4977(5)	0.3454(6)	0.7088(3)	0.046(1)
N(21)	0.5186(5)	0.4021(6)	0.8784(4)	0.049(1)
C(23)	0.6113(7)	0.3212(7)	0.7945(4)	0.048(1)
C(22)	0.3036(6)	0.4451(7)	0.7068(4)	0.044(1)
C(21)	0.3279(6)	0.5057(7)	0.8821(4)	0.044(1)
C(24)	0.5911(9)	0.2715(11)	0.6143(6)	0.066(2)
N(15)	0.4347(5)	0.2518(6)	0.3242(3)	0.046(1)
N(11)	0.7320(5)	0.0569(6)	0.2591(3)	0.047(1)
N(14)	0.1686(5)	0.3043(6)	0.2123(3)	0.043(1)
C(17)	0.4748(6)	0.1212(7)	0.1656(4)	0.041(1)
N(13)	0.1946(6)	0.1871(7)	0.0604(4)	0.052(1)
C(16)	0.5372(6)	0.1506(7)	0.2551(4)	0.041(1)
C(15)	0.2776(6)	0.2037(7)	0.1435(4)	0.037(1)
C(14)	0.2506(7)	0.3241(8)	0.2961(4)	0.046(1)
N(12)	0.6254(5)	0.0085(6)	0.1139(3)	0.050(1)
C(12)	0.8627(8)	0.0361(9)	0.3433(4)	0.049(1)
C(13)	0.7740(7)	-0.0233(8)	0.1733(4)	0.050(1)
C(11)	0.8479(11)	-0.1081(11)	0.4417(5)	0.069(2)

[a]U$_{eq}$ is defined as one-third of the trace of the orthogonalized U$_{ij}$ tensor.

Table A1.16 Fractional Coordinates and Equivalent Isotropic Displacement Parameters [Å^2] of cyanuric acid + melamine), **9a**

Atom	x/a	y/b	z/c	U_{eq}[a]
N(2)	0.0879(3)	0.0000	0.3511(12)	0.026(1)
N(1)	0.2114(2)	0.1228(3)	0.1158(8)	0.025(1)
C(2)	0.1293(2)	0.1217(4)	0.2674(10)	0.026(1)
C(1)	0.2529(3)	0.0000	0.0420(14)	0.023(1)
O(2)	0.3247(12)	0.0000	0.1382(50)	0.026(3)
O(1)	0.0832(6)	0.2355(9)	0.2944(25)	0.027(2)
N(4)	0.3360(17)	0.0000	0.0517(65)	0.028(6)
N(3)	0.0973(8)	0.2381(15)	0.3887(31)	0.024(3)

[a]U_{eq} is defined as one-third of the trace of the orthogonalized U_{ij} tensor.

Table A1.17 Fractional Coordinates and Equivalent Isotropic Displacement Parameters [Å^2] of trithiocyanuric acid + melamine), **9b**

Atom	x/a	y/b	z/c	U_{eq}[a]
N(4)	0.0877(3)	0.0000	0.3053(14)	0.025(1)
N(3)	0.2115(2)	0.1226(3)	0.1161(9)	0.024(1)
C(2)	0.1289(3)	0.1213(4)	0.2681(12)	0.025(1)
C(1)	0.2522(4)	0.0000	0.0449(17)	0.023(2)
S(1)	0.0934(4)	0.2371(5)	0.3634(17)	0.053(2)
N(1)	0.0798(11)	0.2359(17)	0.2633(48)	0.023(6)
N(2)	0.3212(12)	0.0000	-0.1745(57)	0.022(6)
S(2)	0.3331(5)	0.0000	-0.0702(23)	0.052(3)

[a]U_{eq} is defined as one-third of the trace of the orthogonalized U_{ij} tensor.

Table A1.18 Fractional Coordinates and Equivalent Isotropic Displacement Parameters [Å^2] of Trithiocyanuric acid + 4,4'-bipyridyl + benzene, **10a**

Atom	x/a	y/b	z/c	U$_{eq}$^{a}
S(15)	0.4757(1)	0.7270(1)	0.3620(1)	0.043(1)
S(13)	0.9800(1)	0.4111(1)	0.7293(1)	0.048(1)
S(11)	0.2342(1)	0.6153(1)	0.9005(1)	0.061(1)
N(16)	0.3739(3)	0.6593(2)	0.6355(2)	0.036(1)
C(21)	-0.3963(3)	0.9607(2)	0.5142(2)	0.036(1)
C(23)	-0.0531(4)	0.8696(3)	0.4405(3)	0.046(1)
N(14)	0.7055(3)	0.5770(2)	0.5607(2)	0.037(1)
C(15)	0.5177(3)	0.6511(2)	0.5256(2)	0.034(1)
N(12)	0.5991(3)	0.5221(2)	0.7932(2)	0.040(1)
C(26)	-0.3457(4)	0.8970(3)	0.6486(3)	0.048(1)
C(13)	0.7538(3)	0.5065(2)	0.6919(2)	0.036(1)
N(24)	-0.0067(3)	0.8083(2)	0.5699(2)	0.042(1)
C(25)	-0.1530(4)	0.8227(3)	0.6718(3)	0.050(1)
C(22)	-0.2433(3)	0.9453(3)	0.4087(3)	0.044(1)
C(11)	0.4090(3)	0.5985(3)	0.7697(2)	0.038(1)
C(32)	0.3681(15)	0.9161(10)	0.0145(5)	0.123(2)
C(31)	0.3024(11)	1.0570(11)	0.0053(5)	0.124(2)
C(33)	0.5667(18)	0.860(7)	0.0086(5)	0.122(2)
H(23)	0.0475(41)	0.8619(27)	0.3709(28)	0.049(7)
H(26)	-0.4415(44)	0.9004(29)	0.7257(31)	0.060(8)
H(14)	0.7929(41)	0.5731(27)	0.4937(29)	0.046(7)
H(22)	-0.2631(41)	0.9883(29)	0.3162(31)	0.056(8)
H(12)	0.6280(40)	0.4826(28)	0.8750(29)	0.049(8)
H(25)	-0.1214(4)	0.7764(30)	0.7641(31)	0.059(8)
H(16)	0.2427(53)	0.7100(35)	0.6155(33)	0.080(10)
H(31)	0.1776(81)	1.0854(61)	0.0109(54)	0.144(25)
H(32)	0.2666(93)	0.8621(66)	0.0190(60)	0.178(26)
H(33)	0.6066(90)	0.7661(65)	0.0139(56)	0.166(25)

^{a}U$_{eq}$ is defined as one-third of the trace of the orthogonalized U$_{ij}$ tensor.

353

Table A1.19 Fractional Coordinates and Equivalent Isotropic Displacement Parameters [Å²] of Trithiocyanuric acid + 4,4'-bipyridyl + toluene, **10b**

Atom	x/a	y/b	z/c	U_{eq} [a]
S(23)	-0.0276(2)	0.7242(2)	-0.1392(2)	0.050(1)
S(22)	0.4802(2)	0.4203(2)	0.2265(2)	0.055(1)
S(21)	-0.2620(3)	0.6208(3)	0.3969(2)	0.078(1)
N(23)	-0.1254(8)	0.6632(6)	0.1327(5)	0.042(1)
C(11)	0.8962(8)	0.0391(7)	-0.0133(6)	0.040(2)
C(15)	0.5564(10)	0.1329(8)	0.0619(7)	0.051(2)
N(22)	0.2043(7)	0.5796(6)	0.0585(5)	0.040(2)
C(12)	0.8423(10)	0.0982(8)	-0.1467(7)	0.053(2)
C(23)	0.0167(8)	0.6525(7)	0.0242(6)	0.039(2)
C(16)	0.7474(9)	0.0571(8)	0.0918(8)	0.051(2)
N(21)	0.1018(7)	0.5305(7)	0.2890(6)	0.047(2)
C(22)	0.2548(9)	0.5123(7)	0.1899(6)	0.041(2)
N(14)	0.5063(7)	0.1881(6)	-0.0667(6)	0.048(1)
C(21)	-0.0887(9)	0.6041(8)	0.2668(7)	0.048(2)
C(13)	0.6479(10)	0.1720(9)	-0.1680(8)	0.060(2)
C(4)	0.9720(27)	0.1184(19)	-0.5106(15)	0.134(5)
C(3)	0.6239(56)	0.0387(50)	-0.4805(40)	0.387(21)
C(5)	0.7661(42)	0.1080(32)	-0.4984(24)	0.219(9)
C(2)	0.8348(53)	-0.1315(38)	-0.4787(31)	0.307(15)
C(6)	0.8490(32)	-0.0158(27)	-0.4903(19)	0.171(7)
C(7)	0.8592(49)	0.2378(36)	-0.5181(30)	0.301(14)
H(16)	0.7713(105)	0.0241(79)	0.1887(78)	0.069(23)
H(15)	0.4484(101)	0.1363(72)	0.1438(71)	0.061(20)
H(12)	0.9390(95)	0.0952(69)	-0.2257(67)	0.051(19)
H(13)	0.6230(99)	0.2074(75)	-0.2653(76)	0.065(21)
H(21)	0.1252(95)	0.4881(72)	0.3658(69)	0.046(21)
H(22)	0.2859(139)	0.5801(84)	-0.0161(81)	0.076(26)
H(23)	-0.2518(139)	0.7025(102)	0.1114(94)	0.112(34)

[a] U_{eq} is defined as one-third of the trace of the orthogonalized U_{ij} tensor.

Table A1.20 Fractional Coordinates and Equivalent Isotropic Displacement
Parameters [Å^2] of Trithiocyanuric acid + 4,4'-bipyridyl + p-Xylene, **10c**

Atom	x/a	y/b	z/c	U$_{eq}$^{a}
C(11)	0.1540(13)	0.4761(12)	0.3386(7)	0.095(5)
C(12)	0.0723(14)	0.4867(16)	0.4217(9)	0.074(5)
C(13)	0.0633(13)	0.3877(15)	0.4666(10)	0.067(5)
C(14)	-0.0071(15)	0.3950(13)	0.5422(10)	0.075(5)
C(21)	0.3399(15)	0.4697(16)	0.1514(8)	0.134(8)
C(22)	0.4219(18)	0.4815(22)	0.0741(11)	0.089(6)
C(23)	0.4954(23)	0.3858(15)	0.0240(15)	0.099(7)
C(24)	0.5688(16)	0.4048(22)	-0.0487(12)	0.089(7)
N(31)	0.7886(8)	0.1010(7)	-0.4436(4)	0.039(3)
S(31)	0.7537(3)	0.2045(3)	-0.3161(2)	0.064(1)
C(31)	0.6968(10)	0.1744(9)	-0.3842(5)	0.035(3)
S(32)	0.8706(3)	-0.0138(3)	-0.5752(2)	0.051(1)
N(32)	0.6100(8)	0.1249(7)	-0.5020(4)	0.038(2)
C(32)	0.7529(10)	0.0713(9)	-0.5060(6)	0.036(3)
S(33)	0.3355(3)	0.2454(3)	-0.4452(2)	0.048(1)
N(33)	0.5547(8)	0.2174(7)	-0.3863(4)	0.034(2)
C(33)	0.5028(10)	0.1925(9)	-0.4445(6)	0.034(3)
C(41)	0.5493(10)	0.4616(9)	0.4666(5)	0.033(3)
C(42)	0.4973(10)	0.4350(10)	0.4100(5)	0.046(3)
C(43)	0.5926(11)	0.3632(10)	0.3504(6)	0.045(3)
N(44)	0.7330(9)	0.3131(8)	0.3422(4)	0.042(3)
C(45)	0.7836(11)	0.3395(10)	0.3961(6)	0.049(3)
C(46)	0.6961(10)	0.4106(9)	0.4583(5)	0.042(3)
C(51)	0.1641(10)	0.5173(9)	-0.1476(6)	0.036(3)
C(52)	0.3041(11)	0.4571(11)	-0.1506(6)	0.060(4)
C(53)	0.3933(12)	0.3843(11)	-0.2112(7)	0.066(4)
N(54)	0.3485(9)	0.3652(8)	-0.2695(5)	0.044(3)
C(55)	0.2119(11)	0.4242(10)	-0.2663(6)	0.044(3)
C(56)	0.1167(11)	0.4990(10)	-0.2080(6)	0.050(3)
C(57)	0.0648(10)	0.5985(9)	-0.0822(6)	0.035(3)
C(58)	0.1193(11)	0.6214(9)	-0.0248(6)	0.044(1)
C(59)	0.0246(11)	0.6935(9)	0.0354(5)	0.043(3)
S(61)	-0.5574(3)	1.1074(3)	0.3712(2)	0.044(1)
C(61)	-0.4533(11)	1.0193(9)	0.2968(5)	0.031(3)
N(61)	-0.2838(8)	0.8811(7)	0.1717(4)	0.036(2)
S(62)	-0.0479(3)	0.8147(3)	0.2247(2)	0.047(1)
N(62)	-0.5035(8)	1.0057(8)	0.2382(4)	0.040(2)
C(62)	-0.2172(10)	0.8864(9)	0.2277(5)	0.027(3)
S(63)	-0.4993(3)	0.9332(3)	0.1066(2)	0.060(1)
N(63)	-0.3086(7)	0.9537(7)	0.2893(4)	0.038(3)
C(63)	-0.4262(10)	0.9414(9)	0.1740(5)	0.033(3)
S(71)	0.1348(3)	1.1583(3)	0.2762(2)	0.056(1)
N(71)	-0.448(8)	1.0773(7)	0.1057(4)	0.031(2)
C(71)	0.0651(10)	1.1217(9)	0.2142(5)	0.031(3)
S(72)	-0.3138(3)	1.2120(3)	0.1694(2)	0.042(1)
C(72)	-0.1407(10)	1.1519(9)	0.1641(5)	0.031(3)

Table A1.20 (*continued*)

N(72)	-0.0794(8)	1.1699(7)	0.2180(4)	0.036(2)
S(73)	0.2063(3)	0.9330(3)	0.0265(2)	0.046(1)
N(73)	0.1462(8)	1.0464(7)	0.1550(4)	0.040(3)
C(73)	0.0983(10)	1.0218(9)	0.0985(5)	0.040(3)
N(510)	-0.1142(9)	0.7425(7)	0.0431(5)	0.038(2)
C(511)	-0.0803(10)	0.6513(10)	-0.0724(6)	0.047(3)
H(11C)	0.1457(13)	0.5585(12)	0.3180(7)	0.142
H(11B)	0.1140(13)	0.4374(12)	0.3111(7)	0.142
H(11A)	0.2532(13)	0.4256(12)	0.3348(7)	0.142
H(13)	0.1077(13)	0.3082(15)	0.4453(10)	0.081
H(14)	-0.0115(15)	0.3225(13)	0.5691(10)	0.091
H(21C)	0.3437(15)	0.3845(16)	0.1607(8)	0.201
H(21B)	0.2420(15)	0.5254(16)	0.1571(8)	0.201
H(21A)	0.3808(15)	0.4914(16)	0.1867(8)	0.201
H(223)	0.4965(23)	0.3053(15)	0.0389(15)	0.119
H(24)	0.6132(16)	0.3371(22)	-0.0812(12)	0.107
H(31)	0.8777(8)	0.0697(7)	-0.4426(4)	0.047
H(32)	0.5831(8)	0.1151(7)	-0.5407(4)	0.046
H(33)	0.4930(8)	0.2627(7)	-0.3496(4)	0.041
H(42)	0.3994(10)	0.4655(10)	0.4127(5)	0.055
H(43)	0.5554(11)	0.3486(10)	0.3129(6)	0.053
H(45)	0.8822(11)	0.3084(10)	0.3914(6)	0.059
H(46)	0.7362(10)	0.4242(9)	0.4948(5)	0.050
H(52)	0.3412(11)	0.4647(11)	-0.1112(6)	0.072
H(53)	0.4902(12)	0.3461(11)	-0.2118(7)	0.079
H(55)	0.1770(11)	0.4148(10)	-0.3062(6)	0.052
H(56)	0.0205(11)	0.5375(10)	-0.2088(6)	0.059
H(58)	0.2173(11)	0 .5887(9)	-0.0275(6)	0.053
H(59)	0.0619(11)	0.7080(9)	0.0729(5)	0.051
H(61)	-0.2311(8)	0.8365(7)	0.1329(4)	0.043
H(62)	-0.5944(8)	1.0417(8)	0.2423(4)	0.048
H(63)	-0.2729(7)	0.9553(7)	0.3263(4)	0.046
H(71)	-0.0788(8)	1.0647(7)	0.0706(4)	0.037
H(72)	-0.1352(8)	1.2140(7)	0.2565(4)	0.043
H(73)	0.2364(8)	1.0109(7)	0.1529(4)	0.048
H(511)	-0.2652(11)	0.7593(10)	-0.0063(6)	0.057
H(512)	-0.1222(10)	0.6385(10)	-0.1083(6)	0.057

[a] U_{eq} is defined as one-third of the trace of the orthogonalized U_{ij} tensor.

Table A1.21 Fractional Coordinates and Equivalent Isotropic Displacement Parameters [Å²] of Trithiocyanuric acid + 4,4'-bipyridyl + o-xylene, **10d**

Atom	x/a	y/b	z/c	U_eq[a]
S(13)	0.0302(2)	0.2795(1)	0.1381(1)	0.055(1)
S(11)	-0.4810(2)	0.5733(1)	-0.2250(1)	0.058(1)
S(12)	0.2609(2)	0.3787(2)	-0.3947(1)	0.068(1)
N(13)	0.1239(5)	0.3367(4)	-0.1315(4)	0.044(1)
C(21)	0.8963(6)	0.0385(4)	-0.0134(4)	0.044(1)
N(12)	-0.2024(5)	0.4197(4)	-0.0591(4)	0.045(1)
C(25)	0.5595(7)	0.1345(6)	0.0617(5)	0.060(1)
C(13)	-0.0159(6)	0.3478(4)	0.0234(4)	0.041(1)
N(11)	-0.1035(5)	0.4655(4)	-0.2874(4)	0.045(1)
C(12)	0.0878(6)	0.3940(5)	-0.2654(4)	0.044(1)
N(24)	0.5059(5)	0.1878(4)	-0.0646(4)	0.051(1)
C(23)	0.8374(8)	0.0949(6)	-0.1429(5)	0.068(2)
C(11)	-0.2554(6)	0.4837(4)	-0.1879(4)	0.043(1)
C(22)	0.7495(7)	0.0608(6)	0.0915(5)	0.060(1)
C(21)	0.6453(7)	0.1672(7)	-0.1639(6)	0.072(2)
C(4)	-0.0971(70)	0.2325(26)	0.4832(21)	0.298(22)
C(3)	-0.2649(46)	0.1190(39)	0.5024(17)	0.377(25)
C(5)	0.1772(74)	0.1242(29)	0.4741(16)	0.305(26)
C(1)	0.0651(29)	-0.0916(14)	0.5038(8)	0.148(4)
C(2)	-0.1651(23)	-0.0080(23)	0.5137(11)	0.162(4)
C(7)	-0.3157(125)	-0.0530(141)	0.5063(106)	1.499(154)
H(12)	-0.2814(62)	0.4275(40)	0.0027(44)	0.033(11)
H(22)	0.7720(77)	0.0356(54)	0.1768(60)	0.069(15)
H(25)	0.4582(81)	0.1526(52)	0.1302(56)	0.068(15)
H(11)	-0.1281(60)	0.5003(42)	-0.3596(46)	0.031(12)
H(23)	0.9185(81)	0.0866(53)	-0.2134(58)	0.064(16)
H(21)	0.6177(107)	0.2047(76)	-0.2473(79)	0.119(25)
H(13)	0.2398(96)	0.2926(63)	-0.1141(62)	0.086(19)

[a]U_{eq} is defined as one-third of the trace of the orthogonalized U_{ij} tensor.

Table A1.22 Fractional Coordinates and Equivalent Isotropic Displacement Parameters [$Å^2$] of Trithiocyanuric acid + 4,4'-bipyridyl + m-xylene, **10e**

Atom	x/a	y/b	z/c	U_{eq}^a
S(33)	0.3383(3)	0.7219(2)	0.2772(3)	0.060(1)
S(22)	1.4957(3)	0.6680(2)	0.6127(2)	0.060(1)
S(31)	0.8137(3)	0.5610(2)	0.3076(3)	0.066(1)
S(32)	0.6975(3)	0.9696(2)	0.5530(3)	0.065(1)
S(21)	1.0324(3)	0.8363(3)	0.5421(3)	0.072(1)
S(23)	1.1430(3)	0.4044(3)	0.3413(3)	0.073(1)
N(33)	0.5786(8)	0.6509(7)	0.3012(3)	0.049(2)
N(23)	1.3073(8)	0.5515(7)	0.4783(7)	0.053(3)
N(32)	0.5312(7)	0.8346(7)	0.4074(7)	0.048(2)
N(22)	1.1055(8)	0.6227(7)	0.4495(7)	0.053(3)
C(33)	0.4894(9)	0.7350(9)	0.3312(8)	0.044(3)
N(110)	1.5019(9)	0.4567(7)	0.1401(7)	0.054(2)
C(23)	1.1859(10)	0.5290(9)	0.4243(9)	0.052(3)
N(21)	1.2577(7)	0.7371(7)	0.5703(7)	0.049(2)
C(32)	0.6512(9)	0.8520(9)	0.4620(9)	0.048(3)
C(15)	1.4452(11)	-0.0401(9)	-0.2144(10)	0.064(3)
C(16)	1.4806(10)	0.0568(9)	-0.1341(9)	0.061(3)
N(14)	1.3305(9)	-0.0522(8)	-0.2729(8)	0.061(3)
C(112)	1.3408(11)	0.3267(10)	0.0359(10)	0.068(4)
C(22)	1.3472(9)	0.6522(8)	0.5519(8)	0.044(3)
C(11)	1.3978(10)	0.1495(9)	-0.1090(9)	0.050(3)
N(31)	0.7334(8)	0.7596(7)	0.4274(7)	0.056(3)
C(12)	1.2800(10)	0.1386(9)	-0.1699(9)	0.056(3)
C(18)	1.5611(11)	0.2931(9)	0.0054(9)	0.061(3)
C(17)	1.4322(10)	0.2582(9)	-0.0218(9)	0.050(3)
C(31)	0.7034(10)	0.6605(8)	0.3461(9)	0.049(3)
C(111)	1.3787(12)	0.4231(9)	0.1136(10)	0.067(4)
C(21)	1.1350(9)	0.7278(9)	0.5194(9)	0.049(3)
C(19)	1.5901(11)	0.3924(10)	0.0851(10)	0.067(4)
C(13)	1.2501(11)	0.0371(10)	-0.2498(10)	0.063(3)
C(7)	1.8245(20)	-0.0783(22)	-0.1626(18)	0.152(8)
C(4)	1.9104(35)	0.2574(57)	0.0537(35)	0.251(28)
C(2)	1.8521(17)	0.0846(18)	0.0069(27)	0.140(8)
C(1)	1.8663(18)	0.0544(28)	-0.1108(29)	0.150(10)
C(3)	1.8786(29)	0.2157(30)	0.1251(37)	0.208(18)
C(5)	1.9341(29)	0.2726(31)	-0.0352(49)	0.177(20)
C(6)	1.9121(22)	0.1457(54)	-0.1616(32)	0.243(21)
C(8)	1.9649(30)	0.3288(71)	-0.1027(52)	0.459(46)
H(33A)	0.5554(8)	0.5889(7)	0.2518(7)	0.059
H(23A)	1.3631(8)	0.4969(7)	0.4642(7)	0.064
H(32A)	0.4772(7)	0.8908(7)	0.4219(7)	0.058
H(22A)	1.0285(8)	0.6139(7)	0.4177(7)	0.064
H(21A)	1.2791(7)	0.8013(7)	0.6172(7)	0.059
H(15A)	1.5037(11)	-0.1009(9)	-0.2293(10)	0.077
H(16A)	1.5615(10)	0.0604(9)	-0.0959(9)	0.074
H(11B)	1.2531(11)	0.3065(10)	0.0214(10)	0.081

Table A1.22 (*continued*)

H(31A)	0.8101(8)	0.7647(7)	0.4597(7)	0.067
H(12A)	1.2209(10)	0.1991(9)	-0.1537(9)	0.068
H(18A)	1.6270(11)	0.2494(9)	-0.0303(9)	0.074
H(11C)	1.3150(12)	0.4687(9)	0.1507(10)	0.081
H(19A)	1.6769(11)	0.4157(10)	0.1013(10)	0.081
H(13A)	1.1698(11)	0.0311(10)	-0.2894(10)	0.076

[a]U_{eq} is defined as one-third of the trace of the orthogonalized U_{ij} tensor.

Table A1.23 Fractional Coordinates and Equivalent Isotropic Displacement Parameters [Å] of Trithiocyanuric acid + 4,4'-bipyridyl + anthracene, **10f**

Atom	x/a	y/b	z/c	U_{eq}[a]
S(43)	0.4758(3)	0.3144(3)	0.3843(3)	0.046(1)
S(41)	0.9776(3)	0.4704(3)	0.3140(3)	0.045(1)
S(35)	1.1107(3)	1.1648(3)	0.7228(3)	0.045(1)
S(45)	0.8934(3)	0.8109(2)	0.5871(2)	0.042(1)
S(31)	1.6450(3)	1.3765(3)	0.7092(3)	0.053(1)
S(33)	1.2719(3)	0.8696(3)	0.4767(3)	0.045(1)
N(44)	0.6998(9)	0.5581(7)	0.4789(7)	0.035(2)
N(42)	0.7342(9)	0.4046(7)	0.3609(7)	0.033(2)
N(36)	1.3731(9)	1.2565(8)	0.7067(7)	0.032(2)
N(46)	0.9109(9)	0.6248(8)	0.4437(7)	0.039(2)
N(34)	1.2157(9)	1.0337(7)	0.6070(7)	0.034(2)
N(32)	1.4412(8)	1.1294(8)	0.5964(7)	0.034(2)
C(21)	1.5090(10)	1.7524(9)	1.0035(9)	0.029(2)
C(35)	1.2367(11)	1.1508(9)	0.6777(9)	0.033(3)
C(27)	1.5558(11)	1.8881(9)	1.0810(9)	0.032(2)
C(33)	1.3107(10)	1.0167(10)	0.5620(9)	0.031(2)
C(45)	0.8331(11)	0.6594(10)	0.4993(8)	0.032(2)
N(29)	1.6393(10)	2.1448(8)	1.2230(7)	0.039(2)
C(210)	1.5074(13)	2.0442(11)	1.1964(10)	0.046(3)
C(28)	1.7289(12)	2.1181(10)	1.1783(10)	0.047(3)
C(43)	0.6441(11)	0.4300(10)	0.4096(9)	0.033(3)
C(26)	1.3738(13)	1.6454(10)	0.9754(10)	0.049(3)
N(24)	1.4274(9)	1.5001(8)	0.8554(7)	0.035(2)
C(211)	1.4648(12)	1.9176(11)	1.1277(10)	0.047(3)
C(25)	1.3368(12)	1.5226(10)	0.9016(10)	0.045(3)
C(41)	0.8694(11)	0.4990(9)	0.3746(8)	0.031(2)
C(22)	1.6055(12)	1.7275(11)	0.9601(10)	0.052(3)
C(27)	1.6936(12)	1.9936(10)	1.1088(10)	0.044(3)
C(31)	1.4817(11)	1.2514(9)	0.6705(9)	0.034(3)
C(23)	1.5580(13)	1.6003(11)	0.8851(10)	0.053(3)
C(13)	0.9156(13)	0.9345(13)	0.8815(10)	0.056(4)
C(15)	0.8955(13)	1.1405(15)	0.8613(12)	0.061(4)
C(14)	0.9464(12)	0.8671(11)	0.9297(10)	0.052(3)
C(12)	0.9698(12)	0.8671(11)	0.9490(10)	0.047(3)
C(17)	1.0132(18)	1.3353(15)	1.0326(18)	0.089(6)
C(16)	0.9316(16)	1.2721(16)	0.9127(16)	0.074(4)
C(11)	0.9373(14)	0.7304(13)	0.9018(14)	0.070(4)
H(44A)	0.6463(9)	0.5760(7)	0.5123(7)	0.042
H(42A)	0.7040(9)	0.3243(7)	0.3190(7)	0.039
H(36A)	1.3916(9)	1.3319(8)	0.7511(7)	0.038
H(46A)	0.9941(9)	0.6870(8)	0.4522(7)	0.046
H(34A)	1.1337(9)	0.9644(7)	0.5898(7)	0.041
H(32A)	1.504398	1.1231(8)	0.5687(7)	0.041
H(21A)	1.4415(13)	2.0596(11)	1.2251(10)	0.055
H(28A)	1.8211(12)	2.1877(10)	1.1949(10)	0.056
H(26A)	1.3073(13)	1.6557(10)	1.0059(10)	0.059

Table A1.23 (*continued*)

H(21B)	1.3718(12)	1.8501(11)	1.1125(10)	0.056
H(25A)	1.2443(12)	1.4523(10)	0.8834(10)	0.054
H(22A)	1.7010(12)	1.7944(11)	0.9805(10)	0.062
H(27A)	1.7614(12)	1.9808(10)	1.0811(10)	0.052
H(23A)	1.6231(13)	1.5864(11)	0.8546(10)	0.064
H(13A)	0.8580(13)	0.8909(13)	0.8032(10)	0.068
H(15A)	0.8384(13)	1.0994(15)	0.7827(12)	0.073
H(17A)	1.0327(18)	1.4226(15)	1.0660(18)	0.107
H(16A)	0.9017(16)	1.3198(16)	0.8675(16)	0.089
H(11A)	0.8803(14)	0.6863(13)	0.8235(14)	0.084

[a]U_{eq} is defined as one-third of the trace of the orthogonalized U_{ij} tensor.

Table A1.24 Fractional Coordinates and Equivalent Isotropic Displacement Parameters [Å²] of cyanuric acid + silver nitrate, **Ag₂CA**

Atom	x/a	y/b	z/c	U_{eq}[a]
Ag(1)	0.0000	0.0000	-0.5000	0.019(1)
Ag(2)	0.0000	0.1844(1)	-0.7500	0.026(1)
O(3)	0.0974(3)	0.2217(3)	-0.4258(7)	0.022(1)
N(3)	0.1420(4)	0.0559(4)	-0.3481(7)	0.016(1)
C(3)	0.1609(4)	0.1581(4)	-0.3394(8)	0.014(1)
Ag(3)	0.4343(1)	-0.0903(1)	-0.0767(1)	0.024(1)
O(2)	0.1982(4)	-0.1054(3)	-0.2827(7)	0.024(1)
N(2)	0.3146(4)	0.0221(4)	-0.1750(7)	0.015(1)
N(1)	0.2545(4)	0.1893(4)	-0.2342(8)	0.019(1)
C(2)	0.2179(5)	-0.0116(4)	-0.2684(9)	0.014(1)
C(1)	0.3324(5)	0.1230(5)	-0.1547(9)	0.016(1)
O(1)	0.4173(3)	0.1611(3)	-0.0717(7)	0.025(1)

[a] U_{eq} is defined as one-third of the trace of the orthogonalized U_{ij} tensor.

362

2. Appendices for PART 2 (A2)

Disodium croconate trihydrate I

Table A2.1a Fractional Coordinates and Equivalent Isotropic Displacement Parameters [Å²] of I.

Atom	x/a	y/b	z/c	U_{eq}[a]
Na(1)	0.2469(1)	0.4489(1)	0.0146(1)	0.015(1)
Na(2)	0.2759(1)	0.7149(1)	0.8794(1)	0.020(1)
O(2)	0.2430(1)	0.3921(1)	0.4171(1)	0.015(1)
O(3)	0.3657(1)	0.3417(1)	0.6937(1)	0.016(1)
O(4)	0.3605(1)	0.5346(1)	0.8409(1)	0.015(1)
O(5)	0.2417(1)	0.6996(1)	0.6525(1)	0.016(1)
C(5)	0.2613(1)	0.6084(1)	0.6250(1)	0.011(1)
C(4)	0.3201(1)	0.5242(1)	0.7196(1)	0.011(1)
C(2)	0.2622(1)	0.4544(1)	0.5079(1)	0.010(1)
O(1)	0.1873(1)	0.6141(1)	0.3899(1)	0.015(1)
C(3)	0.3214(1)	0.4292(1)	0.6472(1)	0.011(1)
C(1)	0.2312(1)	0.5653(1)	0.4940(1)	0.011(1)
O(12)	0.4025(1)	0.3040(1)	0.9545(1)	0.015(1)
O(11)	0.1202(1)	0.5839(1)	0.1234(1)	0.017(1)
O(10)	0.1046(1)	0.3385(1)	0.1549(1)	0.017(1)
H(10B)	0.1865(25)	0.2760(7)	0.1679(18)	0.050(5)
H(12B)	0.3393(24)	0.2370(5)	0.9479(17)	0.047(5)
H(12A)	0.4055(26)	0.3171(12)	0.8664(5)	0.044(5)
H(11B)	0.1478(29)	0.5835(14)	0.2165(2)	0.056(5)
H(10A)	0.1391(26)	0.3595(13)	0.2444(5)	0.048(5)
H(11A)	0.1557(27)	0.6544(4)	0.1159(17)	0.051(5)

[a]U_{eq} is defined as one-third of the trace of the orthogonalized U_{ij} tensor.

Table A2.1b Rigid-Body Model Libration Corrections for Bond Distances and "Hirshfeld Rigid-Bond" Test I

Bond	Bond Distance		Components of the Correction			Vibration Along the Interatomic Bond			
	Obsd	Calcd	Del(L)	Del(M)	Del(N)	I to J	J to I	Difference	Sqrt(Diff)
C(1) - C(2)	1.4681	1.4705	0.0018	-0.0016	-0.0002	0.0102	0.0099	0.0003	0.0172
C(2) - C(3)	1.4665	1.4686	-0.0007	-0.0021	-0.0001	0.0108	0.0112	0.0004	0.0209
C(3) - C(4)	1.4657	1.4679	-0.0022	0.0003	0	0.0101	0.0095	0.0006	0.0240
C(4) - C(5)	1.4713	1.4736	-0.0007	0.0022	0.0001	0.0110	0.0114	0.0004	0.0199
C(1) - C(5)	1.4686	1.4707	-0.0018	-0.0011	-0.0002	0.0121	0.0123	0.0002	0.0141
O(1) - C(1)	1.2452	1.2471	0	-0.0019	-0.0002	0.0099	0.0104	0.0005	0.0233
O(2) - C(2)	1.2465	1.2483	-0.0018	-0.0003	0	0.0098	0.0098	0	0.0055
O(3) - C(3)	1.2497	1.2517	-0.0011	0.0017	0.0001	0.0080	0.0096	0.0016	0.0400
O(4) - C(4)	1.2555	1.2573	0.0012	0.0014	0.0001	0.0102	0.0108	0.0006	0.0252
O(5) - C(5)	1.2445	1.2465	0.0018	-0.0008	0	0.0086	0.0091	0.0005	0.0225

Sqrt(Sum(DelJ**2)/Nrb) = 0.0007

Table A2.1c Multipole populations I

Atom	M-	D1-	D0	D1+	Q1-	Q0	Q1+	Q2-	Q2+	O1-	O0	O1+	O2-	O2+	O3-	O3+	H0	H1+	H1-	H2+	H2-	H3+	H3-	H4+	H4-
Na(1)	0.48(7)	-0.15(8)	0.12(9)	0.09(7)	-0.03(7)	-0.04(8)	0.09(6)	0.14(7)	0.19(10)	0.06(7)	-0.14(8)	-0.03(7)	0.10(6)	0.10(7)	0.11(7)	0.13(7)	0.07(7)	0.19(7)	0.02(6)	0.09(7)	-0.17(6)	0.03(6)	-0.14(7)	0.13(6)	0.06(6)
Na(2)	0.48(7)	-0.15(8)	0.12(9)	0.09(7)	-0.03(7)	-0.04(8)	0.09(6)	0.14(7)	0.19(10)	0.06(7)	-0.14(8)	-0.03(7)	0.10(6)	0.10(7)	0.11(7)	0.13(7)	0.07(7)	0.19(7)	0.02(6)	0.09(7)	-0.17(6)	0.03(6)	-0.14(7)	0.13(6)	0.06(6)
C(1)	4.07(3)	-0.01(1)	0.03(2)	0.01(1)	-0.01(1)	0.18(2)	-0.04(1)	-0.01(2)	-0.11(1)	-0.02(1)	0.25(1)	-0.01(1)	0.03(2)	0.16(1)	-0.02(1)	0.02(1)									
C(2)	4.07(3)	-0.01(1)	0.03(2)	0.01(1)	-0.01(1)	0.18(2)	-0.04(1)	-0.01(2)	-0.11(1)	-0.02(1)	0.25(1)	-0.01(1)	0.03(2)	0.16(1)	-0.02(1)	0.02(1)									
C(3)	4.07(3)	-0.01(1)	0.03(2)	0.01(1)	-0.01(1)	0.18(2)	-0.04(1)	-0.01(2)	-0.11(1)	-0.02(1)	0.25(1)	-0.01(1)	0.03(2)	0.16(1)	-0.02(1)	0.02(1)									
C(4)	4.07(3)	-0.01(1)	0.03(2)	0.01(1)	-0.01(1)	0.18(2)	-0.04(1)	-0.01(2)	-0.11(1)	-0.02(1)	0.25(1)	-0.01(1)	0.03(2)	0.16(1)	-0.02(1)	0.02(1)									
C(5)	4.07(3)	-0.01(1)	0.03(2)	0.01(1)	-0.01(1)	0.18(2)	-0.04(1)	-0.01(2)	-0.11(1)	-0.02(1)	0.25(1)	-0.01(1)	0.03(2)	0.16(1)	-0.02(1)	0.02(1)									
O(1)	6.13(2)	0.03(1)	-0.07(2)	-0.01(1)	-0.03(1)	-0.07(2)	0.01(1)	-0.00(1)	-0.04(1)	0.00(1)	0.01(1)	-0.01(1)	-0.01(1)	0.02(1)	0.00(1)	-0.01(1)									
O(2)	6.13(2)	0.03(1)	-0.07(2)	-0.01(1)	-0.03(1)	-0.07(2)	0.01(1)	-0.00(1)	-0.04(1)	0.00(1)	0.01(1)	-0.01(1)	-0.01(1)	0.02(1)	0.00(1)	-0.01(1)									
O(3)	6.13(2)	0.03(1)	-0.07(2)	-0.01(1)	-0.03(1)	-0.07(2)	0.01(1)	-0.00(1)	-0.04(1)	0.00(1)	0.01(1)	-0.01(1)	-0.01(1)	0.02(1)	0.00(1)	-0.01(1)									
O(4)	6.13(2)	0.03(1)	-0.07(2)	-0.01(1)	-0.03(1)	-0.07(2)	0.01(1)	-0.00(1)	-0.04(1)	0.00(1)	0.01(1)	-0.01(1)	-0.01(1)	0.02(1)	0.00(1)	-0.01(1)									
O(5)	6.13(2)	0.03(1)	-0.07(2)	-0.01(1)	-0.03(1)	-0.07(2)	0.01(1)	-0.00(1)	-0.04(1)	0.00(1)	0.01(1)	-0.01(1)	-0.01(1)	0.02(1)	0.00(1)	-0.01(1)									

Table A2.1c *(continued)*

O(10)	6.10(6)	0.05(4)	-0.03(5)	-0.17(5)	-0.16(5)	0.04(4)	0.17(4)	0.02(4)	0.08(4)	0.03(3)	-0.02(3)	-0.04(3)	-0.02(3)	-0.03(2)	-0.00(3)	-0.02(3)
O(11)	6.18(6)	0.04(4)	-0.05(5)	-0.02(5)	0.02(5)	0.11(4)	0.05(4)	0.11(4)	0.03(4)	0.09(3)	-0.03(3)	-0.05(3)	0.01(3)	0.01(2)	0.02(3)	-0.03(3)
O(12)	6.11(6)	0.01(3)	-0.05(5)	-0.04(5)	-0.05(5)	0.06(4)	0.11(4)	0.15(4)	0.09(4)	0.08(3)	-0.03(3)	-0.02(3)	0.05(3)	0.01(2)	-0.01(3)	-0.03(3)
(H10A)	0.91(7)	0.02(4)	-0.10(4)	0.01(5)												
(H10B)	1.02(7)	-0.01(4)	-0.11(4)	0.20(5)												
(H11A)	0.84(7)	-0.03(4)	0.06(4)	0.16(5)												
(H11B)	0.91(7)	0.06(4)	-0.05(4)	0.02(5)												
(H12A)	1.04(7)	-0.06(4)	-0.05(4)	0.07(5)												
(H12B)	0.88(7)	0.02(4)	-0.06(4)	0.07(5)												

Disodium croconate trihydrate
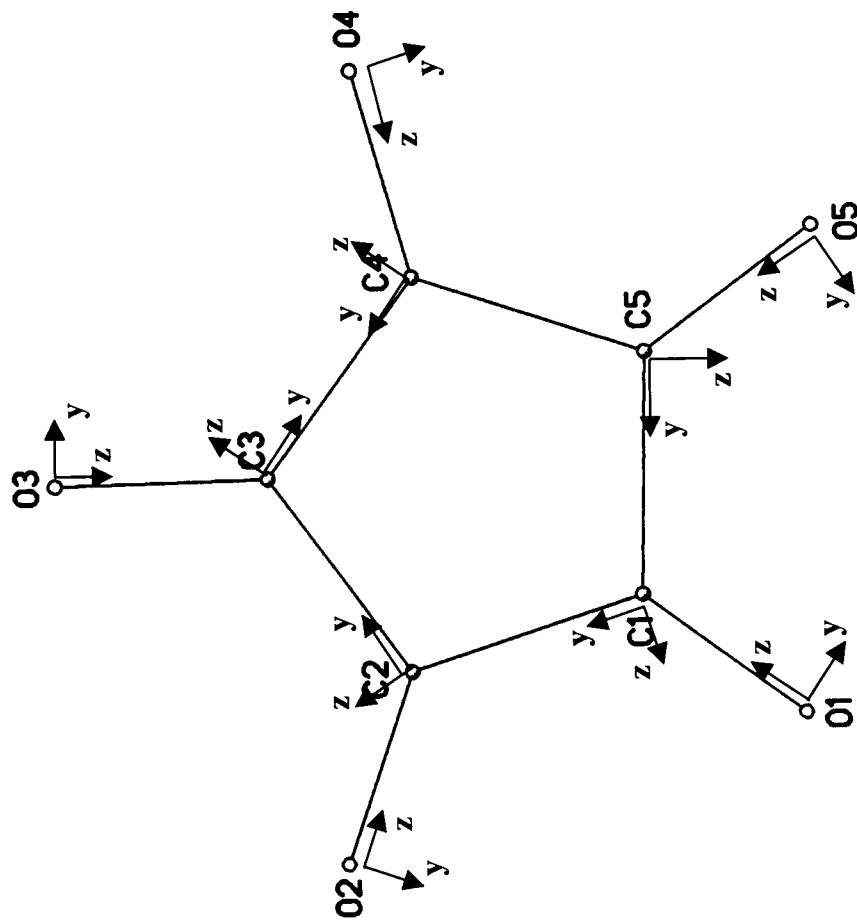
A2.1d Definition of local coordination

Disodium croconate trihydrate
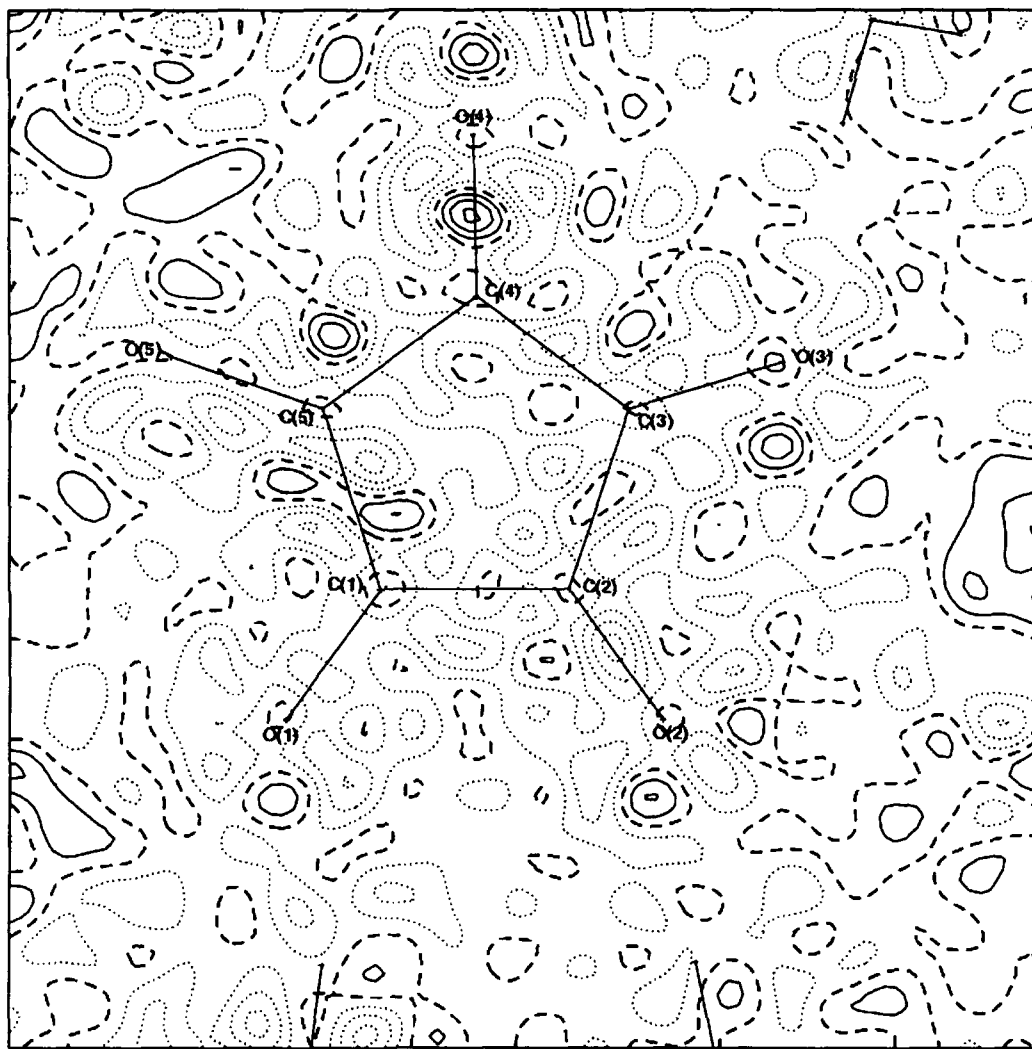
A2.1e Residual electron density map in the plane of the croconate ring (contours at 0.1 eÅ^{-3})

Disodium squarate trihydrate II

Table A2.2a Fractional Coordinates and Equivalent Isotropic Displacement Parameters [Å²] of II

Atom	x/a	y/b	z/c	U_{eq}[a]
Na(1)	0.7644(1)	0.5059(1)	0.0265(1)	0.010(1)
Na(2)	0.5928(1)	0.6321(1)	0.4021(1)	0.011(1)
O(1)	0.4411(1)	0.3365(1)	0.0873(1)	0.010(1)
O(4)	0.2225(1)	0.0849(1)	0.2957(1)	0.012(1)
O(3)	0.0273(1)	-0.3430(1)	-0.0943(1)	0.010(1)
O(2)	0.2568(1)	-0.1011(1)	-0.2982(1)	0.011(1)
C(3)	0.1458(1)	-0.1569(1)	-0.0419(1)	0.007(1)
C(4)	0.2335(1)	0.0381(1)	0.1350(1)	0.008(1)
C(2)	0.2476(1)	-0.0465(1)	-0.1341(1)	0.008(1)
C(1)	0.3332(1)	0.1505(1)	0.0402(1)	0.007(1)
O(7)	0.4208(1)	0.7826(1)	0.2826(1)	0.013(1)
O(6)	0.2595(1)	0.5307(1)	0.4798(1)	0.013(1)
O(5)	0.9397(1)	0.7735(1)	0.3463(1)	0.014(1)
H(7B)	0.5240(18)	0.9014(13)	0.2842(20)	0.040(4)
H(6B)	0.2594(23)	0.6529(12)	0.5638(15)	0.043(4)
H(6A)	0.1445(18)	0.4643(21)	0.3576(11)	0.060(5)
H(5B)	1.0222(20)	0.7992(21)	0.4677(10)	0.040(4)
H(5A)	1.0231(26)	0.8938(17)	0.3402(26)	0.071(5)
H(7A)	0.3225(20)	0.8303(22)	0.3259(21)	0.052(4)

[a]U_{eq} is defined as one-third of the trace of the orthogonalized U_{ij} tensor.

Table A2.2b Rigid-Body Model Libration Corrections for Bond Distances and "Hirshfeld Rigid-Bond" Test II

Bond	Bond Distance		Components of the Correction			Vibration Along the Interatomic Bond			
	Obsd	Calcd	Del(L)	Del(M)	Del(N)	I to J	J to I	Difference	Sqrt(Diff)
C(1) - C(2)	1.4695	1.4704	0.0001	0.0009	0.0001	0.0066	0.0066	0.0001	0.00+83
C(2) - C(3)	1.4596	1.4623	0.0026	-0.0010	0.0001	0.0074	0.0075	0.0002	0.0128
C(3) - C(4)	1.4692	1.4702	0	-0.0010	0	0.0067	0.0064	0.0003	0.0181
C(1) - C(4)	1.4843	1.4871	0.0026	-0.0010	0.0001	0.0075	0.0079	0.0004	0.0192
O(1) - C(1)	1.2606	1.2620	0.0016	0	0.0002	0.0061	0.0071	0.0010	0.0315
O(2) - C(2)	1.2668	1.2686	0.0015	-0.0012	0	0.0057	0.0066	0.0009	0.0302
O(3) - C(3)	1.2601	1.2615	-0.0016	0	0	0.0063	0.0070	0.0008	0.0276
O(4) - C(4)	1.2488	1.2506	-0.0016	0.0012	0	0.0058	0.0067	0.0008	0.0290

Sqrt(Sum(DelIJ**2)/Nrb) = 0.0007

Table A2.2c Multipole populations II

Atom	M1	D1+	D1-	D0	Q0	Q1+	Q1-	Q2+	Q2-	O0	O1+	O1-	O2+	O2-	O3+	O3-	H0	H1+	H1-	H2+	H2-	H3+	H3-	H4+	H4-
Na(1)	0.42(7)	-0.08(6)	0.14(5)	-0.14(10)	-0.16(6)	-0.22(7)	-0.11(8)	0.01(7)	-0.17(6)	0.06(6)	-0.15(6)	0.25(5)	-0.05(4)	-0.01(5)	-0.08(4)	0.07(5)	0.06(7)	0.04(6)	0.16(6)	-0.10(6)	0.01(5)	-0.02(5)	-0.05(5)	0.12(5)	0.27(5)
Na(2)	0.42(7)	-0.08(6)	0.14(5)	-0.14(10)	-0.16(6)	-0.22(7)	-0.11(8)	0.01(7)	-0.17(6)	0.06(6)	-0.15(6)	0.25(5)	-0.05(4)	-0.01(5)	-0.08(4)	0.07(5)	0.06(7)	0.04(6)	0.16(6)	-0.10(6)	0.01(5)	-0.02(5)	-0.05(5)	0.12(5)	0.27(5)
C(1)	4.14(3)	0.01(1)	-0.01(1)	0.01(1)	0.24(1)	0.01(1)	-0.01(1)	-0.09(1)	-0.00(1)	0.32(1)	0.03(1)	-0.02(1)	0.19(1)	-0.00(1)	-0.00(1)	0.01(1)									
C(2)	4.14(3)	0.01(1)	-0.01(1)	0.01(1)	0.24(1)	0.01(1)	-0.01(1)	-0.09(1)	-0.00(1)	0.32(1)	0.03(1)	-0.02(1)	0.19(1)	-0.00(1)	-0.00(1)	0.01(1)									
C(3)	4.14(3)	0.01(1)	-0.01(1)	0.01(1)	0.24(1)	0.01(1)	-0.01(1)	-0.09(1)	-0.00(1)	0.32(1)	0.03(1)	-0.02(1)	0.19(1)	-0.00(1)	-0.00(1)	0.01(1)									
C(4)	4.14(3)	0.01(1)	-0.01(1)	0.01(1)	0.24(1)	0.01(1)	-0.01(1)	-0.09(1)	-0.00(1)	0.32(1)	0.03(1)	-0.02(1)	0.19(1)	-0.00(1)	-0.00(1)	0.01(1)									
O(1)	6.15(2)	0.00(1)	0.01(1)	-0.11(1)	-0.10(1)	0.01(1)	0.02(1)	-0.01(1)	-0.01(1)	0.04(1)	0.00(1)	0.01(1)	0.02(1)	-0.01(1)	0.01(1)	0.02(1)									
O(2)	6.15(2)	0.00(1)	0.01(1)	-0.11(1)	-0.10(1)	0.01(1)	0.02(1)	-0.01(1)	-0.01(1)	0.04(1)	0.00(1)	0.01(1)	0.02(1)	-0.01(1)	0.01(1)	0.02(1)									
O(3)	6.15(2)	0.00(1)	0.01(1)	-0.11(1)	-0.10(1)	0.01(1)	0.02(1)	-0.01(1)	-0.01(1)	0.04(1)	0.00(1)	0.01(1)	0.02(1)	-0.01(1)	0.01(1)	0.02(1)									
O(4)	6.15(2)	0.00(1)	0.01(1)	-0.11(1)	-0.10(1)	0.01(1)	0.02(1)	-0.01(1)	-0.01(1)	0.04(1)	0.00(1)	0.01(1)	0.02(1)	-0.01(1)	0.01(1)	0.02(1)									
O(5)	6.12(4)	0.03(2)	-0.02(3)	-0.04(3)	-0.11(3)	0.02(2)	-0.01(2)	0.07(2)	0.01(2)	0.09(2)	-0.03(2)	-0.01(2)	0.04(2)	0.01(2)	0.02(2)	-0.04(2)									
O(6)	6.13(4)	-0.01(2)	-0.10(3)	-0.01(3)	-0.03(3)	-0.01(2)	0.08(2)	0.04(2)	-0.02(2)	0.08(2)	0.03(2)	-0.03(2)	0.06(2)	0.01(2)	-0.01(2)	-0.04(2)									
O(7)	6.14(4)	-0.01(2)	-0.08(2)	-0.08(3)	-0.04(3)	-0.09(2)	0.02(2)	0.05(2)	-0.03(2)	0.08(2)	0.02(2)	-0.08(2)	0.03(2)	0.00(2)	0.02(2)	-0.04(2)									
(H5A)	0.96(4)	0.12(3)	0.03(3)	0.26(4)																					
(H5B)	0.97(4)	-0.07(2)	-0.01(3)	0.15(3)																					

Kappa values

	κ	κ'
Na	1.18	0.96
O	0.99	0.86
C	0.99	0.96
H	1.15	1.20

Table A2.2c (*continued*)

(H6A)	0.92(5)	0.03(3)	-0.04(3)	0.32(4)
(H6B)	0.83(4)	0.02(2)	-0.05(3)	0.20(3)
(H7A)	1.03(4)	-0.10(3)	-0.00(3)	0.27(4)
(H7B)	0.86(4)	0.08(2)	-0.06(2)	0.20(3)

Disodium squarate trihydrate
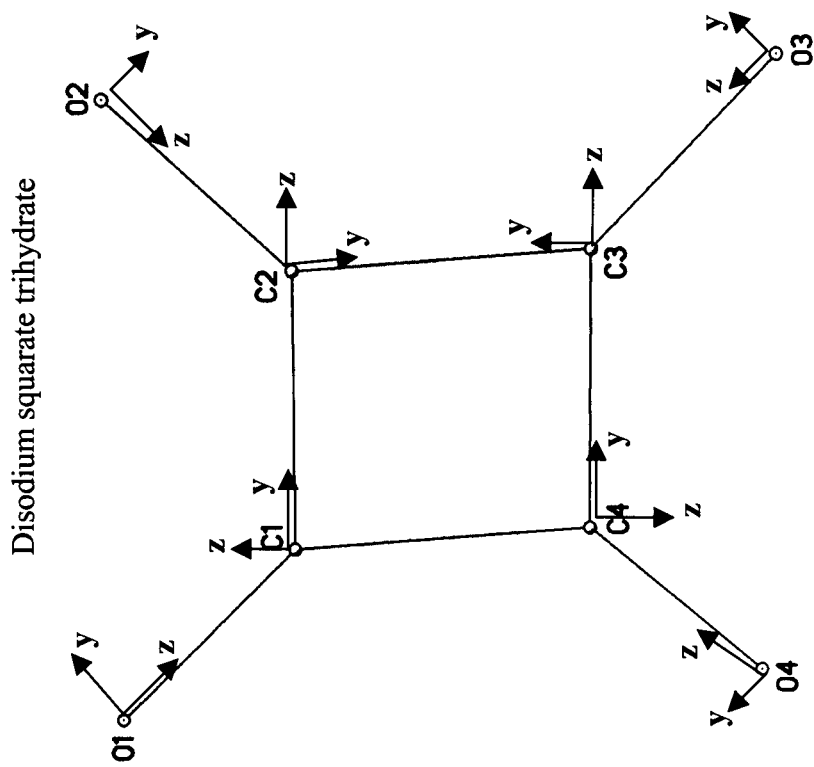
A2.2d Definition of local coordination

371

Disodium squarate trihydrate
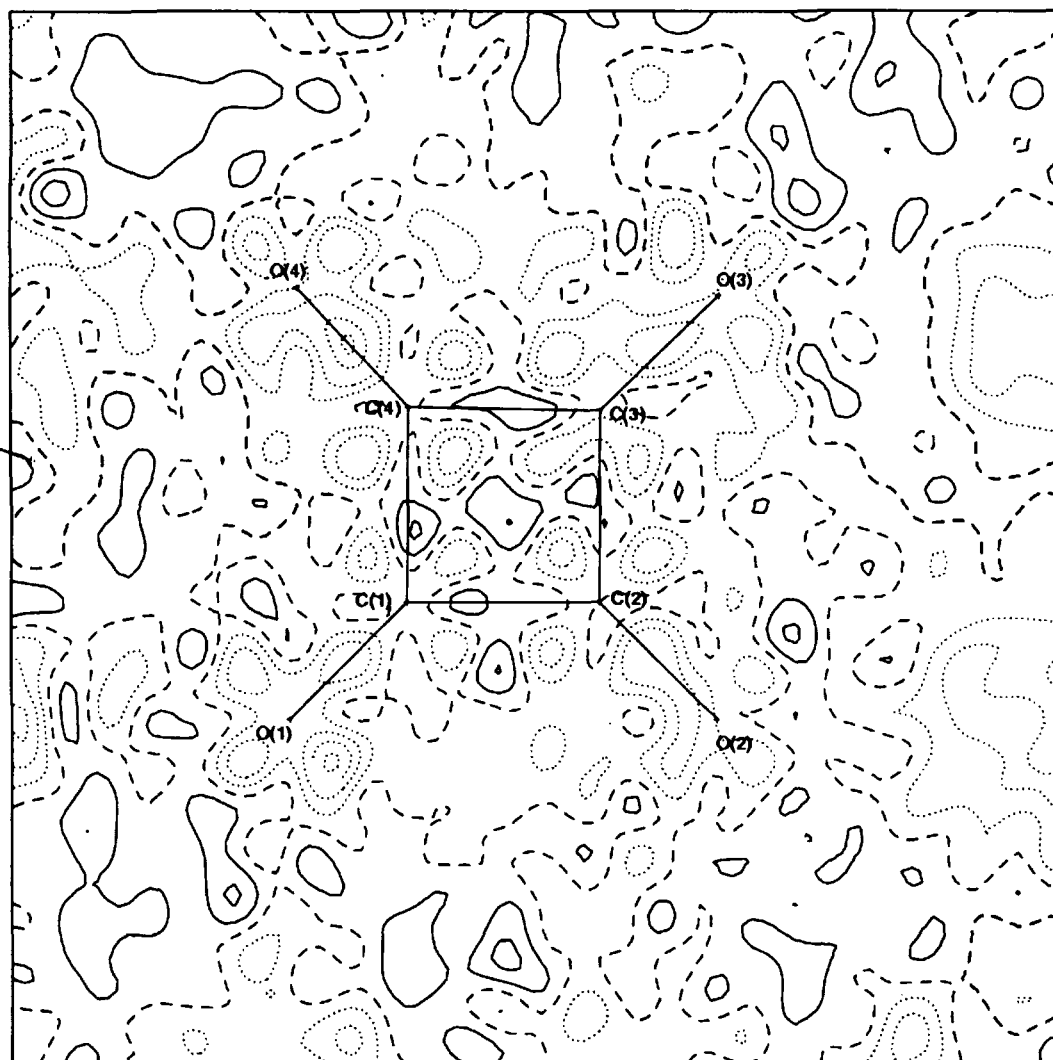
A2.2e Residual electron density map in the plane of the squarate ring (contours at 0.1 eÅ^{-3})

Piperazine oxalate III

Table A2.3a Fractional Coordinates and Equivalent Isotropic Displacement Parameters [Å²] of III

Atom	x/a	y/b	z/c	$U_{eq}{}^a$
O(2)	0.2443(1)	0.8997(1)	0.3819(1)	0.014(1)
O(4)	0.3129(1)	1.3289(1)	0.4201(1)	0.013(1)
O(3)	0.1799(1)	1.4894(1)	0.3333(1)	0.013(1)
C(2)	0.2324(1)	1.3182(1)	0.3687(1)	0.010(1)
C(1)	0.1882(1)	1.0722(1)	0.3424(1)	0.011(1)
O(1)	0.1102(1)	1.0516(1)	0.2894(1)	0.020(1)
N(1)	0.0716(1)	0.4833(1)	0.1048(1)	0.012(1)
C(11)	0.0424(1)	0.2738(1)	0.0290(1)	0.014(1)
C(10)	-0.0034(1)	0.6485(1)	0.0956(1)	0.014(1)
H(11B)	-0.0082(6)	0.1840(20)	0.0577(10)	0.017(3)
H(10B)	0.0227(8)	0.7995(15)	0.1508(10)	0.024(3)
H(10A)	-0.0543(6)	0.5508(21)	0.1202(11)	0.023(3)
H(1B)	0.1216(6)	0.5727(23)	0.0842(12)	0.030(3)
H(11A)	0.1017(6)	0.1670(21)	0.0409(14)	0.033(4)
H(1A)	0.0998(10)	0.4283(29)	0.1889(5)	0.039(4)
H(2)	0.2157(10)	0.7386(13)	0.3650(15)	0.045(4)

$^a U_{eq}$ is defined as one-third of the trace of the orthogonalized U_{ij} tensor.

Table A2.3b Rigid-Body Model Libration Corrections for Bond Distances and "Hirshfeld Rigid-Bond" Test III

Bond	Bond Distance		Components of the Correction			Vibration Along the Interatomic Bond			
	Obsd	Calcd	Del(L)	Del(M)	Del(N)	I to J	J to I	Difference	Sqrt(Diff)
O(1)-C(1)	1.2159	1.1958	-0.0258	-0.0385	-0.0002	0.0086(2)	0.0094(2)	0.0008(3)	0.0282
O(2)-C(1)	1.3131	1.2846	-0.0243	0.0430	0.0003	0.0091(2)	0.0097(2)	0.0005(3)	0.0227
O(3)-C(2)	1.2693	1.2442	0.0250	-0.0409	-0.0002	0.0082(2)	0.0090(2)	0.0008(3)	0.0281
O(4)-C(2)	1.2414	1.2170	0.0241	0.0402	0	0.0085(2)	0.0094(2)	0.0009(3)	0.0293
C(1)-C(2)	1.5545	1.6226	-0.0682	-0.0024	0.0002	0.0089(2)	0.0088(2)	0.0001(3)	0.0084

$$\text{Sqrt(Sum(DelIJ}^{**}2)/\text{Nrb}) = 0.0007$$

Table A2.3c Multipole populations III

Atom	M1	D1+	D1-	D0	Q0	Q1+	Q1-	Q2+	Q2-	O0	O1+	O1-	O2+	O2-	O3+	O3-
O(2)	6.20(3)	0.03(2)	-0.03(2)	0.00(2)	0.11(2)	0.04(2)	0.02(2)	-0.06(2)	0.03(2)	0.12(2)	-0.01(1)	0.00(2)	0.03(2)	0.00(1)	-0.02(2)	0.01(2)
O(4)	6.17(3)	-0.01(2)	0.03(2)	-0.06(2)	-0.02(2)	0.06(2)	-0.01(2)	-0.13(2)	0.02(2)	0.03(2)	0.02(2)	0.02(2)	0.02(2)	0.00(2)	0.00(1)	-0.01(1)
O(3)	6.18(3)	0.04(2)	-0.01(2)	-0.07(2)	0.00(2)	0.02(2)	-0.05(2)	-0.13(2)	0.04(2)	0.06(2)	0.01(2)	0.00(2)	0.03(2)	0.01(1)	0.03(1)	0.00(1)
O(1)	6.10(3)	-0.01(2)	0.00(2)	-0.04(2)	-0.05(3)	-0.05(2)	0.02(2)	-0.16(2)	-0.04(2)	0.00(2)	-0.01(2)	0.03(2)	0.06(2)	0.01(2)	0.01(2)	0.03(2)
N(1)	5.05(4)	-0.05(2)	0.04(2)	0.01(2)	0.03(2)	0.06(2)	0.04(2)	0.00(2)	-0.06(2)	0.17(2)	-0.01(2)	-0.03(2)	-0.02(2)	0.02(2)	-0.01(2)	-0.14(2)
C(2)	4.14(5)	0.04(2)	0.07(2)	0.01(2)	0.21(2)	0.07(2)	-0.08(2)	-0.22(2)	-0.01(2)	0.27(3)	-0.02(2)	0.03(3)	0.22(2)	0.01(2)	0.02(2)	0.00(2)
C(1)	4.08(5)	-0.02(2)	-0.07(2)	0.11(3)	0.23(3)	-0.03(2)	0.00(2)	-0.27(2)	0.02(2)	0.31(3)	0.03(2)	0.00(3)	0.26(2)	-0.01(2)	0.02(2)	-0.03(2)
C(11)	4.31(5)	0.02(2)	0.02(2)	0.07(3)	0.04(2)	0.01(2)	-0.03(2)	-0.11(2)	-0.01(2)	0.20(2)	-0.01(2)	0.01(2)	-0.01(2)	-0.04(2)	-0.07(2)	-0.19(2)
C(10)	4.17(5)	0.04(2)	0.06(2)	0.00(2)	0.07(2)	-0.01(2)	-0.08(2)	-0.09(2)	-0.03(2)	0.22(2)	0.04(2)	0.02(2)	0.00(2)	0.04(2)	-0.04(2)	-0.22(2)
H(11B)	0.88(3)	0.06(2)	-0.02(2)	0.11(2)												
H(10B)	0.89(3)	0.02(2)	0.05(2)	0.12(2)												
H(10A)	0.81(3)	-0.06(2)	0.08(2)	0.10(2)												
H(1B)	0.72(3)	0.02(2)	0.00(2)	0.17(3)												
H(11A)	0.91(3)	-0.01(2)	0.04(2)	0.15(3)												
H(1A)	0.77(3)	0.05(2)	-0.07(2)	0.20(3)												
H(2)	0.63(3)	-0.04(2)	-0.03(2)	0.09(3)												

Kappa values

	κ	κ'
O	1.00	0.90
N	1.00	0.97
C	1.01	0.97
H	1.21	1.20

374

Piperazine oxalate
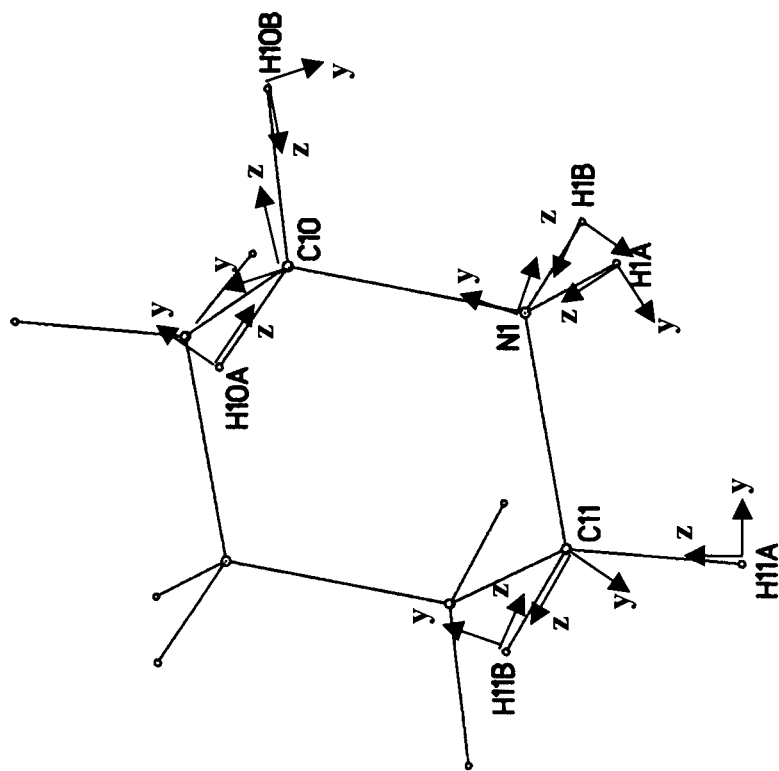
A2.3d Definition of local coordination systems

Piperazine oxalate
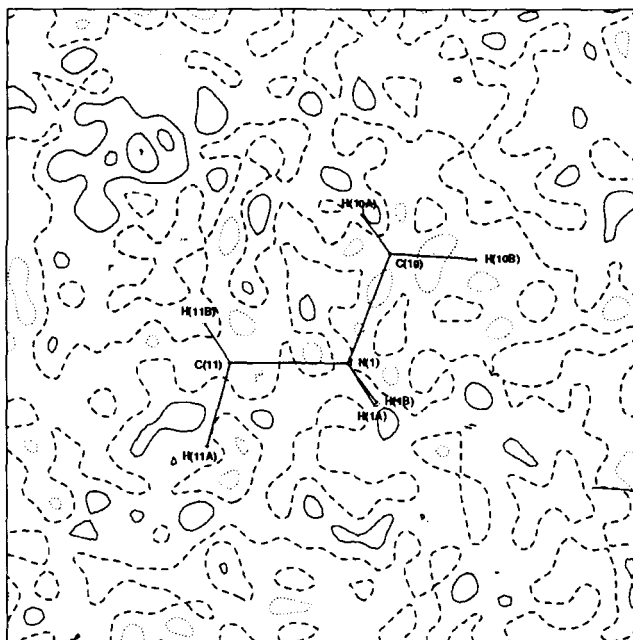
Residual electron density map in the plane containing C(11), N(1) and C(10) atoms (contours at 0.1 e$\mathring{A}^{-3}$)
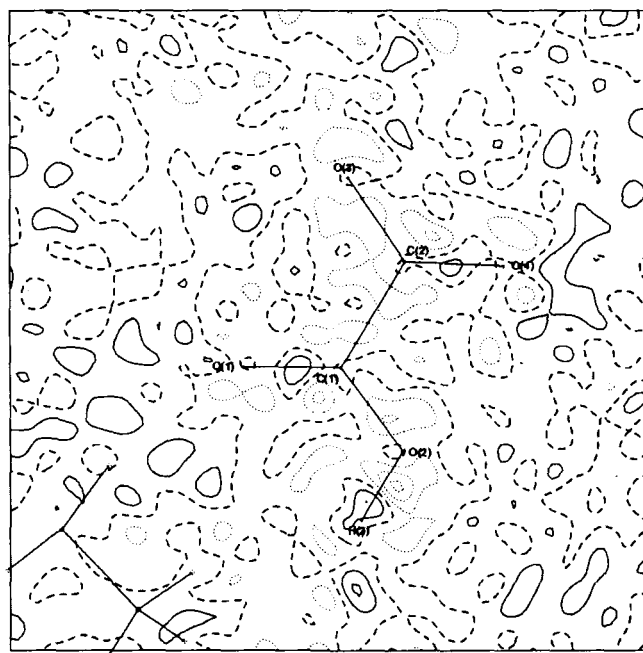
Residual electron density map in the plane containing O(1), C(1) and O(2) atoms (contours at 0.1 e$\mathring{A}^{-3}$)

A2.3e

376

Thiodiglycollic acid-4,4'-bipyridine IV

Table A2.4a Fractional Coordinates and Equivalent Isotropic Displacement Parameters [Å²] of IV

Atom	x/a	y/b	z/c	$U_{eq}{}^a$
S(1)	0.7357(3)	0.9140(3)	0.0348(2)	0.020(1)
C(10)	1.3563(12)	-0.1520(12)	0.6004(8)	0.016(1)
O(13B)	0.8854(12)	0.4960(11)	0.1851(7)	0.022(1)
C(5)	1.2542(12)	-0.0086(13)	0.5127(8)	0.016(1)
N(2)	1.5506(12)	-0.4200(12)	0.7666(8)	0.019(1)
N(1)	1.0613(12)	0.2610(13)	0.3468(8)	0.021(2)
O(14B)	1.2489(11)	0.5976(12)	0.0677(7)	0.025(2)
C(13)	0.7418(13)	0.6319(13)	0.2124(8)	0.018(2)
C(14)	1.0973(13)	0.7277(13)	0.0928(8)	0.018(2)
C(9)	1.4985(14)	-0.3055(14)	0.5717(8)	0.019(2)
O(14A)	1.0665(12)	0.7964(12)	0.1783(7)	0.025(2)
C(3)	1.1138(13)	0.1459(14)	0.5419(8)	0.019(2)
O(13A)	0.6939(12)	0.6667(13)	0.3084(7)	0.026(2)
C(8)	1.3148(14)	-0.1377(15)	0.7153(9)	0.021(2)
C(7)	1.5907(14)	-0.4344(14)	0.6565(9)	0.021(2)
C(12)	0.9694(14)	0.7836(14)	-0.0017(8)	0.020(2)
C(6)	1.4147(15)	-0.2736(15)	0.7946(9)	0.022(2)
C(4)	1.2945(15)	-0.0227(15)	0.3975(9)	0.021(2)
C(2)	1.0224(14)	0.2756(14)	0.4568(9)	0.021(2)
C(1)	1.1954(16)	0.1138(16)	0.3183(9)	0.023(2)
C(11)	0.6414(15)	0.7404(15)	0.1101(9)	0.022(2)
H(3)	1.0824(239)	0.1642(237)	0.6299(43)	0.025(43)
H(9)	1.5378(260)	-0.3194(276)	0.4834(47)	0.033(47)
H(11B)	0.5044(125)	0.8198(253)	0.1409(176)	0.039(53)
H(6)	1.3849(301)	-0.2584(287)	0.8832(48)	0.041(55)
H(2)	0.9115(182)	0.3897(167)	0.4842(158)	0.030(46)
H(4)	1.4001(181)	-0.1364(159)	0.3656(148)	0.027(43)

Table A2.4a *(continued)*

H(12A)	0.9809(253)	0.6617(147)	-0.0355(149)	0.026(43)
H(7)	1.7049(172)	-0.5512(158)	0.6359(153)	0.027(43)
H(8)	1.2196(274)	-0.0365(275)	0.7448(169)	0.035(51)
H(1)	1.2215(260)	0.0970(259)	0.2299(45)	0.031(47)
H(11A)	0.6492(254)	0.6523(208)	0.0490(121)	0.029(45)
H(12B)	1.0231(272)	0.8631(251)	-0.0731(118)	0.041(54)
H(13B)	0.9426(333)	0.4220(320)	0.2570(126)	0.063(73)
H(14B)	1.3246(303)	0.5404(362)	0.1353(137)	0.068(80)

[a]U_{eq} is defined as one-third of the trace of the orthogonalized U_{ij} tensor.

Table A2.4b Rigid-Body Model Libration Corrections for Bond Distances and "Hirshfeld Rigid-Bond" Test IV

Bond	Bond Distance		Components of the Correction			Vibration Along the Interatomic Bond			Sqrt(Diff)
	Obsd	Calcd	Del(L)	Del(M)	Del(N)	I to J	J to I	Difference	
N(1)-C(1)	1.3375	1.3408	0.0001	0.0038	-0.0002	0.0229	0.0244	0.0015	0.0384
N(1)-C(2)	1.3380	1.3418	0.0006	-0.0041	0	0.0208	0.0224	0.0016	0.0402
N(2)-C(6)	1.3377	1.3410	-0.0001	-0.0038	0.0001	0.0196	0.0201	0.0004	0.0208
N(2)-C(7)	1.3398	1.3437	-0.0006	0.0041	0.0001	0.0189	0.0204	0.0015	0.0383
C(1)-C(4)	1.3872	1.3880	0.0007	-0.0002	-0.0002	0.0140	0.0138	0.0002	0.0137
C(2)-C(3)	1.3860	1.3868	0.0008	-0.0005	-0.0002	0.0142	0.0140	0.0002	0.0157
C(3)-C(5)	1.3996	1.4031	0.0001	0.0040	-0.0002	0.0177	0.0179	0.0002	0.0140
C(4)-C(5)	1.3992	1.4032	0.0007	-0.0043	-0.0001	0.0161	0.0162	0.0001	0.0084
C(5)-C(10)	1.4848	1.4856	0.0008	-0.0003	-0.0003	0.0120	0.0118	0.0002	0.0146
C(6)-C(8)	1.3876	1.3884	-0.0007	0.0002	0.0002	0.0130	0.0133	0.0003	0.0185
C(7)-C(9)	1.3832	1.3840	-0.0007	0.0005	0.0002	0.0144	0.0144	0	0.0047
C(8)-C(10)	1.3964	1.4004	-0.0007	0.0043	0.0001	0.0164	0.0160	0.0004	0.0212
C(9)-C(10)	1.3986	1.4020	-0.0001	-0.0039	0.0001	0.0171	0.0174	0.0003	0.0174

Sqrt(Sum(DelJ**2)/Nrb) = 0.0008
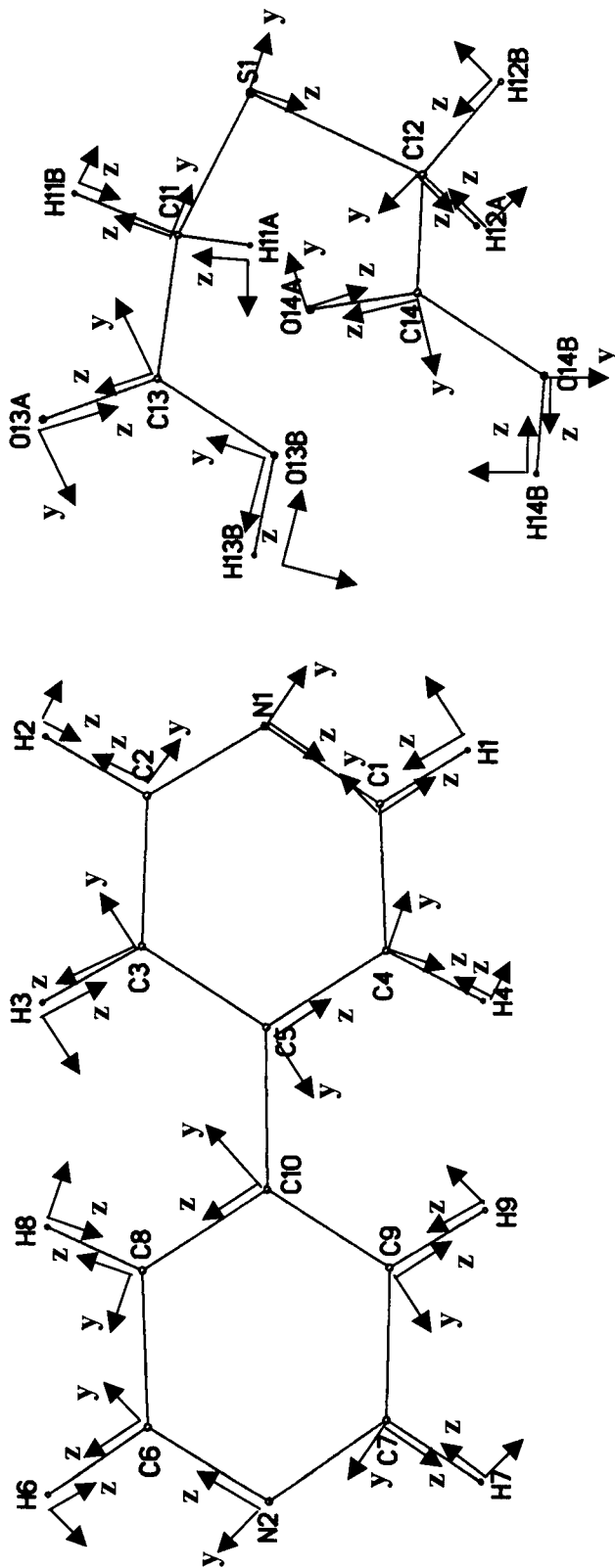
Table A2.4c Multipole populations IV

Atom	M1	D1+	D1-	D0	Q0	Q1+	Q1-	Q2+	Q2-	O0	O1+	O1-	O2+	O2-	O3+	O3-	HO	H1+	H1-	H2+	H2-	H3+	H3-	H4+	H4-
S(1)	6.36(8)	0.02(2)	-0.03(2)	-0.02(2)	-0.26(3)	0.25(3)	0.25(3)	0.09(3)	0.03(3)	-0.01(3)	0.17(2)	-0.07(2)	-0.06(2)	0.04(2)	-0.02(2)	-0.06(2)	-0.05(2)	0.04(3)	-0.08(3)	0.13(2)	-0.17(2)	0.05(3)	0.12(2)	0.06(3)	-0.12(2)
O(13A)	6.07(5)	-0.06(3)	-0.02(3)	-0.04(4)	-0.19(5)	-0.03(4)	-0.10(4)	-0.20(3)	-0.02(3)	-0.03(3)	0.06(3)	0.00(3)	0.04(2)	0.02(2)	0.01(2)	0.05(2)									
O(14A)	6.12(5)	0.00(3)	0.05(3)	0.04(4)	-0.16(4)	-0.16(4)	-0.10(4)	-0.05(3)	-0.12(3)	0.05(3)	-0.01(3)	0.01(3)	-0.03(2)	0.00(2)	-0.02(2)	-0.02(2)									
O(13B)	6.31(4)	0.02(3)	-0.01(4)	-0.04(3)	0.13(3)	-0.01(3)	-0.02(3)	0.13(4)	0.02(3)	0.09(2)	-0.06(2)	-0.08(2)	-0.01(2)	-0.06(2)	-0.06(2)	0.04(2)									
O(14B)	6.26(5)	-0.06(3)	-0.01(4)	-0.01(3)	0.13(3)	-0.13(3)	0.01(3)	0.16(4)	0.03(3)	0.02(3)	0.03(2)	-0.01(2)	0.09(2)	-0.02(2)	-0.032	0.023									
N(1)	5.12(5)	0.03(3)	-0.04(3)	-0.09(4)	-0.01(4)	-0.08(3)	0.10(3)	-0.14(3)	0.07(3)	0.15(3)	-0.07(3)	0.03(3)	0.08(3)	-0.02(3)	0.02(2)	-0.03(2)									
N(2)	5.08(5)	-0.02(3)	-0.06(3)	-0.13(4)	-0.08(4)	0.04(3)	0.12(3)	-0.08(3)	0.02(3)	0.17(3)	0.01(3)	-0.02(3)	0.09(3)	-0.03(3)	-0.04(3)	-0.03(2)									
C(1)	3.97(8)	-0.05(3)	0.03(4)	-0.01(4)	-0.07(4)	0.03(3)	0.05(4)	-0.18(4)	-0.04(3)	0.22(4)	-0.02(3)	-0.06(4)	0.16(4)	0.00(3)	0.04(3)	-0.07(3)									
C(2)	4.04(8)	0.02(3)	-0.06(4)	-0.06(4)	0.03(4)	0.04(3)	0.04(4)	-0.13(4)	-0.05(3)	0.31(4)	-0.01(3)	0.11(4)	0.17(3)	0.00(3)	-0.01(3)	0.06(3)									
C(3)	4.17(8)	0.00(3)	-0.03(4)	-0.04(4)	0.08(4)	0.04(3)	-0.10(4)	-0.12(3)	0.02(3)	0.25(4)	0.01(3)	0.09(4)	0.17(3)	0.11(3)	-0.05(3)	0.03(3)									
C(4)	4.04(7)	0.03(3)	0.06(4)	0.05(4)	0.01(4)	-0.01(3)	-0.12(4)	-0.15(4)	0.02(3)	0.17(4)	0.01(3)	-0.04(4)	0.19(3)	0.05(3)	0.04(3)	-0.02(3)									
C(5)	4.11(7)	-0.03(3)	0.02(4)	0.03(4)	0.12(4)	0.03(3)	0.08(3)	-0.21(3)	0.03(3)	0.26(4)	-0.02(3)	-0.05(4)	0.19(3)	-0.01(3)	-0.08(3)	0.00(3)									
C(6)	4.07(8)	-0.01(3)	0.08(4)	-0.10(4)	-0.02(4)	0.02(3)	0.01(4)	-0.19(4)	0.00(3)	0.27(4)	0.02(3)	0.05(4)	0.23(3)	-0.05(3)	-0.05(3)	0.01(3)									
C(7)	3.78(7)	-0.02(3)	-0.04(4)	-0.03(4)	0.00(4)	-0.09(3)	0.09(4)	-0.14(4)	-0.06(3)	0.28(4)	0.08(3)	0.01(4)	0.14(3)	0.09(3)	-0.02(3)	-0.01(3)									
C(8)	4.08(8)	0.01(3)	-0.02(4)	-0.06(5)	0.04(4)	-0.02(3)	-0.08(4)	-0.12(4)	-0.04(3)	0.16(4)	-0.03(3)	0.01(4)	0.23(3)	-0.05(3)	-0.01(3)	0.01(3)									
C(9)	4.08(8)	0.00(3)	-0.01(4)	-0.02(4)	0.01(4)	-0.11(3)	-0.07(4)	-0.10(3)	-0.06(3)	0.27(4)	0.02(3)	0.02(4)	0.22(3)	0.09(3)	-0.0(3)	-0.06(3)									
C(10)	4.12(7)	0.04(3)	0.04(4)	0.09(4)	0.10(4)	-0.06(3)	0.00(3)	-0.16(3)	0.09(3)	0.20(4)	-0.03(3)	0.04(4)	0.18(3)	0.02(3)	-0.07(3)	-0.04(3)									
C(11)	4.21(7)	-0.02(3)	0.09(4)	-0.10(4)	-0.04(4)	0.04(3)	-0.02(3)	-0.11(3)	0.09(3)	0.26(4)	0.13(3)	0.10(3)	-0.03(3)	0.00(3)	0.07(3)	-0.13(3)									
C(12)	4.44(7)	-0.03(3)	-0.02(4)	0.16(4)	0.01(4)	0.05(3)	-0.01(3)	0.00(3)	0.11(3)	0.21(3)	0.04(3)	0.04(3)	0.00(3)	0.04(3)	0.04(3)	-0.25(3)									
C(13)	4.09(7)	-0.08(3)	0.01(4)	0.11(5)	0.24(4)	-0.04(3)	0.00(4)	-0.15(3)	0.04(3)	0.27(4)	-0.04(4)	0.01(4)	0.25(3)	-0.01(3)	-0.06(3)	-0.02(3)									
C(14)	4.08(7)	-0.04(3)	-0.05(3)	0.11(4)	0.16(4)	-0.03(3)	-0.02(4)	-0.22(3)	-0.05(3)	0.25(4)	-0.06(3)	0.01(4)	0.33(4)	-0.01(3)	-0.04(3)	0.04(3)									
H(1)	0.82(4)	0.07(3)	0.03(3)	0.18(3)																					
H(2)	0.79(4)	0.02(4)	-0.08(3)	0.12(3)																					
H(3)	0.73(4)	0.00(3)	0.00(3)	0.10(3)																					
H(4)	0.82(4)	0.01(3)	0.04(3)	0.16(3)																					
H(6)	0.91(5)	-0.02(3)	0.01(3)	0.20(4)																					
H(7)	0.85(4)	0.08(3)	-0.03(3)	0.15(3)																					
H(8)	0.90(6)	-0.07(3)	0.08(3)	0.05(4)																					

Kappa values

	κ	κ'
S	1.04	1.16
O	1.00	0.92
N	0.99	0.96
C	1.01	1.01
H	1.22	1.20

Table A2.4c (*continued*)

H(9)	0.74(4)	0.03(3)	-0.01(3)	0.17(4)
H(11A)	0.73(4)	-0.09(3)	0.07(3)	0.04(3)
H(11B)	0.94(5)	-0.03(3)	0.04(3)	0.17(4)
H(12A)	0.76(4)	-0.02(3)	-0.08(3)	0.09(3)
H(12B)	0.79(5)	0.01(3)	-0.11(3)	0.14(4)
H(13B)	0.79(5)	0.09(3)	-0.03(3)	0.07(4)
H(14B)	0.83(5)	-0.07(3)	0.04(3)	0.09(5)

Thiodiglycollic acid-4,4'-bipyridine

A2.4d Definition of local coordination

381

Thiodiglycollic acid-4,4'-bipyridine

Residual electron density map in the plane containing C(11), S(1) and C(12) atoms (contours at 0.1 eÅ^{-3})

A2.4e Residual electron density map in the plane of the bipyridyl ring (contours at 0.1 eÅ^{-3})

Melamine V

Table A2.5a Fractional Coordinates and Equivalent Isotropic Displacement Parameters [Å²] of V

Atom	x/a	y/b	z/c	$U_{eq}{}^a$
N(5)	0.5175(1)	0.1908(1)	0.1166(1)	0.012(1)
N(4)	0.5006(1)	0.4974(1)	0.1811(1)	0.014(1)
N(6)	0.2104(1)	0.3380(1)	0.0604(1)	0.013(1)
C(3)	0.3235(1)	0.1949(1)	0.0640(1)	0.011(1)
C(2)	0.5996(1)	0.3471(1)	0.1729(1)	0.012(1)
N(3)	0.2346(1)	0.0376(1)	0.0131(1)	0.015(1)
C(1)	0.3074(1)	0.4861(1)	0.1210(1)	0.012(1)
N(2)	0.7931(1)	0.3515(1)	0.2232(1)	0.016(1)
N(1)	0.2009(1)	0.6323(1)	0.1229(1)	0.016(1)
H(3B)	0.3192(18)	-0.0517(16)	-0.0158(16)	0.031(4)
H(2B)	0.8530(22)	0.4659(12)	0.2705(17)	0.039(4)
H(1B)	0.0614(8)	0.6368(20)	0.0624(15)	0.034(4)
H(3A)	0.0989(9)	0.0571(22)	-0.0512(14)	0.037(5)
H(1A)	0.2685(25)	0.7501(13)	0.1545(19)	0.050(5)
H(2A)	0.8616(23)	0.2321(11)	0.2345(20)	0.048(5)

$^a U_{eq}$ is defined as one-third of the trace of the orthogonalized U_{ij} tensor.

383

Table A2.5b Rigid-Body Model Libration Corrections for Bond Distances and "Hirshfeld Rigid-Bond" Test V

Bond	Bond Distance		Components of the Correction			Vibration Along the Interatomic Bond			
	Obsd	Calcd	Del(L)	Del(M)	Del(N)	I to J	J to I	Difference	Sqrt(Diff)
N(1)-C(1)	1.3415	1.3427	0.0012	0	0	0.0087	0.0093	0.0005	0.0229
N(2)-C(2)	1.3378	1.3392	-0.0007	-0.0012	-0.0001	0.0098	0.0102	0.0004	0.0203
N(3)-C(3)	1.3624	1.3638	-0.0006	0.0013	0.0002	0.0090	0.0096	0.0006	0.0236
N(4)-C(1)	1.3469	1.3483	-0.0006	-0.0013	0	0.0104	0.0105	0.0001	0.0118
N(4)-C(2)	1.3499	1.3511	0.0012	-0.0001	0	0.0090	0.0097	0.0007	0.0270
N(5)-C(2)	1.3542	1.3556	-0.0006	0.0012	0.0001	0.0095	0.0099	0.0004	0.0189
N(5)-C(3)	1.3427	1.3441	-0.0007	-0.0012	-0.0001	0.0100	0.0107	0.0006	0.0254
N(6)-C(1)	1.3527	1.3541	-0.0005	0.0013	0.0001	0.0103	0.0105	0.0002	0.0133
N(6)-C(3)	1.3414	1.3427	0.0012	0.0001	-0.0001	0.0092	0.0102	0.0011	0.0325

$Sqrt(Sum(DelIJ^{**}2)/Nrb) = 0.0006$

Table A2.5c Multipole populations V

Atom	M1	D1+	D1-	D0	Q0	Q1+	Q1-	Q2+	Q2-	O0	O1+	O1-	O2+	O2-	O3+	O3-
C(1)	4.13(2)	-0.02(1)	0.01(1)	-0.01(1)	0.18(1)	-0.02(1)	-0.03(2)	-0.27(1)	0.02(1)	0.33(1)	0.00(1)	0.01(1)	0.23(1)	-0.02(1)	0.01(1)	-0.01(1)
C(2)	4.13(2)	-0.02(1)	0.01(1)	-0.01(1)	0.18(1)	-0.03(1)	-0.03(1)	-0.27(1)	0.02(1)	0.33(1)	0.00(1)	0.01(1)	0.23(1)	-0.02(1)	0.01(1)	-0.01(1)
C(3)	4.13(2)	-0.02(1)	0.01(1)	-0.01(1)	0.18(1)	-0.03(1)	-0.03(1)	-0.27(1)	0.02(1)	0.33(1)	0.00(1)	0.01(1)	0.23(1)	-0.02(1)	0.01(1)	-0.01(1)
N(1)	5.24(2)	-0.01(1)	0.02(1)	0.06(2)	0.11(2)	0.00(1)	-0.02(1)	-0.04(1)	-0.01(1)	0.20(1)	-0.02(1)	0.03(1)	0.12(1)	0.00(1)	-0.02(1)	-0.04(1)
N(2)	5.24(2)	-0.01(1)	0.02(1)	0.06(2)	0.11(2)	0.00(1)	-0.02(1)	-0.04(1)	-0.01(1)	0.20(1)	-0.02(1)	0.03(1)	0.12(1)	0.00(1)	-0.02(1)	-0.04(1)
N(3)	5.24(2)	-0.01(1)	0.02(1)	0.06(2)	0.11(2)	0.00(1)	-0.02(1)	-0.04(1)	-0.01(1)	0.20(1)	-0.02(1)	0.03(1)	0.12(1)	0.00(1)	-0.02(1)	-0.04(1)
N(4)	5.07(2)	0.00(1)	-0.11(1)	-0.07(1)	0.06(1)	-0.02(1)	0.07(1)	-0.10(1)	-0.03(1)	0.10(1)	0.00(1)	-0.02(1)	0.06(1)	0.02(1)	0.01(1)	-0.03(1)
N(5)	5.07(2)	0.00(1)	-0.11(1)	-0.07(1)	0.06(1)	-0.02(1)	0.07(1)	-0.10(1)	-0.03(1)	0.10(1)	0.00(1)	-0.02(1)	0.06(1)	0.02(1)	0.01(1)	-0.03(1)
N(6)	5.07(2)	0.00(1)	-0.11(1)	-0.07(1)	0.06(1)	-0.02(1)	0.07(1)	-0.10(1)	-0.03(1)	0.10(1)	0.00(1)	-0.02(1)	0.06(1)	0.02(1)	0.01(1)	-0.03(1)
H(1A)	0.88(3)	0.02(2)	0.01(2)	0.16(2)												
H(1B)	0.70(3)	-0.01(2)	-0.06(2)	0.11(2)												
H(2A)	0.82(3)	0.01(2)	0.10(2)	0.18(2)												
H(2B)	0.71(3)	0.01(2)	0.07(2)	0.10(2)												
H(3A)	0.77(3)	0.05(2)	0.02(2)	0.12(2)												
H(3B)	0.86(3)	0.01(2)	-0.01(2)	0.14(2)												

Kappa values

	κ	κ'
N	1.00	0.96
C	1.00	1.01
H	1.21	1.20

Melamine
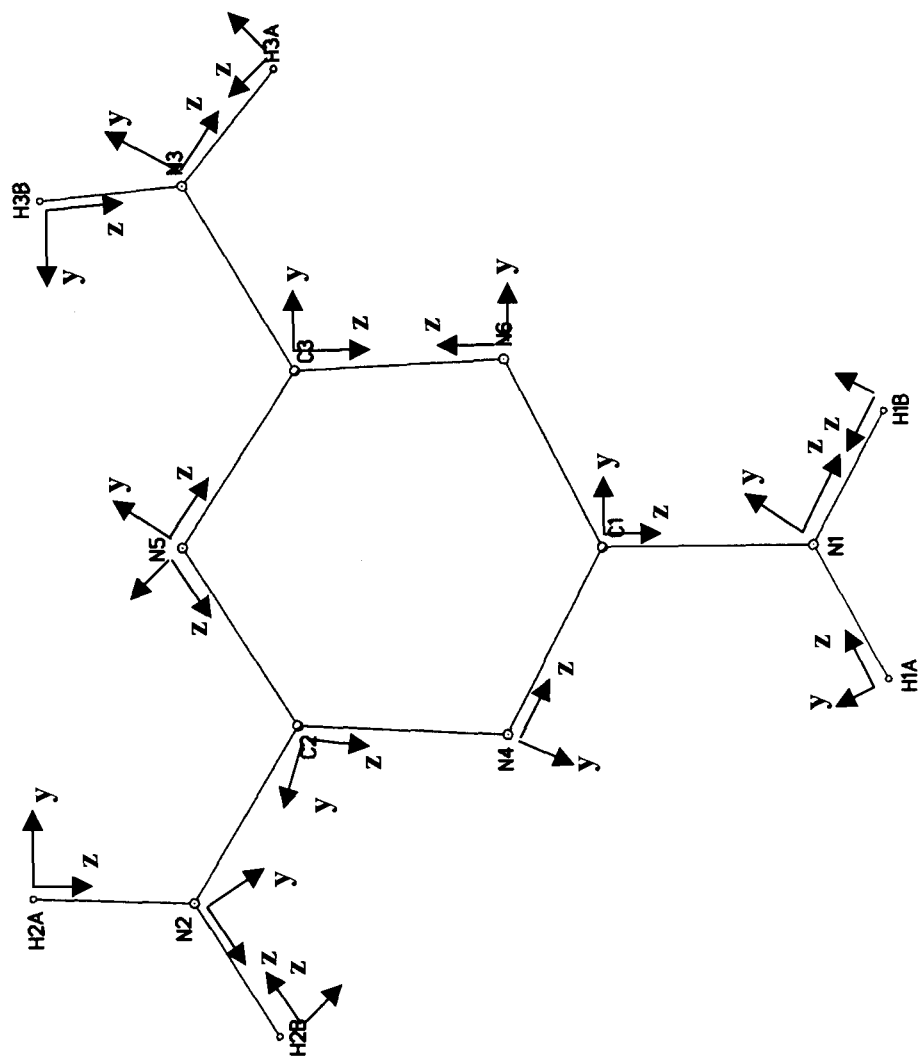
A2.5d Definition of local coordination systems

385

Melamine
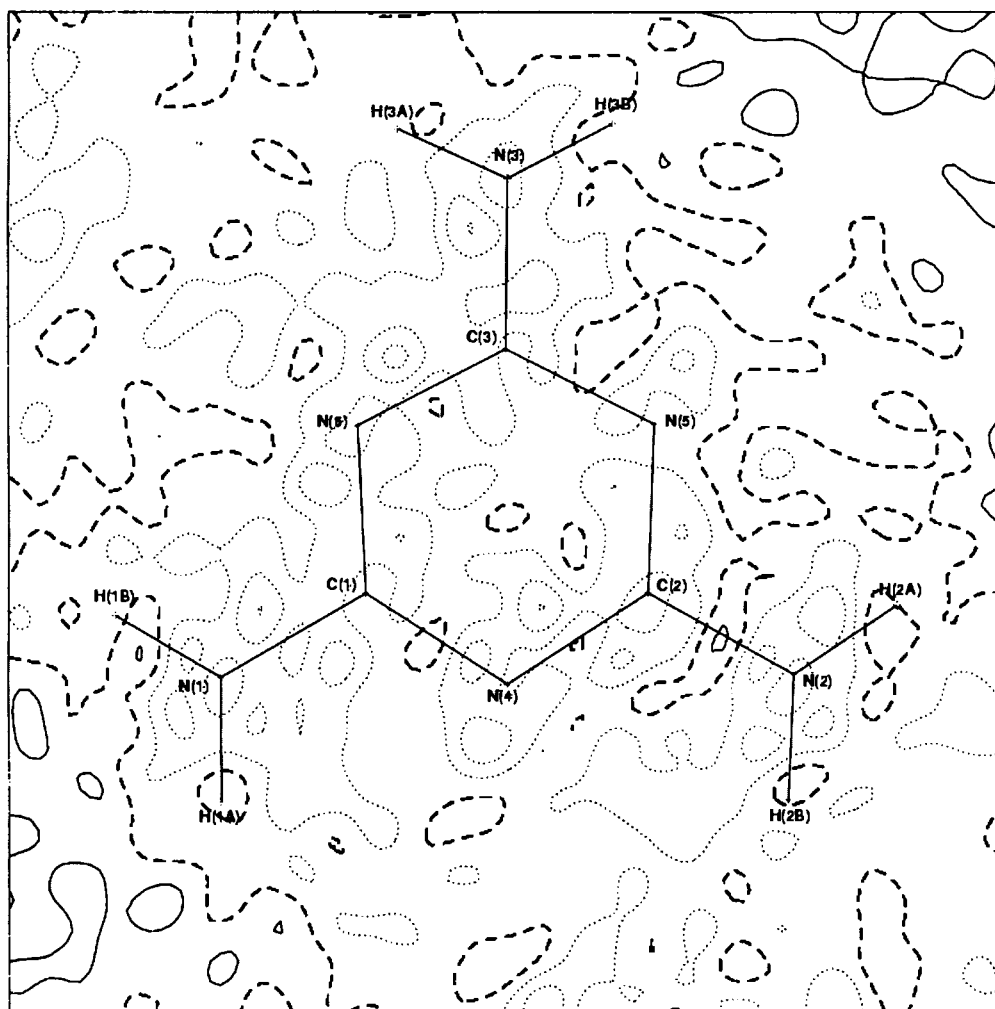
A2.5e Residual electron density map in the plane of the triazine ring (contours at 0.1 eÅ⁻³)

Thionicotinamide VI

TableA2.6a Fractional Coordinates and Equivalent Isotropic Displacement Parameters [Å²] of **VI**

Atom	x/a	y/b	z/c	$U_{eq}{}^a$
S(1)	0.6445(1)	0.1753(1)	0.0762(1)	0.017(1)
C(6)	0.8283(2)	0.0546(1)	0.1335(1)	0.014(1)
N(2)	0.8413(2)	-0.0612(1)	0.1020(1)	0.020(1)
C(5)	0.9796(2)	-0.0194(1)	0.2892(1)	0.016(1)
N(1)	1.2814(2)	0.2147(1)	0.3291(1)	0.018(1)
C(4)	0.9827(2)	0.0739(1)	0.2249(1)	0.013(1)
C(3)	1.1352(2)	0.1895(1)	0.2488(1)	0.015(1)
C(2)	1.2762(2)	0.1233(1)	0.3903(1)	0.020(1)
C(1)	1.1293(2)	0.0062(1)	0.3733(1)	0.019(1)
H(2A)	0.9518(2)	-0.1308(1)	0.1395(1)	0.024
H(2B)	0.7408(2)	-0.0801(1)	0.0404(1)	0.024
H(5)	0.8629(2)	-0.1101(1)	0.2740(1)	0.019
H(3)	1.1346(2)	0.2627(1)	0.1995(1)	0.018
H(2)	1.3924(2)	0.1423(1)	0.4557(1)	0.023
H(1)	1.1305(2)	-0.0643(1)	0.4245(1)	0.023

^{a} U_{eq} is defined as one-third of the trace of the orthogonalized U_{ij} tensor.

Table A2.6b Rigid-Body Model Libration Corrections for Bond Distances and "Hirshfeld Rigid-Bond" Test **VI**

Bond	Bond Distance		Components of the Correction			Vibration Along the Interatomic Bond			Sqrt(Diff)
	Obsd	Calcd	Del(L)	Del(M)	Del(N)	I to J	J to I	Difference	
S(1)-C(6)	1.6791	1.6819	-0.0010	-0.0026	-0.0007	0.0106	0.0122	0.0016	0.0405
N(1)-C(2)	1.3489	1.3515	-0.0009	-0.0022	0.0013	0.0188	0.0198	0.0010	0.0315
N(1)-C(3)	1.3365	1.3382	0.0016	-0.0009	-0.0002	0.0142	0.0142	0.0001	0.0097
N(2)-C(6)	1.3210	1.3240	-0.0007	0.0028	0.0009	0.0100	0.0113	0.0012	0.0349
C(1)-C(2)	1.3844	1.3878	-0.0007	0.0031	-0.0011	0.0177	0.0177	0.0000	0.0045
C(1)-C(5)	1.3944	1.3963	0.0017	-0.0009	-0.0002	0.0153	0.0152	0.0001	0.0084
C(3)-C(4)	1.4000	1.4033	0.0008	-0.0031	0.0010	0.0110	0.0108	0.0001	0.0121

Table A2.6b (*continued*)

C(4)-C(5)	1.3951	1.3977	-0.0023	-0.0009	0.0013	0.0134	0.0134	0.0000	0.0050
C(5)-C(6)	1.4888	1.4907	-0.0007	0.0018	-0.0004	0.0125	0.0132	0.0007	0.0273

Sqrt(Sum(DelJ**2)/Nrb) = 0.0008

Table A2.6c Multipole populations VI

Atom	M1	D1+	D1-	D0	Q0	Q1+	Q1-	Q2+	Q2-	O0	O1+	O1-	O2+	O2-	O3+	O3-	H0	H1+	H1-	H2+	H2-	H3+	H3-	H4+	H4-
S(1)	6.58(5)	-0.03(2)	0.01(2)	-0.06(2)	-0.16(2)	-0.09(2)	-0.06(2)	0.00(2)	0.04(2)	0.09(2)	0.01(2)	0.01(2)	0.02(2)	0.00(2)	-0.01(2)	-0.01(2)	-0.07(2)	-0.07(2)	0.02(2)	0.01(2)	0.03(2)	0.05(2)	-0.04(2)	-0.10(2)	0.02(2)
N(1)	5.05(4)	0.03(2)	-0.11(2)	-0.07(2)	0.06(3)	-0.02(2)	0.03(2)	-0.06(2)	-0.02(2)	0.11(2)	0.02(2)	0.04(2)	0.07(2)	0.00(2)	-0.02(2)	-0.03(2)									
N(2)	5.26(4)	0.01(2)	0.02(2)	-0.04(3)	-0.07(2)	-0.03(2)	-0.04(2)	-0.03(3)	0.03(2)	0.20(2)	-0.08(2)	0.03(2)	0.18(2)	-0.06(2)	-0.03(2)	-0.04(2)									
C(1)	4.25(6)	0.02(2)	0.04(3)	0.07(3)	0.09(3)	0.00(2)	0.01(3)	-0.18(3)	0.02(3)	0.27(3)	-0.01(2)	-0.04(3)	0.17(2)	0.03(3)	-0.04(3)	-0.01(3)									
C(2)	4.22(6)	0.01(3)	0.03(3)	0.00(3)	0.12(3)	0.04(2)	-0.01(3)	-0.16(3)	0.03(3)	0.26(3)	0.00(2)	0.00(3)	0.20(3)	0.04(3)	0.00(3)	-0.03(3)									
C(3)	4.19(5)	-0.05(2)	0.06(3)	0.05(3)	0.08(3)	-0.01(2)	-0.02(3)	-0.18(2)	0.00(2)	0.34(3)	0.02(2)	0.02(3)	0.16(2)	-0.02(2)	0.00(2)	0.02(2)									
C(4)	4.01(5)	0.00(2)	0.04(3)	0.03(3)	0.08(3)	0.01(2)	0.00(2)	-0.15(2)	0.02(2)	0.25(3)	0.00(2)	-0.05(3)	0.27(2)	-0.01(2)	0.02(2)	0.00(2)									
C(5)	4.03(6)	-0.02(2)	0.03(3)	-0.03(3)	0.10(3)	-0.02(2)	-0.02(3)	-0.18(3)	-0.02(2)	0.24(3)	0.03(2)	0.00(3)	0.14(2)	0.02(2)	0.01(2)	0.01(2)									
C(6)	3.93(4)	-0.03(2)	-0.11(2)	-0.01(3)	0.09(3)	-0.01(2)	0.00(2)	-0.21(2)	0.04(2)	0.24(3)	-0.02(2)	-0.04(3)	0.18(2)	0.00(2)	0.03(2)	-0.04(2)									
H(1)	0.77(3)	0.03(2)	0.03(2)	0.05(2)																					
H(2)	0.79(3)	0.02(2)	0.06(2)	0.09(2)																					
H(3)	0.70(3)	0.02(2)	0.02(2)	0.10(2)																					
H(5)	0.78(3)	-0.08(2)	-0.03(2)	0.14(2)																					
H(2A)	0.73(3)	0.11(2)	0.05(2)	0.19(2)																					
H(2B)	0.71(3)	0.07(2)	-0.04(2)	0.07(2)																					

Kappa values

	κ	κ'
S	1.00	0.97
N	0.99	0.94
C	1.00	0.95
H	1.18	1.20
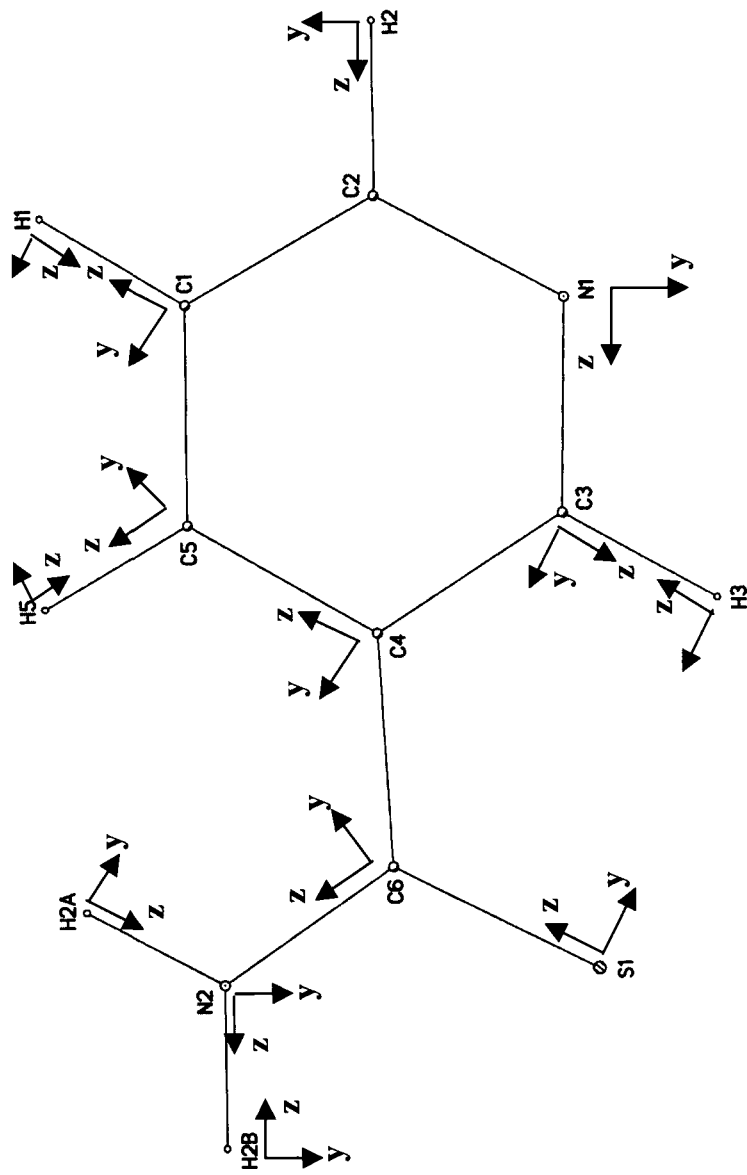
Thionicotinamide

A2.6d Definition of local coordination systems

389

Thionicotinamide
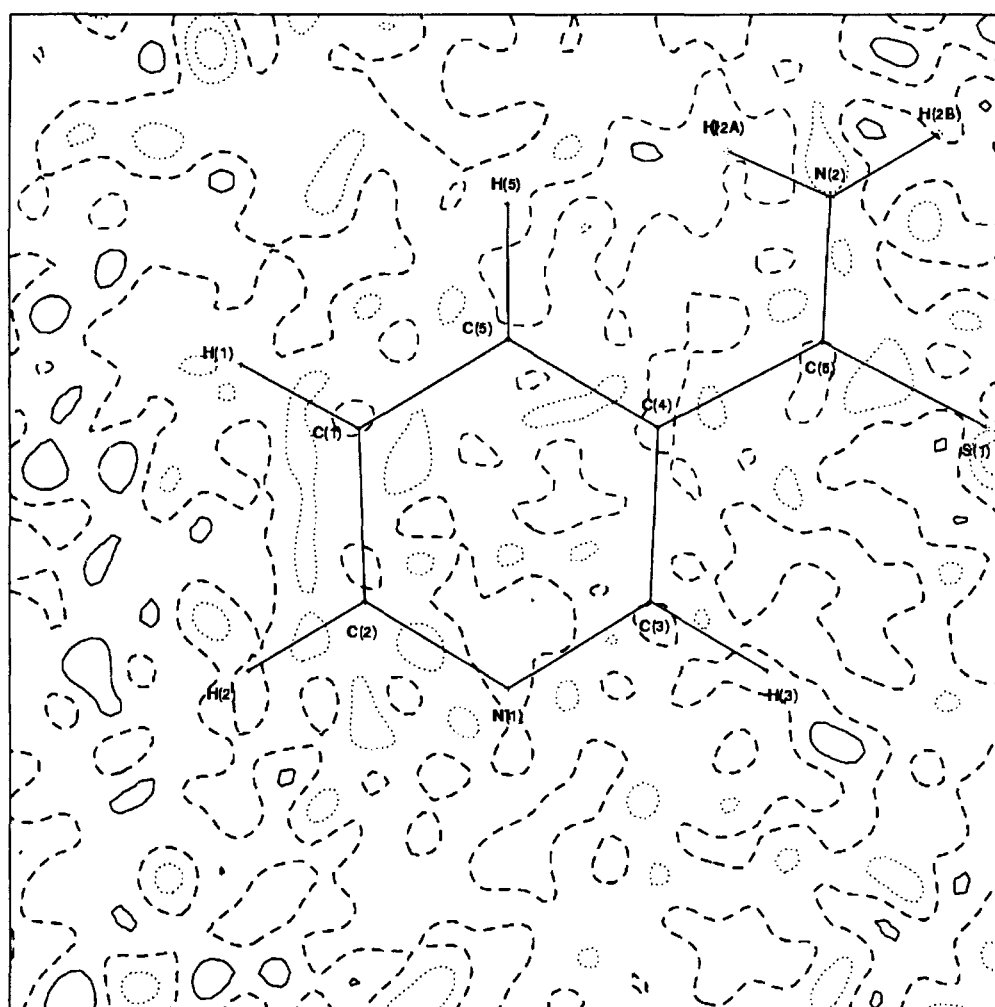
A2.6e Residual electron density map in the plane of the pyridyl ring (contours at 0.1 eÅ^{-3})

Thioacetamide VII

Table A2.7a Fractional Coordinates and Equivalent Isotropic Displacement Parameters [Å²] of VII

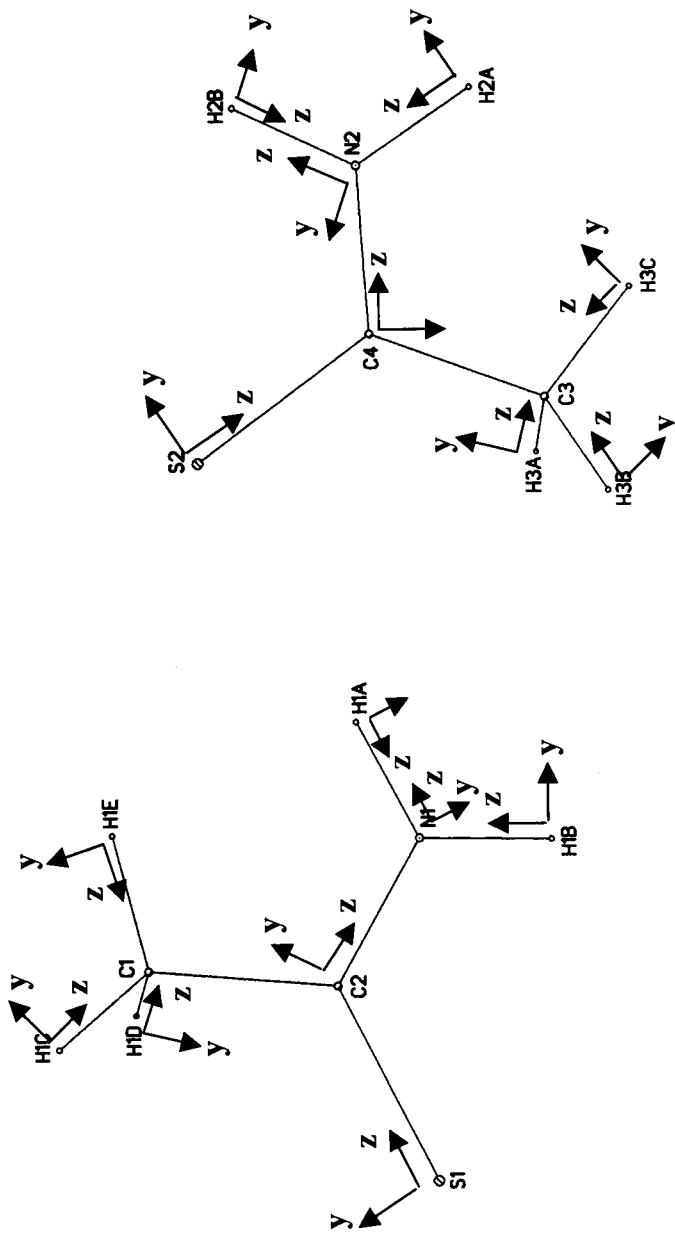| Atom	x/a	y/b	z/c	U_{eq}[a]
S(1)	0.3235(1)	0.6867(1)	0.2486(1)	0.020(1)
S(2)	0.2193(1)	0.1888(1)	-0.0383(1)	0.021(1)
N(2)	0.2955(2)	-0.0599(1)	0.0386(1)	0.021(1)
C(4)	0.2310(2)	0.0603(1)	0.0626(1)	0.016(1)
C(2)	0.2854(2)	0.5609(1)	0.1462(1)	0.018(1)
N(1)	0.2727(2)	0.4336(1)	0.1780(1)	0.027(1)
C(3)	0.1684(2)	0.0768(1)	0.1851(1)	0.023(1)
C(1)	0.2621(2)	0.5887(1)	0.0100(1)	0.028(1)
H(2B)	0.3403(27)	-0.0779(19)	-0.0434(9)	0.045(5)
H(1B)	0.2906(33)	0.4087(21)	0.2689(5)	0.058(7)
H(1D)	0.1318(15)	0.6509(15)	-0.0140(16)	0.036(5)
H(1A)	0.2507(30)	0.3582(13)	0.1146(13)	0.043(5)
H(3C)	0.1552(38)	-0.0236(11)	0.2244(22)	0.088(9)
H(2A)	0.2942(32)	-0.1350(14)	0.1021(14)	0.051(6)
H(3B)	0.2674(27)	0.1368(19)	0.2510(17)	0.065(7)
H(3A)	0.0235(12)	0.1214(19)	0.1735(21)	0.065(7)
H(1C)	0.3853(21)	0.6416(20)	-0.0172(22)	0.072(7)
H(1E)	0.2406(29)	0.4923(10)	-0.0390(16)	0.056(6)

[a] U_{eq} is defined as one-third of the trace of the orthogonalized U_{ij} tensor.

Table A2.7b Multipole populations VII

Atom	M1	D1+	D1-	D0	Q0	Q1+	Q1-	Q2+	Q2-	O0	O1+	O1-	O2+	O2-	O3+	O3-	H0	H1+	H1-	H2+	H2-	H3+	H3-	H4+	H4-
S(1)	6.64(6)	0.10(3)	0.01(3)	0.09(3)	-0.01(4)	0.01(3)	-0.25(3)	-0.10(3)	-0.16(3)	0.14(3)	0.02(3)	-0.02(3)	0.10(3)	0.01(2)	-0.01(3)	-0.04(3)	-0.02(4)	-0.14(4)	0.00(3)	-0.05(3)	-0.07(4)	-0.05(3)	0.03(3)	0.00(3)	-0.03(3)
N(1)	5.18(8)	0.11(4)	-0.10(5)	-0.06(5)	-0.15(5)	-0.03(4)	-0.15(5)	-0.03(5)	-0.07(5)	0.25(4)	0.01(4)	0.02(4)	0.22(4)	0.00(3)	0.02(4)	-0.02(4)									
C(1)	4.18(1)	-0.23(5)	0.02(5)	-0.01(6)	0.04(6)	-0.06(5)	0.06(5)	0.03(5)	0.03(5)	0.10(5)	-0.09(5)	0.08(5)	-0.03(4)	0.04(4)	-0.03(4)	-0.21(4)									
C(2)	4.02(8)	0.05(4)	0.02(4)	-0.01(5)	0.01(5)	0.06(4)	-0.17(4)	-0.22(4)	0.01(3)	0.26(5)	0.01(4)	-0.07(5)	0.13(4)	-0.06(4)	-0.01(3)	-0.05(3)									
S(2)	6.60(6)	0.01(3)	0.00(3)	0.01(3)	-0.22(3)	-0.11(3)	0.25(3)	0.06(3)	-0.20(3)	0.05(3)	-0.02(3)	0.00(3)	0.06(3)	0.00(2)	-0.06(3)	-0.01(3)	-0.10(4)	0.02(4)	0.00(3)	-0.05(4)	-0.07(3)	0.06(3)	-0.07(4)	0.03(3)	-0.05(3)
N(2)	5.31(8)	-0.01(4)	0.02(5)	0.05(5)	0.06(5)	0.12(4)	-0.06(5)	-0.07(5)	-0.01(4)	0.28(3)	-0.02(3)	0.06(4)	0.13(3)	-0.01(3)	0.02(3)	-0.01(4)									
C(3)	4.03(1)	0.00(5)	0.03(5)	-0.07(5)	-0.07(5)	0.03(4)	0.09(4)	0.02(5)	0.01(4)	0.14(4)	-0.02(4)	0.06(4)	-0.07(4)	-0.26(4)	-0.12(4)	-0.25(4)									
C(4)	4.11(8)	0.01(3)	-0.08(4)	-0.08(5)	0.12(5)	-0.02(4)	0.04(4)	-0.26(4)	-0.08(3)	0.30(4)	0.07(4)	0.10(5)	0.19(4)	-0.03(4)	0.03(3)	0.01(3)									
H(1A)	0.80(5)	-0.01(4)	0.01(3)	0.30(4)																					
H(1B)	0.66(6)	-0.10(4)	0.01(4)	0.17(5)																					
H(1C)	0.89(7)	-0.21(4)	-0.09(4)	0.18(6)																					
H(1D)	0.77(6)	-0.02(3)	-0.03(3)	0.10(4)																					
H(1E)	0.87(6)	-0.07(3)	0.04(4)	0.19(5)																					
H(2A)	0.67(5)	0.07(3)	0.01(3)	0.23(4)																					
H(2B)	0.69(5)	0.09(3)	-0.01(3)	0.10(4)																					
H(3A)	0.83(7)	0.10(4)	-0.03(4)	0.30(5)																					
H(3B)	0.83(6)	0.06(4)	-0.10(4)	0.30(5)																					
H(3C)	0.93(8)	0.02(4)	0.01(4)	0.32(6)																					

Kappa values

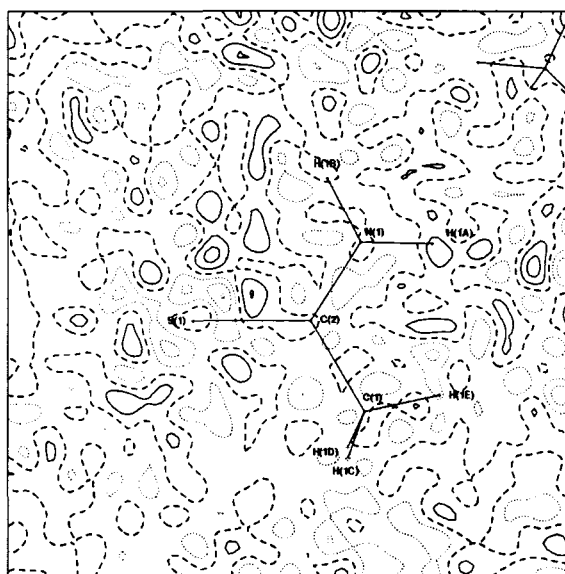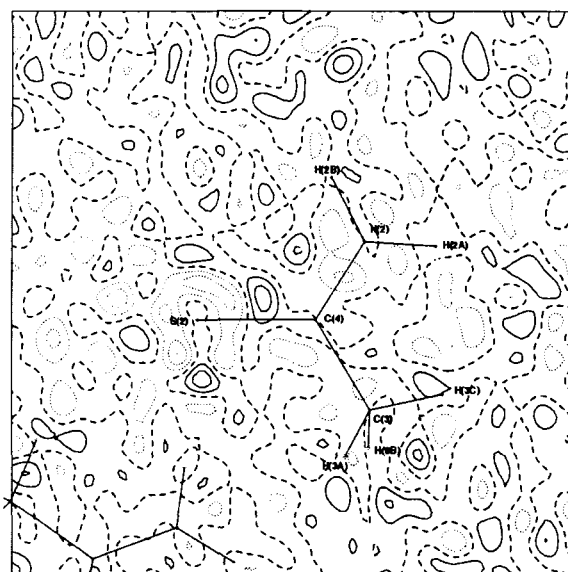|	κ	κ'
S	1.01	1.00
N	0.92	0.92
C	1.00	0.96
H	1.23	1.20

Thioacetamide

A2.7c Definition of local coordination systems

Thioacetamide

Residual electron density map in the plane containing the atoms
S(1), C(2) and N(1) in rotamer I (contours at 0.1 eÅ^{-3})

Residual electron density map in the plane containing the atoms
S(2), C(4) and N(2) in rotamer II (contours at 0.1 eÅ^{-3})

A2.7d